frontiers | Research Topics

Dynamic functional connectivity in neuropsychiatric disorders: Methods and applications, volume II

Edited by
Zaixu Cui, Feng Liu, Wenbin Guo, Yuqi Cheng and Zhifen Liu

Published in
Frontiers in Neuroscience

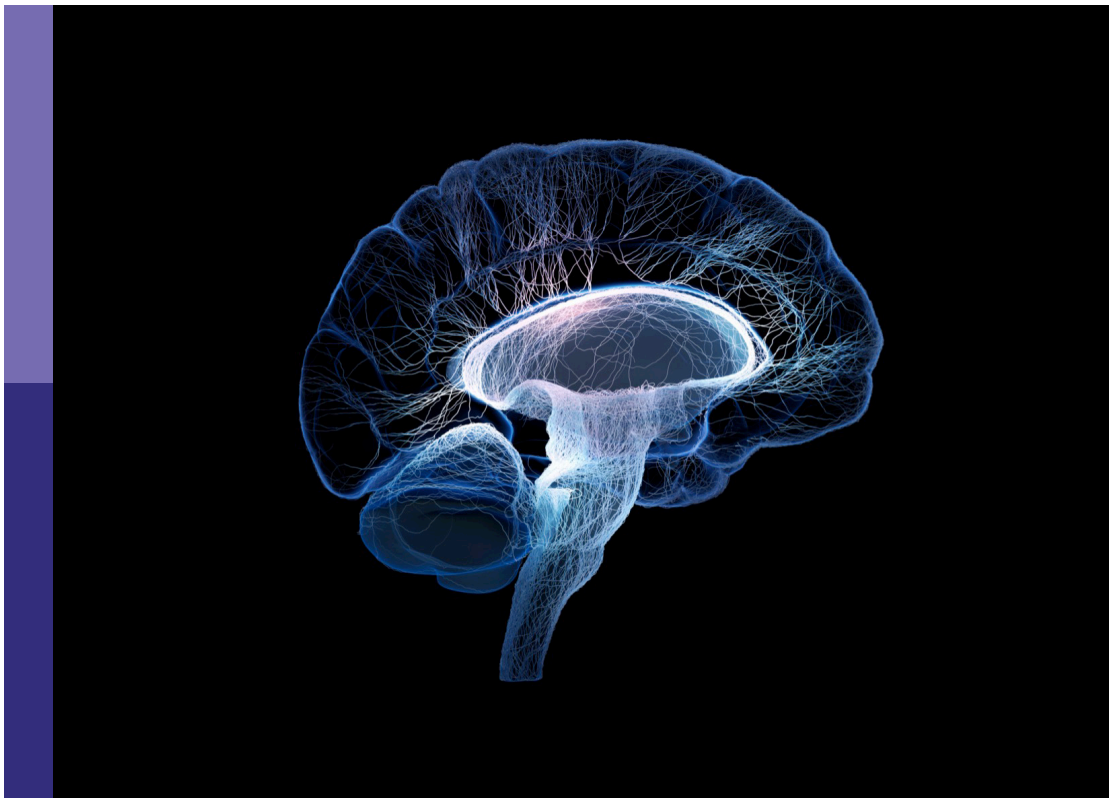

ISSN 1664-8714
ISBN 978-2-83251-021-6
DOI 10.3389/978-2-83251-021-6

About Frontiers

Frontiers is more than just an open access publisher of scholarly articles: it is a pioneering approach to the world of academia, radically improving the way scholarly research is managed. The grand vision of Frontiers is a world where all people have an equal opportunity to seek, share and generate knowledge. Frontiers provides immediate and permanent online open access to all its publications, but this alone is not enough to realize our grand goals.

Frontiers journal series

The Frontiers journal series is a multi-tier and interdisciplinary set of open-access, online journals, promising a paradigm shift from the current review, selection and dissemination processes in academic publishing. All Frontiers journals are driven by researchers for researchers; therefore, they constitute a service to the scholarly community. At the same time, the *Frontiers journal series* operates on a revolutionary invention, the tiered publishing system, initially addressing specific communities of scholars, and gradually climbing up to broader public understanding, thus serving the interests of the lay society, too.

Dedication to quality

Each Frontiers article is a landmark of the highest quality, thanks to genuinely collaborative interactions between authors and review editors, who include some of the world's best academicians. Research must be certified by peers before entering a stream of knowledge that may eventually reach the public - and shape society; therefore, Frontiers only applies the most rigorous and unbiased reviews. Frontiers revolutionizes research publishing by freely delivering the most outstanding research, evaluated with no bias from both the academic and social point of view. By applying the most advanced information technologies, Frontiers is catapulting scholarly publishing into a new generation.

What are Frontiers Research Topics?

Frontiers Research Topics are very popular trademarks of the *Frontiers journals series*: they are collections of at least ten articles, all centered on a particular subject. With their unique mix of varied contributions from Original Research to Review Articles, Frontiers Research Topics unify the most influential researchers, the latest key findings and historical advances in a hot research area.

Find out more on how to host your own Frontiers Research Topic or contribute to one as an author by contacting the Frontiers editorial office: frontiersin.org/about/contact

Dynamic functional connectivity in neuropsychiatric disorders: Methods and applications, volume II

Topic editors

Zaixu Cui — Chinese Institute for Brain Research, Beijing (CIBR), China
Feng Liu — Tianjin Medical University General Hospital, China
Wenbin Guo — Central South University, China
Yuqi Cheng — The First Affiliated Hospital of Kunming Medical University, China
Zhifen Liu — First Hospital of Shanxi Medical University, China

Citation

Cui, Z., Liu, F., Guo, W., Cheng, Y., Liu, Z., eds. (2022). *Dynamic functional connectivity in neuropsychiatric disorders: Methods and applications, volume II*. Lausanne: Frontiers Media SA. doi: 10.3389/978-2-83251-021-6

Table of contents

frontiers | Frontiers in Neuroscience

TYPE Editorial
PUBLISHED 28 November 2022
DOI 10.3389/fnins.2022.1092718

OPEN ACCESS

EDITED AND REVIEWED BY
Vince D. Calhoun,
Georgia State University, United States

*CORRESPONDENCE
Wenbin Guo
guowenbin76@csu.edu.cn

SPECIALTY SECTION
This article was submitted to Brain Imaging Methods, a section of the journal Frontiers in Neuroscience

RECEIVED 08 November 2022
ACCEPTED 16 November 2022
PUBLISHED 28 November 2022

CITATION
Fu X, Liu F, Cui Z, Cheng Y, Liu Z and Guo W (2022) Editorial: Dynamic functional connectivity in neuropsychiatric disorders: Methods and applications, volume II. *Front. Neurosci.* 16:1092718. doi: 10.3389/fnins.2022.1092718

Editorial: Dynamic functional connectivity in neuropsychiatric disorders: Methods and applications, volume II

Xiaoya Fu[1], Feng Liu[2], Zaixu Cui[3], Yuqi Cheng[4,5], Zhifen Liu[6,7] and Wenbin Guo[1,8]*

[1]Department of Psychiatry, National Clinical Research Center for Mental Disorders, The Second Xiangya Hospital of Central South University, Changsha, China, [2]Department of Radiology, Tianjin Medical University General Hospital, Tianjin, China, [3]Chinese Institute for Brain Research, Beijing, China, [4]Department of Psychiatry, The First Affiliated Hospital of Kunming Medical University, Kunming, China, [5]Yunnan Clinical Research Center for Mental Disorders, The First Affiliated Hospital of Kunming Medical University, Kunming, China, [6]Department of Psychiatry, First Hospital of Shanxi Medical University, Taiyuan, China, [7]Shanxi Key Laboratory of Artificial Intelligence Assisted Diagnosis and Treatment for Mental Disorder, First Hospital of Shanxi Medical University, Taiyuan, China, [8]Department of Psychiatry, The Third People's Hospital of Foshan, Foshan, China

KEYWORDS

structural MRI, functional MRI, cognitive deficits, depression, anxiety

Editorial on the Research Topic
Dynamic functional connectivity in neuropsychiatric disorders: Methods and applications, volume II

In 2010, the Global Burden of Disease Study (GBD) reported that the disease burden of neuropsychiatric disorders accounted for 10.4% of global disability-adjusted life years (DALYs). Psychiatric disorders, the fifth leading cause of DALYs, accounted for 7.4% of global DALYs, while neurological disorders accounted for 3% of global DALYs (Whiteford et al., 2015). As the population grows and ages, the global burden of neuropsychiatric diseases continues to increase, which makes neuropsychiatric disorders a prominent health issue.

Patients with neuropsychiatric disorders show multiple problems regarding to emotion, cognition, behavior, and physical symptoms. The neuropathological alterations underlying these somatic discomforts and functional deficits have been one of the critical concerns of researchers. Magnetic resonance imaging (MRI), a safe and non-invasive way to detect changes in brain structure and function, has been one of the most important tools for studying neuropathological changes in neuropsychiatric diseases. Since the discovery of resting-state functional connectivity (FC) by Biswal et al. (1995) and the subsequent introduction of the default mode network (Biswal et al., 1995; Raichle et al., 2001), functional MRI has greatly broadened and deepened our understanding of brain function over the past two decades. However, the focus shifts toward temporal fluctuations in blood-oxygen-level-dependent (BOLD) FC in the brain, considering the rapidly changing neural activity of the brain. In addition to focusing on the

dynamics of FC, the temporal fluctuations of the amplitude of low-frequency fluctuation (ALFF), regional homogeneity (ReHo), and other metrics commonly used in resting-state functional MRI have also been explored for investigating the neuropathological alterations of neuropsychiatric disorders.

This issue is a continuum of our previous topic (Fu et al., 2020). In this Research Topic, we received several articles applying neuroimaging tools to reveal the dynamic function of the brain and articles focusing on neuropsychiatric disorders with other imaging analyses. In the end, a total of 18 papers are included in this Research Topic. We found that the concerns of many studies shifted from a particular disorder to more specific symptoms. Given the heterogeneous manifestations of neuropsychiatric disorders, this symptom delineation might be more conducive to the exploration of the neuropathological mechanisms underlying specific symptoms. In addition, many studies explored the correlation of imaging findings with clinical symptoms and the robustness of differences between groups. These attempts might have a positive influence on the clinical application of these imaging tools.

Of these 18 articles, only 2 articles examined neurological disorders, and the other 16 articles focused on psychiatric disorders. Major depressive disorders (MDD) were the most discussed disorders. Suicide, non-suicidal self-injury, childhood trauma, and medication efficacy were the main focus of these MDD studies.

MDD was responsible for the highest proportion of neuropsychiatric disorder DALYs (Whiteford et al., 2015). Both suicide and non-suicidal self-injury are strongly associated with MDD. Li W. et al. and He et al. examined the neural basis of suicide ideation (SI) of patients of MDD by using different imaging analyses in various brain regions. Li W. et al. used a dynamic FC to study a critical brain region of a default mode network, the PCC, which has been reported to be associated with suicidal ideation in depressed patients in structural and functional MRI studies (Schmaal et al., 2020). He et al. focused on the neuropathological alterations of cingulo-opercular network in MDD patients with SI by using structural and functional neuroimaging. Besides SI, non-suicidal self-injury (NSSI) is also a symptom worthy of note, especially in adolescent MDD. Both NSSI and SI exhibited robust relationships to attempted suicide (Klonsky et al., 2013). Liu H. et al. used an electrophysiological approach to explore the difference in P300 in adolescent MDD patients with NSSI. Yang C. et al. concentrated on suicide attempts (SA) in patients with MDD, and they found that elevated activity in the cingulum functioning may be related to SA.

The associations between childhood trauma and multiple psychiatric disorders have been reported in many previous studies (Varese et al., 2012; McKay et al., 2021). Childhood trauma is a significant predictor of depression severity (Hopfinger et al., 2016). Chen et al. investigated the functional MRI data of female MDD patients with and without childhood trauma and healthy controls. But no ALFF difference was found between MDD patients with childhood trauma and those without. Luo et al. also showed an interest in the impact of childhood trauma on the brain function of patients with MDD. They used multiple dynamic functional MRI indices throughout the whole brain, and examined the aberrant temporal fluctuations of brain function from various perspectives.

As a non-invasive examination, MRI is also very promising in predicting drug efficacy. Two articles in this special issue examined the possibility that MRI is used to predict drug efficacy for two kinds of medical intervention, respectively. Zhang A. et al. separated patients with MDD into a responsive group and a non-responsive group based on the reduction rate of the scores of Hamilton Depression Rating Scale (HAMD-17) after 2-week SSRI treatment and found that there were differences in ReHo in the right parahippocampal gyrus and the middle temporal gyrus between groups. Compared to the study of Zhang A. et al., Zhang F. et al. focused on a novel antidepressant, ketamine, an N-methyl-D-aspartate (NMDA) antagonist. The responders in this study were defined as having an improvement in the Montgomery-Asberg Scale (MADRS) scores $\geq$ 50% after six intravenous injections of ketamine over 12 days. Zhang F. et al. found that responders had lower values of degree centrality in the right middle frontal gyrus (MFG) and stronger FC between the MFG and the right supplementary motor area (SMA) than non-responders.

Besides studies concerning MDD, there are also studies in this special issue that focus on dynamic brain function changes in other psychiatric disorders. Kong et al. investigated network homogeneity (NH) of the default mode network in 57 first-diagnosis drug-naïve schizophrenic patients and 50 healthy controls. Fateh et al. evaluated the dynamic FC within six subdivisions of the insula to investigate whether the dysregulated dynamic FC in insula was related to social dysfunction in patients with attention deficit hyperactivity disorder (ADHD). Liu D. et al. examined both static and dynamic functional brain network in adults with problematic smartphone use. It is important to note that although both the International Classification of Diseases (11 Edition, ICD-11) and Diagnostic and Statistical Manual of Mental Disorders (Fifth Edition, DSM-5) now include a diagnosis of gaming disorder (Gaming Disorder in ICD-11 and Internet Gaming Disorder in DSM-5), problematic smartphone use is not currently a disease. Liu D. et al. found no group difference between participants with and without problematic smartphone use, however the severity of problematic smartphone use was correlated with FC strength as well as temporal variability. Yang, Li, et al. conducted the only comparative study on psychiatric disorders in this special issue. They recruited patients with schizophrenia (SZ), major depressive disorder (MDD) and bipolar disorder (BD) and healthy controls to examine the common and specific neuroanatomical characteristics.

There are three articles in this special issue involved in other diseases rather than psychiatric disorders. Yang, Zhao, et al., and Su et al. all concerned about systemic lupus erythematosus (SLE), an autoimmune disease sometimes involving the nervous system, called neuropsychiatric systemic lupus (NPSLE). The study of Su et al. demonstrated that patients with NPSLE showed atrophic subcortical gray matter and functional alterations in the default mode network, salience network, sensorimotor network, and cerebellum. Yang, Zhao, et al. explored the static and dynamic ALFF in SLE patients with cognitive impairment (CI). Patients with SLE showed altered dynamic ALFF no matter with or without CI, and SLE patients with CI also had changed static ALFF. Nevertheless, compared to SLE patients without CI, those with cognitive impairment only showed higher static ALFF in the right parahippocampal gyrus, but no difference in dynamic ALFF was found between these two groups. Wang, Wang, et al. used FC to discriminate between migraineurs and tension-type headache, which share many similarities in clinical practice.

Notably, three articles in this special issue introduced novel analysis methods for neuropsychiatric disorders. These three articles all proposed improvements and reflections on the application of image analysis to disease diagnosis. Wang, Fu, et al. used the random support vector machine (SVM) cluster, a machine-learning framework, to extract an optimized random SVM cluster that performs well in classifying patients with autism spectrum disorder (ASD) and healthy controls. Song et al. proposed a novel brain-network-constrained multi-view sparse canonical correlation analysis (BN-MSCCA), which combined the structural and functional MRI data as well as diagnosis information to explore the schizophrenia-related biomarkers. Both articles introduced multiple or multimodal features when testing the diagnostic model. Li Y. et al. combined uncertain brain networks and a novel discriminative feature selection method based on a statistical index (dfsSI) to optimize the time consumption, computational cost and the classification accuracy.

Overall, the articles in this special issue applied various imaging analysis methods, with a particular focus on the dynamic changes in brain function. These articles explored the underlying neural basis of neuropsychiatric disorders and also presented several novel approaches. It is hoped that clinicians and researchers will benefit from them.

Author contributions

All authors listed have made a substantial, direct, and intellectual contribution to the work and approved it for publication.

Funding

This study was supported by grants from the National Natural Science Foundation of China (Grant No. 82171508), Natural Science Foundation of Hunan (Grant No. 2020JJ4784), Science and Technology Program of Hunan Province (Grant No. 2020SK53413), and Natural Science Foundation of Tianjin (Grant No. 18JCQNJC10900).

Conflict of interest

The authors declare that the research was conducted in the absence of any commercial or financial relationships that could be construed as a potential conflict of interest.

Publisher's note

All claims expressed in this article are solely those of the authors and do not necessarily represent those of their affiliated organizations, or those of the publisher, the editors and the reviewers. Any product that may be evaluated in this article, or claim that may be made by its manufacturer, is not guaranteed or endorsed by the publisher.

References

Biswal, B., Yetkin, F. Z., Haughton, V. M., and Hyde, J. S. (1995). Functional connectivity in the motor cortex of resting human brain using echo-planar MRI. *Magn. Reson. Med.* 34, 537–541. doi: 10.1002/mrm.1910340409

Fu, X., Liu, F., Cui, Z., and Guo, W. (2020). Editorial: Dynamic functional connectivity in neuropsychiatric disorders: methods and applications. *Front. Neurosci.* 14, 332. doi: 10.3389/fnins.2020.00332

Hopfinger, L., Berking, M., Bockting, C. L. H., and Ebert, D. D. (2016). Emotion regulation mediates the effect of childhood trauma on depression. *J. Affect. Disord.* 198, 189–197. doi: 10.1016/j.jad.2016.03.050

Klonsky, E. D., May, A. M., and Glenn, C. R. (2013). The relationship between nonsuicidal self-injury and attempted suicide: Converging evidence from four samples. *J. Abnormal Psychol.* 122, 231–237. doi: 10.1037/a0030278

McKay, M. T., Cannon, M., Chambers, D., Conroy, R. M., Coughlan, H., Dodd, P., et al. (2021). Childhood trauma and adult mental disorder: A systematic review and meta-analysis of longitudinal cohort studies. *Acta Psychiatr. Scand.* 143, 189–205. doi: 10.1111/acps.13268

Raichle, M. E., MacLeod, A. M., Snyder, A. Z., Powers, W. J., Gusnard, D. A., and Shulman, G. L. (2001). A default mode of brain function. *Proc. Natl. Acad. Sci. U S A.* 98, 676–682. doi: 10.1073/pnas.98.2.676

Schmaal, L., van Harmelen, A.-L., Chatzi, V., Lippard, E. T. C., Toenders, Y. J., Averill, L. A., et al. (2020). Imaging suicidal thoughts and behaviors: a comprehensive review of 2 decades of neuroimaging studies. *Mol. Psychiat.* 25, 408–427. doi: 10.1038/s41380-019-0587-x

Varese, F., Smeets, F., Drukker, M., Lieverse, R., Lataster, T., Viechtbauer, W., et al. (2012). Childhood adversities increase the risk of psychosis: a meta-analysis of patient-control, prospective- and cross-sectional cohort studies. *Schizophr. Bull.* 38, 661–671. doi: 10.1093/schbul/sbs050

Whiteford, H. A., Ferrari, A. J., Degenhardt, L., Feigin, V., and Vos, T. (2015). The global burden of mental, neurological and substance use disorders: An analysis from the global burden of disease study 2010. *PLoS ONE* 10, e0116820. doi: 10.1371/journal.pone.0116820

frontiers in Neuroscience

CLINICAL TRIAL
published: 16 February 2022
doi: 10.3389/fnins.2022.831278

Resting-State fMRI in Predicting Response to Treatment With SSRIs in First-Episode, Drug-Naive Patients With Major Depressive Disorder

Aixia Zhang[1,2†], Xin Wang[1,2†], Jianying Li[1,2], Lin Jing[1,2], Xiaodong Hu[1,2], Hejun Li[1,2], Chunxia Yang[1,2], Kerang Zhang[1,2] and Ning Sun[1,2,3*]*

[1] Department of Psychiatry, First Hospital of Shanxi Medical University, Taiyuan, China, [2] First Clinical Medical College of Shanxi Medical University, Taiyuan, China, [3] Department of Mental Health, Shanxi Medical University, Taiyuan, China

OPEN ACCESS

Edited by:
Wenbin Guo,
Central South University, China

Reviewed by:
Chun Wang,
Nanjing Brain Hospital Affiliated to Nanjing Medical University, China
Daihui Peng,
Shanghai Jiao Tong University, China

***Correspondence:**
Kerang Zhang
atomsxmu@vip.163.com
Ning Sun
sunning@sxmu.edu.con

[†] These authors have contributed equally to this work

Specialty section:
This article was submitted to Brain Imaging Methods, a section of the journal Frontiers in Neuroscience

Received: 08 December 2021
Accepted: 27 January 2022
Published: 16 February 2022

Citation:
Zhang A, Wang X, Li J, Jing L, Hu X, Li H, Yang C, Zhang K and Sun N (2022) Resting-State fMRI in Predicting Response to Treatment With SSRIs in First-Episode, Drug-Naive Patients With Major Depressive Disorder. Front. Neurosci. 16:831278. doi: 10.3389/fnins.2022.831278

Objective: For major depressive disorder (MDD), there has been a lack of neuroimaging markers of efficacy of pharmacological treatment. In this study, we aimed to explore the neuroimaging mechanisms in patients with first-episode MDD and identify markers that predict the efficacy of 5-hydroxytryptamine reuptake inhibitors (SSRIs) with the use of resting-state brain imaging technology.

Methods: A total of 101 patients with first-episode MDD and 53 normal controls were finally included in this study. Based on the reduction rate of the score of Hamilton Depression Rating Scale (HAMD-17) during the 2-week SSRI treatment, 31 patients were assigned into the unresponsive group and 32 were assigned into the responsive group. The brain function was compared between patients with MDD and normal controls, and the diagnostic value of brain function was analyzed. With brain regions showing differences between patients with MDD and normal controls as a mask, and the brain function between the responsive and unresponsive groups were compared. Correlations between brain function the HAMD-17 score reduction rate during the 2-week SSRI treatment were analyzed.

Results: Compared to normal controls, patients with MDD showed increased ReHo in the left parahippocampal gyrus and right parahippocampal gyrus, decreased ReHo in the right middle occipital gyrus, and decreased functional connectivity between the right and left parahippocampal gyri, right middle occipital gyrus and middle temporal gyrus. Receiver operator characteristic (ROC) curve analysis showed that the area under the curve (AUC) was 0.544 (95% CI: 0.445–0.644) for ReHo and 0.822 (95% CI: 0.734–0.909) for functional connectivity. Logistic regression pooling of the differences in ReHo mean time series with the functional connectivity mean time series was performed for the ROC curve analysis, which showed an AUC of 0.832 (95% CI: 0.752–0.911). Compared to the responsive group, the unresponsive group showed elevated ReHo in the right parahippocampal gyrus and lower functional connectivity in the middle temporal gyrus. We also found that the ReHo value was negatively correlated with the HAMD-17 score reduction after 2 weeks of SSRI treatment.

Conclusion: Altered resting-state brain function in some regions might be a neurobiological marker for the diagnosis of MDD, and ReHo values are expected to be predictors of patient response to treatment with SSRIs.

Clinical Trial Registration: [http://www.chictr.org.cn/], identifier [ChiCTR1900028722].

Keywords: major depressive disorder, resting-state functional MRI, SSRIs, regional homogeneity, functional connectivity

INTRODUCTION

Major depressive disorder (MDD) is one of the most common psychiatric disorders associated with severe impairments of quality of life and social function. However, the response and remission rates of MDD remain low as the pathogenesis is still unclear at present. In clinical practice, only 30% of patients are clinically cured by medication, with an response rate of 40–50% (Trivedi et al., 2006; Rush, 2007). Approximately 30% of patients develop refractory depression, and around 70% of patients require several courses of treatment or repeated "trial and error" treatment to achieve remission (McIntyre et al., 2014). A study showed that symptom improvement after 2 weeks of treatment with antidepressants was predictive of clinical remission after 6–8 weeks of treatment, and that patients with MDD who did not respond to antidepressant treatment for 2 weeks had a final remission rate of only 4% if the regimen was unchanged (Szegedi et al., 2009). *Post-hoc* analyses of several clinical trials have also shown that non-response at the end of 2 weeks of antidepressant treatment was predictive of poor treatment outcome after 6–8 weeks (Szegedi et al., 2003; Posternak and Zimmerman, 2005; Papakostas et al., 2006; Taylor et al., 2006; Stassen et al., 2007; Henkel et al., 2009; Hennings et al., 2009; van Calker et al., 2009; Tadić et al., 2010). A study illustrated that non-response at the end of 2 weeks of treatment with 5-hydroxytryptamine reuptake inhibitors (SSRIs) can be considered a valid predictor of poor treatment outcome, indicating that an alternate medication or a combination of drugs could be commenced (Tadić et al., 2016). Therefore, understanding the neuropathological mechanisms of MDD and exploring biomarkers of early therapeutic responses in patients with MDD can provide a basis for clinicians to develop treatment strategies in clinical practice.

Resting-state functional magnetic resonance imaging (MRI) studies have mainly focused on the differences in functional brain activities at rest, while task-state functional MRI studies mainly focused on functional brain activities during tasks; these studies have been proven to be reproducible for the brain imaging procedures and verifiable for the results. At present, the studies of brain function mainly focus on evaluating local functional changes; with brain regions of interest (ROIs) as connection nodes, the spontaneous activities between brain regions are observed, which are used as connection coefficients of brain function to reflect the functional connection between brain regions. Regional homogeneity (ReHo) is used as a measure of regional synchronization of the functional magnetic resonance imaging (fMRI) time course, and has been widely used in clinical studies on MDD. Previous studies on MDD based on resting-state fMRI have revealed abnormalities in several brain regions and functional connections, with more consistent findings involving the prefrontal-amygdala-striatal-medial thalamic regions in the emotion regulation loop. Subsequent studies showed that increased activity in the amygdala and ventrolateral prefrontal cortex at baseline was predictive of poor response to antidepressants, while increased activity in the hippocampus was associated with improvement in depressive symptoms (Williams et al., 2015). During the treatment of MDD with duloxetine, improvement in depressive symptoms was associated with reduced orbitofrontal functional connectivity in the default network; in contrast, reduced orbitofrontal functional connectivity in the default network was associated with poor response to escitalopram in elderly patients with MDD. Meanwhile, increased levels of functional connections in the orbitofrontal cortex prior to treatment were associated with better response to antidepressants (Pizzagalli, 2011). A study showed that a single dose of antidepressants was fast enough to cause significant changes in functional connections in the brain (Schaefer et al., 2014); through brain imaging scans on healthy subjects before and after administration of a single dose of 5-hydroxytryptamine reuptake inhibitors (SSRIs), this study found that functional connections in their brains significantly altered within 3 h. In this study, the whole-brain analysis showed that single doses of 5-hydroxytryptamine reuptake inhibitors (SSRIs) rapidly reduced the level of internal functional connectivity in most brain regions; however, in the cerebellum and thalamus, the level of brain functional connections was increased. It was evident that resting-state fMRI technology has the potential to reflect and identify objective neurobiological markers of psychiatric disorders, and can be used to determine which indicators to use for the early diagnosis and outcome prediction of psychiatric disorders.

MATERIALS AND METHODS

Collection and Evaluation of Clinical Data

Subject Selection

A total of 167 first-episode and treatment-naive patients with MDD were recruited from the inpatient and outpatient department of mental health of the First Hospital of Shanxi Medical University from September 2009 to December 2018. All

the patients were assessed at baseline with the use of MRI and symptom scales, including the Hamilton Depression Rating Scale (HAMD-17) to assess depressive symptoms and the Hamilton Anxiety Rating Scale (HAMA) to assess anxiety symptoms. Eighty healthy controls were recruited from the community and the university, and none of them were relatives of the patients. All the participants provided informed consent.

Patients with MDD were diagnosed and screened by two experienced psychiatrists with the following inclusion criteria: (1) Han Chinese; (2) aged 18–60 years; (3) right-handed; (4) diagnosed with first-episode MDD based on the DSM-IV criteria and untreated; (5) HAMD-17 score $>$ 17 and HAMA-14 score $<$ 14; (6) having provided informed consent for this study. The exclusion criteria were: (1) with MDD or bipolar disorder secondary to organic diseases or antipsychotic drugs; (2) meeting the DSM-IV-TR criteria for Axis I disorders such as alcohol or drug dependence, traumatic stress, and schizoid affective disorder; (3) with severe organic diseases such as neurological diseases, severe liver and kidney dysfunction, cardiovascular diseases, and craniocerebral trauma; (4) with severe suicidal and self-injurious thoughts, history of suicide attempts (suicide-related score $\geq$ 2 in the HAMD-17), obvious impulsivity, or uncooperativeness; (5) breastfeeding or pregnant women; (6) with contraindications to the MRI scan.

Treatment for the Subjects

The untreated patients with first-episode MDD were given standardized antidepressant medication after enrollment. The drugs were SSRIs, including fluoxetine dispersible tablets (Eli Lilly; 10–40 mg/day), escitalopram tablets (Janssen; 5–20 mg/day), citalopram tablets (Envac; 10–40 mg/day), and sertraline tablets (Pfizer; 25–200 mg/day). All the drugs were initiated at small doses and adjusted based on the patients' own conditions. Patients with insomnia were given short-term benzodiazepines or supportive psychotherapy as appropriate. Other antidepressants, antipsychotics, electroconvulsive therapy, or other physical therapies were not used within the 2-week treatment period in this study. The patients' symptoms were evaluated and recorded before treatment and at 2 weeks after the initiation of treatment.

Clinical Data Collection

General Demographic Information

The demographic information of participants, including sex, age, education, marital status, smoking, alcohol consumption, substance abuse, family history, etc., was recorded using the case report form (CRF) developed by our department.

Scales for Clinical Symptoms

The Hamilton Depression Rating Scale (HAMD-17) was used to assess depressive symptoms of the patients and the HAMA was used to assess anxiety symptoms.

Resting-State Functional Magnetic Resonance Imaging

The MRI scans were performed using a Magnetom Trio (A Tim System) 3T whole-body magnetic resonance imaging device manufactured by Siemens. All the subjects underwent MRI scanning after fully informed of the procedure, approximate time required, and possible adverse reactions to the examination. At the time of scanning, the subjects were placed in a supine position, had their heads fixed with sponge pads and wore headphones to reduce the noise they hear. They were required to keep their eyes closed while remaining awake, and refrain from talking, moving or falling asleep. The subjects were also given an alarm bell to end the scan if they were intolerant. A cranial localization scan was first performed, followed by a resting-state scan and a whole-brain stereo 3D high-resolution T1-weighted scan.

A total of 32 layers were obtained with the use of the following parameters: TR (repetition time) = 2,000 ms, TE (echo time) = 30 ms, FOV (field of view) = 240 $\times$ 240 mm2, FA (flip angle) = 90°, acquisition matrix = 64 $\times$ 64, THK (thickness) = 3 mm, and gap = 3.99 mm. The subjects were scanned at a total of 212 time points, with the duration of scanning being 8 min and 6 s.

Analysis of Resting-State Functional Magnetic Resonance Imaging Data

Preprocessing of Resting-State Functional Magnetic Resonance Imaging Data

The resting-state fMRI data was preprocessed using DPARSF[1] based on the SPM8 software (Chao-Gan and Yu-Feng, 2010). The procedures are as follows: (1) the first 10 time points were discarded to allow the magnetic field to reach a steady state; (2) a time-layer correction was performed to exclude the discrepancies caused by intermittent image acquisition; (3) head movement correction was performed by aligning images at all time points to the first image to exclude possible head movements; (4) the single shot echo planar imaging (EPI) template was used for spatial normalization, and the data were normalized to montreal neurological institute (MNI) space and resampled to achieve a voxel size of 3 $\times$ 3 $\times$ 3 mm^3; (5) the images were smoothed with a 6-mm FWHM (full-width at half maximum) kernel for subsequent analysis of functional connection; however, for the ReHo (regional homogeneity) analysis, no smoothing was performed; (6) the smoothed data were filtered for frequencies of 0.01–0.08 Hz; (7) the filtered images were delinearized to remove the drift; and (8) regressions were performed on six cephalomotor parameters, as well as cerebrospinal fluid and white matter signals using the preprocessed data. As regression of whole-brain signals would exaggerate the negative correlations between functional connections, it was not performed to ensure the stability of the results. Finally, ReHo and ROI-based functional connection measures were calculated.

The image quality of raw data was checked by experienced neuroimaging physicians to exclude obvious anatomical abnormalities and artifacts in the MRI data of all participants. Then, all images normalized in data space were checked for obvious alignment errors during data preprocessing. Data with artifacts or non-standard alignments were excluded after inspection. Finally, subjects with head movements greater than

[1] http://rfmri.org/dpabi

2.0 mm in the x, y, and z directions or rotations greater than 2.0 degrees were excluded.

Statistical Analyses

After exclusion of patients with unusable data, a total of 101 patients with MDD and 53 normal controls were included in the study. Data analyses were performed using SPM8 software-based DPARSF (see text footnote 1), and independent samples *t*-test was used to compare ReHo, low-frequency oscillatory amplitudes (ALFF)/low-frequency amplitude ratios (fALFF), and brain regions with significant differences in whole-brain functional connections between patients and normal controls. The ROI-based whole-brain functional connectivity was calculated and Fisher's z transformation was performed using the Gaussian random field (GRF) method. For all the above analyses, $P < 0.05$ indicated statistical significance. Then, receiver operator characteristic (ROC) curves were used to analyze the diagnostic value of resting-state fMRI for MDD.

After 2 weeks of treatment with SSRIs, the patients were divided into the unresponsive group (n = 31) and the responsive group (n = 32) based on their HAMD-17 scores (unresponsive: reduction rate $\leq$ 20%, responsive: reduction rate $\geq$ 50%). With brain regions showing significant difference between patients and normal controls as masks, independent samples *t*-test was performed to compare ReHo, ALFF/fALFF, and ROI-based functional connectivity across the whole brain at baseline between the responsive and unresponsive groups. After the ROI-based functional connectivity was calculated, Fisher's Z transformation was performed, with AlphaSim used for correction. The threshold for statistical significance for a single voxel was set at $p < 0.01$ (uncorrected) and $p < 0.05$ (corrected). Finally, the mean time series of the brain regions with difference between the responsive and unresponsive groups were extracted and used in a partial correlation analysis with the rate of HAMD reduction during the 2-week treatment, with age, sex, and education as covariates.

TABLE 1 | | General demographic information and clinical characteristics of the patients with major depressive disorder (MDD) and normal controls.

Variables	MDD patients (n = 101)	HCs (n = 53)	*P*-value
Age, years ($\bar{x} \pm s$)	34.50 ± 11.091	35.92 ± 9.23	0.814[a]
Sex (F/M)	56/45	26/27	0.747[b]
Education, years ($\bar{x} \pm s$)	4.25 ± 1.39	4.47 ± 1.20	0.329[a]
HAMD-17 scores ($\bar{x} \pm s$)	23.4 ± 2.3	NA	–

[a] *t-test.*
[b] χ^2 *test.*
Education: 1 = illiterate, 2 = elementary school, 3 = junior high school, 4 = senior high school, 5 = junior college, 6 = undergraduate, 7 = graduate and above.

TABLE 2 | | General demographic data and clinical characteristics of the responsive and unresponsive groups.

Variables	The effective group (n = 32)	The ineffective group (n = 31)	*P*-value
Age, years ($\bar{x} \pm s$)	34.59 ± 10.21	36.29 ± 12.49	0.577[a]
Sex (F/M)	18/14	13/16	0.189[b]
Education, years ($\bar{x} \pm s$)	4.48 ± 1.57	4.10 ± 1.51	0.348[a]
HAMD-17 scores (0 w) ($\bar{x} \pm s$)	21.74 ± 4.03	20.65 ± 3.05	0.245[a]
HAMD-17 scores (2 w) ($\bar{x} \pm s$)	7.58 ± 3.75	17.92 ± 3.37	0.000[a]

[a] *t-test.*
[b] χ^2 *test.*
Education: 1 = illiterate, 2 = elementary school, 3 = junior high school, 4 = senior high school, 5 = junior college, 6 = undergraduate, 7 = graduate and above.

RESULTS

General Demographic Data and Clinical Characteristics

A total of 101 patients with MDD and 53 normal controls with satisfactory resting-state fMRI data were included in the analyses. The general demographic data and clinical characteristics of the patients with MDD and normal controls are presented in **Table 1**. According to results of independent samples *t*-test for age and education and chi-square test for sex, there were no significant differences in age (t = −0.236, p = 0.814), sex (x^2 = 0.104, p = 0.747), and education (t = 0.980, p = 0.329) between the two groups.

After 2 weeks of SSRI treatment, the patients were divided into the unresponsive group (n = 31) and the responsive group (n = 32) based on their HAMD-17 scores. The general demographic data and clinical characteristics of the responsive and unresponsive groups are presented in **Table 2**. According to results of independent sample *t*-test for age, education and HAMD-17 scores and chi-square test for sex, there were no significant differences in age (t = −0.566, p = 0.577), sex (X^2 = 1.724, p = 0.189), and education (t = 1.175, p = 0.245) between the two groups.

Resting-State Functional Magnetic Resonance Imaging Results

ALFF/fALFF

The result of independent samples *t*-test showed that there was no significant difference in ALFF/fALFF between patients with MDD and the normal controls.

TABLE 3 | | ReHo of brain regions showing significant difference between patients with major depressive disorder (MDD) and normal controls.

Regions	Voxel size	BA	Left/ Right	MNI peak coordinates			Peak *t* value
				x	y	z	
MDD > NCs							
Parahippocampal gyrus	456	–	Left	−27	−27	−18	4.837
	119	–	Right	9	−24	6	4.572
MDD < NCs							
Interoccipital gyrus	176	–	Right	27	−84	24	−4.122

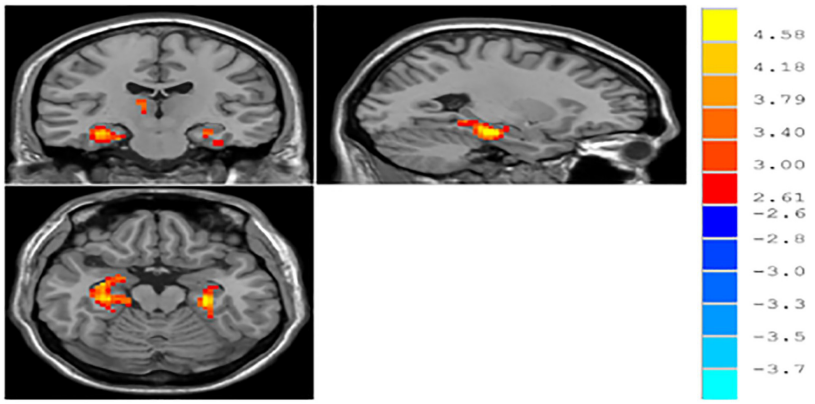

FIGURE 1 | | Brain regions with different ReHo between patients with major depressive disorder (MDD) and normal controls.

ReHo

The result of independent samples *t*-test showed that, after GRF correction, ReHo significantly increased in the left parahippocampal gyrus and right parahippocampal gyrus and significantly decreased in the right middle occipital gyrus in patients with MDD, as compared with normal controls ($p < 0.05$) (see **Table 3** and **Figure 1**).

Differences in Regions of Interest-Based Functional Connections Between the Patients With Major Depressive Disorder and Normal Controls

According to the independent samples *t*-test with GRF correction, the functional connections between the left and right parahippocampal gyri and between the right middle occipital gyrus and middle temporal gyrus significantly decreased in patients with MDD, as compared with normal controls ($p < 0.05$) (see **Table 4** and **Figure 2**).

ROC curve analysis was performed by extracting brain regions with different ReHo values with the mean time series of the whole brain functional connections in patients with MDD and normal controls. The curves were plotted with the horizontal coordinate as (1–specificity) and the vertical coordinate as sensitivity. The Youden index of the ROC curve was further calculated as sensitivity + specificity −1. The maximum value of the Youden index was used as the basis for the optimal threshold to calculate the sensitivity and specificity. As shown in **Figure 3**, the area under the curve (AUC) for ReHo was 0.544 (95% CI: 0.445–0.644), and the AUC for functional connectivity was 0.822 (95% CI: 0.734–0.909). Logistic regression of mean time series of ReHo with the mean time series of functional connections was performed for the ROC curve analysis, which showed that the AUC was 0.832 (95% CI: 0.752–0.911), with a sensitivity of 93.1% and specificity of 75.5% (see **Figure 4**).

TABLE 4 | | Differences in regions of interest (ROI)-based functional connections between patients with major depressive disorder (MDD) and normal controls.

Regions	Voxel size	BA	Left/ Right	MNI peak coordinates			Peak *t* value
				x	y	z	
MDD < NCs							
Temporal pole: middle temporal gyrus	57	–	Right	42	21	−39	−23.081
	44	–	Left	−45	18	−36	−19.406
Middle temporal gyrus	56	–	Left	−69	−18	−9	−12.79

Comparison of Resting-State Brain Function Between the Responsive and Unresponsive Groups

ALFF/fALFF

There were no significant differences in brain areas between the effective and ineffective groups in the ALFF/fALFF ratio using the independent samples *t*-test.

ReHo

ReHo values in the right parahippocampal gyrus significantly reduced in the responsive group as compared with the unresponsive group, while no significant difference was found in the right middle occipital gyrus and the left parahippocampal gyrus, as shown in **Table 5** and **Figure 5**.

Regions of Interest-Based Functional Connectivity

The result showed that functional connections of the middle temporal gyrus in the unresponsive group were significantly lower than those in the responsive group ($p < 0.05$), as shown in **Table 6** and **Figure 6**.

Correlations Between Changes in Resting-State Brain Function and Treatment Efficacy

The result showed that there was a negative correlation between changes in resting-state ReHo and the HAMD-17 score reduction rate when controlling for sex, age, and education ($r = -0.265$, $p = 0.028$), as shown in **Figure 7**.

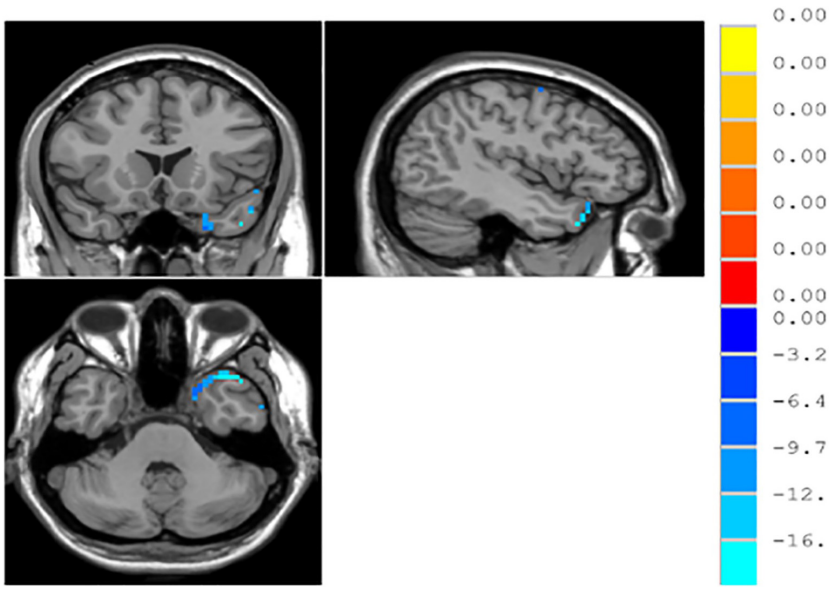

FIGURE 2 | | Regions of interest (ROI)-based functional connections in patients with major depressive disorder (MDD) and normal controls.

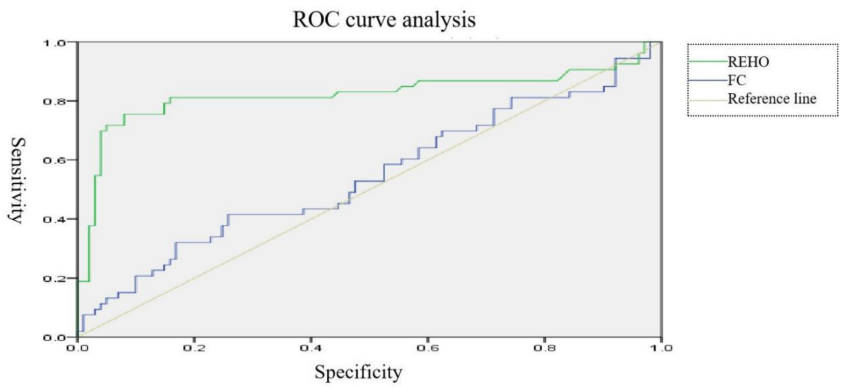

FIGURE 3 | | ROC curves for patients with major depressive disorder (MDD).

Correlation Between Regions of Interest-Based Functional Connectivity and Treatment Efficacy

According to the analysis, no correlation was found between changes in resting-state functional connectivity and the HAMD-17 score reduction rate ($R = 0.116$, $p = 0.386$).

DISCUSSION

The limbic system is the center of human emotions, behaviors, and memories, and it helps to control stress responses, attention, sexual instincts, etc. The limbic system consists of a complex set of structures, including the cingulate gyrus, parahippocampal gyrus, hippocampal structures, septa, and piriform lobe. As studies advances, the scope of the limbic system has been gradually expanded, and now includes areas that are similar to cortical structures of the limbic lobe, such as the temporal lobe, the posterior part of the frontal orbital gyrus, the anterior part of the insula, and some subcortical structures that are closer in function and connection, such as the septum, amygdala, hypothalamus, superior colliculus, anterior thalamic nucleus, and medial region of the midbrain tegmentum. The hippocampal structures, parahippocampal gyrus and internal olfactory area, dentate gyrus, cingulate gyrus, papillae, and amygdala are interconnected through the Papez loop and connected extensively to other brain structures, such as the neocortex, thalamus, and brainstem. Therefore, researchers inferred that the role of the limbic system is to enable information exchange between the midbrain, mesencephalon, and neocortical structures. The limbic system is involved in mediating instinctive and emotional behaviors through connections with the hypothalamus and the autonomic nervous system, which regulates involuntary body functions. The limbic system is also involved in higher psychoneurological and visceral activities; if damaged, it can lead to mental disorders

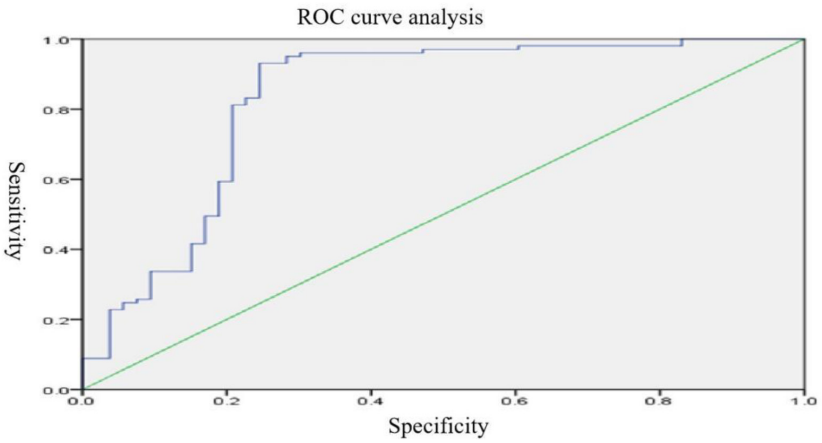

FIGURE 4 | | Resting-state ROC curves for major depressive disorder (MDD).

such as hallucinations, emotional and memory disturbances, abnormal behaviors, unresponsiveness, and impairment of visceral activities.

In this study, no brain regions significantly differed in ALFF/fALFF between patients with MDD and normal controls; increased ReHo was found in the left parahippocampal gyrus and right parahippocampal gyrus and decreased ReHo was found in the right middle occipital gyrus. With brain regions showing different ReHo values between patients with MDD and normal controls as ROIs, it was found that the functional connectivity between the right and left parahippocampal gyri and between the right middle occipital gyrus and middle temporal gyrus were reduced in the patients with MDD. Previous studies have found increased fALFF values in the left supraoccipital gyrus and decreased fALFF values in the left parahippocampal gyrus in patients with MDD, as compared to normal controls (Liu et al., 2013). Fan et al. (2013) found that patients with MDD, compared to normal controls, had increased ALFF values in the right parahippocampal gyrus and decreased ALFF values in the left angular gyrus and left middle occipital gyrus. With regard to ReHo, a study found that patients with MDD showed reduced ReHo values in the right orbitofrontal cortex, cingulate gyrus, ventral anterior cingulate, posterior cingulate, and insula, as well as in the left dorsal anterior cingulate, nucleus accumbens, thalamus, temporal lobe, posterior cerebellum, and bilateral occipital lobes (Yao et al., 2009). Studies on resting-state functional connectivity in MDD selected different ROIs. Using the cingulate gyrus as the ROI, studies found that the anterior subgenual cingulate gyrus had enhanced connectivity to the dorsomedial frontal lobe and left dorsolateral frontal lobe and decreased connectivity to the insula, amygdala, and precuneus in in patients with MDD (Wang et al., 2012; Connolly et al., 2013). Using the amygdala as the ROI, studies have shown that patients with MDD have decreased functional connectivity of the amygdala with the ventral lateral prefrontal lobe, insula,

TABLE 5 | | Brain regions with different resting-state ReHo between the responsive and unresponsive groups.

Regions	Voxel size	Left/ Right	MNI peak coordinates			Peak *t* value
			x	y	z	
The effective group < ineffective group						
Parahippocampal gyrus	18	Right	30	−12	−27	−3.1133

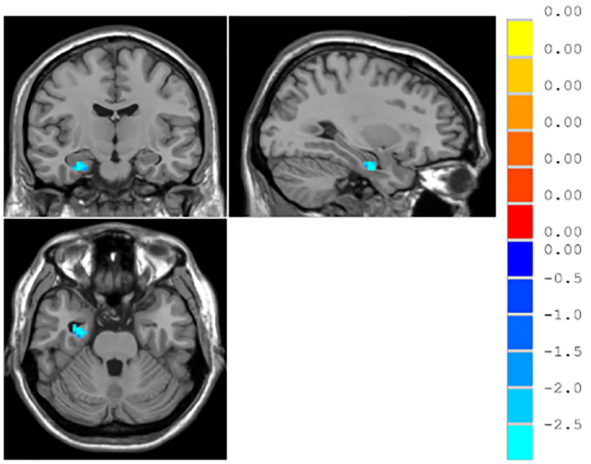

FIGURE 5 | | Brain regions with different resting-state ReHo between the responsive and unresponsive groups.

TABLE 6 | | Brain regions with different functional connectivity between the responsive and unresponsive groups.

Regions	Voxel size	BA	Left/ Right	MNI peak coordinates			Peak *t* value
				x	y	z	
The effective group < ineffective group							
Middle temporal gyrus	21	–	Left	−54	−21	0	−2.4946

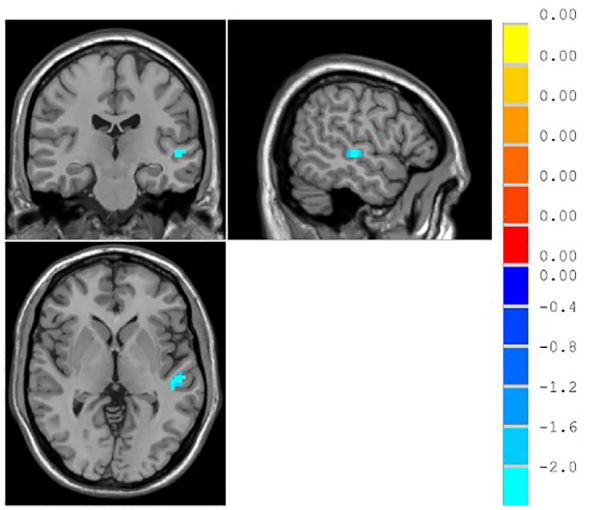

FIGURE 6 | | Brain regions with different functional connectivity between the responsive and unresponsive groups.

middle temporal/superior gyrus, cerebellum and occipital lobe and enhanced functional connectivity with the bilateral temporal poles; the amygdala also had reduced functional connectivity with the left ventral prefrontal lobe (Tang et al., 2013; Ramasubbu et al., 2014). Using the hippocampus as the ROI, a study found that patients with MDD had enhanced functional connectivity of the hippocampus with the bilateral limbic system, temporal lobe, and inferior/medial prefrontal lobe and reduced functional connectivity with the bilateral prefrontal, occipital, and parietal lobes, as well as the cerebellum (Cao et al., 2012). ReHo-mean time series and the averaged functionally connected time series were used in the logistic regression for the ROC curve analysis with a discrimination of 83%, indicating that resting-state MRI provided a high diagnostic value for MDD.

This study explored the association between the efficacy of SSRIs for MDD and resting-state brain function. It found that after 2 weeks of treatment with SSRIs, there was no difference in ALFF/fALFF between the unresponsive group and the responsive group, while elevated ReHo values were found in the right parahippocampal gyrus. We also found that the unresponsive group had lower functional connectivity in the middle temporal gyrus. Previous studies have shown that the activity of the bilateral frontal middle lobes, parahippocampal gyrus, and cerebellum might be related to patient responses to drugs (Alexopoulos et al., 2012). Differences in the correlations between resting-state functional connectivity and treatment outcomes might be resulted from different grouping method or analyses of data from patients with different severities of MDD.

In summary, the inconsistent results of resting-state fMRI studies on MDD might be attributed to the following factors. First, the different diagnostic criteria for MDD used in these studies led to differences in study samples; second, the status of patients with MDD was different across studies; and third, the different methods of data collection, processing, and analysis might have an impact on the results. Based on resting-state fMRI imaging, the present study found that the mechanisms of MDD and the prediction of responses to SSRIs might involve abnormalities in brain regions associated with affective disorders, especially in the limbic system, including the hippocampus, parahippocampal gyrus, cingulate gyrus, and temporal lobe.

Despite the strengths in our study, some limitations should also be noted. Firstly, there is a lack of longitudinal MRI data due to great loss to follow-up. A follow-up plan has been developed to expand our sample and prepare for further long-term longitudinal follow-up studies. Secondly, it has been demonstrated in previous studies that the duration of illness before treatment in patients with depression is associated with greater volume loss in some brain regions. However, this was not included the data collected for this study. Thirdly, the range of age in this study was broad, and the effects of brain development and aging were not taken into account. Finally, the reproducibility of the study results was relatively low. Hopefully, future studies using multiple imaging methods and multicenter data can further validate the results of this study and provide guidance for the prediction of treatment efficacy and individualized treatment for patients with MDD.

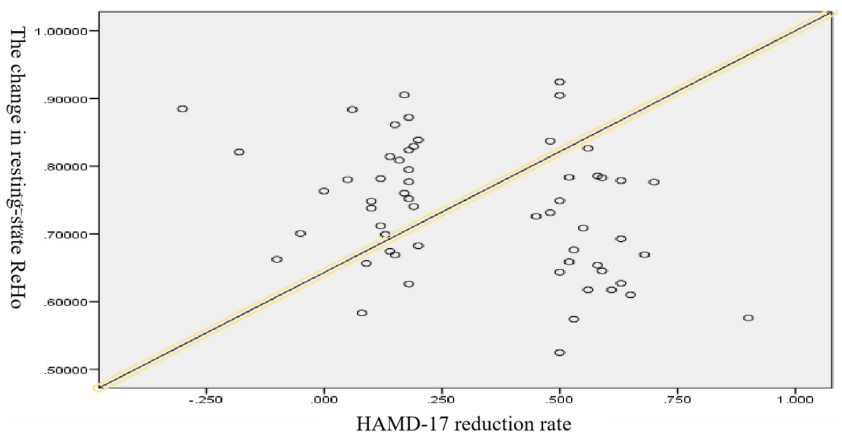

FIGURE 7 | | Scatterplot of major depressive disorder (MDD) based on ReHo and HAMD-17 score reduction rate.

CONCLUSION

Through analyses of the fMRI data and treatment response of patients with MDD, this study suggested that altered resting-state function in some brain regions might be a neurobiological marker for the diagnosis of MDD and that the degree of impairment in resting-state ReHo at baseline is expected to be a predictor of the efficacy of SSRIs in patients with MDD.

DATA AVAILABILITY STATEMENT

The raw data supporting the conclusions of this article will be made available by the authors, without undue reservation.

ETHICS STATEMENT

The studies involving human participants were reviewed and approved by the First Hospital of Shanxi Medical University. The patients/participants provided their written informed consent to participate in this study. Written informed consent was obtained from the individual(s) for the publication of any potentially identifiable images or data included in this article.

AUTHOR CONTRIBUTIONS

KZ and NS designed the experiments. AZ, XW, JL, LJ, XH, HL, and CY performed the clinical data collection and assessment. AZ and XW performed the neuroimaging data analysis and wrote the draft. All the authors discussed the results and reviewed the manuscript.

FUNDING

This study was supported by the National Natural Science Youth Fund Project (81601192), 136 Medical Rejuvenation Project of Shanxi Province, and Program for the Outstanding Innovative Teams of Higher Learning Institutions of Shanxi.

REFERENCES

Alexopoulos, G., Hoptman, M., Kanellopoulos, D., Murphy, C., Lim, K., and Gunning, F. (2012). Functional connectivity in the cognitive control network and the default mode network in late-life depression. *J. Affect. Disord.* 139, 56–65. doi: 10.1016/j.jad.2011.12.002

Cao, X., Liu, Z., Xu, C., Li, J., Gao, Q., Sun, N., et al. (2012). Disrupted resting-state functional connectivity of the hippocampus in medication-naïve patients with major depressive disorder. *J. Affect. Disord.* 141, 194–203. doi: 10.1016/j.jad.2012.03.002

Chao-Gan, Y., and Yu-Feng, Z. (2010). DPARSF: a MATLAB Toolbox for "Pipeline" Data Analysis of Resting-State fMRI. *Front. Syst. Neurosci.* 4:13. doi: 10.3389/fnsys.2010.00013

Connolly, C., Wu, J., Ho, T., Hoeft, F., Wolkowitz, O., Eisendrath, S., et al. (2013). Resting-state functional connectivity of subgenual anterior cingulate cortex in depressed adolescents. *Biol. Psychiatry* 74, 898–907. doi: 10.1016/j.biopsych.2013.05.036

Fan, T., Wu, X., Yao, L., and Dong, J. (2013). Abnormal baseline brain activity in suicidal and non-suicidal patients with major depressive disorder. *Neurosci. Lett.* 534, 35–40. doi: 10.1016/j.neulet.2012.11.032

Henkel, V., Seemüller, F., Obermeier, M., Adli, M., Bauer, M., Mundt, C., et al. (2009). Does early improvement triggered by antidepressants predict response/remission? Analysis of data from a naturalistic study on a large sample of inpatients with major depression. *J. Affect. Disord.* 115, 439–449. doi: 10.1016/j.jad.2008.10.011

Hennings, J., Owashi, T., Binder, E., Horstmann, S., Menke, A., Kloiber, S., et al. (2009). Clinical characteristics and treatment outcome in a representative sample of depressed inpatients - findings from the Munich Antidepressant Response Signature (MARS) project. *J. Psychiatr. Res.* 43, 215–229. doi: 10.1016/j.jpsychires.2008.05.002

Liu, F., Guo, W., Liu, L., Long, Z., Ma, C., Xue, Z., et al. (2013). Abnormal amplitude low-frequency oscillations in medication-naive, first-episode patients with major depressive disorder: a resting-state fMRI study. *J. Affect. Disord.* 146, 401–406. doi: 10.1016/j.jad.2012.10.001

McIntyre, R., Filteau, M., Martin, L., Patry, S., Carvalho, A., Cha, D., et al. (2014). Treatment-resistant depression: definitions, review of the evidence, and algorithmic approach. *J. Affect. Disord.* 156, 1–7. doi: 10.1016/j.jad.2013.10.043

Papakostas, G., Perlis, R., Scalia, M., Petersen, T., and Fava, M. (2006). A meta-analysis of early sustained response rates between antidepressants and placebo for the treatment of major depressive disorder. *J. Clin. Psychopharmacol.* 26, 56–60. doi: 10.1097/01.jcp.0000195042.62724.76

Pizzagalli, D. A. (2011). Frontocingulate dysfunction in depression: toward biomarkers of treatment response. *Neuropsychopharmacology* 36, 183–206. doi: 10.1038/npp.2010.166

Posternak, M., and Zimmerman, M. (2005). Is there a delay in the antidepressant effect? A meta-analysis. *J. Clin. Psychiatry* 66, 148–158. doi: 10.4088/jcp.v66n0201

Ramasubbu, R., Konduru, N., Cortese, F., Bray, S., Gaxiola-Valdez, I., and Goodyear, B. (2014). Reduced intrinsic connectivity of amygdala in adults with major depressive disorder. *Front. Psychiatry* 5:17. doi: 10.3389/fpsyt.2014.00017

Rush, A. J. (2007). STAR*D: what have we learned? *Am. J. Psychiatry* 164, 201–204. doi: 10.1176/ajp.2007.164.2.201

Schaefer, A., Burmann, I., Regenthal, R., Arélin, K., Barth, C., Pampel, A., et al. (2014). Serotonergic modulation of intrinsic functional connectivity. *Curr. Biol.* 24, 2314–2318. doi: 10.1016/j.cub.2014.08.024

Stassen, H., Angst, J., Hell, D., Scharfetter, C., and Szegedi, A. (2007). Is there a common resilience mechanism underlying antidepressant drug response? Evidence from 2848 patients. *J. Clin. Psychiatry* 68, 1195–1205. doi: 10.4088/jcp.v68n0805

Szegedi, A., Jansen, W., van Willigenburg, A., van der Meulen, E., Stassen, H., and Thase, M. (2009). Early improvement in the first 2 weeks as a predictor of treatment outcome in patients with major depressive disorder: a meta-analysis including 6562 patients. *J. Clin. Psychiatry* 70, 344–353. doi: 10.4088/jcp.07m03780

Szegedi, A., Müller, M., Anghelescu, I., Klawe, C., Kohnen, R., and Benkert, O. (2003). Early improvement under mirtazapine and paroxetine predicts later stable response and remission with high sensitivity in patients with major depression. *J. Clin. Psychiatry* 64, 413–420. doi: 10.4088/jcp.v64n0410

Tadić, A., Helmreich, I., Mergl, R., Hautzinger, M., Kohnen, R., Henkel, V., et al. (2010). Early improvement is a predictor of treatment outcome in patients with mild major, minor or subsyndromal depression. *J. Affect. Disord.* 120, 86–93. doi: 10.1016/j.jad.2009.04.014

Tadić, A., Wachtlin, D., Berger, M., Braus, D., van Calker, D., Dahmen, N., et al. (2016). Randomized controlled study of early medication change for non-improvers to antidepressant therapy in major depression–The EMC trial. *Eur. Neuropsychopharmacol.* 26, 705–716. doi: 10.1016/j.euroneuro.2016.02.003

Tang, Y., Kong, L., Wu, F., Womer, F., Jiang, W., Cao, Y., et al. (2013). Decreased functional connectivity between the amygdala and the left ventral prefrontal cortex in treatment-naive patients with major depressive disorder: a resting-state functional magnetic resonance imaging study. *Psychol. Med.* 43, 1921–1927. doi: 10.1017/s0033291712002759

Taylor, M., Freemantle, N., Geddes, J., and Bhagwagar, Z. (2006). Early onset of selective serotonin reuptake inhibitor antidepressant action: systematic review

and meta-analysis. *Arch. Gen. Psychiatry* 63, 1217–1223. doi: 10.1001/archpsyc.63.11.1217

Trivedi, M., Rush, A., Wisniewski, S., Nierenberg, A., Warden, D., Ritz, L., et al. (2006). Evaluation of outcomes with citalopram for depression using measurement-based care in STAR*D: implications for clinical practice. *Am. J. Psychiatry* 163, 28–40. doi: 10.1176/appi.ajp.163.1.28

van Calker, D., Zobel, I., Dykierek, P., Deimel, C., Kech, S., Lieb, K., et al. (2009). Time course of response to antidepressants: predictive value of early improvement and effect of additional psychotherapy. *J. Affect. Disord.* 114, 243–253. doi: 10.1016/j.jad.2008.07.023

Wang, L., Dai, W., Su, Y., Wang, G., Tan, Y., Jin, Z., et al. (2012). Amplitude of low-frequency oscillations in first-episode, treatment-naive patients with major depressive disorder: a resting-state functional MRI study. *PLoS One* 7:e48658. doi: 10.1371/journal.pone.0048658

Williams, L., Korgaonkar, M., Song, Y., Paton, R., Eagles, S., Goldstein-Piekarski, A., et al. (2015). Amygdala Reactivity to Emotional Faces in the Prediction of General and Medication-Specific Responses to Antidepressant Treatment in the Randomized iSPOT-D Trial. *Neuropsychopharmacology* 40, 2398–2408. doi: 10.1038/npp.2015.89

Yao, Z., Wang, L., Lu, Q., Liu, H., and Teng, G. (2009). Regional homogeneity in depression and its relationship with separate depressive symptom clusters: a resting-state fMRI study. *J. Affect. Disord.* 115, 430–438. doi: 10.1016/j.jad.2008.10.013

Conflict of Interest: The authors declare that the research was conducted in the absence of any commercial or financial relationships that could be construed as a potential conflict of interest.

Publisher's Note: All claims expressed in this article are solely those of the authors and do not necessarily represent those of their affiliated organizations, or those of the publisher, the editors and the reviewers. Any product that may be evaluated in this article, or claim that may be made by its manufacturer, is not guaranteed or endorsed by the publisher.

frontiers in Neuroscience

ORIGINAL RESEARCH
published: 02 March 2022
doi: 10.3389/fnins.2022.856366

Identifying Changes of Brain Regional Homogeneity and Cingulo-Opercular Network Connectivity in First-Episode, Drug-Naïve Depressive Patients With Suicidal Ideation

Mengxin He[1,2], Liangliang Ping[1,3], Zhaosong Chu[1], Chunqiang Zeng[1], Zonglin Shen[1,2,4] and Xiufeng Xu[2,4]**

[1] Department of Psychiatry, First Affiliated Hospital of Kunming Medical University, Kunming, China, [2] Mental Health Institute of Yunnan, First Affiliated Hospital of Kunming Medical University, Kunming, China, [3] Department of Psychiatry, Xiamen Xianyue Hospital, Xiamen, China, [4] Yunnan Clinical Research Center for Mental Disorders, First Affiliated Hospital of Kunming Medical University, Kunming, China

OPEN ACCESS

Edited by:
Wenbin Guo,
Central South University, China

Reviewed by:
Gang Zhu,
China Medical University, China
Xiancang Ma,
First Affiliated Hospital of Xi'an Jiaotong University, China

***Correspondence:**
Zonglin Shen
shenzl1987@163.com
Xiufeng Xu
xfxu2004@sina.com

Specialty section:
This article was submitted to Brain Imaging Methods, a section of the journal Frontiers in Neuroscience

Received: 17 January 2022
Accepted: 31 January 2022
Published: 02 March 2022

Citation:
He M, Ping L, Chu Z, Zeng C, Shen Z and Xu X (2022) Identifying Changes of Brain Regional Homogeneity and Cingulo-Opercular Network Connectivity in First-Episode, Drug-Naïve Depressive Patients With Suicidal Ideation. Front. Neurosci. 16:856366. doi: 10.3389/fnins.2022.856366

Objective: Adult patients with major depressive disorder (MDD) may not actively reveal their suicidal ideation (SI). Therefore, this study is committed to finding the alterations in the cingulo-opercular network (CON) that are closely related to SI with multi-imaging methods, thus providing neuroimaging basis for SI.

Method: A total of 198 participants (129 MDD patients and 69 healthy controls) were recruited and evaluated with the Montgomery–Asberg Depression Rating Scale (MADRS). The healthy individuals formed the HC group, while the MDD patients were subdivided into no SI MDD (NSI, $n = 32$), mild SI MDD (MSI, $n = 64$), and severe SI MDD (SSI, $n = 33$) according to their MADRS item 10. We obtained MRI data of all participants and applied regional homogeneity (ReHo) analysis to verify a previous finding that links CON abnormality to SI. In addition, we employed the structural covariance network (SCN) analysis to investigate the correlation between abnormal structural connectivity of CON and SI severity.

Results: Compared to those of the HC group, MDD ReHo values and gray matter volume (GMV) were consistently found abnormal in CON. ReHo values and GMV of the right orbital inferior frontal gyrus (ORBinf.R) in the MDD group decreased with the increase of SI. Compared to the HC group, the MDD patients showed enhanced structural connectivity of three pairs of brain regions in CON [ACC.L–left superior frontal gyrus (SFG.L), SFG.L–left middle temporal gyrus (MTG.L), and the SFG.L–left post-central gyrus (PoCG.L)]. Compared with that of the NSI and MSI groups, the structural connectivity of three pairs of brain regions in CON is enhanced in the SSI

groups [ORBinf.L–right ventral posterior cingulate gyrus (VPCC.R), VPCC.R–SFG.R, and SFG.R–PoCG.R].

Conclusion: Our findings showed the distinctive ReHo, GMV, and SCN pattern of CON in MDD patients with SI; and with the severity of suicide, abnormal brain regions increased. Our finding suggested that MDD patients with different severity of SI have different neuroimaging changes.

Keywords: major depressive disorder, suicidal ideation, regional homogeneity, functional MRI, structure connectivity

INTRODUCTION

Major depressive disorder (MDD) is a common disease affecting more than 264 million people worldwide (World Health Organization, 2017). Depression is different from mood swings and short-term emotional responses to challenges in daily life, and long-term moderate or severe depression may become a serious illness. At its worst, depression can lead to suicide, and nearly 800,000 people die by suicide each year (World Health Organization, 2017). To a large extent, the results of the suicide risk assessment can be attributed to the subjective willingness of patients (Walker et al., 2015). Suicide incurs unacceptably high costs for society, families, and individuals (Walker et al., 2015). MDD patients with (vs. without) suicidal ideation (SI) (Cooper et al., 1994) have a higher rate of suicide attempts (Pfaff and Almeida, 2004; Du et al., 2017). SI can be considered the first step on the road to a suicide attempt (Ding et al., 2016). SI can lead to suicide attempts and may be caused by biological factors (van Heeringen et al., 2014). The degree of heritability of symptoms of depression, such as physical symptoms, guilt, and SI, has been shown to vary (h2 range, 0–35%) (Fried and Nesse, 2015). SI has a higher heritability coefficient than do other symptoms (Kappelmann et al., 2021). In addition, SI is driven by neurobiological processes; it is not merely a symptom of depression (Fried and Nesse, 2015; Du et al., 2017). Identifying SI helps to reduce suicide attempts (Ding et al., 2016).

Although the risk assessment of MDD patients can be carried out by suicide scales, an investigative study found that adults may not seek help by disclosing SI (McGillivray et al., 2022). MDD patients with mild or severe SI can develop anxiety symptoms, but people tend to pay more attention to patients with severe SI while ignoring those with mild SI. This results in poor efficacy for these patients and even severe, chronic, or even treatment-resistant depression (Lieberman et al., 2020). Therefore, studying the neural mechanisms of SI at different severity may prevent this condition. MRI has been widely used as a non-invasive method of studying brain structure and function in depressive suicide attempters (Fried and Nesse, 2015; Du et al., 2017). Neuroimaging may also be able to provide reliable indicators of SI. Elucidating the neuroimaging characteristics of SI in MDD could help clinicians to intervene early and thereby reduce the risk of suicide. While the prefrontal cortex (PFC) has been proved to be associated with SI in previous studies (Myung et al., 2016), it is generally believed that SI is related to abnormal neural network connectivity and not limited to a single brain region (Chase et al., 2017; Bani-Fatemi et al., 2018; Schmaal et al., 2020).

Recent studies have reported that disconnection of the cingulo-opercular network (CON) is the key to many mental illnesses (Jollant et al., 2010). Components of the CON include the anterior cingulate cortex (ACC), PFC, parietal cortex, and basal ganglia. These are major brain regions associated with MDD (Dosenbach et al., 2007; Kaiser et al., 2015). CON helps to flexibly control target-oriented performance and has been shown to participate in maintaining the stability of executive function cross-testing in the main cognitive control and SI processing (Dosenbach et al., 2007; Yang et al., 2020). In addition, research has suggested that key areas of the CON are related to suicide in MDD (Dosenbach et al., 2007; Bani-Fatemi et al., 2018; Yang et al., 2020). For example, it was recently reported that abnormality of brain regions in the CON is related to the severity of MDD symptoms (Sylvester et al., 2012; Rappaport et al., 2020). Since MDD patients with SI tend to have higher depression scores than those without SI, and CON is associated with disease severity, it is suggested that CON may reflect SI in MDD.

Regional homogeneity (ReHo) can reflect the temporal homogeneity of blood oxygen level-dependent signals in a certain region, revealing the temporal homogeneity of activity in various brain regions in the resting-state functional network (Yan et al., 2021). The ReHo analysis can be used to explore the neural activity of abnormal brain regions in the functional network. Structural covariance network (SCN) is an established measure of the cortex–cortex connectivity, which shows a good correspondence with transcribed brain networks and anatomical connectivity inferred from white matter fiber tract imaging (Gong et al., 2012). As a unique measure of connectivity, SCN can be used to investigate communication factors between anatomically connected non-adjacent brain regions where there is information exchange between synapses of non-adjacent neurons, forming macro-level structural covariance (Alexander-Bloch et al., 2013). In addition, SCN can provide a model for understanding progressive cortical abnormalities in mental disorders (Crossley et al., 2014). The relationship between functional ReHo and SCN changes should be explored because this information will help to increase our understanding of the mechanism of SI at the level of brain function and structural connectivity.

We propose the hypothesis that SI at different severity in MDD patients is associated with different changes of CON. ReHo value and SCN analysis method based on gray matter volume (GMV)

can reflect the characteristics of CON in functional and structural connectivity and may better reveal whether the changes of CON varied with different SI severity.

MATERIALS AND METHODS

Participants

First-episode, drug-naïve adults diagnosed with MDD were recruited from the psychiatric outpatient and inpatient departments of psychiatry in the First Affiliated Hospital of Kunming Medical University between 2015 and 2017. To mitigate the influence of vascular factors on brain structure, the participants in this study were adults under the age of 45 (Kendler et al., 2009). The psychiatric diagnosis was based on the DSM-IV, and at least two psychiatrists were in agreement (vanPraag, 1990). Hamilton Anxiety Scale (HAMA) was used to assess the severity of participants' anxiety symptoms (Hamilton, 1960). All of the patients had been diagnosed with MDD for the first time and had never received anti-sedatives or systemic psychotherapy. An HC group was matched for age, gender, education level, and dominant hand. The exclusion criteria of MDD patients were as follows: previous brain injury with loss of consciousness, history of cortisol drug use, history of substance abuse, previous neurological disease, pregnancy, diagnosis of another mental illness or neurological disease, received electroconvulsive therapy for MDD, and dominant left hand. The exclusion criteria of the HC group were as follows: previous brain injury with loss of consciousness, pregnancy, history of psychiatric or neurological disease, and dominant left hand. The research protocol was approved by the First Affiliated Hospital of Kunming Medical University's ethics committee. All participants were provided with details about the study, and their consent was obtained.

Subgroups

To better study whether the brain abnormality model is related to the severity of SI, the 10th item of the Montgomery–Asberg Depression Rating Scale (MADRS) measures SI on a scale of 0–6, representing the feeling that life is not worth living, the feeling that a natural death would be welcome, suicidal thoughts, and preparations for suicide (Montgomery and Åsberg, 1979). In the past, only patients with scores $\geq$4 were studied (Murrough et al., 2015). A MADRS 10th item score $\geq$4 indicating severe SI is consistent with other suicide-related scale assessments (Montgomery and Åsberg, 1979; Murrough et al., 2015). To verify the hypothesis of this current study, we extended on previous research and MDD patients with scores from 1 to 3 and $\geq$4. All recruited patients were divided into three groups: no SI (NSI, 0 points), mild SI (MSI, 1–3 points), and severe SI (SSI, $\geq$4 points).

Image Acquisition

Magnetic resonance (MR) images were captured by an experienced radiologist using an Achieva 3.0 Tesla MRI system (Philips, Eindhoven, Netherlands) with a 16-channel phased-array head coil. T1- and T2-weighted scans were obtained for all of the participants to rule out the presence of brain abnormalities. High-resolution three-dimensional MRI scans were acquired using a fast-spoiled gradient recalled acquisition (FSPGR) sequence with the following parameters: repetition time (TR) = 7.38 ms, echo time (TE) = 3.4 ms, matrix size = 256 mm × 256 mm, field of view (FOV) = 250 × 250 mm, flip angle = 8°, slice thickness = 0.6 mm, slices = 230 with no gap, and acquisition time = 6 min 53 s.

The functional image data at rest were obtained by using the echo-planar imaging sequence with the following parameters: TR = 2,200 ms, TE = 35 ms, flip angle = 90°, FOV = 230 mm × 230 mm, matrix size = 128 × 128 mm, slice thickness = 3.0 mm without interlayer spacing, slices = 50, scan duration time = 17 min 40 s.

Functional MRI Preprocessing and Regional Homogeneity Calculation

Data preprocessing was performed in Matlab 2018b using the resting-state functional MRI (fMRI) analysis package (DPABI[1]); the first 10 images of the initial MRI signal were discarded to reduce the effect of pre-subject instability, head motion correction, and smoothing constraints. Participants were not displaced by more than 1.5 mm in the x-, y-, or z-axes, temporally bandpass filtered (0.01–0.08 Hz) and linearly detrended, imaging data space was normalized to Montreal Neurological Institute (MNI) space and resampled to 3 × 3 × 3 mm^3, and 24 head motion parameters were obtained.

Regional homogeneity analysis was conducted by the software DPABI for the MDD and HC groups. The time series of a given voxel with the time series of its nearest neighbors is generated by calculating the Kendall coefficient (KCC) for each ReHo to be mapped (neighboring voxels were set as 26) (Yan et al., 2021). Normalization to ReHo was performed by dividing the KCC between voxels by the average KCC of the whole brain to reduce the effect of individual differences (Tononi et al., 1998).

Gray Matter Volume Preprocessing

FreeSurfer 7.0 software[2] was used to process images to estimate GMV. The pre-processing included motion correction, averaging of multiple volume T1-weighted images, stripping non-brain tissues by using hybrid watershed/cortical surface deformation, automated Talairach deformation, segmentation of gray matter tissue, subdivision of white matter boundary and smoothing, intensity normalization, gray matter boundary network identification, automatic topology correction, surface deformation, and optimal positioning of intensity gradient gray/white matter boundary. The location of the gray matter/cerebrospinal fluid boundary was used to transform the maximum intensity definition to other tissue types. The entire cortex of each participant was visually inspected, and the segmentation was manually edited for inaccuracies (Fischl, 2004). The cortex was then divided based on the Destrieux atlas (Destrieux et al., 2010). This produced a vector of estimated cortical volumes for each bilateral frontal lobe, the anterior cingulate gyrus, the posterior cingulate cortex (PCC), the thalamus, the parietal lobe, the temporal lobe, and the basal

[1]http://rfmri.org/DPABI

[2]https://surfer.nmr.mgh.harvard.edu

ganglia in the CON (58 brain regions) for each participant (see **Figure 2A** and details provided in the **Supplementary Material**).

Statistical Analysis

The demographics and clinical characteristics of the participants were analyzed using SPSS 18.0. ANOVA was used to test demographic differences among three MDD groups and the HC group.

Regional Homogeneity Analysis

A voxel-based ANOVA comparison of the whole brain ReHo maps among the MDD and HC groups was performed in REST package viewer1.8.[3] The statistical threshold was set at $p < 0.05$ after false discovery rate (FDR) correction with an extent cluster of 100 contiguous voxels or greater using age, sex, and education level as covariates. The ReHo values of each MDD patient were extracted from the brain regions with abnormal ReHo, which are based on Matlab using the DPABI (see text footnote 1). The correlations between abnormal ReHo and MADRS total scores and 10th item scores were determined using Pearson's correlation analyses, controlling for age, gender, and education level ($p < 0.05$).

Gray Matter Volume Analysis

Analysis of covariance (ANCOVA) was used to test the GMV values of CON (58 brain regions) among three MDD groups and the HC group in which age, gender, and education level were used as covariates. Then *post hoc t*-tests were conducted to identify differences in the GMV values between each pair of groups by using the same covariates mentioned above. Then *post hoc t*-tests were used to compare among MDD subgroups, by using age, sex, education level, and illness duration as covariates. To correct for multiple comparisons, the FDR was controlled at 5% using the Benjamini–Hochberg procedure (Benjamini and Hochberg, 1995).

Structural Covariance Network Analysis

Gray matter volume was used as the morphological measurement in this study, and Pearson's correlation was used to calculate structural covariance. A Pearson's correlation coefficient was calculated for the estimated GMV values of each pair of cortical regions. First, age, gender, and illness duration were regressed on the GMV estimates (Alexander-Bloch et al., 2013; Wannan et al., 2019). An r-to-z transformation was performed on all correlation coefficients to improve normality. Separate connection matrixes were produced for each of the three patient groups and the HC group to quantify the strength of the connection between the pair of regions. A two-sample *t*-test was used to independently test the structural covariance between the MDD groups and the control group for each area pair. A non-parametric permutation test (10,000 permutations) was used to determine the statistical significance of between-group differences in the network. Non-parametric methods were used to identify the null distribution of the data, enabling the use of non-standard test statistics (Wannan et al., 2019). FDR was controlled to correct for multiple comparisons (Benjamini and Hochberg, 1995).

[3]http://restfmri.net/forum/REST_V1.8

RESULTS

Participants' Characteristics

Table 1 shows the demographics and clinical characteristics of the participants. There were no significant differences in gender, age, and education level between 129 patients and 69 HCs. The 198 participants were classified as follows: 32 NSI, 64 MSI, 33 SSI, and 69 HC. The four groups showed no differences in age, gender, education level, or illness duration. The NSI and MSI groups scored lower than the SSI group for total MADRS score (NSI group $t = 1.62$, $p < 0.001$; MSI group $t = 1.37$, $p < 0.001$) and MADRS 10th item score (NSI group $t = 0.14$, $p < 0.001$; ESC group $t = 0.12$, $p < 0.001$). There was no significant difference in the MADRS total scores between NSI and MSI, but both were lower than the score in the SSI group. The MSI and SSI groups scored higher than the NSI group for HAMA total score (**Table 1**).

Regional Homogeneity and Correlation Results

Figure 1A and **Table 2** show the ANOVA of the ReHo value between the MDD and HC groups with age, gender, and education level as covariates. Compared with the HC group, there were lower ReHo values in the left PCC, the left triangular of the inferior frontal gyrus (IFGtriang), the left post-central gyrus (PoCG), the left inferior parietal gyrus (IPL), the left superior temporal gyrus (STG), the left temporal pole gyrus (TPO), and the bilateral middle temporal gyrus (MTG) in the MDD group, as well as higher ReHo values in the left ACC, the left cerebellum (CE), the right median cingulate cortex (MCC), the right middle frontal gyrus (MFG), the right orbital inferior frontal gyrus (ORBinf), and the right precentral gyrus (PreCG) in the MDD group. Disrupted ReHo is the core brain region of CON at rest (Dosenbach et al., 2007; Kaiser et al., 2015). We used the REX toolbox to extract the mean value of ReHo in different brain regions of the MDD group; after controlling for age, gender, and education level, the right orbital inferior frontal gyrus (ORBinf.R) ($r = -0.41$, $p < 0.01$) and the right middle frontal gyrus (MFG.R) were significantly correlated with SI severity (MADRS 10th item, 0–6 scores) in the MDD group ($r = 0.46$, $p < 0.01$) (**Figure 1B**).

Gray Matter Volume Results

Gray matter volume was found abnormal in regions of the left ACC (ACC.L), the left superior frontal gyrus (SFG.L), the left middle temporal gyrus (MTG.L), and the ORBinf.R in the MDD and HC groups by ANCOVA (**Table 3**).

Compared with the HC group, the three MDD groups have decreased GMV of the ACC.L and SFG.L. *Post hoc* analysis revealed that GMV of the ACC.L and SFG.L in the NSI group; the ACC.L, SFG.L, and ORBinf.R. in the MSI group; and the ACC.L, MTG.L, SFG.L, PoCG.L, PoCG.R, ORBinf.R, and right ventral posterior cingulate gyrus (vPCC.R) in the SSI group

TABLE 1 | The demographics and clinical characteristics of the participants.

Variables (mean ± SD)	MDD	HC	*p*-Value
Gender (male/female)	39/90	20/49	0.13[a]
Age (years)	32.4 ± 7.6	32.9 ± 7.5	0.63[a]
Education level (years)	12.0 ± 4.3	13.0 ± 4.0	0.19[a]

Variables (mean ± SD)	NSI	MSI	SSI	HC	*p*-Value
Gender (male/female)	11/21	18/46	10/23	20/49	0.73[b]
Age (years)	33.3 ± 7.7	31.9 ± 7.5	31.9 ± 7.8	32.9 ± 7.5	0.70[b]
Education level (years)	12.1 ± 3.9	12.0 ± 4.4	12.3 ± 4.1	13.0 ± 4.0	0.94[b]
MADRS total score	26.279 ± 6.0*	28.64 ± 6.3*	37.18 ± 6.7*	–	0.00[c]
MADRS 10th item(suicidal ideation)	0*	2 ± 0.61*	4.19 ± 0.59*		0.00[c]
HAMA score	18.03 ± 4.69*	24.41 ± 5.90*	25.41 ± 6.26*		0.01[c]
Illness duration (months)	14.00 ± 19.24	13.12 ± 17.81	12.39 ± 16.34	–	0.74[b]

MDD, major depressive disorder; MADRS, Montgomery–Asberg Depression Rating Scale; HAMA, Hamilton Anxiety Scale; LSD, least significant difference.
[a]The p-values were obtained by two-sample t-test.
[b]The p-values were obtained by ANOVA.
[c]The p-values were obtained by chi-square test; LSD correction was used for post hoc comparison.
**Compared to MDD groups. $p < 0.05$ MADRS score: SSI > NSI, MSI; HAMA score: MSI, SSI > NSI.*

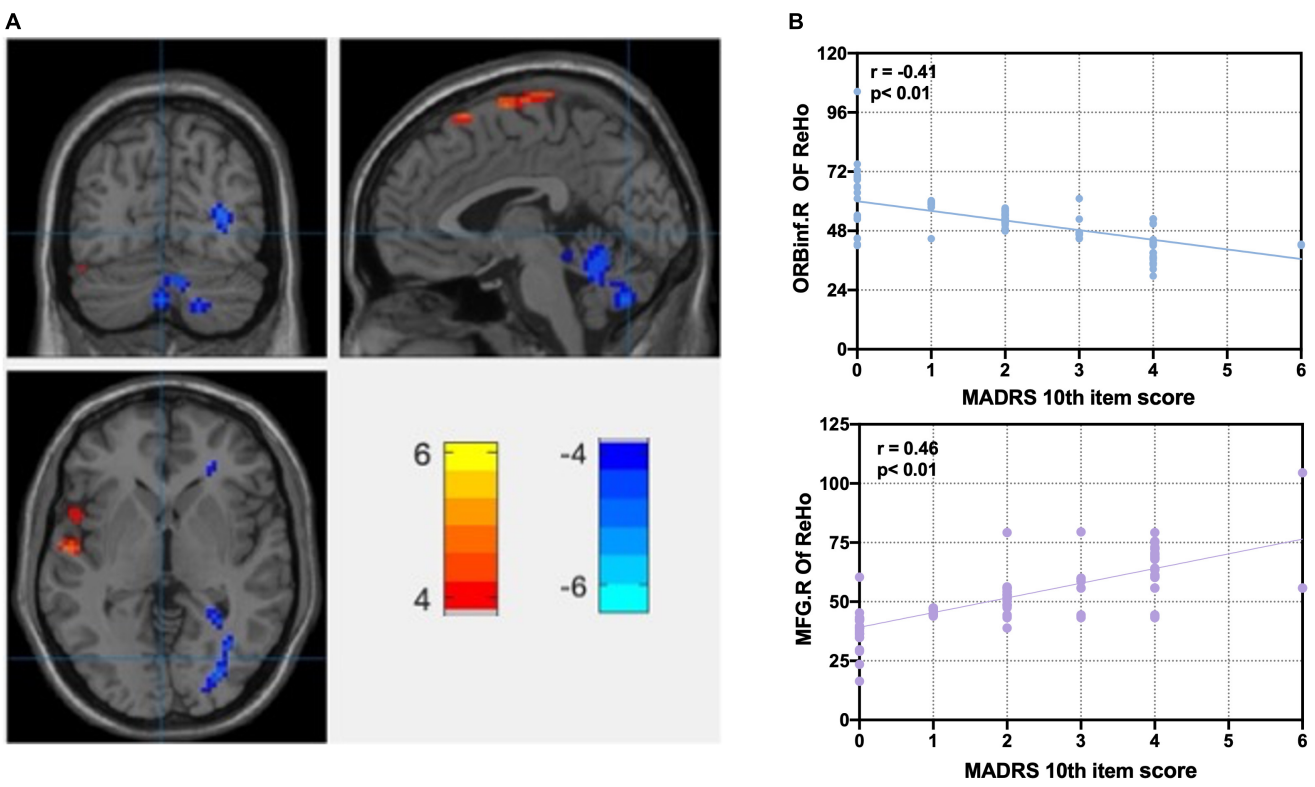

FIGURE 1 | Correlation analysis of significant ReHo differences between MDD and HC groups with MADRS 10th item score. **(A)** Statistical map depicts higher and lower ReHo of MDD compared with HC groups. Abnormal ReHo of anterior cingulate cortex, prefrontal lobe, parietal cortex, and cerebellum. Disrupted regional homogeneity of the core brain region of CON at rest. **(B)** Correlation analyses between ReHo and MADRS 10th item score. Blue denotes lower ReHo, and red denotes higher ReHo. L, left side; R, right side; ReHo, regional homogeneity; ORBinf, right orbital inferior frontal gyrus; MFG, middle frontal gyrus; MADRS, Montgomery–Asberg Depression Rating Scale; FDR, false discovery rate; MDD, major depressive disorder. FDR $p < 0.05$. MADRS 10th item score: suicidal ideation, 0–6 score.

decreased (FDR correction) (**Table 3**). The GMV of the ACC.L was smaller in the SSI group than in the NSI group (FDR correction) (**Figure 2B**).

Compared with NSI, GMV of ORBinf.R decreased in SSI and MSI. Compared with MSI, the GMV of ORBinf.R in the SSI group was remarkably reduced (FDR correction) (**Figure 2B**).

TABLE 2 | Regional homogeneity analysis between MDD and HC groups.

Cluster locationHC > MDD	Hemisphere	Peak (MNI)			Number of voxels	*Z*-value
		x	y	z		
Posterior cingulate cortex, PCC	L	−6	−54	6	32	4.2727
Triangular of Inferior frontal gyrus, IFGtriang	L	−48	27	24	36	4.3395
Post-central, PoCG	L	−60	−18	33	38	3.9647
Inferior parietal gyrus, IPL	L	−36	−42	42	38	5.0662
Superior temporal gyrus, STG	L	−54	−9	0	40	4.9904
Temporal pole gyrus, TPO	L	−51	9	−3	14	4.3405
Middle temporal gyrus, MTG	L	−51	−66	21	45	4.0296
Middle temporal gyrus, MTG	R	63	−18	−12	56	4.0296
HC < MDD						
Anterior cingulate cortex, ACC	L	14	30	21	125	−4.3745
Cerebellum, CE	L	−3	−39	−12	28	−4.178
Median cingulate cortex, MCC	R	12	−33	39	66	−4.0981
Middle frontal gyrus, MFG	R	39	9	60	43	4.2547
Orbital inferior frontal gyrus, ORBinf	R	33	−21	9	75	−4.4684
Precentral gyrus, PreCG	R	18	−51	15	40	−6.4008

MNI, Montreal Neurological Institute; ReHo, regional homogeneity; L, left hemisphere; R, right hemisphere; MDD, major depressive disorder; FDR, false discovery rate. FDR $p < 0.05$.

Structural Covariance Network Results

Compared with the HC group, SCNs of the ACC.L–SFG.L (HC $r = 0.32$, $z = 0.33$; NSI $r = 0.52$, $z = 0.57$, MSI $r = 0.48$, $z = 0.52$; and SSI $r = 0.72$, $z = 0.90$) and SFG.L–TMG.L (HC $r = 0.40$; $z = 0.42$, NSI $r = 0.56$, $z = 0.63$; MSI $r = 0.54$ $z = 0.60$, and SSI $r = 0.68$, $z = 0.97$) increased in the NSI, MSI, and SSI groups. The SCN of SFG.L–PoCG.L (HC $r = 0.49$, $z = 0.53$; NSI $r = 0.52$, $z = 0.56$; MSI $r = 0.54$, $z = 0.59$ and SSI $r = 0.87$, $z = 1.32$) increased in SSI (FDR $p < 0.05$) (**Figure 3**, left).

The structural connectivity related to SI is mainly the following three pairs: OrBInf.R–vPCC.R (HC $r = 0.29$, $z = 0.29$; NSI $r = 0.27$, $z = 0.28$, MSI $r = 0.47$, $z = 0.52$ and SSI $r = 0.56$, $z = 0.71$; SSI > MSI > NSI, HC); vPCC.R–SFG.R (HC $r = 0.50$, $z = 0.55$; NSI $r = 0.48$, $z = 0.50$; MSI $r = 0.68$, $z = 0.80$ and SSI $r = 0.70$, $z = 1.03$; SSI, MSI > NSI), and SFG.R–PoCG.R (HC $r = 0.31$, $z = 0.33$; NSI $r = 0.31$, $z = 0.32$; MSI $r = 0.33$, $z = 0.35$ and SSI $r = 0.41$, $z = 0.44$ SSI > MSI, NSI, HC). SCN increased with the increase of Si severity (FDR $p < 0.05$) (**Figure 3**, right).

DISCUSSION

Using multimodal imaging analyses, we explored the underlying neuropathological mechanisms associated with SI severity in MDD patients. From analyses of whole-brain ReHo values, we found ReHo changes within the CON. Specifically, ReHo changes of the right middle frontal gyrus and orbital inferior frontal gyrus are negatively correlated with SI severity. Compared to HC, MDD patients were found to have abnormal ReHo and GMV in the ACC.L. GMV of the ORBinf.R was negatively correlated with SI severity. This suggests that there is heterogeneity in the function and structure of CON in MDD patients with SI of different severity. Previous studies have demonstrated intercorrelation between defects in brain structural connection and brain dysfunctions (Honey et al., 2009). Changes in functional dynamics are usually caused by changes in structures; at the same time, long-term functional changes can lead to structural changes through synaptic plasticity (Hagmann et al., 2010). The present study builds upon this structural network analysis and is the first to explore alterations in the structural connectivity of the NSI, MSI, and SSI.

Compared with the HC group, with brain regions with abnormal ReHo located in CON (Dosenbach et al., 2007; Jollant et al., 2011), the MDD patients showed lower ReHo of the ACC.L (Boes et al., 2018). The ACC.L is a key region associated with MDD (Boes et al., 2018; Crowell et al., 2019; Cole et al., 2020; Rappaport et al., 2020). We investigated that the ORBinf.R ($r = -0.41$, $p < 0.01$) was significantly correlated with SI severity (MADRS 10th item, 0–6 scores) at the rest of the MDD group. The ORBinf is a part of the orbitofrontal cortex (OFC) in CON that participates in decision-making, reward learning (Izquierdo, 2017), emotional processes, and cognitive control (Kuusinen et al., 2018). Interestingly, poor decision-making about risk and safety is associated with lateral activation changes in both individuals with SI and their first-degree relatives, indicating that lesions in the OFC (BA47) may be a biomarker of increased risk of suicide (Ding et al., 2016; Johnston et al., 2017). Furthermore, our study also showed that the ReHo values of ORBinf.R in CON are negatively correlated with SI severity.

Compared with the HC group, the MDD patients showed atrophy of the ACC.L, and atrophy of the ACC.L may be related to MDD (Boes et al., 2018). In CON, we found the reduction GMV of the ORBinf.R and decreased GMV with increased SI severity. The magnitude of ORBinf.R volume atrophy and lower ReHo has also been found to be positively correlated with SI score in CON (Yang et al., 2020). A prior analysis showed that reduction in OFC volume (Arnone et al., 2011) and cortical

TABLE 3 | Analysis of covariance of gray matter volume among MDD and HC groups.

ANCOVA results	**Hemisphere**		***F***	***p***	
Anterior cingulate cortex, ACC	L		7.07	0.008	
Superior frontal gyrus, SFG	L		6.01	0.01	
Middle temporal gyrus, MTG	L		6.77	0.01	
Orbital inferior frontal gyrus, ORBinf	R		8.27	0.005	
NSI ($n = 32$) < HC ($n = 69$)	**Hemisphere**	**NSI**	**HC**	**T**	***p***
Anterior cingulate cortex, ACC	L	4, 138 ± 396	4, 351 ± 467	8.27	0.001
Superior frontal gyrus, SFG	L	1, 570 ± 165	1, 826 ± 190	6.38	0.003
MSI ($n = 64$) < HC ($n = 69$)	**Hemisphere**	**MSI**	**HC**	**T**	***p***
Anterior cingulate cortex, ACC	L	3, 858 ± 380	4, 351 ± 467	8.70	0.0003
Superior frontal gyrus, SFG	L	1, 599 ± 195	1, 826 ± 190	5.82	0.004
Orbital inferior frontal gyrus, ORBinf	R	869 ± 107	1, 002 ± 178	7.00	0.002
SSI ($n = 33$) < HC ($n = 69$)	**Hemisphere**	**SSI**	**HC**	**T**	***p***
Anterior cingulate cortex, ACC	L	3, 590 ± 508	4, 351 ± 467	10.01	<0.0001
Middle temporal gyrus, MTG	L	6, 764 ± 1, 360	7, 292 ± 1, 232	5.81	0.004
Superior frontal gyrus, SFG	L	1, 269 ± 187	1, 826 ± 190	6.52	0.002
Post-central gyrus, PoCG	L	3, 011 ± 613	3, 790 ± 558	5.12	0.003
Orbital inferior frontal gyrus, ORBinf	R	821 ± 118	1, 002 ± 178	8.43	0.001
Ventral posterior cingulate cortex, vPCC	R	697 ± 148	861 ± 131	4.43	0.012

The F values were obtained using ANCOVA for age, gender, and education level as covariates.
The post hoc t-tests were used to compare among MDD and HC groups.
FDR, $p < 0.05$, healthy group (HC), no suicidal ideation (NSI), mild suicidal ideation (MSI), and severe suicidal ideation (SSI).
L, left hemisphere; R, right hemisphere; MDD, major depressive disorder; ANCOVA, analysis of covariance; FDR, false discovery rate.

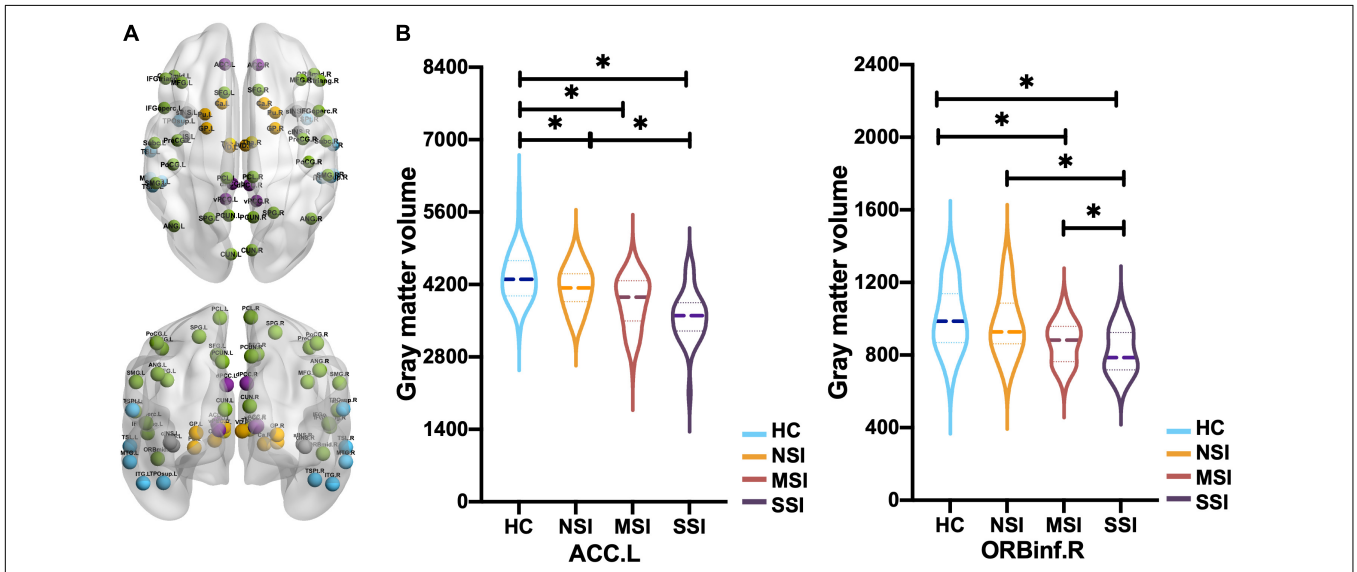

FIGURE 2 | Comparison of gray matter volume (GMV) of 58 brain regions in CON. **(A)** Frontal and parietal lobe (green), cingulate gyrus (purple), temporal lobe (blue), insula (gray), basal ganglia (orange), and thalamus (gold) in CON (58 regions). **(B)** The left anterior cingulate gyrus (ACC.L) of three major depressive disorder (MDD) groups has a smaller GMV than the HC, and NSI > SSI. The right orbital inferior frontal gyrus (ORBinf.R), MSI, and SSI have smaller GMV than HC, and NSI > MSI > SSI [*$p < 0.05$, false discovery rate (FDR)]. Healthy group (HC), no suicidal ideation (NSI), mild suicidal ideation (MSI), and severe suicidal ideation (SSI).

thickness (Suh et al., 2019) in MDD patients was associated with SI (Wagner et al., 2011). The results of the GMV analysis were consistent with the previous ReHo analysis, which also used multimodal imaging analysis to verify the reliability of results. As far as we know, there have been few studies on the structure of the CON focusing on SI at different severity, and most related

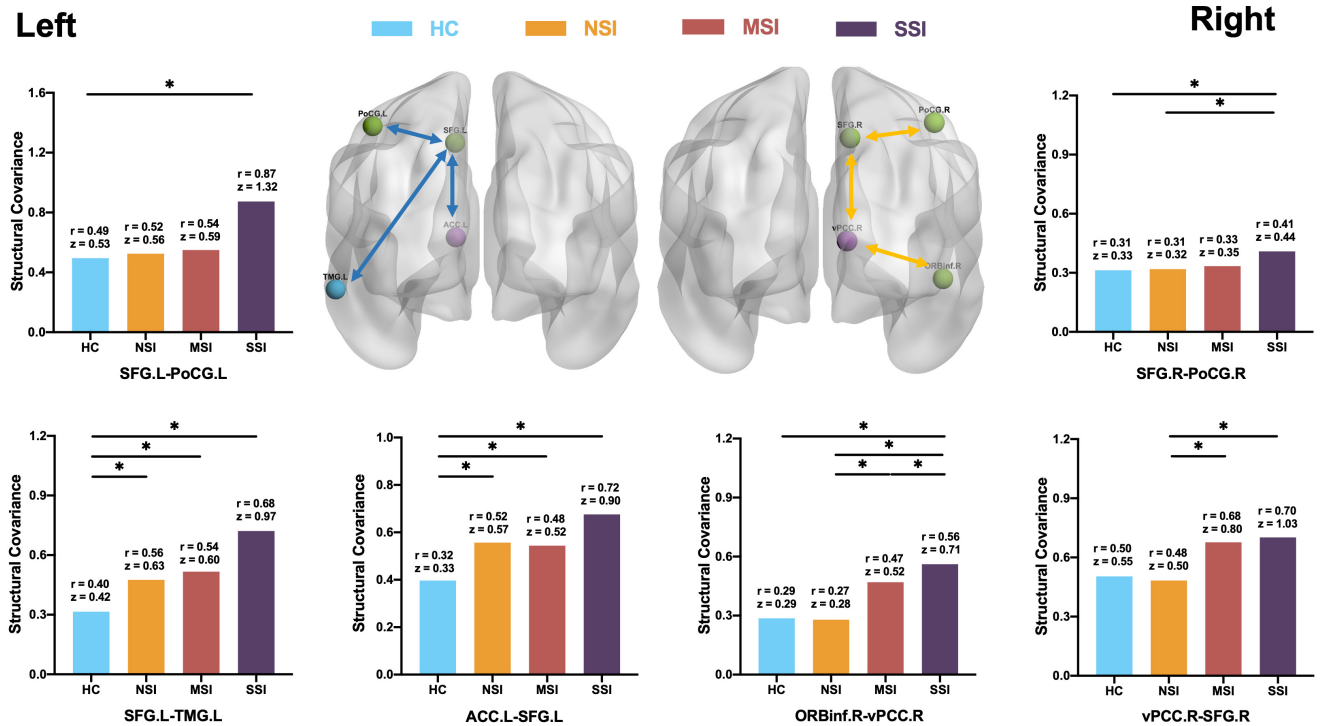

FIGURE 3 | Comparison of CON structural covariance network. **(Left side)** Compared with HC, there is an abnormal increase in the structural covariance of the three MDD groups. The network is concentrated on the left side of the brain. The three pairs include the anterior cingulate gyrus (ACC)–superior frontal gyrus (SFG), SFG–post-central gyrus (PoCG), and SFG–middle temporal gyrus (MTG). **(Right side)** The comparison of the three MDD groups is found to be concentrated on the right side of the brain; three pairs include ORBinf–ventral posterior cingulate gyrus (vPCC), vPCC-SFG, and SFG–PoCG; structural covariance increases with increasing suicidal ideation. There is no difference between HC and NSI. Healthy group (HC), no suicidal ideation (NSI), mild suicidal ideation (MSI), and severe suicidal ideation (SSI). Blue line, comparison between MDD group and HC; yellow line, comparison between MDD three groups. *$p < 0.05$, false discovery rate (FDR).

research has focused on functional abnormalities, which are often due to structural abnormalities (Fried and Nesse, 2015).

Unlike the structural networks of the HC group, network connectivity in the MDD groups was abnormal, and as the severity of illness abnormality spread from the ACC.L to the SFG.L, this then affected the left central posterior gyrus and left middle temporal gyrus; this finding is consistent with a series of studies (Repple et al., 2020; Yang et al., 2020). The cingulate gyrus forms a C-shape adjacent to the prefrontal lobe (Williams(ed.), 2021). As MDD progresses, abnormal information transmission by SFG.L neurons or reduction of regional nutrition results in increased structural connectivity between the two brain regions, and SFG.L is also affected (Raj et al., 2012; Weickenmeier et al., 2018) by shrinkage and abnormal structural connectivity. A functional brain network study of repetitive transcranial magnetic stimulation (TMS) treatment of MDD (Philip et al., 2018) found that the ACC.L of the pathological neural network was connected to the left prefrontal lobe; after receiving TMS treatment, abnormalities of the frontal and parietal network are improved in clinically cured patients (Belleau et al., 2019). Our results on the MDD and HC groups are basically consistent with previous structural and functional network studies, indicating the feasibility of SCN analysis.

In the present study, MDD patients with SI at different severity showed not only specific differences in ReHo and GMV but also characteristic structural connectivity between brain regions in the SCN. Abnormal structural connectivity related to SI was concentrated in the right hemisphere of the CON in three circuits: ORBinf.R–vPCC.R, vPCC.R–SFG.R, and SFG.R–PoCG.R. The concentration in the right hemisphere may be because the right OFC is closely involved in cognitive control and decision-making (Ding et al., 2016; Johnston et al., 2017). Efferent nerve fibers traveling from the OFC to the cingulate gyrus enable it to influence behavior and physiological responses (Burks et al., 2018). As a result, ORBinf.R atrophy (Yang et al., 2020) affects the communication of information between the right-sided CON brain regions, resulting in the spread of vPCC.R abnormalities to the frontal and parietal regions. Eventually, the CON is progressively damaged with SI increases. GMV atrophy of the ORBinf.R and ORBinf.R–vPCC.R circuit abnormality may be associated with SI at different severity and used as a marker for suicide prediction and assessment in the future.

Our findings are consistent with previous studies that demonstrated that MDD is a degenerative mental illness dominated by disrupted ReHo (Späti et al., 2015) and GMV

atrophy (Schmaal et al., 2020; Zhang et al., 2020; Stein et al., 2021). By using ReHo and SCN analysis (Lerch et al., 2006; Alexander-Bloch et al., 2013), we found that compared with healthy people, MDD patients had functional and structural defects in the CON and showed disrupted ReHo and GMV atrophy in the ACC.L and abnormal structural connectivity of the ACC.L–SFG.L (Boes et al., 2018; Crowell et al., 2019; Cole et al., 2020; Rappaport et al., 2020). MDD with SI at different severity has specific functional defects and structural network changes located in the ORBinf.R of CON (Yang et al., 2020) and showed disrupted ReHo and GMV atrophy in the ORBinf.R and abnormal structural connectivity of the ORBinf.R–vPCC.R (Kappelmann et al., 2021). Our finding suggested that MDD patients with different severity of SI have different neuroimaging changes.

LIMITATIONS AND FUTURE DIRECTIONS

A significant limitation of this study is its cross-sectional design. A longitudinal study is required to confirm the results. The number of MDD patients with severe SI is small in the present study. Participants in this study were not professionally assessed by SI and were simply grouped according to the MADRS for SI, which should be further analyzed in detail using the professional suicide assessment scale in the future.

DATA AVAILABILITY STATEMENT

The datasets presented in this article are not readily available because the data are currently part of a longitudinal study that is ongoing. However, they can be obtained by contacting the corresponding author. Requests to access the datasets should be directed to corresponding author XX, xfxu2004@sina.com.

ETHICS STATEMENT

The studies involving human participants were reviewed and approved by the Ethics Review Board of Kunming Medical College First Affiliated Hospital [Ethics Review L No. 50(2016)]. The patients/participants provided their written informed consent to participate in this study.

AUTHOR CONTRIBUTIONS

XX and ZS participated in the conception and design, data analysis, and interpretation of the research. MH contributed to the conception and design of the project, data collection and analysis, and the writing and revision of the manuscript. LP, ZC, and CZ contributed to data analysis. All authors critically revised the draft version of the manuscript and approved the final manuscript.

FUNDING

This study was funded by the National Natural Science Foundation of China (81660237), Yunnan Basic Research Projects-Union Foundation [2019FE001(-144)], Yunnan Health Training Project of High Level Talents (H-2018090), and Yunnan Provincial Health Institute Research Project (2018NS0109).

SUPPLEMENTARY MATERIAL

The Supplementary Material for this article can be found online at: https://www.frontiersin.org/articles/10.3389/fnins.2022.856366/full#supplementary-material

REFERENCES

Alexander-Bloch, A., Giedd, J. N., and Bullmore, E. (2013). Imaging structural co-variance between human brain regions. *Nat. Rev. Neurosci.* 14, 322–336. doi: 10.1038/nrn3465

Arnone, D., Mcintosh, A., Ebmeier, K., Munafò, M. R., and Anderson, I. (2011). Magnetic resonance imaging studies in unipolar depression: systematic review and meta-regression analyses. *Eur. Neuropsychopharmacol.* 22, 1–16. doi: 10.1016/j.euroneuro.2011.05.003

Bani-Fatemi, A., Tasmim, S., Graff-Guerrero, A., Gerretsen, P., Strauss, J., Kolla, N., et al. (2018). Structural and functional alterations of the suicidal brain: an updated review of neuroimaging studies. *Psychiatry Res. Neuroimaging* 278, 77–91. doi: 10.1016/j.pscychresns.2018.05.008

Belleau, E. L., Treadway, M. T., and Pizzagalli, D. A. (2019). The impact of stress and major depressive disorder on hippocampal and medial prefrontal cortex morphology. *Biol. Psychiatry* 85, 443–453. doi: 10.1016/j.biopsych.2018.09.031

Benjamini, Y., and Hochberg, Y. (1995). Controlling the false discovery rate - a practical and powerful approach to multiple testing. *J. R. Statist. Soc. B* 57, 289–300. doi: 10.2307/2346101

Boes, A. D., Uitermarkt, B. D., Albazron, F. M., Lan, M. J., Liston, C., Pascual-Leone, A., et al. (2018). Rostral anterior cingulate cortex is a structural correlate of repetitive TMS treatment response in depression. *Brain Stimul.* 11, 575–581. doi: 10.1016/j.brs.2018.01.029

Burks, J. D., Conner, A. K., Bonney, P. A., Glenn, C. A., Baker, C. M., Boettcher, L. B., et al. (2018). Anatomy and white matter connections of the orbitofrontal gyrus. *J. Neurosurg.* 128, 1865–1872. doi: 10.3171/2017.3.JNS162070

Chase, H. W., Segreti, A. M., Keller, T. A., Cherkassky, V. L., Just, M. A., Pan, L. A., et al. (2017). Alterations of functional connectivity and intrinsic activity within the cingulate cortex of suicidal ideators. *J. Affect. Disord.* 212, 78–85. doi: 10.1016/j.jad.2017.01.013

Cole, E. J., Stimpson, K. H., Bentzley, B. S., Gulser, M., Cherian, K., Tischler, C., et al. (2020). Stanford accelerated intelligent neuromodulation therapy for treatment-resistant depression. *Am. J. Psychiatry* 177, 716–726. doi: 10.1176/appi.ajp.2019.19070720

Cooper, L., Crum, R., and Ford, D. (1994). Identifying suicidal ideation in general medical patients. *JAMA* 272, 1757–1762. doi: 10.1001/jama.272.22.1757

Crossley, N. A., Mechelli, A., Scott, J., Carletti, F., Fox, P. T., McGuire, P., et al. (2014). The hubs of the human connectome are generally implicated in the anatomy of brain disorders. *Brain* 137, 2382–2395. doi: 10.1093/brain/awu132

Crowell, A. L., Riva-Posse, P., Holtzheimer, P. E., Garlow, S. J., Kelley, M. E., Gross, R. E., et al. (2019). Long-Term outcomes of subcallosal cingulate deep brain stimulation for treatment-resistant depression. *Am. J. Psychiatry* 176, 949–956. doi: 10.1176/appi.ajp.2019.18121427

Destrieux, C., Fischl, B., Dale, A., and Halgren, E. (2010). Automatic parcellation of human cortical gyri and sulci using standard anatomical nomenclature. *Neuroimage* 53, 1–15. doi: 10.1016/j.neuroimage.2010.06.010

Ding, Y., Pereira, F., Hoehne, A., Beaulieu, M.-M., Lepage, M., Turecki, G., et al. (2016). Altered brain processing of decision-making in healthy first-degree biological relatives of suicide completers. *Mol. Psychiatry* 22, 1149–1154. doi: 10.1038/mp.2016.221

Dosenbach, N., Fair, D., Miezin, F., Cohen, A., Wenger, K., Dosenbach, R., et al. (2007). Distinct brain networks for adaptive and stable task control in humans. *Proc. Natl. Acad. Sci. U.S.A.* 104, 11073–11078. doi: 10.1073/pnas.0704320104

Du, L., Zeng, J., Liu, H., Tang, D., Meng, H., Li, Y., et al. (2017). Fronto-limbic disconnection in depressed patients with suicidal ideation: a resting-state functional connectivity study. *J. Affect. Disord.* 215, 213–217. doi: 10.1016/j.jad.2017.02.027

Fischl, B. (2004). Automatically parcellating the human cerebral cortex. *Cereb. Cortex* 14, 11–22. doi: 10.1093/cercor/bhg087

Fried, E. I., and Nesse, R. M. (2015). Depression sum-scores don't add up: why analyzing specific depression symptoms is essential. *BMC Medicine* 13:72. doi: 10.1186/s12916-015-0325-4

Gong, G., He, Y., Chen, Z. J., and Evans, A. C. (2012). Convergence and divergence of thickness correlations with diffusion connections across the human cerebral cortex. *Neuroimage* 59, 1239–1248. doi: 10.1016/j.neuroimage.2011.08.017

Hagmann, P., Sporns, O., Madan, N., Cammoun, L., Pienaar, R., Wedeen, V. J., et al. (2010). White matter maturation reshapes structural connectivity in the late developing human brain. *Proc. Natl. Acad. Sci. U.S.A.* 107, 19067–19072. doi: 10.1073/pnas.1009073107

Hamilton, M. (1960). A rating scale for depression. *J. Neurol. Neurosurg. Psychiatry* 23, 56–62. doi: 10.1136/jnnp.23.1.56

Honey, C. J., Sporns, O., Cammoun, L., Gigandet, X., Thiran, J. P., Meuli, R., et al. (2009). Predicting human resting-state functional connectivity from structural connectivity. *Proc. Natl. Acad. Sci. U.S.A.* 106, 2035–2040. doi: 10.1073/pnas.0811168106

Izquierdo, A. (2017). Functional heterogeneity within rat orbitofrontal cortex in reward learning and decision making. *J. Neurosci.* 37, 10529–10540. doi: 10.1523/JNEUROSCI.1678-17.2017

Johnston, J. A. Y., Wang, F., Liu, J., Blond, B. N., Wallace, A., Liu, J., et al. (2017). Multimodal neuroimaging of frontolimbic structure and function associated with suicide attempts in adolescents and young adults with bipolar disorder. *Am. J. Psychiatry* 174, 667–675. doi: 10.1176/appi.ajp.2016.15050652

Jollant, F., Lawrence, N., Olie, E., Guillaume, S., and Courtet, P. (2011). The suicidal mind and brain: a review of neuropsychological and neuroimaging studies. *World J. Biol. Psychiatry?* 12, 319–339. doi: 10.3109/15622975.2011.556200

Jollant, F., Lawrence, N., Olie, E., O'Daly, O., Malafosse, A., Courtet, P., et al. (2010). Decreased activation of lateral orbitofrontal cortex during risky choices under uncertainty is associated with disadvantageous decision-making and suicidal behavior. *Neuroimage* 51, 1275–1281. doi: 10.1016/j.neuroimage.2010.03.027

Kaiser, R. H., Andrews-Hanna, J. R., Wager, T. D., and Pizzagalli, D. A. (2015). Large-Scale network dysfunction in major depressive disorder. *JAMA Psychiatry* 72:603. doi: 10.1001/jamapsychiatry.2015.0071

Kappelmann, N., Arloth, J., Georgakis, M. K., Czamara, D., Rost, N., Ligthart, S., et al. (2021). Dissecting the association between inflammation. metabolic dysregulation, and specific depressive symptoms. *JAMA Psychiatry* 78:161. doi: 10.1001/jamapsychiatry.2020.3436

Kendler, K., Fiske, A., Gardner, C., and Gatz, M. (2009). Delineation of two genetic pathways to major depression. *Biol. Psychiatry* 65, 808–811. doi: 10.1016/j.biopsych.2008.11.015

Kuusinen, V., Cesnaite, E., Peräkylä, J., Ogawa, K. H., and Hartikainen, K. M. (2018). Orbitofrontal lesion alters brain dynamics of emotion-attention and emotion-cognitive control interaction in humans. *Front. Hum. Neurosci.* 12:437. doi: 10.3389/fnhum.2018.00437

Lerch, J. P., Worsley, K., Shaw, W. P., Greenstein, D. K., Lenroot, R. K., Giedd, J., et al. (2006). Mapping anatomical correlations across cerebral cortex (MACACC) using cortical thickness from MRI. *Neuroimage* 31, 993–1003. doi: 10.1016/j.neuroimage.2006.01.042

Lieberman, L., Petrey, K., Shankman, S. A., Phan, K. L., and Gorka, S. M. (2020). Heightened reactivity to uncertain threat as a neurobehavioral marker of suicidal ideation in individuals with depression and anxiety. *Int. J. Psychophysiol.* 155, 99–104. doi: 10.1016/j.ijpsycho.2020.06.003

McGillivray, L., Rheinberger, D., Wang, J., Burnett, A., and Torok, M. (2022). Non-disclosing youth: a cross sectional study to understand why young people do not disclose suicidal thoughts to their mental health professional. *BMC Psychiatry* 22:3. doi: 10.1186/s12888-021-03636-x

Montgomery, S. A., and Åsberg, M. A. (1979). New depression scale designed to be sensitive to change. *Br. J. Psychiatry* 134, 382–389. doi: 10.1192/bjp.134.4.382

Murrough, J. W., Soleimani, L., Dewilde, K. E., Collins, K. A., Lapidus, K. A., Iacoviello, B. M., et al. (2015). Ketamine for rapid reduction of suicidal ideation: a randomized controlled trial. *Psychol. Med.* 45, 3571–3580. doi: 10.1017/S0033291715001506

Myung, W., Han, C. E., Fava, M., Mischoulon, D., Papakostas, G. I., Heo, J.-Y., et al. (2016). Reduced frontal-subcortical white matter connectivity in association with suicidal ideation in major depressive disorder. *Transl. Psychiatry* 6:e835. doi: 10.1038/tp.2016.110

Pfaff, J., and Almeida, O. (2004). Identifying suicidal ideation among older adults in a general practice setting. *J. Affect. Disord.* 83, 73–77. doi: 10.1016/j.jad.2004.03.006

Philip, N. S., Barredo, J., vant Wout-Frank , M., Tyrka, A. R., Price, L. H., and Carpenter, L. L. (2018). Network mechanisms of clinical response to transcranial magnetic stimulation in posttraumatic stress disorder and major depressive disorder. *Biol. Psychiatry* 83, 263–272. doi: 10.1016/j.biopsych.2017.07.021

Raj, A., Kuceyeski, A., and Weiner, M. A. (2012). Network diffusion model of disease progression in dementia. *Neuron* 73, 1204–1215. doi: 10.1016/j.neuron.2011.12.040

Rappaport, B. I., Kandala, S., Luby, J. L., and Barch, D. M. (2020). Brain reward system dysfunction in adolescence: current. cumulative, and developmental periods of depression. *Am. J. Psychiatry* 177, 754–763. doi: 10.1176/appi.ajp.2019.19030281

Repple, J., Mauritz, M., Meinert, S., de Lange, S. C., Grotegerd, D., Opel, N., et al. (2020). Severity of current depression and remission status are associated with structural connectome alterations in major depressive disorder. *Mol. Psychiatry* 25, 1550–1558. doi: 10.1038/s41380-019-0603-1

Schmaal, L., Pozzi, E. C., Ho, T., van Velzen, L. S., Veer, I. M., Opel, N., et al. (2020). ENIGMA MDD: seven years of global neuroimaging studies of major depression through worldwide data sharing. *Transl. Psychiatry* 10:172. doi: 10.1038/s41398-020-0842-6

Späti, J., Hänggi, J., Doerig, N., Ernst, J., Sambataro, F., Brakowski, J., et al. (2015). Prefrontal thinning affects functional connectivity and regional homogeneity of the anterior cingulate cortex in depression. *Neuropsychopharmacology* 40, 1640–1648. doi: 10.1038/npp.2015.8

Stein, F., Meller, T., Brosch, K., Schmitt, S., Ringwald, K., Pfarr, J. K., et al. (2021). Psychopathological syndromes across affective and psychotic disorders correlate with gray matter volumes. *Schizophr. Bull.* 47, 1740–1750. doi: 10.1093/schbul/sbab037

Suh, J. S., Schneider, M. A., Minuzzi, L., MacQueen, G. M., Strother, S. C., Kennedy, S. H., et al. (2019). Cortical thickness in major depressive disorder: a systematic review and meta-analysis. *Prog. Neuro Psychopharmacol. Biol. Psychiatry* 88, 287–302. doi: 10.1016/j.pnpbp.2018.08.008

Sylvester, C., Corbetta, M., Raichle, M., Rodebaugh, T., Schlaggar, B., Sheline, Y., et al. (2012). Functional network dysfunction in anxiety and anxiety disorders. *Trends Neurosci.* 35, 527–535. doi: 10.1016/j.tins.2012.04.012

Tononi, G., McIntosh, A. R., Russell, D. P., and Edelman, G. M. (1998). Functional clustering: identifying strongly interactive brain regions in neuroimaging data. *Neuroimage* 7, 133–149. doi: 10.1006/nimg.1997.0313

van Heeringen, K., Bijttebier, S., Desmyter, S., Vervaet, M., and Baeken, C. (2014). Is there a neuroanatomical basis of the vulnerability to suicidal behavior? A coordinate-based meta-analysis of structural and functional MRI studies. *Front. Hum. Neurosci.* 8:824. doi: 10.3389/fnhum.2014.00824

vanPraag, H. M. (1990). The DSM-IV (Depression) classification: to be or not to be? *J. Nervous Mental Dis.* 178, 147–149. doi: 10.1097/00005053-199003000-00001

Wagner, G., Koch, K., Schachtzabel, C., Schultz, C., Sauer, H., and Schlösser, R. (2011). Structural brain alterations in patients with major depressive disorder and high risk for suicide: evidence for a distinct neurobiological entity? *Neuroimage* 54, 1607–1614. doi: 10.1016/j.neuroimage.2010.08.082

Walker, E. R., McGee, R. E., and Druss, B. G. (2015). Mortality in mental disorders and global disease burden implications. *JAMA Psychiatry* 72:334. doi: 10.1001/jamapsychiatry.2014.2502

Wannan, C., Cropley, V., Chakravarty, M., Bousman, C., Ganella, E., Bruggemann, J., et al. (2019). Evidence for network-based cortical thickness reductions in schizophrenia. *Am. J. Psychiatry* 176, 1–12. doi: 10.1176/appi.ajp.2019.18040380

Weickenmeier, J., Kuhl, E., and Goriely, A. (2018). Multiphysics of prionlike diseases: progression and atrophy. *Phys. Rev. Lett.* 121:158101. doi: 10.1103/PhysRevLett.121.158101

Williams, M. (ed.) (2021). "The Cingulate Cortex," in *The Neuropathology of Schizophrenia*, (Cham: Springer International Publishing), 111–129. doi: 10.1007/978-3-030-68308-5_7

World Health Organization (2017). *World Health Organization. Depression Fact Sheet. World Health Organization*. Available online at: https://www.who.int/mediacentre/factsheets/%0Dfs369/en/ (accessed January 11, 2020).

Yan, M., He, Y., Cui, X., Liu, F., Li, H., Huang, R., et al. (2021). Disrupted regional homogeneity in melancholic and non-melancholic major depressive disorder at rest. *Front. Psychiatry* 12:618805. doi: 10.3389/fpsyt.2021.618805

Yang, Y., Chattun, M. R., Yan, R., Zhao, K., Chen, Y., Zhu, R., et al. (2020). Atrophy of right inferior frontal orbital gyrus and frontoparietal functional connectivity abnormality in depressed suicide attempters. *Brain Imaging Behav.* 14, 2542–2552. doi: 10.1007/s11682-019-00206-4

Zhang, Y., Li, M., Wang, Q., Hsu, J. S., Deng, W., Ma, X., et al. (2020). A joint study of whole exome sequencing and structural MRI analysis in major depressive disorder. *Psychol. Med.* 50, 384–395. doi: 10.1017/S0033291719000072

Conflict of Interest: The authors declare that the research was conducted in the absence of any commercial or financial relationships that could be construed as a potential conflict of interest.

Publisher's Note: All claims expressed in this article are solely those of the authors and do not necessarily represent those of their affiliated organizations, or those of the publisher, the editors and the reviewers. Any product that may be evaluated in this article, or claim that may be made by its manufacturer, is not guaranteed or endorsed by the publisher.

frontiers in Neuroscience

ORIGINAL RESEARCH
published: 28 March 2022
doi: 10.3389/fnins.2022.849158

Altered Cingulum Functioning in Major Depressive Disorder Patient With Suicide Attempts: A Resting-State Functional Magnetic Resonance Imaging Study

Chunxia Yang[1], Yajuan Duan[2], Lei Lei[2], Penghong Liu[1], Aixia Zhang[1], Gaizhi Li[1], Ning Sun[1,3], Yikun Wang[1], Zhifen Liu[1] and Kerang Zhang[1]**

[1] Department of Psychiatry, First Hospital of Shanxi Medical University, Taiyuan, China, [2] The First Hospital, Shanxi Medical University, Taiyuan, China, [3] Nursing College of Shanxi Medical University, Taiyuan, China

OPEN ACCESS

Edited by:
Nathalie Just,
Copenhagen University Hospital, Denmark

Reviewed by:
Jianzhong Ma,
University of Texas MD Anderson Cancer Center, United States
Hao Guo,
Taiyuan University of Technology, China

***Correspondence:**
Zhifen Liu
liuzhifen5518@163.com
Kerang Zhang
atomsxmu@vip.163.com

Specialty section:
This article was submitted to Brain Imaging Methods, a section of the journal Frontiers in Neuroscience

Received: 05 January 2022
Accepted: 04 March 2022
Published: 28 March 2022

Citation:
Yang C, Duan Y, Lei L, Liu P, Zhang A, Li G, Sun N, Wang Y, Liu Z and Zhang K (2022) Altered Cingulum Functioning in Major Depressive Disorder Patient With Suicide Attempts: A Resting-State Functional Magnetic Resonance Imaging Study. Front. Neurosci. 16:849158. doi: 10.3389/fnins.2022.849158

Background: Major depressive disorder (MDD) with suicide attempts (SA) poses a significant public health issue. This study aims to identify neurobiological markers for MDD with SA on resting-state brain functional magnetic resonance imaging (rs-fMRI).

Methods: Fifty-one unmedicated adult MDD participants, 27 with SA on the Beck Scale for Suicidal Ideation and 24 without SA, underwent rs-fMRI scanning. A group of 30 healthy controls (HC) matched for age, gender, and education-level with MDD were chosen. A whole brain analysis of regional homogeneity (ReHo) was performed on subjects to identify regions where brain activity was associated with SA. Multiple comparison analysis was performed for ReHo. Pearson's correlation analysis was performed between HAMD-SA scores and ReHo. The statistical significance level was set at $p < 0.05$.

Results: We examined whether there were significant differences among the three groups in whole brain ReHo during resting state. Subjects with SA showed significant increase of ReHo in the right Cingulum Post in comparison with those without SA. Subjects with SA showed significant decrease of ReHo in the right Cingulate Gyrus/Precuneus in comparison with HC. The mean ReHo from the significant brain region was associated with HAMD-SA (item 3 of the HAMD) scores ($r = 0.349$, $P = 0.012$) but was not associated with HAMD-24 scores.

Conclusion: These results indicate that SA is associated with altered resting-state brain activity. The pattern of elevated activity in the cingulum functioning may be related to SA. Identifying cingulum activity associated with SA may help to elucidate its pathogenesis and etiology.

Keywords: major depressive disorder, resting-state fMRI, regional homogeneity (ReHo), suicidal attempts, cingulum functioning

INTRODUCTION

Major depressive disorder (MDD) is a worldwide widespread psychiatric disorder associated with premature death by suicide (Saraceno, 2002; Kalin, 2020). The lifetime risk of suicide in patients with MDD ranges from 5 to 11% (Angst et al., 2005; Isometsä, 2014). Approximately 40–70% of those who have attempted or committed suicide were diagnosed with major depressive disorder (Rihmer, 2007). Recent studies suggest that the lifetime prevalence of suicide attempts (SA) in MDD was as high as 31% worldwide (Dong et al., 2019). Although the social and personal costs of suicidal behavior are devastating, clinically, suicide risk in MDD patients is predicted based on a few limited scale tests. However, these tests are largely dependent on the subjective wishes of the patients. Also, patients may be inclined to avoid discussing SA with clinicians (Zalsman et al., 2016). Therefore, it is important to identify markers associated with SA, which may help to develop tests to assess the risk of suicide and also have the potential to create more targeted therapeutic strategies to reverse SA (Schmaal et al., 2020).

In an attempt to identify factors contributing to suicidal behavior, an increasing number of researchers have studied neurobiological markers pointing to functional and structural alterations in the limbic zone of MDD patients with suicidal behavior (Cao et al., 2016; Zhang et al., 2016). Meanwhile, previous studies also found that both psychotherapy (Chaïb et al., 2020) and psychoactive medication (Zalsman et al., 2016) could reduce the risk of suicide. However, there are no objective indicators to quantify this risk yet. Therefore, elucidating the neural basis of suicidal behavior in MDD may provide insights into early intervention and treatment. Resting state functional magnetic resonance imaging (rs-fMRI) studies have found that SA often occurs during mind rest phases, brain processes that occur when subjects are not engaged in any specific mental task (Rush and Beck, 1978). Previous studies showed that SA was associated with a pattern of low self-esteem (Cox et al., 2004; Bhar et al., 2008). Another study showed that two dimensions of rumination, brooding, and reflection, were predictors of suicidal ideation (Miranda and Nolen-Hoeksema, 2007). Moreover, rs-fMRI study explained the neural substrates of depressive rumination and explicit account of functional abnormalities in sgPFC in MDD (Hamilton et al., 2015). Therefore, rs-fMRI is particularly beneficial in finding SA in MDD related brain regions.

In magnetic resonance imaging (MRI), a powerful tool to explore alterations in neural circuits is regional homogeneity (ReHo), which reflects statistical similarity in spontaneous neural activity between spatially adjacent brain tissues (Zhu et al., 2005). ReHo is believed to reflect anatomical, morphological, and intrinsic geometric similarities and topological functional interactions of local brain structures. Abnormal ReHo reflects changes in the temporal aspects of regional neural activity (Jiang and Zuo, 2016). At present, the studies of brain function mainly focus on evaluating local functional changes, and ReHo is used as a measure of regional synchronization of the fMRI time course, and has been widely used in many studies on MDD. ReHo alterations in the prefrontal cortex, thalamus, right supplementary motor area, and primary visual, auditory, and motor cortices have been detected in MDD. A recent study found that lower ReHo in the postcentral gyrus was associated with depressive symptoms in MDD. In addition, a recent study (Xia et al., 2019) provided some evidence for differentiating subgroups of MDD. ReHo may be a transdiagnostic neurobiological basis for reproducible alterations in the assessment of underlying depressive symptoms.

Research has focused on investigating dynamic functional connectivity or networks, which can provide information about dynamic tissue changes in brain strength or space (Bassett and Sporns, 2017). Studies in depressed patients have linked SA to impulsive behavior and executive and emotional processing dysfunction (Myung et al., 2016; Johnston et al., 2017). Notably, executive functions and emotional processing involve brain regions such as the orbitofrontal cortex, anterior cingulate cortex, dorsolateral prefrontal cortex and temporal polar gyrus (Rogers et al., 2004; Olson et al., 2007). Frontal limbic (Du et al., 2017) and orbitofrontal thalamic functional connectivity (Kim et al., 2017) and frontal cortical white matter connectivity (Myung et al., 2016) were reduced in patients with SA compared to MDD patients without SA. Convergent findings suggest the presence of structural and fMRI abnormalities in MDD SA patients (Myung et al., 2016; Du et al., 2017; Kim et al., 2017). The reason for the inconsistency of these research results may be due to the limited research indicators or the different focus of the research objects, some teenagers (Ordaz et al., 2018) and women (Wei et al., 2018). However, there are a few promising studies (Cao et al., 2015; Chen et al., 2021) on suicide and ReHo indicators, which in turn encourages additional related research.

In an effort to characterize MDD patients with concomitant SA, we applied ReHo on resting state fMRI of MDD patients with and without SA. We sought to determine (1) whether MDD patients with SA show a different pattern of local consistency than MDD patients without SA and (2) whether the altered ReHo values could provide a neural marker to predict the severity of SA. By studying ReHo features in MDD patients with SA, we expect to delineate brain regions associated with SA that have the potential to be targeted for subsequent therapies. We also hope to shed further light on the biological details of the brains of MDD patients with SA.

MATERIALS AND METHODS

Participants

The participants consisted of 51 first-episode, drug-naive patients with MDD. All of these patients were recruited from the Department of Psychiatry in the First Hospital of Shanxi Medical University between December 2018 and July 2019. Independent diagnoses by at least two consultant psychiatrists according to Diagnostic and Statistical Manual of Mental Disorders Fourth Edition (DSM-IV) criteria for MDD. The patients were also assessed with the Chinese Version of the Modified Structured Clinical Interview for DSM-IV TR Axis I Disorders Patient Edition (SCID-I/P, 11/2002 revision). At the same time, the subjects were interviewed using the 24-item HAMD. All of the

subjects included in this study meet the following inclusion criteria: (1) aged from 18 to 65 years old; (2) right-handed; (3) diagnosed with first-episode, drug-naive patients based on the DSM-IV criteria; (4) HAMD-17 score >17 and HAMA-14 score <14. The exclusion criteria were: (1) meeting DSM-IV axis I psychiatric disorders; (2) with severe organic diseases such as neurological diseases; (3) obvious impulsivity, or uncooperativeness; (4) pregnant women; (5) contraindications for MRI scans.

The patients were divided into two groups based on whether or not they had a history of suicide attempts. Suicide attempt is defined as a self-destructive act leading to physical harm with some degree of intention to die. Accordingly, 24 patients who attempted suicide were categorized in the group. On the other hand, 27 patients who never attempted suicide were classified in the non-SA group. The Scale for Suicidal Ideation (SSI) was used to assess suicidal ideation as well as the risk of suicide which was not required for the non-SA and HCs group.

None of the subjects were excluded due to excessive head motion during the fMRI scan. In order to explore neurobiological markers for MDD with SA on rs-fMRI, 30 age-, gender-, and education-level-matched healthy controls were selected. Excluded subjects were those who were left-handed, had mental disorders, a neurological illness, or showed abnormalities on brain images.

Written informed consent was obtained from each participant and consent from each participant's guardian was also obtained prior to data acquisition. The Ethical Committee for Medicine of the First Hospital of Shanxi Medical University approved this study.

Magnetic Resonance Imaging Data Acquisition

Data preprocessing was conducted using an A MAGNETOM Trio Tim 3.0 T (Siemens Medical Solutions, Germany) with a 12-channel birdcage head coil located. The head of participants was positioned within a 32-channel head coil. A 3DFLASH sequence was used to obtain high resolution trasaxial T1-weighted anatomical images for voxel-based morphometry (VBM) with the following parameters: 120 sagittal slices, TR = 14 ms, TE = 4.92ms, thickness/skip = 1.5/0.3 mm, FOV = 230 mm × 230 mm, matrix = 256 × 192 mm, flip angle = 25°. The rs-fMRI was performed using an echo planar imaging (EPI) sequence with the following parameters: TR = 2,000 ms, TE = 30 ms, Flip angle = 70°, FOV = 24 cm × 24 cm, matrix = 64 × 64, section thickness = 3 mm, slice gap = 2 mm, acquired over 6 min and 212 volumes were obtained. Anatomic images were obtained with 3D MPRAGE sequence for co-registration with the functional data. The fMRI images were pre-processed in SPM5 (statistics parameter mapping[1]) and REST software for motion correction, band-pass filter (0.01–0.1 Hz), image normalization and 4 mm Gaussian spatial smoothing after Reho calculation. During the scan, all subjects were confirmed that they did not fall asleep.

[1]www.fil.ion.ucl.uk/spm

Regional Homogeneity Analysis

Regional homogeneity is based on the concept that BOLD signal fluctuations in a particular region reflect activity close to neurons at the same frequency, and this time synchronization is limited to groups of neurons performing related functions (Zang et al., 2004). We used the DPARSF software to calculate the ReHo. Individual ReHo maps were generated by calculating Kendall's coefficient of concordance (KCC) of the time series of a given voxel with those of its nearest neighbors (26 voxels) in a voxel-wise analysis. Assuming that a voxel is similar to its neighbors in time, the consistency and similarity of each individual is assessed by calculating the KCC of the time series between a given voxel and its neighbors in voxel analysis. After the ReHo map was calculated on the basis of voxel-by-voxel, the standardized ReHo images were then spatially smoothed with a Gaussian kernel of $8 \times 8 \times 8$ mm^3 full width at half-maximum. Finally, low-frequency fluctuations (LFFs) within a functional cluster were synchronized with neighboring voxels.

Statistical Analyses

All statistical analyses were performed using IBM SPSS Statistics Version 23.0 (SPSS23.0). One-way ANOVAs were conducted to detect the differences among the three groups in terms of age and, years of education. An X^2-test was used to estimate group differences in gender. *T*-tests were conducted to compare the total HAMD score between the two patient groups. A multiple comparison analysis was performed to analyze the ReHo. The ReHo between the patient groups and controls were examined using one-way ANOVA analysis followed by *post-hoc* two-sample *t*-tests. The statistical significance level was set at $p < 0.05$.

To assess the effect of independent of SA, the value of the suicide item (item 3) of the HAMD was subtracted from the HAMD score in order to yield a clinical variable (HAMD-SA) for further analyses. Pearson's correlation analysis was performed between HAMD-SA scores and ReHo.

RESULTS

We examined whether there were differences among the three groups in whole brain ReHo during a resting state. Subjects with SA showed a significant increase of in ReHo in the right Cingulum Post compared to those without SA. Subjects with SA showed a significant decrease of in ReHo in the right Cingulate Gyrus/Precuneus compared to HC. The mean ReHo from the significant brain region was associated with HAMD-SA scores ($r = 0.349$, $P = 0.012$) but was not associated with HAMD-24 scores.

Demographic Data Comparisons

The MDD patients and HC were comparable in age, gender, and years of education with no significant differences. There were no significant differences between the patients with SA and without SA in their total HAMD-24 scores. The average SSI scores of with Suicide Attempts group was 10.04 ± 1.78 (**Table 1**).

TABLE 1 | Demographic and clinical characteristics of all participants.

Variable	With suicide attempts group (*n* = 24)	Without suicide attempts symptoms group (*n* = 27)	HCs group (*n* = 30)	x^2/t/F-Value	*P*-value
Gender (M/F)	8/16	14/13	16/14	1.26	0.289[a]
Age (years)	33.46 ± 9.47	30.96 ± 11.68	32.83 ± 8.42	0.45	0.640[b]
Education (years)	13.21 ± 4.45	13.41 ± 4.72	15.63 ± 3.41	2.90	0.061[b]
HAMD-17 total scores	20.83 ± 3.61	23.00 ± 3.09	–	1.06	0.308[c]
HAMD-24 total scores	26.54 ± 4.21	27.93 ± 3.97	–	0.14	0.714[c]

[a]*P-value for chi-square test.*
[b]*P-values for one-way ANOVA.*
[c]*P-values for two-sample t-test.*

Regional Homogeneity Regions Differences in Suicide Attempts Symptoms Group, Non-suicide Attempts Symptoms Group, and Healthy Controls Group

We examined whether there were differences among the three groups in whole brain ReHo during resting state. Significant differences in ReHo were observed among the three groups for the right Cingulum Post (**Table 2** and **Figure 1A**).

Compared to the non-SA group, the SA group showed increased brain activity in the Right Cingulum Post (see **Table 2** and **Figure 1B**). Compared to the HCs group, the SA group showed decreased brain activity in the right Cingulate Gyrus/Precuneus (see **Table 2** and **Figure 1C**).

Correlations Between HAMD-SA (item 3 of the HAMD) Scores and Regional Homogeneity

Mean ReHo from the significant brain region was associated with HAMD-SA (item 3 of the HAMD) scores ($r = 0.349$, $P = 0.012$) (see **Figure 2**) but was not associated with HAMD-24 scores.

DISCUSSION

At the initial assessment, because patients and clinicians may be relatively unaware of each other, suicide patients may deny SA during an interview. Some patients may deliberately obstruct interventions to prevent suicide (Brook et al., 2006). Identifying neurophysiologic markers is of great importance for objectively diagnosing SA in MDD patients. The results of our present study show that the SA group demonstrated increased local consistency of neural activity in the right cingulate relative to the NSA group; however, it demonstrated less local consistency in the right Cingulate/Precuneus relative to the HC group. In addition, the mean ReHo of right cingulate from the significant brain region correlated with the HAMD-SA score, but was not associated with HAMD-24 scores. Finding these ReHo-altered functional brain regions may shed light on the pathophysiological mechanism of suicide in MDD patients.

Cingulate has been the subject of intense research, with anterior cingulate cortex (ACC) volume loss being one of the most consistent findings (Arnone et al., 2012). ACC is involved in cognitive functioning and is executive functioning (Breukelaar et al., 2017), and impaired executive functioning may be a neuropsychological risk factor for suicidal behavior (Westheide et al., 2008). It has been reported that there was a volume decrease in the rostral anterior cingulate in patients with suicidal MDD compared to non-suicidal MDD patients (Wagner et al., 2011; Li et al., 2019). An autopsy study revealed that the number and length of dendritic branches in the anterior cingulate gyrus were significantly reduced in depressed suicide completers compared to controls (Hercher et al., 2010). A recent study reported decreased ACC activity in adolescents with a history of suicide attempts and depression compared to adolescents with a history of depression only (Pan et al., 2011). However, our study illustrates increasing right cingulate functioning in MDD patients with SA. Therefore, we speculate that the ReHo changes of ACC in depression and suicide should be similar, which may be related to the common pathophysiological mechanism of depression and suicide in this region.

Recent brain functional imaging studies have found that the precuneus is associated with many high levels cognitive functions, such as episodic memory, self-related information processing. Previous studies mostly focused on the local functional consistency of precuneus in depression, and little attention has been paid on suicide. Of the two suicide-related ReHo studies, one was that ReHo in the left precuneus was higher in the SA group than in the normal control group (Cao et al., 2015), the other study found lower ReHo of the right cuneus in the SA group compared with the NSA group (Chen et al., 2021). No such result was found in our study. However, there are many studies on ReHo indicators of depression. Liu et al. (2012) study found that compared to the healthy controls, MDD patients had significantly decreased ReHo in right precuneus. Moreover, other studies found that there were significant lower in ReHo in left anterior cingulate cortex and bilateral precuneus in MDD group compared with the control group (Lai, 2018). These are consistent with the results of our study. However, findings that are inconsistent with ours were reported, including those those in the study of Zhang et al. (2021) where it was shown that ReHo in the right precuneus lobe of patients with SA depression was significantly increased compared with healthy controls. Studies reported that relative to patients with LOD (later adult onset depression, age 30–44), patients with EOD (early adult onset

TABLE 2 | Regions showing significant differences in regional homogeneity (ReHo) among major depressive disorder (MDD) with/without suicide attempts (SA) and healthy controls.

Area		Cluster size (voxels) mm^3	BA	Side	MNI Co-ordinates[a]			F/T-value[b]
					x	y	z	
Differences among three groups								
HCs > with suicide attempts group	Cingulum post	4,617	23	Left	−3	−39	24	11.6288
	Cingulate Gyrus/Precuneus	189	–	Right	12	−51	27	2.7282
Without suicide attempts group < with suicide attempts group	Cingulum Post	1,188	–	Right	3	−42	15	−3.2385

[a] *Co-ordinates of primary peak locations in the Montreal Neurological Institute space.*
[b] *T-statistical value of peak voxel showing ReHo differences between groups.*
BA, Brodmann area.
H represents healthy controls, Y represents depressed patients with SA, and N represents depressed patients without SA.

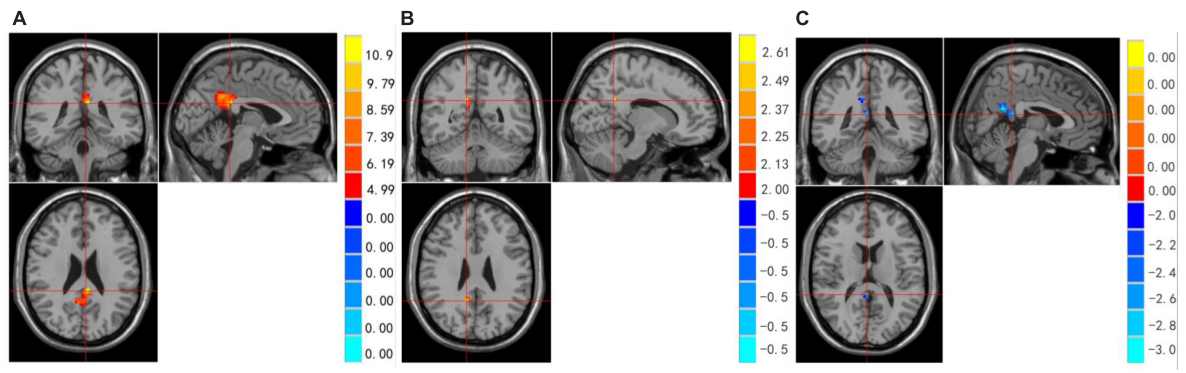

FIGURE 1 | (A–C) Regions showing significant differences in ReHo among MDD with/without SA and healthy controls. Red represents HCs > with suicide attempts group brain area, blue represents without suicide attempts group < with suicide attempts group brain area.

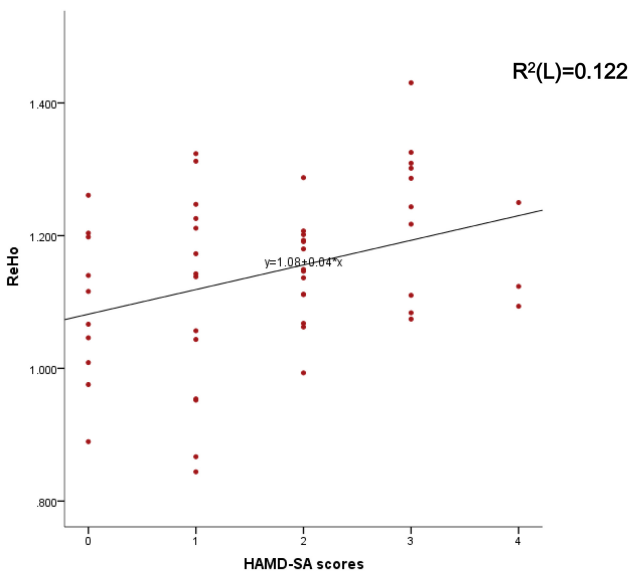

FIGURE 2 | Represents the correlation between the mean ReHo of the right Cingulate Gyrus and HAMD-SA scores.

depression, age 18–29) displayed significantly increased ReHo in the left precuneus (Chen et al., 2012; Shen et al., 2017). In our study, we did not have similar observations on the left precuneus, probably reflecting the idiosyncrasies of the different study subjects. The reason for the similarities and differences of these results may also be that precuneus is not necessarily a dysfunctional brain area caused by suicide, but may be a specific indicator of depression.

Regarding the correlation between ReHo and HAMD, a study found that the right cuneus of SI was positively correlated with HAM-D (Chen et al., 2021). Another study (Modinos et al., 2014) found that the volume of anterior cingulate gyrus negatively correlated with suicidal symptoms. The correlation analysis of another study (Zhang et al., 2021) showed that there was no significant correlation between the BDI-II score and the ReHo value of the precuneus in the SA group. Our study found that the mean ReHo in the right cingulate gyrus was correlated with HAMD-SA scores, but was not associated with HAMD-24 scores. It also indirectly illustrates that structural and functional abnormalities of the cingulate gyrus may be closely related to the symptoms of suicide.

Our study had some limitations: first, the sample size for MDD patients was relatively small. A larger sample size is needed to replicate the results we presented here. Second, our study was a cross-sectional design, and the data were insufficient to establish a causal relationship between depressive symptoms and suicidal behavior. Future studies using longitudinal designs will be useful for examining the causal relationship between depression and SA. Third, we only studied suicidal ideation in MDD patients. Future studies are needed to examine the role of the right cingulate gyrus in suicidal behavior in patients with other mental disorders, such as schizophrenia. Last but not least, it has been demonstrated that periods of untreated depression are associated with greater volume loss in some brain regions. We will certainly pay attention to this point in future studies. Therefore, our findings should be considered preliminary and should be confirmed before firm conclusions can be drawn.

CONCLUSION

Our study showed that SA in depressed patients was associated with alterations in resting state brain activity. Our results suggest that the neural basis of psychopathology in depressed patients with suicidal ideation may involve functional abnormalities in multiple brain regions. The pattern of increased local functional activity in the right cingulate may be related to SA. Identifying cingulate activity may help elucidate the etiology and pathogenesis associated with SA.

DATA AVAILABILITY STATEMENT

The raw data supporting the conclusions of this article will be made available by the authors, without undue reservation.

ETHICS STATEMENT

The studies involving human participants were reviewed and approved by Medical Research Ethics Committee of Shanxi Medical University. The patients/participants provided their written informed consent to participate in this study.

AUTHOR CONTRIBUTIONS

KZ and ZL designed and supervised this study. NS, YW, GL, and CY were responsible for data analysis and manuscript drafting. PL and LL revised the manuscript. YD and AZ participated in sample collection and carried out the experimental procedures. All authors reviewed and approved the final manuscript.

FUNDING

This work was supported by the National Natural Science Foundation of China (82171534), National Natural Science Youth Fund Project (82001802), Natural Science Foundation of Shanxi Province (20210302123251 and 20210302123257), a research project supported by the Shanxi Scholarship Council of China (HGKY2019098), Natural Science Foundation of Shanxi Province for youth (20210302124193), and 136 Medical Rejuvenation Project of Shanxi Province.

ACKNOWLEDGMENTS

We sincerely thank the patients and their families, as well as the healthy volunteers for their participation, and all the medical staff involved in the collection of specimens.

REFERENCES

Angst, J., Angst, F., Gerber-Werder, R., and Gamma, A. (2005). Suicide in 406 mood-disorder patients with and without long-term medication: a 40 to 44 years' follow-up. *Arch. Suicide Res.* 9, 279–300. doi: 10.1080/13811110590929488

Arnone, D., McIntosh, A. M., Ebmeier, K. P., Munafò, M. R., and Anderson, I. M. (2012). Magnetic resonance imaging studies in unipolar depression: systematic review and meta-regression analyses. *Eur. Neuropsychopharmacol.* 22, 1–16. doi: 10.1016/j.euroneuro.2011.05.003

Bassett, D. S., and Sporns, O. (2017). Network neuroscience. *Nat. Neurosci.* 20, 353–364. doi: 10.1038/nn.4502

Bhar, S., Ghahramanlou-Holloway, M., Brown, G., and Beck, A. T. (2008). Self-esteem and suicide ideation in psychiatric outpatients. *Suicide Life Threat. Behav.* 38, 511–516. doi: 10.1521/suli.2008.38.5.511

Breukelaar, I. A., Antees, C., Grieve, S. M., Foster, S. L., Gomes, L., Williams, L. M., et al. (2017). Cognitive control network anatomy correlates with neurocognitive behavior: a longitudinal study. *Human Brain Mapp.* 38, 631–643. doi: 10.1002/hbm.23401

Brook, R., Klap, R., Liao, D., and Wells, K. B. (2006). Mental health care for adults with suicide ideation. *Gen. Hosp. Psychiatry* 28, 271–277. doi: 10.1016/j.genhosppsych.2006.01.001

Cao, J., Chen, J. M., Kuang, L., Ai, M., Fang, W. D., Gan, Y., et al. (2015). Abnormal regional homogeneity in young adult suicide attempters with no diagnosable psychiatric disorder: a resting state functional magnetic imaging study. *Psychiatry Res.* 231, 95–102. doi: 10.1016/j.pscychresns.2014.10.011

Cao, J., Chen, X., Chen, J., Ai, M., Gan, Y., Wang, W., et al. (2016). Resting-state functional MRI of abnormal baseline brain activity in young depressed patients with and without suicidal behavior. *J. Affect. Disord.* 205, 252–263. doi: 10.1016/j.jad.2016.07.002

Chaïb, L. S., Lopez-Castroman, J., and Abbar, M. (2020). Group post-admission cognitive therapy for suicidality vs individual supportive therapy for the prevention of repeat suicide attempts: a randomized controlled trial. *Trials* 21:889. doi: 10.1186/s13063-020-04816-y

Chen, J. D., Liu, F., Xun, G. L., Chen, H. F., Hu, M. R., Guo, X. F., et al. (2012). Early and late onset, first-episode, treatment-naive depression: same clinical symptoms, different regional neural activities. *J. Affect. Disord.* 143, 56–63. doi: 10.1016/j.jad.2012.05.025

Chen, V. C., Chou, Y. S., Tsai, Y. H., Huang, Y. C., McIntyre, R. S., and Weng, J. C. (2021). Resting-state functional connectivity and brain network abnormalities in depressive patients with suicidal ideation. *Brain Topogr.* 34, 234–244. doi: 10.1007/s10548-020-00817-x

Cox, B. J., Enns, M. W., and Clara, I. P. (2004). Psychological dimensions associated with suicidal ideation and attempts in the National Comorbidity Survey. *Suicide Life Threat. Behav.* 34, 209–219. doi: 10.1521/suli.34.3.209.42781

Dong, M., Zeng, L. N., Lu, L., Li, X. H., Ungvari, G. S., Ng, C. H., et al. (2019). Prevalence of suicide attempt in individuals with major depressive disorder: a meta-analysis of observational surveys. *Psychol. Med.* 49, 1691–1704. doi: 10.1017/S0033291718002301

Du, L., Zeng, J., Liu, H., Tang, D., Meng, H., Li, Y., et al. (2017). Fronto-limbic disconnection in depressed patients with suicidal ideation: a resting-state functional connectivity study. *J. Affect. Disord.* 215, 213–217. doi: 10.1016/j.jad.2017.02.027

Hamilton, J. P., Farmer, M., Fogelman, P., and Gotlib, I. H. (2015). Depressive rumination, the default-mode network, and the dark matter of clinical neuroscience. *Biol. Psychiatry* 78, 224–230. doi: 10.1016/j.biopsych.2015.02.020

Hercher, C., Canetti, L., Turecki, G., and Mechawar, N. (2010). Anterior cingulate pyramidal neurons display altered dendritic branching in depressed suicides. *J. Psychiatr. Res.* 44, 286–293. doi: 10.1016/j.jpsychires.2009.08.011

Isometsä, E. (2014). Suicidal behaviour in mood disorders–who, when, and why? *Can. J. Psychiatry* 59, 120–130. doi: 10.1177/070674371405900303

Jiang, L., and Zuo, X. N. (2016). Regional homogeneity: a multimodal, multiscale neuroimaging marker of the human connectome. *Neuroscientist* 22, 486–505. doi: 10.1177/1073858415595004

Johnston, J., Wang, F., Liu, J., Blond, B. N., Wallace, A., Liu, J., et al. (2017). Multimodal neuroimaging of frontolimbic structure and function associated with suicide attempts in adolescents and young adults with bipolar disorder. *Am. J. Psychiatry* 174, 667–675. doi: 10.1176/appi.ajp.2016.15050652

Kalin, N. H. (2020). Insights into suicide and depression. *Am. J. Psychiatry* 177, 877–880. doi: 10.1176/appi.ajp.2020.20081207

Kim, K., Kim, S. W., Myung, W., Han, C. E., Fava, M., Mischoulon, D., et al. (2017). Reduced orbitofrontal-thalamic functional connectivity related to suicidal ideation in patients with major depressive disorder. *Sci. Rep.* 7:15772. doi: 10.1038/s41598-017-15926-0

Lai, C. H. (2018). The regional homogeneity of cingulate-precuneus regions: the putative biomarker for depression and anxiety. *J.Affect. Disord.* 229, 171–176. doi: 10.1016/j.jad.2017.12.086

Li, J., Duan, X., Cui, Q., Chen, H., and Liao, W. (2019). More than just statics: temporal dynamics of intrinsic brain activity predicts the suicidal ideation in depressed patients. *Psychol. med.* 49, 852–860. doi: 10.1017/S0033291718001502

Liu, F., Hu, M., Wang, S., Guo, W., Zhao, J., Li, J., et al. (2012). Abnormal regional spontaneous neural activity in first-episode, treatment-naive patients with late-life depression: a resting-state fMRI study. *Prog. Neuro Psychopharmacol. Biol. Psychiatry* 39, 326–331. doi: 10.1016/j.pnpbp.2012.07.004

Miranda, R., and Nolen-Hoeksema, S. (2007). Brooding and reflection: rumination predicts suicidal ideation at 1-year follow-up in a community sample. *Behav. Res. Ther.* 45, 3088–3095. doi: 10.1016/j.brat.2007.07.015

Modinos, G., Allen, P., Frascarelli, M., Tognin, S., Valmaggia, L., Xenaki, L., et al. (2014). Are we really mapping psychosis risk? *Psychol. Med.* 44, 3491–3501. doi: 10.1017/S0033291714000865

Myung, W., Han, C. E., Fava, M., Mischoulon, D., Papakostas, G. I., Heo, J. Y., et al. (2016). Reduced frontal-subcortical white matter connectivity in association with suicidal ideation in major depressive disorder. *Transl. Psychiatry* 6:e835. doi: 10.1038/tp.2016.110

Olson, I. R., Plotzker, A., and Ezzyat, Y. (2007). The enigmatic temporal pole: a review of findings on social and emotional processing. *Brain* 130, 1718–1731. doi: 10.1093/brain/awm052

Ordaz, S. J., Goyer, M. S., Ho, T. C., Singh, M. K., and Gotlib, I. H. (2018). Network basis of suicidal ideation in depressed adolescents. *J. Affect. Disord.* 226, 92–99. doi: 10.1016/j.jad.2017.09.021

Pan, L. A., Batezati-Alves, S. C., Almeida, J. R., Segreti, A., Akkal, D., Hassel, S., et al. (2011). Dissociable patterns of neural activity during response inhibition in depressed adolescents with and without suicidal behavior. *J. Am. Acad. Child Adolesc. Psychiatry* 50, 602.e–611.e. doi: 10.1016/j.jaac.2011.03.018

Rihmer, Z. (2007). Suicide risk in mood disorders. *Curr. Opin. psychiatry* 20, 17–22. doi: 10.1097/YCO.0b013e3280106868

Rogers, M. A., Kasai, K., Koji, M., Fukuda, R., Iwanami, A., Nakagome, K., et al. (2004). Executive and prefrontal dysfunction in unipolar depression: a review of neuropsychological and imaging evidence. *Neurosci. Res.* 50, 1–11. doi: 10.1016/j.neures.2004.05.003

Rush, A. J., and Beck, A. T. (1978). Cognitive therapy of depression and suicide. *Am. J. Psychother.* 32, 201–219. doi: 10.1176/appi.psychotherapy.1978.32.2.201

Saraceno, B. (2002). The WHO World Health Report 2001 on mental health. *Epidemiol. Psichiatr. Soc.* 11, 83–87. doi: 10.1017/s1121189x00005546

Schmaal, L., van Harmelen, A. L., Chatzi, V., Lippard, E., Toenders, Y. J., Averill, L. A., et al. (2020). Imaging suicidal thoughts and behaviors: a comprehensive review of 2 decades of neuroimaging studies. *Mol. Psychiatry* 25, 408–427. doi: 10.1038/s41380-019-0587-x

Shen, Z., Jiang, L., Yang, S., Ye, J., Dai, N., Liu, X., et al. (2017). Identify changes of brain regional homogeneity in early and later adult onset patients with first-episode depression using resting-state fMRI. *PLoS One* 12:e0184712. doi: 10.1371/journal.pone.0184712

Wagner, G., Koch, K., Schachtzabel, C., Schultz, C. C., Sauer, H., and Schlösser, R. G. (2011). Structural brain alterations in patients with major depressive disorder and high risk for suicide: evidence for a distinct neurobiological entity. *Neuroimage* 54, 1607–1614. doi: 10.1016/j.neuroimage.2010.08.082

Wei, S., Chang, M., Zhang, R., Jiang, X., Wang, F., and Tang, Y. (2018). Amygdala functional connectivity in female patients with major depressive disorder with and without suicidal ideation. *Ann. Gen. Psychiatry* 17, 37. doi: 10.1186/s12991-018-0208-0

Westheide, J., Quednow, B. B., Kuhn, K. U., Hoppe, C., Cooper-Mahkorn, D., Hawellek, B., et al. (2008). Executive performance of depressed suicide attempters: the role of suicidal ideation. *Eur. Arch. Psychiatry Clin. Neurosci.* 258, 414–421. doi: 10.1007/s00406-008-0811-1

Xia, M., Si, T., Sun, X., Ma, Q., Liu, B., Wang, L., et al. (2019). Reproducibility of functional brain alterations in major depressive disorder: evidence from a multisite resting-state functional MRI study with 1,434 individuals. *Neuroimage* 189, 700–714. doi: 10.1016/j.neuroimage.2019.01.074

Zalsman, G., Hawton, K., Wasserman, D., van Heeringen, K., Arensman, E., Sarchiapone, M., et al. (2016). Suicide prevention strategies revisited: 10–year systematic review. *Lancet Psychiatry* 3, 646–659. doi: 10.1016/S2215-0366(16)30030-X

Zang, Y., Jiang, T., Lu, Y., He, Y., and Tian, L. (2004). Regional homogeneity approach to fMRI data analysis. *Neuroimage* 22, 394–400. doi: 10.1016/j.neuroimage.2003.12.030

Zhang, B., Qi, S., Liu, S., Liu, X., Wei, X., and Ming, D. (2021). Altered spontaneous neural activity in the precuneus, middle and superior frontal gyri, and hippocampus in college students with subclinical depression. *BMC Psychiatry* 21:280. doi: 10.1186/s12888-021-03292-1

Zhang, S., Chen, J. M., Kuang, L., Cao, J., Zhang, H., Ai, M., et al. (2016). Association between abnormal default mode network activity and suicidality in depressed adolescents. *BMC Psychiatry* 16:337.

Zhu, C. Z., Zang, Y. F., Liang, M., Tian, L. X., He, Y., Li, X. B., et al. (2005). Discriminative analysis of brain function at resting-state for attention-deficit/hyperactivity disorder. *Med. Image Comput. Comput. Assist. Interv.* 8, 468–475. doi: 10.1007/11566489_58

Conflict of Interest: The authors declare that the research was conducted in the absence of any commercial or financial relationships that could be construed as a potential conflict of interest.

Publisher's Note: All claims expressed in this article are solely those of the authors and do not necessarily represent those of their affiliated organizations, or those of the publisher, the editors and the reviewers. Any product that may be evaluated in this article, or claim that may be made by its manufacturer, is not guaranteed or endorsed by the publisher.

frontiers | Frontiers in Neuroscience

CLINICAL TRIAL
published: 26 April 2022
doi: 10.3389/fnins.2022.851111

Functional Connectivity Features of Resting-State Functional Magnetic Resonance Imaging May Distinguish Migraine From Tension-Type Headache

Yajuan Wang[1], Yingshuang Wang[1], Lihong Bu[2], Shaoyang Wang[3], Xinhui Xie[4], Fuchun Lin[5†] and Zheman Xiao[1*†]*

[1] Department of Neurology, Renmin Hospital of Wuhan University, Wuhan, China, [2] Positron Emission Tomography-Computer Tomography (PET-CT)/Magnetic Resonance Imaging (MRI) Center, Renmin Hospital of Wuhan University, Wuhan, China, [3] Department of Emergency, People's Hospital of Rizhao, Rizhao, China, [4] Department of Psychiatry, Renmin Hospital of Wuhan University, Wuhan, China, [5] State Key Laboratory of Magnetic Resonance and Atomic and Molecular Physics, National Center for Magnetic Resonance in Wuhan, Wuhan Institute of Physics and Mathematics, Innovation Academy for Precision Measurement Science and Technology, Chinese Academy of Sciences, Wuhan, China

OPEN ACCESS

Edited by:
Yuqi Cheng,
The First Affiliated Hospital of Kunming Medical University, China

Reviewed by:
Weidan Pu,
Central South University, China
Jianping Wu,
Virginia Tech, United States

***Correspondence:**
Fuchun Lin.
fclin@wipm.ac.cn
Zheman Xiao
zmxiao@whu.edu.cn

† These authors have contributed equally to this work and share last authorship

Specialty section:
This article was submitted to Brain Imaging Methods, a section of the journal Frontiers in Neuroscience

Received: *09 January 2022*
Accepted: *14 March 2022*
Published: *26 April 2022*

Citation:
Wang Y, Wang Y, Bu L, Wang S, Xie X, Lin F and Xiao Z (2022) Functional Connectivity Features of Resting-State Functional Magnetic Resonance Imaging May Distinguish Migraine From Tension-Type Headache. Front. Neurosci. 16:851111. doi: 10.3389/fnins.2022.851111

Background: Migraineurs often exhibited abnormalities in cognition, emotion, and resting-state functional connectivity (rsFC), whereas patients with tension-type headache (TTH) rarely exhibited these abnormalities. The aim of this study is to explore whether rsFC alterations in brain regions related to cognition and emotion could be used to distinguish patients with migraine from patients with TTH.

Methods: In this study, Montreal Cognitive Assessment (MoCA), Self-Rating Anxiety Scale (SAS), Self-Rating Depression Scale (SDS), and rsFC analyses were used to assess the cognition, anxiety, and depression of 24 healthy controls (HCs), 24 migraineurs, and 24 patients with TTH. Due to their important roles in neuropsychological functions, the bilateral amygdala and hippocampus were chosen as seed regions for rsFC analyses. We further assessed the accuracy of the potential rsFC alterations for distinguishing migraineurs from non-migraineurs (including HCs and patients with TTH) by the receiver operating characteristic (ROC) analysis. Associations between headache characteristics and rsFC features were calculated using a multi-linear regression model. This clinical trial protocol has been registered in the Chinese Clinical Trial Registry (registry number: ChiCTR1900024307, Registered: 5 July 2019-Retrospectively registered, http://www.chictr.org.cn/showproj.aspx?proj=40817).

Results: Migraineurs showed lower MoCA scores (p = 0.010) and higher SAS scores (p = 0.017) than HCs. Migraineurs also showed decreased rsFC in the bilateral calcarine/cuneus, lingual gyrus (seed: left amygdala), and bilateral calcarine/cuneus (seed: left hippocampus) in comparison to HCs and patients with TTH. These rsFC features demonstrated significant distinguishing capabilities and got a sensitivity of 82.6% and specificity of 81.8% with an area under the curve (AUC) of 0.868. rsFC

alterations showed a significant correlation with headache frequency in migraineurs ($p = 0.001$, $Pc = 0.020$).

Conclusion: The rsFC of amygdala and hippocampus with occipital lobe can be used to distinguish patients with migraine from patients with TTH.

Clinical Trial Registration: [http://www.chictr.org.cn/showproj.aspx?proj=40817], identifier [ChiCTR1900024307].

Keywords: migraine, tension-type headache, cognition, emotion, functional connectivity, resting state functional magnetic resonance image

INTRODUCTION

Migraine is the second most common primary headache disorder after tension-type headache (TTH) (Stovner et al., 2007), and the second leading cause of disability worldwide (Feigin et al., 2019). Migraine and TTH exhibit many similarities in clinical practice (Vargas, 2008). Approximately 37% of patients who were initially diagnosed with TTH developed migraine-like attacks in the late stage (Lipton et al., 2002). Because functional impairments, such as neuropsychological dysfunction and neuroimaging abnormalities, caused by migraine are more serious than those caused by TTH, it is urgent to distinguish patients with migraine from patients with TTH.

Migraineurs often exhibited abnormalities in cognition, psychological function, and resting-state functional connectivity (rsFC), whereas patients with TTH rarely exhibited these functional impairments (Vuralli et al., 2018; Skorobogatykh et al., 2019). The interaction between neuropsychological performance and neuroimaging features may be one of the potential characteristics to distinguish patients with migraine from patients with TTH. The amygdala and hippocampus are the key brain regions related to cognition and emotion (Montagne et al., 2019; de Carvalho et al., 2021; Dogra et al., 2021; Duan et al., 2021; Mateus-Pinheiro et al., 2021; Nguyen et al., 2021). The alterations in rsFC of the two brain regions have been reported in migraineurs when compared to healthy controls (HCs) (Hadjikhani et al., 2013; Zhu et al., 2021). However, there is a lack of studies to directly compare functional brain connectivity between migraine and TTH. As a result, it remains unknown whether these abovementioned rsFC alterations are specific to migraine or just a general marker of recurrent episodes of headache. To clarify this issue, we have performed the current study.

In this study, we conducted neuropsychological tests and seed-based rsFC analyses on age-, sex- and educational years-matched HCs, migraineurs, and patients with TTH. The bilateral amygdala and hippocampus were chosen as seed regions because of their important roles in cognition and emotion. We further assessed the accuracy of the potential rsFC alterations for distinguishing migraineurs from non-migraineurs (including HCs and patients with TTH) by the receiver operating characteristic (ROC) analysis. Moreover, we examined their associations with headache characteristics in migraine and TTH groups. The aim of this study is to explore whether the rsFC alterations with brain regions (amygdala and hippocampus) related to cognition and emotion can be used to distinguish patients with migraine from patients with TTH.

Abbreviations: ANCOVA, analysis of covariance; ANOVA, analysis of variance; AUC, area under the curve; FD, framewise displacement; FDR, false discovery rate; fMRI, functional MRI; ICHD-3, international classification of headache disorders, 3th Edition; MNI, Montreal Neurological Institute; MoCA, Montreal Cognitive Assessment; MRI, magnetic resonance imaging; ROC, receiver operating characteristic; rsFC, resting-state functional connectivity; SAS, self-rating anxiety scale; SDS, self-rating depression scale; TTH, tension-type headache; VBM, voxel-based morphometry.

MATERIALS AND METHODS

Participants

All participants were recruited from the Renmin Hospital of Wuhan University from July 2018 to December 2019. A total of 24 HCs, 24 patients with migraine, and 24 patients with TTH were included in this study. The age, gender ratio, and years of education were matched across the three groups. Patients with migraine and patients with TTH were diagnosed by two neurologists according to the International Classification of Headache Disorders, 3th Edition (ICHD-3) (Olesen et al., 2018). Patients were included if they: (1) were between 18 and 60 years old and had more than 6 years of education, (2) experienced headache at least once a month in the last 3 months, and (3) had a history of migraine or TTH for at least 6 months. Patients were excluded if they: (1) had contraindications for magnetic resonance imaging (MRI), (2) had any other diseases in addition to migraine or TTH, (3) had a history of alcohol or drug abuse, and (4) were pregnant or lactating. HCs had no known diseases. The exclusion criteria for HCs were the same as those for patients. To minimize the effects of an impending headache or a prior headache, all patients were headache-free for at least 72 h at the time of the MRI scan. Our clinical trial protocol has been registered in the Chinese Clinical Trial Registry(registry number: ChiCTR1900024307).[1]

Assessment of Cognition, Anxiety, and Depression

The cognitive function of participants was assessed using the Montreal Cognitive Assessment (MoCA), which evaluated six cognitive domains with a total score of 30, including

[1]http://www.chictr.org.cn

visuospatial/executive functions, naming, attention, language, abstraction, delay recall, and orientation. A MoCA score ≥26 indicates normal cognition. Participants' anxiety and depression states were assessed using the Self-Rating Anxiety Scale (SAS) and Self-Rating Depression Scale (SDS), respectively. The higher the scores of SAS and SDS, the more serious the symptoms of anxiety and depression.

Magnetic Resonance Imaging Acquisition

Resting-state functional MRI (fMRI) scans were acquired on a General Electric (Signa HDxt) 3.0T scanner, which had a standard 8-channel head coil and used echo-planar imaging with the following parameters: repetition time = 2,000 ms; echo time = 30 ms; flip angle = 90°; acquisition matrix = 64 × 64; field of view = 220 mm × 220 mm; and slice thickness = 4 mm with a 0.6-mm gap. Each volume consisted of 31 axial slices, and each run contained 240 volumes. During fMRI scanning, all subjects were instructed to close their eyes and rest, and not to think about anything or fall asleep.

Image Pre-processing

Image pre-processing was performed using the DPARSF software.[2] The first 10 volumes were discarded to avoid signal instability. Slice-timing and head-motion correction were conducted on the remaining 230 volumes. We used the Friston 24 parameter model to eliminate the effects of head motion (Friston et al., 1996). Any participants with head motion greater than 2.5 mm or 2.5° in any direction were excluded from this study. As a result, one HC, one migraineur, and two patients with TTH were discarded, and a total of 23 HCs, 23 migraineurs, and 22 patients with TTH were ultimately included for further analyses. We compared framewise displacement (FD) among the HC, migraine, and TTH groups to avoid the effect of microscopic head motions. The mean FD scores did not differ among the three groups ($p > 0.05$) and were used as a covariate for intergroup comparisons. Then, the realigned images were normalized to the Montreal Neurological Institute (MNI) space, resampled to a 3-mm isotropic voxel, and smoothened with a 4-mm full width at half maximum isotropic Gaussian kernel. After these steps, the processed data were detrended, and the white matter and cerebrospinal fluid signals were removed by a regression analysis. Finally, temporal bandpass filtering (0.01–0.1 Hz) was applied to reduce the effects of low-frequency drift and high-frequency noise.

[2]http://rfmri.org/DPARSF

Seed-Based Resting-State Functional Connectivity Analyses

Previous studies have shown that migraineurs exhibited alterations in the rsFC of amygdala and hippocampus (Hadjikhani et al., 2013; Zhu et al., 2021), and the two brain regions were associated with cognition and emotion (Montagne et al., 2019; de Carvalho et al., 2021; Dogra et al., 2021; Duan et al., 2021; Mateus-Pinheiro et al., 2021; Nguyen et al., 2021). Considering the differences in neuropsychological performance between migraine and TTH (Waldie et al., 2002; Gil-Gouveia et al., 2015, 2016; Huang et al., 2017; Puledda et al., 2017; Karsan and Goadsby, 2018; Vuralli et al., 2018), we chose the bilateral amygdala and hippocampus as seed regions for rsFC analyses, to explore the potential rsFC features that may distinguish the two types of headache. The average time series were calculated for each seed in each subject. Then, the Pearson correlation coefficient was calculated between the average time course of the seed and that of each voxel of the whole brain. A Fisher's z-transformation was applied to improve the normality of the

TABLE 1 | Demographic, psychometric, and headache characteristics of all participants.

	HC (n = 24)	Migraine (n = 24)	TTH (n = 24)	$F/\chi^2/t$	P-value	η^2/Cohen's φ /Cohen's d
Age (years)	33.29 ± 9.34	30.75 ± 6.89	36.21 ± 9.23	2.442[a]	0.095[a]	0.066[a]
Female (%)	14 (58%)	18 (75%)	17 (71%)	1.661[b]	0.436[b]	0.263[b]
Educational level (years)	15.08 ± 2.19	14.29 ± 3.03	13.33 ± 2.37	2.825[a]	0.066[a]	0.076[a]
MoCA	28.73 ± 2.00	25.94 ± 1.95	26.33 ± 3.06	5.180[a]	**0.010[a]***	0.131[a]
SAS	25.60 ± 4.48	35.16 ± 9.81	31.50 ± 8.49	4.210[a]	**0.022[a]***	0.109[a]
SDS	27.60 ± 6.95	32.53 ± 9.49	29.08 ± 8.59	1.225[a]	0.305[a]	0.034[a]
Disease duration (years)	NA	6.80 ± 4.28	5.00 ± 5.15	1.288[c]	0.205[c]	0.380[c]
Headache frequency (n/month)	NA	2.25 ± 1.85	7.75 ± 10.20	−2.597[c]	**0.016[c]***	−0.750[c]
Single-attack duration (hours)	NA	17.39 ± 17.52	8.52 ± 9.33	2.104[c]	**0.043[c]***	0.632[c]
Headache intensity (0–10)	NA	7.23 ± 1.53	4.96 ± 1.32	5.154[c]	**<0.001[c]***	1.589[c]

Categorical variables are reported as numbers and percentages; continuous variables are reported as means ± standard deviations (SDs). Demographic and clinical characteristics were analyzed for all study subjects (n = 72), although only 68 subjects were ultimately subjected to resting-state functional connectivity (rsFC) analysis due to the exclusion of one HC, one migraine patient, and two TTH patients after head-motion control.

[a]F-values, [a]p-values, and [a]η^2 for the age, educational level, and neuropsychological scores in the three groups were obtained using one-way ANOVA.

[b]χ^2-values, [b]p-values, and [b]cohen's φ for the gender distribution in the three groups were obtained using chi-squared analysis.

[c]T-values, [c]p-values, and [c]cohen's d for the headache characteristics in migraine and TTH groups were obtained using Welch's two-sample t-test.

**p-value < 0.05.*

HC, healthy control; TTH, tension-type headache; MoCA, Montreal Cognitive Assessment; SAS, self-rating anxiety scale; SDS, self-rating depression scale; ANOVA, analysis of variance.

correlation coefficient (Wang et al., 2006). Finally, the rsFC maps of each seed were obtained for each subject.

Statistical Analysis

We used the R software (R version 3.6.1) for statistical analysis. Potential differences in demographic and psychometric among the HC, migraine, and TTH groups were evaluated using one-way analysis of variance (ANOVA) and *post-hoc* analysis for continuous variables, and chi-squared tests for categorical variables. Potential differences in headache characteristics between migraine and TTH groups were evaluated using Welch's two-sample *t*-test. The value of $p < 0.05$ was considered as statistically significant.

A whole-brain voxel-wise analysis of intergroup differences in the rsFC for each seed was performed using one-way analysis of covariance (ANCOVA), with age, gender, years of education, and mean FD as covariates. Statistical differences were set at a threshold of false discovery rate (FDR) corrected $p < 0.05$ at the voxel level. *Post-hoc* multiple comparisons were performed on the clusters that showed significant differences in one-way ANCOVA using Tukey's test, to test pair-wise differences between the groups (HC vs. migraine, HC vs. TTH, and migraine vs. TTH). The accuracy of the potential rsFC alterations for distinguishing migraineurs from non-migraineurs (including HCs and patients with TTH) was assessed using the ROC analysis. The optimal cut-off for classifying migraineurs vs. non-migraineurs based on these rsFC alterations was calculated using Youden's index (J = sensitivity + specificity–1). The optimal cut-off was determined as the point with the maximum index value.

Additionally, the multiple linear regression model was performed to examine the associations between headache characteristics and the altered rsFC. In the model, the averaged rsFC strengths in the significant regions were used as dependent variables, and headache characteristics (disease duration, headache frequency, single-attack duration, and headache intensity) were used as independent variables, with age, gender, and years of education as covariates. A threshold of $\alpha = 0.05$ was applied to consider regression weights significant, and the Bonferroni correction was used for multiple comparisons.

RESULTS

Basic Characteristics and Intergroup Comparisons

The demographic, psychometric, and headache characteristics of our study population ($n = 72$, including 24 HCs, 24 migraines, and 24 TTH) are summarized in **Table 1**. Notably, demographic and clinical characteristics were analyzed for all study subjects ($n = 72$) although only 68 subjects were ultimately used for the rsFC analysis due to the exclusion of one HC, one migraine patient, and two patients with TTH after head-motion control. The study population had a female proportion of 68%, an age range from 18 to 54 years old at baseline (mean ± SD: 33.4 ± 8.7) and education of 14.2 ± 2.6 years. The difference in age, gender ratio, and educational years among the three groups did not reach statistical significance ($p > 0.05$; **Table 1**). Cognitive performances (i.e., MoCA) significantly differed among the three groups ($p = 0.010$; **Table 1**) with lower scores on MoCA in migraine than HC ($p = 0.010$; **Figure 1A**), where lower scores represent a worse cognitive function. The affected cognitive domains in migraineurs were visuospatial/executive functions ($p = 0.045$; **Figure 1D**) and attention ($p = 0.046$; **Figure 1D**) in comparison with HCs. Participants' anxiety states (i.e., SAS) significantly differed among the three groups ($p = 0.022$; **Table 1**) with higher scores on SAS in migraine than HC ($p = 0.017$; **Figure 1B**), where higher scores represent more severe anxiety symptom. The difference in participants' depression states (i.e., SDS) among the three groups did not reach statistical significance ($p > 0.05$; **Table 1**, **Figure 1C**). There were no significant differences in MoCA, SAS, and SDS between TTH and HCs. Headache characteristics of migraine and TTH were assessed in terms of disease duration, headache frequency, single-attack duration, and headache intensity. Migraineurs exhibited less frequent episodes ($p = 0.016$; **Table 1**), a longer single-attack duration ($p = 0.043$; **Table 1**), and a higher headache intensity ($p < 0.001$; **Table 1**) in comparison with TTH. There were no significant differences in the disease duration between migraine and TTH groups.

Seed-Based Resting-State Functional Connectivity

A significant result from one-way ANCOVA for the seed-based rsFC among HC, migraine, and TTH groups is shown in **Table 2**. Using the left amygdala as a seed, there were significant differences in rsFC with the bilateral calcarine/cuneus and bilateral lingual gyrus. For the left hippocampus, there were significant differences in rsFC with the bilateral calcarine/cuneus. No significant differences in rsFC were observed using the right amygdala or the right hippocampus as seeds.

Post-hoc *t*-tests were then performed on the clusters that showed significant differences in one-way ANCOVA, to test pair-wise differences between the groups (HC vs. migraine, HC vs. TTH, and migraine vs. TTH). Using the left amygdala as a seed, migraineurs showed decreased rsFC with the bilateral calcarine/cuneus (compared to HC: $p < 0.001$; compared to TTH: $p < 0.001$; **Figures 2A,B**), left lingual gyrus (compared to HC: $p = 0.003$; compared to TTH: $p < 0.001$; **Figures 2C,D**) and right lingual gyrus (compared to HC: $p < 0.001$; compared to TTH: $p < 0.001$; **Figures 2E,F**). Using the left hippocampus as a seed, patients with migraine showed decreased rsFC with the left calcarine/cuneus (compared to HC: $p < 0.001$; compared to TTH: $p = 0.003$; **Figures 3A,B**) and right calcarine/cuneus (compared to HC: $p < 0.001$; compared to TTH: $p = 0.003$; **Figures 3C,D**). There were no significant differences in rsFC between HCs and patients with TTH.

Classification of Migraineurs and Non-migraineurs Based on the Altered Resting-State Functional Connectivity

The accuracy of these rsFC alterations in discriminating migraineurs from non-migraineurs including (HCs and patients

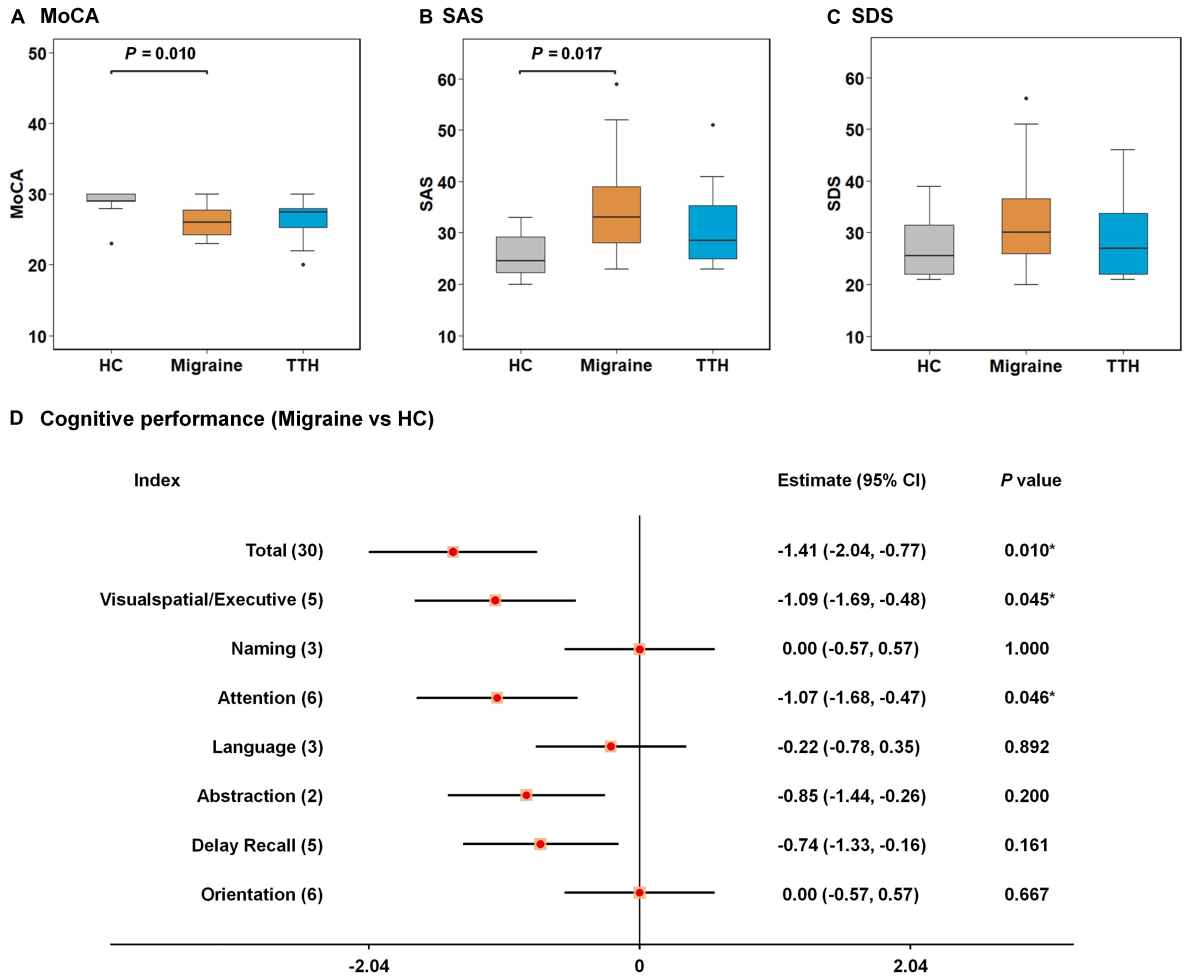

FIGURE 1 | Intergroup differences in neuropsychological tests among healthy control (HC), migraine, and TTH groups. Migraineurs showed lower scores on MoCA **(A)** and higher scores on SAS **(B)** than HCs; no significant differences in SDS were observed among the three groups **(C)**; the affected cognitive domains in migraineurs were visuospatial/executive functions and attention in comparison with HCs **(D)**. The intergroup differences were tested using one-way ANOVA and *post-hoc* analysis. Significant *p*-values for each pair of intergroup comparisons were depicted at the top of each figure **(A–C)**; differences in cognitive performances between migraineurs and HCs were assessed by Welch's two-sample *t*-test, and were demonstrated by 95% CI and *p*-values. **p*-value < 0.05 **(D)**. TTH, tension-type headache; MoCA, Montreal Cognitive Assessment; SAS, self-rating anxiety Scale; SDS, self-rating depression scale; ANOVA, analysis of variance; CI, confidence interval.

TABLE 2 | Brain regions showing significant differences in rsFC among the HC, migraine and TTH groups.

Seed	Regions of differences	Peak coordinates (MNI)			Cluster size (voxels)	Peak *F*	η^2
		X	Y	Z			
Amy_L	Bilateral calcarine/cuneus	−3	−72	18	568	18.87	0.354
	Left lingual gyrus	−21	−66	−18	75	11.74	0.254
	Right lingual gyrus	15	−69	−18	37	11.03	0.242
Hip_L	Left calcarine/cuneus	−15	−60	15	148	17.02	0.330
	Right calcarine/cuneus	12	−63	15	39	11.67	0.253

The intergroup differences among the three groups were tested using one-way ANCOVA with age, gender, educational years, and mean FD values as covariates. A threshold of $p < 0.05$ (FDR corrected) at voxel level was considered statistically different.
Amy_L, left amygdala; Hip_L, left hippocampus; MNI, Montreal Neurological Institute; HC, healthy control; TTH, tension-type headache; ANCOVA, analysis of covariance; FD, framewise displacement; FDR, false discovery rate.

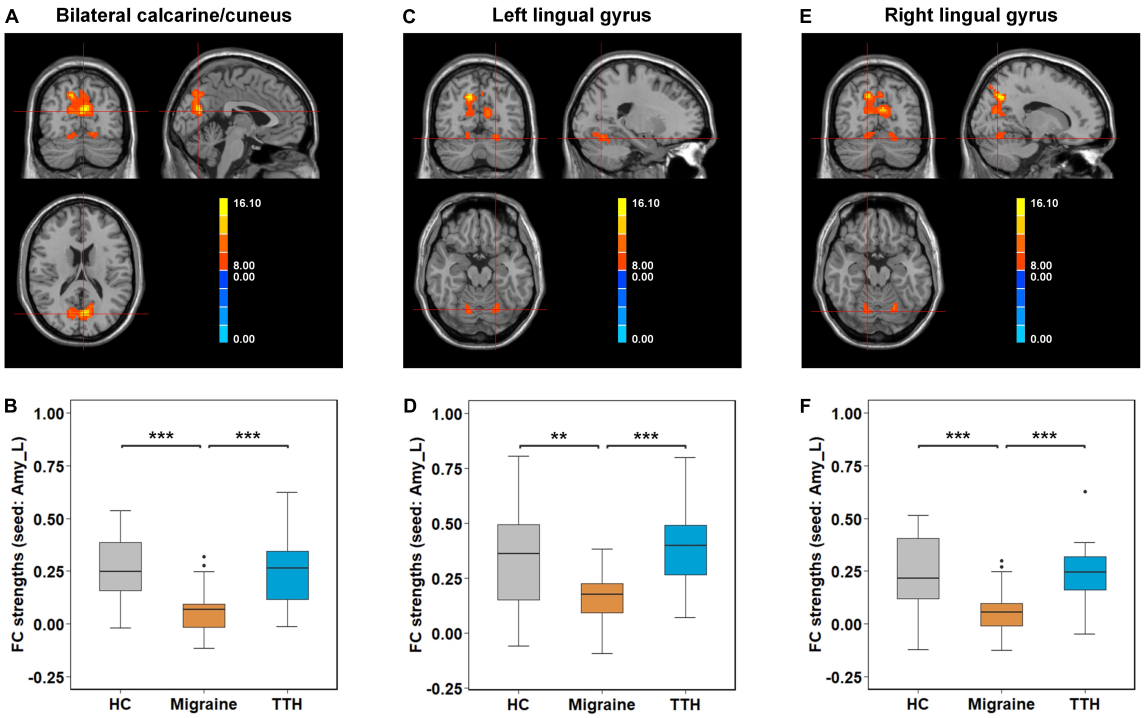

FIGURE 2 | Intergroup differences in rsFC strengths (seed: left amygdala). Migraineurs showed decreased rsFC of left amygdala with bilateral calcarine/cuneus (–3,–72, 18) **(A,B)**, left lingual gyrus (–21,–66,–18) **(C,D)**, and right lingual gyrus (15,–69,–18) **(E,F)** in comparison with HCs and patients with TTH. The pair-wise differences in the significant clusters observed in one-way ANCOVA (**Table 2**) were tested using *post-hoc t*-tests. **p*-value < 0.05; ***p*-value < 0.01; ****p*-value < 0.001. rsFC, resting-state functional connectivity; Amy_L, left amygdala; HC, healthy control; TTH, tension-type headache; ANCOVA, analysis of covariance.

with TTH) was assessed by the ROC analysis. Based on the rsFC between the left amygdala and bilateral calcarine/cuneus, the area under the curve (AUC), optimal cut-off, sensitivity, and specificity of discriminating migraineurs from HCs (**Figure 4A**) and of discriminating migraineurs from patients with TTH (**Figure 4D**) were 0.839, 0.111, 82.6%, and 82.6% and 0.822, 0.096, 78.3%, and 81.8%, respectively. Based on the rsFC between the left amygdala and left lingual gyrus, the AUC, optimal cut-off, sensitivity, and specificity of discriminating migraineurs from HCs (**Figure 4B**) and for discriminating migraineurs from patients with TTH (**Figure 4E**) were 0.732, 0.261, 87%, and 60.9% and 0.868, 0.242, 82.6%, and 81.8%, respectively. Based on the rsFC between the left amygdala and right lingual gyrus, the AUC, optimal cut-off, sensitivity, and specificity of discriminating migraineurs from HCs (**Figure 4C**) and of discriminating migraineurs from patients with TTH (**Figure 4F**) were 0.828, 0.121, 82.6%, and 73.9% and 0.830, 0.114, 78.3%, and 86.4%, respectively.

Based on the rsFC between the left hippocampus and left calcarine/cuneus, the AUC, optimal cut-off, sensitivity, and specificity were 0.830, 0.124, 69.6%, and 82.6% for discriminating migraineurs from HCs (**Figure 5A**), and 0.779, 0.100, 65.2%, and 86.4% for discriminating migraineurs from patients with TTH (**Figure 5C**). Based on the rsFC between the left hippocampus and right calcarine/cuneus, the AUC, optimal cut-off, sensitivity, and specificity were 0.854, 0.269, 95.7%, and 60.9% for discriminating migraineurs from HCs (**Figure 5B**), and 0.783, 0.216, 82.6%, and 63.6% for discriminating migraineurs from patients with TTH (**Figure 5D**).

Associations Between Headache Characteristics and the Altered Resting-State Functional Connectivity

Next, we examined associations between headache characteristics (including disease duration, headache frequency, single-attack duration, and headache intensity) and the altered rsFC in migraine and TTH groups. In the migraine group, the rsFC strength of the left amygdala with the bilateral calcarine/cuneus was associated with headache frequency (p = 0.029); the rsFC strength of the left amygdala with the left lingual gyrus was associated with disease duration (p = 0.030), headache frequency (p = 0.001, Pc = 0.020, **Figure 6**), single-attack duration (p = 0.012), and headache intensity (p = 0.011); the rsFC strength of the left amygdala with the right lingual gyrus was associated with headache frequency (p = 0.049). However, in the migraine group, only the association of headache frequency with rsFC within the left amygdala and left lingual gyrus survived the Bonferroni correction (**Figure 6**). In the TTH group, there were no significant associations between headache characteristics and rsFC strengths. Using the left hippocampus as a seed, there were no significant associations between headache characteristics

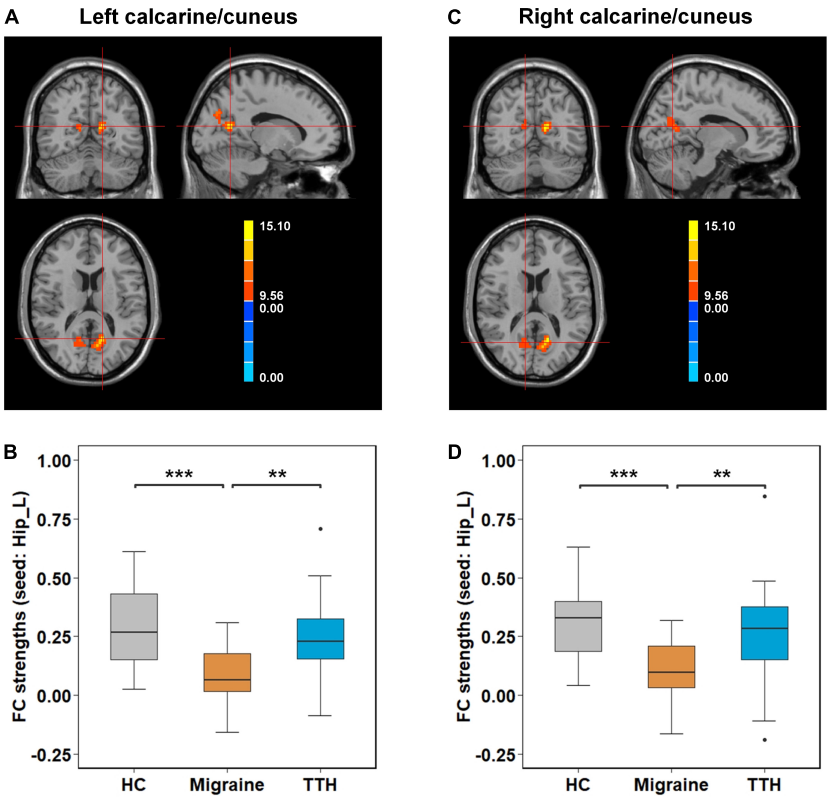

FIGURE 3 | Intergroup differences in rsFC strengths (seed: left hippocampus). Migraineurs showed decreased rsFC of left hippocampus with left calcarine/cuneus (–15,–60, 15) **(A,B)** and right calcarine/cuneus (12,–63, 15) **(C,D)** in comparison with HCs and patients with TTH. The pair-wise differences in the significant clusters observed in one-way ANCOVA (**Table 2**) were tested using *post-hoc t*-tests. **p*-value < 0.05; ***p*-value < 0.01; ****p*-value < 0.001. rsFC, resting-state functional connectivity; Hip_L, left hippocampus; HCs, healthy controls; TTH, tension-type headache; ANCOVA, analysis of covariance.

and rsFC strengths in the migraine or TTH group. Specific β coefficients and *p*-values can be found in Additional File 1.

DISCUSSION

In this study, we found that compared with HCs and patients with TTH, migraineurs exhibited impaired cognition and increased anxiety, which showed lower MoCA scores and higher SAS scores. The rsFC features of amygdala and hippocampus with the occipital lobe, such as the bilateral calcarine/cuneus and lingual gyrus, could significantly distinguish migraineurs from non-migraineurs (including HCs and patients with TTH). Moreover, the rsFC strength of the left amygdala with the left lingual gyrus was associated with headache frequency in migraineurs. These findings suggested that the rsFC features might be applied into clinical practice in the future to distinguish migraineurs from patients with TTH.

Impaired Cognition and Increased Anxiety in Migraineurs

Migraineurs frequently experienced cognitive and psychological dysfunction, such as difficulty in concentration, anxiety, and unhappiness (Gil-Gouveia et al., 2015; Huang et al., 2017; Puledda et al., 2017; Karsan and Goadsby, 2018; Vuralli et al., 2018). Impaired cognitive and psychological functions may distinguish migraineurs from patients with other types of headaches (Vuralli et al., 2018). Although TTH is the most common primary headache disorder, the neuropsychological performance in patients with TTH has not been thoroughly investigated as patients with migraine. Two prospective comparative studies showed that the cognitive and psychological functions of patients with TTH were similar to those of HCs, but different from those from migraineurs (Waldie et al., 2002; Gil-Gouveia et al., 2016). In this study, we found that migraineurs exhibited impaired cognition, which was characterized by the impairment of visuospatial/executive functions and attention, as well as increased anxiety, which were generally consistent with previous studies (Gil-Gouveia et al., 2015; Huang et al., 2017; Puledda et al., 2017; Karsan and Goadsby, 2018; Vuralli et al., 2018). Additionally, the neuropsychological scores (i.e., MoCA, SAS, and SDS) of patients with TTH were intermediate between those of migraineurs and HCs. These findings confirmed that impaired cognition and increased anxiety were more severe in patients with migraine than in patients with TTH. Therefore, we suppose that the brain functional changes with brain regions related to cognition

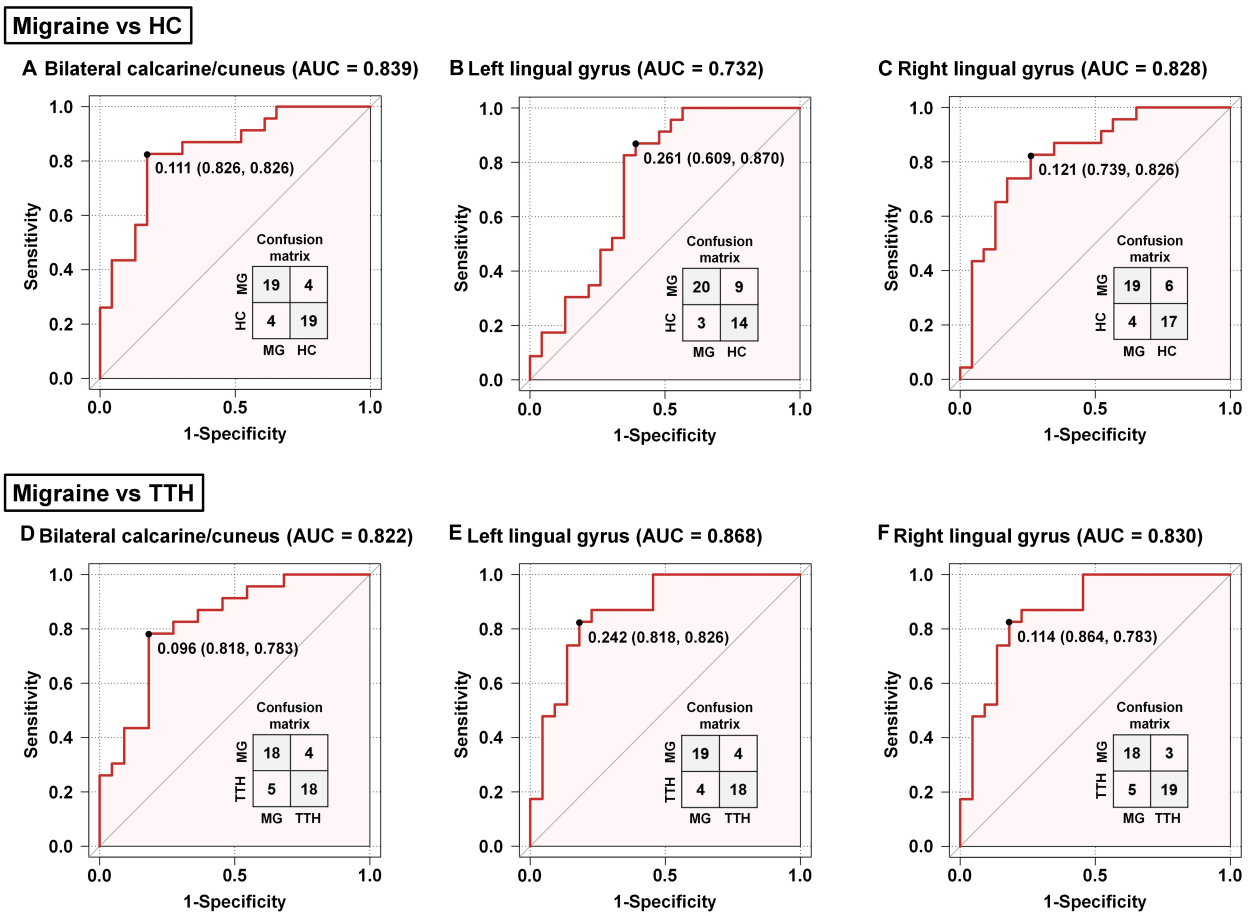

FIGURE 4 | Classification of migraineurs and non-migraineurs based on the rsFC alterations (seed: left amygdala). Classification of migraineurs and HCs **(A–C)**; classification of migraineurs and patients with TTH **(D–F)**. The point on each ROC curve represents the optimal cut-off (specificity and sensitivity). MG, migraine; HC, healthy controls; TTH, tension-type headache; ROC, receiver operating characteristic; AUC, area under the curve.

and emotion may distinguish patients with migraine from patients with TTH.

Resting-State Functional Connectivity Alterations in Migraineurs and Their Discriminative Ability

As a hypothesis-driven fMRI study, the bilateral amygdala and hippocampus, which are known to be associated with cognition and emotion in well-replicated studies (Montagne et al., 2019; de Carvalho et al., 2021; Dogra et al., 2021; Duan et al., 2021; Mateus-Pinheiro et al., 2021; Nguyen et al., 2021), were selected as seed regions for subsequent rsFC analyses. Our results indicated that migraineurs showed decreased rsFC mainly in the occipital lobe, such as the bilateral calcarine/cuneus and lingual gyrus, using the left amygdala and left hippocampus as seeds. Similarly, the rsFC alterations in the occipital lobe have been identified as the most specific imaging markers to distinguish patients with migraine from HCs or patients with other chronic pain disorders, such as chronic low back pain and fibromyalgia, using fMRI-based machine learning approach (Tu et al., 2020) and network mapping technique (Burke et al., 2020). However, previous studies did not include other types of headache. As a result, they did not reveal whether these alterations in rsFC are specific to migraine or a general marker of recurrent episodes of headache. In this study, we found that the altered rsFC of the amygdala and hippocampus with the occipital lobe can be used to distinguish migraineurs from not only the HCs but also patients with TTH. When distinguishing migraineurs from HCs, the rsFC between the left hippocampus and right calcarine/cuneus achieved the highest AUC. When distinguishing migraineurs from patients with TTH, the rsFC between the left amygdala and left lingual gyrus achieved the highest AUC. Notably, previously observed rsFC abnormalities in migraineurs did not exist in patients with TTH, suggesting that these abnormalities may be unique to migraine, not just a general sign of recurrent headache.

When the right amygdala and right hippocampus were selected as seeds, we did not observe any difference in rsFC among the three groups. This may be related to the inherent left lateralization of the brain of migraine patients, which is consistent with previous neuroimaging studies (Maniyar et al., 2014; Gaist et al., 2018; Burke et al., 2020). A positron emission tomography

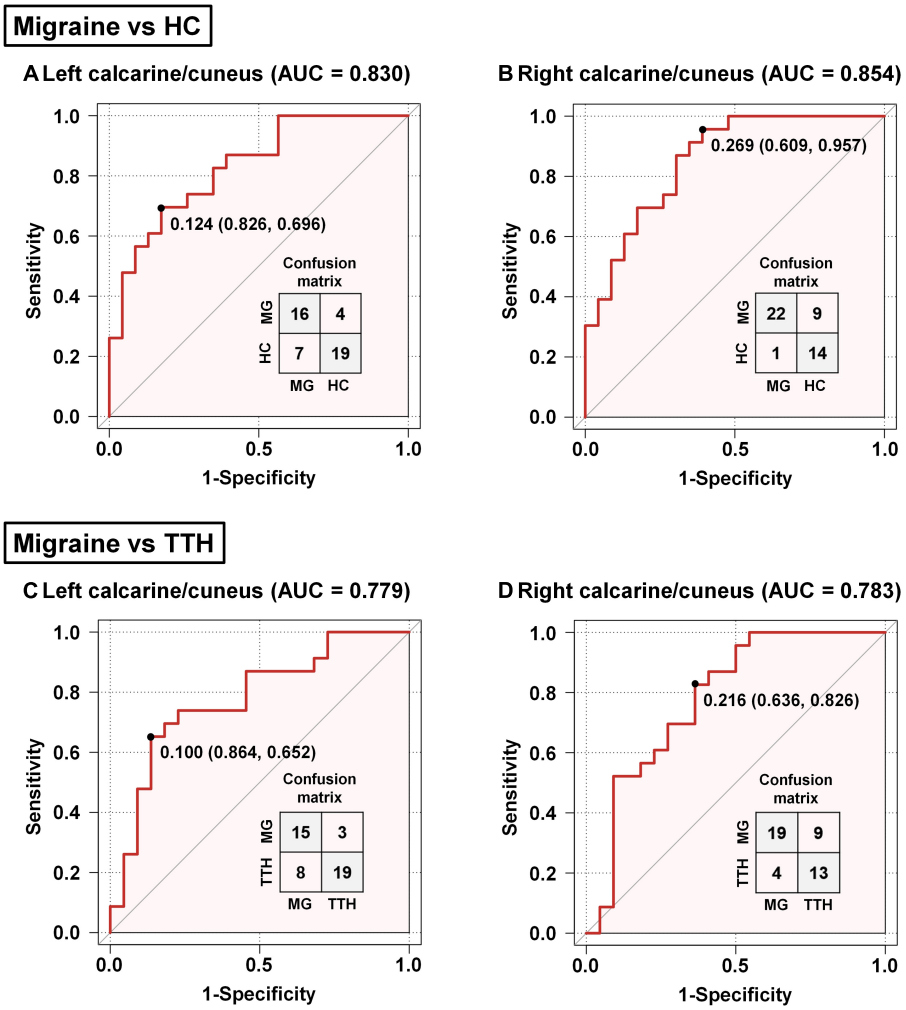

FIGURE 5 | Classification of migraineurs and non-migraineurs based on the rsFC alterations (seed: left hippocampus). Classification of migraineurs and HCs **(A,B)**; classification of migraineurs and patients with TTH **(C,D)**. The point on each ROC curve represents the optimal cut-off (specificity and sensitivity). MG, migraine; HC, healthy controls; TTH, tension-type headache; ROC, receiver operating characteristic; AUC, area under the curve.

(PET) study investigated photic hypersensitivity of migraineurs and reported peak hypermetabolism mainly occurred in the left extrastriate cortex (Maniyar et al., 2014), and a cortical thickness study identified increased left visual cortex thickness of migraine patients (Gaist et al., 2018). Moreover, a recent voxel-based morphometry (VBM) meta-analysis reported that migraine atrophy coordinates were mainly connected to a cluster in the left visual cortex (Burke et al., 2020). Future studies are needed to explore the significance of left lateralization.

A Correlation Analysis Between Headache Characteristics and Resting-State Functional Connectivity Alterations

Further, a correlation analysis showed that the rsFC strength of the left amygdala with the left lingual gyrus was associated with headache frequency in migraineurs. This result supported previous findings that the migraine attack frequency could be predicted by fMRI-based machine learning approaches (Mu et al., 2020; Tu et al., 2020). In clinical practice, the migraine attack frequency is often assessed by self-report, resulting in the measurement of headache frequency to become inaccurate and unreliable (Berger et al., 2018; Haywood et al., 2018). Because attack frequency is a risk factor for migraine progression, objective measurements are needed to accurately estimate migraine progression. Our results and previous finding (Mu et al., 2020; Tu et al., 2020) suggested that neuroimaging markers might be used to predict factors for the estimation of migraine progression.

Limitations

There are several limitations to our study. Firstly, we did not include other primary headache disorders, such as cluster

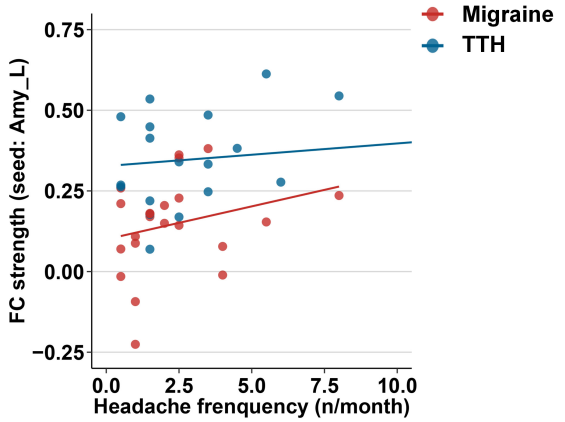

FIGURE 6 | Associations between the rsFC strength of the left amygdala with the left lingual gyrus and headache frequency in migraine (red) and TTH (blue) groups. Only the association in migraine group (red) reached statistical significance after Bonferroni correction. The associations of headache characteristics with rsFC strengths in the significant regions were tested using multiple linear regression model with age, gender, and educational years as covariates. Specific β coefficients and *p*-values can be found in Additional File 1. TTH, tension-type headache.

headache or other trigeminal autonomic cephalalgias. We included patients with TTH in our study because TTH is the most common primary headache disorder and the most common misdiagnosed migraine. We also included patients with other primary headache disorders in the next diagnostic trials. Secondly, we used pre-specified seed points as a hypothesis-driven approach to reduce the "researcher degrees of freedom," but this method might miss some potential rsFC alterations. A combination of hypothesis-driven and data-driven approaches will be more appropriate for future studies with larger sample sizes. Thirdly, we compared changes in rsFC in patients who were not in the current headache episode, but it was not clear whether the changes were persistent during the headache episode. Future studies are needed to explore whether our results were symptom-dependent or trait indicators. Fourthly, our study yielded a relatively high AUC value, implying a good differentiation for migraineurs by using these rsFC changes. Nevertheless, it should be noted that this did not mean that our method can be directly applied to clinical practice. Fifthly, only MoCA, SAS, and SDS were used to assess the cognition, anxiety, and depression of the study population, which would not comprehensively reflect neuropsychological function. More detailed and comprehensive neuropsychological tests are needed in the future. Sixthly, we did not assess whether the participants met the diagnosis of anxiety disorder, potentially allowing the results to be influenced by a comorbid anxiety disorder. Seventhly, the small sample size of our study might reduce the statistical power of the study. A rigorous clinical diagnostic trial with sufficient sample size is needed to further validate our results.

CONCLUSION

Compared with HCs and patients with TTH, migraineurs exhibited impaired cognition, increased anxiety, and significant rsFC alterations. The rsFC features of amygdala and hippocampus with occipital lobe could significantly distinguish migraineurs from non-migraineurs (including HCs and patients with TTH) and the rsFC strength of the left amygdala with the left lingual gyrus was associated with headache frequency in migraineurs. These findings offer the possibility of developing objective criteria to distinguish migraine from TTH.

DATA AVAILABILITY STATEMENT

All data generated or analyzed during this study are included in this article and **Supplementary Material**.

ETHICS STATEMENT

The studies involving human participants were reviewed and approved by the Clinical Research Ethics Committee of Renmin Hospital of Wuhan University. The patients/participants provided their written informed consent to participate in this study.

AUTHOR CONTRIBUTIONS

YaW analyzed the data and drafted the manuscript. YiW and LB collected the data. SW analyzed the data. XX revised the manuscript. FL analyzed the data and revised the manuscript. ZX designed and conceptualized the study. All authors contributed to the article and approved the submitted version.

FUNDING

This work was supported by grants from the National Natural Science Foundation of China (Grant Nos. 81971055, 81471133, and 82101292) and the Frontier Scientific Significant Breakthrough Project of CAS (Grant No. QYZDB-SSW-SLH046).

ACKNOWLEDGMENTS

The imaging data for this study were obtained from the PET-CT/MRI Center, Renmin Hospital of Wuhan University.

SUPPLEMENTARY MATERIAL

The Supplementary Material for this article can be found online at: https://www.frontiersin.org/articles/10.3389/fnins.2022.851111/full#supplementary-material

REFERENCES

Berger, S. E., Vachon-Presseau, É, Abdullah, T. B., Baria, A. T., Schnitzer, T. J., and Apkarian, A. V. (2018). Hippocampal morphology mediates biased memories of chronic pain. *Neuroimage* 166, 86–98. doi: 10.1016/j.neuroimage.2017.10.030

Burke, M. J., Joutsa, J., Cohen, A. L., Soussand, L., Cooke, D., Burstein, R., et al. (2020). Mapping migraine to a common brain network. *Brain* 143, 541–553. doi: 10.1093/brain/awz405

de Carvalho, C. R., Lopes, M. W., Constantino, L. C., Hoeller, A. A., de Melo, H. M., Guarnieri, R., et al. (2021). The ERK phosphorylation levels in the amygdala predict anxiety symptoms in humans and MEK/ERK inhibition dissociates innate and learned defensive behaviors in rats. *Mol. Psychiatry* 26, 7257–7269. doi: 10.1038/s41380-021-01203-0

Dogra, S., Stansley, B. J., Xiang, Z., Qian, W., Gogliotti, R. G., Nicoletti, F., et al. (2021). Activating mGlu(3) Metabotropic Glutamate Receptors Rescues Schizophrenia-like Cognitive Deficits Through Metaplastic Adaptations Within the Hippocampus. *Biol. Psychiatry* 90, 385–398. doi: 10.1016/j.biopsych.2021.02.970

Duan, K., Gu, Q., Petralia, R. S., Wang, Y. X., Panja, D., Liu, X., et al. (2021). Mitophagy in the basolateral amygdala mediates increased anxiety induced by aversive social experience. *Neuron* 109, 3793.e–3809.e. doi: 10.1016/j.neuron.2021.09.008

Feigin, V. L., Nichols, E., Alam, T., Bannick, M. S., Beghi, E., and Blake, N. (2019). Global, regional, and national burden of neurological disorders, 1990-2016: a systematic analysis for the Global Burden of Disease Study 2016. *Lancet Neurol.* 18, 459–480. doi: 10.1016/s1474-4422(18)30499-x

Friston, K. J., Stephan, K. M., Heather, J. D., Frith, C. D., Ioannides, A. A., Liu, L. C., et al. (1996). A multivariate analysis of evoked responses in EEG and MEG data. *Neuroimage* 3, 167–174. doi: 10.1006/nimg.1996.0018

Gaist, D., Hougaard, A., Garde, E., Reislev, N. L., Wiwie, R., Iversen, P., et al. (2018). Migraine with visual aura associated with thicker visual cortex. *Brain* 141, 776–785. doi: 10.1093/brain/awx382

Gil-Gouveia, R., Oliveira, A., and Pavão Martins, I. (2016). Clinical Utility of the Mig-SCog. *Headache* 56, 941–951. doi: 10.1111/head.12806

Gil-Gouveia, R., Oliveira, A. G., and Martins, I. P. (2015). Assessment of cognitive dysfunction during migraine attacks: a systematic review. *J. Neurol.* 262, 654–665. doi: 10.1007/s00415-014-7603-5

Hadjikhani, N., Ward, N., Boshyan, J., Napadow, V., Maeda, Y., Truini, A., et al. (2013). The missing link: enhanced functional connectivity between amygdala and visceroceptive cortex in migraine. *Cephalalgia* 33, 1264–1268. doi: 10.1177/0333102413490344

Haywood, K. L., Mars, T. S., Potter, R., Patel, S., Matharu, M., and Underwood, M. (2018). Assessing the impact of headaches and the outcomes of treatment: a systematic review of patient-reported outcome measures (PROMs). *Cephalalgia* 38, 1374–1386. doi: 10.1177/0333102417731348

Huang, L., Juan Dong, H., Wang, X., Wang, Y., and Xiao, Z. (2017). Duration and frequency of migraines affect cognitive function: evidence from neuropsychological tests and event-related potentials. *J. Headache Pain* 18:54. doi: 10.1186/s10194-017-0758-6

Karsan, N., and Goadsby, P. J. (2018). Biological insights from the premonitory symptoms of migraine. *Nat. Rev. Neurol.* 14, 699–710. doi: 10.1038/s41582-018-0098-4

Lipton, R. B., Cady, R. K., Stewart, W. F., Wilks, K., and Hall, C. (2002). Diagnostic lessons from the spectrum study. *Neurology* 58, S27–S31. doi: 10.1212/wnl.58.9_suppl_6.s27

Maniyar, F. H., Sprenger, T., Schankin, C., and Goadsby, P. J. (2014). Photic hypersensitivity in the premonitory phase of migraine–a positron emission tomography study. *Eur. J. Neurol.* 21, 1178–1183. doi: 10.1111/ene.12451

Mateus-Pinheiro, A., Patrício, P., Alves, N. D., Martins-Macedo, J., Caetano, I., Silveira-Rosa, T., et al. (2021). Hippocampal cytogenesis abrogation impairs inter-regional communication between the hippocampus and prefrontal cortex and promotes the time-dependent manifestation of emotional and cognitive deficits. *Mol. Psychiatry* 26, 7154–7166. doi: 10.1038/s41380-021-01287-8

Montagne, A., Huuskonen, M. T., Rajagopal, G., Sweeney, M. D., Nation, D. A., Sepehrband, F., et al. (2019). Undetectable gadolinium brain retention in individuals with an age-dependent blood-brain barrier breakdown in the hippocampus and mild cognitive impairment. *Alzheimers Dement* 15, 1568–1575. doi: 10.1016/j.jalz.2019.07.012

Mu, J., Chen, T., Quan, S., Wang, C., Zhao, L., and Liu, J. (2020). Neuroimaging features of whole-brain functional connectivity predict attack frequency of migraine. *Hum. Brain Mapp.* 41, 984–993. doi: 10.1002/hbm.24854

Nguyen, C., Mondoloni, S., Le Borgne, T., Centeno, I., Come, M., Jehl, J., et al. (2021). Nicotine inhibits the VTA-to-amygdala dopamine pathway to promote anxiety. *Neuron* 109, 2604–2615.e9. doi: 10.1016/j.neuron.2021.06.013

Olesen, J., Bes, A., Kunkel, R., Lance, J. W., Nappi, G., Pfaffenrath, V., et al. (2018). Headache Classification Committee of the International Headache Society (IHS) The International Classification of Headache Disorders, 3rd edition. *Cephalalgia* 38, 1–211. doi: 10.1177/0333102417738202

Puledda, F., Messina, R., and Goadsby, P. J. (2017). An update on migraine: current understanding and future directions. *J. Neurol.* 264, 2031–2039. doi: 10.1007/s00415-017-8434-y

Skorobogatykh, K., van Hoogstraten, W. S., Degan, D., Prischepa, A., Savitskaya, A., Ileen, B. M., et al. (2019). Functional connectivity studies in migraine: what have we learned? *J. Headache Pain* 20:108. doi: 10.1186/s10194-019-1047-3

Stovner, L., Hagen, K., Jensen, R., Katsarava, Z., Lipton, R., Scher, A., et al. (2007). The global burden of headache: a documentation of headache prevalence and disability worldwide. *Cephalalgia* 27, 193–210. doi: 10.1111/j.1468-2982.2007.01288.x

Tu, Y., Zeng, F., Lan, L., Li, Z., Maleki, N., Liu, B., et al. (2020). An fMRI-based neural marker for migraine without aura. *Neurology* 94, e741–e751. doi: 10.1212/wnl.0000000000008962

Vargas, B. B. (2008). Tension-type headache and migraine: two points on a continuum? *Curr. Pain Headache Rep.* 12, 433–436. doi: 10.1007/s11916-008-0073-7

Vuralli, D., Ayata, C., and Bolay, H. (2018). Cognitive dysfunction and migraine. *J. Headache Pain* 19:109. doi: 10.1186/s10194-018-0933-4

Waldie, K. E., Hausmann, M., Milne, B. J., and Poulton, R. (2002). Migraine and cognitive function: a life-course study. *Neurology* 59, 904–908. doi: 10.1212/wnl.59.6.904

Wang, L., Zang, Y., He, Y., Liang, M., Zhang, X., Tian, L., et al. (2006). Changes in hippocampal connectivity in the early stages of Alzheimer's disease: evidence from resting state fMRI. *Neuroimage* 31, 496–504. doi: 10.1016/j.neuroimage.2005.12.033

Zhu, Y., Dai, L., Zhao, H., Ji, B., Yu, Y., Dai, H., et al. (2021). Alterations in Effective Connectivity of the Hippocampus in Migraine without Aura. *J. Pain Res.* 14, 3333–3343. doi: 10.2147/jpr.s327945

Conflict of Interest: The authors declare that the research was conducted in the absence of any commercial or financial relationships that could be construed as a potential conflict of interest.

frontiers | Frontiers in Neuroscience

ORIGINAL RESEARCH
published: 29 April 2022
doi: 10.3389/fnins.2022.889105

Depression Classification Using Frequent Subgraph Mining Based on Pattern Growth of Frequent Edge in Functional Magnetic Resonance Imaging Uncertain Network

Yao Li[1], Zihao Zhou[2], Qifan Li[1], Tao Li[1], Ibegbu Nnamdi Julian[1], Hao Guo[1] and Junjie Chen[1]**

[1] College of Information and Computer, Taiyuan University of Technology, Taiyuan, China, [2] College of Mathematics, Taiyuan University of Technology, Taiyuan, China

OPEN ACCESS

Edited by:
Wenbin Guo,
Central South University, China

Reviewed by:
Qi Li,
Changchun University of Science and Technology, China
Lingzhong Fan,
Institute of Automation (CAS), China

***Correspondence:**
Hao Guo
feiyu_guo@sina.com
Junjie Chen
chenjj@tyut.edu.cn

Specialty section:
This article was submitted to Brain Imaging Methods, a section of the journal Frontiers in Neuroscience

Received: 03 March 2022
Accepted: 01 April 2022
Published: 29 April 2022

Citation:
Li Y, Zhou Z, Li Q, Li T, Julian IN, Guo H and Chen J (2022) Depression Classification Using Frequent Subgraph Mining Based on Pattern Growth of Frequent Edge in Functional Magnetic Resonance Imaging Uncertain Network. Front. Neurosci. 16:889105. doi: 10.3389/fnins.2022.889105

The brain network structure is highly uncertain due to the noise in imaging signals and evaluation methods. Recent works have shown that uncertain brain networks could capture uncertain information with regards to functional connections. Most of the existing research studies covering uncertain brain networks used graph mining methods for analysis; for example, the mining uncertain subgraph patterns (MUSE) method was used to mine frequent subgraphs and the discriminative feature selection for uncertain graph classification (DUG) method was used to select discriminant subgraphs. However, these methods led to a lack of effective discriminative information; this reduced the classification accuracy for brain diseases. Therefore, considering these problems, we propose an approximate frequent subgraph mining algorithm based on pattern growth of frequent edge (unFEPG) for uncertain brain networks and a novel discriminative feature selection method based on statistical index (dfsSI) to perform graph mining and selection. Results showed that compared with the conventional methods, the unFEPG and dfsSI methods achieved a higher classification accuracy. Furthermore, to demonstrate the efficacy of the proposed method, we used consistent discriminative subgraph patterns based on thresholding and weighting approaches to compare the classification performance of uncertain networks and certain networks in a bidirectional manner. Results showed that classification performance of the uncertain network was superior to that of the certain network within a defined sparsity range. This indicated that if a better classification performance is to be achieved, it is necessary to select a certain brain network with a higher threshold or an uncertain brain network model. Moreover, if the uncertain brain network model was selected, it is necessary to make full use of the uncertain information of its functional connection.

Keywords: frequent subgraph mining, discriminative feature selection, machine learning, classification, fMRI, depression, uncertain brain network

INTRODUCTION

Over recent years, the use of neuroimaging technology to investigate the interaction of brain regions has gained has attracted much attention and recognition (Richardson, 2010). The Blood Oxygen Level-Dependent (BOLD) signal is now routinely used as a neurophysiological indicator for resting-state functional magnetic resonance imaging (rs-fMRI) to detect endogenous or spontaneous activity in the brain neurons. According to BOLD signals, a functional connectivity network can be built and then applied to research the pathological mechanisms underlying brain diseases. This theory has been widely applied to the diagnosis of brain diseases, including schizophrenia (Steardo et al., 2020), depression (Sen et al., 2019), attention deficit syndrome (Riaz et al., 2020), and Alzheimer's disease (Shao et al., 2020).

Recent researchers have stated that uncertainty is inherent in graph data connections and that this is due to problems associated with data acquisition, the accuracy of equipment, and evaluation methods (Yuan et al., 2016; Khan et al., 2018b; de Ridder et al., 2019). These challenges suggest that it is only possible to provide the probability of a link in the graph, rather than precise values. For instance, the acquisition of fMRI data is influenced by a variety of distinct factors, like subject age (Wig, 2017), head movement (Vakamudi et al., 2019), scanning time (Hagler et al., 2019), vasoconstriction (An et al., 2015), heartbeat and respiration (Pinto et al., 2017; Tong et al., 2019), arterial blood pressure (Steiner et al., 2020), and arterial carbon dioxide concentration (Driver et al., 2016; Prokopiou et al., 2018). Moreover, increasing evidence suggests that even in the resting state, the neural activity in the brain still exhibits transient and subtle dynamics (Kudela et al., 2017; Zhao et al., 2020). However, most studies considered that the interaction of brain regions remains unchanged during the resting state, so as to construct a brain functional network. Therefore, they can be concluded that the functional connections between brain regions are highly uncertain if the rs-fMRI data is employed to build the brain network. These functional connections are obtained by considering processing steps, such as the analysis of temporal correlations in spontaneous BOLD signal oscillations, where each edge refers to a probability to calculate the likelihood that the functional connection exists in the brain.

Previous studies have applied traditional brain network analysis based on certain network for the diagnosis of brain diseases (Sporns, 2011, 2018; Farahani et al., 2020; Zhao et al., 2021). This theory claims deciding whether there is an edge between two brain regions; this is resolved using a threshold or a threshold range (Zhou Z. et al., 2020). The employment of binary networks helps to measuring the network properties and diminishing the burden caused by the generation of graphs. However, the employment of the threshold approach to construct a certain network unavoidably results in the loss of uncertain information (Kong et al., 2013; Hamdi et al., 2018; Zhang et al., 2018). Simultaneously, in exiting researches, there is no gold standard for deciding how to choose the optimal threshold for constructing the effective certain network (Garrison et al., 2015).

To settle the issues of threshold selection in traditional network, researchers selected a small range of thresholds to evade sensitivity related to the selection of a threshold (Jie et al., 2014); however, this method may result in incomplete results or even misdirecting results if the network properties are unsteady within a larger threshold range (Graham et al., 2009; Zhang et al., 2018). Based on this problem, some researchers have proposed the minimum spanning tree (MST) method to build brain networks (Jackson and Read, 2010a; Stam et al., 2014). However, the MST may miss the emphasize of low weight connections and clusters in the interaction of the brain regions (Tewarie et al., 2015), in particularly, from loops formed by low weight links (Li et al., 2011). Moreover, MST analysis may be less sensitive to small differences in the signal-to-noise ratio between subjects because the MST was only lied in the rank of the link weights of the strongest network connections (Van Dellen et al., 2018). In addition, although MST analysis is not dependent on the section of the threshold, it is influenced by the network scale. which further effect the classification performance (Van Dellen et al., 2018). In addition, there are other studies that used direct functional connectivity strength as a feature for classification (Zhang et al., 2021). Although this method also effectively avoids the problems caused by threshold selection, it does not construct a brain network and lacks information relating to network topology properties; thus, whether the network is connected or disconnected becomes irrelevant.

Considering above problems, the concept of the uncertain network was introduced to characterize the uncertainty of functional connections (Kong et al., 2013; Cao et al., 2015a,b; Saha et al., 2021). Uncertain networks are based on uncertain graph theory, where each node represents one object and each edge is related to probabilities so that we can quantify the chances that a pair of nodes exit (Khan et al., 2018b; Ke et al., 2020). In neuroimaging, each node in an uncertain network refers to a brain region, and each edge refers to a probabilistic connection; this indicates the likelihood that a functional connection exists in the brain. Over the past few years, uncertain networks have been successfully applied to the field of neuroimaging. For example, Kong et al. (2013) proposed the discriminative feature selection for uncertain graph classification (DUG) algorithm to mine discriminative subgraphs in uncertain brain network using fMRI data and used this to classify Alzheimer's disease and normal controls. In another study, Cao et al. (2015b) proposed an uncertain graph mining framework based on current data mining techniques and then verified the framework using a bipolar dataset and identified abnormal subgraph patterns in fMRI data. In addition, Saha et al. (2021) reported how to compute a novel concept of betweenness centrality in an uncertain brain network and used subjects with autism to validate the efficacy of the proposed solution.

As an important topological feature of an uncertain network, a "frequent subgraph" represents the connected patterns that appear most often in the network; this is an essential approach for characterize uncertain graph (Zou et al., 2009; Kong and Yu, 2014; Yuan et al., 2016; Chen et al., 2019). This approach not only models the network connectivity patterns around nodes but also capture changes on local areas. That is,

subgraph patterns could balance local topological information with global graph topological information (Kong and Yu, 2014; Cao et al., 2015b). Therefore, in the analysis of uncertain brain networks, most researchers usually used subgraph patterns to quantify uncertain brain networks and applied them to explore brain diseases (Kong et al., 2013; Cao et al., 2015b). Specifically, the mining uncertain subgraph patterns (MUSE) algorithm was mainly used to mine the frequent subgraphs of uncertain brain networks, and the DUG method was used to select discriminative subgraphs. Although the MUSE algorithm has been successfully applied to extract frequent subgraphs, a limitation of this algorithm is that the time complexity is quite high (Papapetrou et al., 2011). Therefore, in the present study, we improved on this algorithm and then proposed an approximate algorithm; that is, we developed a frequent subgraph pattern mining algorithm based on pattern growth of frequent edge in an uncertain network (unFEPG). In this algorithm, pattern growth of frequent edge was employed to substitute the original pruning process exploited to frequent subgraphs. This decreased the time consumption of the method and gives an effective solution to the excessive computational cost of the MUSE algorithm which arose from too many subgraph features being extracted.

Previous researchers proposed the DUG method to identify discriminative subgraph features in uncertain graphs based on a statistical index (Kong et al., 2013; Cao et al., 2015b). Specifically, based on the discrimination score function, dynamic programming was used to calculate the probability distribution of each subgraph. Then, combined with the theory of the discrimination score function in a certain graph, the discrimination score (statistical index) of each subgraph was calculated. Based on discrimination score, discriminative subgraphs were selected. The DUG method was able to obtain the discrimination score in an effective manner but also caused excessive computational consumption due to the use of the dynamic programming method. In addition, previous studies reported that the classification accuracy of brain diseases obtained by the DUG method was too low; that is, this method could not effectively extract biomarkers for specific brain diseases (Kong et al., 2013). Thus, in this paper, we propose a novel discriminative feature selection method that is based on the statistical index (dfsSI). Unlike the DUG method, the statistical index (mean value) was directly calculated as the probability distribution of a subgraph for each subgraph pattern in positive and negative samples. Next, based on the theory of the discrimination score function in a certain graph, the discrimination score for each subgraph was calculated and discriminative subgraphs were selected accordingly.

Considering the inherent uncertainty in graphs and the limitations imposed by a certain brain network, this paper introduced uncertain graph theory to construct an uncertain brain network and then used the approximate algorithm (unFEPG) to mine frequent subgraphs within the uncertain brain network. Next, discriminative subgraphs were selected using the statistical index (dfsSI) and the discriminative score function. Finally, the discriminative subgraph features were used for classification. Results show that the MUSE and dfsSI method achieves better classification accuracy than the traditional DUG method. Furthermore, to further prove the efficacy of the proposed method, this paper also compared an uncertain brain network with a certain brain network in a bidirectional manner based on a unified subgraph model. Results showed that under certain sparsity conditions (that is, under certain threshold conditions), the classification performance of the uncertain brain network was better than that of the certain network. In addition, we also evaluated the generalization performance of the classification model constructed by the proposed method using our dataset and an independent validation dataset respectively. We also discuss the number of features, model parameters, and classifier parameters.

MATERIALS AND METHODS

Method Framework

Figure 1 shows the entire flowchart. Specifically, this process focuses on the analysis of uncertain brain network and includes the following parts:

(1) Data acquisition and preprocessing.

(2) Group independent component (IC) analysis.

According to fMRI data, the ICs are estimated.

(3) Construction of uncertain brain networks in which the correlation method is used to construct an uncertain brain network.

(4) Mining frequent subgraphs of uncertain networks using the approximate algorithm method, based on pattern growth of frequent edge, to obtain a frequent subgraph pattern.

(5) Selection of discriminative features utilizing the statistical index and the discrimination score function to obtain discriminative subgraph features.

(6) Support vector machine classification.

A support vector machine (SVM) based on radial basis function (RBF) kernel function is used for classification.

(7) Comparison of the uncertain and certain brain networks.

The uncertain discriminative subgraph is fitted with a threshold and the certain discriminative subgraph is weighted to obtain a consistent subgraph mode. On this basis, the classification performance of the certain and uncertain networks can be compared in a bidirectional manner.

Data Acquisition and Preprocessing

Following the recommendations of the Shanxi Medical Ethics Committee (reference no. 2012013), all subjects needed to provide their consent to participate. All participants provided written informed consent in accordance with the Declaration of Helsinki, including 38 subjects with first-time, drug-free, major depression disorder (MDD) as the depression group and 28 age and gender-matched healthy volunteers as the normal control (NC) group. All subjects were righthanded. Participants in the depression group participants were first-time, drug-free patients identified by the criteria provided by the American Manual of Diagnostic and Statistical Manual of Mental Disorders, Fourth

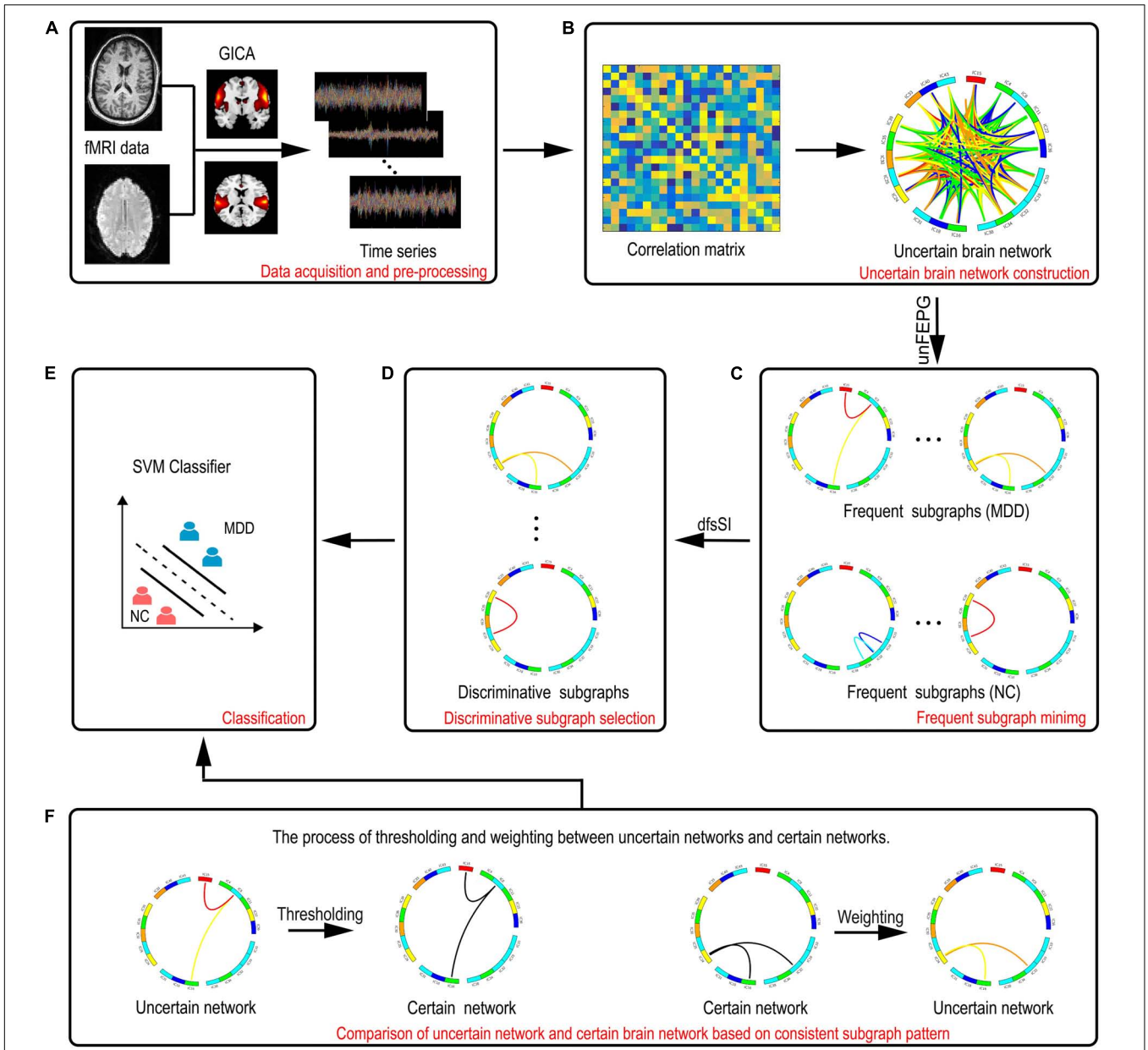

FIGURE 1 | A description of the entire framework for the proposed method. **(A)** Data acquisition and preprocessing. **(B)** Construction of the uncertain brain network. **(C)** Frequent subgraph mining. **(D)** Discriminative subgraph selection. **(E)** Classification. **(F)** Comparison of the uncertain network and certain brain network based on consistent subgraph patterns. The left graph represents thresholding of discriminative subgraphs in the uncertain network. The right graph represents the weighting of discriminative subgraphs in the certain network.

Edition (DSM-IV) (First and Gibbon, 1997). The severity of depression was determined by the 24 Hamilton rating scale for depression (HAMD) (Williams, 1988) and the clinical global impression of severity (CGI-S) (Guy, 1976). Using a 3T magnetic resonance scanner (Siemens Trio 3-Tesla scanner, Siemens, Erlangen, Germany), resting-state functional magnetic resonance scans were performed on 28 normal and 38 patients with depression. Detailed information relating to the subjects is shown in **Table 1**. The power analysis for subject inclusion is shown in **Supplementary Text S1**.

Data acquisition was completed by the First Hospital of Shanxi Medical University and all scans were performed by radiologists who were familiar with the operation of the MRI scanner. All patients underwent complete physical and neurological examinations, standard laboratory tests, and extensive neuropsychological assessments. During the scanning period, subjects were asked to close their eyes, relax, and not to think about anything specific, but to remain awake and not to fall asleep. Scanning parameters were set as follows: 33 axial slices; repetition time (TR) = 2000 ms; echo time

TABLE 1 | Demographic and clinical characteristics of the subjects.

	NC (n = 28)	MDD (n = 38)	P-value
Age	26.60 ± 9.4 (17–51)	28.40 ± 9.68 (17–49)	0.44[a]
Gender (Female/Male)	15/13	23/15	0.57[b]
Handedness (Right/Left)	28/0	38/0	–
HAMD	N/A	22.80 ± 13.30 (15–42)	–

Data are presented as the range (mean ± standard deviation). NC, normal controls; MDD, major depressive disorder; HAMD, Hamilton Depression Rating Scale. [a]P-value was calculated by two-sample two-tailed t-test; [b]P-value was computed by two-tailed Pearson's chi-square test.

(TE) = 30 ms; slice thickness/skip = 4/0 mm; field of view (FOV) = 192 × 192 mm; matrix size = 64 × 64 mm; flip angle = 90°; volumes = 248. Detailed scanning parameters are given in **Supplementary Text S2**.

Data preprocessing was performed in SPM8 software[1]. First, the dataset was corrected for slice time and head motion. From the final total of 66 subjects, data were not included from any subject with a head movement greater than 3 mm or with rotation greater than 3°. Then, we performed co-registration for spatial correction. Next, images underwent 12-dimensional optimal affine transformation into the standardized Montreal Neurological Institute (MNI) space, using 3 mm voxels. Smoothing was further performed to eliminate the differences between brain structures in different subjects and to improve the signal-to-noise ratio. Linear dimensionality reduction and bandpass filtering (0.01–0.10 Hz) were finally performed to eliminate the effects of line frequency drift and high frequency physiological noise. In addition, we used head, white matter and cerebrospinal fluid signals as covariates for regression analysis to remove nuisance information from images. However, we did not regress global brain signals (Li et al., 2019).

Group Independent Component Analysis

In the current study, group independent component analysis (GICA) was used to analyze the fMRI data. GICA was carried using the GIFT package[2]. Specifically, the minimum description length (MDL) criterion was applied to estimate the optimal number of decomposition components (Koechlin and Summerfield, 2007) in the normal group and in the depression group. On this basis, we set the final number of ICs to 54. Next, the ICs of each subject was decomposed using the Infomax algorithm, thus resulting in 54 independent spatial components in each subject. The principle of this algorithm was to minimize the mutual information among the components of the output by maximizing the mutual information between the input and the output (Du and Fan, 2013). To strengthen the stability and reliability of the ICs, the Infomax algorithm was run 20 times on ICASSO[3] by randomly initializing the decomposition matrix; after these repetitions, the same convergence threshold (Nenert et al., 2014) was acquired. Finally, the GICA3 (the third method based on group independent component analysis) algorithm was adopted to reconstruct the data such that the spatial distribution and time series of the ICs of the subjects (Erhardt et al., 2011) could be obtained. See **Supplementary Text S3** and **Supplementary Table S1** for a detailed explanation relating to the rationality for selecting the 54 ICs.

The ICs extracted by the GICA in this paper not only included the components-of-interest from the brain network but they also included other unrelated components and components with more noise. Therefore, it was necessary to use a prior template matching method to screen out these ICs and to further confirm the components-of-interest using a manual inspection method (Jafri et al., 2008). The screening criteria used for the exclusion of intrinsic connection network components included the following conditions: larger activation areas, where the multiple regression coefficients matched the prior template; the distribution of the main activation regions in the gray matter; the overlap of these regions with known components, such as blood vessels and head movements in low frequency space; and the domination of the power spectrum for the time series in activation regions by low frequency power (Allen et al., 2011). Finally, 32 unrelated or noisy components were removed, and 22 brain network components were retained; these intrinsic connectivity network components were identified as being part of the auditory network, sensorimotor network, visual network, default mode network (DMN), attention network, or frontal lobe network. These 22 brain network components were common regions for the two groups of subjects.

Construction of the Uncertain Brain Network

Uncertain Graph Theory

Definition 1 (Uncertain Graphs)

Uncertain graphs are undirected graphs with uncertainties represented as $\widetilde{G} = (V, E, p)$ (Khan et al., 2018b; Ke et al., 2020). Of these, $V = \{v_1, v_2, ..., v_n\}$ refers to the node set, $E \subseteq V \times V$refers to the probabilistic edge set, and $p : E \rightarrow (0, 1]$ is a function denoting the likelihood of the existence of each edge in E. That is, $p(e)$ denotes the probability of the edge about $e \in E$. A certain graph is a special case of uncertain graph, where the probability of its edges $[p(e)]$ is 1.

An uncertain graph $\widetilde{G}$ may include a great quantity of instances, each of which is a certain graph, represented by G. **Figure 2** shows an example of an fMRI uncertain brain network including thirteen nodes and thirteen edges.

If all edges $E(G)$ in the graph G are extracted from $E(\widetilde{G})$ in terms of the probability $p(e)$ and $E(G) \subseteq E(\widetilde{G})$, then a certain graph $G = (V, E)$ can be implied from an uncertain graph $\widetilde{G}$ (denoted as $\widetilde{G} \Rightarrow G$). G is an instance of $\widetilde{G}$, and all instances consists of a set $W(\widetilde{G}) = \{G | \widetilde{G} \Rightarrow G\}$. The probability that a certain graph $G \in W(\widetilde{G})$ is implied from an uncertain graph $\widetilde{G}$, which is defined by Eq. 1 (Khan et al., 2018b; Ke et al., 2020).

$$\Pr[\widetilde{G} \Rightarrow G] = \prod_{e \in E(G)} \Pr_{\widetilde{G}}(e) \prod_{e \in E(\widetilde{G}) - E(G)} (1 - \Pr_{\widetilde{G}}(e)) \quad (1)$$

[1]http://www.fil.ion.ucl.ac.uk/spm

[2]https://trendscenter.org/software/gift/

[3]http://www.cis.hut.fi/projects/ica/icasso

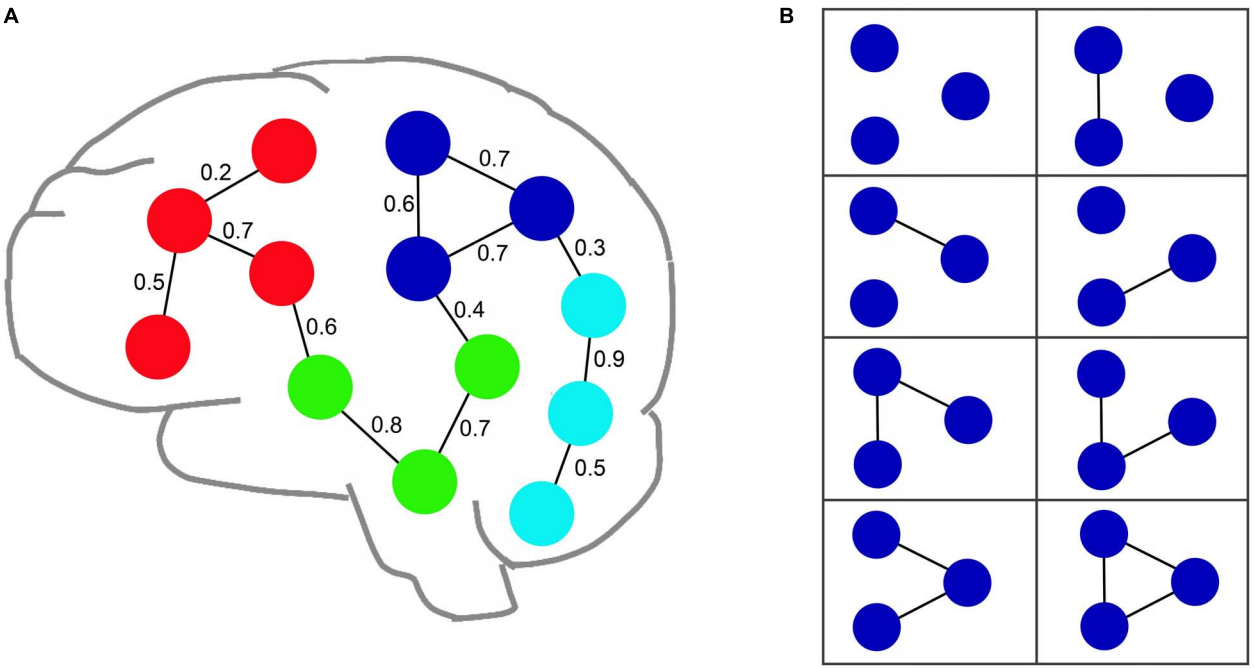

FIGURE 2 | An example of an uncertain fMRI brain network. **(A)** Illustrates an uncertain brain network with thirteen nodes and thirteen edges. The value of edge denotes the probability value of each edge. **(B)** Shows all possible instances for an uncertain graph composed of the blue nodes shown in **(A)**.

In Eq. 1, e refers to the edge of an uncertain graph; $E(G)$ refers to the edge sets of graph G; $E(\widetilde{G})$ refers to the edge sets of graph $\widetilde{G}$; $\Pr_{\widetilde{G}}(e)$ refers to the existence probability for an edge $e \in E(\widetilde{G})$.

Notably, the uncertain graph was similar with the weighted graph in terms of its form. However, the largest difference between the two graphs is the understanding of weights. An uncertain graph can be considered as a special edge-weighted graph (Zou et al., 2010) in which the weights refer to the probability of an edge existing between a pair of nodes, thus considering the noisy measurements of the underlying truth. Edge probabilities are semantically different from edge weights, and there is no meaningful way to perform such a casting (Khan et al., 2018b). Moreover, with an uncertainty graph, we can set a threshold probability value and decide to ignore any component with an existence probability below that threshold (Khan et al., 2018b). In recent years, uncertain graphs have been applied to many fields, especially biological networks, mobile *ad hoc* networks, social networks, and other applications where edges are assigned a probability of existence due to a range of factors, such as noisy measurements, the lack of precise information, and inconsistent, incorrect, and potentially ambiguous sources of information (Zhang et al., 2017; Khan et al., 2018a; Li et al., 2020; Saha et al., 2021).

Construction of Uncertain Brain Networks

An uncertain brain network is based on uncertain graph theory in which each node represents a region of interest and each edge is associated with a probability $p(e)$ that relates to the likelihood that a functional connection exists in the brain. In exiting studies, uncertain brain networks were mainly constructed based on Pearson's correlation method (Kong et al., 2013; Cao et al., 2015a,b; Saha et al., 2021). Therefore, in this paper, we used Pearson's correlation method to construct an uncertain brain network. Specifically, the locations in the cerebral cortex that corresponded to the remaining 22 ICs (after removing noise components) were used as the nodes of the uncertain brain network. For each subject, a 22 × 22 correlation matrix was obtained based on Pearson's correlation method; this was calculated by Eq. 2.

$$r_{i,j} = \frac{cov(i,j)}{\sigma_i \sigma_j} \tag{2}$$

In Eq. 2, $r_{i,j}$ denotes the correlation coefficient of the time series relating to the independent component i (IC i) and independent component j (IC j). $cov(i,j)$ denotes the covariance of the two independent component time series. $\sigma_i$and σ_j represent the standard deviations of the time series about the two ICs, respectively.

Given that the edges of the uncertain network were associated with a probability that illustrates the likelihood of whether this edge should exist or not, the correlation matrix was processed according to Eq. 3.

$$b_{ij} = \begin{cases} r_{ij}, r_{ij} \geq 0 \\ 0, r_{ij} < 0 \end{cases} \tag{3}$$

In Eq. 3, b_{ij} denotes the edge value of IC i of IC j in the uncertain brain network model (Kong et al., 2013; Saha et al., 2021). Positive correlations were used as edge values (uncertain

links) among different brain regions to form uncertain networks (Kong et al., 2013; Cao et al., 2015a; Tokuda et al., 2018).

Frequent Subgraph Mining of Uncertain Brain Networks

Subgraph Theory

Definition 2 (Subgraph)

In definition 2 (subgraph), $g = (V', E')$ and $G = (V, E)$ denote two certain graphs, separately. If $V' \in V$and $E' \in E$, then g denotes a subgraph of G, or G contains a subgraph g (denoted as $g \subseteq G$) (Kong and Yu, 2014).

Given an uncertain graph, the probability of $\widetilde{G}$containing subgraph g is expressed by Eq. 4.

$$\Pr[g \subseteq \widetilde{G}] = \sum_{e \in E(g)} \Pr(\widetilde{G} \Rightarrow G) \cdot I(g \subseteq G) = \begin{cases} \prod_{e \in E(g)} p(e), E(g) \subseteq E(\widetilde{G}) \\ 0, \text{otherwise} \end{cases} \quad (4)$$

In Eq. 4, e refers to an edge of the uncertain graph; $E(g)$ refers to all edges in the graph g; $E(\widetilde{G})$ refers to all edges in the graph $\widetilde{G}$; $\Pr(\widetilde{G} \Rightarrow G)$ have the same meaning as in Eq. 1; when $g \subseteq G$, then $I(g \subseteq G) = 1$, if not, then $I(g \subseteq G) = 0$; $p(e)$ represents the probability of the edge about $e \in E(g)$.

Definition 3 (Support Degree)

Definition 3 (support degree) assumes that the uncertain graph dataset $W(\widetilde{D})$ including all of the certain graph set D is a probability distribution; the support degree of subgraph g in the middle is a probability distribution, as defined by Eq. 5.

$$\begin{bmatrix} g_1 & g_2 & \cdots & g_m \\ \Pr(g_1) & \Pr(g_2) & \ldots & \Pr(g_m) \end{bmatrix} \quad (5)$$

In Eq. 6, the different subgraph patterns of $W(\widetilde{D})$ are $g_1, g_2 \ldots, g_m$; $\Pr(g_k) = \Pr[g_k \subseteq \widetilde{G_i}](k = 1, \ldots, m; i = 1, \ldots, n)$ represents the probability of $\widetilde{G_i}$ including subgraph g which can be referred to as the support degree of subgraph g_k(Li et al., 2012); m refers to the number of subgraph patterns, n refers to the number of uncertain graphs; k refers to kth subgraph patterns; i refers to the ith uncertain graph. Based on this, the expected support degree of subgraph g_k is defined by Eq. 6.

$$Esup(g_k, \widetilde{D}) = \frac{1}{n} \sum_{i=1}^{n} \Pr[g_k \subseteq \widetilde{G}_i] \quad (6)$$

In Eq. 6, $\Pr[g_k \subseteq \widetilde{G}_i]$ has the same meaning as in Eq. 6. If the $Esup(g_k, \widetilde{D})$ is more than the threshold *minsup*, then the subgraph is regarded as a frequent subgraph.

Frequent Subgraph Mining Based on the Pattern Growth of Frequent Edges

Frequent subgraph patterns are an important structural feature of uncertain networks and balance local with global graph topological information (Zou et al., 2009; Kong and Yu, 2014; Yuan et al., 2016; Chen et al., 2019). Considering the limitations of MUSE algorithm, in the present study, we improved the algorithm and proposed an approximate algorithm: a frequent subgraph pattern mining algorithm based on pattern growth of frequent edge in an uncertain network (unFEPG) in which pattern growth of frequent edge was employed to substitute the original pruning process on the frequent subgraph. The specific idea and process used by the algorithm was as follows.

We assumed that the given uncertain graph dataset $\widetilde{D} = \{\widetilde{G}_1, \widetilde{G}_2, \ldots, \widetilde{G}_n\}$contained n uncertain graphs and that $\widetilde{G}_i$ represents the ith uncertain graph in $\widetilde{D}$. Then, $y = [y_1, y_2, \ldots, y_n]^T$denotes the class labels vector and the class labels are given by $y_i \in \{-1, +1\}$. From this, the graph for the depression group in this study can be represented as $\widetilde{D}_{MDD} = \{\widetilde{G}_i | \widetilde{G}_i \in \widetilde{D} \wedge y_i \in +1\}$ while that for the normal group is represented as $\widetilde{D}_{NC} = \{\widetilde{G}_i | \widetilde{G}_i \in \widetilde{D} \wedge y_i \in -1\}$.

The main concept behind the unFEPG algorithm is to construct a multi-layer sub-search space and select frequent subgraphs from all subgraphs contained in each layer of the sub-search space in all sub-search space. The frequent subgraphs in all sub-search spaces constituted the frequent subgraphs in the MDD group and the NC group. Of these, all subgraphs in each layer sub-search space were obtained using the unFEPG method. The unFEPG algorithm mainly consists of the following steps. Firstly, we took the edges in uncertain brain networks as the subgraphs of the 1-layer search space, calculated the expected support degree (Eq. 7) corresponding to each edge and compared this with the threshold *minsup*. Finally, the edge whose expected support degree was greater than or equal to *minsup* was regarded as a frequent edge and added to the 1-subgraph pattern set in corresponding sub-search space (notably, the frequent edges here were also frequent subgraphs), and the number of frequent edges k was set as the number of subgraph search spaces. Secondly, based on the 1-subgraph pattern set, we used the pattern growth of frequent edge method to construct the i-layer (i = 2,3,. . .,k) sub-search space. Next, we judged all subgraphs in the i-layer sub-search space to assess whether they were frequent according to the rules of frequent subgraphs. If the conditions were met, then we defined this as a frequent subgraph and added it to the i-subgraph pattern set in corresponding sub-search space. Finally, if the i-subgraph pattern set was null or $i \geq k$, then ended the search of sub-search space process and search the next sub-search space. Otherwise, set $i = i+1$, iterate (2)-(3). In the next section, each step was described in detail.

The specific steps required to obtain the 1-subgraph pattern set are as follows. Given the input uncertain graph dataset $\widetilde{D} = \{\widetilde{G}_1, \widetilde{G}_2, \ldots, \widetilde{G}_n\}$ and the threshold *minsup*; then all the subgraph patterns in $\widetilde{D}$ constitute the whole search space. First, the edges in the uncertain brain networks were regarded as subgraphs of the 1-layer search space. Then, the expected support degree (Eq. 7) of each edge in the MDD group and the NC group was calculated and compared with the threshold *minsup*. If the expected support degree of the edge was greater than *minsup*, then the edge was

denoted as a frequent edge and added to the 1-subgraph pattern set. Note, the frequent edges observed during this step were frequent subgraphs. If the 1-subgraph pattern set contains the edges m_1, m_2, ..., m_k, then the whole search space can be divided into k sub-search spaces that do not intersect each other, where the i-subgraph pattern set was distributed in the i-layer of the search space. In addition, to reduce the comparison of repeated graphs, we did not include edges with subscripts less than i in the i-th sub-search space.

The specific steps used to acquire the i-subgraph pattern in corresponding sub-search space were as follows. (1) based on the 1-subgraph pattern set, the pattern growth of frequent edge method was adopted to construct the i-layer (i = 2,3,. . .,k) sub-search space. (2) The pattern growth of frequent edge method is based on the frequent edges in the 1-subgraph pattern set, each frequent edge is selected to be added to the i-1 subgraph pattern set in a retrospective manner. Here, to reduce the comparison of repeated graphs and computation cost, frequent edges were only selected if their subscripts were less than i in the 1-layer subgraph pattern set. (3) according to the rules of frequent subgraphs, all subgraphs in the i-layer sub-search space were only judged if they are frequent subgraphs. When a subgraph satisfied the conditions required by frequent subgraphs, then it was regarded as a frequent subgraph and added to the i-subgraph pattern set in the sub-search space. The specific condition for a subgraph to be a frequent subgraph was that the subgraph must be connected, and its expected support was greater than or equal to *minsup*. (4) the process was terminated if the i-subgraph pattern set was null or $i \geq k$ and search the next sub-search space. Otherwise, set $i = i$+1, iterate (2)-(3). The detailed algorithm for this process is shown in **Tables 2**, **3**. **Supplementary Text S4** shows an example to illustrate the unFEPG algorithm. Note that in the i-subgraph pattern set, the frequent subgraphs are all i edges.

Based on the uncertain brain networks in the MDD group and NC group, we were able to obtain each layer subgraph pattern set (that is, frequent subgraphs in each layer search space). These frequent subgraphs constituted the final frequent subgraphs of the two groups of subjects.

Discriminative Subgraph Feature Selection for Uncertain Brain Networks

The number of frequent subgraphs extracted by uncertain brain networks was very large. If all frequent subgraphs participated in the classification, then this would reduce the classification performance. Not all frequent subgraphs had discriminative ability; in fact, only a few subgraphs are known to possess discriminative ability (Guo et al., 2017). Thus, it was necessary to select discriminative subgraphs as classification features. In previous studies, researches usually measured the discrimination score for each subgraph to select discriminative subgraphs (Guo et al., 2017, 2018; Cui et al., 2018). The larger the discriminative score, the stronger the discriminative ability of the subgraph. In conventional certain networks, the discrimination scores of the subgraph features were applied into discriminative subgraph mining, in which the edge of each network was certain. On this basis, there is clear certainty relating to the number of times the subgraph feature appears in the network. Accordingly, a discriminative subgraph can be selected according to the discrimination scores (for example, the difference in frequency for which a subgraph features in two groups of subjects) (Guo et al., 2017). However, when the uncertainty of the edges was presented in the form of a graphs (i.e., an uncertain network), a subgraph feature only existed in a graph with a specific probability. Thus, the discrimination scores for a subgraph feature were no longer certain values; rather, they were random variables with probability distributions (Gao and Wang, 2010). Therefore, due to the uncertainty of the edges being taken into account, the selection of discriminative subgraphs in the uncertain brain network was every different from that of a conventional certain network (Kong et al., 2013). **Supplementary Figure S1** shows an example to illustrate the differences of discriminative capabilities between subgraphs from uncertain and certain networks.

Considering the problem of low classification accuracy of discriminative subgraphs in existing uncertain brain network research, we combined the calculation method used to define the discriminative score in certain and uncertain networks and proposed a novel discriminative feature selection method based

TABLE 2 | Algorithm for frequent subgraph mining based on frequent edges.

Input: The uncertain graph dataset $\widetilde{D}$ and minimum expected support degree *minsup*

Recursive subgraphs mining:

(1) Traverse $\widetilde{D}$ to acquire all 1-layer sub-search space in $\widetilde{D}$, and calculate the expected support degree $Esup(g, \widetilde{D})$ according to formular 7.

(2) If $Esup(g, \widetilde{D}) \geq minsup$ of the subgraph (frequent edge) in the 1-layer search space, then add it to the 1-subgraph pattern set M and the frequent subgraph pattern dataset R.

(3) Set the number of subgraph sub-search spaces as k according to the number of subgraphs in M.

(4) For each subgraph in M, employ the algorithm for pattern growth given in Table 3 to acquire the i-layer ($i = 2,3,\ldots,k$) corresponding sub-search space N.

(5) For the subgraph in i-layer (i = 2,3,. . .,k) search space N, use formular 7 to calculate the expected support $Esup$; similarly, if $Esup \geq minsup$ in the i-layer ($i = 2,3,\ldots,k$) sub-search space, then add it the i-subgraph pattern set in i-layer ($i = 2,3,\ldots,k$) sub-search space and the frequent subgraph pattern dataset R.

(6) $i = i$+1, repeat steps 4 and 5 until i-subgraph pattern set was null or $i \geq k$ and search the next sub-search space.

Output:

The frequent subgraph pattern dataset R from $\widetilde{D}$.

TABLE 3 | Algorithm for pattern growth.

Input: The (i-1)-subgraph pattern set in (i-1)-layer (i = 2,3,. . .,k) sub-search space and the 1-subgraph pattern set M.

Pattern growth:

(1) Label the sub-search space where the (i-1)-subgraph pattern is defined as i-1.

(2) For each subgraph pattern (frequent edge) in M, if it has a label > i-1, then add it to the (i-1)-subgraph pattern set to acquire the new subgraph s (the number of edge in the subgraph is i).

(3) If subgraph s is connected, then add it to the i-layer (i = 2,3,. . .,k) sub-search space N.

Output:

The i-layer (i = 2,3,. . .,k) sub-search space N.

on statistical index (dfsSI) to select discriminative subgraph features from an uncertain brain network.

First, the selection method used for a discriminative subgraph in a certain network was referenced. In a certain network, a discriminative subgraph was obtained by counting the number of times a subgraph appeared in positive and negative samples and then applying this to the discriminative score function to calculate the discriminative score. The higher the discriminative score, the stronger the discriminative ability of the subgraph. As mentioned earlier, a certain network can be regarded as a special uncertain network with a probability of 1 on each edge. On this basis, the number of times a subgraph appears can be regarded as the sum of the probabilities in a positive and negative sample. This was the methodology applied in the current study. In addition, considering the balance between sample sizes, we further introduced the statistical index method for uncertain networks. In other words, the statistical index was introduced to calculate the probability distribution of a subgraph appearing in the two groups of subjects respectively. Then, we applied this into the discriminative score function to calculate a discriminative score for each subgraph.

Many statistical indicators have been used in existing studies, including mean, median, and range (Chen, 2014; Franceschelli et al., 2017; Ben-Aharon et al., 2019). In this study, we adopted the mean index as a statistical index as this has been widely applied to discriminative subgraph mining in uncertain networks (Zou et al., 2009, 2010; Kong et al., 2013). The mathematical definition of the mean values for this study were given as shown in Eqs 7, 8.

$$Mean(g, \underset{MDD}{\widetilde{D}}) = \frac{1}{M}\sum_{i=1}^{M} \Pr[g \subseteq \widetilde{G_i}] \tag{7}$$

$$Mean(g, \underset{NC}{\widetilde{D}}) = \frac{1}{N}\sum_{i=1}^{N} \Pr[g \subseteq \widetilde{G_i}] \tag{8}$$

In Eqs 7, 8, $\underset{MDD}{\widetilde{D}}$ represents the set of uncertain networks for the depression group; $\underset{NC}{\widetilde{D}}$ represents the set of uncertain networks for the normal group; $\widetilde{G_i}$ represents the uncertain brain network for the ith subject; g represents a frequent subgraph; $\sum_{i=1}^{N} \Pr[g \subseteq \widetilde{G_i}]$ represents the corresponding probability values for subgraph g contained in $\widetilde{G_i}$; M refers to the number of subjects in the depression group; and N refers to the number of subjects in the normal group. After calculating the mean value for frequent subgraphs, we then carried out the discriminative score function to obtain discriminative scores for frequent subgraphs. In uncertain graph theory, the common discriminative score functions contain confidence (Jin and Wang, 2011), frequency ratio (Yan et al., 2008), G-test score (Gao and Wang, 2010), and Hillbert Schmidt independence criterion (HSIC) (Kong et al., 2011). The confidence method possesses good subgraph discrimination ability and a strong generalization ability, which has been widely applied in previous researches (Jackson and Read, 2010a,b). Therefore, in the present study, we used the confidence method as the discriminative score function to select discriminative subgraphs. We measured the confidence values of the frequent subgraphs respectively for the MDD group and the NC group. Then we arranged the two group values in reverse order, and selected the top-k values in the two groups as discriminative subgraph features. Finally, we acquired $2k$ discriminative subgraphs. The specific definition was expressed by Eqs 9, 10.

$$Confidence(n^g_{MDD}, n^g_{NC}) = \frac{n^g_{MDD}}{n^g_{MDD} + n^g_{NC}} \tag{9}$$

$$Confidence(n^g_{MDD}, n^g_{NC}) = \frac{n^g_{\mathrm{NC}}}{n^g_{MDD} + n^g_{NC}} \tag{10}$$

In Eqs 10, 11, n^g_{MDD} refers to $Mean(g, \underset{MDD}{\widetilde{D}})$; n^g_{NC} refers to $Mean(g, \underset{NC}{\widetilde{D}})$.

Classification

The discriminative subgraph was selected using the dfsSI method (that is, the mean value was used as the statistical index value and applied to the discriminative score function to select the discriminative subgraph). Then, the classification model was constructed according to the discriminative subgraph feature. In this study, we adopted a SVM classifier based on the RBF kernel for classification. Here, we used the LIBSVM toolkit in MATLAB to classify our data[4].

We adopted the 10-fold cross validation to evaluate classification performance. The samples were randomly divided into 10 parts, with one part regarded as the test set and the other nine as the training set. Finally, the average of 10 results was measured to assess the performance of the classifier. In addition, to increase the accuracy of our results, the 10-fold cross-validation was repeated 100 experiments in the experiment, and the average value of the 100 experiments was considered as the final result.

RESULTS

Intrinsic Connectivity Network

In this study, we chose 22 ICs using GICA. **Supplementary Figure S2** shows the spatial maps of these 22 ICs. In terms of the spatial maps of each IC, the inherently connected network to which they belong was determined, as shown in **Supplementary Figure S2**.

These 22 ICs were similar to those identified in previous work (Beckmann et al., 2005; Calhoun et al., 2008; Smith et al., 2009; Allen et al., 2011). Here, we described these 22 ICs in detail. Resting-state networks are grouped by their anatomical and functional properties. IC 15 forms a rather prototypical representation of the large parts of the auditory system (AUD), mainly including bilateral activation of the

[4]http://www.csie.ntu.edu.tw/~cjlin/libsvm/

superior temporal gyrus (Seifritz et al., 2002; Specht and Reul, 2006). The Sensorimotor networks (SM) were captured by five components (ICs 4, 8,11, 22, and 36) situated in the vicinity of the central sulcus, mainly including activation of the left precentral gyrus, right postcentral gyrus, bilateral activation of the paracentral lobule, supramarginal gyrus and supplementary motor area (Krienen and Buckner, 2009; Abouelseoud et al., 2010). The visual system (VIS) is also represented by six components (ICs 10, 19, 32, 34, and 38) in good agreement with the anatomical and functional delineations of occipital cortex. The main active regions were the lingual gyrus, cuneiform lobe, suboccipital gyrus, talus gyrus and middle temporal gyrus (Grill-Spector and Malach, 2004). The DMN was captured by three independent components (ICs 16, 18, and 31); the main active regions were located in the precuneus lobe, lingual gyrus and temporal lobe etc. The attention network (ATTN) was captured by six independent components (ICs 24, 25, 30, 35 39, and 40); the main active regions were located in the frontal lobe, parietal lobe, precuneus lobe, temporal lobe and angular gyrus (Corbetta and Shulman, 2002; Vincent et al., 2008). Finally, frontal networks (FRONT; ICs 33 and 43) known to mediate executive as well as memory and language functions was observed, whose active regions were located in the medial prefrontal cortex and parietal lobe (Koechlin et al., 2003; Koechlin and Summerfield, 2007).

Frequent Subgraph Patterns and Discriminative Subgraph Patterns

After constructing the uncertain brain network, the unFEPG algorithm was separately used to mine the frequent subgraphs from the NC and MDD groups. When the *minsup* parameter was set to 0.25, 289 frequent subgraphs were mined from the NC group and 192 from the MDD group. Specific information relating to the frequent subgraphs is given in **Supplementary Table S2**.

According to the frequent subgraphs, the dfsSI algorithm was used to calculate discriminative scores for the frequent subgraphs. Then, discriminative subgraphs from the NC group and MDD group were selected based on discriminative scores. To ensure a balanced number of subgraph features, we respectively selected the top 15 frequent subgraphs with the highest discriminative scores from the two groups of subjects as the discriminative subgraph features to perform classification, as shown in **Figure 3** (see Section "The Influence of the Number of Features" for a discussion of the number of subgraph features). To analyze the difference of the discriminative subgraphs between the two groups, we combined 15 discriminative subgraphs from each group, as shown in **Figure 4A**. Results showed that the abnormal components obtained by the two sets of discriminative subgraphs were almost identical, and included IC16, IC32, IC34, IC4, IC8, IC15, IC24, IC25, IC33, IC18, IC38, and IC35. On this basis, we counted the number of times each IC appeared in all discriminative subgraphs to select the most discriminative components for MDD, as shown in **Figure 4B**. The results showed that the top 3 abnormal components were IC16, IC32, and IC34. Of these, IC16 occurred the most frequently in the abnormal components (seven times). This was followed by IC32 and IC34 respectively (occurring six times each).

Classification Results

Based on the discriminative subgraph features, we next assessed classification performance by calculating classification accuracy, sensitivity, and specificity, and the area under the curve (ROC).

We evaluated classification performance based on probability values representing functional connections (PV-FC), the unFEPG method and by combining the unFEPG method with the dfsSI method; then, we compared these two outcomes with the traditional DUG method. First, the DUG method applied Pearson's correlation method to construct an uncertain brain network. Secondly, the probability distribution for each current subgraph was calculated based on dynamic programming, in which a current subgraph was selected based on a DFS-code tree in gSpan. Then, based on the probability distribution and the values obtained by discriminant score function (confidence) for each current subgraph, statistical indicator (discriminative scores) was acquired. Furthermore, we set the minimum expected frequency (*min_sup*) and the minimum discriminative score (θ), and then compared the expected frequency and discriminative scores for each current subgraph with *min_sup* (*min_sup* was set as 0.25) and θ. If these values were greater than *min_sup* and θ, then the current subgraph was added to the discriminative subgraph set. Otherwise, the sub-tree of the current subgraph was pruned by the branch-and-bound algorithm. Next, a recursion process based on a depth-first search was carried out to identify other discriminative subgraphs. Finally, the top 15 discriminative subgraphs were selected as subgraph features for classification. The classification results for these methods are summarized in **Table 4**. We found that the accuracy of the unFEPG method, when combined with the dfsSI method, reached 92.9%; this was higher than other three methods (PV-FC, the unFEPG method and the traditional DUG method).

COMPARISON OF UNCERTAIN AND CERTAIN BRAIN NETWORKS

Considering inconsistency between uncertain and certain graphs with regards to subgraph features, and their different forms of feature characteristics, we used consistent discriminative subgraph patterns to bidirectionally compare the classification performance of uncertain networks and certain networks.

Thresholding Discriminative Subgraphs in Uncertain Brain Networks

To assure that the subgraph patterns were consistent when comparing the classification performance of uncertain and certain networks, we first carried the discriminative subgraph acquired from uncertain brain networks as subgraph features, and then utilized the thresholding method to map them to the certain network. The specific thresholding method process

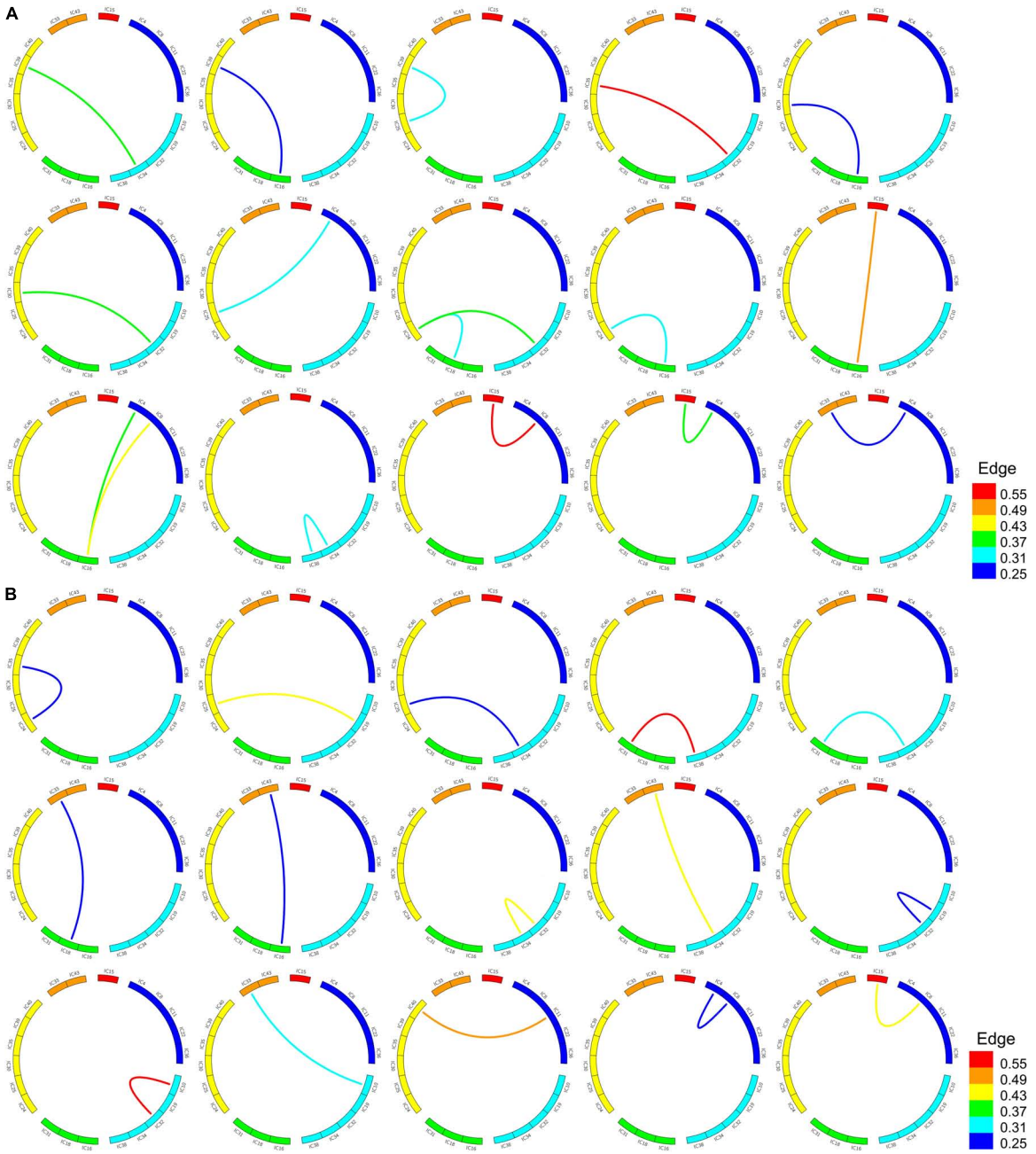

FIGURE 3 | Frequent subgraphs of MDD and NC group. **(A)** Represent top 15 discriminative subgraphs in MDD group. Edge refers to the edges are assigned with a probability of existence in MDD group. **(B)** Represent top 15 discriminative subgraphs in NC group. Edge refers to the edges are assigned with a probability of existence in NC group.

is as follows. First, the probability values for all edges in the uncertain brain network were ordered in reverse order. Then, based on the selected sparsity, the minimum weight at which an edge can exist was regarded as *min_weight*. When the value of an edge of a subgraph in the uncertain network was larger than *min_weight*, then the edge existed in a certain network, and *vice versa*. Accordingly, we acquired the discriminative subgraph patters for the corresponding certain network. Here, note that we obtained distinct subgraph features for a certain network if the sparsity was set distinctly, and the mapped subgraph pattern for a certain network was not necessarily exited. When the mapped subgraph feature was exitent in the certain network, this was represented as 1 (and 0 it not exitent). Using this method, we were able to construct a classification feature matrix for a certain graph. **Figure 5** shows an example of thresholding.

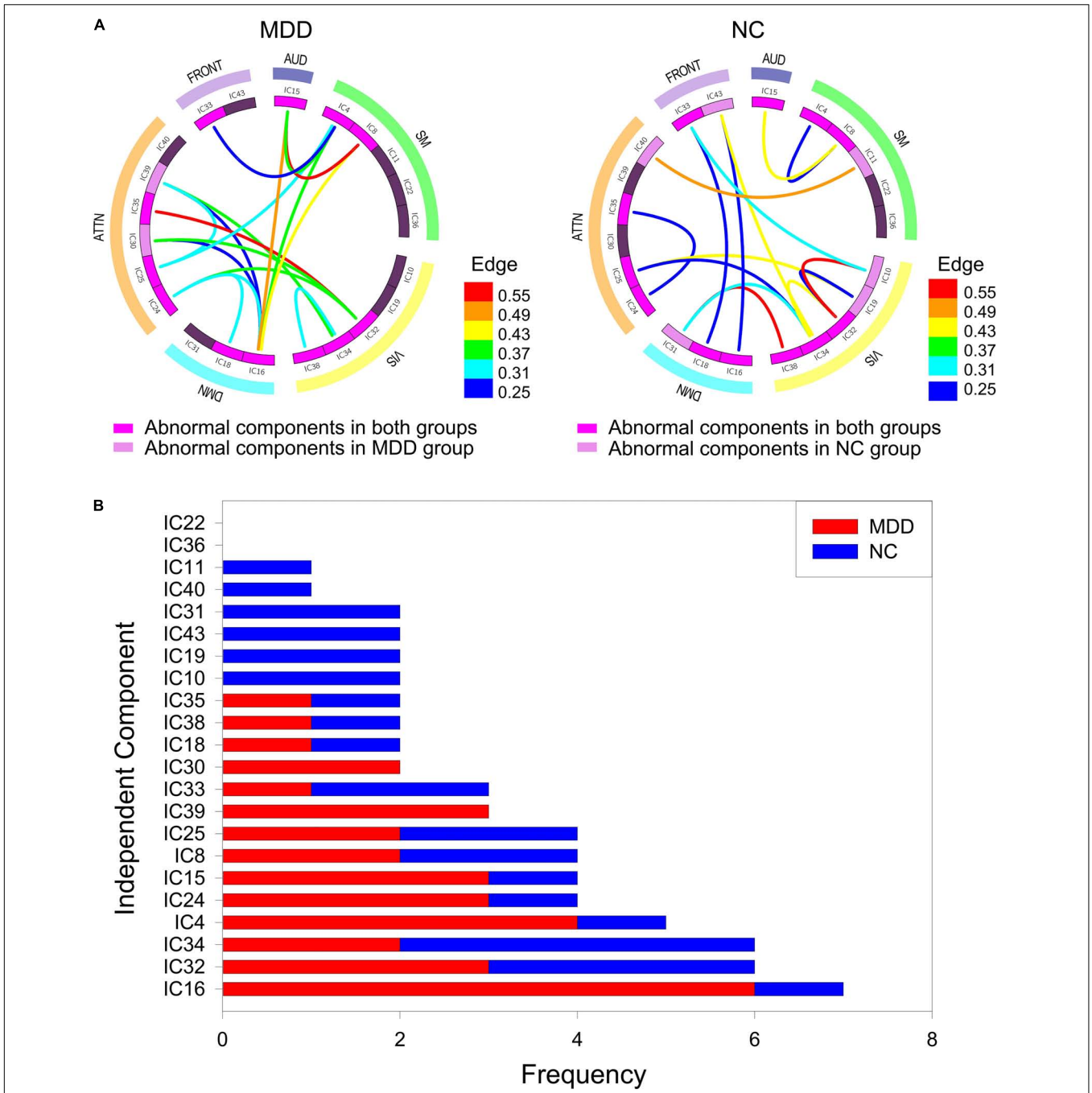

FIGURE 4 | The abnormal independent components of subgraph feature. **(A)** Represents all discriminative subgraphs were combined in each group. AUD, auditory network; SM, sensorimotor network; VIS, visual network; DMN, default mode network; ATTN, attentional network; FRONT, frontal network. Edge refers to the edges are assigned with a probability of existence. **(B)** Represents a statistical chart about the occurrences of these independent components in **(A)**.

The detailed steps taken to perform thresholding for discriminative subgraphs in an uncertain brain network were as follows. First, after construction of the uncertain brain network, we separately used the unFEPG algorithm to the NC group and then to the MDD group to obtain corresponding frequent subgraphs. Next, we used the dfsSI method to measure discriminative scores and extracted the top k subgraph features from the NC group and the MDD group as discriminative subgraph features; ranging features were set to 10–130 with a step size of 10. Then, based on the specific sparsity in a certain brain network, and by applying the thresholding method, the discriminative subgraph features in the uncertain network were changed into the corresponding discriminative subgraph in the certain network. Accordingly,

TABLE 4 | Comparison of classification performance for different researches.

Method	Research	Disease	Accuracy	Sensitivity	Specificity
Frequent subgraph mining of uncertain graphs	PV-FC	MDD	77.85%	81.18%	72.43%
	unFEPG method	MDD	79.15%	86.58%	65.29%
	unFEPG and dfsSI method	MDD	92.90%	93.40%	85.83%
	DUG method (Kong et al., 2013)	ADNI	71.70%	–	–
		MDD	81.04%	88.50%	68.26%

The PV-FC method represents probability values representing functional connections. The unFEPG method represents frequent subgraph pattern mining algorithm based on pattern growth of frequent edge. The unFEPG and dfsSI method represents combining frequent subgraph pattern mining algorithm based on pattern growth of frequent edge and discriminative feature selection method based on statistical index. The DUG method represents the traditional discriminative feature selection for uncertain graph classification algorithm. MDD, major depressive disorder; ADNI, Alzheimer's disease.

we were able to construct a corresponding classification feature matrix for the certain brain network. Finally, SVMs were adopted to carry out classification and the 10-fold cross-validation was repeated 100 experiments to validate the classification performance.

Weighting of Discriminative Subgraphs in the Certain Brain Network

In this part of the study, we used the well-known gSpan algorithm (Yan, 2002) to extract frequent subgraphs from the certain network. Due its high efficiency for graph traversal and subgraph mining, the gSpan algorithm has been widely employed in neuroimaging (Du et al., 2016; see **Supplementary Text S5**). To ensure the consistency of this experiment, the maximum total number of discrimination subgraphs for the certain network was set at 130.

Next, we first took the discriminative subgraph patterns obtained from certain networks as subgraph features, and then proposed the weighting method to map them to the uncertain network. The specific weighting method process was as follows. The weight of each edge in the certain network was separated into two values: 0 and 1; in other words, the edge of certain network includes two states, existent and non-existent. During the procedure of subgraph conversion, each edge weight in the certain network was regarded as the probability of the edge in the uncertain network. Here, it should be noted that according to the specific sparsity, the discriminative subgraph features of each certain network must include a corresponding uncertain discriminative subgraph. An example of weighting is shown in **Figure 5**.

The detailed steps used to weight discriminative subgraphs in the certain brain network were as follows. First, a corresponding certain network was constructed by ranging different sparsity from 0.05 to 0.4, with a step size of 0.05. Second, based on each brain network being constructed with a specific sparsity, the gSpan algorithm was used to mine frequent subgraphs. Third, the discriminative score was calculated using the frequency differences for the NC group and MDD group. The top k subgraph features for the NC group and the MDD group were then extracted as discriminative subgraph features for the certain brain network; ranging features were set to 10–130 with a step size of 10. Then, for each specific sparsity, based on the weighting method, the discriminative subgraph features in the certain brain network constructed by the specific sparsity were mapped into the corresponding discriminative subgraph in the uncertain network. On this basis, we were able to construct a corresponding classification feature matrix for the uncertain brain network, based on the certain brain network constructed by each specific sparsity. Finally, SVMs were adopted to carry out classification and 10-fold cross-validation was repeated 100 experiments to validate classification performance.

Comparison of Classification Results

Thresholding Discriminative Subgraphs in the Uncertain Brain Network

Based on the sparsity in the certain brain network, we used the thresholding method to map discriminative subgraph features of the uncertain brain network to the certain network. Then, under these consistent discriminative subgraph patterns, classification performance was compared between the uncertain network and the certain brain network. Classification results are shown in **Figure 6**; following the thresholding of discriminative subgraphs for the uncertain network and when considering all discriminative subgraph features, the classification accuracy for the uncertain brain network was better than that of the certain brain network with a sparsity of 0.05–0.25 and was lower than that of the certain brain network with a sparsity of 0.3–0.4.

Weighting Subgraphs in the Certain Brain Network

Based on the weighting method, the discriminative subgraphs obtained from the certain brain network constructed by each specific sparsity were matched to the uncertain brain network. Then, under these consistent and discriminative subgraph patterns, we compared the classification performance between the certain network and the uncertain brain network. The classification results are shown in **Figure 7**. With increasing sparsity, the classification accuracy of the uncertain network was consistently higher than that of the certain network. The classification accuracy of the uncertain network was consistently lower than that of the certain network until the sparsity reached 0.35.

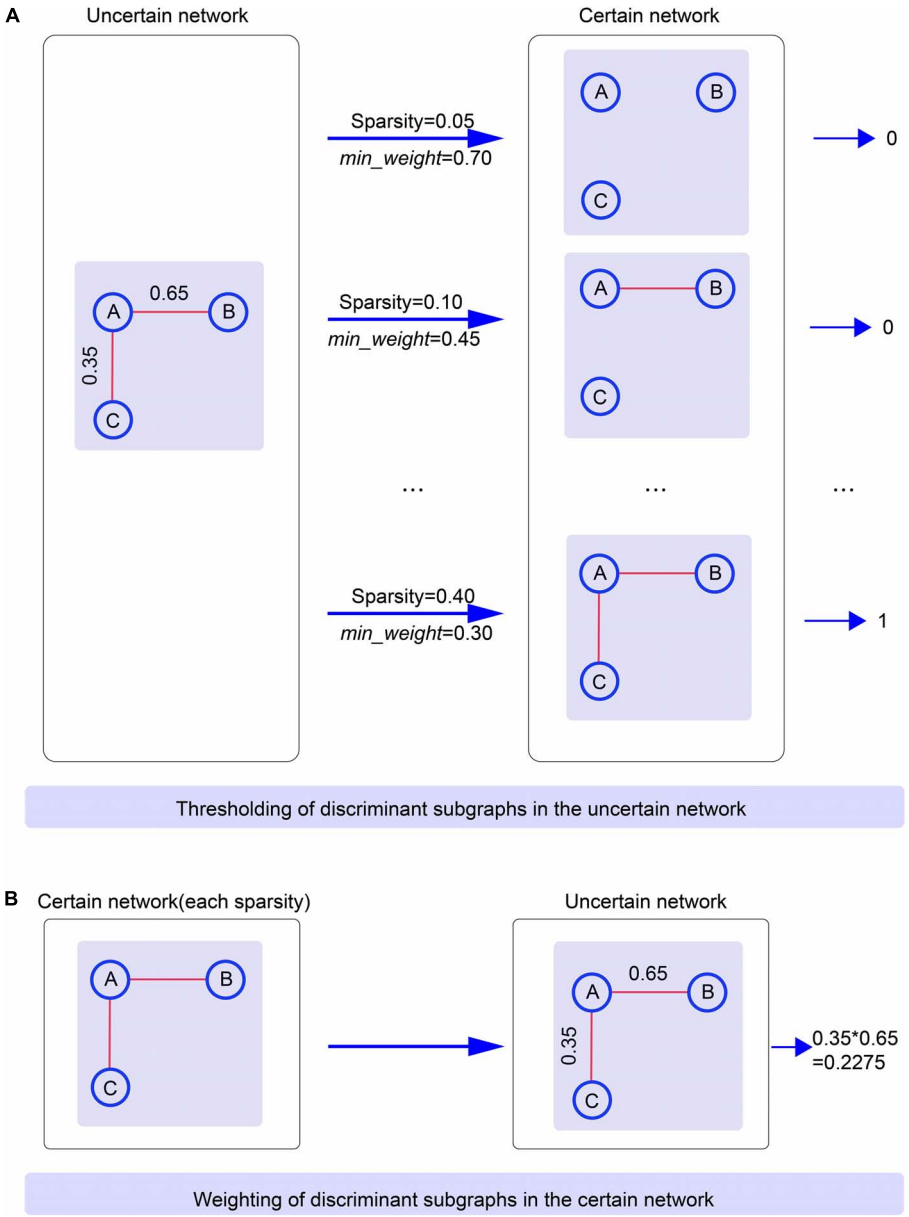

FIGURE 5 | The process of thresholding and weighting between uncertain networks and certain brain networks. Specific clarification is that **(A)** Illustrates the thresholding of discriminant subgraphs in the uncertain network. **(B)** Illustrates the weighting of discriminant subgraphs in the certain network.

DISCUSSION

Considering the inability to provide effective classification information in the existing subgraph mining and selection methods of uncertain brain network (Papapetrou et al., 2011; Kong et al., 2013), we proposed unFEPG and dfsSI algorithm for subgraph mining and selection in uncertain network. First, we constructed an uncertain brain network to represent the uncertain information with regards to functional connection. Then, the unFEPG algorithm was used to mine frequent subgraphs. Next, dfsSI algorithm was used to select the discriminant subgraph. Finally, SVM was used for classification. The results show that compared with the conventional methods, our uncertain brain network classification method greatly improved the diagnostic accuracy for depression's disease.

Abnormal Components

The best classification performance was obtained when 30 frequent subgraph patterns were selected as discriminative subgraph patterns (NC: 15; MDD: 15). Therefore, we analyzed the most discriminative abnormal components obtained by 30 discriminative subgraphs. First, the number of times each IC appeared in all discriminative subgraphs was determined. Then, the top three components were considered to be the most

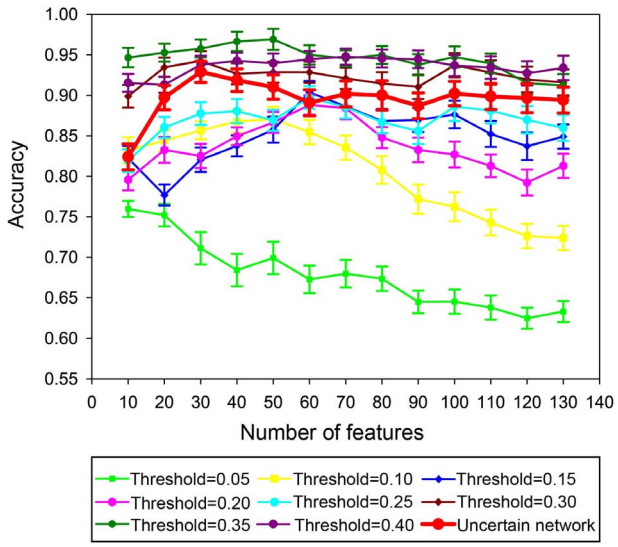

FIGURE 6 | Classification performance using the thresholding method to map discriminative subgraph features of the uncertain brain network to the certain network. The ordinate denotes the accuracy, and the abscissa indicates different feature numbers.

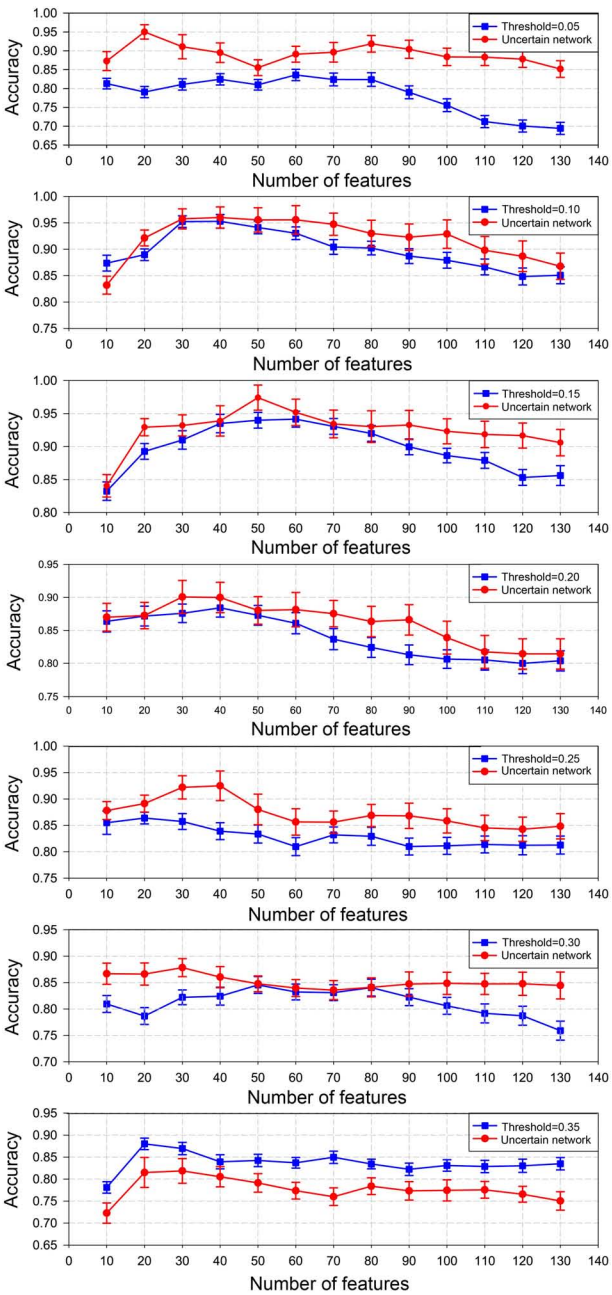

FIGURE 7 | Classification performance using the weighting method to map discriminative subgraph features of the certain brain network to the uncertain network. The ordinate denotes the accuracy, and the abscissa indicates different feature numbers.

discriminative components (IC16, IC32, and IC34). Of these, IC16 was contained in the DMN. The DMN can be regarded as a high-level cognitive network system; the main function of this network is self-reference. In previous studies, researchers confirmed that the default network was significantly associated with depression (Chen et al., 2015; Zhou H.-X. et al., 2020). In addition, the remaining two discriminative components, IC32 and IC34, were contained in the visual network. The visual network is mainly responsible for the preliminary information processing of stimuli and is regulated by specific regions, such as attention. Existing studies have shown that the pathological mechanisms underlying MDD are related to the visual network; when the visual processing time was significantly increased, the connection pattern was abnormal (Wang et al., 2019). These abnormalities may relate to the selective attention and working memory disorders that occur in depressive patients (Moreno-Ortega et al., 2019). Therefore, the abnormal component results obtained in this experiment are consistent with those in the literature. In addition, we further discussed the pathological mechanism of depression from the brain regions to which the discriminative ICs belong (see **Supplementary Text S6**). According to brain regions, it could also be concluded that the markers of depression in current study were the same as the existing research.

Classification Results

The PV-FC, the unFEPG method, the combined unFEPG and dfsSI method, and the traditional DUG method, were respectively applied to the MDD and NC groups for classification purposes, as shown in **Table 4**. The classification results of the method proposed in this paper (a combination of the unFEPG and dfsSI methods) were higher than those of the PV-FC, the unFEPG and traditional DUG methods. Among the other three methods, PV-FC has the lowest accuracy. This suggested that the classification performance can be improved after using graph theory to measure and characterize the uncertain brain network. Conversely, the classification results obtained by the unFEPG and dfsSI method were higher than those obtained from the unFEPG method. This may be due to the selection of the

most discriminative subgraph features on the basis of frequent subgraphs. However, the unFEPG method only utilized frequent subgraph feature mining and did not select discriminative subgraphs. This made led to the inclusion of more features with too much redundant information, fewer features related to class labels, and significant information loss. Accordingly, the generalization ability of the model was reduced (Nouinou et al., 2018). This result was also confirmed by the classification results relating to the selection of the number of discriminative subgraph features (see section "Classification Results"). In the current study, we considered the influence of the number of discriminative subgraph features to evaluate the classification model; the number of discriminative subgraph features ranged from 10 to 100, with a step size of 10. We found that when the number of discriminative subgraph features exceeded 30 and gradually increased, the classification results gradually decreased. This result suggests that some frequent subgraph features were not strongly correlated with brain diseases and could not effectively classify brain diseases (i.e., MDD). Therefore, it is necessary to select more discriminative subgraph features to perform classification when using frequent subgraphs.

The classification results obtained by the unFEPG and dfsSI method was higher than the traditional DUG method. This may be because the unFEPG and dfsSI method fully considered uncertain information in the uncertain brain network. The DUG method was predominantly based on the number of occurrences for each subgraph feature and then used dynamic programming to calculate the probability distribution of all possible occurrences for each subgraph in all samples. For example, for a selected subgraph, the number of possible occurrences of the subgraph in all uncertain brain networks was set as 0-n (n is the number of subjects). Next, the dynamic programming method was used to calculate the probability distribution of the subgraph in which the number of occurrences of the subgraph was i (i = 0,...,n). Furthermore, the score of the subgraph for when the number of occurrences of the subgraph was i was calculated based on the discriminant score function theory in the certain brain network. Finally, based on the probability distribution of all possible occurrences and the corresponding scores, the discriminant score of the subgraph was calculated by using statistical indicators.

However, the unFEPG and dfsSI method did not consider the number of possible occurrences of the subgraph feature in all sample sets, calculate the probability distribution for all possible occurrences, and then determine the discriminant score of a subgraph by measuring statistical indicators. Instead, our method was inspired by a certain brain network that can be regarded as a special uncertain brain network with a probability of 1 for each edge. From the perspective of probability, that is, starting from the uncertain information contained in the uncertain brain network, the number of occurrences of the subgraphs in the discriminant score function was regarded as the sum of the probabilities in all samples. Furthermore, considering the balance between sample sizes, the sum of the probabilities of a subgraph was transformed into a mean probability which was then applied to the discriminant score function to calculate the discriminant score of a subgraph. That is, the uncertain information contained in the uncertain brain network was fully considered. Moreover, compared with the DUG method, the time consumption associated with our combined method was greatly reduced. This result implies that more effective discriminative subgraph features in the uncertain brain network would be selected, the ability to distinguish differences between the MDD and NC groups would be improved, and more accurate biological markers of depression would be obtained when the uncertain information of the uncertain brain network was considered.

Furthermore, we used thresholding and weighting methods to generate consistent discriminative subgraph patterns for uncertain networks and certain networks, and bidirectionally compared the classification performance of these network models. We found that the classification performance of the uncertain network was superior to that of the certain network within a defined sparsity range (**Figures 6**, **7**), regardless of the thresholding method (discriminative subgraphs from the uncertain brain network were converted to the certain brain network) or weighting method (discriminative subgraphs of the certain brain network were converted to the uncertain brain network). The underlying reason is that the number of edges, and the information contained in the certain network, also increased when the sparsity gradually increased. The frequent subgraph pattern of the certain network might be superior to the subgraph pattern of the corresponding uncertain network; thus, the classification accuracy of the certain network was greater than that of the uncertain network.

These results show that the classification accuracy for brain diseases was related to the effective information contained within its subgraph features. To achieve a better classification performance, it is necessary to select a certain brain network with a higher threshold or an uncertain brain network model. Moreover, if an uncertain brain network model is selected, then it is necessary to make full use of the uncertain information related to its functional connections.

The Discussion of Time Complexity Between This Algorithm and Mining Uncertain Subgraph Patterns Algorithm

Previous studies mainly used three methods for the data-driven analysis of uncertain graphs, including frequent subgraph pattern mining, clustering algorithm calculation for uncertain graphs, and shortest and minimum generation based trees (Potamias et al., 2010; Khan et al., 2018b). The frequent subgraph pattern mining has been used in the field of neuroimaging. Therefore, we proposed to use this novel approximate frequent subgraph algorithm in the current study based on the fact that it has been widely used to apply the frequent subgraph algorithm (the MUSE algorithm; Zou et al., 2009; Kong et al., 2013) on uncertain graphs.

Although the traditional MUSE algorithm adopts the approximation algorithm, alongside expected support and spatial clipping technology, to reduce temporal and space complexity, the computational consumption incurred by this technique is still large (Papapetrou et al., 2011). Therefore, we improved upon

this algorithm and proposed an approximation algorithm to generate the unFEPG algorithm, in which the pattern growth of frequent edge was applied to replace the original pruning process on frequent subgraphs. This technique reduced the time complexity associated with the algorithm, thus improving upon the traditional method which takes too long because it considers too many subgraph patterns during frequent subgraph mining. Specifically, the traditional algorithm uses the APRIOR property to crop the entire search space. In contrast, in our research, we adopted the pattern growth method; that is, we replaced the traditional pruning process with the growth of frequent edges on the frequent subgraph, thus reducing time consumption. In addition, the traditional algorithm incorporated the subgraph isomorphism algorithm when calculating the expected support, although the judgment required by subgraph isomorphism is still time-consuming (Huan et al., 2003). However, the unFEPG algorithm proposed in this study encoded edges and applied the depth-first search method, so that we were able to prune the search space within the database. This allowed for additional optimization due to early termination and efficient scheduling to avert expensive subgraph isomorphism tests.

In conclusion, this proposed algorithm was superior to the traditional MUSE algorithm in terms of computational consumption. The computational cost for the two algorithms was investigated in each minimum support threshold (*minsup*) using the same dataset. Same as this article, *minsup* was selected from 0.15 to 0.35, with a step size of 0.05; results are shown in **Figure 8**.

The Validation of Generalization Performance for the Classification Results

We verified the generalization performance of the proposed method from two aspects. On the one hand, we divided our datasets into a training set and a validation set (they are the same site), where the validation set did not participate in the construction of the classification model at all and did not participate in the process of subgraph feature extraction and selection, but was used directly to validate classification model. On the other hand, we introduced independent validation datasets from other sites and used them to evaluate the generalization performance of classification models.

We randomly divided our dataset into training set and validation set with a ratio of 7:3. As for the training set, after these processes of network construction, subgraph mining, and the selection of discriminative subgraphs, we used the 10-fold cross-validation method to obtain multiple SVM classification models. The generalization performance of the classification model was then evaluated using the validation set. Specifically, the training set data was randomly divided into 10 equal parts, one of which was used as the validation set (Sn) and the remainder as the training set (S-n). S-n was then divided into two parts (training set TR and test set TE). Since different SVM parameter settings led to different results, based on training set TR, classifiers were constructed by choosing different parameters (c, g) values, and the (c, g) value that gave the highest classification accuracy regarding training set TR was determined to be the best parameter. Here, similar to manuscript (c, g) value was set in the [−5, 5] range with a step size of 1. In this way, ten different classification models were built. Then, we used each classification models to predict validation dataset. Finally, the accuracy of each model was averaged as final classification accuracy in this cross-validation. Furthermore, to increase the robustness of our results, dataset partitioning was repeated 20 times and the 10-fold cross-validation in training dataset was repeated 100 times in the experiment, and the mean of the 20*100 results was taken as the final test result. The results are shown in **Supplementary Text S7**, indicating that under each method, the difference between the test accuracy and the classification results obtained in **Table 4** of this paper, about 2–5%, except the subgraph feature with sparsity 0.5. The method proposed in this paper differed by 3%, and finally achieved a test accuracy of 89.56%, which shows that the method proposed in this paper could obtain a satisfactory generalization performance in our dataset.

In addition, we used all site and each site dataset as independent validation datasets to verify the generalization performance of the classifier constructed in this paper. The dataset is obtained from DecNef Project Brain Data Repository[5]. See Tanaka et al. (2021) for the specific demographic information of the subjects. Similar to the validation of above generalization performance. We mainly applied separately the datasets of each site and all site into each of classifiers to perform prediction. The classification results are shown in **Supplementary Text S7**. The results show that the classifier constructed in this paper has reached more than 70% on all independent data sets, and the accuracy in the HUH dataset was the highest, reaching 75%, which is higher than the results in the existing research (Yamashita et al., 2020). This also indicated that the features obtained by the proposed method can construct an effective MDD classifier. For a detailed discussion, see **Supplementary Text S7**.

METHODOLOGY

Many parameters were considered in this study. We found that the final classification performance was different when the parameter selection was different. These parameters mainly referred to the feature number, the support degree *minsup* for frequent subgraph mining, the penalty factor *c* in the SVM model, and the kernel parameter *g* in the kernel function. In the next section, we discuss each of these parameters individually.

The Influence of the Number of Features

In this paper, the unFEPG method was used to obtain the frequent subgraphs of the uncertain brain network, and the dfsSI method was used to calculate the discriminant scores and sort them to select the frequent subgraphs corresponding to the top-*k* discriminant scores as the discriminant subgraphs for classification. Here, the selection of the *k* value will affect the classification, that is, the number of discriminative subgraph features was different, and the classification was different.

[5]https://bicr-resource.atr.jp/decnefpro/

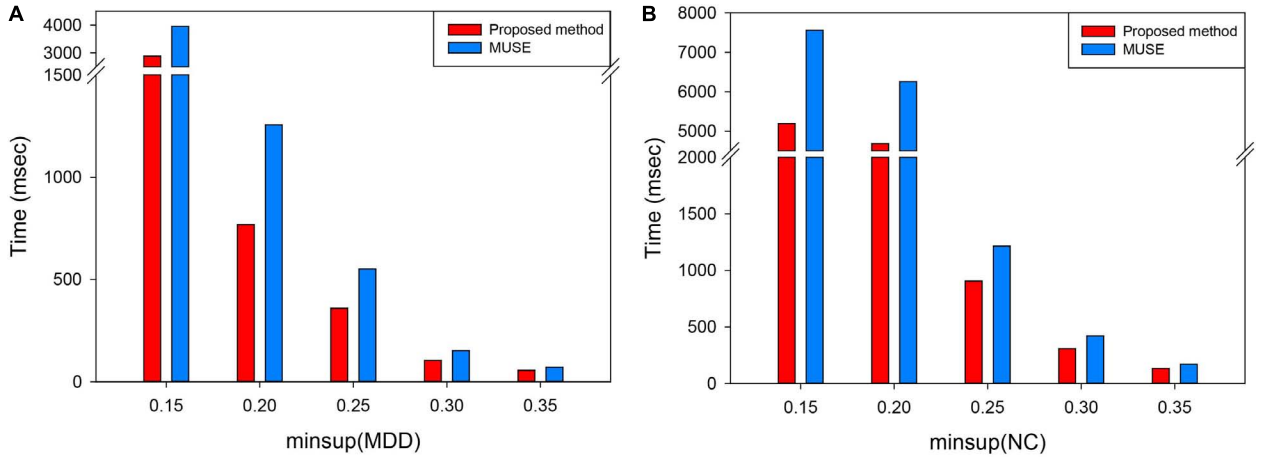

FIGURE 8 | Time complexity under each *minsup* in two groups of subjects. **(A)** Refers to the execution time mining frequent subgraph under each *minsup* in MDD group. **(B)** Refers to the execution time mining frequent subgraph under each *minsup* in NC group. MUSE represents traditional the mining uncertain subgraph patterns algorithm. The proposed method represents unFEPG and dfsSI methods. "msec" refers to millisecond.

Therefore, in present study, the number of features was set to 10–130 with a step size of 10. The classification model was respectively constructed and the effect of the number of features on the classification performance was analyzed. It should be noted that when the number of features was larger than 130, the discriminant score value was almost similar or even smaller. This illustrated that the discriminative ability of these subgraphs was not too great. Thus, in present study, the maximum feature number of the discriminative subgraph was set at 130. As is shown in **Figure 9**, the results show that as the number of features increased, the classification performance gradually decrease after the initial increase. When the number of features was 30, the highest classification accuracy is achieved. The potential reason is that if the feature number is too small, the difference between the MDD group and the NC group is not well expressed; on the contrary, if the number of features is too large, the redundant features would be included, so that affect the construction of the classifier.

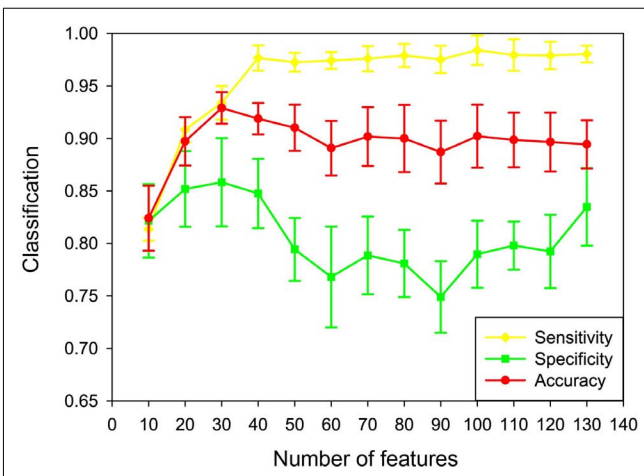

FIGURE 9 | Classification performance based on different feature numbers in the uncertain brain network. Yellow denotes the sensitivity in different feature numbers. Green denotes the specificity in different feature numbers. Red denotes the accuracy in different feature numbers.

The Influence of the *min_sup* of unFEPG Method

Based on fMRI data, mining frequent subgraphs from uncertain networks includes the minimum expected support degree (*min_sup*), which affects the number of frequent subgraphs mined from the uncertain network. In present study, the *min_sup* was set to 0.05–0.35 with a step size of 0.05. These *min_sup* was chosen to analyze the classification performance and the other parameters being fixed. **Figure 10** show that the classification result was the highest when the *min_sup* was set to 0.25. The potential reason is when the *min_sup* selected is too large, many effective frequent subgraph features may be missed at the mining stage, which caused the classification performance is lower. When the *min_sup* selected is too small, the sizes of the frequent subgraphs will be too large, which caused the redundancy of discriminative subgraph features. This also affected the classification performance. The result indicated that if we want to obtain effective frequent subgraphs, the *min_sup* setting should be moderate.

The Influence of Support Vector Machine Classification Parameters *c* and *g*

In the classification process, the two parameters of the SVM model, the penalty factor *c* and the kernel parameter *g*, strongly effect the classification, and thus it is important to finding the optimal values (Chapelle et al., 2002). The penalty factor *c* is applied to adjust the range of confidence intervals in data subspace. The kernel parameter *g* of the RBF is involved to decide

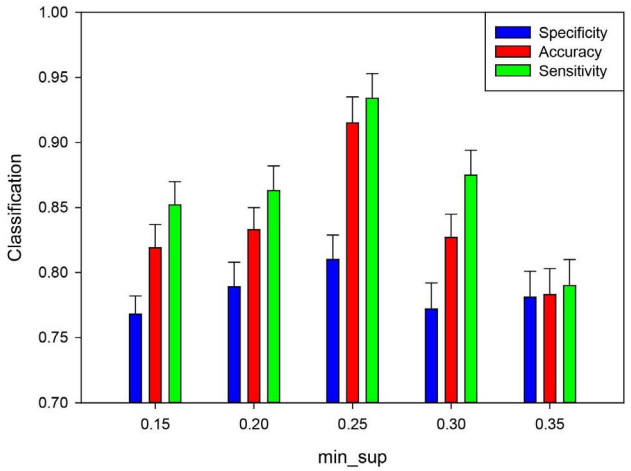

FIGURE 10 | Effect of the minimum support degree (*minsup*) of unFEPG method on the classification performance. Green denotes the sensitivity in different feature numbers. Blue denotes the specificity in different feature numbers. Red denotes the accuracy in different feature numbers.

the function for mapping data to a high-dimensional feature space. Selecting the optimal (c, g) can improve the construction of classification model. For given values of (c, g), we utilized the K-fold cross-validation method to obtain the training set validation accuracy. The values of (c, g) that generated the highest validation classification accuracy were selected as the optimum parameters. The ranges of parameter settings applied for c and g were $[2^{-5}, 2^{5}]$ and $[2^{-8}, 2^{2}]$, with a step of 1. **Figure 11** displays the results of parameter optimization of (c, g) when using classification features as training sets. The results show that when $c = 0.25$ and $g = 0.5$, the classification accuracy of the training sets was the highest, reaching 93.85%.

Limitation

We must also note some limitations of our new method in that the frequent subgraph mining proposed in this paper was a simplified approximate algorithm. This greatly reduced the running time of the algorithm but may have led to the omission of some frequent subgraphs. Therefore, future research should focus on how to further optimize the frequent subgraph mining algorithm for uncertain networks without increasing its computation time. In addition, at the network construction level, we constructed a resting state uncertain brain network in a static form. However, increasing evidence suggests that even in the resting state, the neural activity in the brain still exhibits transient and subtle dynamics. Moreover, these dynamic changes are essential for understanding the basic characteristics relating to brain organization and may be significantly correlated with the pathological mechanisms underlying brain diseases; consequently, these changes may

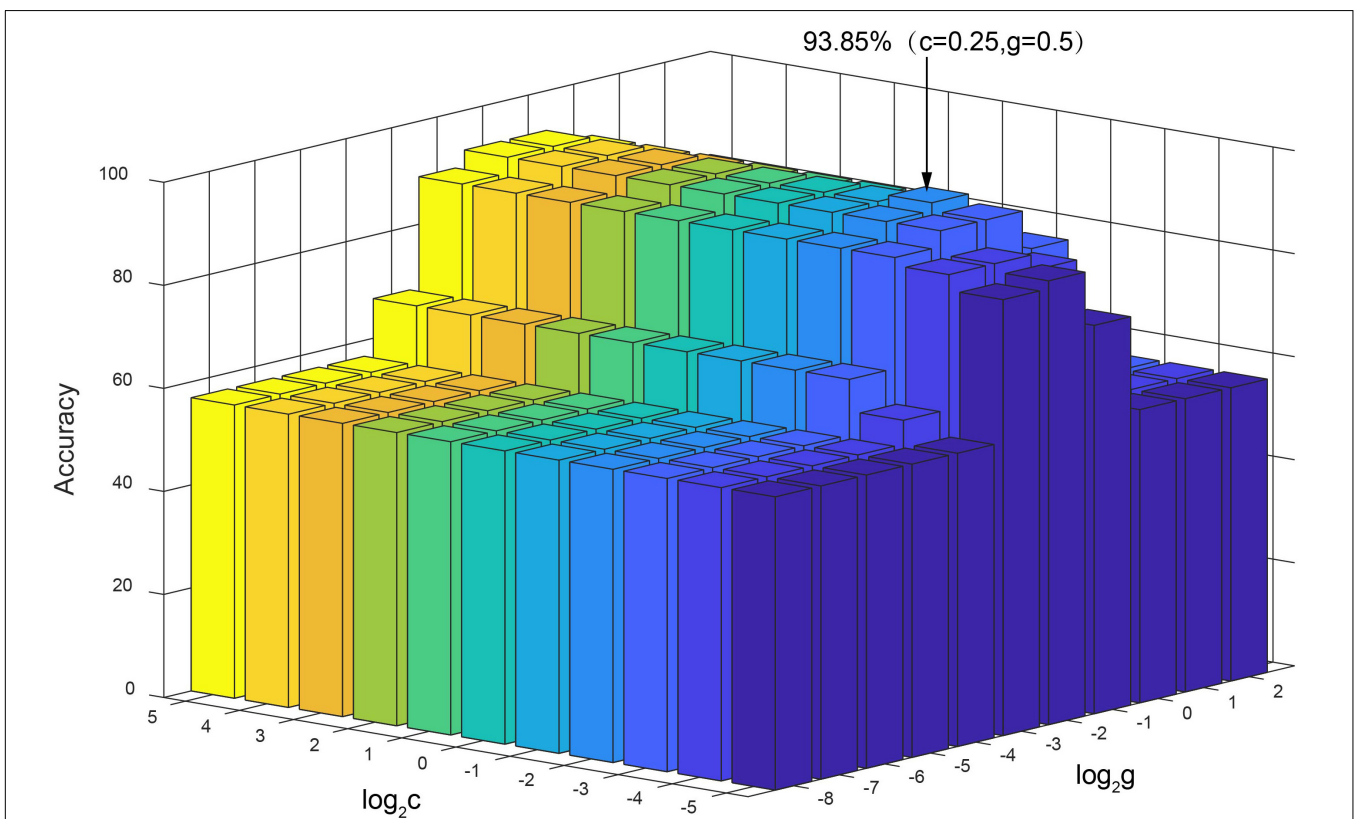

FIGURE 11 | Training classification accuracy of different SVM parameters (c, g).

provide useful information for disease classification (Kudela et al., 2017; Zhao et al., 2020). Therefore, dynamic uncertain brain networks could be introduced for the diagnosis of brain diseases and the exploration of pathological mechanisms in future studies. At the feature extraction level, we adopted subgraph features to represent the topology information of uncertain brain networks, which ignore the local topological property information of uncertain brain networks. In future studies, researchers can combine the local properties of uncertain brain networks [e.g., betweenness centrality and shortest paths (Saha et al., 2021)] to comprehensively characterize the topological information of uncertain brain networks, thus fuse multi-feature to further improve classification validity of the model. At the subgraph selection level, we calculated the discriminative score of frequent subgraphs through the statistical index (i.e., mean) value. However, study has shown that the mean index may not be robust to extreme values (Kong et al., 2013). Therefore, in future research, index such as extreme index (Chen, 2014) can be introduced to satisfy the sensitivity of extreme values between subgraph patterns in uncertain brain networks. At the classification model level, we used traditional machine learning——SVM to classify and diagnose depression. In future research, based on the uncertain brain network model, we can introduce deep learning models such as graph neural network (Zhao et al., 2021) to improve brain psychiatric diseases.

CONCLUSION

Studies have shown that certain brain networks inevitably lead to the loss of uncertain information with regards to functional connections. Therefore, uncertain brain networks are proposed to represent uncertain information with regards to functional connections. The frequent subgraph mining (MUSE) method and the discriminative subgraph method (DUG) cannot effectively extract sufficient subgraph features, thus leading to low classification accuracy in the existing uncertain brain network studies. Therefore, in the present study, we used the unFEPG method to mine frequent subgraphs and used the dfsSI method to select discriminative subgraphs from the perspective of probability, in which uncertain information in the uncertain brain network was fully used to improve the ability to identify differences between the MDD and NC groups. The result showed that the unFEPG and dfsSI method obtained a higher classification accuracy. In addition, to further verify the efficacy of the method proposed in this study, we adopted weighting and thresholding methods to unify the subgraph pattern between the uncertain network and the certain network. The classification performance of the uncertain network was superior to that of the certain network within a defined sparsity range. This meant that a satisfactory effect can be obtained from a certain brain network irrespective of whether a higher threshold or an uncertain brain network model was selected. Moreover, if the uncertain brain network model was selected, it is necessary to make full use of the uncertain information held by its functional connections.

DATA AVAILABILITY STATEMENT

The raw data supporting the conclusions of this article will be made available by the authors, without undue reservation.

ETHICS STATEMENT

The studies involving human participants were reviewed and approved by the Medical Ethics Committee of Shanxi Province (reference number: 2012013). The patients/participants provided their written informed consent to participate in this study.

AUTHOR CONTRIBUTIONS

YL was responsible for the study design and writing the manuscript. ZZ, QL, and TL performed the statistical analysis. IJ integrated the experimental data. HG and JC provided the conception and design of the work. All the authors approved the final version of the manuscript.

FUNDING

This study was supported by research grants from the National Natural Science Foundation of China (61672374, 61741212, 61876124, 61873178, and 61472270), Natural Science Foundation of Shanxi Province (201803D31043 and 201801D121135), CERNET Innovation Project (NGII20170712), Key Research and Development (R&D) Projects of Shanxi Provincial Department of Science and Technology Basic Research (201803D31043, 20210302123129, 20210302124166, and 20210302123099). The sponsors had no role in the design or execution of the study, the collection, management, analysis, and interpretation of the data, or preparation, review, and approval of the manuscript.

ACKNOWLEDGMENTS

We would like to thank Shanxi Xinhan Information Technology Co., Ltd. to provide data analysis services. In section "Validation of Generalization Performance for the Classification Results," the part data used in the preparation of this work were obtained from the DecNef Project Brain Data Repository (https://bicr-resource.atr.jp/srpbsopen/), collected as part of the Japanese Strategic Research Program for the Promotion of Brain Science (SRPBS) supported by the Japanese Advanced Research and Development Programs for Medical Innovation (AMED).

SUPPLEMENTARY MATERIAL

The Supplementary Material for this article can be found online at: https://www.frontiersin.org/articles/10.3389/fnins.2022.889105/full#supplementary-material

REFERENCES

Abouelseoud, A., Starck, T., Remes, J., Nikkinen, J., Tervonen, O., and Kiviniemi, V. (2010). The effect of model order selection in group PICA. *Hum. Brain Mapp.* 31, 1207–1216. doi: 10.1002/hbm.20929

Allen, E. A., Erhardt, E. B., Damaraju, E., Gruner, W., Segall, J. M., Silva, R. F., et al. (2011). A baseline for the multivariate comparison of resting-state networks. *Front. Syst. Neurosci.* 5:2. doi: 10.3389/fnsys.2011.00002

An, H., Rajeev, O., Huang, D., Yang, J., Li, J., Yu, F., et al. (2015). Influence of internal carotid artery stenosis, blood pressure, glycated hemoglobin, and hemoglobin level on fMRI signals of stroke patients. *Neurol. Res.* 37, 502–509. doi: 10.1179/1743132815Y.0000000004

Beckmann, C. F., DeLuca, M., Devlin, J. T., and Smith, S. M. (2005). Investigations into resting-state connectivity using independent component analysis. *Philos. Trans. R. Soc. B Biol. Sci.* 360, 1001–1013. doi: 10.1098/rstb.2005.1634

Ben-Aharon, O., Magnezi, R., Leshno, M., and Goldstein, D. A. (2019). Median survival or mean survival: which measure is the most appropriate for patients, physicians, and policymakers? *Oncologist* 24, 1469–1478. doi: 10.1634/theoncologist.2019-0175

Calhoun, V. D., Kiehl, K. A., and Pearlson, G. D. (2008). Modulation of temporally coherent brain networks estimated using ICA at rest and during cognitive tasks. *Hum. Brain Mapp.* 29, 828–838. doi: 10.1002/hbm.20581

Cao, B., Kong, X., and Yu, P. S. (2015a). A review of heterogeneous data mining for brain disorder identification. *Brain Inf.* 2, 253–264. doi: 10.1007/s40708-015-0021-3

Cao, B., Zhan, L., Kong, X., Yu, P. S., Vizueta, N., Altshuler, L. L., et al. (2015b). "Identification of discriminative subgraph patterns in fMRI brain networks in bipolar affective disorder," in *Brain Informatics and Health*, eds Y. Guo, K. Friston, F. Aldo, S. Hill, and H. Peng (Cham: Springer International Publishing), 105–114. doi: 10.1007/978-3-319-23344-4_11

Chapelle, O., Vapnik, V., Bousquet, O., and Mukherjee, S. (2002). Choosing multiple parameters for support vector machines. *Mach. Learn.* 46, 131–159. doi: 10.1023/A:1012450327387

Chen, E. J. (2014). Range statistics and equivalence tests. *J. Simul.* 8, 143–150. doi: 10.1057/jos.2013.23

Chen, Y., Wang, C., Zhu, X., Tan, Y., and Zhong, Y. (2015). Aberrant connectivity within the default mode network in first-episode, treatment-naïve major depressive disorder. *J. Affect. Disord.* 183, 49–56. doi: 10.1016/j.jad.2015.04.052

Chen, Y., Zhao, X., Lin, X., Wang, Y., and Guo, D. (2019). Efficient mining of frequent patterns on uncertain graphs. *IEEE Trans. Knowl. Data Eng.* 31:1. doi: 10.1109/TKDE.2018.2830336

Corbetta, M., and Shulman, G. L. (2002). Control of goal-directed and stimulus-driven attention in the brain. *Nat. Rev. Neurosci.* 3, 201–215. doi: 10.1038/nrn755

Cui, X., Xiang, J., Guo, H., Yin, G., Zhang, H., Lan, F., et al. (2018). Classification of Alzheimer's disease, mild cognitive impairment, and normal controls with subnetwork selection and graph kernel principal component analysis based on minimum spanning tree brain functional network. *Front. Comput. Neurosci.* 12:31. doi: 10.3389/fncom.2018.00031

de Ridder, M., Klein, K., Yang, J., Yang, P., Lagopoulos, J., Hickie, I., et al. (2019). An uncertainty visual analytics framework for fMRI functional connectivity. *Neuroinformatics* 17, 211–223. doi: 10.1007/s12021-018-9395-8

Driver, I. D., Whittaker, J. R., Bright, M. G., Muthukumaraswamy, S. D., and Murphy, K. (2016). Arterial CO_2 fluctuations modulate neuronal rhythmicity: implications for MEG and fMRI studies of resting-state networks. *J. Neurosci.* 36, 8541–8550. doi: 10.1523/JNEUROSCI.4263-15.2016

Du, J., Wang, L., Jie, B., and Zhang, D. (2016). Network-based classification of ADHD patients using discriminative subnetwork selection and graph kernel PCA. *Comput. Med. Imaging Graph.* 52, 82–88. doi: 10.1016/j.compmedimag.2016.04.004

Du, Y., and Fan, Y. (2013). Group information guided ICA for fMRI data analysis. *Neuroimage* 69, 157–197. doi: 10.1016/j.neuroimage.2012.11.008

Erhardt, E. B., Rachakonda, S., Bedrick, E. J., Allen, E. A., Adali, T., and Calhoun, V. D. (2011). Comparison of multi-subject ICA methods for analysis of fMRI data. *Hum. Brain Mapp.* 32, 2075–2095. doi: 10.1002/hbm.21170

Farahani, F. V., Karwowski, W., and Lighthall, N. R. (2020). Application of graph theory for identifying connectivity patterns in human brain networks: a systematic review. *Front. Neurosci.* 13:585. doi: 10.3389/fnins.2019.00585

First, M. B., and Gibbon, M. (1997). *User's Guide for the Structured Clinical Interview for DSM-IV Axis I Disorders: SCID-1 Clinician Version*. Washington, DC: American Psychiatric Pub.

Franceschelli, M., Giua, A., and Pisano, A. (2017). Finite-time consensus on the median value with robustness properties. *IEEE Trans. Automat. Control* 62, 1652–1667. doi: 10.1109/TAC.2016.2590602

Gao, C., and Wang, J. (2010). "Direct mining of discriminative patterns for classifying uncertain data," in *Proceedings of the 16th ACM SIGKDD International Conference on Knowledge Discovery and Data Mining* (Washington, DC: Association for Computing Machinery), 861–870. doi: 10.1145/1835804.1835913

Garrison, K. A., Scheinost, D., Finn, E. S., Shen, X., and Constable, R. T. (2015). The (in)stability of functional brain network measures across thresholds. *Neuroimage* 118, 651–661. doi: 10.1016/j.neuroimage.2015.05.046

Graham, S., Bellmore, A., Nishina, A., and Juvonen, J. (2009). "It Must Be Me": ethnic diversity and attributions for peer victimization in middle school. *J. Youth Adolesc.* 38, 487–499. doi: 10.1007/s10964-008-9386-4

Grill-Spector, K., and Malach, R. (2004). The human visual cortex. *Annu. Rev. Neurosci.* 27, 649–677.

Guo, H., Yan, P., Cheng, C., Li, Y., Chen, J., Xu, Y., et al. (2018). fMRI classification method with multiple feature fusion based on minimum spanning tree analysis. *Psychiatry Res. Neuroimaging* 277, 14–27. doi: 10.1016/j.pscychresns.2018.05.001

Guo, H., Zhang, F., Chen, J., Xu, Y., and Xiang, J. (2017). Machine learning classification combining multiple features of a hyper-network of fMRI data in Alzheimer's disease. *Front. Neurosci.* 11:615. doi: 10.3389/fnins.2017.00615

Guy, W. (1976). ECDEU Assessment Manual for Psychopharmacology. Rockville: Public Health Service, Alcohol, Drug Abuse, and Mental Health Administration.

Hagler, D. J., Hatton, S., Cornejo, M. D., Makowski, C., Fair, D. A., Dick, A. S., et al. (2019). Image processing and analysis methods for the adolescent brain cognitive development study. *Neuroimage* 202:116091. doi: 10.1016/j.neuroimage.2019.116091

Hamdi, S. M., Aydin, B., Boubrahimi, S. F., Angryk, R., Krishnamurthy, L. C., and Morris, R. (2018). "Biomarker detection from fMRI-based complete functional connectivity networks," in *Proceedings of the 2018 IEEE First International Conference on Artificial Intelligence and Knowledge Engineering (AIKE)* (Piscataway, NJ: IEEE), 17–24. doi: 10.1109/AIKE.2018.00011

Huan, J., Wang, W., and Prins, J. (2003). "Efficient mining of frequent subgraphs in the presence of isomorphism," in *Proceedings of the 3rd IEEE International Conference on Data Mining (ICDM 2003)* (Piscataway, NJ: IEEE), 549–552. doi: 10.1109/ICDM.2003.1250974

Jackson, T. S., and Read, N. (2010a). Theory of minimum spanning trees. I. Mean-field theory and strongly disordered spin-glass model. *Phys. Rev. E Stat. Nonlin. Soft Matter Phys.* 81:021130. doi: 10.1103/PhysRevLett.85.840

Jackson, T. S., and Read, N. (2010b). Theory of minimum spanning trees. II. Exact graphical methods and perturbation expansion at the percolation threshold. *Phys. Rev. E Stat. Nonlin. Soft Matter Phys.* 81:021131. doi: 10.1103/PhysRevE.81.021131

Jafri, M. J., Pearlson, G. D., Stevens, M., and Calhoun, V. D. (2008). A method for functional network connectivity among spatially independent resting-state components in schizophrenia. *Neuroimage* 39, 1666–1681. doi: 10.1016/j.neuroimage.2007.11.001

Jie, B., Zhang, D., Wee, C.-Y., and Dinggang, S. (2014). Topological graph kernel on multiple thresholded functional connectivity networks for mild cognitive impairment classification. *Hum. Brain Mapp.* 35, 2876–2897. doi: 10.1002/hbm.22353

Jin, N., and Wang, W. (2011). "LTS: discriminative subgraph mining by learning from search history," in *Proceedings of the 2011 IEEE 27th International Conference on Data Engineering* (Hannover: IEEE), 207–218.

Ke, X., Khan, A., Hasan, M. A., and Rezvansangsari, R. (2020). Reliability maximization in uncertain graphs. *IEEE Trans. Knowl. Data Eng.* 1. [Epub ahead of print]. doi: 10.1109/TKDE.2020.2987570

Khan, A., Ye, Y., and Chen, L. (2018b). On uncertain graphs. *Synth. Lect. Data Manage.* 10, 1–94. doi: 10.2200/S00862ED1V01Y201807DTM048

Khan, A., Bonchi, F., Gullo, F., and Nufer, A. (2018a). "Conditional reliability in uncertain graphs," in *Proceedings of the IEEE Transactions on Knowledge and*

Data Engineering (Piscataway, NJ: IEEE), 2078–2092. doi: 10.1109/TKDE.2018.2816653

Koechlin, E., Ody, C., and Kouneiher, F. (2003). The architecture of cognitive control in the human prefrontal cortex. *Science* 302, 1181–1185. doi: 10.1126/science.1088545

Koechlin, E., and Summerfield, C. (2007). An information theoretical approach to prefrontal executive function. *Trends Cogn. Sci.* 11, 229–235. doi: 10.1016/j.tics.2007.04.005

Kong, X., Fan, W., and Yu, P. S. (2011). "Dual active feature and sample selection for graph classification," in *Proceedings of the 17th ACM SIGKDD International Conference on Knowledge Discovery and Data Mining*, San Diego, CA, 654–662. doi: 10.1145/2020408.2020511

Kong, X., and Yu, P. S. (2014). Brain network analysis: a data mining perspective. *ACM SIGKDD Explor. Newslett.* 15, 30–38. doi: 10.1145/2641190.2641196

Kong, X., Yu, P. S., Wang, X., and Ragin, A. B. (2013). "Discriminative feature selection for uncertain graph classification," in *Proceedings of the 2013 SIAM International Conference on Data Mining* (Philadelphia, PA: SIAM), 82–93. doi: 10.1137/1.9781611972832.10

Krienen, F. M., and Buckner, R. L. (2009). Segregated fronto-cerebellar circuits revealed by intrinsic functional connectivity. *Cereb. Cortex* 19, 2485–2497. doi: 10.1093/cercor/bhp135

Kudela, M., Harezlak, J., and Lindquist, M. A. (2017). Assessing uncertainty in dynamic functional connectivity. *Neuroimage* 149, 165–177. doi: 10.1016/j.neuroimage.2017.01.056

Li, C., Wang, H., de Haan, W., Stam, C. J., and Van Mieghem, P. (2011). The correlation of metrics in complex networks with applications in functional brain networks. *J. Stat. Mech. Theory Exp.* 11:11018. doi: 10.1088/1742-5468/2011/11/p11018

Li, F., Xie, W., Jiang, Y., and Fan, Z. (2020). "A comparative study of uncertain knowledge representation methods," in *Proceedings of the 2020 IEEE 4th Information Technology, Networking, Electronic and Automation Control Conference (ITNEC)*, Chongqing, 2038–2042. doi: 10.1109/ITNEC48623.2020.9084983

Li, J., Kong, R., Liégeois, R., Orban, C., Tan, Y., Sun, N., et al. (2019). Global signal regression strengthens association between resting-state functional connectivity and behavior. *Neuroimage* 196, 126–141. doi: 10.1016/j.neuroimage.2019.04.016

Li, J., Zou, Z., and Gao, H. (2012). Mining frequent subgraphs over uncertain graph databases under probabilistic semantics. *VLDB J.* 21, 753–777. doi: 10.1007/s00778-012-0268-8

Moreno-Ortega, M., Prudic, J., Rowny, S., Patel, G. H., Kangarlu, A., Lee, S., et al. (2019). Resting state functional connectivity predictors of treatment response to electroconvulsive therapy in depression. *Sci. Rep.* 9:5071. doi: 10.1038/s41598-019-41175-4

Nenert, R., Allendorfer, J. B., and Szaflarski, J. P. (2014). A model for visual memory encoding. *PLoS One* 9:e107761. doi: 10.1371/journal.pone.0107761

Nouinou, S., Afia, A. E., and Fkihi, S. E. (2018). "Overview on last advances of feature selection," in *Proceedings of the International Conference on Learning and Optimization Algorithms: Theory and Applications* (Rabat: Association for Computing Machinery), 1–6. doi: 10.1007/978-3-319-67588-6_1

Papapetrou, O., Ioannou, E., and Skoutas, D. (2011). "Efficient discovery of frequent subgraph patterns in uncertain graph databases," in *Proceedings of the 14th International Conference on Extending Database Technology* (Uppsala: ACM), 355–366.

Pinto, J., Nunes, S., Bianciardi, M., Dias, A., Silveira, L. M., Wald, L. L., et al. (2017). Improved 7 Tesla resting-state fMRI connectivity measurements by cluster-based modeling of respiratory volume and heart rate effects. *Neuroimage* 153, 262–272. doi: 10.1016/j.neuroimage.2017.04.009

Potamias, M., Bonchi, F., Gionis, A., and Kollios, G. (2010). k-nearest neighbors in uncertain graphs. *Proc. VLDB Endow.* 3, 997–1008. doi: 10.14778/1920841.1920967

Prokopiou, P. C., Pattinson, K. T. S., Wise, R. G., and Mitsis, G. D. (2018). Modeling of dynamic cerebrovascular reactivity to spontaneous and externally induced CO_2 fluctuations in the human brain using BOLD-fMRI. *Neuroimage* 186, 533–548. doi: 10.1016/j.neuroimage.2018.10.084

Riaz, A., Asad, M., Alonso, E., and Slabaugh, G. (2020). DeepFMRI: end-to-end deep learning for functional connectivity and classification of ADHD using fMRI. *J. Neurosci. Methods* 335:108506. doi: 10.1016/j.jneumeth.2019.108506

Richardson, M. (2010). Current themes in neuroimaging of epilepsy: brain networks, dynamic phenomena, and clinical relevance. *Clin. Neurophysiol.* 121, 1153–1175. doi: 10.1016/j.clinph.2010.01.004

Saha, A., Brokkelkamp, R., Velaj, Y., Khan, A., and Bonchi, F. (2021). Shortest paths and centrality in uncertain networks. *Proc. VLDB Endow.* 14, 1188–1201. doi: 10.14778/3450980.3450988

Seifritz, E., Esposito, F., Hennel, F., Mustovic, H., Neuhoff, J. G., Bilecen, D., et al. (2002). Spatiotemporal pattern of neural processing in the human auditory cortex. *Science* 297, 1706–1708. doi: 10.1126/science.1074355

Sen, B., Mueller, B., Klimes-Dougan, B., Cullen, K., and Parhi, K. K. (2019). "Classification of major depressive disorder from resting-state fMRI," in *Proceedings of the 2019 41st Annual International Conference of the IEEE Engineering in Medicine & Biology Society (EMBC)* (Piscataway, NJ: IEEE), 3511–3514. doi: 10.1109/EMBC.2019.8856453

Shao, W., Peng, Y., Zu, C., Wang, M., and Zhang, D. (2020). Hypergraph based multi-task feature selection for multimodal classification of Alzheimer's disease. *Comput. Med. Imaging Graph.* 80:101663. doi: 10.1016/j.compmedimag.2019.101663

Smith, S. M., Fox, P. T., Miller, K. L., Glahn, D. C., Fox, P. M., Mackay, C. E., et al. (2009). Correspondence of the brain's functional architecture during activation and rest. *Proc. Natl. Acad. Sci. U.S.A.* 106:13040. doi: 10.1073/pnas.0905267106

Specht, K., and Reul, J. (2006). Functional segregation of the temporal lobes into highly differentiated subsystems for auditory perception: an auditory rapid event-related fMRI-task. *Neuroimage* 20, 169–173. doi: 10.1016/j.neuroimage.2003.07.034

Sporns, O. (2011). The human connectome: a complex network. *Ann. N. Y. Acad. Sci.* 1224, 109–125. doi: 10.1111/j.1749-6632.2010.05888.x

Sporns, O. (2018). Graph theory methods: applications in brain networks. *Dialogues Clin. Neurosci.* 20, 111–121. doi: 10.31887/DCNS.2018.20.2/osporns

Stam, C. J., Tewarie, P., Van Dellen, E., Van Straaten, E. C. W., Hillebrand, A., and Van Mieghem, P. (2014). The trees and the forest: characterization of complex brain networks with minimum spanning trees. *Int. J. Psychophysiol.* 92, 129–138. doi: 10.1016/j.ijpsycho.2014.04.001

Steardo, L., Carbone, E. A., Filippis, R. D., Pisanu, C., and Fazio, P. D. (2020). Application of support vector machine on fMRI data as biomarkers in schizophrenia diagnosis: a systematic review. *Front. Psychiatry* 11:588. doi: 10.3389/fpsyt.2020.00588

Steiner, A. R., Rousseau-Blass, F., Schroeter, A., Hartnack, S., and Bettschart-Wolfensberger, R. (2020). Systematic review: anaesthetic protocols and management as confounders in rodent blood oxygen level dependent functional magnetic resonance imaging (BOLD fMRI)–part a: effects of changes in physiological parameters. *Front. Neurosci.* 14:577119. doi: 10.3389/fnins.2020.577119

Tanaka, S. C., Yamashita, A., Yahata, N., Itahashi, T., Lisi, G., Yamada, T., et al. (2021). A multi-site, multi-disorder resting-state magnetic resonance image database. *Sci. Data* 8:227. doi: 10.1038/s41597-021-01004-8

Tewarie, P., Van, D. E., Hillebrand, A., and Stam, C. J. (2015). The minimum spanning tree: an unbiased method for brain network analysis. *Neuroimage* 104, 177–188. doi: 10.1016/j.neuroimage.2014.10.015

Tokuda, T., Yoshimoto, J., Shimizu, Y., Okada, G., Takamura, M., Okamoto, Y., et al. (2018). Identification of depression subtypes and relevant brain regions using a data-driven approach. *Sci. Rep.* 8:14082. doi: 10.1038/s41598-018-32521-z

Tong, Y., Hocke, L. M., and Frederick, B. B. (2019). Low frequency systemic hemodynamic "Noise" in resting state BOLD fMRI: characteristics, causes, implications, mitigation strategies, and applications. *Front. Neurosci.* 13:787. doi: 10.3389/fnins.2019.00787

Vakamudi, K., Posse, S., Jung, R., Cushnyr, B., and Chohan, M. O. (2019). Real-time presurgical resting-state fMRI in patients with brain tumors: quality control and comparison with task-fMRI and intraoperative mapping. *Hum. Brain Mapp.* 41, 797–814. doi: 10.1002/hbm.24840

Van Dellen, E., Sommer, I. E., Bohlken, M. M., Tewarie, P., Draaisma, L., Zalesky, A., et al. (2018). Minimum spanning tree analysis of the human connectome. *Hum. Brain Mapp.* 39, 2455–2471. doi: 10.1002/hbm.24014

Vincent, J. L., Kahn, I., Snyder, A. Z., Raichle, M. E., and Buckner, R. L. (2008). Evidence for a frontoparietal control system revealed by intrinsic functional connectivity. *J. Neurophysiol.* 100, 3328–3342. doi: 10.1152/jn.90355.2008

Wang, Q., Poh, J. S., Wen, D. J., Broekman, B. F. P., Chong, Y.-S., Yap, F., et al. (2019). Functional and structural networks of lateral and medial orbitofrontal cortex as potential neural pathways for depression in childhood. *Depress. Anxiety* 36, 365–374. doi: 10.1002/da.22874

Wig, G. S. (2017). Segregated systems of human brain networks. *Trends Cogn. Sci.* 21, 981–996. doi: 10.1016/j.tics.2017.09.006

Williams, J. B. (1988). A structured interview guide for the Hamilton Depression Rating Scale. *Arch. Gen. Psychiatry* 45, 742–747. doi: 10.1001/archpsyc.1988.01800320058007

Yamashita, A., Sakai, Y., Yamada, T., Yahata, N., Kunimatsu, A., Okada, N., et al. (2020). Generalizable brain network markers of major depressive disorder across multiple imaging sites. *PLoS Biol.* 18:e3000966. doi: 10.1371/journal.pbio.3000966

Yan, X. (2002). "gSpan: graph-based substructure pattern mining," in *Proceedings of the 2002 IEEE International Conference on Data Mining* (Piscataway, NJ: IEEE), 721–724. doi: 10.1109/ICDM.2002.1184038

Yan, X., Cheng, H., Han, J., and Yu, P. S. (2008). "Mining significant graph patterns by leap search," in *Proceedings of the 2008 ACM SIGMOD International Conference on Management of Data (SIGMOD)*, Vancouver, BC, 433–444. doi: 10.1145/1376616.1376662

Yuan, Y., Wang, G., Chen, L., and Ning, B. (2016). Efficient pattern matching on big uncertain graphs. *Inf. Sci.* 339, 369–394. doi: 10.1016/j.ins.2015.12.034

Zhang, D., Huang, J., Jie, B., Du, J., Tu, L., and Liu, M. (2018). Ordinal pattern: a new descriptor for brain connectivity networks. *IEEE Trans. Med. Imaging* 37, 1711–1722. doi: 10.1109/TMI.2018.2798500

Zhang, Y., Lin, H., Yang, Z., Wang, J., and Liu, Y. (2017). An uncertain model-based approach for identifying dynamic protein complexes in uncertain protein-protein interaction networks. *BMC Genomics* 18(Suppl. 7):743. doi: 10.1186/s12864-017-4131-6

Zhang, Y., Wu, W., Toll, R. T., Naparstek, S., and Etkin, A. (2021). Identification of psychiatric disorder subtypes from FC patterns in rsEEG. *Nat. Biomed. Eng.* 5, 309–323. doi: 10.1038/s41551-020-00614-8

Zhao, F., Chen, Z., Rekik, I., Lee, S. W., and Shen, D. (2020). Diagnosis of autism spectrum disorder using central-moment features from low- and high-order dynamic resting-state functional connectivity networks. *Front. Neurosci.* 14:258. doi: 10.3389/fnins.2020.00258

Zhao, K., Duka, B., Xie, H., Oathes, D. J., Calhoun, V., and Zhang, Y. (2021). A dynamic graph convolutional neural network framework reveals new insights into connectome dysfunctions in ADHD. *Neuroimage* 246:118774. doi: 10.1016/j.neuroimage.2021.118774

Zhou, H.-X., Chen, X., Shen, Y.-Q., Li, L., Chen, N.-X., Zhu, Z.-C., et al. (2020). Rumination and the default mode network: meta-analysis of brain imaging studies and implications for depression. *Neuroimage* 206:116287. doi: 10.1016/j.neuroimage.2019.116287

Zhou, Z., Chen, X., Zhang, Y., Qiao, L., Yu, R., Pan, G., et al. (2020). Brain network construction and classification toolbox (BrainNetClass). *Hum. Brain Mapp.* 41, 2808–2826. doi: 10.1002/hbm.24979

Zou, Z., Li, J., Gao, H., and Zhang, S. (2009). "Frequent subgraph pattern mining on uncertain graph data," in *Proceeding of the 18th ACM Conference on Information and Knowledge Management, CIKM'09*, Hong Kong, 583–592. doi: 10.1145/1645953.1646028

Zou, Z., Li, J., Gao, H., and Zhang, S. (2010). Mining frequent subgraph patterns from uncertain graph data: mining large uncertain and probabilistic databases. *IEEE Trans. Knowl. Data Eng.* 22, 1203–1218. doi: 10.1109/TKDE.2010.80

Conflict of Interest: The authors declare that the research was conducted in the absence of any commercial or financial relationships that could be construed as a potential conflict of interest.

Publisher's Note: All claims expressed in this article are solely those of the authors and do not necessarily represent those of their affiliated organizations, or those of the publisher, the editors and the reviewers. Any product that may be evaluated in this article, or claim that may be made by its manufacturer, is not guaranteed or endorsed by the publisher.

frontiers | Frontiers in Neuroscience

ORIGINAL RESEARCH
published: 02 May 2022
doi: 10.3389/fnins.2022.839194

Structural and Functional Characterization of Gray Matter Alterations in Female Patients With Neuropsychiatric Systemic Lupus

*Li Su[1,2,3], Zhizheng Zhuo[4], Yunyun Duan[4], Jing Huang[5], Xiaolu Qiu[5], Mengtao Li[2,3], Yaou Liu[4] and Xiaofeng Zeng[2,3]**

[1] Department of Rheumatology and Clinical Immunology, Xuanwu Hospital, Capital Medical University, Beijing, China, [2] Department of Rheumatology and Clinical Immunology, Peking Union Medical College Hospital, Chinese Academy of Medical Sciences & Peking Union Medical College, Beijing, China, [3] Key Laboratory of Rheumatology and Clinical Rheumatology, National Clinical Research Center for Dermatologic and Immunologic Diseases, Ministry of Education, Beijing, China, [4] Department of Radiology, Beijing Tiantan Hospital, Capital Medical University, Beijing, China, [5] Department of Radiology, Xuanwu Hospital, Capital Medical University, Beijing, China

Objective: To investigate morphological and functional alterations within gray matter (GM) in female patients with neuropsychiatric systemic lupus (NPSLE) and to explore their clinical significance.

Methods: 54 female patients with SLE (30 NPSLE and 24 non-NPSLE) and 32 matched healthy controls were recruited. All subjects received a quantitative MRI scan (FLAIR, 3DT1, resting-state functional MRI). GM volume (GMV), fractional amplitude of low-frequency fluctuation (fALFF), regional homogeneity (ReHo), and degree of centrality (DC) were obtained. Between-group comparison, clinical correlation, and discrimination of NPSLE from non-NPSLE were achieved by voxel-based analysis, cerebellar seed-based functional connectivity analysis, regression analysis, and support vector machine (SVM), respectively.

Results: Patients with NPSLE showed overt subcortical GM atrophy without significantly abnormal brain functions in the same region compared with controls. The dysfunction within the left superior temporal gyri (L-STG) was found precede the GM volumetric loss. The function of the nodes in default mode network (DMN) and salience network (SN) were weakened in NPSLE patients compared to controls. The function of the cerebellar posterior lobes was significantly activated in non-NPSLE patients but attenuated along with GM atrophy and presented higher connectivity with L-STG and DMN in NPSLE patients, while the variation of the functional activities in the sensorimotor network (SMN) was the opposite. These structural and functional alterations were mainly correlated with disease burden and anti-phospholipid antibodies (aPLs) (r ranges from -1.53 to 1.29). The ReHos in the bilateral cerebellar posterior lobes showed high discriminative power in identifying patients with NPSLE with accuracy of 87%.

Conclusion: Patients with NPSLE exhibit both structural and functional alterations in the GM of the brain, which especially involved the deep GM, the cognitive, and sensorimotor regions, reflecting a reorganization to compensate for the disease damage to the brain which was attenuated along with pathologic burden and cerebral vascular

OPEN ACCESS

Edited by:
Yuqi Cheng,
The First Affiliated Hospital of Kunming Medical University, China

Reviewed by:
Baoci Shan,
Institute of High Energy Physics (CAS), China
Xize Jia,
Hangzhou Normal University, China
Dongbao Zhao,
Changhai Hospital, China

****Correspondence:***
Xiaofeng Zeng
zengxfpumc@163.com

Specialty section:
This article was submitted to Brain Imaging Methods, a section of the journal Frontiers in Neuroscience

Received: *19 December 2021*
Accepted: *05 April 2022*
Published: *02 May 2022*

Citation:
Su L, Zhuo Z, Duan Y, Huang J, Qiu X, Li M, Liu Y and Zeng X (2022) Structural and Functional Characterization of Gray Matter Alterations in Female Patients With Neuropsychiatric Systemic Lupus. Front. Neurosci. 16:839194. doi: 10.3389/fnins.2022.839194

risk factors. The GM within the left temporal lobe may be one of the direct targets of lupus-related inflammatory attack. The function of the cerebellar posterior lobes might play an essential role in compensating for cortical functional disturbances and may contribute to identifying patients with suspected NPSLE in clinical practice.

Keywords: neurosychiatric systemic lupus, gray matter, resting sate fMRI, female, cerebellar seed-based functional connectivity

INTRODUCTION

Systemic lupus erythematosus (SLE) is a chronic autoimmune disorder involving multiple organ systems, typically presents in females of childbearing age, with the incidence ratio of female to male is around 9:1 (Mok et al., 1999). The role of female reproductive hormones in the development of the disease has been reported (Costenbader et al., 2007). Neuropsychiatric systemic lupus (NPSLE) is one of the most common manifestations of lupus, affecting 21–95% of patients with SLE and related to high disability and mortality (Pamfil et al., 2015). The central nervous system is involved in approximately 90% of patients with NPSLE, with various clinical manifestations, including cognitive impairment, headache, mood disorders, cerebrovascular disease, psychosis, seizures, and acute confusional state, etc. (Pamfil et al., 2015).

The pathogenesis of NPSLE is not yet fully clear, but several mechanisms are implicated, including autoimmune inflammatory neuronal damage, vasculitis and vasculopathy with ischemia, precocious atherosclerosis, and embolisms (Cohen et al., 2017; Gelb et al., 2018). The diagnosis of NPSLE in clinical practice still requires the judgment of experienced physicians. Correct attribution of neuropsychiatric events to NPSLE or an alternative etiology is still a challenge, considering the absence of a diagnostic gold standard. Magnetic resonance imaging (MRI) of the brain has been applied to SLE for years, but the findings are nonspecific; the most common presentations of conventional MRI are cerebral atrophy (15–20%), diffused white matter (WM) lesions or hyperintensities (30–75%), focal lesions after stroke, etc (Sarbu et al., 2015). However, more than 40% of patients with NPSLE showed no remarkable changes on conventional MRI (Luyendijk et al., 2011). Hence, advanced brain imaging techniques (e.g., structural and resting state functional MRI) have been applied into this field to successfully characterize the brain microstructural and functional abnormalities, to study *in vivo* neural mechanisms of neurologic and psychiatric manifestations of the disease invisible with only structural imaging, attempting to help classify and evaluate patients with suspected NPSLE in clinical practice (Sarbu et al., 2017). Resting state (RS) functional connectivity (FC) abnormalities have been reported both in NPSLE patients and non-NPSLE patients (Nystedt et al., 2019; Bonacchi et al., 2020; Cao et al., 2021), suggesting reorganizations of the neuronal networks may take place even before the onset of neuropsychiatric symptoms, and may be adaptive or maladaptive to the brain functional impairments.

Meanwhile, previous neuroimaging studies suggest that lupus patients have characteristic subcortical and regional gray matter atrophy when compared to controls (Jung et al., 2010; Kalinowska-Łyszczarz et al., 2018), and that these group differences may be more significant in NPSLE patients. However, other functional MRI research of SLE patients indicated an apparent lack of overlap between gray matter volume reduction and functional alterations. The different patterns of relationship between the structure and function of brain found in the disease worth exploring more deeply (Lin et al., 2011).

In this context, by using structural and resting state functional MRI, we aimed to investigate the morphological and functional alterations of the gray matter and their possible inter-relationship in female patients with NPSLE, and to explore their potential clinical significance. This approach increased the homogeneousness of the enrolled subjects and the accuracy of the results.

MATERIALS AND METHODS

Participants

Seventy-four female patients (including 40 NPSLE and 34 non-NPSLE) were randomly recruited from the Department of Rheumatology and Immunology in Peking Union Medical College Hospital, fulfilling at least four of the American College of Rheumatology (ACR) classification criteria for SLE (Smith and Shmerling, 1999) between Jan 2017 and Dec 2018. Thirty-six female age-matched healthy controls (HCs) were enrolled. Primary CNS NPSLE manifestations were defined according to the ACR definition and the Systemic Lupus International Collaborating Clinics (SLICC) model B criteria (Bortoluzzi et al., 2018). All the clinical information of patients with SLE was verified by an experienced rheumatologist and an experienced neurologist. The diagnosis of cognitive disorder and mood disorder were made by the neurologist according to the routine screening tests [Mini-Mental State Exam (MMSE), Montreal Cognitive Assessment (MoCA), Hamilton Anxiety Scale (HAMA), and Hamilton Depression Scale (HAMD)]. The inclusion criteria also included age between 18 and 65 years and right handedness. The exclusion criteria were as follows: (Mok et al., 1999) taking psychoactive medication or alcohol/drug abuse; (Costenbader et al., 2007) any current or past diagnosed primary mental illness; (Pamfil et al., 2015) secondary NPSLE due to infections, electrolyte disturbances, hypertension, or other causes; (Cohen et al., 2017) any evident MRI lesions in the HCs; (Gelb et al., 2018) further contraindications to MRI scan; and (Sarbu et al., 2015) poor MRI image quality, e.g., overt motion and susceptibility artifacts, and low signal-to-noise ratio. From the original cohort, 20 patients with SLE and 4 HCs were excluded due to Mok et al. (1999) incomplete records of medical

history (n = 6); (Costenbader et al., 2007) secondary NPSLE (n = 5); (Pamfil et al., 2015) remittent mild headache as the single neuropsychiatric symptom (n = 3); and (Cohen et al., 2017) poor MRI data quality (n = 10). The remaining 30 patients with primary CNS NPSLE with at least one classified neuropsychiatric symptom, 24 patients with non-NPSLE and 32 healthy volunteers were finally enrolled. All the patients had received treatment with steroids and immunosuppressors. Disease activity was assessed using the Systemic Lupus Erythematosus Diseases Activity Index 2000 (SLEDAI-2k) scores. Accumulative disease damage was assessed with the Systemic Lupus International Collaborating Clinics/American College of Rheumatology (SLICC/ACR) damage index (SDI) scores. The demographics, clinical data (disease duration, manifestations of SLE, current medications, and immunological data) were registered. The interval between clinical evaluations and MRI scans was within 7 days. The study protocol was approved by the Ethics Committee at the Peking Union Medical College Hospital. All participants gave their written informed consent.

Image Acquisition

The conventional MR sequences [T2 and fluid-attenuated inversion recovery (FLAIR)], high-resolution T1-weighted imaging [3DT1], and resting state functional MRI [rs-fMRI] were performed on a 3.0-Tesla MR system (Siemens Magnetom Trio Tim System, Siemens Healthcare GmbH, Erlangen, Germany) using a 32-channel head coil. Axial T2-weighted images and FLAIR images with 4-mm slice thickness were acquired for lesion identification. High-resolution anatomical images were acquired using T1-weighted three-dimensional volumetric magnetization-prepared rapidly acquired gradient-echo (MPRAGE) sequence: repetition time (TR) = 1600 ms; echo time (TE) = 2.13 ms; flip angle (FA) = 9°; inversion time (TI) = 1000 ms; in-plane resolution 1 × 1 mm^2; slice thickness = 1 mm; matrix = 256 × 224; 176 axial slices. Rs-fMRI data were collected using a gradient rapid echo-echo planar imaging (GRE-EPI) sequence: TR = 2000 ms; TE = 30 ms; FA = 90°; in-plane resolution = 3.5 × 3.5 mm^2; slice thickness = 3 mm; slice gap = 1 mm; matrix = 64 × 64; 35 axial slices. The MRI scans of the patients with SLE were acquired at least 4 weeks from the last relapse and treatment to minimize their confounding effects on the following analysis.

Magnetic Resonance Imaging Image Processing

The fMRI images were preprocessed by using DAPARSF (Data Processing Assistant for Resting-State fMRI, Advanced Edition[1]). Preprocessing steps include removing the first 10 time points, slice timing correction, realigning fMRI volumes, reorienting fMRI and T1 images, coregistering the structural T1 image to functional MRI image, segmenting the structural T1 with DARTEL (Diffeomorphic Anatomical Registration Through Exponentiated Lie Algebra) and then warping these images into Montreal Neurological Institute (MNI) space, regressing the nuisance covariates (including signal linear drift, head motion parameters, mean signals within white matter and CSF), warping the processed fMRI images into MNI space with the normalization parameters derived from the structural T1 segmentation and normalization, and resampling the fMRI voxel into 3 mm × 3 mm × 3 mm. In our preprocessing steps, smoothing was not carried out to preserve the signal details.

The fractional low frequency amplitude (fALFF) within the 0.01-0.1 Hz band was calculated, and then the fMRI signals were filtered with the frequency band of 0.01-0.1 Hz to reflect the low-frequency oscillator fluctuations of resting state fMRI signals. The regional homogeneity (ReHo) to measure the similarity of time series within local brain areas and degree centrality (DC) to measure the importance of local brain areas in the functional connectivity were obtained by using the filtered images. Z-score maps of all the parameter images were obtained and smoothed by a 4-mm full width at half maximum Gaussian kernel for the following voxel-based statistical analysis. Additionally, the segmented and normalized gray matter (GM) images in MNI space were modulated and smoothed for voxel-based morphometry (VBM) analysis.

The CONN (Whitfield-Gabrieli and Nieto-Castanon, 2012) v.20.b toolbox[2] is used for resting-state functional connectivity analysis. Pre-processing of the data used the default pipeline of CONN included discard the first 10 time points, slice-timing correction, functional realignment and unwarping, structural segmentation, functional and structural normalization in the MNI-space (normalization of the co-registered T1 image and EPI volumes with a voxel size of 2 × 2 × 2mm), functional outlier detection (ART-based scrubbing) and smoothing (8-mm FWHM Gaussian filter). Then, the toolbox step to a denoising procedure: the confounding effects such as the white matter, cerebrospinal fluid, realignment results, scrubbing results, and the rest were regressed out of the fMRI time series, and after that, the data were bandpass-filtered with the default CONN values (0.008–0.09 Hz) and linear detrended.

Seed Based Connectivity Analysis (Seed-To-Voxel Analysis)

According to FSL Harvard-Oxford atlas in CONN, bilateral cerebellar Crus I & Crus II and only right cerebellar Crus II were used as the seeds, respectively. Their BOLD response was correlated with those of each voxel in the rest of the brain.

Statistical Analysis

The statistical analysis was performed using SPSS (SPSS for Windows, version 25.0; IBM, Armonk, NY, United States), the statistics toolbox in MATLAB (MATLAB 2019a) and Statistical Parametric Mapping (SPM12[3]).

The values are expressed as the mean and standard deviation (SD) for normally distributed variables and median and interquartile range (IQR) for parameters without a normal distribution.

One-way ANOVA and *post hoc* comparison and Student's t-test were used for variables with a normal distribution. The

[1]http://rfmri.org/DPARSF

[2]http://www.nitrc.org/projects/conn

[3]https://www.fil.ion.ucl.ac.uk/spm/

Wilcoxon and Kruskal-Wallis test, *post hoc* analysis and Mann-Whitney U test were used for variables that were not normally distributed. Multiple comparisons were performed by Bonferroni correction. P value < .05 was deemed statistically significant.

For voxel-based statistical analysis of GM structural and functional measures, nonparametric one-way ANOVA [permutation test with 5000 permutations and familywise error (FWE) correction for multiple comparisons with $p < 0.05$] with age and total intracranial volume [TIV, only for GM volume (GMV)] as covariates were first performed, followed by nonparametric two-sample analysis (permutation test with 5000 permutations and FWE correction for multiple comparisons $p < 0.05$) to compare each pair of groups.

For seed-to-voxel analysis, one-way ANOVA was used to compare the differences in functional connectivity between NPSLE, non-NPSLE and HCs groups. Then, multiple comparisons were adjusted by applying the correction of False discovery rate (FDR) ($p < 0.05$).

Linear regression analyses were performed to find the associations between the MRI and clinical features with adjustment for age for SLE patients (including both NPSLE and non-NPSLE).

Logistic regression analysis was performed to evaluate the ability [by sensitivity, specificity, and area under the curve (AUC)] of structural and functional MRI measures to distinguish between patients with NPSLE and patients with non-NPSLE.

Support Vector Machine for Discriminating Patients With Neuropsychiatric Systemic Lupus From Patients With Non-neuropsychiatric Systemic Lupus

Support vector machine with linear kernel (SVM, using libsvm[4]) was adopted to identify patients and further distinguish different types of patients with SLE by using structural and functional features, which showed statistically significant differences between groups. Multivariate logistic regression was first used for feature selection. Leave-one-out cross-validation was adopted to train and evaluate the SVM model. Accuracy, sensitivity, specificity, precision, recall, and F1-score were used to evaluate the performance of the classification.

RESULTS

Demographic Characteristics and Clinical Findings

All demographic and clinical characteristics are summarized in **Table 1**. There was no significant difference in disease duration, SLEDAI scores, the rate of patients with SLEDAI ≥ 5, anti-ribosomal P protein antibody, antiphospholipid antibodies (aPLs), traditional vascular risk factors or current medication between patients with NPSLE and non-NPSLE (all $p > 0.05$). However, patients with NPSLE showed higher Systemic Lupus International Collaborating Clinics/American College of Rheumatology(SLICC/ACR) Damage Index (SDI) scores compared to the patients with non-NPSLE, which was mainly due to the neurological involvement ($p < 0.05$).

The current study included 10(33.3%) patients with active NPSLE. The median time interval between the first NP event to the imaging assessment was 32.5 (40.4) months, while the median time interval between the last NP event to the imaging assessment was 9.2 (16.4) months. The neuropsychiatric manifestations of patients with NPSLE included seizure disorders ($n = 13$, 43.3%), cognitive disorder ($n = 12$, 40%), demyelinating syndrome ($n = 9$, 30%), mood disorder ($n = 9$, 30%), severe headache ($n = 7$, 23.3%), psychosis ($n = 6$, 20.0%), acute confusional state and cerebrovascular events ($n = 5$, 16.7%, respectively).

On conventional MRI, patients with NPSLE showed significantly increased lesion volume, when compared with patients with non-NPSLE [0.0 (0.0, 1164.0) vs 2188.0 (0.0, 6176.0), $p = 0.002$].

Gray Matter Volumetric Alterations in Systemic Lupus Erythematosus

Compared to HCs, patients with non-NPSLE presented no significant GM atrophy, while patients with NPSLE presented widespread GM atrophy in the cortical cortex including the frontal (e.g., rectus gyrus and precentral gyrus), temporal (e.g., superior/inferior temporal gyrus), parietal (e.g., postcentral and precuneus gyrus) and occipital (e.g., fusiform, lingual gyrus and calcarine) cortex, subcortical nuclei (e.g., thalamus, hippocampus, and putamen) and cerebellum (**Figure 1** and **Table 2**).

Compared to patients with non-NPSLE, patients with NPSLE presented GM atrophy in the left superior temporal gyrus, right thalamus, and bilateral putamen (**Figure 1** and **Table 2**).

Gray Matter Functional Alterations in Systemic Lupus Erythematosus

Compared to HCs, patients with non-NPSLE presented increased fALFF in the left inferior occipital lobe and decreased fALFF in the bilateral postcentral and paracentral lobules; patients with NPSLE presented decreased fALFF in the left medial superior frontal gyrus, left anterior cingulum, and bilateral middle cingulate. Compared to non-NPSLE, patients with NPSLE presented increased fALFF in the bilateral postcentral gyrus (**Figure 2** and **Table 2**).

Compared to HCs, patients with non-NPSLE presented increased ReHo in the left cerebellar posterior lobe (L-Crus II, L-Crus I) and decreased ReHo in the left superior temporal gyrus, left postcentral gyrus, and right precentral gyrus; patients with NPSLE presented increased ReHo in the right fusiform and lingual gyrus and decreased ReHo in the left anterior cingulum gyrus, left superior temporal gyrus, right insula, and cerebellar vermis. Compared to non-NPSLE, patients with NPSLE presented decreased ReHo in the bilateral cerebellar posterior lobes (Crus II, Crus I) (**Figure 2** and **Table 2**).

Compared to HCs, patients with non-NPSLE presented decreased DC in the right postcentral gyrus. No difference was

[4]http://www.csie.ntu.edu.tw/~cjlin/libsvm/

TABLE 1 | Demographic and clinical characteristics of SLE patients with and without neuropsychiatric manifestations.

	non-NPSLE	NPSLE	P value
	(*n* = 24)	(*n* = 30)	
Age, mean (SD), years	29.1 (10.0)	32.5 (12.8)	0.30
Duration, median (IQR), years	28.0 (10.5, 54.0)	66.0 (12.0, 168.0)	**0.060**
SLEDAI score, median (IQR)	4.0 (1.0, 7.5)	6.0 (3.0, 12.0)	**0.061**
SLEDAI score ≥ 5, n (%)	9 (38%)	18 (62%)	0.10
Non-neurological SLEDAI score, median (IQR)	4.0 (1.0, 7.5)	4.0 (2.0, 8.0)	0.55
SLICC SDI score, median (IQR)	0.0 (0.0, 0.0)	1.0 (0.0, 1.0)	**< 0.001**
Active NP, n (%)		10 (33.3%)	
Period between 1st NP event to scanning, median (IQR), months		32.5 (40.4)	
Period between last NP event to scanning, median (IQR), months		9.2 (16.4)	
Cumulative organ system involvement, n (%)			
Cutaneous	15 (63%)	22 (73%)	0.56
Vasculitis	6 (25%)	6 (20%)	0.75
Articular	12 (50%)	14 (47%)	1.00
Serositis	6 (25%)	10 (33%)	0.56
Renal	12 (50%)	18 (60%)	0.58
Hematologic	18 (75%)	19 (63%)	0.39
Interstitial pneumonia	2 (8%)	6 (20%)	0.28
Cardiac	0 (0%)	3 (10%)	0.25
Manifestations of NP, n (%)			
Seizure disorder		13(43.3%)	
Cerebrovascular events		5(16.7%)	
Acute confusional state		5(16.7%)	
Psychosis		6(20.0%)	
Cognitive disorder		12(40.0%)	
Mood disorder		9(30.0%)	
Severe headache		7(23.3%)	
Demyelinating syndrome		9(30.0%)	
Laboratory findings, n (%)			
Anti-dsDNA (+)	12 (50%)	18 (60%)	0.58
Anti-ribosomal P (+)	8 (33%)	15 (50%)	0.27
aPLs (+)	5 (21%)	12 (40%)	0.15
Hypocomplementemia	19 (79%)	28 (93%)	0.22
Complications, n (%)			
Sjogren' syndrome	2 (8%)	7 (23%)	0.27
Hashimoto's disease	1 (4%)	5 (17%)	0.21
Smoking	0 (0%)	0 (0%)	
Hypertension	1 (4%)	7 (23%)	0.063
Diabetes	1 (4%)	1 (3%)	1.00
Dyslipidemia	0 (0%)	4 (13%)	0.12
Current medication, n(%)			
Glucocorticoids	21 (88%)	29 (97%)	0.31
Cumulative dose of steroids, median (IQR)	11.2 (3.9, 14.6)	11.4 (7.2, 29.4)	0.16
Low dose of steroids (Pred < 10mg/d)	15 (63%)	15 (52%)	0.58
DMARDs	20 (83%)	24 (83%)	1.00
Anticoagulants/antiplatelets	4 (17%)	9 (31%)	0.34
Lipid lowering agents	2 (8%)	9 (31%)	0.086
Vasodilators	0 (0%)	4 (14%)	0.12
cMRI Imaging			
Lesion Volume, median (IQR)	0.0 (0.0, 1164.0)	2188.0 (0.0, 6176.0)	**0.002**

Values are mean ± SD, median (IQR), or number (%).
P values are for Wilcoxon's rank sum test on continuous variables and for Fisher's exact test on categorical variables.
**Include Cyclophosphamide, Mycophenolate Mofetil, Azathioprine, Methotrexate, Ciclosporin, and Tacrolimus.*
SD, standard deviation; IQR, interquartile range; SLE, systemic lupus erythematosus; anti-dsDNA, anti-double strand DNA antibody; aPLs, anti-phospholipid antibodies; SLEDAI, Systemic Lupus Erythematosus Disease Activity Index; SLICC SDI, Systemic Lupus International Collaborating Clinics/American College of Rheumatology Damage Index; DMARDs, disease modifying antirheumatic drugs; cMRI, conventional MRI.
The bold values mean p < 0.05 or nearly to 0.05.

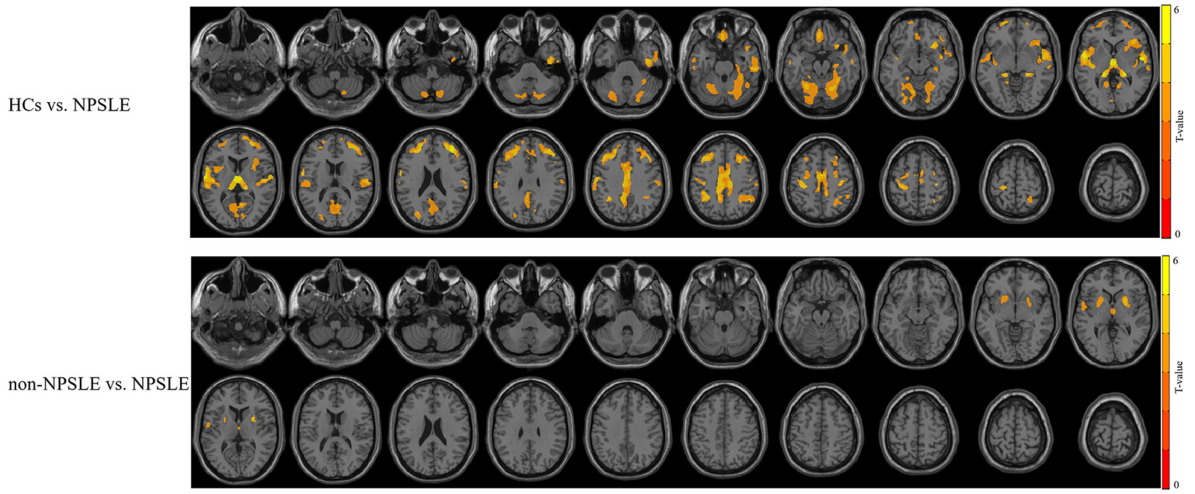

FIGURE 1 | The different patterns of GM atrophy in patients with NPSLE and non-NPSLE. The colored bar indicates the statistical T distribution between groups.

found between HCs and patients with NPSLE or between patients with non-NPSLE and those with NPSLE (**Figure 2** and **Table 2**).

Cerebellar Seed-Based Functional Connectivity Alterations in Systemic Lupus Erythematosus

According to the results from the structural and functional imaging data analysis mentioned above, we found that the cerebellar posterior lobes might play a crucial role in the compensation for the disease damage. We next did the seed-based functional connectivity analysis with using the cerebellar posterior lobes (Crus I, Crus II) as the seeds, to further investigate the potential interaction of the cerebellar posterior lobes with other cognitive networks in SLE.

Figure 3 and **Table 3** summarized the voxel-wise differences of RS FC between subgroups, with the cerebellar posterior lobes as the seeds. Compared to non-NPSLE patients, NPSLE patients exhibited hyperconnectivity between the bilateral Crus I & II region and the left-posterior superior temporal gyrus (L-pSTG), left planum temporale and left parietal operculum. Specifically, with a seed placed at the right cerebellar Crus II, an essential node for the cerebellum network, the NPSLE group had increased FC of the posterior cingulate gyrus, precuneous cortex, left posterior temporal fusiform cortex and left posterior parahippocampal gyrus within the posterior DMN, but reduced FC of the L-pSTG and left planum temporale as compared to the non-NPSLE group.

Correlations of Magnetic Resonance Imaging Indices With Clinical Variables

As shown in **Table 4**, lesion volume presented significant negative correlations with GM volume (GMV) in the bilateral putamen and GMV in the right thalamus and ReHo in the left cerebellum.

Disease duration presented negative correlations with ReHo in the left cerebellum and positive correlations with ReHo in the right precentral cortex and DC in the right postcentral gyrus.

Systemic Lupus Erythematosus Diseases Activity Index (SLEDAI) scores presented a positive correlation with DC in the right postcentral cortex and a negative correlation with fALFF in the left inferior occipital gyrus.

SDI scores presented negative correlations with GMV in the right cerebellum/fusiform/lingual/hippocampus/bilateral thalamus, GMV in the left cerebellum/fusiform/lingual gyrus, GMV in the right inferior frontal/precentral/postcentral/superior temporal/insula/putamen, GMV in the left inferior frontal/precentral/postcentral/superior temporal/insula, GMV in the right thalamus, and GMV in the left superior temporal gyrus and a positive correlation with DC in the cerebellar posterior lobe.

Cumulative doses of steroids presented significant positive correlations with ReHo in the left and right cerebellum and negative correlations with ReHo in the right precentral gyrus and DC in the right postcentral gyrus.

Hypertension was positively correlated with ReHo in the left postcentral/paracentral lobule and DC in the right postcentral gyrus.

Anti-phospholipid antibodies (aPLs) presented a mildly negative correlation with fALFF and ReHo at the whole brain level, fALFF in the left inferior occipital region and a mildly positive correlation with ReHo in the left anterior cingulum.

Logistic Analysis for the Discrimination of Patients With Neuropsychiatric Systemic Lupus From Non-neuropsychiatric Systemic Lupus

For the discrimination of patients with NPSLE from non-NPSLE, logistic analysis results showed structural features, with the top 3 leading AUCs being GMV in the right thalamus, left putamen and left superior temporal, and functional features with the top 3 leading AUCs being ReHo in the bilateral cerebellum and left postcentral gyrus (**Figure 4**).

TABLE 2 | Statistically significant structural and functional alterations in SLE patients using voxel-based analysis.

MR features	Between groups	Brain areas	cluster size (voxels)	Peak MNI coordinate			Peak T
				X	Y	Z	
Gray matter volume	HCs vs NPSLE	Right cerebellar anterior and posterior lobe/bilateral thalamus	8392	–1.5	–10.5	7.5	5.56
		Left cerebellar anterior and posterior lobe	4443	–28.5	–55.5	–18	4.55
		Right inferior and middle temporal gyrus/right fusiform gyrus	1972	37.5	–10.5	–36	5.03
		Left inferior temporal gyrus	285	–57	–12	–18	3.95
		Right insula/right superior temporal gyrus	6169	27	22	–13	5.13
		Left rectus gyrus	1123	–3	37.5	–22.5	4.47
		Left superior and middle frontal gyrus	3990	–31	29	46	4.54
		Left superior temporal gyrus/left postcentral gyrus/left insula	6156	–53	–1	1	5.17
		Right superior and middle frontal gyrus	4267	36	40	26	5.17
		Bilateral cingulum and bilateral precuneus	10240	–2	–6	49	5.09
		Left middle occipital gyrus	424	–24	–75	22.5	4.1696
		Right middle cingulum	225	–1.5	39	31.5	3.952
		Left inferior parietal gyrus	608	–35	–46	41	4.53
		Right superior and inferior parietal gyrus	1314	28.5	–55.5	45	4.6806
		Right superior and middle frontal gyrus	268	25.5	–3	54	3.9186
	Non-NPSLE vs NPSLE	Left putamen	739	–22.5	7.5	1.5	4.0225
		Right putamen	701	24	6	6	4.4821
		Bilateral thalamus	269	3	–10.5	3	3.7348
		Left superior temporal gyrus	390	–55.6	–6	6	4.0848
ReHo	HCs vs non-NPSLE	Left cerebellar posteiro lobe	48	–48	–54	–45	–3.7567
		Left superior temporal; pole	73	–39	9	–27	5.0354
		Right precentral gyrus	36	9	–21	78	3.2704
		Left postcentral gyrus	50	0	–30	72	3.4827
	HCs vs NPSLE	Left superior temporal pole	40	–39	15	–21	3.9901
		Right Fusiform/right lingual gyrus	51	27	–69	6	–3.9288
		Right insula	42	42	15	–6	4.1044
		Left anterior Cingulum	41	–3	42	–3	3.7632
		Vermis_4_5	32	–3	–35	–1	3.6127
	Non-NPSLE vs NPSLE	Left cerebellar posterior lobe	150	–51	–54	–45	4.1608
		Right cerebellar posterior lobe	59	33	–51	–42	3.6234
DC	HCs vs non-NPSLE	Right postcentral gyrus	30	30	–36	72	3.3265
	HCs vs NPSLE	Right cerebellar posterior lobe	30	6	–93	–36	–3.4111
fALFF	HCs vs non-NPSLE	Left inferior occipital gyrus	32	–30	–81	–12	–3.5115
		Left postcentral gyrus	120	–3	–33	75	3.5695
	HCs vs NPSLE	Left superior medial frontal gyrus/left anterior cingulum	108	–3	48	33	4.4221
		Bilateral middle cingulum_	201	1	23	32	4.66
	non-NPSLE vs NPSLE	left Postcentral Gyrus	39	–15	–45	72	–3.1991

Peak T, peak T value.

Support Vector Machine Classification for the Discrimination of Patients With Systemic Lupus Erythematosus From Healthy Controls and Patients With Neuropsychiatric Systemic Lupus From Non-neuropsychiatric Systemic Lupus

As shown in **Table 5**, the structural and functional features were selected by logistic regression with coefficients of $p < 0.005$ and $p < 0.001$ to investigate the robust features. The classification performance had accuracies of 94.44% and 87.04% for features with $p < 0.005$ and $p < 0.001$ for the discrimination of patients with NPSLE from patients with non-NPSLE, respectively. The most robust MRI features were ReHo in the bilateral cerebellar posterior lobes.

DISCUSSION

In this study, we adopted a well-validated quantitative MRI approach (3D T1, T2/FLAIR, and rs-fMRI) to investigate the structural and functional characteristics of GM in patients with

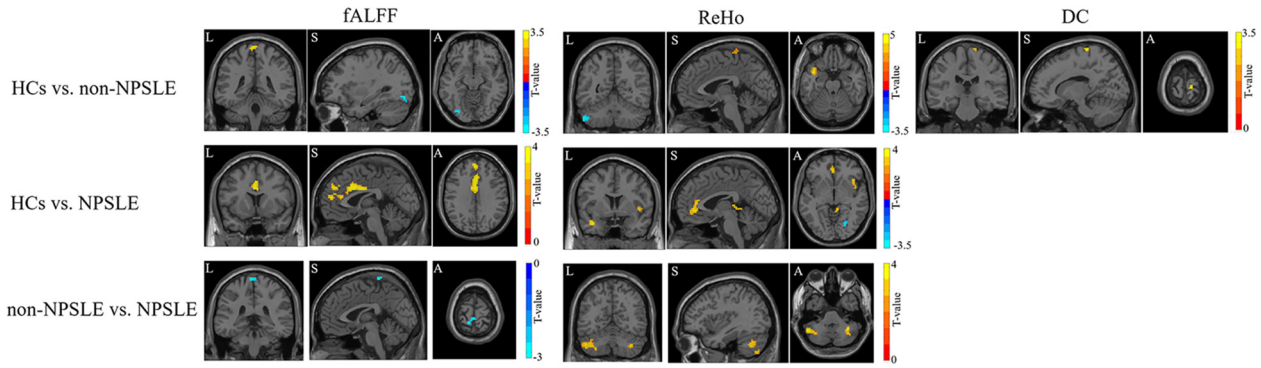

FIGURE 2 | The fALFF, ReHo and DC changes in patients with NPSLE and non-NPSLE. The colored bar indicates the statistical T distribution between groups.

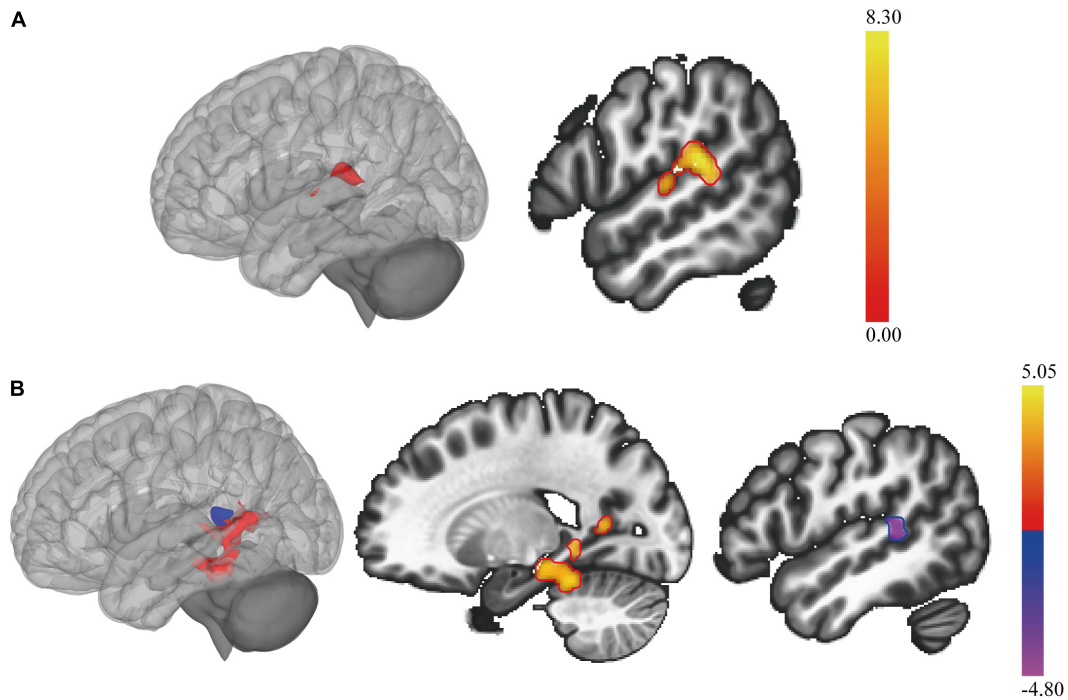

FIGURE 3 | The cerebellar seed-based resting state functional connectivity (RS FC) changes in patients with NPSLE and non-NPSLE. **(A)**: Clusters of abnormal RS FC between subgroups of patients with SLE, as the bilateral cerebellar posterior lobes (cerebellar Crus I & Crus II) being the seed. **(B)**: Clusters of abnormal RS FC between subgroups of patients with SLE, as the right cerebellar Crus II being the seed. The colored bar indicates the statistical T distribution between groups.

NPSLE compared with patients with non-NPSLE and HCs. Then, we correlated MRI abnormalities with clinical variables to study the clinical relevance of our findings. Finally, we introduced SVM, the more advanced discriminative approach, to identify potential MRI imaging biomarkers to assist the diagnosis of NPSLE.

In accordance with previous MRI imaging studies, we found widespread GM atrophy in patients with NPSLE (Appenzeller et al., 2007; Jung et al., 2010; Piga et al., 2015; Liu et al., 2018), with significant subcortical GM (the right thalamus and bilateral putamen) atrophy as compared to patients with non-NPSLE, as showed in **Figure 1** and **Table 2**. SLE is bound to cause cerebral atrophy through autoantibody and cytokine induced vascular damage, blood-brain barrier (BBB) impairment, inflammatory neurotoxicity, and other uncovered mechanisms (Sibbitt et al., 2010; Prechl and Czirjak, 2015; Cohen et al., 2017; Schwartz et al., 2019). However, subcortical GM atrophy is not specific for NPSLE: it can also be found in other neuropsychiatric diseases, such as Parkinson's disease, Alzheimer's disease, multiple sclerosis, depression, and autism (Orhun et al., 2019). Subcortical GM atrophy in NPSLE might be a mixture of several mechanisms, including vulnerability of this territory to hemodynamic and hypoxic impairment (Chiang et al., 2019; Eslami et al., 2019). It is putatively linked to cognitive

decline. However, Kalinowska-Łyszczarz et al. (2018) found no correlations between subcortical atrophy and cognitive deficits in SLE. They concluded the cognitive impairment in SLE is independent of brain atrophy or lesion volume. Notably, in our present study, we also found no significant functional alterations in basal ganglia or thalamus in SLE patients, suggesting that the

TABLE 3 | Clusters of abnormal RS FC between HC and SLE patients and between subgroups of SLE patients, as the parts of the cerebellar posterior lobes (Crus I, Crus II) being the seeds.

Contrast	Clusters	Size	X	Y	Z	F	P_{FDR}
Seed: bilateral cerebellar Crus I & Crus II							
NPSLE>HCs							NS
non-NPSLE>HCs							NS
NPSLE>non-NPSLE	Left planum temporale Left parietal operculum cortex L-pSTG	274	–54	–32	+16	7.35	0.018
Seed: right cerebellar Crus II							
NPSLE>HCs							NS
non-NPSLE>HCs							NS
NPSLE>non-NPSLE	Posterior cingulate gyrus L cerebellum 4 5 Precuneous cortex	339	–12	–42	2	4.97	0.012
	Posterior cingulate gyrus	259	20	–44	0	4.60	0.022
	L cerebellum 4 5 Posterior temporal fusiform cortex L posterior Parahippocampal gyrus	213	–60	–40	–10	–5.39	0.025
NPSLE<non-NPSLE	L planum temporale L-pSTG	233	–22	–40	10	4.93	0.023

L, left; L-pSTG, left posterior superior temporal gyrus.

TABLE 4 | The clinical associations of MRI measurements with clinical variables using linear regression in SLE patients (including both NPSLE and non-NPSLE).

Features	Brain regions	Disease duration (months)	SLEDAI scores	SDI scores	Cumulative steroid dose (g)	Lesion volume	Hypertension	aPLs
GMV	right cerebellum/fusiform/lingual/ hippocampus/bilateral thalamus			–0.37 (0.035)				
	Left cerebellum/fusiform/lingual gyrus			–0.46 (0.008)				
	right inferior frontal/precentral/postcentral/ superior temporal/insula/putamen			–0.40 (0.021)				
	left inferior frontal/precentral/postcentral/ superior temporal/insula			–0.33 (0.049)				
	left putamen					–0.49 (< 0.001)		
	right putamen					–0.40 (0.001)		
	right thalamus			–0.44 (0.008)		–0.32 (0.028)		
	left superior temporal			–0.36 (0.020)				
fALFF	whole brain							–0.14 (0.037)
	left inferior occipital		–0.49 (0.003)					–0.12 (0.024)
ReHo	whole brain							–0.16 (0.039)
	left cerebellum	–1.53 (0.001)			1.29 (0.003)			
	right precentral	1.15 (0.032)			–1.17 (0.020)			
	left postcentral/paracentral lobule						0.32 (0.033)	
	left anterior cingulum							0.14 (0.024)
	left cerebellum	–1.31 (0.005)			0.87 (0.041)	–0.41 (0.033)		
DC	right postcentral	0.75 (0.034)	0.36 (0.03)		–0.87 (0.009)		0.31 (0.002)	
	cerebellar posterior lobe			0.55 (0.009)				

The results are presented with the regression coefficients and the corresponding p values. Statistical significance of two-sided $p < 0.05$ was adopted.

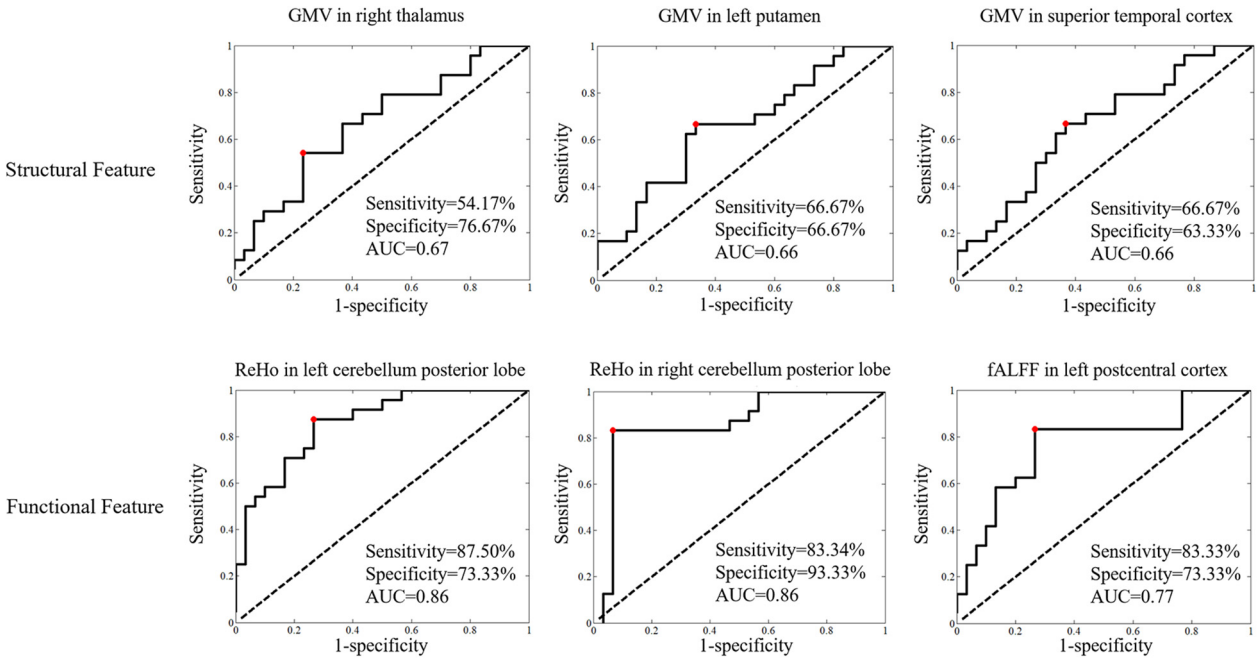

FIGURE 4 | The logistic regression analyses of the structural and functional features in statistically significant brain regions for discrimination of patients with NPSLE from those with non-NPSLE (features with the top 3 leading AUCs are presented). Classificational sensitivity, specificity and AUC are presented at the cut-off point (red).

TABLE 5 | SVM classification results for the diagnosis of SLE from HCs and NPSLE from non-NPSLE using statistically significant structural and functional features selected by logistic regression with $p < 0.005$ and $p < 0.001$, respectively.

	Feature numbers	Accuracy (%)	Sensitivity (%)	Specificity (%)	Precision (%)	Recall (%)	F1 score
MRI features (logistic regression with $p < 0.005$)							
HCs vs non-NPSLE+NPSLE	9	97.67	98.15	96.88	98.15	98.15	0.98
HCs+non-NPSLE vs NPSLE	10	93.02	96.67	91.07	85.29	96.67	0.91
HCs vs non-NPSLE	12	94.64	875	100	100	87.50	0.93
HCs vs NPSLE	9	100	100	100	100	100	100
non-NPSLE vs NPSLE	5	94.44	96.67	91.67	93.55	96.67	0.95
MRI features (logistic regression with $p < 0.001$)							
HCs vs non-NPSLE+NPSLE	9	97.67	98.15	96.88	98.15	98.15	0.98
HCs+non-NPSLE vs NPSLE	8	95.35	93.33	96.43	93.33	93.33	0.93
HCs vs non-NPSLE	5	94.64	91.67	96.88	95.65	91.67	0.94
HCs vs NPSLE	8	100	100	100	100	100	100
non-NPSLE vs NPSLE	2	87.04	90.00	83.33	87.10	90.00	0.89

function of subcortical nuclei is relatively intact in SLE, similar with the results we previously found in neuromyelitis optica (NMO) (Liu et al., 2015). The dissociation of morphological and functional alterations in GM within this region in SLE may further support the hypothesis of brain reorganization to compensate for the functional impairments caused by neuronal injury in SLE.

In what follows, as showed in **Figure 2** and **Table 2**, we found that in patients with non-NPSLE, the function of the left superior temporal gyri (L-STG) within default mode network (DMN) was decreased without detectable volumetric reduction, while in patients with NPSLE, the functional impairment of the same region was conspicuous with significant atrophy. L-STG is involved in limbic system connecting closely with hippocampus. These regions play crucial roles in social cognition and emotion regulation. Microstructural and functional alterations of this area were previously reported in patients with autoimmune encephalitis (e.g., anti-NMDAR) with schizophrenia-like psychiatric manifestations as the initial presentation (Bost et al., 2016). Meanwhile, prior studies using mouse models and *in vitro* experiments demonstrated that anti-double stranded DNA antibody and anti-ribosomal P protein antibody could cross react with neuron surface receptors including NMDARs (DeGiorgio et al., 2001), mainly injuring

the hippocampus, inducing neuronal death and leading to cognitive disorders and memory loss. Taken together, our data thus verified *in vivo* the L-STG is one of the potential neural substrates of neuropsychiatric impairment in patients with SLE (Kowal et al., 2006; Schwarting et al., 2019). Besides, choric neurological histopathological lesions characterized by non-specific focal vasculopathy have already been found in the brain tissue of patients with non-NPSLE, while in that of patients with NPSLE, it progresses into more specific lesions including diffuse vasculopathy and microthrombi, which is related to clinical neuropsychiatric symptoms (Cohen et al., 2017). Therefore, hypothetically, NPSLE is considered the consequence of these cumulative pathological damages to the nervous system when exceeding a certain threshold (Petri et al., 2008; Kozora et al., 2012; Cohen et al., 2017; Schwartz et al., 2019). On the basis of these findings and hypothesis, we speculated that the GM within the left temporal lobe including the L-STG may be one of the direct targets of lupus-related inflammatory attack, in which it exhibited a progressive pathological change.

In accordance with previous fMRI studies (Desmond et al., 2003; Hester and Garavan, 2004; Ren et al., 2012), we also found that (**Figure 2** and **Table 2**), to compensate for the cerebral regional dysfunction, the areas in cerebellar posterior lobes were significantly activated in patients with non-NPSLE. Thus, cerebellar posterior lobes, an area which has a role in working memory, language processing and other executive tasks and is also included within the DMN (Schmahmann et al., 2019), may play a central role in the adaptability and plasticity of the brain to limit the functional impairment that has been caused by the disease. However, in patients with NPSLE as we found, while the GM volume within the cerebellar posterior lobes significantly reduced, its functional activities were attenuated as well, with increased FC of the ROIs within the posterior DMN and the regions around the L-STG. Increased cerebellar RS FC has been found in many neurological (Simioni et al., 2016) and neuropsychiatric (Feng et al., 2017) diseases. Bonacchi et al. (2020) identified that higher RS FC in the left cerebellar crus I was associated with worse memory performance. Taken together, these findings indicated a probable maladaptive rewiring and a trend of decompensation of the cerebellum to the disease damage in the state of NPSLE (Nystedt et al., 2019). In addition, other studies have demonstrated that compensatory functional signals decreased in SLE patients with disease duration of more than 10 years, indicating that the compensatory activations could be weakened by irreversible neural injuries (Mackay et al., 2011).

In line with the recently published literature (Bonacchi et al., 2020), the cerebral clusters in which we observed significant functional alterations during resting state in patients with NPSLE as compared with controls were the bilateral middle cingulate, the left superior temporal gyri, the bilateral cerebellar posterior lobes and the left medial superior frontal gyri within DMN, the right insula and the left anterior cingulate within salience network (SN), and the precentral and postcentral gyri within sensorimotor network (SMN). These neural networks are organized in balance. Previous research have verified the DMN and the SMN are anti-correlated, both regulated by the SN (Fox et al., 2005; Huang et al., 2015; Wang et al., 2019; Russo et al., 2020). The SN plays a critical role in attention and attributing saliency to external or internal originated events or stimuli and thus exerts control and balance on the DMN and other networks including the SMN (Shott et al., 2012; Martino et al., 2016). During resting state, the DMN is activated while the SMN is inhibited through the SN in healthy subjects. In patients with NPSLE, we observed attenuation of the DMN and the SN, and increased activation of the SMN during resting state. DMN abnormalities have been consistently verified in several neurological (Hohenfeld et al., 2018; Valsasina et al., 2019; Preziosa et al., 2020) and psychiatric (Chahine et al., 2017) disorders. As previous research reported (Barraclough et al., 2019), the DMN was indicated to have attenuated deactivation during performing cognitive tasks, and hypoconnectivities within it and between the cognitive networks during resting state (Nystedt et al., 2018) in NPSLE patients, which was interpreted as a compensatory mechanism resulting in preserved cognitive performance. Meanwhile, as previous fMRI studies reported, the RS FC within SN is severely impaired in major depression (Philip et al., 2018). However, Bonacchi et al. (2020) found increased RS FC in the left insular cortex with more severe depression, and decreased RS FC in the right anterior cingulate cortex with better memory performance within SN, suggesting an adaptive mechanism, probably contributing to a more efficient performance of the SN on cognitive tasks. Taken together, we speculated that the increased function of the nodes within SMN might be the consequence of the disinhibition of it, due to weakened control and regulation from the attenuated SN and DMN (Lin et al., 2011; Nystedt et al., 2018; Papadaki et al., 2018), which was also reported in previous studies (Nystedt et al., 2018), and may partially explain the inattention, hyperactivity and impulsivity in patients with NPSLE as reported in prior literature (Garcia et al., 2013; Gao et al., 2015).

By correlation analysis, we verified that the widespread GM atrophy in patients with NPSLE was negatively correlated with SDI scores. Meanwhile, the subcortical GM atrophy was negatively correlated with lesion volume (**Table 3**). These results suggested that the distribution and the degree of brain GM atrophy in NPSLE patients could be an indicator of disease burden (Mak et al., 2016; Liu et al., 2018). In addition, we found that the characteristic functional alterations in the cerebellar posterior lobes and the sensorimotor center as detailed above were associated with disease duration, SDI scores, lesion volume, hypertension, and aPLs, which was consistent with previous evidence, reflecting a reduction of the brain adaptability to maintain normal function along with severe pathologic burden and multiple cerebral vascular risk factors (Rocca et al., 2006; Mackay et al., 2011; Cohen et al., 2017; Papadaki et al., 2018). However, it is worth noting that the functional alterations in GM within these regions was negatively associated with cumulative corticosteroid use, which might suggest a therapeutic effect for corticosteroids and requires further study.

In addition, the SVM analysis (**Figure 3** and **Table 4**) further confirmed that the combination of the ReHo of the bilateral cerebellar posterior lobes may be a potential imaging biomarker in early diagnosis of NPSLE, with both sensitivity and specificity above 0.8. Our results provided relatively satisfactory proof of the notion that the diagnostic process of NPSLE could be aided by

objective MRI imaging parameters rather than merely physician assessment (Zirkzee et al., 2012; Fanouriakis et al., 2016).

There are some limitations in our study. First, the sample size is relatively small. However, sample sizes of this magnitude have been confirmed to have adequate signal sensitivity to obtain statistical significance as a pilot study. Certainly, further studies are needed to confirm the present observations on a larger sample, with longitudinal follow-up and assistance of neuropsychiatric assessments. Second, the patients recruited in our study had all received treatment with steroids and immunosuppressors. However, this limitation is inherent to this type of study. Third, the educational level of the subjects should be considered as a potential confounder in the future study. Forth, there were around 1/3 patients with active NPSLE, which might probably influence the results due to active inflammation. However, the median SLEDAI scores and the rate of patients with SLEDAI score ≥ 5 between the NPSLE and non-NPSLE groups had no significant difference, which had balanced the potential confounder. Fifth, the patients enrolled in the NPSLE group were heterogeneous, according to the different NP manifestations the patients had. However, in the present pilot study, we aimed to investigate the overall characteristics of the GM in patients with NPSLE, and we planned to refine the patients with NPSLE in the future study. Despite its exploratory nature, this quantitative MRI pilot study offers valuable insights into the brain reorganizational capacity in SLE patients, as well as indicates for the first time the functional parameter of the cerebellar posterior lobes may be a potential imaging biomarker to aid the early diagnosis of NPSLE. Further investigation of the underlying lupus-related vascular damage and BBB impairment in SLE patients using other advanced quantitative MRI techniques (e.g., high-resolution MR angiography, MR permeability imaging, susceptibility weighted imaging, and quantitative susceptibility mapping) is, therefore, an essential next step.

CONCLUSION

In this study, characteristic deep nuclei atrophy and functional alteration pattern in GM within brain networks were identified in patients with NPSLE as compared with matched groups, which especially involved the cognitive and sensorimotor regions, and mainly associated with disease burden and aPLs. The different forms of the relationship between the structural and functional changes in patients with NPSLE and non-NPSLE reflected a compensatory mechanism of the brain to maintain normal function, which was attenuated along with pathologic burden and cerebral vascular risk factors. We also, for the first time, demonstrated *in vivo* that the GM within the left temporal lobe may be one of the direct targets of lupus-related inflammatory attack. Finally, we found that the function of the cerebellar posterior lobes might play an essential role in compensating for cortical functional disturbances and may contribute to identifying patients with suspected NPSLE in clinical practice. Larger longitudinal studies are required to further validate these data.

DATA AVAILABILITY STATEMENT

The original contributions presented in the study are included in the article/supplementary material, further inquiries can be directed to the corresponding author.

ETHICS STATEMENT

The studies involving human participants were reviewed and approved by the Ethics Committee at the Peking Union Medical College Hospital. The patients/participants provided their written informed consent to participate in this study.

AUTHOR CONTRIBUTIONS

LS was responsible for the study design, patient recruit, data acquisition, and manuscript drafting. ZZ was responsible for the data analysis and manuscript drafting. YD, JH, XQ, and ML help the data acquisition and manuscript editing. YL and XZ were responsible for the study design, manuscript review, and final approval of this manuscript. All authors contributed to the article and approved the submitted version.

FUNDING

This study was supported by the Natural Science Foundation of Beijing Municipality, Grant/Award Number: 7133244; Beijing Nova Program, Grant/Award Number: xx2013045; National Natural Science Foundation of China, Grant/Award Numbers: 81571597, 81571631, and 81870958; The Chinese National Key Research and Development Program, Grant/Award Numbers: 2017YFC0907601, 2017YFC0907602, and 2017YFC090760.

REFERENCES

Appenzeller, S., Bonilha, L., Rio, P. A., Min, Li L, Costallat, L. T., and Cendes, F. (2007). Longitudinal analysis of gray and white matter loss in patients with systemic lupus erythematosus. *Neuroimage* 34, 694–701. doi: 10.1016/j.neuroimage.2006.09.029

Barraclough, M., McKie, S., Parker, B., Jackson, A., Pemberton, P., Elliott, R., et al. (2019). Altered cognitive function in systemic lupus erythematosus and associations with inflammation and functional and structural brain changes. *Ann. Rheum. Dis.* 78, 934–940. doi: 10.1136/annrheumdis-2018-214677

Bonacchi, R., Rocca, M. A., Ramirez, G. A., Bozzolo, E. P., Canti, V., Preziosa, P., et al. (2020). Resting state network functional connectivity abnormalities in systemic lupus erythematosus: correlations with neuropsychiatric impairment. *Mol. Psychiatry* 20:907. doi: 10.1038/s41380-020-00907-z

Bortoluzzi, A., Scire, C. A., and Govoni, M. (2018). Attribution of neuropsychiatric manifestations to systemic lupus erythematosus. *Front. Med. (Lausanne).* 5:68. doi: 10.3389/fmed.2018.00068

Bost, C., Pascual, O., and Honnorat, J. (2016). Autoimmune encephalitis in psychiatric institutions: current perspectives. *Neuropsychiatr. Dis. Treat.* 12, 2775–2787. doi: 10.2147/NDT.S82380

Cao, Z. Y., Wang, N., Jia, J. T., Zhang, H. Y., Shang, S. A., Hu, J. J., et al. (2021). Abnormal topological organization in systemic lupus erythematosus: a resting-state functional magnetic resonance imaging analysis. *Brain Imaging Behav.* 15, 14–24. doi: 10.1007/s11682-019-00228-y

Chahine, G., Richter, A., Wolter, S., Goya-Maldonado, R., and Gruber, O. (2017). Disruptions in the left frontoparietal network underlie resting state endophenotypic markers in schizophrenia. *Hum. Brain Mapp.* 38, 1741–1750. doi: 10.1002/hbm.23477

Chiang, F. L., Wang, Q., Yu, F. F., Romero, R. S., Huang, S. Y., Fox, P. M., et al. (2019). Localised grey matter atrophy in multiple sclerosis is network-based: a coordinate-based meta-analysis. *Clin. Radiol.* 74, 816.e19-816.e28. doi: 10.1016/j.crad.2019.07.005

Cohen, D., Rijnink, E. C., Nabuurs, R. J., Steup-Beekman, G. M., Versluis, M. J., Emmer, B. J., et al. (2017). Brain histopathology in patients with systemic lupus erythematosus: identification of lesions associated with clinical neuropsychiatric lupus syndromes and the role of complement. *Rheumatology (Oxford)* 56, 77–86. doi: 10.1093/rheumatology/kew341

Costenbader, K. H., Feskanich, D., Stampfer, M. J., and Karlson, E. W. (2007). Reproductive and menopausal factors and risk of systemic lupus erythematosus in women. *Arthritis Rheum.* 56, 1251–1262. doi: 10.1002/art.22510

DeGiorgio, L. A., Konstantinov, K. N., Lee, S. C., Hardin, J. A., Volpe, B. T., and Diamond, B. (2001). A subset of lupus anti-DNA antibodies cross-reacts with the NR2 glutamate receptor in systemic lupus erythematosus. *Nat. Med.* 7, 1189–1193. doi: 10.1038/nm1101-1189

Desmond, J. E., Chen, S. H., DeRosa, E., Pryor, M. R., Pfefferbaum, A., and Sullivan, E. V. (2003). Increased frontocerebellar activation in alcoholics during verbal working memory: an fMRI study. *Neuroimage* 19, 1510–1520. doi: 10.1016/s1053-8119(03)00102-2

Eslami, V., Tahsili-Fahadan, P., Rivera-Lara, L., Gandhi, D., Ali, H., Parry-Jones, A., et al. (2019). Influence of intracerebral hemorrhage location on outcomes in patients with severe intraventricular hemorrhage. *Stroke* 50, 1688–1695. doi: 10.1161/STROKEAHA.118.024187

Fanouriakis, A., Pamfil, C., Rednic, S., Sidiropoulos, P., Bertsias, G., and Boumpas, D. T. (2016). Is it primary neuropsychiatric systemic lupus erythematosus? Performance of existing attribution models using physician judgment as the gold standard. *Clin. Exp. Rheumatol.* 34, 910–917.

Feng, X., Li, L., Zhang, M., Yang, X., Tian, M., Xie, W., et al. (2017). Dyslexic children show atypical cerebellar activation and cerebro-cerebellar functional connectivity in orthographic and phonological processing. *Cerebellum* 16, 496–507. doi: 10.1007/s12311-016-0829-2

Fox, M. D., Snyder, A. Z., Vincent, J. L., Corbetta, M., Van Essen, D. C., and Raichle, M. E. (2005). The human brain is intrinsically organized into dynamic, anticorrelated functional networks. *Proc. Natl. Acad. Sci. U.S.A.* 102, 9673–9678. doi: 10.1073/pnas.0504136102

Gao, Y., Lo, Y., and Mok, M. Y. (2015). Symptoms of attention deficit hyperactivity disorder in patients with systemic lupus erythematosus. *Lupus* 24, 1498–1504. doi: 10.1177/0961203315593817

Garcia, R. J., Francis, L., Dawood, M., Lai, Z. W., Faraone, S. V., and Perl, A. (2013). Attention deficit and hyperactivity disorder scores are elevated and respond to N-acetylcysteine treatment in patients with systemic lupus erythematosus. *Arthritis Rheum.* 65, 1313–1318. doi: 10.1002/art.37893

Gelb, S., Stock, A. D., Anzi, S., Putterman, C., and Ben-Zvi, A. (2018). Mechanisms of neuropsychiatric lupus: The relative roles of the blood-cerebrospinal fluid barrier versus blood-brain barrier. *J. Autoimmun.* 91, 34–44. doi: 10.1016/j.jaut.2018.03.001

Hester, R., and Garavan, H. (2004). Executive dysfunction in cocaine addiction: evidence for discordant frontal, cingulate, and cerebellar activity. *J. Neurosci.* 24, 11017–11022. doi: 10.1523/JNEUROSCI.3321-04.2004

Hohenfeld, C., Werner, C. J., and Reetz, K. (2018). Resting-state connectivity in neurodegenerative disorders: Is there potential for an imaging biomarker? *Neuroimage Clin.* 18, 849–870. doi: 10.1016/j.nicl.2018.03.013

Huang, S., Li, Y., Zhang, W., Zhang, B., Liu, X., Mo, L., et al. (2015). Multisensory competition is modulated by sensory pathway interactions with fronto-sensorimotor and default-mode network regions. *J. Neurosci.* 35, 9064–9077. doi: 10.1523/JNEUROSCI.3760-14.2015

Jung, R. E., Segall, J. M., Grazioplene, R. G., Qualls, C., Sibbitt, W. L., and Roldan, C. A. (2010). Cortical thickness and subcortical gray matter reductions in neuropsychiatric systemic lupus erythematosus. *PLoS One* 5:e9302. doi: 10.1371/journal.pone.0009302

Kalinowska-Łyszczarz, A., Pawlak, M. A., Pietrzak, A., Pawlak-Bus, K., Leszczynski, P., Puszczewicz, M., et al. (2018). Subcortical gray matter atrophy is associated with cognitive deficit in multiple sclerosis but not in systemic lupus erythematosus patients. *Lupus* 27, 610–620. doi: 10.1177/0961203317735186

Kowal, C., Degiorgio, L. A., Lee, J. Y., Edgar, M. A., Huerta, P. T., Volpe, B. T., et al. (2006). Human lupus autoantibodies against NMDA receptors mediate cognitive impairment. *Proc. Natl. Acad. Sci. U.S.A.* 103, 19854–19859. doi: 10.1073/pnas.0608397104

Kozora, E., Filley, C. M., Zhang, L., Brown, M. S., Miller, D. E., Arciniegas, D. B., et al. (2012). Immune function and brain abnormalities in patients with systemic lupus erythematosus without overt neuropsychiatric manifestations. *Lupus* 21, 402–411. doi: 10.1177/0961203311429116

Lin, Y., Zou, Q. H., Wang, J., Wang, Y., Zhou, D. Q., Zhang, R. H., et al. (2011). Localization of cerebral functional deficits in patients with non-neuropsychiatric systemic lupus erythematosus. *Hum. Brain Mapp.* 32, 1847–1855. doi: 10.1002/hbm.21158

Liu, S., Cheng, Y., Zhao, Y., Yu, H., Lai, A., Lv, Z., et al. (2018). Clinical factors associated with brain volume reduction in systemic lupus erythematosus patients without major neuropsychiatric manifestations. *Front. Psychiatry* 9:8. doi: 10.3389/fpsyt.2018.00008

Liu, Y., Duan, Y., Huang, J., Ren, Z., Ye, J., Dong, H., et al. (2015). Multimodal quantitative mr imaging of the thalamus in multiple sclerosis and neuromyelitis optica. *Radiology* 277, 784–792. doi: 10.1148/radiol.2015142786

Luyendijk, J., Steens, S. C., Ouwendijk, W. J., Steup-Beekman, G. M., Bollen, E. L., van der Grond, J., et al. (2011). Neuropsychiatric systemic lupus erythematosus: lessons learned from magnetic resonance imaging. *Arthritis Rheum.* 63, 722–732. doi: 10.1002/art.30157

Mackay, M., Bussa, M. P., Aranow, C., Ulug, A. M., Volpe, B. T., Huerta, P. T., et al. (2011). Differences in regional brain activation patterns assessed by functional magnetic resonance imaging in patients with systemic lupus erythematosus stratified by disease duration. *Mol. Med.* 17, 1349–1356. doi: 10.2119/molmed.2011.00185

Mak, A., Ho, R. C., Tng, H. Y., Koh, H. L., Chong, J. S., and Zhou, J. (2016). Early cerebral volume reductions and their associations with reduced lupus disease activity in patients with newly-diagnosed systemic lupus erythematosus. *Sci. Rep.* 6:22231. doi: 10.1038/srep22231

Martino, M., Magioncalda, P., Huang, Z., Conio, B., Piaggio, N., Duncan, N. W., et al. (2016). Contrasting variability patterns in the default mode and sensorimotor networks balance in bipolar depression and mania. *Proc. Natl. Acad. Sci. U.S.A.* 113, 4824–4829. doi: 10.1073/pnas.1517558113

Mok, C. C., Lau, C. S., Chan, T. M., and Wong, R. W. (1999). Clinical characteristics and outcome of southern Chinese males with systemic lupus erythematosus. *Lupus* 8, 188–196. doi: 10.1191/096120399678847605

Nystedt, J., Mannfolk, P., Jonsen, A., Bengtsson, A., Nilsson, P., Sundgren, P. C., et al. (2018). Functional connectivity changes in systemic lupus erythematosus: a resting-state study. *Brain Connect.* 8, 220–234. doi: 10.1089/brain.2017.0557

Nystedt, J., Mannfolk, P., Jonsen, A., Nilsson, P., Strandberg, T. O., and Sundgren, P. C. (2019). Functional connectivity changes in core resting state networks are associated with cognitive performance in systemic lupus erythematosus. *J. Comp. Neurol.* 527, 1837–1856. doi: 10.1002/cne.24656

Orhun, G., Tuzun, E., Bilgic, B., Ergin Ozcan, P., Sencer, S., Barburoglu, M., et al. (2019). Brain volume changes in patients with acute brain dysfunction due to sepsis. *Neurocrit. Care* 32, 459–468. doi: 10.1007/s12028-019-00759-8

Pamfil, C., Fanouriakis, A., Damian, L., Rinzis, M., Sidiropoulos, P., Tsivgoulis, G., et al. (2015). EULAR recommendations for neuropsychiatric systemic lupus erythematosus vs usual care: results from two European centres. *Rheumatology (Oxford)* 54, 1270–1278. doi: 10.1093/rheumatology/keu482

Papadaki, E., Fanouriakis, A., Kavroulakis, E., Karageorgou, D., Sidiropoulos, P., Bertsias, G., et al. (2018). Neuropsychiatric lupus or not? Cerebral hypoperfusion by perfusion-weighted MRI in normal-appearing white matter in primary neuropsychiatric lupus erythematosus. *Ann. Rheum. Dis.* 77, 441–448. doi: 10.1136/annrheumdis-2017-212285

Petri, M., Naqibuddin, M., Carson, K. A., Wallace, D. J., Weisman, M. H., Holliday, S. L., et al. (2008). Brain magnetic resonance imaging in newly diagnosed systemic lupus erythematosus. *J. Rheumatol.* 35, 2348–2354. doi: 10.3899/jrheum.071010

Philip, N. S., Barredo, J., van 't Wout-Frank, M., Tyrka, A. R., Price, L. H., and Carpenter, L. L. (2018). Network mechanisms of clinical response to transcranial magnetic stimulation in posttraumatic stress disorder and major depressive disorder. *Biol. Psychiatry.* 83, 263–272. doi: 10.1016/j.biopsych.2017.07.021

Piga, M., Peltz, M. T., Montaldo, C., Perra, D., Sanna, G., Cauli, A., et al. (2015). Twenty-year brain magnetic resonance imaging follow-up study in systemic lupus erythematosus: factors associated with accrual of damage and central nervous system involvement. *Autoimmun. Rev.* 14, 510–516. doi: 10.1016/j.autrev.2015.01.010

Prechl, J., and Czirjak, L. (2015). The endothelial deprotection hypothesis for lupus pathogenesis: the dual role of C1q as a mediator of clearance and regulator of endothelial permeability. *F1000Reserch* 4:24. doi: 10.12688/f1000research.6075.2

Preziosa, P., Rocca, M. A., Ramirez, G. A., Bozzolo, E. P., Canti, V., Pagani, E., et al. (2020). Structural and functional brain connectomes in patients with systemic lupus erythematosus. *Eur. J. Neurol.* 27:113–e2. doi: 10.1111/ene.14041

Ren, T., Ho, R. C., and Mak, A. (2012). Dysfunctional cortico-basal ganglia-thalamic circuit and altered hippocampal-amygdala activity on cognitive set-shifting in non-neuropsychiatric systemic lupus erythematosus. *Arthritis Rheum.* 64, 4048–4059. doi: 10.1002/art.34660

Rocca, M. A., Agosta, F., Mezzapesa, D. M., Ciboddo, G., Falini, A., Comi, G., et al. (2006). An fMRI study of the motor system in patients with neuropsychiatric systemic lupus erythematosus. *Neuroimage* 30, 478–484. doi: 10.1016/j.neuroimage.2005.09.047

Russo, D., Martino, M., Magioncalda, P., Inglese, M., Amore, M., and Northoff, G. (2020). Opposing changes in the functional architecture of large-scale networks in bipolar mania and depression. *Schizophr. Bull.* 46, 971–980. doi: 10.1093/schbul/sbaa004

Sarbu, N., Alobeidi, F., Toledano, P., Espinosa, G., Giles, I., Rahman, A., et al. (2015). Brain abnormalities in newly diagnosed neuropsychiatric lupus: systematic MRI approach and correlation with clinical and laboratory data in a large multicenter cohort. *Autoimmun. Rev.* 14, 153–159. doi: 10.1016/j.autrev.2014.11.001

Sarbu, N., Toledano, P., Calvo, A., Roura, E., Sarbu, M. I., Espinosa, G., et al. (2017). Advanced MRI techniques: biomarkers in neuropsychiatric lupus. *Lupus* 26, 510–516. doi: 10.1177/0961203316674820

Schmahmann, J. D., Guell, X., Stoodley, C. J., and Halko, M. A. (2019). The theory and neuroscience of cerebellar cognition. *Annu. Rev. Neurosci.* 42, 337–364. doi: 10.1146/annurev-neuro-070918-050258

Schwarting, A., Mockel, T., Lutgendorf, F., Triantafyllias, K., Grella, S., Boedecker, S., et al. (2019). Fatigue in SLE: diagnostic and pathogenic impact of anti-N-methyl-D-aspartate receptor (NMDAR) autoantibodies. *Ann. Rheum. Dis.* 78, 1226–1234. doi: 10.1136/annrheumdis-2019-215098

Schwartz, N., Stock, A. D., and Putterman, C. (2019). Neuropsychiatric lupus: new mechanistic insights and future treatment directions. *Nat. Rev. Rheumatol.* 15, 137–152. doi: 10.1038/s41584-018-0156-8

Shott, M. E., Filoteo, J. V., Jappe, L. M., Pryor, T., Maddox, W. T., Rollin, M. D., et al. (2012). Altered implicit category learning in anorexia nervosa. *Neuropsychology* 26, 191–201. doi: 10.1037/a0026771

Sibbitt, W. L. Jr., Brooks, W. M., Kornfeld, M., Hart, B. L., Bankhurst, A. D., and Roldan, C. A. (2010). Magnetic resonance imaging and brain histopathology in neuropsychiatric systemic lupus erythematosus. *Semin. Arthritis Rheum.* 40, 32–52. doi: 10.1016/j.semarthrit.2009.08.005

Simioni, A. C., Dagher, A., and Fellows, L. K. (2016). Compensatory striatal-cerebellar connectivity in mild-moderate Parkinson's disease. *Neuroimage Clin.* 10, 54–62. doi: 10.1016/j.nicl.2015.11.005

Smith, E. L., and Shmerling, R. H. (1999). The American College of Rheumatology criteria for the classification of systemic lupus erythematosus: strengths, weaknesses, and opportunities for improvement. *Lupus* 8, 586–595. doi: 10.1191/096120399680411317

Valsasina, P., Hidalgo de la Cruz, M., Filippi, M., and Rocca, M. A. (2019). Characterizing rapid fluctuations of resting state functional connectivity in demyelinating, neurodegenerative, and psychiatric conditions: from static to time-varying analysis. *Front. Neurosci.* 13:618. doi: 10.3389/fnins.2019.00618

Wang, P., Kong, R., Kong, X., Liegeois, R., Orban, C., Deco, G., et al. (2019). Inversion of a large-scale circuit model reveals a cortical hierarchy in the dynamic resting human brain. *Sci. Adv.* 5:eaat7854. doi: 10.1126/sciadv.aat7854

Whitfield-Gabrieli, S., and Nieto-Castanon, A. (2012). Conn: a functional connectivity toolbox for correlated and anticorrelated brain networks. *Brain Connect.* 2, 125–141. doi: 10.1089/brain.2012.0073

Zirkzee, E. J., Steup-Beekman, G. M., van der Mast, R. C., Bollen, E. L., van der Wee, N. J., Baptist, E., et al. (2012). Prospective study of clinical phenotypes in neuropsychiatric systemic lupus erythematosus; multidisciplinary approach to diagnosis and therapy. *J. Rheumatol.* 39, 2118–2126. doi: 10.3899/jrheum.120545

Conflict of Interest: The authors declare that the research was conducted in the absence of any commercial or financial relationships that could be construed as a potential conflict of interest.

Publisher's Note: All claims expressed in this article are solely those of the authors and do not necessarily represent those of their affiliated organizations, or those of the publisher, the editors and the reviewers. Any product that may be evaluated in this article, or claim that may be made by its manufacturer, is not guaranteed or endorsed by the publisher.

frontiers | Frontiers in Neuroscience

ORIGINAL RESEARCH
published: 09 May 2022
doi: 10.3389/fnins.2022.852799

Altered Variability and Concordance of Dynamic Resting-State Functional Magnetic Resonance Imaging Indices in Patients With Major Depressive Disorder and Childhood Trauma

Qianyi Luo[1], Huiwen Yu[1], Juran Chen[1], Xinyi Lin[1], Zhiyao Wu[1], Jiazheng Yao[1], Yuhong Li[1], Huawang Wu[2] and Hongjun Peng[1]**

[1] Department of Clinical Psychology, The Affiliated Brain Hospital of Guangzhou Medical University, Guangzhou, China,
[2] Department of Radiology, The Affiliated Brain Hospital of Guangzhou Medical University, Guangzhou, China

Childhood trauma is a non-specific risk factor for major depressive disorder (MDD). resting-state functional magnetic resonance imaging (R-fMRI) studies have demonstrated changes in regional brain activity in patients with MDD who experienced childhood trauma. However, previous studies have mainly focused on static characteristics of regional brain activity. This study aimed to determine the specific brain regions associated with MDD with childhood trauma by performing temporal dynamic analysis of R-fMRI data in three groups of patients: patients with childhood trauma-associated MDD (n = 48), patients without childhood trauma-associated MDD (n = 30), and healthy controls (n = 103). Dynamics and concordance of R-fMRI indices were calculated and analyzed. In patients with childhood trauma-associated MDD, a lower dynamic amplitude of low-frequency fluctuations was found in the left lingual gyrus, whereas a lower dynamic degree of centrality was observed in the right lingual gyrus and right calcarine cortex. Patients with childhood trauma-associated MDD showed a lower voxel-wise concordance in the left middle temporal and bilateral calcarine cortices. Moreover, group differences (depressed or not) significantly moderated the relationship between voxel-wise concordance in the right calcarine cortex and childhood trauma history. Overall, patients with childhood trauma-associated MDD demonstrated aberrant variability and concordance in intrinsic brain activity. These aberrances may be an underlying neurobiological mechanism that explains MDD from the perspective of temporal dynamics.

Keywords: major depressive disorder, childhood trauma, resting-state functional magnetic resonance imaging, concordance, temporal dynamics

OPEN ACCESS

Edited by:
Feng Liu,
Tianjin Medical University General Hospital, China

Reviewed by:
Yann Quidé,
University of New South Wales, Australia
Bochao Cheng,
Sichuan University, China

****Correspondence:***
Huawang Wu
huawangwu1@163.com
Hongjun Peng
pengdoctor2@163.com

Specialty section:
This article was submitted to Brain Imaging Methods, a section of the journal Frontiers in Neuroscience

Received: *11 January 2022*
Accepted: *18 March 2022*
Published: *09 May 2022*

Citation:
Luo Q, Yu H, Chen J, Lin X, Wu Z, Yao J, Li Y, Wu H and Peng H (2022) Altered Variability and Concordance of Dynamic Resting-State Functional Magnetic Resonance Imaging Indices in Patients With Major Depressive Disorder and Childhood Trauma. Front. Neurosci. 16:852799. doi: 10.3389/fnins.2022.852799

INTRODUCTION

Major depressive disorder (MDD) is a common mental illness that affects over 350 million people. It is a heterogeneous clinical syndrome that can include symptoms of disturbed mood, difficulty concentrating, bodily complaints, self-loathing, delusions of guilt, indecision, and even a strong wish to die (de Kwaasteniet et al., 2013; McCarron et al., 2021). MDD is a major leading

cause of disability and has an approximate 12-month prevalence of 6% worldwide (Kessler and Bromet, 2013). The onset and development of MDD is a complicated process and involves various factors, including genetic vulnerability (Howard et al., 2019), stressful life events and circumstances (Hammen, 2005; Southwick et al., 2005), dysfunctional cognition (Gotlib and Joormann, 2010; Figueroa et al., 2015), interpersonal dysfunction (Hammen and Brennan, 2002), female sex (Kuehner, 2017; Salk et al., 2017), and childhood trauma (Huh et al., 2017; Nelson et al., 2017).

Childhood trauma is a non-specific risk factor for MDD. Patients with childhood trauma-associated MDD have a worse treatment response (Nikkheslat et al., 2020). According to existing studies, among individuals with childhood trauma, 54% suffer from depression, 64% are addicted to illicit drugs, and 67% have experienced suicidal ideation (Dube et al., 2003). Childhood trauma consists of emotional, physical, and sexual abuse, and emotional and physical neglect (Danese and Baldwin, 2017), and has been closely associated with numerous psychiatric disorders such as MDD (Yu M. et al., 2019), bipolar disorder (Begemann et al., 2021), post-traumatic stress disorder (Kisely et al., 2018), and borderline personality disorder (Nicol et al., 2015). The neurobiological mechanisms underlying the association remain unclear. Yu M. et al. (2019) found that traumatic childhood experiences and dimensional symptoms are linked to aberrant network architecture in MDD, providing strong evidence for the negative impact of childhood trauma. Furthermore, Heim et al. (2008) and Du et al. (2016), observed an aberrant amplitude of low-frequency fluctuation (ALFF) and fractional amplitude of low-frequency fluctuation (fALFF) in patients with MDD across widespread brain regions relative to healthy controls, demonstrating that childhood trauma might lead to brain dysfunction and increased risk of MDD. Similarly, in a multimodal study, Duncan et al. (2015) found that childhood trauma causes long-term functional and structural effects in the brain.

Although previous studies have provided insights into the neurobiological mechanisms underlying MDD in patients who experienced childhood trauma, they did not examine variability and concordance in intrinsic brain activity. Brain activity fluctuates and changes over time in response to context and activity and underlies temporal-dynamic integration in the brain (Park et al., 2018). A number of studies have captured the temporal dynamic patterns of intrinsic brain activity using the sliding window method. Evidence has indicated that aberrant variability and concordance of resting-state functional magnetic resonance imaging (R-fMRI) indices are related to the mechanisms underlying MDD (Hutchison et al., 2013; Allen et al., 2014; Xue et al., 2020). Regarding aberrant variability, Zhao, Lei and colleagues reported significantly decreased dynamic ALFF (dALFF) in the emotion network in depressed patients (Zhao et al., 2021). Xue et al. (2020) observed a consistently decreased dynamic regional homogeneity (dReHo) in patients with MDD in both fusiform gyri, the right temporal pole, and the hippocampus relative to healthy controls. Additionally, Zhang et al. (2022) revealed the relationship between brain dynamic working patterns and chronic stress in adolescent MDD using the dynamic functional connectivity (FC) method. Zhu et al. (2020) reported abnormal cerebellar-cerebral dynamic FC changes in MDD. As for abnormal concordance, Zhu et al. (2019) reported decreased volume-wise concordance in patients with MDD relative to healthy controls. To characterize the local characteristics of the single voxel, ALFF and its normalized version fALFF have been used to compute the mean value of amplitudes within the 0.01–0.1 Hz low-frequency range from a Fourier decomposition of the blood oxygenation level-dependent (BOLD) time course (Zang et al., 2007; Zou et al., 2008). Regional homogeneity (ReHo) was developed to represent the level of regional brain activity coherence (Zang et al., 2004). Voxel-mirrored homotopic connectivity (VMHC) was adopted as the Pearson's correlation coefficient between the time series of each voxel in one hemisphere and the time series of its symmetrical counterpart in the opposite hemisphere (Zuo et al., 2010b). Global signal connectivity (GSCorr) was considered as the Pearson's correlation coefficient between the averaged time series and the time series of each voxel within the entire gray matter (Hahamy et al., 2014; Yang et al., 2017; Zhang et al., 2019). To depict the functional importance of the specific voxel, degree centrality (DC) was developed to calculate FC within the whole brain using the graph-theoretical approach (Buckner et al., 2009; Tomasi and Volkow, 2010; Zuo et al., 2012; Liu et al., 2015). Collectively, those R-fMRI indices have been applied widely to investigate aberrant intrinsic brain activity in depressed patients, which has enabled significant breakthroughs in the exploration of MDD neurobiological mechanisms (Guo et al., 2012; Liu et al., 2013, 2014; Shen et al., 2015; Gong et al., 2020; Ebneabbasi et al., 2021; Zhou et al., 2021). Therefore, in this study, we extensively applied dALFF, dynamic fALFF (dfALFF), dReHo, dynamic voxel mirrored homotopic connectivity (dVMHC), dynamic global signal correlation (dGSCorr), and dynamic DC (dDC) to investigate functional alterations of the brain in patients with MDD who experienced childhood trauma.

Previous studies have not explored alterations in variability and concordance of brain activity in MDD with childhood trauma. This study compared temporal dynamics analysis data based on R-fMRI images acquired from patients with MDD who experienced childhood trauma with data from patients with MDD who did not experience childhood trauma as well as healthy controls. We hypothesized that patients with MDD who experienced childhood trauma exhibit aberrant dynamic regional brain activity and concordance and that the concordance is associated with the severity of childhood trauma.

MATERIALS AND METHODS

Participants

We recruited 78 patients with MDD and 108 healthy subjects for this study. MDD diagnosis was made by two psychiatrists with extensive experience using the DSM-5 diagnostic criteria. We used the Hamilton Depressive Rating Scale (HAMD) (Helmreich et al., 2012) to assess the depression severity (for those with MDD). It is well established that the Childhood Trauma Questionnaire (CTQ) is a reliable tool to evaluate the negative

influence of maltreatment experience (Wu et al., 2022). Prior studies have proved that the CTQ has high validity in different countries (Kim et al., 2013; Isvoranu et al., 2017; Zhang et al., 2020; Petrikova et al., 2021). Using the CTQ cutoff points for the CTQ subscale scores to determine whether participants with and without traumatic experience has been widely validated and accepted (Jansen et al., 2016; Xie et al., 2018; Monteleone et al., 2020). Hence, we followed the same criterion to identify whether the participants suffered childhood maltreatment. To summarize, we used the cutoff point for the CTQ subscales score to distinguish the participants with and without childhood trauma, and the CTQ total score was used to quantify the severity of childhood maltreatment history. The CTQ total score and its subscale scores were used as continuous variables in this study. According to different types of childhood maltreatment, the CTQ can be divided into the following subscales: (i) emotional neglect (EN), (ii) physical neglect (PN), (iii) emotional abuse (EA), (iv) physical abuse (PA), and (vi) sexual abuse (SA) (Xie et al., 2018). The detailed cutoff points of CTQ subscales are shown below: (i) EN score $\geq$ 15, (ii) PN score $\geq$ 10, (iii) EA score $\geq$ 13, (iv) PA score $\geq$ 10, and SA score $\geq$ 8 (Jansen et al., 2016; Xie et al., 2018). Participants with any above-threshold score in the childhood trauma subtype will be considered as exposed to childhood maltreatment and will be included in our study. All participants received an assessment of the negative impact of traumatic history.

Based on whether each participant with or without traumatic history (using the cutoff points of the CTQ subscales to identify the participants with trauma exposure), had or had not been diagnosed with MDD (diagnosis of the patient with MDD was made by two psychiatrists), participants were divided into MDD with childhood trauma group (n = 48), MDD without childhood trauma group (n = 30), and healthy control group (n = 108). Patients with MDD were recruited from the inpatient department of the Affiliated Brain Hospital of Guangzhou Medical University. Correspondingly, 108 age-, gender-, and education-matched healthy controls were recruited from the advertising and nearby community. We excluded patients who (i) did not have a first episode of depression, (ii) had a history of any other major mental illness and physical disorder, (iii) had a family history of any other major mental illness and physical disorder, (iv) were taking psychiatric medication before (non-drug-naive), (v) received systemic psychotherapy and electroconvulsive therapy before, and (vi) were with contraindication for R-fMRI. The study was approved by the Ethics Committee of the Affiliated Brain Hospital of Guangzhou Medical University. All participants offered their written informed consent before the data collection.

Magnetic Resonance Imaging Data Acquisition

MRI images were obtained using a 3T Philips scanner at the radiology department of The Affiliated Brain Hospital of Guangzhou Medical University in China. (i) Resting-state functional scans were performed using a gradient-echo echoplanar imaging sequence with the parameters listed below: TR = 2,000 ms, TE = 30 ms, number of slices = 33, flip angle = 90°, matrix = 64 × 64, field of view = 220 × 220 mm^2, and slice thickness = 4 mm with 0.6 mm interslice gap. The whole scanning process included 240 time points, lasting for 8 min. (ii) High-resolution 3D T1 images were acquired with the parameters listed below: TR/TE = 8.2/3.7 ms, number of slices = 188, slice thickness = 1 mm, flip angle = 7°, acquisition matrix = 256 × 256, and voxel size = 1 mm × 1 mm × 1 mm. All participants were instructed to close their eyes, relax, remain motionless, and keep awake.

Magnetic Resonance Imaging Data Preprocessing

Using the DPARSF toolbox (DPARSFA[1]) to preprocess the R-fMRI images, first, we removed the first ten volumes to allow data to reach equilibrium; second, we performed slice timing and head motion. Notably, the mean framewise displacement (FD) based on the Jenkinson model (FD-Jenkinson) was computed by averaging the FD from every time point for each subject (Jenkinson et al., 2002). We included only subjects with relatively low head motion (criteria: mean FD < 0.2 mm). Third, we conducted structural image alignment with a six-degree-of-freedom linear transformation to align the T1 image to the functional image; subsequently, we segmented the transformed structural images into the cerebrospinal fluid, white matter, and gray matter (Ashburner and Friston, 2005); Then, we spatially normalized the motion-corrected functional images into standard MNI space with 3 mm × 3 mm × 3 mm using the normalization parameters estimated during unified segmentation. The normalized images of the resulting ALFF and fALFF were then smoothed using a 4-mm FWHM Gaussian kernel. Subsequently, we treated Friston 24-head motion parameters, the white matter signal, and the CSF signal as the nuisance covariates to regress out (Friston et al., 1996). As for calculating ReHo, VMHC, and DC, the normalized images were subjected to nuisance regression to regress out Friston 24-head motion parameters, the white matter signal, and the CSF signal (Friston et al., 1996). Finally, the images were filtered with a temporal band-pass filter between 0.01 and 0.08 Hz.

Dynamic Resting-State Functional Magnetic Resonance Imaging Indices Calculation

Dynamic indices were computed using the temporal dynamic analysis toolkits on DPABI (Yan et al., 2016) (DPABI,[2] version 4.5). We used the sliding-window approach to explore alterations in variability and concordance of dynamic R-fMRI indices throughout the whole brain. For the calculation of the dynamic R-fMRI indices, window length is an essential but open parameter. Prior research has pointed out that 50 TRs window length is the most suitable parameter to maintain the balance between achieving reliable estimates of intrinsic brain activity (with a longer window length) and capturing high-speed shifting

[1] www.restfmri.net/forum/DPARSF

[2] http://rfmri.org/dpabi

dynamic brain activity (with a shorter window length) (Liao et al., 2019; Cui et al., 2020; Liu et al., 2021). Thus, a sliding window length of 50 TRs and a step size of 1 TR were selected to analyze the dynamic R-fMRI indices in this study.

The time series of each subject was divided into 181 windows. In each window, R-fMRI metrics, including ALFF, fALFF, ReHo, GSCorr, VMHC, and DC, were calculated. Then, the following dynamic indices were analyzed: dALFF, dfALFF, dReHo, dGSCorr, dVMHC, and dDC. Images for calculating ALFF and fALFF were smoothed but not filtered; the images for calculating the other indices were filtered but not smoothed. A standard deviation (SD) across the windows was then computed to represent the dynamic indices. Finally, smoothing and Z standardization were executed on the SD maps (apart from dALFF and dfALFF, which were smoothed before). Window sizes of 30 TRs and 70 TRs were also computed (refer to **Supplementary Data**).

Computation of Multiple Resting-State Functional Magnetic Resonance Imaging Indices

Interdependence among the following six R-fMRI brain activity indices was investigated:

(i) ALFF and fALFF: Above all, we transformed the time course into the frequency domain to acquire the corresponding power spectrum by using a Fast Fourier Transform. Then, we computed the square root at each frequency of the power spectrum. In particular, the averaged square root within the 0.01–0.1 Hz low-frequency range was considered the ALFF value (Zang et al., 2007). Moreover, fALFF was accepted as the ratio of the power spectrum within the 0.01–0.1 Hz low-frequency range to that of the whole frequency range (Zou et al., 2008). Owing to the high colinearity between ALFF and fALFF, we only included the fALFF value in the subsequent concordance calculation, as it improves specificity and sensitivity when examining regional brain activity (Zou et al., 2008; Zuo et al., 2010a; Yan et al., 2013).

(ii) ReHo: ReHo was adopted to represent the level of regional brain activity coherence. It was accepted as Kendall's coefficient of concordance of the BOLD time course of a specific voxel with its 26 neighboring voxels' time course (Zang et al., 2004).

(iii) GSCorr: GSCorr was considered the Pearson's correlation coefficient between the averaged time series and time series of each voxel within the entire gray matter (Hahamy et al., 2014; Yang et al., 2017; Zhang et al., 2019). Afterward, the above GSCorr values underwent Fisher's z-transformation to reach distribution normality.

(iv) VMHC: VMHC was adopted as the Pearson's correlation coefficient between the time series of each voxel in one hemisphere and the time series of its symmetrical counterpart in the opposite hemisphere (Zuo et al., 2010b). Subsequently, the above VMHC values underwent Fisher's z-transformation to reach distribution normality.

(v) DC: We computed the Pearson's correlation coefficients between the time series of all the pairwise voxels within the entire gray matter. This correspondingly resulted in the FC matrix of the entire gray matter. DC was accepted as the sum of positive FC (defined as FC values above a threshold of 0.25) between a given voxel and the rest of the voxels (Buckner et al., 2009; Zuo et al., 2012).

Our study is an exploratory analysis and aims to examine the aberrant variability and concordance of dynamic resting-state fMRI indices (i.e., dALFF, dfALFF, dReHo, dVMHC, dGSCorr, and dDC) in patients with MDD who experienced childhood trauma. Following extensive exploratory analysis, we observed significant variability differences in dALFF and dDC.

TABLE 1 | Demographic and clinical scale scores of MDD with childhood trauma, MDD without childhood trauma, and HC group.

	MDD with childhood trauma (n = 48)	MDD without childhood trauma (n = 30)	HC (n = 103)	F/t/x^2	p-value
Age (years), mean ± SD	28.1 ± 6.524	29.07 ± 7.913	27.03 ± 6.591	1.185	0.308
Gender (male/female)	24/23	11/19	44/59	2.436	0.119
Educational level (years), mean ± SD	12.92 ± 3.319	13.73 ± 3.35	14.32 ± 2.598	3.778*	0.025
MDD onset age	27.9 ± 6.722	28.00 ± 7.424	26.94 ± 7.268	2.122	0.560
HAMD score	29.46 ± 8.543	29.73 ± 5.458	–	0.025	0.876
HAMA score	16.65 ± 6.849	19.7 ± 6.276	–	3.91	0.052
Mean FD (mm)	0.564 ± 0.021	0.582 ± 0.021	0.561 ± 0.017	0.141	0.869
CTQ score	55.33 ± 12.575	29.7 ± 4.535	38.09 ± 9.126	78.385**	<0.001
Emotional neglect	18.04 ± 3.984	7.43 ± 2.921	11.15 ± 4.729	66.043**	<0.001
Physical neglect	12.19 ± 3.486	5.77 ± 1.04	8.31 ± 2.927	51.169**	<0.001
Emotional abuse	11.02 ± 4.987	5.73 ± 1.165	7.06 ± 2.678	30.897**	<0.001
Physical abuse	8.06 ± 4.503	5.57 ± 1.165	6.07 ± 1.767	11.035**	<0.001
Sexual abuse	6.02 ± 2.686	5.2 ± 0.407	5.5 ± 1.065	2.754	0.066

*$p < 0.05$, **$p < 0.01$.
MDD, major depressive disorder; CTQ, childhood trauma questionnaire; HC, healthy control.

However, no significant variability difference was identified for the other metrics.

Concordance Analysis

Concordance values were computed based on Kendall's W coefficient. Two types of concordance indices were calculated: (i) volume-wise concordance, computed as the global level concordance index across voxels; and (ii) voxel-wise concordance, computed as the voxel-level concordance across time windows of each subject.

Statistical Analysis

Statistical analyses were conducted using SPSS software version 19.0 (IBM Corp., Armonk, NY, United States). Demographic data, clinical scale scores, and volume-wise concordance were compared between groups using the chi-square test and one-way ANOVA with *post hoc* Bonferroni correction. To compare voxel-wise concordance and standardized SD maps between groups, one-way ANOVA with *post hoc* Bonferroni correction for multiple comparisons was conducted. Significant results are obtained from the multiple comparisons with Bonferroni correction *post hoc* tests. Family-wise error correction (FWE) was conducted with a significance threshold of $p < 0.05$ and a cluster size of > 15 voxels (Wang et al., 2014). Mean dynamic index values were extracted from brain regions showing significant intergroup differences in the voxel-wise dynamic analyses. In the multiple comparisons in regions with differences in dDC, $p < 0.05/2 = 0.025$ was accepted as significant owing to dDC analysis resulting in two significant clusters. In the multiple comparisons in regions with differences in voxel-wise concordance, $p < 0.05/3 = 0.016$ was accepted as significant (voxel-wise concordance analysis resulting in three significant clusters). Pearson's correlation analyses were used to explore the associations of voxel-wise concordance with CTQ score in all participants [$p < 0.05/18 = 0.0027$, with Bonferroni correction of 18 being due to three clusters and 6 scales (i.e., CTQ scale and its five subscales)]. In addition, to further quantitatively compare correlation coefficients between groups, we used a regression model with group moderating the associations of dynamic indices with CTQ score ($p < 0.05/3 = 0.016$, with Bonferroni correction of 3 due to three clusters). In this study, age, gender, and education were considered as control variables.

TABLE 2 | Regions with differences in dynamic R-fMRI indices among the MDD with childhood trauma, MDD without childhood trauma, and HC groups.

Anatomical region	Peak MNI			Cluster size	*F*
	x	*y*	*z*		
dALFF					
Left lingual	0	−81	3	36	11.6394
dDC					
Right lingual	9	−81	0	26	12.7027
Right calcarine	12	−63	18	78	11.8277

dALFF, dynamics of amplitude of low-frequency fluctuations; dDC, dynamics of degree centrality; MDD, major depressive disorder; HC, healthy control.

RESULTS

Demographic Data

As shown in **Table 1**, no significant differences were found between the patients with MDD-associated childhood trauma, patients without MDD-associated childhood trauma, and control groups with respect to demographic data, Hamilton Anxiety Rating Scale score, and Hamilton Depressive Rating Scale score. However, the CTQ score and its subscale scores significantly differed between groups.

Dynamics of Resting-State Functional Magnetic Resonance Imaging Indices

Intergroup differences in dALFF were detected in the left lingual gyrus (**Table 2** and **Figure 1**), whereas differences in dDC were observed in the right lingual gyrus and the right calcarine cortex (**Table 2** and **Figure 1**). The *post hoc* testing showed that dALFF and dDC were lower in the patients with childhood trauma-associated MDD group than in the patients without childhood trauma-associated MDD and the control group (**Table 3** and **Figure 1**). Other dynamic indices did not significantly differ between groups.

Volume-Wise Concordance of Resting-State Functional Magnetic Resonance Imaging Indices

Mean volume-wise concordance values significantly differed among the three groups ($p = 0.001$). The *post hoc* testing showed that mean concordance was lower in the patients with childhood trauma-associated MDD group than in the control group. SD values of volume-wise concordance did not significantly differ between the three groups ($p = 0.996$; **Figure 2** and **Table 4**).

Voxel-Wise Concordance of Resting-State Functional Magnetic Resonance Imaging Indices

Significant differences were observed in the left middle temporal and bilateral calcarine cortices when comparing voxel-wise concordance between the groups (**Figure 3** and **Table 5**). Multiple comparisons showed that the concordance of these regions in the patients with childhood trauma-associated MDD group was lower than that in the other two groups (**Figure 3** and **Table 6**).

Correlation Analysis and Multiple Linear Regression Analysis

We further examined the associations of dALFF and dDC with the CTQ total score. As shown in **Figure 4** and **Table 7**, the correlation analyses revealed that childhood trauma history was negatively correlated with voxel-wise concordance in the left middle temporal ($r = -0.166$, $p = 0.026$), left calcarine ($r = -0.160$, $p = 0.032$), and right calcarine ($r = -0.165$, $p = 0.027$), respectively.

Moreover, multiple linear regression analysis (Baron and Kenny, 1986) was used to investigate whether a history of childhood trauma has the same effect on dALFF and dDC in

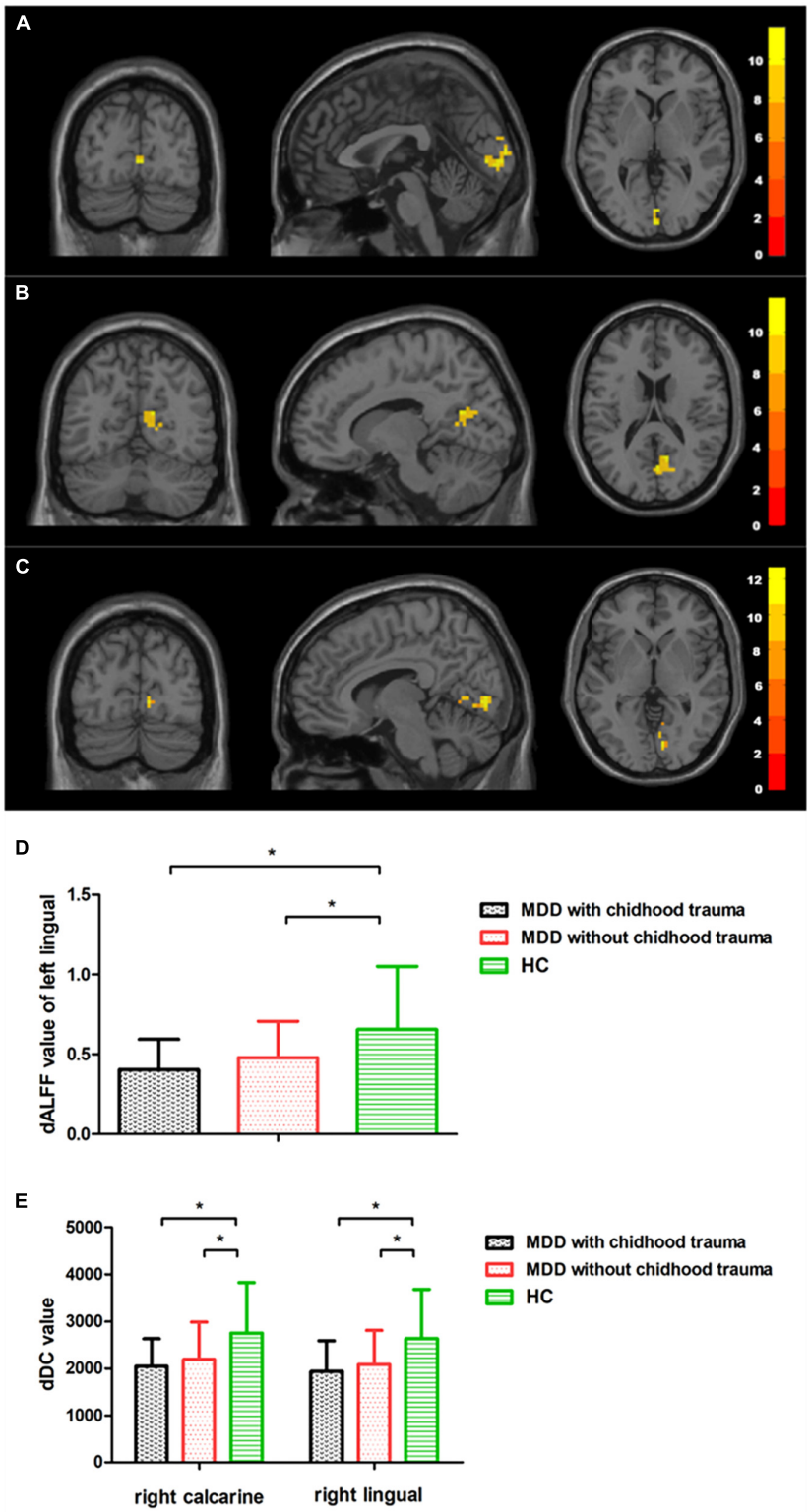

FIGURE 1 | Regions with differences in dALFF and dDC between the MDD with childhood trauma, MDD without childhood trauma, and HC groups and *post hoc* analysis. **(A)** The intergroup difference in dALFF in the left lingual gyrus. **(B,C)** The intergroup difference in dDC in the right lingual gyrus and the right calcarine cortex, respectively. **(D,E)** The multiple comparisons in regions with differences in dALFF and dDC, respectively. MDD, major depressive disorder; HC, healthy control; dALFF, dynamics of amplitude of low-frequency fluctuations; dDC, dynamics of degree centrality. * means the *p*-value has reached a significant level. In the multiple comparisons in regions with differences in dDC, $p < 0.05/1 = 0.05$ was accepted as significant. In the multiple comparisons in regions with differences in dDC, $p < 0.05/2 = 0.025$ was accepted as significant.

TABLE 3 | Multiple comparisons in regions with differences in dALFF and dDC.

Dynamic R-fMRI indices	Anatomical region	(I)	(J)	Mean difference (I-J)	*p*	95% CI	
dALFF	Left lingual	MDD with childhood trauma	MDD without childhood trauma	−0.0622708	0.413	−0.212051	0.08751
			HC	−0.2512045*	<0.001	−0.363675	−0.138734
		MDD without childhood trauma	MDD with childhood trauma	0.0622708	0.413	−0.08751	0.212051
			HC	−0.1889337*	0.006	−0.32245	−0.055417
		HC	MDD with childhood trauma	0.2512045*	<0.001	0.138734	0.363675
			MDD without childhood trauma	0.1889337*	0.006	0.055417	0.32245
dDC	Right lingual	MDD with childhood trauma	MDD without childhood trauma	−114.333	0.589	−531.23	302.56
			HC	−696.346*	<0.001	−1009.4	−383.3
		MDD without childhood trauma	MDD with childhood trauma	114.333	0.589	−302.56	531.23
			HC	−582.013*	0.002	−953.64	−210.38
		HC	MDD with childhood trauma	696.346*	<0.001	383.3	1009.4
			MDD without childhood trauma	582.013*	0.002	210.38	953.64
	Right calcarine	MDD with childhood trauma	MDD without childhood trauma	2043.499*	<0.001	1646.31	2440.69
			HC	−708.469*	<0.001	−1006.72	−410.22
		MDD without childhood trauma	MDD with childhood trauma	−2043.499*	<0.001	−2440.69	−1646.31
			HC	−2751.968*	<0.001	−3106.03	−2397.91
		HC	MDD with childhood trauma	708.469*	<0.001	410.22	1006.72
			MDD without childhood trauma	2751.968*	<0.001	2397.91	3106.03

*P_{adjust} was set as 0.05/2 = 0.025. MDD, major depressive disorder; HC, healthy control.

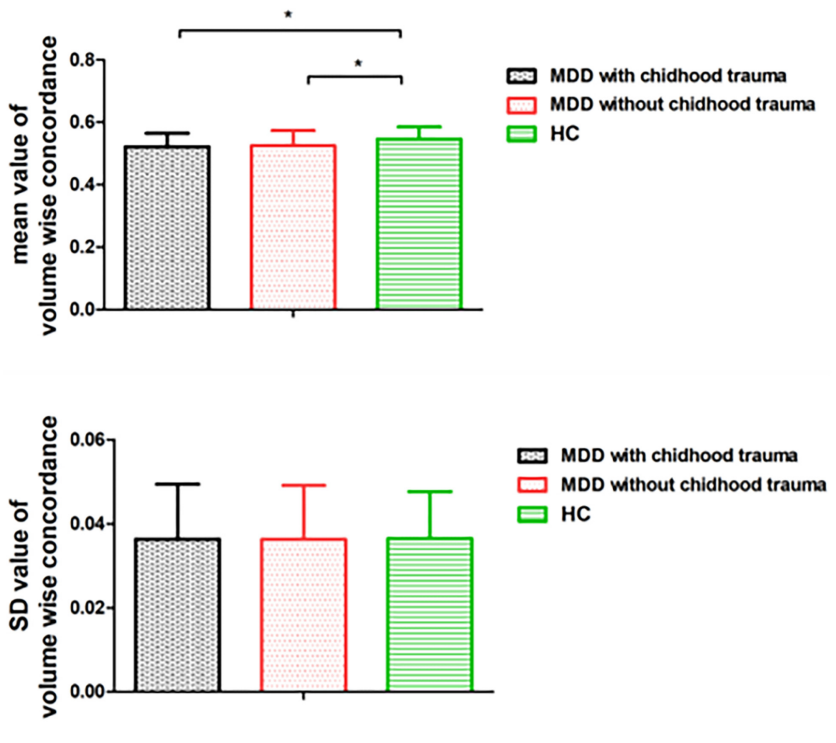

FIGURE 2 | Comparison of volume wise concordance among the MDD with childhood trauma, MDD without childhood trauma, and HC groups. MDD, major depressive disorder; HC, healthy control. *$p < 0.05$.

individuals with and without depression. We defined group difference (depressed or not), CTQ total score, and their interaction as independent variables; functional concordance was defined as the dependent variable; age, gender, and education were considered as nuisance covariates. To avoid multicollinearity, we performed mean centering for all the independent variables before constructing the interaction terms (Holmbeck, 1997). As shown in **Table 8**, further regression

TABLE 4 | Comparison of volume wise concordance among the MDD with childhood trauma, MDD without childhood trauma, and HC groups.

	MDD with childhood trauma	MDD without childhood trauma	HC	*F*	*p*
Mean	0.521 ± 0.043	0.524 ± 0.048	0.546 ± 0.038	7.068	0.001
SD	0.036 ± 0.013	0.036 ± 0.012	0.036 ± 0.011	0.004	0.996

MDD, major depressive disorder; HC, healthy control.

analyses showed an interaction of group and childhood trauma history on dALFF of the left lingual gyrus ($F = 6.798$, $p < 0.001$), dDC of the right lingual gyrus ($F = 5.423$, $p < 0.001$), and dDC of the right calcarine cortex ($F = 5.529$, $p < 0.001$).

DISCUSSION

This study adopted temporal dynamic analysis to examine aberrant variability and concordance of intrinsic brain activity in patients with childhood trauma-associated MDD. Several findings were interesting: (i) patients with childhood trauma-associated MDD exhibited lower dALFF in the left lingual gyrus and lower dDC in the right calcarine cortex as well as the right lingual gyrus relative to healthy subjects; (ii) patients with childhood trauma-associated MDD showed decreased volume-wise concordance compared with healthy controls; (iii) decreased voxel-wise concordance was observed in the left middle temporal cortex and bilateral calcarine cortices in patients with childhood trauma-associated MDD; and (iv) multiple linear regression

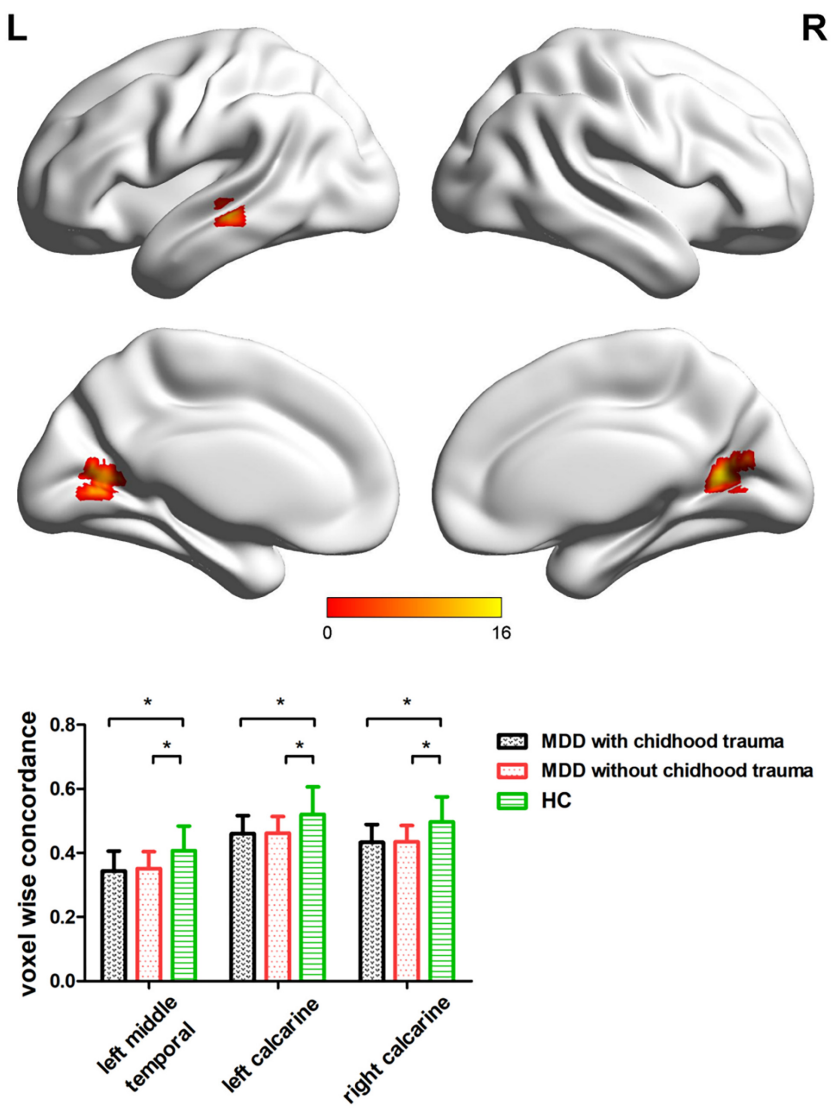

FIGURE 3 | Regions with differences in the voxel wise concordance of R-fMRI indices among the MDD with childhood trauma, MDD without childhood trauma, and HC groups and *post-hoc* analysis. MDD, major depressive disorder; HC, healthy control. * means the *p*-value has reached a significant level. In the multiple comparisons in regions with differences in voxel-wise concordance, $p < 0.05/3 = 0.016$ was accepted as significant (voxel-wise concordance analysis resulting in three significant clusters).

TABLE 5 | Regions with differences in the voxel-wise concordance of R-fMRI indices among the MDD with childhood trauma, MDD without childhood trauma, and HC groups.

Anatomical region	Peak MNI			Cluster size	*F*
	x	*y*	*z*		
Left middle temporal	−60	−27	−6	36	15.8445
Left calcarine	−21	−69	15	57	11.8452
Right calcarine	21	−60	9	68	15.5341

analysis revealed that history of childhood trauma had a different impact on aberrant brain functional concordance in depressed patients and healthy subjects. However, dynamic R-fMRI index and functional concordance analyses showed no significant differences between the MDD with childhood trauma group and the MDD without childhood trauma group, which may be related to our small sample size.

Patients with childhood trauma-associated MDD had lower dALFF (mainly detected in the left lingual gyrus) and dDC (mainly detected in the right lingual gyrus and right calcarine cortex) than healthy subjects, suggesting stable but inflexible intrinsic brain activity in patients with childhood trauma-associated MDD. Previous studies have suggested that dysfunction in the lingual gyrus and calcarine cortex is closely linked to the development of MDD in patients with previous childhood trauma. Childhood trauma has been associated with impairment of emotion regulation, involving the multiprocess of emotion regulatory stages that precede and follow psychological regulatory implementation (Bonanno and Burton, 2013). Preliminary investigations that focused on the neural basis of emotion dysregulation have reported that activation in specific brain areas (including the lingual gyrus and calcarine cortex) is associated with attentional deployment, cognitive change, and response modulation (Sheppes et al., 2015).

Greater activation in the left lingual gyrus has been observed during the processing of the sadness emotion (Groves et al., 2018), suggesting that different patterns of brain activation in the lingual gyrus might be related to the underlying neural mechanisms of depression. Moreover, Daniels et al. (2012) identified a positive relationship between the history of childhood trauma and higher activation in the lingual gyrus. Evidence from temporal dynamics analysis has also revealed a key role for the lingual gyrus in processing negative emotions. In a neuroimaging study of brain dynamics in depressed patients, Zhang et al. (2021) detected significantly lower dALFF in patients with MDD relative to healthy subjects, which is in line with our findings. In a dynamic functional network connectivity analysis, Zhi et al. (2018) found that depressed patients exhibited decreased harmonic centrality values in the lingual gyrus, which was correlated with clinical symptom severity and self-cognition. In depressed patients with suicidal ideation, an aberrant dynamic functional connection between the lingual gyrus and habenula has been detected (Qiao et al., 2020). Considering the findings of prior studies as well as this study, abnormal brain activity variability in the lingual gyrus might indicate disrupted dynamic intrinsic brain activity in patients with MDD. Moreover, the lingual gyrus is widely involved in distinguishing emotional facial expressions and verbal declarative memory (Kitada et al., 2010); difficulties with these processes are common in patients with childhood trauma-associated MDD. The lingual gyrus dysfunction in patients with childhood trauma-associated MDD might reflect an increased ability to identify and encode adverse experiences in verbal declarative memory (Kitada et al., 2010). In conclusion, the alterations in variability in the lingual gyrus might be specific to the additive effects of MDD and childhood trauma history.

We detected a significant decrease in dDC in the right lingual gyrus and right calcarine cortex. Calcarine cortex dysfunction is frequently observed in patients with MDD and is closely related to depression severity. A previous study has confirmed a relationship between increased depressive symptoms and increased FC between the calcarine cortex and basolateral amygdala in veterans with MDD (McGlade et al., 2020). Additionally, a previous meta-analysis reported decreased cortical thickness in the left calcarine cortex and lingual gyrus in depressed patients compared with healthy controls (Suh et al., 2019). Similarly, decreased normalized cerebral blood flow in the right calcarine cortex in early-onset MDD patients has been observed, providing more experimental evidence for the contribution of calcarine dysfunction to the development of depression (Liao et al., 2017). More powerful evidence from FC analysis detected significantly reduced FC between the right posterior insular gyrus, calcarine cortex, and lingual gyrus in adolescents with MDD (Hu et al., 2019). Notably, childhood trauma might also cause calcarine cortex dysfunction (Luo et al., 2022). In addition to statistical analysis, dynamic analysis has also revealed a key role of abnormal calcarine variability in contributing to the negative impact of depression from the perspective of temporal dynamics. Decreased dALFF has been previously detected in the calcarine cortex (Zhang et al., 2021), which is consistent with our findings and further confirms the relationship between the development of depression and abnormal brain variability in the calcarine cortex. Similarly, by examining alterations in dfALFF, Hu, L. and colleagues identified altered variability in the calcarine cortex in depressed patients with mild cognitive impairment relative to those without mild cognitive impairment (Yu Y. et al., 2019). Furthermore, Li et al. (2021) surprisingly found that baseline functional stability in the calcarine cortex could effectively predict improvement of clinical symptoms in depressed patients. The altered variability in the calcarine cortex observed in our study may be a core neurobiological feature of MDD with childhood trauma.

Intergroup differences were found in functional voxel-wise and volume-wise concordance. Specifically, patients with childhood trauma-associated MDD showed decreased voxel-wise concordance in the left middle temporal, left calcarine, and right calcarine cortices compared with healthy controls; volume-wise concordance was also lower in patients with childhood trauma-associated MDD. The temporal gyrus is involved in language and memory function (Eichenbaum et al., 2007), whereas the calcarine cortex plays a key role in integrating "visuopsychic" and "visuosensory" processing (Ffytche and Catani, 2005). In a previous study, adults who experienced

TABLE 6 | Multiple comparisons in regions with differences in voxel-wise concordance.

Anatomical region	(I)	(J)	Mean difference (I-J)	*p*	95% CI	
Right calcarine	MDD with childhood trauma	MDD without childhood trauma	−0.001788	0.911	−0.03344	0.02986
		HC	−0.063534*	<0.001	−0.0873	−0.03977
	MDD without childhood trauma	MDD with childhood trauma	0.001788	0.911	−0.02986	0.03344
		HC	−0.061746*	<0.001	−0.08996	−0.03353
	HC	MDD with childhood trauma	0.063534*	<0.001	0.03977	0.0873
		MDD without childhood trauma	0.061746*	<0.001	0.03353	0.08996
Left calcarine	MDD with childhood trauma	MDD without childhood trauma	−0.002346	0.891	−0.03622	0.03153
		HC	−0.060463*	<0.001	−0.0859	−0.03503
	MDD without childhood trauma	MDD with childhood trauma	0.002346	0.891	−0.03153	0.03622
		HC	−0.058117*	<0.001	−0.08831	−0.02792
	HC	MDD with childhood trauma	0.060463*	<0.001	0.03503	0.0859
		MDD without childhood trauma	0.058117*	<0.001	0.02792	0.08831
Left middle temporal	MDD with CT	MDD without childhood trauma	−0.007787	0.63	−0.03959	0.02402
		HC	−0.063079*	<0.001	−0.08696	−0.0392
	MDD without childhood trauma	MDD with childhood trauma	0.007787	0.63	−0.02402	0.03959
		HC	−0.055292*	<0.001	−0.08364	−0.02694
	HC	MDD with childhood trauma	0.063079*	<0.001	0.0392	0.08696
		MDD without childhood trauma	0.055292*	<0.001	0.02694	0.08364

*P_{adjust} was set as 0.05/3 = 0.016.
MDD, major depressive disorder; HC, healthy control.

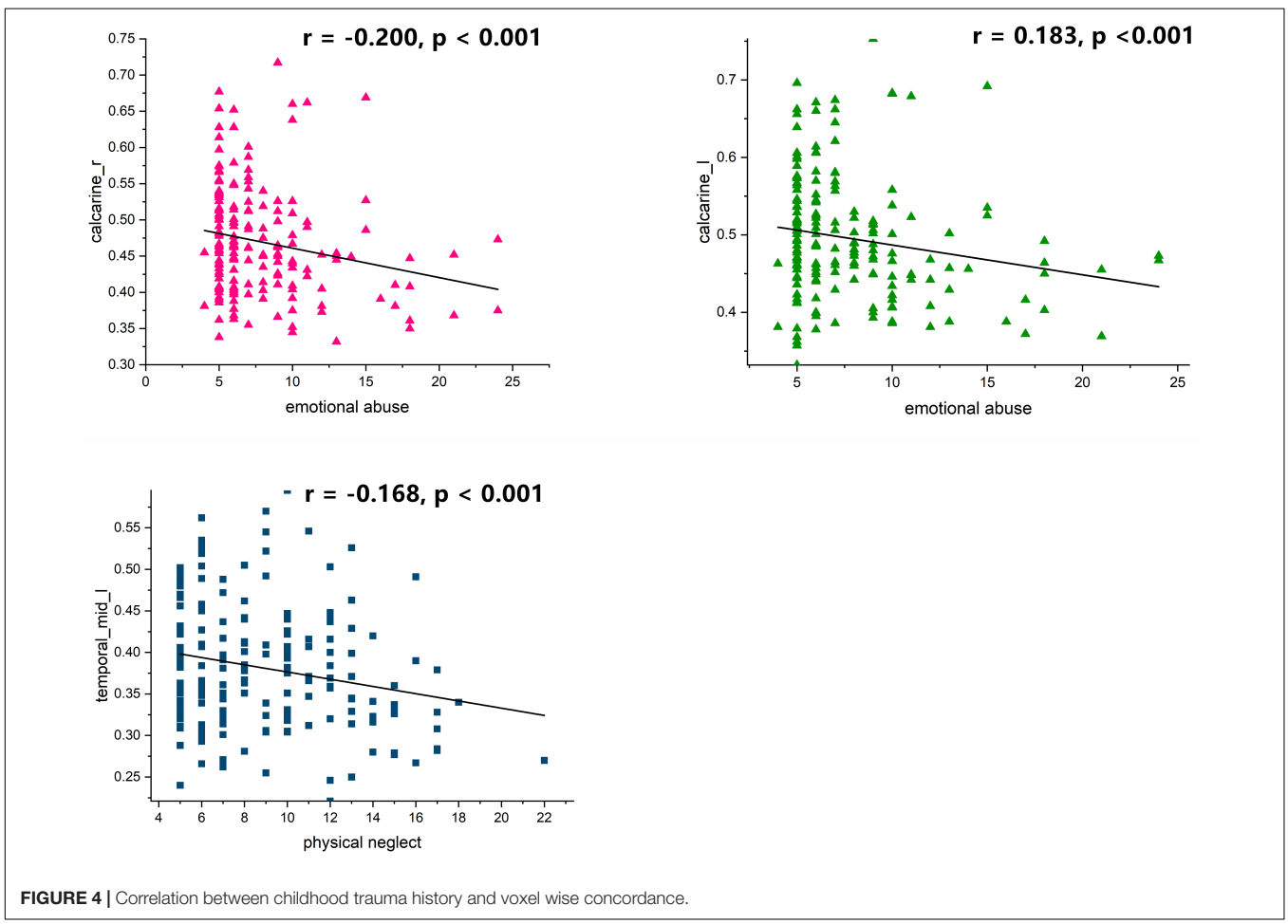

FIGURE 4 | Correlation between childhood trauma history and voxel wise concordance.

TABLE 7 | Correlation between voxel wise concordance and childhood trauma.

	Emotional abuse	Physical abuse	Sexual abuse	Emotional neglect	Physical neglect	Total score of CTQ
Right calcarine	−0.200*	−0.221*	0.042	−0.13	−0.100	−0.165
Left calcarine	−0.183*	−0.136	−0.001	−0.149	−0.072	−0.160
Left middle temporal	−0.124	−0.160	0.108	−0.125	−0.168*	−0.166

P_{adjust} was set as 0.05/18 = 0.0027.

TABLE 8 | Multiple linear regressions analyses between childhood trauma history and dynamic indices.

Model		Unstandardized coefficients	Standardized coefficients	*t*	*p*	95% confidence interval	
		B	Beta			Lower bound	Upper bound
dALFF of left lingual gyrus	Age	0.011	0.224	3.215*	0.002	0.004	0.018
	Education	−0.018	−0.156	−2.193	0.03	−0.034	−0.002
	Gender	0.038	0.055	0.794	0.428	−0.056	0.132
	Group	0.232	0.334	4.633*	<0.001	0.133	0.33
	CTQ total score	−0.004	−0.158	−2.097	0.037	−0.008	0.000
	Group * CTQ total score	−0.0012	−0.004	−0.058	0.954	0.000	0.000
dDC of right lingual gyrus	Age	14.176	0.099	1.392	0.166	−5.92	34.272
	Education	−11.806	−0.036	−0.499	0.618	−58.513	34.901
	Gender	−123.058	−0.063	−0.896	0.371	−394.124	148.007
	Group	626.742	0.319	4.339*	<0.001	341.682	911.802
	CTQ total score	−12.595	−0.17	−2.204	0.029	−23.875	−1.315
	Group * CTQ total score	−0.011	−0.136	−1.836	0.068	−0.023	0.001
dDC of right calcarine cortex	Age	12.291	0.087	1.227	0.221	−7.472	32.053
	Education	−13.183	−0.041	−0.566	0.572	−59.114	32.748
	Gender	−104.621	−0.054	−0.775	0.44	−371.183	161.942
	Group	636.274	0.329	4.48*	<0.001	355.95	916.599
	CTQ total score	−11.588	−0.159	−2.062*	0.041	−22.68	−0.495
	Group * CTQ total score	−0.013	−0.158	−2.145	0.033	−0.025	−0.001

P_{adjust} was set as 0.05/3 = 0.016.

childhood trauma had increased activation in the left middle temporal gyrus and left superior frontal gyrus, indicating an association between middle temporal gyrus dysfunction and underlying neurophysiological MDD mechanisms (Heany et al., 2018). Furthermore, increased FC between the calcarine cortex and amygdala has been shown in patients with post-traumatic stress disorder, which demonstrates that the calcarine cortex plays an essential role in the processing of fear and threat cues (Morey et al., 2015). Moreover, R-fMRI metrics have been shown to have a high concordance in cortical and subcortical areas across the whole time window (Yan et al., 2017). Voxel-wise concordance might characterize the homogeneity between the various R-fMRI metrics (Lou et al., 2021). Therefore, aberrant functional concordance in the left middle temporal and left and right calcarine cortices might reflect the impaired integrative function of intrinsic brain activity.

In our multiple linear regression analyses of dynamic indices and childhood trauma history, group differences (depressed or not) significantly moderated the relationship between dALFF and dDC and childhood trauma history, indicating that childhood trauma has a significantly different impact on aberrant brain functional concordance in depressed patients and healthy subjects. This result highlights the key role of childhood trauma in mental health development and provides evidence that it is detrimental.

Limitations and Future Directions

This study had several limitations. First, we used a cross-sectional approach, which does not examine cause and effect. Second, the sample size was small, which is probably why we could not detect a difference between MDD patients with and without childhood trauma. Future large-scale studies are warranted. Moreover, childhood trauma subtype analyses were not conducted due to the small sample size. Future studies should focus on the impact of a single subtype of childhood trauma, such as neglect or abuse. Third, childhood trauma was assessed retrospectively *via* self-report; although the CTQ is reliable and widely used, evaluation of traumatic history using an objective tool would have been preferable.

CONCLUSION

Patients with childhood trauma-associated MDD demonstrated aberrant variability and concordance in intrinsic brain activity.

These aberrances may be an underlying neurobiological mechanism that explains MDD from the perspective of temporal dynamics.

DATA AVAILABILITY STATEMENT

The original contributions presented in the study are included in the article/**Supplementary Material**, further inquiries can be directed to the corresponding author/s.

ETHICS STATEMENT

The studies involving human participants were reviewed and approved by the Ethics Committee of the Affiliated Brain Hospital of Guangzhou Medical University. The patients/participants provided their written informed consent to participate in this study.

AUTHOR CONTRIBUTIONS

HP, HW, and QL designed the study and drafted the primary manuscript. HW, ZW, and QL supervised the recruitment and made statistical analyses. JC, QL, and YL took part in recruitment and data management. HP and HW made further revisions to the manuscript. All authors had read and approved the final manuscript.

FUNDING

This study design was supported by the Guangdong Natural Science Foundation, China (2015A030313800) to HP. The data collection of the study was also supported by the Guangzhou Municipal Key Discipline in Medicine for Guangzhou Brain Hospital (GBH2014-ZD04) to HP.

ACKNOWLEDGMENTS

We thank Liwen Bianji (Edanz) (https://www.liwenbianji.cn) for editing the language of a draft of this manuscript.

SUPPLEMENTARY MATERIAL

The Supplementary Material for this article can be found online at: https://www.frontiersin.org/articles/10.3389/fnins.2022.852799/full#supplementary-material

REFERENCES

Allen, E. A., Damaraju, E., Plis, S. M., Erhardt, E. B., and Eichele, T. (2014). Tracking whole-brain connectivity dynamics in the resting state. *Cereb. Cortex* 24, 663–676. doi: 10.1093/cercor/bhs352

Ashburner, J., and Friston, K. J. (2005). Unified segmentation. *Neuroimage* 26, 839–851. doi: 10.1016/j.neuroimage.2005.02.018

Baron, R. M., and Kenny, D. A. (1986). The moderator-mediator variable distinction in social psychological research: conceptual, strategic, and statistical considerations. *J. Pers. Soc. Psychol.* 51, 1173–1182. doi: 10.1037//0022-3514.51.6.1173

Begemann, M., Schutte, M., van Dellen, E., Abramovic, L., and Boks, M. P. (2021). Childhood trauma is associated with reduced frontal gray matter volume: a large transdiagnostic structural MRI study. *Psychol. Med.* [Online ahead of print]. doi: 10.1017/S0033291721002087

Bonanno, G. A., and Burton, C. L. (2013). Regulatory flexibility: an individual differences perspective on coping and emotion regulation. *Perspect. Psychol. Sci.* 8, 591–612. doi: 10.1177/1745691613504116

Buckner, R. L., Sepulcre, J., Talukdar, T., Krienen, F. M., and Liu, H. (2009). Cortical hubs revealed by intrinsic functional connectivity: mapping, assessment of stability, and relation to Alzheimer's disease. *J. Neurosci.* 29, 1860–1873. doi: 10.1523/JNEUROSCI.5062-08.2009

Cui, Q., Sheng, W., Chen, Y., Pang, Y., and Lu, F. (2020). Dynamic changes of amplitude of low-frequency fluctuations in patients with generalized anxiety disorder. *Hum. Brain Mapp.* 41, 1667–1676. doi: 10.1002/hbm.24902

Danese, A., and Baldwin, J. R. (2017). Hidden wounds? inflammatory links between childhood trauma and psychopathology. *Annu. Rev. Psychol.* 68, 517–544. doi: 10.1146/annurev-psych-010416-044208

Daniels, J. K., Coupland, N. J., Hegadoren, K. M., Rowe, B. H., and Densmore, M. (2012). Neural and behavioral correlates of peritraumatic dissociation in an acutely traumatized sample. *J. Clin. Psychiatry* 73, 420–426. doi: 10.4088/JCP.10m06642

de Kwaasteniet, B., Ruhe, E., Caan, M., Rive, M., and Olabarriaga, S. (2013). Relation between structural and functional connectivity in major depressive disorder. *Biol. Psychiatry* 74, 40–47. doi: 10.1016/j.biopsych.2012.12.024

Du, L., Wang, J., Meng, B., Yong, N., and Yang, X. (2016). Early life stress affects limited regional brain activity in depression. *Sci. Rep.* 6:25338. doi: 10.1038/srep25338

Dube, S. R., Felitti, V. J., Dong, M., Chapman, D. P., and Giles, W. H. (2003). Childhood abuse, neglect, and household dysfunction and the risk of illicit drug use: the adverse childhood experiences study. *Pediatrics* 111, 564–572. doi: 10.1542/peds.111.3.564

Duncan, N. W., Hayes, D. J., Wiebking, C., Tiret, B., and Pietruska, K. (2015). Negative childhood experiences alter a prefrontal-insular-motor cortical network in healthy adults: a preliminary multimodal rsfMRI-fMRI-MRS-dMRI study. *Hum. Brain Map.* 36, 4622–4637. doi: 10.1002/hbm.22941

Ebneabbasi, A., Mahdipour, M., Nejati, V., Li, M., and Liebe, T. (2021). Emotion processing and regulation in major depressive disorder: a 7T resting-state fMRI study. *Hum. Brain Map.* 42, 797–810. doi: 10.1002/hbm.25263

Eichenbaum, H., Yonelinas, A. P., and Ranganath, C. (2007). The medial temporal lobe and recognition memory. *Annu. Rev. Neurosci.* 30, 123–152. doi: 10.1146/annurev.neuro.30.051606.094328

Ffytche, D. H., andCatani, M. (2005). Beyond localization: from hodology to function. *Philos Trans. R Soc. Lond. B Biol. Sci.* 360, 767–779. doi: 10.1098/rstb.2005.1621

Figueroa, C. A., Ruhe, H. G., Koeter, M. W., Spinhoven, P., and Van der Does, W. (2015). Cognitive reactivity versus dysfunctional cognitions and the prediction of relapse in recurrent major depressive disorder. *J. Clin. Psychiatry* 76, e1306–e1312. doi: 10.4088/JCP.14m09268

Friston, K. J., Williams, S., Howard, R., Frackowiak, R. S., and Turner, R. (1996). Movement-related effects in fMRI time-series. *Magn. Reson. Med.* 35, 346–355. doi: 10.1002/mrm.1910350312

Gong, J., Wang, J., Qiu, S., Chen, P., and Luo, Z. (2020). Common and distinct patterns of intrinsic brain activity alterations in major depression and bipolar disorder: voxel-based meta-analysis. *Transl. Psychiatry* 10:353. doi: 10.1038/s41398-020-01036-5

Gotlib, I. H., and Joormann, J. (2010). Cognition and depression: current status and future directions. *Annu. Rev. Clin. Psychol.* 6, 285–312. doi: 10.1146/annurev.clinpsy.121208.131305

Groves, S. J., Pitcher, T. L., Melzer, T. R., Jordan, J., and Carter, J. D. (2018). Brain activation during processing of genuine facial emotion in depression: preliminary findings. *J. Affect. Disord.* 225, 91–96. doi: 10.1016/j.jad.2017.07.049

Guo, W. B., Liu, F., Xue, Z. M., Xu, X. J., and Wu, R. R. (2012). Alterations of the amplitude of low-frequency fluctuations in treatment-resistant and treatment-response depression: a resting-state fMRI study. *Prog. Neuropsychopharmacol. Biol. Psychiatry* 37, 153–160. doi: 10.1016/j.pnpbp.2012.01.011

Hahamy, A., Calhoun, V., Pearlson, G., Harel, M., and Stern, N. (2014). Save the global: global signal connectivity as a tool for studying clinical populations with functional magnetic resonance imaging. *Brain Connect.* 4, 395–403. doi: 10.1089/brain.2014.0244

Hammen, C. (2005). Stress and depression. *Annu. Rev. Clin. Psychol.* 1, 293–319. doi: 10.1146/annurev.clinpsy.1.102803.143938

Hammen, C., and Brennan, P. A. (2002). Interpersonal dysfunction in depressed women: impairments independent of depressive symptoms. *J. Affect. Disord.* 72, 145–156. doi: 10.1016/s0165-0327(01)00455-4

Heany, S. J., Groenewold, N. A., Uhlmann, A., Dalvie, S., and Stein, D. J. (2018). The neural correlates of Childhood Trauma Questionnaire scores in adults: a meta-analysis and review of functional magnetic resonance imaging studies. *Dev. Psychopathol.* 30, 1475–1485. doi: 10.1017/S0954579417001717

Heim, C., Newport, D. J., Mletzko, T., Miller, A. H., and Nemeroff, C. B. (2008). The link between childhood trauma and depression: insights from HPA axis studies in humans. *Psychoneuroendocrinology* 33, 693–710. doi: 10.1016/j.psyneuen.2008.03.008

Helmreich, I., Wagner, S., Mergl, R., Allgaier, A. K., and Hautzinger, M. (2012). Sensitivity to changes during antidepressant treatment: a comparison of unidimensional subscales of the Inventory of Depressive Symptomatology (IDS-C) and the Hamilton Depression Rating Scale (HAMD) in patients with mild major, minor or subsyndromal depression. *Eur. Arch. Psychiatry Clin. Neurosci.* 262, 291–304. doi: 10.1007/s00406-011-0263-x

Holmbeck, G. N. (1997). Toward terminological, conceptual, and statistical clarity in the study of mediators and moderators: examples from the child-clinical and pediatric psychology literatures. *J Consult Clin Psychol* 65, 599–610. doi: 10.1037//0022-006x.65.4.599

Howard, D. M., Adams, M. J., Clarke, T. K., Hafferty, J. D., and Gibson, J. (2019). Genome-wide meta-analysis of depression identifies 102 independent variants and highlights the importance of the prefrontal brain regions. *Nat. Neurosci.* 22, 343–352. doi: 10.1038/s41593-018-0326-7

Hu, L., Xiao, M., Ai, M., Wang, W., and Chen, J. (2019). Disruption of resting-state functional connectivity of right posterior insula in adolescents and young adults with major depressive disorder. *J. Affect. Disord.* 257, 23–30. doi: 10.1016/j.jad.2019.06.057

Huh, H. J., Kim, K. H., Lee, H. K., and Chae, J. H. (2017). The relationship between childhood trauma and the severity of adulthood depression and anxiety symptoms in a clinical sample: the mediating role of cognitive emotion regulation strategies. *J. Affect. Disord.* 213, 44–50. doi: 10.1016/j.jad.2017.02.009

Hutchison, R. M., Womelsdorf, T., Allen, E. A., Bandettini, P. A., and Calhoun, V. D. (2013). Dynamic functional connectivity: promise, issues, and interpretations. *Neuroimage* 80, 360–378. doi: 10.1016/j.neuroimage.2013.05.079

Isvoranu, A. M., van Borkulo, C. D., Boyette, L. L., Wigman, J. T., and Vinkers, C. H. (2017). A network approach to psychosis: pathways between childhood trauma and psychotic symptoms. *Schizophr. Bull.* 43, 187–196. doi: 10.1093/schbul/sbw055

Jansen, K., Cardoso, T. A., Fries, G. R., Branco, J. C., and Silva, R. A. (2016). Childhood trauma, family history, and their association with mood disorders in early adulthood. *Acta Psychiatr. Scand.* 134, 281–286. doi: 10.1111/acps.12551

Jenkinson, M., Bannister, P., Brady, M., and Smith, S. (2002). Improved optimization for the robust and accurate linear registration and motion correction of brain images. *Neuroimage* 17, 825–841. doi: 10.1016/s1053-8119(02)91132-8

Kessler, R. C., and Bromet, E. J. (2013). The epidemiology of depression across cultures. *Annu. Rev. Public Health* 34, 119–138. doi: 10.1146/annurev-publhealth-031912-114409

Kim, D., Bae, H., Han, C., Oh, H. Y., and Macdonald, K. (2013). Psychometric properties of the Childhood Trauma Questionnaire-Short Form (CTQ-SF) in Korean patients with schizophrenia. *Schizoph. Res.* 144, 93–98. doi: 10.1016/j.schres.2012.12.020

Kisely, S., Abajobir, A. A., Mills, R., Strathearn, L., and Clavarino, A. (2018). Child maltreatment and mental health problems in adulthood: birth cohort study. *Br. J. Psychiatry* 213, 698–703. doi: 10.1192/bjp.2018.207

Kitada, R., Johnsrude, I. S., Kochiyama, T., and Lederman, S. J. (2010). Brain networks involved in haptic and visual identification of facial expressions of emotion: an fMRI study. *Neuroimage* 49, 1677–1689. doi: 10.1016/j.neuroimage.2009.09.014

Kuehner, C. (2017). Why is depression more common among women than among men? *Lancet Psychiatry* 4, 146–158. doi: 10.1016/S2215-0366(16)30263-2

Li, X., Zhang, Y., Meng, C., Zhang, C., and Zhao, W. (2021). Functional stability predicts depressive and cognitive improvement in major depressive disorder: a longitudinal functional MRI study. *Prog. Neuropsychopharmacol. Biol. Psychiatry* 111:110396. doi: 10.1016/j.pnpbp.2021.110396

Liao, W., Li, J., Ji, G. J., Wu, G. R., and Long, Z. (2019). Endless fluctuations: temporal dynamics of the amplitude of low frequency fluctuations. *IEEE Trans. Med. Imaging* 38, 2523–2532. doi: 10.1109/TMI.2019.2904555

Liao, W., Wang, Z., Zhang, X., Shu, H., and Wang, Z. (2017). Cerebral blood flow changes in remitted early- and late-onset depression patients. *Oncotarget* 8, 76214–76222. doi: 10.18632/oncotarget.19185

Liu, F., Guo, W., Liu, L., Long, Z., and Ma, C. (2013). Abnormal amplitude low-frequency oscillations in medication-naive, first-episode patients with major depressive disorder: a resting-state fMRI study. *J. Affect. Disord.* 146, 401–406. doi: 10.1016/j.jad.2012.10.001

Liu, F., Zhu, C., Wang, Y., Guo, W., and Li, M. (2015). Disrupted cortical hubs in functional brain networks in social anxiety disorder. *Clin. Neurophysiol.* 126, 1711–1716. doi: 10.1016/j.clinph.2014.11.014

Liu, J., Bu, X., Hu, X., Li, H., and Cao, L. (2021). Temporal variability of regional intrinsic neural activity in drug-naive patients with obsessive-compulsive disorder. *Hum. Brain Map.* 42, 3792–3803. doi: 10.1002/hbm.25465

Liu, J., Ren, L., Womer, F. Y., Wang, J., and Fan, G. (2014). Alterations in amplitude of low frequency fluctuation in treatment-naive major depressive disorder measured with resting-state fMRI. *Hum. Brain Map.* 35, 4979–4988. doi: 10.1002/hbm.22526

Lou, F., Tao, J., Zhou, R., Chen, S., and Qian, A. (2021). Altered variability and concordance of dynamic resting-state fMRI indices in patients with attention deficit hyperactivity disorder. *Front. Neurosci.* 15:731596. doi: 10.3389/fnins.2021.731596

Luo, Q., Chen, J., Li, Y., Wu, Z., and Lin, X. (2022). Altered regional brain activity and functional connectivity patterns in major depressive disorder: a function of childhood trauma or diagnosis? *J. Psychiatr. Res.* 147, 237–247. doi: 10.1016/j.jpsychires.2022.01.038

McCarron, R. M., Shapiro, B., Rawles, J., and Luo, J. (2021). Depression. *Ann. Intern. Med.* 174, C65–C80. doi: 10.7326/AITC202105180

McGlade, E., Rogowska, J., DiMuzio, J., Bueler, E., and Sheth, C. (2020). Neurobiological evidence of sexual dimorphism in limbic circuitry of US Veterans. *J. Affect. Disord.* 274, 1091–1101. doi: 10.1016/j.jad.2020.05.016

Monteleone, A. M., Marciello, F., Cascino, G., Cimino, M., and Ruzzi, V. (2020). Early traumatic experiences impair the functioning of both components of the endogenous stress response system in adult people with eating disorders. *Psychoneuroendocrinology* 115:104644. doi: 10.1016/j.psyneuen.2020.104644

Morey, R. A., Dunsmoor, J. E., Haswell, C. C., Brown, V. M., and Vora, A. (2015). Fear learning circuitry is biased toward generalization of fear associations in posttraumatic stress disorder. *Transl. Psychiatry* 5:e700. doi: 10.1038/tp.2015.196

Nelson, J., Klumparendt, A., Doebler, P., and Ehring, T. (2017). Childhood maltreatment and characteristics of adult depression: meta-analysis. *Br. J. Psychiatry* 210, 96–104. doi: 10.1192/bjp.bp.115.180752

Nicol, K., Pope, M., Romaniuk, L., and Hall, J. (2015). Childhood trauma, midbrain activation and psychotic symptoms in borderline personality disorder. *Transl. Psychiatry* 5:e559. doi: 10.1038/tp.2015.53

Nikkheslat, N., McLaughlin, A. P., Hastings, C., Zajkowska, Z., and Nettis, M. A. (2020). Childhood trauma, HPA axis activity and antidepressant response in patients with depression. *Brain Behav. Immun.* 87, 229–237. doi: 10.1016/j.bbi.2019.11.024

Park, H. J., Friston, K. J., Pae, C., Park, B., and Razi, A. (2018). Dynamic effective connectivity in resting state fMRI. *Neuroimage* 180(Pt B), 594–608. doi: 10.1016/j.neuroimage.2017.11.033

Petrikova, M., Kascakova, N., Furstova, J., Hasto, J., and Tavel, P. (2021). Validation and adaptation of the slovak version of the Childhood Trauma Questionnaire (CTQ). *Int. J. Environ. Res. Public Health* 18:2440 doi: 10.3390/ijerph18052440

Qiao, D., Zhang, A., Sun, N., Yang, C., and Li, J. (2020). Altered static and dynamic functional connectivity of habenula associated with suicidal ideation in first-episode, drug-naive patients with major depressive disorder. *Front. Psychiatry* 11:608197. doi: 10.3389/fpsyt.2020.608197

Salk, R. H., Hyde, J. S., and Abramson, L. Y. (2017). Gender differences in depression in representative national samples: meta-analyses of diagnoses and symptoms. *Psychol. Bull.* 143, 783–822. doi: 10.1037/bul0000102

Shen, Y., Yao, J., Jiang, X., Zhang, L., and Xu, L. (2015). Sub-hubs of baseline functional brain networks are related to early improvement following two-week pharmacological therapy for major depressive disorder. *Hum. Brain Map.* 36, 2915–2927. doi: 10.1002/hbm.22817

Sheppes, G., Suri, G., and Gross, J. J. (2015). Emotion regulation and psychopathology. *Annu. Rev. Clin. Psychol.* 11, 379–405. doi: 10.1146/annurev-clinpsy-032814-112739

Southwick, S. M., Vythilingam, M., and Charney, D. S. (2005). The psychobiology of depression and resilience to stress: implications for prevention and treatment. *Annu. Rev. Clin. Psychol.* 1, 255–291. doi: 10.1146/annurev.clinpsy.1.102803.143948

Suh, J. S., Schneider, M. A., Minuzzi, L., MacQueen, G. M., and Strother, S. C. (2019). Cortical thickness in major depressive disorder: a systematic review and meta-analysis. *Prog. Neuropsychopharmacol. Biol. Psychiatry* 88, 287–302. doi: 10.1016/j.pnpbp.2018.08.008

Tomasi, D., and Volkow, N. D. (2010). Functional connectivity density mapping. *Proc. Natl. Acad. Sci. U. S. A.* 107, 9885–9890. doi: 10.1073/pnas.1001414107

Wang, D., Qin, W., Liu, Y., Zhang, Y., and Jiang, T. (2014). Altered resting-state network connectivity in congenital blind. *Hum. Brain Map.* 35, 2573–2581. doi: 10.1002/hbm.22350

Wu, Z., Liu, Z., Jiang, Z., Fu, X., and Deng, Q. (2022). Overprotection and overcontrol in childhood: an evaluation on reliability and validity of 33-item expanded Childhood Trauma Questionnaire (CTQ-33), Chinese version. *Asian J. Psychiatr.* 68:102962. doi: 10.1016/j.ajp.2021.102962

Xie, P., Wu, K., Zheng, Y., Guo, Y., and Yang, Y. (2018). Prevalence of childhood trauma and correlations between childhood trauma, suicidal ideation, and social support in patients with depression, bipolar disorder, and schizophrenia in southern China. *J. Affect. Disord.* 228, 41–48. doi: 10.1016/j.jad.2017.11.011

Xue, K., Liang, S., Yang, B., Zhu, D., and Xie, Y. (2020). Local dynamic spontaneous brain activity changes in first-episode, treatment-naive patients with major depressive disorder and their associated gene expression profiles. *Psychol. Med.* [Online ahead of print]. doi: 10.1017/S0033291720003876

Yan, C., Yang, Z., Colcombe, S. J., Zuo, X., and Milham, M. P. (2017). Concordance among indices of intrinsic brain function: insights from inter-individual variation and temporal dynamics. *Sci. Bull.* 62, 1572–1584. doi: 10.1016/j.scib.2017.09.015

Yan, C. G., Craddock, R. C., Zuo, X. N., Zang, Y. F., and Milham, M. P. (2013). Standardizing the intrinsic brain: towards robust measurement of inter-individual variation in 1000 functional connectomes. *Neuroimage* 80, 246–262. doi: 10.1016/j.neuroimage.2013.04.081

Yan, C. G., Wang, X. D., Zuo, X. N., and Zang, Y. F. (2016). DPABI: data processing & analysis for (resting-state) brain imaging. *Neuroinformatics* 14, 339–351. doi: 10.1007/s12021-016-9299-4

Yang, G. J., Murray, J. D., Glasser, M., Pearlson, G. D., and Krystal, J. H. (2017). Altered global signal topography in Schizophrenia. *Cereb. Cortex* 27, 5156–5169. doi: 10.1093/cercor/bhw297

Yu, M., Linn, K. A., Shinohara, R. T., Oathes, D. J., and Cook, P. A. (2019a). Childhood trauma history is linked to abnormal brain connectivity in major depression. *Proc. Natl. Acad. Sci. U. S. A.* 116, 8582–8590. doi: 10.1073/pnas.1900801116

Yu, Y., Li, Z., Lin, Y., Yu, J., and Peng, G. (2019b). Depression affects intrinsic brain activity in patients with mild cognitive impairment. *Front. Neurosci.* 13:1333. doi: 10.3389/fnins.2019.01333

Zang, Y., Jiang, T., Lu, Y., He, Y., and Tian, L. (2004). Regional homogeneity approach to fMRI data analysis. *Neuroimage* 22, 394–400. doi: 10.1016/j.neuroimage.2003.12.030

Zang, Y. F., He, Y., Zhu, C. Z., Cao, Q. J., and Sui, M. Q. (2007). Altered baseline brain activity in children with ADHD revealed by resting-state functional MRI. *Brain Dev.* 29, 83–91. doi: 10.1016/j.braindev.2006.07.002

Zhang, H., Tao, Y., Xu, H., Zou, S., and Deng, F. (2022). Associations between childhood chronic stress and dynamic functional connectivity in drug-naive, first-episode adolescent MDD. *J. Affect. Disord.* 299, 85–92. doi: 10.1016/j.jad.2021.11.050

Zhang, J., Magioncalda, P., Huang, Z., Tan, Z., and Hu, X. (2019). Altered global signal topography and its different regional localization in motor cortex and hippocampus in mania and depression. *Schizophr. Bull.* 45, 902–910. doi: 10.1093/schbul/sby138

Zhang, L., Zhang, R., Han, S., Womer, F. Y., and Wei, Y. (2021). Three major psychiatric disorders share specific dynamic alterations of intrinsic brain activity. *Schizophr. Res.* [Online ahead of print]. doi: 10.1016/j.schres.2021.06.014

Zhang, S., Lin, X., Yang, T., Zhang, S., and Pan, Y. (2020). Prevalence of childhood trauma among adults with affective disorder using the Childhood Trauma Questionnaire: a meta-analysis. *J. Affect. Disord.* 276, 546–554. doi: 10.1016/j.jad.2020.07.001

Zhao, L., Wang, D., Xue, S. W., Tan, Z., and Wang, Y. (2021). Aberrant state-related dynamic amplitude of low-frequency fluctuations of the emotion network in major depressive disorder. *J. Psychiatr. Res.* 133, 23–31. doi: 10.1016/j.jpsychires.2020.12.003

Zhi, D., Calhoun, V. D., Lv, L., Ma, X., and Ke, Q. (2018). Aberrant dynamic functional network connectivity and graph properties in major depressive disorder. *Front. Psychiatry* 9:339. doi: 10.3389/fpsyt.2018.00339

Zhou, W., Yuan, Z., Yingliang, D., Chaoyong, X., and Ning, Z. (2021). Differential patterns of dynamic functional connectivity variability in major depressive disorder treated with cognitive behavioral therapy. *J. Affect. Disord.* 291, 322–328. doi: 10.1016/j.jad.2021.05.017

Zhu, D. M., Yang, Y., Zhang, Y., Wang, C., and Wang, Y. (2020). Cerebellar-cerebral dynamic functional connectivity alterations in major depressive disorder. *J. Affect. Disord.* 275, 319–328. doi: 10.1016/j.jad.2020.06.062

Zhu, J., Zhang, Y., Zhang, B., Yang, Y., and Wang, Y. (2019). Abnormal coupling among spontaneous brain activity metrics and cognitive deficits in major depressive disorder. *J. Affect. Disord.* 252, 74–83. doi: 10.1016/j.jad.2019.04.030

Zou, Q. H., Zhu, C. Z., Yang, Y., Zuo, X. N., and Long, X. Y. (2008). An improved approach to detection of amplitude of low-frequency fluctuation (ALFF) for resting-state fMRI: fractional ALFF. *J. Neurosci. Methods* 172, 137–141. doi: 10.1016/j.jneumeth.2008.04.012

Zuo, X. N., Di Martino, A., Kelly, C., Shehzad, Z. E., and Gee, D. G. (2010a). The oscillating brain: complex and reliable. *Neuroimage* 49, 1432–1445. doi: 10.1016/j.neuroimage.2009.09.037

Zuo, X. N., Kelly, C., Di Martino, A., Mennes, M., and Margulies, D. S. (2010b). Growing together and growing apart: regional and sex differences in the lifespan developmental trajectories of functional homotopy. *J. Neurosci.* 30, 15034–15043. doi: 10.1523/JNEUROSCI.2612-10.2010

Zuo, X. N., Ehmke, R., Mennes, M., Imperati, D., and Castellanos, F. X. (2012). Network centrality in the human functional connectome. *Cereb. Cortex* 22, 1862–1875. doi: 10.1093/cercor/bhr269

Conflict of Interest: The authors declare that the research was conducted in the absence of any commercial or financial relationships that could be construed as a potential conflict of interest.

Publisher's Note: All claims expressed in this article are solely those of the authors and do not necessarily represent those of their affiliated organizations, or those of the publisher, the editors and the reviewers. Any product that may be evaluated in this article, or claim that may be made by its manufacturer, is not guaranteed or endorsed by the publisher.

frontiers | Frontiers in Neuroscience

ORIGINAL RESEARCH
published: 17 May 2022
doi: 10.3389/fnins.2022.900330

Identification of Pathogenetic Brain Regions *via* Neuroimaging Data for Diagnosis of Autism Spectrum Disorders

Yu Wang[1,2,3], *Yu Fu*[1,2,3]* *and Xun Luo*[1,2,3]

[1] *Hunan Provincial Key Laboratory of Intelligent Computing and Language Information Processing, Hunan Normal University, Changsha, China,* [2] *College of Information Science and Engineering, Hunan Normal University, Changsha, China,* [3] *Hunan Xiangjiang Artificial Intelligence Academy, Changsha, China*

Autism spectrum disorder (ASD) is a kind of neurodevelopmental disorder that often occurs in children and has a hidden onset. Patients usually have lagged development of communication ability and social behavior and thus suffer an unhealthy physical and mental state. Evidence has indicated that diseases related to ASD have commonalities in brain imaging characteristics. This study aims to study the pathogenesis of ASD based on brain imaging data to locate the ASD-related brain regions. Specifically, we collected the functional magnetic resonance image data of 479 patients with ASD and 478 normal subjects matched in age and gender and used a machine-learning framework named random support vector machine cluster to extract distinctive brain regions from the preprocessed data. According to the experimental results, compared with other existing approaches, the method used in this study can more accurately distinguish patients from normal individuals based on brain imaging data. At the same time, this study found that the development of ASD was highly correlated with certain brain regions, e.g., lingual gyrus, superior frontal gyrus, medial gyrus, insular lobe, and olfactory cortex. This study explores the effectiveness of a novel machine-learning approach in the study of ASD brain imaging and provides a reference brain area for the medical research and clinical treatment of ASD.

Keywords: autism spectrum disorders, fMRI, pathogenic brain regions identification, disease diagnosis, random SVM cluster

OPEN ACCESS

Edited by:
Wenbin Guo,
Central South University, China

Reviewed by:
Leyi Wei,
Shandong University, China
Lei Du,
Northwestern Polytechnical University, China

***Correspondence:**
Yu Fu
fuyuhnnu@163.com

Specialty section:
This article was submitted to Brain Imaging Methods, a section of the journal Frontiers in Neuroscience

Received: *20 March 2022*
Accepted: *11 April 2022*
Published: *17 May 2022*

Citation:
Wang Y, Fu Y and Luo X (2022) Identification of Pathogenetic Brain Regions via Neuroimaging Data for Diagnosis of Autism Spectrum Disorders. Front. Neurosci. 16:900330. doi: 10.3389/fnins.2022.900330

INTRODUCTION

Autism spectrum disorder (ASD) is a kind of brain developmental disorder with complex etiology and hidden onset (Lord et al., 2018). It is most often diagnosed in teenagers and children because of the high plasticity of their brain function. Children with ASD will suffer various difficulties in early development, including slow response to sensory information (e.g., hearing, smell, and taste), lagged language learning, limited interest, difficulty interacting with others, etc. (Vallianatos et al., 2018; McKinnon et al., 2019; Kang et al., 2020; Santore et al., 2020). Currently, there is no specific therapy for ASD in the clinic, which will cause the long-term economic burden of family and social support (Helkkula et al., 2020). Considering that the ages of patients are relatively small, it is difficult to diagnose based on the general quantitative evaluation of social behavior in clinics. Therefore,

looking for characteristic biomarkers to help clinical workers make accurate clinical decisions in the early stage is an important research direction at present (Frye et al., 2019).

Magnetic resonance imaging (MRI) is a commonly applied technique for diagnosing brain diseases in clinical, which can intuitively show the location and degree of brain lesions. MRI is currently playing a major auxiliary role in the treatment and research of complex brain diseases, such as ASD (Hao et al., 2017; Du et al., 2019; Dryburgh et al., 2020; Yang et al., 2021). Specifically, functional MRI (fMRI) is a new neuroimaging technique that can measure the hemodynamic changes caused by neuronal activity and generate a time series to reflect the activity characteristics of certain brain regions. Some open-access datasets, such as autism brain imaging data exchange (ABIDE), usually contain sufficient fMRI data, which greatly promotes the development of relevant research (Di Martino et al., 2014, 2017). For example, Cheng et al. (2017) conducted a knowledge-based enrichment analysis of fMRI data of patients with autism and healthy controls (HCs) and found that some functional connections (FCs) decreased significantly at the network circuit level. Through specific correlation analysis technology, the correlation networks among multiple regions of interest (ROIs) can be established, which provides a broader perspective in pathogenetic studies (Franzmeier et al., 2019; Noble et al., 2019). For example, Ingalhalikar et al. (2021) obtained fMRI data in ABIDE, proposed a novel technology to eliminate differences between sites, and found several important FCs of patients with ASD.

Efficiency is usually an important factor in imaging data analysis. In recent years, machine-learning algorithms have been increasingly used in dimension reduction and feature extraction in brain imaging data and have played a key role in the research of ASD and many other brain diseases (Abraham et al., 2017; Heinsfeld et al., 2018; Li et al., 2020). Among the existing machine-learning approaches, a support vector machine (SVM) can keep a stable performance in optimizing the feature dimension of samples (Guo et al., 2019; Wei et al., 2019). In the research related to ASD, Chaitra et al. (2020) proposed a new feature-eliminating mechanism to iteratively improve the classification ability of the trivial SVM method and obtained the connected feature subset with better ASD recognition ability. Osredkar et al. (2019) combined SVM and radial kernel function with 4 urine biomarkers to diagnose ASD and found that the levels of 8-hydroxy-2′-deoxyguanosine and 8-isoproterenol in urine can improve the diagnosis performance.

The extraction of the most discriminative features is the central work to ensure the efficiency of SVM. However, most previous studies focused on optimizing single SVM classifiers. The disadvantage of such approaches is that current methods of feature extraction can hardly avoid remaining some important features incorrectly ignored and the screened features can difficult be reconsidered after the optimization of a single SVM classifier. Also, the pathogeny identification in the existing studies is often based on limited data, which may lead to few reliable results and weak generality. Therefore, this study applies a random SVM cluster framework to extract features from fMRI data to classify patients with ASD and HCs (Bi et al., 2018). With the help of ensemble learning, only the features shared by most classifiers are extracted as the important features, which reduces the blindness in feature selection and prevents over-fitting even under a large scale of data. As the results indicate, the optimized random SVM cluster performs well in classifying patients with ASD and HCs, and the feature extraction results are consistent with many existing studies. Compared to the other existing works, this study provides an attractive framework to detect the disease-associated factors of ASD based on the fMRI data.

MATERIALS AND METHODS

Overview

The entire analysis pipeline of this study can be divided into three major parts, which are depicted in **Figure 1**. First, the fMRI data are preprocessed, resulting in the time series for each ROI. Second, a random SVM cluster is constructed to extract the characteristic features. Finally, further analysis is conducted to identify pathogenetic brain regions.

Subjects

All biological data in this study are from the ABIDE database and do not involve bio-standard safety measures and institutional safety procedures. The data acquirement has been approved by relevant departments and complies with relevant standards. The subjects used in this study are determined through further screening. This study has tried to keep as many samples as possible to ensure the robustness of the conclusion. However, it is a necessity to eliminate the data that occur errors while preprocessing. At last, it remains raw fMRI data of 479 patients with ASD and 478 HCs obtained from ABIDE-I for analysis. All HCs have signed written consent and are out of any other neurological diseases. ABIDE database has strict standards for data collection and processing, which ensures the homology of data structure.

The online datasets extendedly provide additional information on subjects, including age, full-scale intelligence quotient (FIQ), performance intelligence quotient (PIQ), and verbal intelligence quotient (VIQ). The latter three indicators are used to quantify the comprehensive performance of the intellectual function. This study evaluated the statistical differences in the above attributions between ASD and HC groups. The basic information of the two groups of subjects is shown in **Table 1**, which indicates no significant difference in all indicators among the participants.

Data Preprocessing

All fMRI data are collected from MRI scanners whereas the subjects are in the resting state, which means all subjects are relaxed without doing any thinking work during the scanning. To conduct data preprocessing, this study uses a Data Processing Assistant for Resting-State fMRI (DPARSF),[1] a widely applied tool in the MATLAB platform that is dedicated to fMRI preprocessing (Karpiel et al., 2019). Specific steps of preprocessing are listed as follows:

[1]http://rfmri.org/dpabi

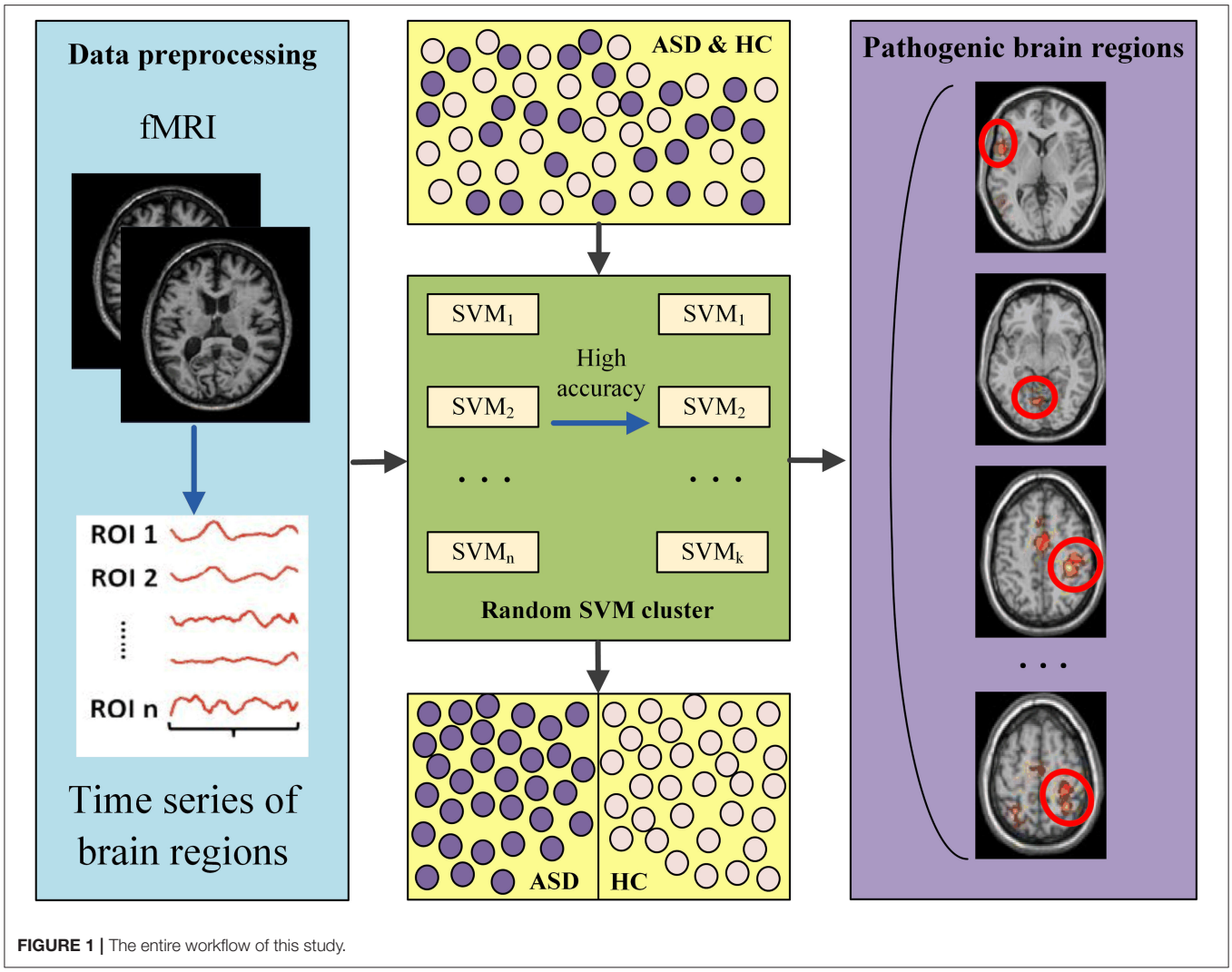

FIGURE 1 | The entire workflow of this study.

TABLE 1 | Basic information of the subjects.

Variable	Patients with ASD	HC subjects	*p*-value
Age	16.70 ± 8.23	17.20 ± 8.06	0.798*
FIQ	105.21 ± 16.56	111.20 ± 12.80	0.000**
PIQ	104.89 ± 17.06	108.61 ± 13.31	0.001**
VIQ	103.25 ± 18.05	110.37 ± 13.50	0.000**

**This study calculated the p-value corresponding to the age through chi-square test.*
***This study calculated the p-values corresponding to FIQ, PIQ, and VIQ using two-sample t-test. All information listed in this table is expressed by the format of "mean ± standard deviation." It shows no statistical difference between two groups of data if the corresponding p-value is >0.05.*

(1) Inputting the raw DCM files and converting the data format to NIFTI;
(2) Deleting the initial 10 time points and slice timing;
(3) Realigning the head movement to eliminate artifact effect;
(4) Readjusting, including standardizing the functional image to echo plane imaging template and smoothing;
(5) Eliminating the residual noise which increases or decreases over time;
(6) Temporal filtering to maintain the fluctuation being within 0.01 ± 0.08 Hz;
(7) Removing covariates and head movements that may affect unnatural BOLD fluctuations.

Construction of Sample Features

Functional connections can reflect the organization and interrelationships among different ROIs even if they are not histologically connected. In this study, FCs are constructed as the features of the samples. Specifically, the weight value of an FC is calculated to represent the tightness of the corresponding ROI–ROI pair. Concrete construction steps are as follows.

(1) Separating all brain images into ROIs according to the automatic anatomical labeling template, which is applied in many fMRI-based studies (Liu et al., 2016). The applied template can generate 116 ROIs in total, of which 90 ROIs belong to the brain whereas the other 26 ROIs belong to

the cerebellum. As a common practice, this study focuses only on the brain and the ROIs in the cerebellum are therefore omitted.

(2) Calculating the Pearson correlation coefficient value between each ROI pair as the FCs. Before the calculation, time series are normalized and further sliced to a uniform length to eliminate the effect of inter-site difference (Esteban et al., 2017; Wang et al., 2022). The higher the coefficient value, the stronger the FC between two ROIs.

(3) Constructing sample features. For each sample, a vector composed of 4,005 (i.e., the number of free combinations among 90 ROIs) weight values of FCs is calculated as the sample feature for subsequent experiments. In other words, the dimensionality of the original sample features is 4,005 in this study.

Construction of the Random Support Vector Machine Cluster

In machine learning, excessively big feature dimensionality may cause mass computing load. However, if the feature dimensionality is too small, a large amount of important information may be lost. Ensemble learning is an effective strategy that can effectively improve the model performance by integrating single classifier to form clusters and generate results through a voting mechanism (Chen et al., 2018a; Wei et al., 2018). According to our previous research, ensemble learning shows great potential in feature selection (Bi et al., 2020, 2021). In this study, this study adopted a method named random SVM cluster to effectively analyze the high-dimensional data, which has performed well in the fMRI-based study of Alzheimer's disease. The concrete procedure details are as follows.

First, the initial sample set S is divided into three subsets, namely, a training set S_1 with 382 subjects, a verifying set S_2 with 96 subjects, and a testing set S_3 with 479 subjects. The size rate is ∼4:1:5. The proportion balance of patients and HCs is kept during the division.

Second, to construct an SVM classifier, M samples are randomly selected from the training set S_1.and a d-dimension sub-feature is generated by randomly selecting d components from the original 4,005-dimension feature. The above procedure improves the diversity of SVM classifiers, which, according to the theory of ensemble learning, will bring significant improvement to the generalization performance of the integrated learner. By repeating the above procedure for n times, n SVMs are derived and the random SVM cluster is constructed accordingly.

Third, the SVM classifiers are further screened for optimization. Specifically, the verification set S_2 is applied to evaluate all constructed SVM classifiers by their respective classification accuracies. The classifiers with classification accuracies lower than 0.5 will be deleted, in that such performance is inferior to the randomly guessing and will passively affect the performance of the overall cluster. After the selection, k superior SVMs ($k < n$) have been selected to form a new cluster.

Finally, sample classification and feature extraction are conducted using the random SVM cluster. Concretely, k screened SVMs in the cluster separately classify the samples in the testing set S_3 and generate the final result through the majority voting mechanism. By calculating the ratio of the number of correctly classified samples to the size of the S_3, the accuracy of the entire cluster is obtained.

Identification of Pathological Brain Regions

The SVM classifiers in this study are generated through the random selection of features and samples, which makes the features of each classifier not the same. At the same time, the classification accuracy of a classifier indicates the significance of its corresponding features. After the screening of classifiers, the remaining features are taken as the important features that have strong classification ability for ASD and HC. In other words, ASD and HC have more obvious differences in these characteristics, which means that the ROIs contained in these characteristics are more prone to functional or structural damage. Further, considering that these features are defined as FCs of ROI–ROI pairs, the ROIs that appear the most in the important features are selected as the pathological brain regions. The specific procedure of pathogeny identification is as follows.

(1) Sorting and determining the superior classifiers. All SVM classifiers are sorted in descending order of classification accuracy. Then, a classifier whose accuracy is greater than a certain threshold of 0.75 would be determined as the superior classifier.

(2) Extracting the optimal features. The appearance frequency of each feature in superior SVM classifiers is calculated. Then, the features with the highest frequencies are extracted as the optimal features, which represent the most discriminative FCs between patients with ASD and HC subjects.

(3) Determining the pathological brain regions of ASD. In this study, this study defined the weight of an ROI as its appearance frequency in optimal features. The ROIs with the highest weights are taken as the pathological brain regions.

RESULTS

Performance Comparison With Existing Methods

To certify the efficiency of the random SVM cluster, this article compared its performance with other common approaches for feature selection. The baseline methods include product-based neural network (PNN), backpropagation neural network (BPNN), K-nearest neighbor (KNN), naïve Bayes classifier (Bayes), single SVM classifier (SVM), random forest (RF), and random SVM cluster (RSVMC). Considering the randomness in sample division and feature selection, all comparative methods have been repeated 50 times to avoid accidental errors. The box plot in **Figure 2** depicts the comparative results.

It could be observed that the applied random SVM cluster was significantly superior to the baseline approaches. It is worth noting that the random forest method, as a typical ensemble learner, performed better than all single learners, which indicates the effectiveness of ensemble learning. Also, the highest accuracy

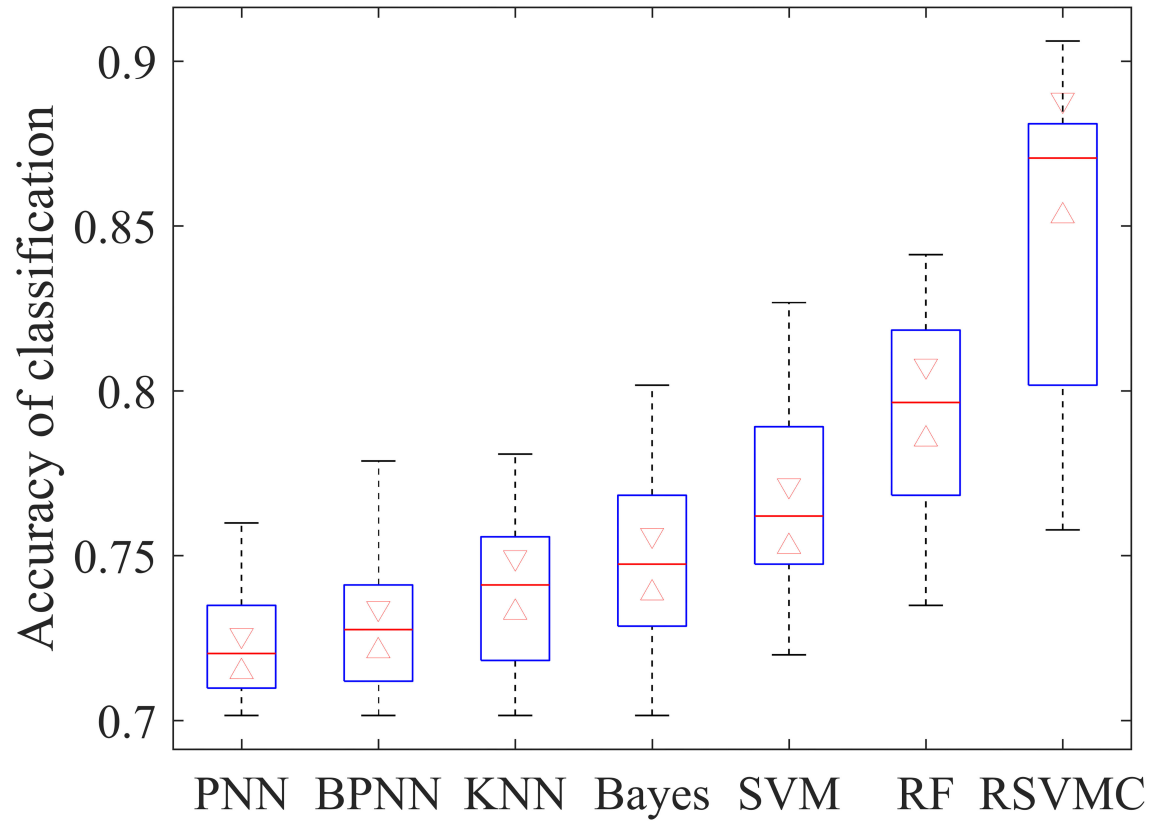

FIGURE 2 | Classification accuracy of different classification method.

of single SVM among all single learners proves the superiority of SVM in brain imaging analysis. Such results implied that the superiority of our method derives from the effective integration of the advantages of SVM and ensemble learning.

To compare the performances of the machine-learning methods, this study further calculated the precision and recall values of all comparative methods. **Figure 3** depicted the Precision-Recall (P-R) curves of all competing methods, where we could observe that the random SVM cluster owned the highest position among all methods, and the superiority of our method is confirmed from another angle.

Parameter Optimization

According to the method definition, the SVM number n and feature dimensionality d are the two important parameters to be optimized, which is critical to finalizing a well-performed random SVM cluster. Parameter optimizing results are shown as follows.

On the one hand, this study conducted experiments to find the optimal number of SVM classifiers in the initial cluster. Specifically, the number of the SVM was gradually increased from 5 to 600 with a step length of 5, during which the accuracy of the random SVM cluster had first increased and then tended to be stable. According to the experimental results depicted in **Figure 4**, it can be observed that when the cluster includes 360 SVMs, the overall performance started to be stable. Thus, the base classifier number n was determined as 360.

On the other hand, this study determined the optimal feature dimensionality. To ensure the performance of the model, the conventional practice is to set the feature dimensionality as the square root of the original feature dimensionality (Belgiu and Drăgu, 2016). However, considering the data complexity of fMRI, such means may cause a great loss of important information, which inspired us to expand and optimize the feature dimensionality. First, this study built the initial cluster with 70 out of 4,005 randomly opted features. The initial number is determined as 70 because it was an approximate value of the square root of 4,005. Subsequently, this study increased the feature dimensionality up to 300 in a step of 2 and calculated the overall accuracy of the cluster in each iteration. Finally, this study took the feature dimensionality corresponding to the highest accuracy as the optimal dimensionality of features. **Figure 5** depicted the results during all iterations, which showed that when the feature dimensionality is determined as 148, the accuracy was 88.1%. It is worth noting that the equivalence of accuracies in two optimization experiments was an accident and these two experiments were carried out successively, which means that in the second experiment, the number of SVM classifiers was determined as 360 according to the former experiment.

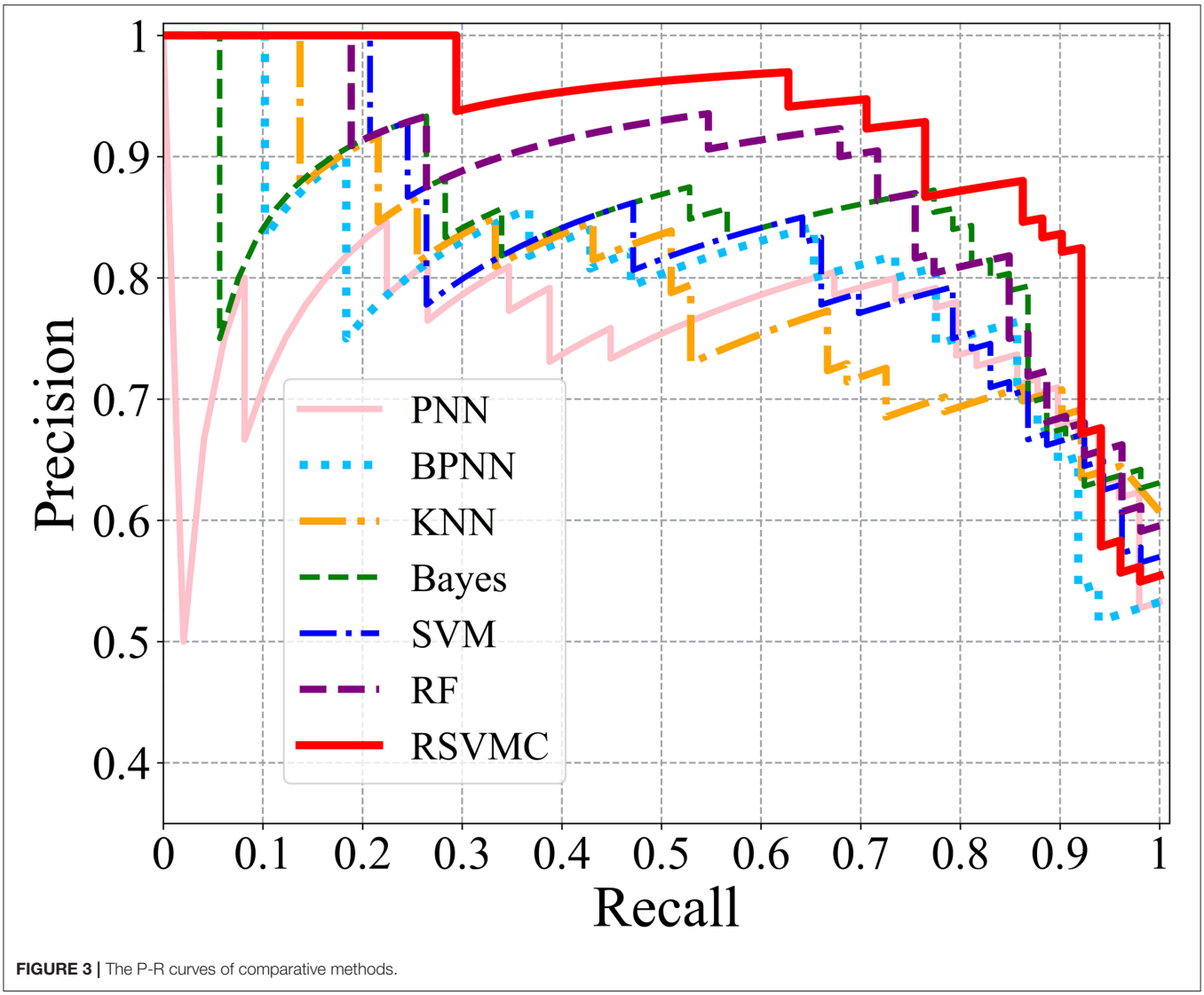

FIGURE 3 | The P-R curves of comparative methods.

Extraction Results of the Pathological Brain Regions

By fitting the optimal number of features to 148, the performance of the random SVM cluster was maximized and the cost of computing resources was concurrently reduced. Consequently, 148 discriminative FCs in patients with ASD and HCs were obtained. The top 20 FCs with the highest frequencies were visualized in **Figure 6**, where the node size that corresponds to each brain region represents the weight of the brain region, that is, the frequency of the brain area. The larger the node, the higher the frequency of brain regions. Subsequently, the frequencies of all 90 ROIs included in the 148 FCs are shown in **Figure 7**.

DISCUSSION

This study utilized an improved SVM learner and achieved the classification accuracy of 88.1% in patients with ASD identification. Compared with other recent endeavors based on ABIDE datasets, our method also shows superiority in classification performance. Liu et al. (2020) proposed a multi-task objective function to extract the dynamic functional connectivity specific to ASD, archiving an accuracy of 76.8%. Wang et al. proposed a new method integrating ensemble learning with sparseness constraints and tested the method on two different sites of data in ABIDE, obtaining accuracies of 72.6 and 71.4%, respectively. Epalle et al. (2021) improved the deep neural network model and tested the proposed classification framework based on cross-validation, achieving the final accuracy value of 78.07%.

As shown in **Figure 7**, the discriminative FCs of ASD mainly existed in the lingual gyrus (LING.R), superior frontal gyrus, medial (SFGmed.R), olfactory cortex (OLF.L), insula (INS.R), parahippocampal gyrus (PHG.R), posterior cingulate gyrus (PCG.R), and fusiform gyrus (FFG.R). On the one hand, our findings were consistent with other existing studies of

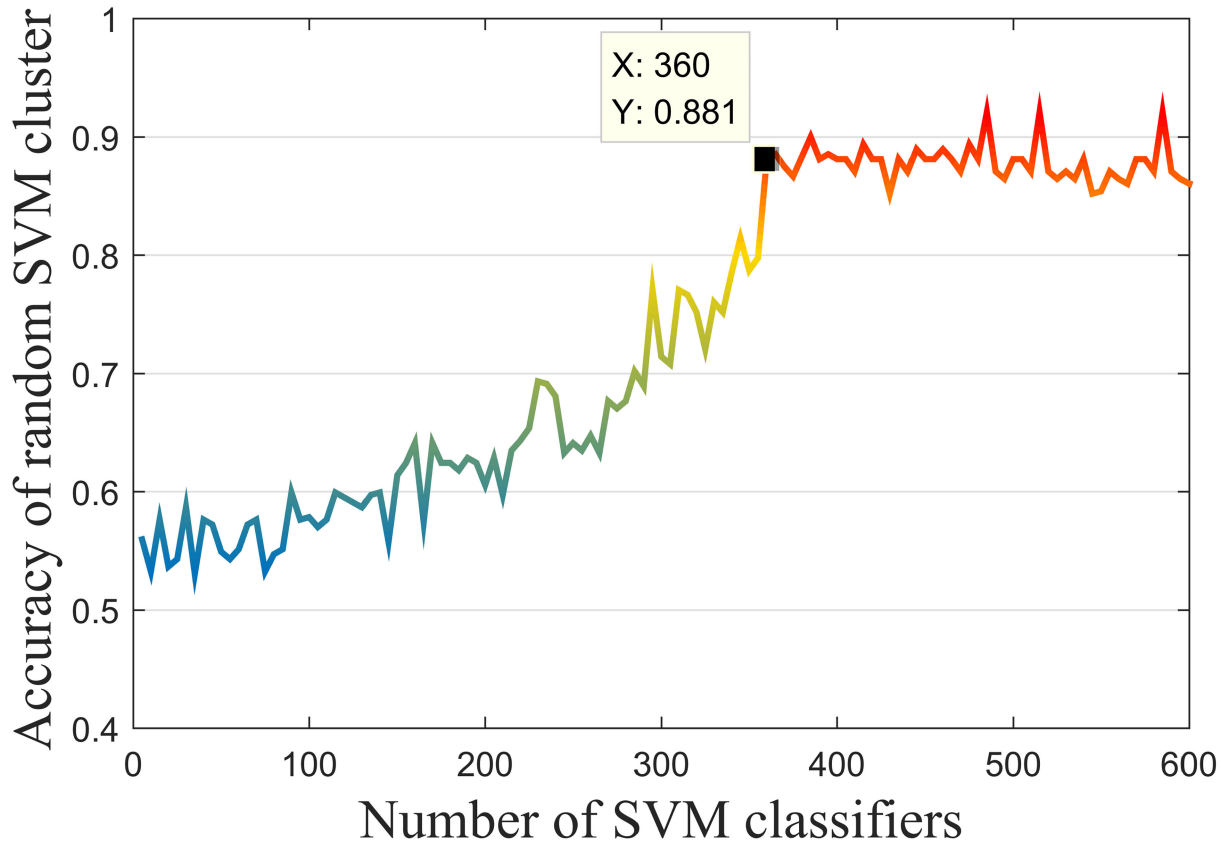

FIGURE 4 | Performance of the random SVM cluster with different number of SVM.

single brain regions. For instance, Herringshaw et al. (2016) utilized meta-analysis methods to quantify the common and consistent brain activation patterns that usually develop the language processing control, and the results showed that the activation of the LING.R in patients with ASD increased. Lee et al. (2020) used a univariate universal linear model to determine the regions of average connectivity differences between male and female subjects with ASD, and the results showed similar gender differences in the tongue gyrus and the posterior cingulate gyrus cortex. Qian et al. (2018) analyzed the time-varying connectivity using the resting-state fMRI data to investigate brain state mutations in children with ASD and finally found abnormal connectivity between INS.R and visual network (and in the middle). Glerean et al. (2016) calculated the correlation between the hemodynamic time courses of each pair of 6-mm isotropic voxels and the proportional inclusiveness between all pairs of subjects, and the results indicated that the subjects who had lower autism quotient scores conversely showed significantly higher nodule intensity in certain brain regions, including FFG.R.

On the other hand, some connection-based studies also verify the results in this article. Huang et al. (2019) enhanced the representation of FC networks by fusing and conveying the public and supplementary information into multiple networks to identify the biomarkers of neuropsychiatric diseases, and the results indicated that OLF.L in subcortical regions is a potential discriminative brain region. Liu and Huang (2020) applied multivariate model analysis to study the connectedness subset of whole-brain FC, finding out that the severity of ASD with SFGmed.R and SFGmed.L changed significantly. Noriega (2019) adopted a sliding-time window method based on an adjusted time span to study whether the time proportion of correlation measure was above or below the average, and the results showed that the FC related to OLF.L was significantly enhanced in controls relative to ASD-severe. Delbruck et al. studied the action observation network of children with ASD and observed that atypical connectomes related to FFG.R showed great significance to the social cognitive defection.

Some other highly-rated ROIs found in our work, such as the PCG.R and PHG.R, were rarely studied in other research about ASD. Nevertheless, certain studies have indicated their potential relation to ASD. For example, PCG.R has been presently found as the tissue correlated with sensation, stereo location, and memory. The hippocampus is an emotion regulation center, which had been long paid special attention in depression research. In addition, as the main cortex of the hippocampus, PHG.R can significantly affect the cognitive and emotional functions of the brain. Thus, the findings in this article may provide a new insight for further exploration of the pathological mechanism of ASD.

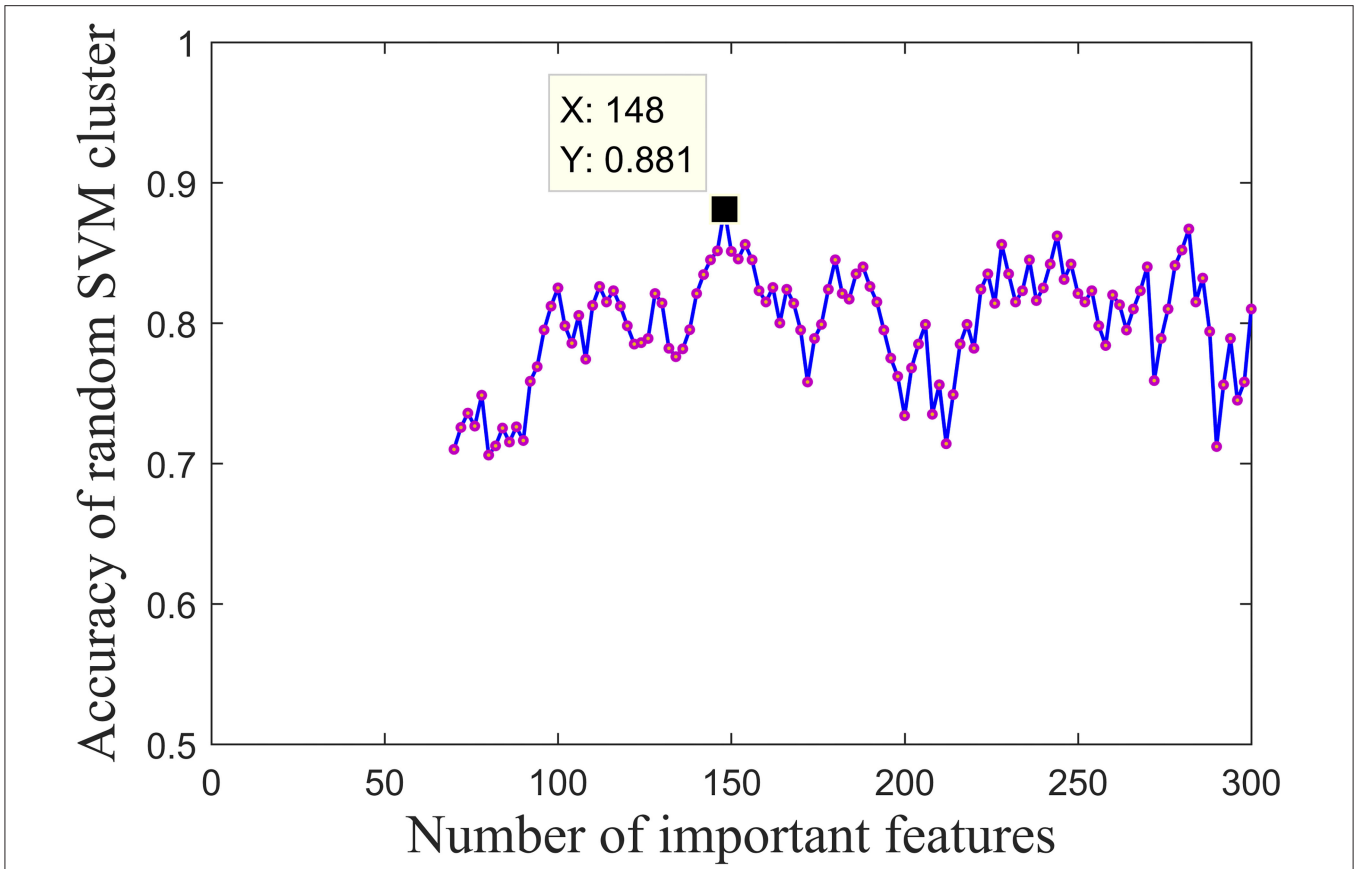

FIGURE 5 | Accuracies of the random SVM cluster with different numbers of important fusion features.

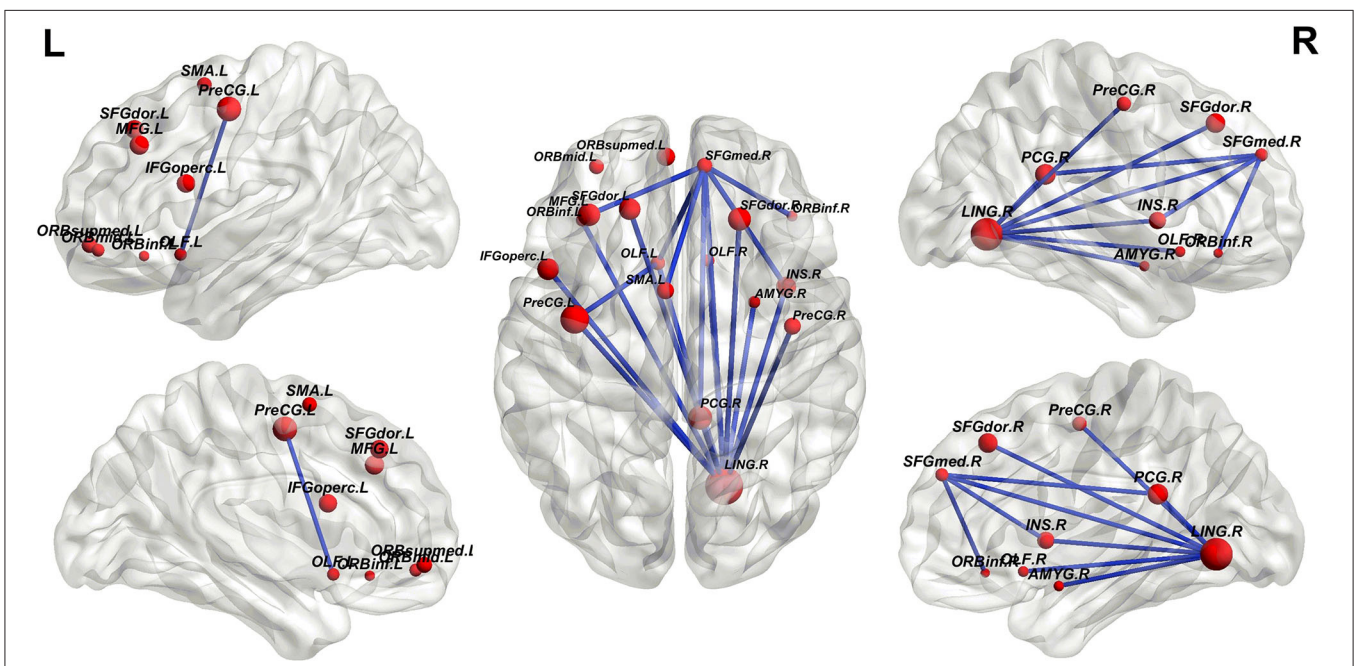

FIGURE 6 | Top 20 functional connections corresponding to the extracted optimal features.

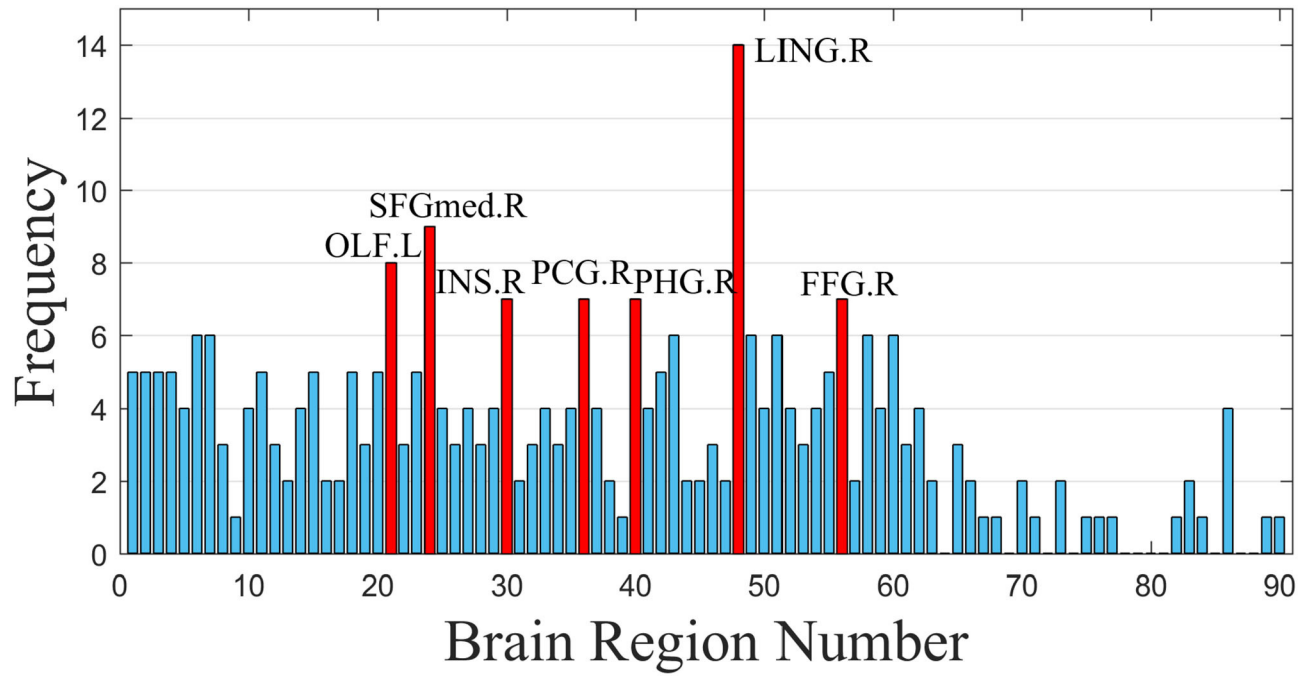

FIGURE 7 | Frequencies of all ROIs.

Despite the satisfactory performance, our study still has limitations. First, in this study, this study uses a normalization strategy to preprocess fMRI data obtained from multiple sites, whereas many advanced approaches have been proposed to eliminate the inter-site differences (Moradi et al., 2017; Wang et al., 2019), which may be applied in future work. Second, this study utilizes the Anatomical Automatic Labeling (AAL) template for brain segmentation, but there are many other proposed templates, e.g., the Harvard-Oxford Atlas template, which may provide some quite different information and help to discover different types of FCs (Lei et al., 2020). Finally, in this study, this study only analyzed the medical imaging data for feature extraction. In the follow-up work, we will try to expand the data types in various ways and may involve genes, cells, electrocardiographs, or other clinical phenotypes for further research (Raka et al., 2017; Wang et al., 2017; Chen et al., 2018b; Du et al., 2020).

CONCLUSION

This article conducted an fMRI-based study for ASD diagnosis using a machine-learning approach named random SVM cluster. Defining the sample features as FCs among ROIs, the pathological factors of ASD were explored. According to the experimental results, discriminative ROIs of patients with ASD and HCs were identified, including LING.R, SFGmed.R, OLF.L, INS.R, PCG.R, PHG.R, and FFG.R. The contributions of our work can be summarized in two key points. On the one hand, an efficient random SVM cluster was applied for ASD diagnosis. On the other hand, some pathological FCs and ROIs highly related to the development of ASD are identified, which can provide valuable references for the medical research and clinical treatment of ASD.

DATA AVAILABILITY STATEMENT

Publicly available datasets were analyzed in this study. This data can be found here: https://ida.loni.usc.edu/login.jsp?project=ABIDE.

ETHICS STATEMENT

This study was carried out in accordance with the recommendations of National Institute of Aging-Alzheimer's Association (NIA-AA) Workgroup Guidelines. The study was approved by Institutional Review Board (IRB) of each participating site, including the Banner Alzheimer's Institute, and was conducted in accordance with Federal Regulations, the Internal Conference on Harmonization (ICH), and Good Clinical Practices (GCP). The patients/participants provided their written informed consent to participate in this study.

AUTHOR CONTRIBUTIONS

YF proposed the design of the work and revised it critically for important intellectual content. XL organized the original draft of the paper and drafted part of the work. YW collected, interpreted the data, and drafted part of the work. YF and XL carried out the experiment for the work. All authors contributed to the article and approved the submitted version.

FUNDING

This work was supported by the National Natural Science Foundation of China (62072173), Natural Science Foundation of Hunan Province, China (2020JJ4432), Key Scientific Research Projects of Department of Education of Hunan Province (20A296), Key Open Project of Key Laboratory of Data Science and Intelligence Education (Hainan Normal University), Ministry of Education (DSIE202101), National Key Research and Development Program of China (2020YFB2104400), the Hunan Provincial Science and Technology Project Foundation (2018TP1018), Medical Humanities and Social Sciences Project of Hunan Normal University, and Innovation & Entrepreneurship Training Program of Hunan Xiangjiang Artificial Intelligence Academy.

REFERENCES

Abraham, A., Milham, M. P., Di Martino, A., Craddock, R. C., Samaras, D., Thirion, B., et al. (2017). Deriving reproducible biomarkers from multi-site resting-state data: an autism-based example. *Neuroimage* 147, 736–745. doi: 10.1016/j.neuroimage.2016.10.045

Belgiu, M., and Drăgu,t, L. (2016). Random forest in remote sensing: a review of applications and future directions. *ISPRS J. Photogram. Remote Sens.* 114, 24–31. doi: 10.1016/j.isprsjprs.2016.01.011

Bi, X-,a, Hu, X., Xie, Y., and Wu, H. (2021). A novel CERNNE approach for predicting Parkinson's disease-associated genes and brain regions based on multimodal imaging genetics data. *Med. Image Anal.* 67, 101830. doi: 10.1016/j.media.2020.101830

Bi, X-,a, Liu, Y., Xie, Y., Hu, X., and Jiang, Q. (2020). Morbigenous brain region and gene detection with a genetically evolved random neural network cluster approach in late mild cognitive impairment. *Bioinformatics* 36, 2561–2568. doi: 10.1093/bioinformatics/btz967

Bi, X-,a, Shu, Q., Sun, Q., and Xu, Q. (2018). Random support vector machine cluster analysis of resting-state fMRI in Alzheimer's disease. *PLoS ONE* 13, e0194479. doi: 10.1371/journal.pone.0194479

Chaitra, N., Vijaya, P., and Deshpande, G. (2020). Diagnostic prediction of autism spectrum disorder using complex network measures in a machine learning framework. *Biomed. Signal Process. Control* 62, 102099. doi: 10.1016/j.bspc.2020.102099

Chen, J.-H., Parsons, S. P., Shokrollahi, M., Wan, A., Vincent, A. D., Yuan, Y., et al. (2018b). Characterization of simultaneous pressure waves as biomarkers for colonic motility assessed by high-resolution colonic manometry. *Front. Physiol.* 9, 1248. doi: 10.3389/fphys.2018.01248

Chen, Q., Meng, Z., Liu, X., Jin, Q., and Su, R. (2018a). Decision variants for the automatic determination of optimal feature subset in RF-RFE. *Genes* 9, 301. doi: 10.3390/genes9060301

Cheng, W., Rolls, E. T., Zhang, J., Sheng, W., Ma, L., Wan, L., et al. (2017). Functional connectivity decreases in autism in emotion, self, and face circuits identified by knowledge-based enrichment analysis. *Neuroimage* 148, 169–178. doi: 10.1016/j.neuroimage.2016.12.068

Di Martino, A., O'connor, D., Chen, B., Alaerts, K., Anderson, J. S., Assaf, M., et al. (2017). Enhancing studies of the connectome in autism using the autism brain imaging data exchange II. *Sci. Data* 4, 1–15. doi: 10.1038/sdata.2017.10

Di Martino, A., Yan, C-G, Li, Q., Denio, E., Castellanos, F. X., Alaerts, K., et al. (2014). The autism brain imaging data exchange: towards a large-scale evaluation of the intrinsic brain architecture in autism. *Mol. Psychiatry* 19, 659–667. doi: 10.1038/mp.2013.78

Dryburgh, E., McKenna, S., and Rekik, I. (2020). Predicting full-scale and verbal intelligence scores from functional connectomic data in individuals with autism spectrum disorder. *Brain Imaging Behav.* 14, 1769–1778. doi: 10.1007/s11682-019-00111-w

Du, L., Liu, K., Yao, X., Risacher, S. L., Han, J., Saykin, A. J., et al. (2020). Detecting genetic associations with brain imaging phenotypes in Alzheimer's disease via a novel structured SCCA approach. *Med. Image Anal.* 61, 101656. doi: 10.1016/j.media.2020.101656

Du, L., Liu, K., Zhu, L., Yao, X., Risacher, S. L., Guo, L., et al. (2019). Identifying progressive imaging genetic patterns via multi-task sparse canonical correlation analysis: a longitudinal study of the ADNI cohort. *Bioinformatics* 35, i474–i83. doi: 10.1093/bioinformatics/btz320

Epalle, T. M., Song, Y., Liu, Z., and Lu, H. (2021). Multi-atlas classification of autism spectrum disorder with hinge loss trained deep architectures: ABIDE I results. *Appl. Soft Comput.* 107, 107375. doi: 10.1016/j.asoc.2021.107375

Esteban, O., Birman, D., Schaer, M., Koyejo, O. O., Poldrack, R. A., and Gorgolewski, K. J. (2017). MRIQC: Advancing the automatic prediction of image quality in MRI from unseen sites. *PLoS ONE* 12, e0184661. doi: 10.1371/journal.pone.0184661

Franzmeier, N., Rubinski, A., Neitzel, J., Kim, Y., Damm, A., Na, D. L., et al. (2019). Functional connectivity associated with tau levels in ageing, Alzheimer's, and small vessel disease. *Brain* 142, 1093–1107. doi: 10.1093/brain/awz026

Frye, R. E., Vassall, S., Kaur, G., Lewis, C., Karim, M., and Rossignol, D. (2019). Emerging biomarkers in autism spectrum disorder: a systematic review. *Ann. Trans. Med.* 7, 792. doi: 10.21037/atm.2019.11.53

Glerean, E., Pan, R. K., Salmi, J., Kujala, R., Lahnakoski, J. M., Roine, U., et al. (2016). Reorganization of functionally connected brain subnetworks in high-functioning autism. *Hum. Brain Mapp.* 37, 1066–1079. doi: 10.1002/hbm.23084

Guo, K., Chai, R., Candra, H., Guo, Y., Song, R., Nguyen, H., et al. (2019). A hybrid fuzzy cognitive map/support vector machine approach for EEG-based emotion classification using compressed sensing. *Int. J. Fuzzy Syst.* 21, 263–273. doi: 10.1007/s40815-018-0567-3

Hao, X., Li, C., Du, L., Yao, X., Yan, J., Risacher, S. L., et al. (2017). Mining outcome-relevant brain imaging genetic associations via three-way sparse canonical correlation analysis in Alzheimer's disease. *Sci. Rep.* 7, 44272. doi: 10.1038/srep44272

Heinsfeld, A. S., Franco, A. R., Craddock, R. C., Buchweitz, A., and Meneguzzi, F. (2018). Identification of autism spectrum disorder using deep learning and the ABIDE dataset. *Neuroimage Clin.* 17, 16–23. doi: 10.1016/j.nicl.2017.08.017

Helkkula, A., Buoye, A. J., Choi, H., Lee, M. K., Liu, S. Q., and Keiningham, T. L. (2020). Parents' burdens of service for children with ASD–implications for service providers. *J. Service Manage.* 31, 1015–1039. doi: 10.1108/JOSM-01-2020-0011

Herringshaw, A. J., Ammons, C. J., DeRamus, T. P., and Kana, R. K. (2016). Hemispheric differences in language processing in autism spectrum disorders: a meta-analysis of neuroimaging studies. *Autism Res.* 9, 1046–1057. doi: 10.1002/aur.1599

Huang, H., Liu, X., Jin, Y., Lee, S. W., Wee, C. Y., and Shen, D. (2019). Enhancing the representation of functional connectivity networks by fusing multi-view information for autism spectrum disorder diagnosis. *Hum. Brain Mapp.* 40, 833–854. doi: 10.1002/hbm.24415

Ingalhalikar, M., Shinde, S., Karmarkar, A., Rajan, A., Rangaprakash, D., and Deshpande, G. (2021). Functional connectivity-based prediction of Autism on site harmonized ABIDE dataset. *IEEE Trans. Biomed. Eng.* 68, 3628–3637. doi: 10.1109/TBME.2021.3080259

Kang, E., Gadow, K. D., and Lerner, M. D. (2020). Atypical communication characteristics, differential diagnosis, and the autism spectrum disorder phenotype in youth. *J. Clin. Child Adolesc. Psychol.* 49, 251–263. doi: 10.1080/15374416.2018.1539912

Karpiel, I., Klose, U., and Drzazga, Z. (2019). Optimization of rs-fMRI parameters in the seed correlation analysis (SCA) in DPARSF toolbox: a preliminary study. *J. Neurosci. Res.* 97, 433–443. doi: 10.1002/jnr.24364

Lee, J. K., Amaral, D. G., Solomon, M., Rogers, S. J., Ozonoff, S., and Nordahl, C. W. (2020). Sex differences in the amygdala resting-state connectome of children with autism spectrum disorder. *Biol Psychiatry Cogn. Neurosci. Neuroimaging* 5, 320–329. doi: 10.1016/j.bpsc.2019.08.004

Lei, B., Zhao, Y., Huang, Z., Hao, X., Zhou, F., Elazab, A., et al. (2020). Adaptive sparse learning using multi-template for neurodegenerative disease diagnosis. *Med. Image Anal.* 61, 101632. doi: 10.1016/j.media.2019.101632

Li, X., Gu, Y., Dvornek, N., Staib, L. H., Ventola, P., and Duncan, J. S. (2020). Multi-site fMRI analysis using privacy-preserving federated learning and domain adaptation: ABIDE results. *Med. Image Anal.* 65, 101765. doi: 10.1016/j.media.2020.101765

Liu, J., Sheng, Y., Lan, W., Guo, R., Wang, Y., and Wang, J. (2020). Improved ASD classification using dynamic functional connectivity and multi-task feature selection. *Pattern Recognit. Lett.* 138, 82–87. doi: 10.1016/j.patrec.2020.07.005

Liu, J., Zhang, X., Yu, C., Duan, Y., Zhuo, J., Cui, Y., et al. (2016). Impaired parahippocampus connectivity in mild cognitive impairment and Alzheimer's disease. *J. Alzheimers Dis.* 49, 1051–1064. doi: 10.3233/JAD-150727

Liu, X., and Huang, H. (2020). Alterations of functional connectivities associated with autism spectrum disorder symptom severity: a multi-site study using multivariate pattern analysis. *Sci. Rep.* 10, 4330. doi: 10.1038/s41598-020-60702-2

Lord, C., Elsabbagh, M., Baird, G., and Veenstra-Vanderweele, J. (2018). Autism spectrum disorder. *Lancet* 392, 508–520. doi: 10.1016/S0140-6736(18)31129-2

McKinnon, C. J., Eggebrecht, A. T., Todorov, A., Wolff, J. J., Elison, J. T., Adams, C. M., et al. (2019). Restricted and repetitive behavior and brain functional connectivity in infants at risk for developing autism spectrum disorder. *Biol. Psychiatry Cogn. Neurosci. Neuroimaging* 4, 50–61. doi: 10.1016/j.bpsc.2018.09.008

Moradi, E., Khundrakpam, B., Lewis, J. D., Evans, A. C., and Tohka, J. (2017). Predicting symptom severity in autism spectrum disorder based on cortical thickness measures in agglomerative data. *Neuroimage* 144, 128–141. doi: 10.1016/j.neuroimage.2016.09.049

Noble, S., Scheinost, D., and Constable, R. T. (2019). A decade of test-retest reliability of functional connectivity: a systematic review and meta-analysis. *Neuroimage* 203, 116157. doi: 10.1016/j.neuroimage.2019.116157

Noriega, G. (2019). Restricted, repetitive, and stereotypical patterns of behavior in autism—an fmri perspective. *IEEE Trans. Neural Syst. Rehabil. Eng.* 27, 1139–1148. doi: 10.1109/TNSRE.2019.2912416

Osredkar, J., Gosar, D., Maček, J., Kumer, K., Fabjan, T., Finderle, P., et al. (2019). Urinary markers of oxidative stress in children with autism spectrum disorder (ASD). *Antioxidants* 8, 187. doi: 10.3390/antiox8060187

Qian, L., Wang, Y., Chu, K., Li, Y., Xiao, C., Xiao, T., et al. (2018). Alterations in hub organization in the white matter structural network in toddlers with autism spectrum disorder: a 2-year follow-up study. *Autism Res.* 11, 1218–1228. doi: 10.1002/aur.1983

Raka, A. G., Naik, G. R., and Chai, R. (2017). Computational algorithms underlying the time-based detection of sudden cardiac arrest via electrocardiographic markers. *Appl. Sci.* 7, 954. doi: 10.3390/app7090954

Santore, L. A., Gerber, A., Gioia, A. N., Bianchi, R., Talledo, F., Peris, T. S., et al. (2020). Felt but not seen: observed restricted repetitive behaviors are associated with self-report—but not parent-report—obsessive-compulsive disorder symptoms in youth with autism spectrum disorder. *Autism* 24, 983–994. doi: 10.1177/1362361320909177

Vallianatos, C. N., Farrehi, C., Friez, M. J., Burmeister, M., Keegan, C. E., and Iwase, S. (2018). Altered gene-regulatory function of KDM5C by a novel mutation associated with autism and intellectual disability. *Front. Mol. Neurosci.* 11, 104. doi: 10.3389/fnmol.2018.00104

Wang, M., Zhang, D., Huang, J., Yap, P.-T., Shen, D., and Liu, M. (2019). Identifying autism spectrum disorder with multi-site fMRI via low-rank domain adaptation. *IEEE Trans. Med. Imaging* 39, 644–655. doi: 10.1109/TMI.2019.2933160

Wang, N., Yao, D., Ma, L., and Liu, M. (2022). Multi-site clustering and nested feature extraction for identifying autism spectrum disorder with resting-state fMRI. *Med. Image Anal.* 75, 102279. doi: 10.1016/j.media.2021.102279

Wang, T., Zhang, X., Li, A., Zhu, M., Liu, S., Qin, W., et al. (2017). Polygenic risk for five psychiatric disorders and cross-disorder and disorder-specific neural connectivity in two independent populations. *Neuroimage Clin.* 14, 441–449. doi: 10.1016/j.nicl.2017.02.011

Wei, L., Chen, H., and Su, R. (2018). M6APred-EL: a sequence-based predictor for identifying N6-methyladenosine sites using ensemble learning. *Mol. Therapy Nucleic Acids* 12, 635–644. doi: 10.1016/j.omtn.2018.07.004

Wei, L., Luan, S., Nagai, L. A. E., Su, R., and Zou, Q. (2019). Exploring sequence-based features for the improved prediction of DNA N4-methylcytosine sites in multiple species. *Bioinformatics* 35, 1326–1333. doi: 10.1093/bioinformatics/bty824

Yang, C., Wang, P., Tan, J., Liu, Q., and Li, X. (2021). Autism spectrum disorder diagnosis using graph attention network based on spatial-constrained sparse functional brain networks. *Comput. Biol. Med.* 139, 104963. doi: 10.1016/j.compbiomed.2021.104963

Conflict of Interest: The authors declare that the research was conducted in the absence of any commercial or financial relationships that could be construed as a potential conflict of interest.

frontiers | Frontiers in Neuroscience

ORIGINAL RESEARCH
published: 31 May 2022
doi: 10.3389/fnins.2022.890596

Abnormal Insular Dynamic Functional Connectivity and Its Relation to Social Dysfunctioning in Children With Attention Deficit/Hyperactivity Disorder

*Ahmed Ameen Fateh[1], Wenxian Huang[2], Tong Mo[1], Xiaoyu Wang[1], Yi Luo[1], Binrang Yang[2], Abla Smahi[3], Diangang Fang[1], Linlin Zhang[2], Xianlei Meng[1] and Hongwu Zeng[1]**

[1] Department of Radiology, Shenzhen Children's Hospital, Shenzhen, China, [2] Children's Healthcare, Mental Health Center, Shenzhen Children's Hospital, Shenzhen, China, [3] Shenzhen Graduate School, Peking University, Shenzhen, China

OPEN ACCESS

Edited by:
Zaixu Cui,
Chinese Institute for Brain Research, China

Reviewed by:
Jia Lu Xia,
Tsinghua University, China
Xiaohua Cao,
First Hospital of Shanxi Medical University, China

***Correspondence:**
Hongwu Zeng
homerzeng@126.com

Specialty section:
This article was submitted to Brain Imaging Methods, a section of the journal Frontiers in Neuroscience

Received: *06 March 2022*
Accepted: *09 May 2022*
Published: *31 May 2022*

Citation:
Fateh AA, Huang W, Mo T, Wang X, Luo Y, Yang B, Smahi A, Fang D, Zhang L, Meng X and Zeng H (2022) Abnormal Insular Dynamic Functional Connectivity and Its Relation to Social Dysfunctioning in Children With Attention Deficit/Hyperactivity Disorder. Front. Neurosci. 16:890596. doi: 10.3389/fnins.2022.890596

Anomalies in large-scale cognitive control networks impacting social attention abilities are hypothesized to be the cause of attention deficit hyperactivity disorder (ADHD). The precise nature of abnormal brain functional connectivity (FC) dynamics including other regions, on the other hand, is unknown. The concept that insular dynamic FC (dFC) among distinct brain regions is dysregulated in children with ADHD was evaluated using Insular subregions, and we studied how these dysregulations lead to social dysfunctioning. Data from 30 children with ADHD and 28 healthy controls (HCs) were evaluated using dynamic resting state functional magnetic resonance imaging (rs-fMRI). We evaluated the dFC within six subdivisions, namely both left and right dorsal anterior insula (dAI), ventral anterior insula (vAI), and posterior insula (PI). Using the insular sub-regions as seeds, we performed group comparison between the two groups. To do so, two sample *t*-tests were used, followed by *post-hoc t*-tests. Compared to the HCs, patients with ADHD exhibited decreased dFC values between right dAI and the left middle frontal gyrus, left postcentral gyrus and right of cerebellum crus, respectively. Results also showed a decreased dFC between left dAI and thalamus, left vAI and left precuneus and left PI with temporal pole. From the standpoint of the dynamic functional connectivity of insular subregions, our findings add to the growing body of evidence on brain dysfunction in ADHD. This research adds to our understanding of the neurocognitive mechanisms behind social functioning deficits in ADHD. Future ADHD research could benefit from merging the dFC approach with task-related fMRI and non-invasive brain stimulation, which could aid in the diagnosis and treatment of the disorder.

Keywords: attention deficit hyperactivity disorder, dynamic functional connectivity, insula, rs-fMRI, social dysfunction

1. INTRODUCTION

Attention Deficit Hyperactivity Disorder (ADHD) is the most commonly diagnosed condition in children, characterized by age-inappropriate problems like inattention, impulsivity, and hyperactivity (Thomas et al., 2015; Sayal et al., 2018). ADHD is therefore related to cognitive, academic, familial, and occupational problems (Usami, 2016). Social functioning is also directly impacted by ADHD. This might be manifested as peer rejection and disagreements. Social dysfunction may negatively affect the short- and long-term prognosis of ADHD youngsters. The activities that encourage social inadequacies are directly linked to ADHD diagnosis in some infants. While children with ADHD crave social interaction, they often struggle to adapt their behavior to their environment due to the nasty, angry tone of their interactions as well as their hyperactive/impulsive behavior. This implicates rule infractions, aggressive and dominating behavior, and physical and verbal animosity. It also includes agitation and intrusion, which are often inappropriate and difficult to remedy (Lahey et al., 2005).

ADHD is linked to functional deficits in the cognitive, academic, familial, and occupational areas of everyday life (Usami, 2016). Social functioning is another crucial aspect of ADHD that is directly affected. This might present itself as peer rejection and disputes with other children and adults. Social dysfunction may have a significant negative impact on the short- and long-term prognosis of children with ADHD. The practices that promote social deficiencies may be a direct result of diagnosing symptoms of ADHD in at least some infants. Some of ADHD's DSM-IV criteria, such as "interrupting or intruding on others," even explicitly relate to poor social conduct (Lahey et al., 2005). Generally, the combination of hyperactivity, impulsivity, and inattention is likely to affect social behavior. Although children with ADHD have a strong desire to interact with others, they typically struggle to adapt their attitude to their surroundings. Two behavioral characteristics are typically linked to social difficulties in children with ADHD, namely the unpleasant, hostile tone of their interactions, as well as their hyperactive/impulsive behavior. Rule violations, antagonistic and dominating behavior, and the use of physical and verbal hostility are examples of the first aspect. These actions may pose a direct threat to others, and they have been proven to be substantial predictors of negative peer nominations in both ADHD and non-ADHD children. Examples of the second aspect comprise restless and invasive conduct, which is frequently inappropriate in the current setting and difficult to remedy (Lahey et al., 2005).

The orbitofrontal cortex (OFC), the amygdala, and the temporal cortex (mostly the superior temporal sulcus-STS) were found to be primary elements of the so called "social brain," in the early 1990s (Brothers, 1990). Afterwards, other areas like the medial prefrontal cortex (mPFC) and the anterior cingulate cortex (ACC), were shown to be primary for social functioning and were therefore included with the initial core (Frith and Frith, 2006; Bickart et al., 2014). Modern definitions of social brain usually incorporate dynamic and hierarchical structure of circuitry entangled in elementary constructs of more automated systems like the identification of socially significant stimuli as well as relatively overlapping circuitry implicated in higher-order operations of the psychological condition. For instance, feelings such as disgust or anger were basically associated with the aversion network where the insula is key component (Buckholtz et al., 2008). This implicates that the insula, among other brain regions in the aversion network, is mediated in aversive behaviors such as avoiding strangers that are not trustworthy. Studies have also demonstrated the implication of the insula in the "social decision making" that enables the selection of flexible behavioral responses to others (Rogers-Carter and Christianson, 2019). More precisely, the insular cortex is anatomically located to connect integrated social sensory cues to the social decision making network, resulting in flexible and adaptive behavioral outcomes to social and emotional stimuli. In line with these findings, Belfi et al. (2015) suggested that subjects with lesion on the insula had aberrant trust expressions. During a trust game, when acting as an investor, these people behaved benevolently (showing misguided trust), and when acting as a trustee, they acted malevolently (infringing their partner's trust). Although the topic of attention, play and social behavior in children with ADHD has been studied for years now, yet, it is unfortunate that tackling the role of the insula in the social dysfunctioning in children with ADHD is still scarce. Large body of research barely mentioned the insula as part of different networks related to social functioning, especially with regard to neuroimaging-based investigations.

The majority of neuroimaging research indicates static brain networks across the course of an fMRI session. These networks show functional connections and interactions between distinct cortical and subcortical brain regions during task execution or at rest. However, because activity in static networks does not clearly display changes that occur over short periods of time during an fMRI scan, dynamic reconfiguration-based methods to discover the modular architectures of changing networks are becoming more popular and the so called dFC was introduced. By partitioning fMRI images into time windows, the interconnections between brain regions can be better understood. Dynamic reconfigurations are more sensitive and able to detect more changes in human brain activity than static reconfigurations (Patil et al., 2021). whether static or dynamic, at rest or task-based, accurately identifying the altered functional connectivity generated by ADHD or any other specific disorder is a critical endeavor that may reveal the disorder's causative factors. Both in childhood and adulthood, imaging studies have revealed structural and functional abnormalities in the brains of ADHD patients. Many evidence from fMRI studies strongly suggest that biomarkers and alterations in interactions within and between different brain connectivity may contribute to the disruption of normal brain functions and cognitive performance, leading to fluctuations in attention in patients with ADHD (Sonuga-Barke and Castellanos, 2007; Shappell et al., 2021). Functional impairments in fronto-cortical and fronto-subcortical networks are basic deficiencies in both children and adults with ADHD, according to Rubia et al. (2014). Consistent with these findings, Guo et al. (2020) questioned the consistency of ADHD diagnosis from childhood to maturity, as well as the similarities and differences in abnormal functional connectivities (FCs) across

ADHD children and adults. To put it another way, they looked at clinical changes and pathophysiological continuity in ADHD patients from childhood to adulthood. On the other hand, a thorough research in the literature yielded to very few researches addressing dFC in ADHD. For instance, Ahmadi et al. (2021) revealed that subtypes of ADHD have generalized anomalies in static FC and dFC between large-scale resting state networks, encompassing cortical and subcortical areas, when compared to typically developing youngsters. They came to the conclusion that dynamic changes in brain FC may better help to explain the pathophysiology of ADHD. Sun et al. (2021) suggested state-dependent dynamic changes in large-scale brain connections and network topologies in ADHD. Yang et al. (2021) found that children with ADHD have more unstable dFC of the amygdala subregions, which may impact their cognitive skills. As a result, it should be indicated that to ensure successful diagnosis, therapy, and prevention, it is critical to research the sophisticated mechanisms underlying ADHD, as well as the functional deficits of the diseased brain. rs-fMRI is one such a non-invasive and safe method of detecting spontaneous brain activity (Lu et al., 2018). Over the last three decades, numerous studies have been conducted to investigate potential imaging changes and biomarkers of ADHD. However, no significant findings were yield to study the dFC of the insula in children with ADHD, and its contribution to social dysfunction.

From a neurobiologic standpoint, ADHD is increasingly being recognized as a disorder resulting from disruptions in large-scale brain networks. Extant studies of brain's FC in ADHD, however, have provided inconsistent outcomes, with some research suggesting hyper- and hypoconnectivity with respect to neurotypical controls and others providing null findings, mostly between the same brain networks, likely due to weak theoretical models, inadequate quantitative approaches, and variation in protocols and measures across data collection silos. Importantly, little is understood about the dynamics of brain connectivity in ADHD, because earlier research assumed that functional linkages across brain regions or networks were stationary. Aiming to overcome these challenges, this study investigated Insular subregions to test the hypothesis that insular dFC among different brain regions is impaired in children with ADHD, and these impairments may play a role in social dysfunction. Furthermore, the neural biomarkers found in children with ADHD were analyzed to see if they might be used as group-level features to distinguish patients with ADHD from HCs. The findings of this study could provide new imaging-based insights that can assist explain the clinical manifestations of ADHD and improve our understanding of the brain mechanism behind its symptoms in the pathway to ADHD.

2. MATERIALS AND METHODS

2.1. Participants and Measures

Shenzhen Children's Hospital provided data with a total of 30 ADHD boys aged between 7 and 10 years and 28 HCs having the same age range. Two experienced psychiatrists assessed all of the patients to ensure that they met the diagnostic criteria for ADHD based on clinical interviews that followed the Diagnostic and Statistical Manual of Mental Disorders, Fourth Edition. The participants and their parents were interviewed using the Schedule for Affective Disorders and Schizophrenia for School-Age Children-Present and Lifetime Version interview (K-SADS-PL; Kaufman et al., 1997). ADHD diagnoses were based on the Diagnostic and Statistical Manual of mental disorders-fourth edition (DSM IV) (Association, 2013). Clinically-referred children who satisfied the DSM-IV criteria (either mixed, mainly inattentive, or predominantly hyperactive/impulsive subtype) were included in this study.

For each ADHD patient, parents, teachers, and other people who are in charge of caring for the kid were asked about the child's behaviors and conducts in various settings, such as at home, school, or with peers. The Conners-3 parent/teacher ratings (Conners, 2008) was used to evaluate ADHD symptoms and associated issues such as disruptive behavior and learning difficulties. The used lengthy Conner-3 version has 105/111 items (parent/teacher) that are graded on a 4-point Likert-scale from 0 (never) to 3 (very much/very frequently). The Conners-3 comprises scales such as hyperactivity/impulsivity, inattention, learning problems, executive functions, aggression, peer relations (content scales); DSM IV-inattention and hyperactivity/impulsivity, DSM IV-conduct disorder, DSM IV-oppositional defiant disorder (symptom scales); ADHD index, Global index. We obtained an internal consistency Cronbach's α (Christiansen et al., 2016) of 0.84 for the content scales and $\alpha = 0.80$ for the symptom scales of the Conners-3 parent rating scale. Children with ADHD who showed persistent patterns of inattention and/or hyperactivity-impulsivity that affect their functioning and development for at least 6 months were diagnosed. Accordingly, healthcare providers examined symptoms of inattention such as: (1) failing to pay close attention to details or making thoughtless blunders, in schoolwork, (2) frequently struggling to maintain focus on chores or recreational activities, (3) frequently ignoring instructions and directions and failing to complete homework or chores (e.g., loses focus, side-tracked), (4) having a hard time keeping track of tasks and activities, (5) during regular activities, the kid is prone to forgetfulness and distraction, (6) frequently misplaces items required for chores and activities (e.g., school materials, pencils, books, tools, eyeglasses), (7) frequently avoids, hates, or is hesitant to accomplish tasks that demand sustained mental effort (such as schoolwork or homework). Symptoms related to hyperactivity and impulsivity were also examined such as: (1) being unable to play or participate in leisure activities in a peaceful manner, (2) talking excessively, (3) having difficulty waiting for their turn, (3) disturbs or invades the privacy of others (e.g., butts into conversations or games). The cognitive function was assessed using the Stroop Color and Word Test (SCWT) (Lee and Chan, 2000) which indeed has effect on the working memory that can, in turn, have behavioral consequences similar to those of externally perceived stimuli. As for the assessment of social functioning, there were specific questions about the number of close friends, the contact with them. Ratings were made on a 4-point scale (less than one, 1–2, 3–4, 5 or more). The quality of ADHD

children's relationships with friends and their reactions to family members visits was also evaluated using a questionnaire of a 5-point scale [from 0 (no contact/reaction at all) to 5 (very well)].

The K-SADS-PL was used to consult the children in HCs group, as well as their parents, to check that they did not fulfill the diagnostic criteria for ADHD or any other mental illnesses. Normal eyesight and hearing were also required, as well as a Full-Scale Intelligence Quotient (FSIQ) $\geq$ 70 calculated using the Wechsler Intelligence Scale for Children, Fourth Edition. Participants with current or previous psychological illnesses, major physical disorders, neurological disorders, or brain injuries were not allowed to participate in this study. The Shenzhen Children's Hospital Medical Research Ethics Committee gave their approval to this study. All of the children agreed to take part in this study, and their parents gave signed informed consent.

2.2. rs-fMRI Data Acquisition

The rs-fMRI data for all participants were obtained using a 3.0-T system scanner (Siemens Magnetom Skyra) at the Radiology Department of Shenzhen Children's Hospital, Shenzhen, China. The rs-fMRI data were acquired using echo-planar imaging (EPI) sequence with the following parameters: repetition time (TR) $= 2,000$ *ms*; echo time $= 30$ *ms*; flip angle$= 90^{\circ}$; matrix size $= 64 \times 64$; 32 axial slices; field of view = 24×24 cm^2; slice thickness $= 3$ *mm* and no gap. Structure 3D-MPRAGE; T1 Repetition Time [TR, ms] = 2,300 ms, Echo Time [TE, ms]= 2.26; Number of Averages $= 1.0$, Slice Thickness $= 1.0$ *mm*, Field of View (FOV)$= 256$ *mm*.

2.3. Data Pre-processing

The DPABI toolkit (Yan et al., 2016) was used to preprocess the data. Because of the volatility of the initial magnetic resonance imaging signal and the participants' adaption to the experimental setup, the first 10 volumes were eliminated. The remaining 220 volumes were first realigned to correct for head-motion before being corrected by the acquisition time delay among different slices. Under the head motion criterion of ± 3 *mm* and no participant was excluded. The pictures were then normalized and resampled into a voxel size of $3 \times 3 \times 3$ mm^3 utilizing an uniform segmentation of anatomical images. The following three steps were engaged in normalization: 1) Each participant's T1 structural images were co-registered to their corresponding functional images; 2) Co-registered T1 images were segmented into gray matter, white matter, and cerebrospinal fluid using transformation parameters that indicated transformation from subject native space to standard Montreal Neurological Institute (MNI) space; 3) Functional images were finally transformed into the standard space using transformation p. Additional regression was applied to nuisance factors, such as 24 head movement parameters, global signal, white matter signal, and cerebrospinal fluid signal, to adjust for physiological noise, such as motion and cardiac and respiratory cycles. Following that, the data were linearly detrended, filtered at 0.01–0.08 Hz, and smoothed with a 6*mm* full-width-at-half-maximum Gaussian kernel.

2.4. Head Motion

The mean framewise displacement (FD) created during the scanning process was removed using Jenkinson's relative root-mean-square technique (Jenkinson et al., 2002). To evaluate the voxel-wise motion differences between the two groups, the mean FD (Jenkinson) was determined. The mean FD did not change substantially between the ADHD and HC groups ($p < 0.6$).

2.5. Static Functional Connectivity Analysis

Seed areas were chosen based on the presence of social dysfunctioning-related anomalies in right and letf dAI, vAI, and PI in FC. The seeds were obtained using cluster analysis, in agreement with earlier literature (Deen et al., 2011), in which the insula was subdivided based on FC pattern clustering. We were primarily interested in the rdAI and rvAI regions, which have been linked to attention and emotion, as well as an outwardly and inwardly oriented system, respectively (Touroutoglou et al., 2012). The right and left hemispheres of the dAI, vAI, and PI were then transformed to MNI 152 standard brain (3-mm resolution) and used as seed regions in the FC analysis in HC and ADHD patients. We used the REST toolbox (http://restfmri.net/forum/index.php) to perform seed-based FC studies to evaluate the aberrant sFC of seed regions in HC and ADHD. Between the mean time course of each seed region and the time course of all other voxels in the entire brain, Pearson's correlation coefficient was derived. To increase the Gaussianity of their distribution, the resulting r maps were turned into z maps using Fisher's r-to-z transformation. We obtained z-score maps for each subject that represented the sFC of the right and left of dAI, vAI, and PI.

2.6. Dynamic Functional Connectivity Analysis

Using the DynamicBC toolbox (Liao et al., 2014), the sliding window method was used to analyze the dFC for each participant. According to previous research, the window length is an open but important parameter in sliding window based resting state dynamic computation (Fateh et al., 2020; Li et al., 2020; Yang et al., 2021). This approach can calculate the time-varying covariance of interregional neural signals, which is the variance of dFC, and reveal the temporal aspects of FC during the full scan period. The sliding window method uses the window length as a crucial parameter.The minimum window length should not be smaller than 1/fmin, as per Leonardi and van de Ville (Leonardi and Van De Ville, 2015), because a very short window length may generate spurious fluctuations. In addition, the fmin represents the time courses' minimal frequency. The dynamic properties of the time series would be made unobservable if the window length was too long. We chose a window length of 50 TRs (i.e., 100s) and a step size of 1 TR because a window length of 50 TR was proposed to maximize the balance between recording a fast altering dynamic relationship and producing credible estimations of the correlations between regions (Liao et al., 2018) (i.e., 2s). In the validation analyses that followed, other window lengths and step sizes were also evaluated. Liao et al. (2018) computed the Fisher's z-transformed Pearson's correlation coefficient between the average time series of each seed region

and the remaining voxels in the whole brain in each window. As a result, each participant received a set of sliding-window correlation maps. Calculating standard deviation values at each voxel across sliding-windows was used to estimate the dFC.

2.7. Statistical Analyses

To see if there was a difference in the dFC of the insular subregion between HCs and ADHD patients, a two-sample *t*-test model was used. Confounding factors such as the mean FD, age, gender, and grade were regressed out. T-statistic images were transformed to z-statistic images, and then thresholder using clusters identified by a z value of > 2.3 and a cluster-level thresholder *p*-value of 0.05, corrected for whole-brain multiple comparison correction using Gaussian random field theory. The regions of interest (ROIs) for the *post-hoc* analysis were chosen from the survivors' brain clusters. The data were corrected by multiple comparisons using Gaussian random field theory (GRF, voxel-wise $p < 0.001$, cluster-wise $p < 0.05$, two-tailed) and the dynamic R-fMRI indices and voxel-wise concordance were compared using a two-sample *t*-test. On these ROIs, a two-tailed, two-sample *t*-test was used to evaluate the differences between two groups (HC vs. ADHD). The statistical significance level is $p < 0.05/6$. (Bonferroni correction). Brain regions data are summarized in **Table 1** and the positions of the Insular sub-regions are depicted in **Figure 1**.

2.8. Validation Analysis

We performed validation analysis for several sliding window lengths besides 50 TR to corroborate our findings of dFC variability derived from 50 TR lengths of the sliding window. As a consequence, we recalculated the primary dFC results with the other two window lengths (30TR and 80TR).

3. RESULTS

3.1. Demographic and Clinical Information

The demographic and clinical characteristics of the ADHD and HC groups were listed in **Table 2**. No differences in sex and mean FD were detected between the two groups. We found a large differences in IQ, working memory and learning problems between the two groups, in a way that these variables were lower in ADHD patients compared to HCs. For social functioning, children with ADHD had a significantly lower number of social contacts, and a poorer quality of social contacts with family members compared to the HCs group. It was also shown that ADHD patients had more problems with social relations with their peers although the effects were marginally significant (i.e., $p < 0.1$).

3.2. Differences of the dFC in the Right dAI, vAI and PI Among ADHD, and HCs

Compared with HCs, patients with ADHD showed significantly decreased dFC between right dAI with left middle frontal gyrus and left postcentral gyrus and between right vAI with right cerebellum crus. No significance was found in the PI. Moreover, no increased dFC has been obtained between the two group. Details regarding information on differences of dFC in between-group are introduced in **Figure 2** and **Table 2**.

3.3. Differences of the dFC in the Left dAI, vAI and PI Among ADHD, and HC

Compared with HCs, patients with ADHD showed significantly decreased dFC between dAI, vAI and PI and left thalamus, left precuneus and right temporal pole, respectively. No increased dFC has been detected between the two group. Details pertaining to the results of between-group differences in dFC of left subregions of insula is presented in **Figure 3** and **Table 2**.

3.4. Validation Analyses

To verify our findings of dFC in insular subregions variability obtained from sliding-window length of 50 TRs (100s), we performed auxiliary analyses with different sliding window

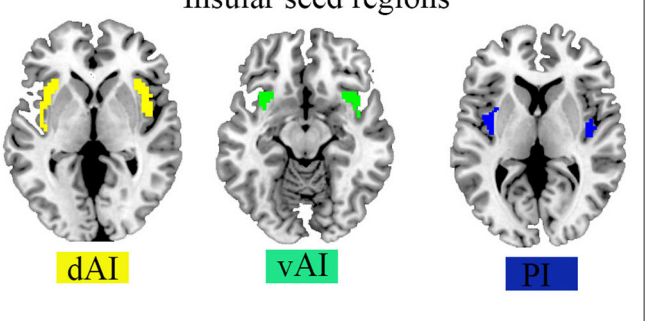

FIGURE 1 | Seed regions of the insula in the Brian.

TABLE 1 | Brain clusters showing significant effects in the dFC of insular subregions.

Seed region	Brain regions	Cluster size Voxels	Z score	M N I X Y Z	ADHD(n = 30) M ± SD	HC(n = 28) M ± SD
Right dAI	Left middle frontal gyrus	80	–5.76	–33 9 36	0.02 ± 0.01	0.05 ± 0.01
Right dAI	Left postcentral gyrus	85	–5.02	–48 –33 63	0.02 ± 0.009	0.05± 0.019
Right vAI	Right cerebelum_crus	91	–5.54	33 –75 –48	–0.13 ± 0.14	–0.001± 0.12
Left dAI	Left thalamus	68	–7.75	–3 –15 3	0.02 ± 0.012	0.05± 0.019
Left vAI	Left precuneus	79	8.1	–42 –60 0	–0.09 ± 0.15	0.02 ± 0.14
Left PI	Right temporal pole	65	–6.27	43 20 –22	0.02 ± 0.0.01	0.05 ± 0.016

SD, Standard Deviation; M, Mean value; dAI, dorsal Anterior Insula; vAI, Ventral Anterior Insula; PI, Posterior Insula.

TABLE 2 | Demographic and clinical information.

Variables	HC ($n = 28$)	ADHD ($n = 30$)	p-values
Age, mean ± SD	8.6 ± 0.97	8.6 ± 0.56	0.11[a]
Sex (male)	28	30	
Grade, mean ± SD	3 ± 0.83	2.6 ± 0.56	0.02[a]
FD, mean ± SD	0.05 ± 0.02	0.06 ± 0.02	0.6[a]
IQ scores, mean ± SD	108.6 ± 10.81	84.3 ± 9.37	< 0.001[a]
Working memory, mean ± SD	19.5 ± 3.10	9.95 ± 2.11	< 0.001[a]
Behavioral problems, mean ± SD	1.12 ± 0.45	0.50 ± 0.40	< 0.001[a]
Anxiety score, mean ± SD	0.54 ± 0.35	0.12 ± 0.10	< 0.01[a]
Learning problems, mean ± SD	1.15 ± 0.5	0.45 ± 0.30	< 0.01[a]
Psychosomatic disorder, mean ± SD	0.21 ± 0.18	0.12 ± 0.30	0.51[a]
IS(time), mean ± SD	18.2 ± 8.5	9 ± 3.5	< 0.01[a]
Number of social contacts	3.2± 0.80	2.98± 0.82	< 0.1[a]
Quality of social contacts-family	3.45 ± 1.07	3.34 ±1.04	< 0.1[a]
Quality of social contacts-friends	3.78 ± 1.50	4.10 ± 1.28	
Problems with social relations with their peers	3.00 ± 2.19	3.04 ± 2.80	< 0.1[a]

HC, healthy control; ADHD, Attention deficit hyperactivity; FD, frame-wise displacement; SD, Standard deviation; a, Two-samplet-test; IS, interference score.

lengths. We recalculated the main results by using two other window lengths (30 TR and 80 TRs) were similar to the main results of 50 TR in our study.The corresponding results are shown in the **Supplementary Materials**. All validation analysis results are presented in **Supplementary Figures S1–S4**.

4. DISCUSSION

Impaired attention, impulsivity and hyperactivity are the solely hallmarks in ADHD. These symptoms are directly related to social dysfunctioning that mostly affects the daily life of ADHD patients, especially kids. Despite its importance to the neuroimaging research community, few studies about dFC in children and adolescents with ADHD have been published so far. Although there are no clinically accurate biomarkers for the diagnosis of ADHD, this study investigated the insula dFC with other brain regions in the hope that such research can promote to the discovery of numerous viable candidate biomarkers, especially those associated to social dysfunctioning. Our findings support the hypothesis that the insular dFC with distinct brain regions is altered, and these deficits may be implicated in social dysfunction. Consistent with our hypothesis, compared to HCs, patients with ADHD showed decreased dFC values between right dAI and the left frontal_mid gyrus, left postcentral gyrus and the right of cerebellum crus. Results also indicated a decreased dFC between left dAI and thalamus, left vAI and left precuneus and left PI with temporal pole mid.

Social dysfunctioning is a broad term that is manifested by various neuropsychiatric disorders. To date, the majority of studies investigating social functioning have relied on self-report, questionnaire-based measures of social function (Hodgetts et al., 2017). In this study, with regard to ADHD, during diagnosis testing, we opted for a number of aspects (i.e., cognitive and executive functioning, working memory, learning problems, and anxiety-related symptoms and other measures; namely the number of social contacts, the quality of social contacts for both family and friends and the problems with social relations with their peers) depending on the available participants' data. These aspects entail other related concepts such as emotion regulation and attention orientation. The current findings, as well as those from earlier studies (Biederman et al., 1993), suggest that children with ADHD frequently experience issues with social relationships. Due to their behavioral problems (e.g., not following the rules when playing a game), these children may not have the same opportunities to make friends. Other impaired functional connectivity that are possibly associated with social dysfunctioning are discussed below considering our dFC's findings. We also found a considerable differences in IQ, working memory and learning problems between the two groups. Many studies have demonstrated that both IQ and working memory are related to learning in a sense that these IQ and working memory would predict reading, writing, and math skills in children (Alloway and Copello, 2013). Our findings are consistent with other existing studies in the literature (Rohrer-Baumgartner et al., 2014) that found in children with below median IQ-score, a larger number of ADHD symptoms were more likely to be accompanied by reports of lower expressive language skills. One possible reason for such lower scores and their implications to the lower expressive language skills is due to impaired (decreased) dFC between the Insula and the frontal middle gyrus since these two regions have been involved in language, self expression and learning. More related interpretations are presented below.

The insula (or insular cortex) is a thin ribbon of gray matter tissue that lies just deep to the lateral brain surface, separating the temporal lobe from the inferior parietal cortex (Broder and Preston, 2011). Taste, visceral sensation, and autonomic control are only a few of the homeostatic activities pertaining to basic survival needs that involve the insula. It was also proved that the insula regulates the sympathetic and parasympathetic nervous systems, which control autonomic activities (Bud Craig, 2009). According to functional connectivity studies and in line with our study, the human insula has at least three different segments (Nomi et al., 2016). A dorsal anterior insula (dAI) subdivision with connections to the frontal, anterior cingulate, and parietal areas is participated in cognitive control processes; a ventral anterior insula (vAI) subdivision has connections to limbic areas and is involved in affective processes; and a mid-posterior insula (PI) subdivision has connections to brain regions for sensorimotor processing (Cereda et al., 2002). Based on our dFC analysis, while studying time-varying patterns of interactions between insular subdivisions and other brain regions, we found

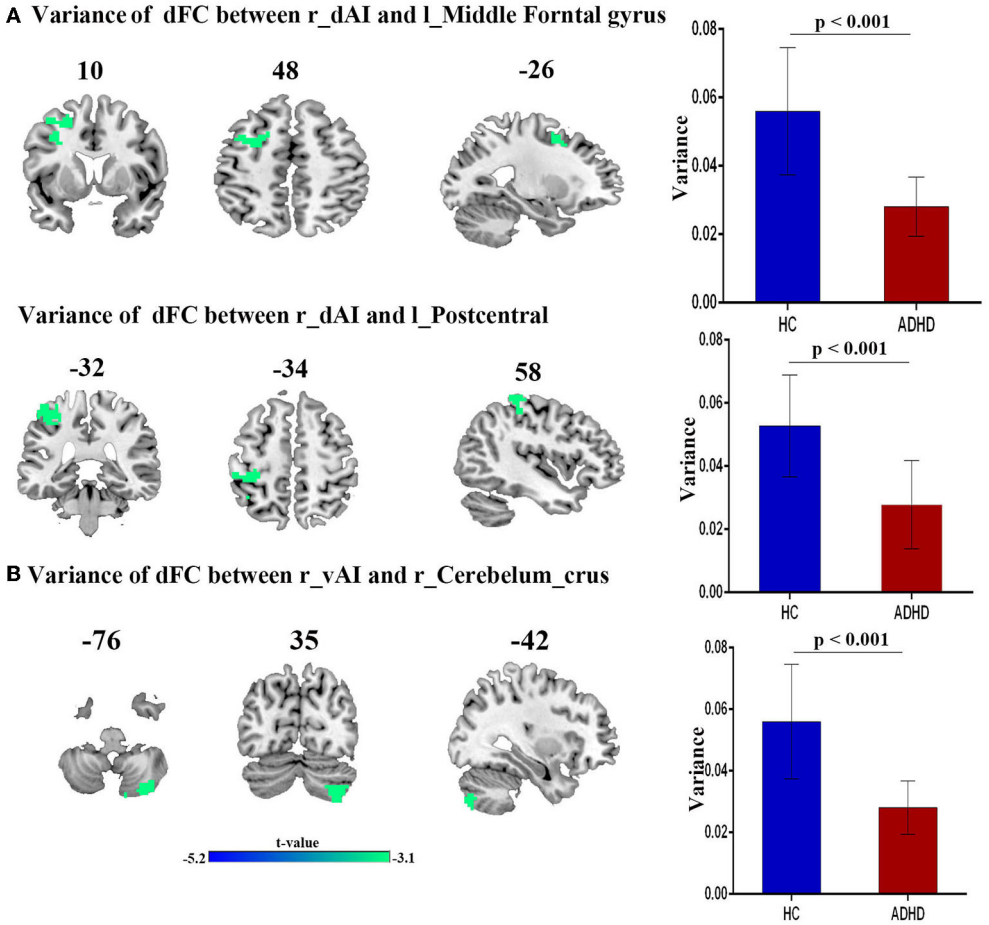

FIGURE 2 | The variance of dFC between the right insula and other brain regions, obtained by comparing HCs and ADHD groups, using two sample *t*-test; **(A)** Between right dAI and Left Middle frontal gyrus (first row) and Left postcentral gyrus (second row). **(B)** Between right vAI and right cerebelum curs.

that the dAI has more changeable connections than the other insular segments. This is consistent with previous research indicating the dAI's functional "diversity," which is engaged across numerous task domains (Penfield and Faulk, 1955; Cereda et al., 2002). On the other hand, recent functional imaging investigations have found that the left or right lateralization of emotional processing is influenced by stimulus valence (positive or negative emotions) (Harrington, 1995), behavior (approach/withdrawal) (Davidson et al., 1990), and subjective state (perception/experience) (Peelen et al., 2010). In regard to the lateralization of the human insula, our findings revealed the following insights: (1) stronger dFC of the insula in the left hemisphere than the right, which was manifested among all subdivisions (2) heterogeneous connectivity between insula subdivisions' profiles. In accordance with these findings, a number of lesion case studies elucidated the role of left insula in executive set-switching (executive functioning) which is mainly associated with ADHD. For instance, Varjačić et al. (2018) suggested support for the role of the left insular cortex in flexible attention switching among stroke survivors. Markostamou et al. (2015) studied the case of a woman with an acute left anterior insular infarction that led to executive (word and design fluency, mental flexibility, sustained attention, inhibitory control) but not language, visuoperceptual, or memory deficits. Conflicting with these findings, by considering the the way we relate language to our interpersonal relationships, while some functional imaging studies reported greater activation in the left insula in equal bilingual young adults (Chee et al., 2004), others demonstrated the brain's ability to sustain proper language without the insula (Duffau et al., 2001). On the other hand, regarding our second finding which supports many relevant recent researches proposing a tripartite organization rather than the traditional anterior-posterior dichotomy. Nomi et al. (2018) elucidated that the functional profiles of the insular subdivisions are both unique and overlapping.

Our decreased dFC results were compatible with other studies (Wang et al., 2020) that found significant decreases in both functional connectivity and global network efficiency. This decrease may correspond to either patients' insula incapability to integrate external sensory information with cognitive abilities including supervisory attentional control (Cieslik et al., 2015) and interior emotion or to the small size of the data sample. The former inference is due to the anatomy of the nervous system whereby the thalamus takes information from "homeostatic

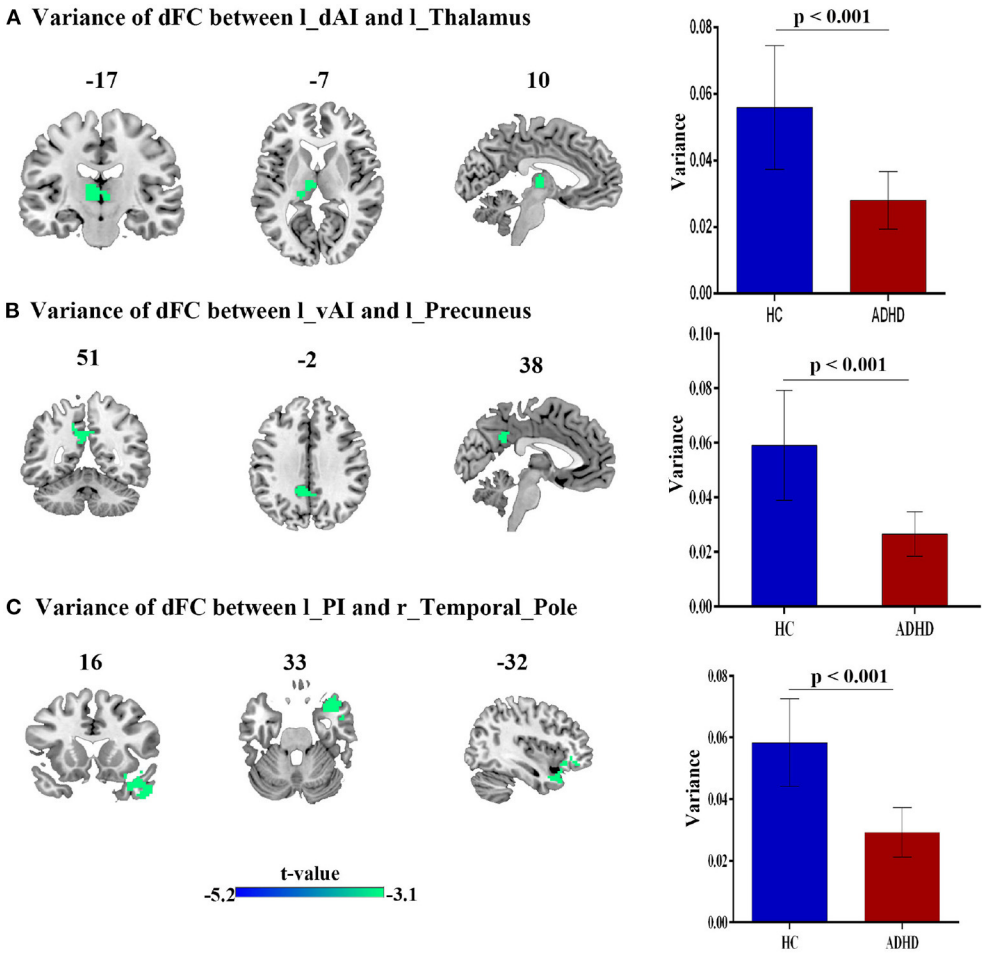

FIGURE 3 | The variance of dFC between the left insula and other brain regions, obtained by comparing HCs and ADHD groups, using two sample *t*-test; **(A)** Between left dAI and Left thalamus. **(B)** Between left vAI and left precuneus, **(C)** between left PI and right temporal_pole_mid.

afferent" sensory pathways and transfers it to the insula, which then sends it to a number of limbic-related regions, including the amygdala.

Another key result of this study is the alteration of dFC between left AI and left thalamus. Consistent with our findings, in regard with social dysfunctioning, the processing of information relevant to gustatory, visceral, and autonomic functions, and even salient information and emotion regulation, is underpinned by connections between the thalamus and the anterior insula (Ghaziri et al., 2018). A decreased FC with limbic regions such as the amygdala, hippocampus, thalamus, and insula in people with subclinical anxiety were reported in Scheinost et al. (2013) and in ADHD adolescents (Rubia et al., 2019). Mills et al. (2012), in turn, also suggested a corticostriatal-thalamic connectivity changes in children with ADHD and they then discussed the relation of these results to patients' working memory ability. Working memory is critical for reasoning, decision-making, and behavior guidance and it is among the core difficulties especially for students with ADHD. We continually handle social cognitive information, whether it's keeping track of friends' viewpoints during conversation, a roomful of colleagues' beliefs during a conference, or the political ideology of someone we just met. Smooth social interaction necessitates keeping track of a variety of social data, such as individual attributes and interpersonal relationships and this referred to social working memory where both the thalamus and the insula are involved (Meyer and Lieberman, 2012). This illustrates our result in a sense that deficits in working memory in children, especially during learning-based activities, can result in children experiencing information overload and thus they may act out behaviorally or withdraw socially. In other words, this disrupted dFC between left AI and left thalamus, a finding that can be interpreted as support for the significant differences we found in IQ, working memory and behavioral problems between the two groups.

Importantly, we found a disrupted dFC between the right dAI and frontal middle gyrus. The implication of the frontal middle gyrus in competencies such as literacy, numeracy has been widely discussed by neuroimaging studies (Koyama et al., 2017). However, in line with our findings, Japee et al. (2015) suggested the role of middle frontal gyrus in the reorienting of attention which indicates the individuals' ability to efficiently pick and guide their attention toward behaviorally relevant information in

their environment. Postcentral gyrus, on the other hand, was also involved in our study whereby dFC analysis showed alterations between this region and the right dAI. Intriguingly, Du et al. (2020) found a stronger within-network connectivity in the insula, the thalamus and the postcentral gyrus among other brain regions that constitute the so called punishment network. From a social psychological standpoint, this study strongly supports our results in such a way that people are compelled to comply out of fear of punishment since a minority position is aversive and it can result in hostility, condemnation, rejection from others, or social isolation. People may be encouraged to adhere to the majority position in order to escape such social penalty. Along with our results, the finding that the postcentral gyrus is amongst the potentially relevant brain areas in punishment processing, represents what could be a previously unknown function for this part of the brain and could provide a new target for researchers.

Our findings also showed altered dFC between left PI and right temporal pole. Generally, temporal areas comprising the temporal sulcus were found to be involved in the so called social attention and face perception particularly (Nummenmaa and Calder, 2009). Social attention refers to the social conduct that underpins joint attention, with the goal of coordinating attention allocation with others. These crucial social abilities are thought to be dependent on the development of attention skills such as (1) detecting eye-direction and (2) allocating attention to the same focus of attention as another human being. These cortical areas are critical in the processing of socially relevant cues such gaze following, eye direction, and head orientation (Hopkins et al., 2014). Conflicting with these findings, other literature interestingly suggested that temporal pole activations are more common in sophisticated emotional tasks like theory of mind activities, but are less common in simpler emotional tasks like emotional face perception or gaze perception tasks (Olson et al., 2007).

To sum up, by interpreting our results, we displayed the insula's ability to be both specialized and integrative and to operate both independently and cooperatively. This could explain how the insula functions as a network hub, coordinating input from various cognitive areas and activities. More replicated research on this area is required in the future especially for more specified aspects associated to social dysfunction such as social inattention.

4.1. Limitations

Power considerations may limit our ability to examine the consequences of medications and comorbidity with other diseases, particularly those with inattention impairments like autism, substance dependence, depression, anxiety or learning disorders. Furthermore, the consequences of head motion are in general a constant source of concern in in ADHD and imaging youth. To deal with the issue of motion, we omitted high-motion subjects as an exclusion criteria, and we suggest considering other methods such as regressing realignment parameters and performing individual-level separation techniques such as independent component analysis. Moreover, this research used cross-sectional data and merely served as a surrogate for maturational effects. Extending and refining dynamic connectivity techniques in ADHD will be possible in the future with larger and longitudinal subject populations.

Furthermore, in task-based fMRI trials, nothing is known about how dynamic functional connections are associated to social dysfunctioning. Although prior research has shown that the insula's static functional connections are altered within the salience and default mode networks (Zhao et al., 2017), there have been few studies that have looked at dynamic functional connections underlying social dysfunctioning during task states (Fong et al., 2019). Future research should look into how dynamic connections between insula subdivisions function in task-based fMRI studies.

Also, in our current configuration, functional connectivity evaluations were conducted using standardized insular sub-region seeds. Individual differences in the size and placement of functional areas may have an impact on connectivity maps. Individualized seeds created from a functional parcellation approach will aid future investigations in overcoming these methodological flaws.

Finally, It should be noted that the current dFC method is just one of several approaches for mapping the dynamic functional connections between distinct brain areas. Graph theoretical approaches (Braun et al., 2015), test statistics tracking time course variations (Zalesky et al., 2014), co-activation pattern identification (Chen et al., 2015), and employing time frequency information (Yang et al., 2014) have all held promise in identifying changes in functional connections that static FC methods fail to capture. Future research should look into how these different measurements can help to better understand the dynamic functional links of the insula subdivisions.

5. CONCLUSION

Clinicians can diagnose psychopathology associated to insular dysfunction and stratify differential remedies by translating basic science into clinically useful facts. To improve our treatments, we must connect the pieces of evidence to fully comprehend any brain region, learn how the brain works, and decode clinical manifestations. The regulation of instrumental parts of the brain, such as the insula, is at the heart of daily life's micro-operations. This study provides evidence that the ability of the insula to serve as a subjective experiencing and feeling center that combines emotional, sensory, cognitive, and motor functions is its primary purpose. Therefore, we suggest that the insula is implicated in social dysfunctioning in childern with ADHD, and hence, aberrant insular dFC and provides an essential connectivity marker associated with a diagnosis of ADHD.

DATA AVAILABILITY STATEMENT

The datasets presented in this article are not readily available due to privacy concerns, and access to the data used in this study is restricted. The data has been used only for research purposes and it does not contain any identifiable information. Requests to access the datasets should be directed to HZ, homerzeng@126.com.

ETHICS STATEMENT

The studies involving human participants were reviewed and approved by the Medical Ethics Committee of Shenzhen Children's Hospital. Written informed consent to participate in this study was provided by the participants' legal guardian/next of kin.

AUTHOR CONTRIBUTIONS

AF, WH, and HZ are design of the work. TM, XW, YL, DF, XM, and LZ collected the data and organize the clinical information's. BY, AS, and HZ review the methods and whole manuscript. AF, WH, and DF analyze the data. AF writes the manuscript. Finally, all authors discussed the results and contributed to the final manuscript.

FUNDING

This work was supported by a grant from Shenzhen Medical and Health Project (No. SZSM202011005).

ACKNOWLEDGMENTS

The authors thank all the individuals who served as research participants.

SUPPLEMENTARY MATERIAL

The Supplementary Material for this article can be found online at: https://www.frontiersin.org/articles/10.3389/fnins.2022.890596/full#supplementary-material

REFERENCES

Ahmadi, M., Kazemi, K., Kuc, K., Cybulska-Klosowicz, A., Helfroush, M. S., and Aarabi, A. (2021). Resting state dynamic functional connectivity in children with attention deficit/hyperactivity disorder. *J. Neural Eng.* 18, 0460d0461. doi: 10.1088/1741-2552/ac16b3

Alloway, T. P., and Copello, E. (2013). Working memory: The what, the why, and the how. *Aust. Educ. Dev. Psychol.* 30, 105–118. doi: 10.1017/edp.2013.13

Association, A. P. (2013). "Dsm 5 diagnostic and statistical manual of mental disorders," in *DSM 5 Diagnostic and Statistical Manual of Mental Disorders* (Washington, DC), 947.

Belfi, A. M., Koscik, T. R., and Tranel, D. (2015). Damage to the insula is associated with abnormal interpersonal trust. *Neuropsychologia* 71, 165–172. doi: 10.1016/j.neuropsychologia.2015.04.003

Bickart, K. C., Dickerson, B. C., and Feldman Barrett, L. (2014). The amygdala as a hub in brain networks that support social life. *Neuropsychologia* 63, 235–248. doi: 10.1016/j.neuropsychologia.2014.08.013

Biederman, J., Faraone, S. V., Spencer, T., Wilens, T., Norman, D., Lapey, K. A., et al. (1993). Patterns of psychiatric comorbidity, cognition, and psychosocial functioning in adults with attention deficit hyperactivity disorder. *Am. J. Psychiatry* 150, 1792–1798. doi: 10.1176/ajp.150.12.1792

Braun, U., Schäfer, A., Walter, H., Erk, S., Romanczuk-Seiferth, N., Haddad, L., et al. (2015). Dynamic reconfiguration of frontal brain networks during executive cognition in humans. *Proc. Natl. Acad. Sci. U.S.A.* 112, 11678–11683. doi: 10.1073/pnas.1422487112

Broder, J., and Preston, R. (2011). "Imaging the head and brain," in *Diagnostic Imaging Emerg. Physician* (Saint Louis, MO: Elsevier), 1–45.

Brothers, L. (1990). The neural basis of primate social communication. *Motiv. Emot.* 14, 81–91. doi: 10.1007/BF00991637

Buckholtz, J. W., Asplund, C. L., Dux, P. E., Zald, D. H., Gore, J. C., Jones, O. D., et al. (2008). The neural correlates of third-party punishment. *Neuron* 60, 930–940. doi: 10.1016/j.neuron.2008.10.016

Bud Craig, A. D. (2009). How do you feel–now? The anterior insula and human awareness. *Nat. Rev. Neurosci.* 10, 59–70. doi: 10.1038/nrn2555

Cereda, C., Ghika, J., Maeder, P., and Bogousslavsky, J. (2002). Strokes restricted to the insular cortex. *Neurology* 59, 1950–1955. doi: 10.1212/01.WNL.0000038905.75660.BD

Chee, M. W. L., Soon, C. S., Lee, H. L., and Pallier, C. (2004). Left insula activation: a marker for language attainment in bilinguals. *Proc. Natl. Acad. Sci. U.S.A.* 101, 15265–15270. doi: 10.1073/pnas.0403703101

Chen, J. E., Chang, C., Greicius, M. D., and Glover, G. H. (2015). Introducing co-activation pattern metrics to quantify spontaneous brain network dynamics. *Neuroimage* 111, 476–488. doi: 10.1016/j.neuroimage.2015.01.057

Christiansen, H., Hirsch, O., Drechsler, R., Wanderer, S., Knospe, E.-L., Günther, T., et al. (2016). German validation of the conners 3u+ 00ae rating scales for parents, teachers, and children. *Z. Kinder. Jugendpsychiatr. Psychother.* 44, 139–147. doi: 10.1024/1422-4917/a000408

Cieslik, E. C., Mueller, V. I., Eickhoff, C. R., Langner, R., and Eickhoff, S. B. (2015). Three key regions for supervisory attentional control: Evidence from neuroimaging meta-analyses. *Neurosci. Biobehav. Rev.* 48, 22–34. doi: 10.1016/j.neubiorev.2014.11.003

Conners, K. (2008). *Conners 3rd Edn manual*. New York, NY: Multi-health systems. Inc..[Google Scholar].

Davidson, R., Ekman, P., Saron, C., Senulis, J., and Friesen, W. (1990). Approach-withdrawal and cerebral asymmetry: emotional expression and brain physiology. *J. Pers. Soc. Psychol.* 58, 330–341. doi: 10.1037/0022-3514.58.2.330

Deen, B., Pitskel, N. B., and Pelphrey, K. A. (2011). Three systems of insular functional connectivity identified with cluster analysis. *Cereb. Cortex* 21, 1498–1506. doi: 10.1093/cercor/bhq186

Du, Y., Wang, Y., Yu, M., Tian, X., and Liu, J. (2020). Resting-state functional connectivity of the punishment network associated with conformity. *Front. Behav. Neurosci.* 14, 617402. doi: 10.3389/fnbeh.2020.617402

Duffau, H., Bauchet, L., Lehéricy, S., and Capelle, L. (2001). Functional compensation of the left dominant insula for language. *Neuroreport* 12, 2159–2163. doi: 10.1097/00001756-200107200-00023

Fateh, A. A., Cui, Q., Duan, X., Yang, Y., Chen, Y., Li, D., et al. (2020). Disrupted dynamic functional connectivity in right amygdalar subregions differentiates bipolar disorder from major depressive disorder. *Psychiatry Res.* 304, 111149. doi: 10.1016/j.pscychresns.2020.111149

Fong, A. H. C., Yoo, K., Rosenberg, M. D., Zhang, S., Li, C.-S. R., Scheinost, D., et al. (2019). Dynamic functional connectivity during task performance and rest predicts individual differences in attention across studies. *Neuroimage* 188, 14–25. doi: 10.1016/j.neuroimage.2018.11.057

Frith, C. D., and Frith, U. (2006). The Neural basis of mentalizing. *Neuron* 50, 531–534. doi: 10.1016/j.neuron.2006.05.001

Ghaziri, J., Tucholka, A., Girard, G., Boucher, O., Houde, J.-C., Descoteaux, M., et al. (2018). Subcortical structural connectivity of insular subregions. *Sci. Rep.* 8, 8596. doi: 10.1038/s41598-018-26995-0

Guo, X., Yao, D., Cao, Q., Liu, L., Zhao, Q., Li, H., et al. (2020). Shared and distinct resting functional connectivity in children and adults with attention-deficit/hyperactivity disorder. *Transl. Psychiatry* 10, 65. doi: 10.1038/s41398-020-0740-y

Harrington, A. (1995). "Unfinished business: models of laterality in the nineteenth century," in *Brain Asymmetry*, eds R. J. Davidson and K. Hugdahl (Washington, DC: The MIT Press), 3–27.

Hodgetts, S., Gallagher, P., Stow, D., Ferrier, I. N., and O'Brien, J. T. (2017). The impact and measurement of social dysfunction in late-life depression: an evaluation of current methods with a focus on wearable technology. *Int. J. Geriatr. Psychiatry* 32, 247–255. doi: 10.1002/gps.4632

Hopkins, W. D., Misiura, M., Reamer, L. A., Schaeffer, J. A., Mareno, M. C., and Schapiro, S. J. (2014). Poor receptive joint attention skills are associated with atypical gray matter asymmetry in the posterior superior temporal gyrus of chimpanzees (Pan troglodytes). *Front. Psychol.* 5, 7. doi: 10.3389/fpsyg.2014.00007

Japee, S., Holiday, K., Satyshur, M. D., Mukai, I., and Ungerleider, L. G. (2015). A role of right middle frontal gyrus in reorienting of attention: a case study. *Front. Syst. Neurosci.* 9, 23. doi: 10.3389/fnsys.2015.00023

Jenkinson, M., Bannister, P., Brady, M., and Smith, S. (2002). Improved optimization for the robust and accurate linear registration and motion correction of brain images. *Neuroimage* 17, 825–841. doi: 10.1006/nimg.2002.1132

Kaufman, J., Birmaher, B., Brent, D., Rao, U., Flynn, C., Moreci, P., et al. (1997). schedule for affective disorders and schizophrenia for school-age children-present and lifetime version (K-SADS-PL): initial reliability and validity data. *J. Am. Acad Child Adolesc. Psychiatry* 36, 980–988. doi: 10.1097/00004583-199707000-00021

Koyama, M. S., O'Connor, D., Shehzad, Z., and Milham, M. P. (2017). Differential contributions of the middle frontal gyrus functional connectivity to literacy and numeracy. *Sci. Rep.* 7, 17548. doi: 10.1038/s41598-017-17702-6

Lahey, B. B., Pelham, W. E., Loney, J., Lee, S. S., and Willcutt, E. (2005). Instability of the DSM-IV subtypes of ADHD from preschool through elementary school. *Arch. Gen. Psychiatry* 62, 896. doi: 10.1001/archpsyc.62.8.896

Lee, T. M., and Chan, C. C. (2000). Stroop interference in chinese and english. *J. Clin. Exp. Neuropsychol.* 22, 465–471. doi: 10.1076/1380-3395(200008)22:4;1-0;FT465

Leonardi, N., and Van De Ville, D. (2015). On spurious and real fluctuations of dynamic functional connectivity during rest. *Neuroimage* 104, 430–436. doi: 10.1016/j.neuroimage.2014.09.007

Li, Y., Zhu, Y., Nguchu, B. A., Wang, Y., Wang, H., Qiu, B., et al. (2020). Dynamic functional connectivity reveals abnormal variability and hyper-connected pattern in autism spectrum disorder. *Autism. Res.* 13, 230–243. doi: 10.1002/aur.2212

Liao, W., Li, J., Duan, X., Cui, Q., Chen, H., and Chen, H. (2018). Static and dynamic connectomics differentiate between depressed patients with and without suicidal ideation. *Hum. Brain Mapp.* 39, 4105–4118. doi: 10.1002/hbm.24235

Liao, W., Wu, G. R., Xu, Q., Ji, G. J., Zhang, Z., Zang, Y. F., et al. (2014). DynamicBC: a MATLAB toolbox for dynamic brain connectome analysis. *Brain Connect.* 4, 780–790. doi: 10.1089/brain.2014.0253

Lu, B., Chen, X., Li, L., Shen, Y., Chen, N., Mei, T., et al. (2018). Aberrant dynamics of spontaneous brain activity and its integration in patients with autism spectrum disorder. *Chin. Sci. Bull.* 63, 1452–1463. doi: 10.1360/N972017-01260

Markostamou, I., Rudolf, J., Tsiptsios, I., and Kosmidis, M. H. (2015). Impaired executive functioning after left anterior insular stroke: a case report. *Neurocase* 21, 148–153. doi: 10.1080/13554794.2013.878725

Meyer, M. L., and Lieberman, M. D. (2012). Social working memory: Neurocognitive networks and directions for future research. *Front. Psychol.* 3, 571. doi: 10.3389/fpsyg.2012.00571

Mills, K. L., Bathula, D., Dias, T. G. C., Iyer, S. P., Fenesy, M. C., Musser, E. D., et al. (2012). Altered cortico-striatal-thalamic connectivity in relation to spatial working memory capacity in children with ADHD. *Front. Psychiatry* 3, 2. doi: 10.3389/fpsyt.2012.00002

Nomi, J. S., Farrant, K., Damaraju, E., Rachakonda, S., Calhoun, V. D., and Uddin, L. Q. (2016). Dynamic functional network connectivity reveals unique and overlapping profiles of insula subdivisions. *Hum. Brain Mapp.* 37, 1770–1787. doi: 10.1002/hbm.23135

Nomi, J. S., Schettini, E., Broce, I., Dick, A. S., and Uddin, L. Q. (2018). Structural connections of functionally defined human insular subdivisions. *Cereb. Cortex* 28, 3445–3456. doi: 10.1093/cercor/bhx211

Nummenmaa, L., and Calder, A. J. (2009). Neural mechanisms of social attention. *Trends Cogn. Sci.* 13, 135–143. doi: 10.1016/j.tics.2008.12.006

Olson, I. R., Plotzker, A., and Ezzyat, Y. (2007). The Enigmatic temporal pole: a review of findings on social and emotional processing. *Brain* 130, 1718–1731. doi: 10.1093/brain/awm052

Patil, A. U., Ghate, S., Madathil, D., Tzeng, O. J. L., Huang, H.-W., and Huang, C.-M. (2021). Static and dynamic functional connectivity supports the configuration of brain networks associated with creative cognition. *Sci. Rep.* 11, 165. doi: 10.1038/s41598-020-80293-2

Peelen, M. V., Atkinson, A. P., and Vuilleumier, P. (2010). Supramodal representations of perceived emotions in the human bbrain. *J. Neurosci.*, 30, 10127–10134. doi: 10.1523/JNEUROSCI.2161-10.2010

Penfield, W., and Faulk, M. E. (1955). The insula; further observations on its function. *Brain* 78, 445–470. doi: 10.1093/brain/78.4.445

Rogers-Carter, M. M., and Christianson, J. P. (2019). An insular view of the social decision-making network. *Neurosci. Biobehav. Rev.* 103, 119–132. doi: 10.1016/j.neubiorev.2019.06.005

Rohrer-Baumgartner, N., Zeiner, P., Egeland, J., Gustavson, K., Skogan, A., Reichborn-Kjennerud, T., et al. (2014). Does IQ influence associations between ADHD symptoms and other cognitive functions in young preschoolers? *Behav Brai Funct.* 10, 16. doi: 10.1186/1744-9081-10-16

Rubia, K., Alegria, A., and Brinson, H. (2014). Imaging the ADHD brain: disorder-specificity, medication effects and clinical translation. *Expert. Rev. Neurother.* 14, 519–538. doi: 10.1586/14737175.2014.907526

Rubia, K., Criaud, M., Wulff, M., Alegria, A., Brinson, H., Barker, G., et al. (2019). Functional connectivity changes associated with fMRI neurofeedback of right inferior frontal cortex in adolescents with ADHD. *Neuroimage* 188, 43–58. doi: 10.1016/j.neuroimage.2018.11.055

Sayal, K., Prasad, V., Daley, D., Ford, T., and Coghill, D. (2018). ADHD in children and young people: prevalence, care pathways, and service provision. *Lancet Psychiatry* 5, 175–186. doi: 10.1016/S2215-0366(17)30167-0

Scheinost, D., Stoica, T., Saksa, J., Papademetris, X., Constable, R. T., Pittenger, C., et al. (2013). Orbitofrontal cortex neurofeedback produces lasting changes in contamination anxiety and resting-state connectivity. *Transl. Psychiatry* 3, e250-e250. doi: 10.1038/tp.2013.24

Shappell, H. M., Duffy, K. A., Rosch, K. S., Pekar, J. J., Mostofsky, S. H., Lindquist, M. A., et al. (2021). Children with attention-deficit/hyperactivity disorder spend more time in hyperconnected network states and less time in segregated network states as revealed by dynamic connectivity analysis. *Neuroimage* 229, 117753. doi: 10.1016/j.neuroimage.2021.117753

Sonuga-Barke, E. J., and Castellanos, F. X. (2007). Spontaneous attentional fluctuations in impaired states and pathological conditions: a neurobiological hypothesis. *Neurosci. Biobehav. Rev.* 31, 977–986. doi: 10.1016/j.neubiorev.2007.02.005

Sun, Y., Lan, Z., Xue, S.-W., Zhao, L., Xiao, Y., Kuai, C., et al. (2021). Brain state-dependent dynamic functional connectivity patterns in attention-deficit/hyperactivity disorder. *J. Psychiatr. Res.* 138, 569–575. doi: 10.1016/j.jpsychires.2021.05.010

Thomas, R., Sanders, S., Doust, J., Beller, E., and Glasziou, P. (2015). Prevalence of attention-deficit/hyperactivity disorder: a systematic review and meta-analysis. *Pediatrics* 135, e994-e1001. doi: 10.1542/peds.2014-3482

Touroutoglou, A., Hollenbeck, M., Dickerson, B. C., and Feldman Barrett, L. (2012). Dissociable large-scale networks anchored in the right anterior insula subserve affective experience and attention. *Neuroimage* 60, 1947. doi: 10.1016/j.neuroimage.2012.02.012

Usami, M. (2016). Functional consequences of attention-deficit hyperactivity disorder on children and their families. *Psychiatry Clin. Neurosci.* 70, 303–317. doi: 10.1111/pcn.12393

Varjačić, A., Mantini, D., Levenstein, J., Slavkova, E. D., Demeyere, N., and Gillebert, C. R. (2018). The role of left insula in executive set-switching: lesion evidence from an acute stroke cohort. *Cortex* 107, 92–101. doi: 10.1016/j.cortex.2017.11.009

Wang, M., Hu, Z., Liu, L., Li, H., Qian, Q., and Niu, H. (2020). Disrupted functional brain connectivity networks in children with attention-deficit/hyperactivity disorder: evidence from resting-state functional near-infrared spectroscopy. *Neurophotonics* 7, 1. doi: 10.1117/1.NPh.7.1.015012

Yan, C.-G., Wang, X.-D., Zuo, X.-N., and Zang, Y.-F. (2016). Dpabi: data processing analysis for (resting-state) brain imaging. *Neuroinformatics* 14, 339–351. doi: 10.1007/s12021-016-9299-4

Yang, Y., Yang, B., Zhang, L., Peng, G., and Fang, D. (2021). Dynamic functional connectivity reveals abnormal variability in the amygdala subregions of children with attention-deficit/hyperactivity disorder. *Front. Neurosci.* 15, 648143. doi: 10.3389/fnins.2021.648143

Yang, Z., Craddock, R. C., Margulies, D. S., Yan, C.-G., and Milham, M. P. (2014). Common intrinsic connectivity states among posteromedial cortex

subdivisions: Insights from analysis of temporal dynamics. *Neuroimage* 93, 124–137. doi: 10.1016/j.neuroimage.2014.02.014

Zalesky, A., Fornito, A., Cocchi, L., Gollo, L. L., and Breakspear, M. (2014). Time-resolved resting-state brain networks. *Proc. Natl. Acad. Sci. U.S.A.* 111, 10341–10346. doi: 10.1073/pnas.1400181111

Zhao, Q., Li, H., Yu, X., Huang, F., Wang, Y., Liu, L., et al. (2017). Abnormal resting-state functional connectivity of insular subregions and disrupted correlation with working memory in adults with attention deficit/hyperactivity disorder. *Front. Psychiatry* 8, 200. doi: 10.3389/fpsyt.2017.00200

Conflict of Interest: The authors declare that the research was conducted in the absence of any commercial or financial relationships that could be construed as a potential conflict of interest.

Publisher's Note: All claims expressed in this article are solely those of the authors and do not necessarily represent those of their affiliated organizations, or those of the publisher, the editors and the reviewers. Any product that may be evaluated in this article, or claim that may be made by its manufacturer, is not guaranteed or endorsed by the publisher.

frontiers | Frontiers in Neuroscience

ORIGINAL RESEARCH
published: 10 June 2022
doi: 10.3389/fnins.2022.919272

Reduced Gray Matter Volume in Orbitofrontal Cortex Across Schizophrenia, Major Depressive Disorder, and Bipolar Disorder: A Comparative Imaging Study

Yongfeng Yang[1,2,3†], Xue Li[1,2,3†], Yue Cui[4,5,6], Kang Liu[1,2,3], Haoyang Qu[7], Yanli Lu[1], Wenqiang Li[1,2,3], Luwen Zhang[1,2,3], Yan Zhang[1,2,3], Jinggui Song[1,2,3] and Luxian Lv[1,2,3]**

[1] Department of Psychiatry, Henan Mental Hospital, Second Affiliated Hospital of Xinxiang Medical University, Xinxiang, China, [2] Henan Key Lab of Biological Psychiatry, Xinxiang Medical University, Xinxiang, China, [3] International Joint Research Laboratory for Psychiatry and Neuroscience of Henan, Xinxiang, China, [4] Brainnetome Center and Institute of Automation, Chinese Academy of Sciences, Beijing, China, [5] National Laboratory of Pattern Recognition, Institute of Automation, Chinese Academy of Sciences, Beijing, China, [6] University of Chinese Academy of Sciences, Beijing, China, [7] Department of Psychiatry, The Second Clinic College of Xinxiang Medical University, Xinxiang, China

OPEN ACCESS

Edited by:
Wenbin Guo,
Central South University, China

Reviewed by:
Jiaojian Wang,
University of Electronic Science and Technology of China, China
Bing Liu,
Beijing Normal University, China

***Correspondence:**
Jinggui Song
songjg62@126.com
Luxian Lv
lvx928@126.com

† These authors have contributed equally to this work and share first authorship

Specialty section:
This article was submitted to Brain Imaging Methods, a section of the journal Frontiers in Neuroscience

Received: *13 April 2022*
Accepted: *02 May 2022*
Published: *10 June 2022*

Citation:
Yang Y, Li X, Cui Y, Liu K, Qu H, Lu Y, Li W, Zhang L, Zhang Y, Song J and Lv L (2022) Reduced Gray Matter Volume in Orbitofrontal Cortex Across Schizophrenia, Major Depressive Disorder, and Bipolar Disorder: A Comparative Imaging Study. Front. Neurosci. 16:919272. doi: 10.3389/fnins.2022.919272

Schizophrenia (SZ), major depressive disorder (MDD), and bipolar disorder (BD) are severe psychiatric disorders and share common characteristics not only in clinical symptoms but also in neuroimaging. The purpose of this study was to examine common and specific neuroanatomical features in individuals with these three psychiatric conditions. In this study, 70 patients with SZ, 85 patients with MDD, 42 patients with BD, and 95 healthy controls (HCs) were recruited. Voxel-based morphometry (VBM) analysis was used to explore brain imaging characteristics. Psychopathology was assessed using the Beck Depression Inventory (BDI), the Beck Anxiety Inventory (BAI), the Young Mania Rating Scale (YMRS), and the Positive and Negative Syndrome Scale (PANSS). Cognition was assessed using the digit symbol substitution test (DSST), forward-digital span (DS), backward-DS, and semantic fluency. Common reduced gray matter volume (GMV) in the orbitofrontal cortex (OFC) region was found across the SZ, MDD, and BD. Specific reduced GMV of brain regions was also found. For patients with SZ, we found reduced GMV in the frontal lobe, temporal pole, occipital lobe, thalamus, hippocampus, and cerebellum. For patients with MDD, we found reduced GMV in the frontal and temporal lobes, insular cortex, and occipital regions. Patients with BD had reduced GMV in the medial OFC, inferior temporal and fusiform regions, insular cortex, hippocampus, and cerebellum. Furthermore, the OFC GMV was correlated with processing speed as assessed with the DSST across four groups ($r = 0.17$, $p = 0.004$) and correlated with the PANSS positive symptoms sub-score in patients with SZ ($r = -0.27$, $p = 0.026$). In conclusion, common OFC alterations in SZ, MDD, and BD provided evidence that this region dysregulation may play a critical role in the pathophysiology of these three psychiatric disorders.

Keywords: schizophrenia, major depressive disorder, bipolar disorder, gray matter volume (GMV), psychopathology

INTRODUCTION

Schizophrenia (SZ), major depressive disorder (MDD), and bipolar disorder (BD) are highly complex psychiatric disorders for which the diagnosis primarily depends on the patient's clinical symptoms and the psychiatrist's experiences. The literature has shown that these psychiatric disorders share some common genetic vulnerability and clinical symptoms (Wang et al., 2017; Cross-Disorder Group of the Psychiatric Genomics Consortium, 2019).

Previous research using voxel-based morphometry (VBM) found that decreased gray matter (GM) volume in the right inferior frontal gyrus was a common abnormality feature in both MDD and BD (Cai et al., 2015). Atrophy or decreased GM volume (GMV) was found in the subgenual anterior cingulate cortex (ACC) in MDD and in the subcallosal ACC (Niida et al., 2014, 2019) and bilateral fronto-insular cortex (Bora et al., 2012) in BD. Further analysis revealed that patients with both MDD and BD showed decreased GMV in the bilateral insula cortex (Wise et al., 2016), left ACC, and right hippocampus (Chen et al., 2018). Patients with SZ showed some evidence of GMV reduction in the prefrontal and temporal cortex (Yuksel et al., 2012; Nenadic et al., 2015; Knochel et al., 2016), bilateral insular cortex (Niida et al., 2019), thalamus, hippocampus, striatum, and cerebellum (Watson et al., 2012; Nenadic et al., 2015). In addition, it was found that patients with both SZ and BD had some common GMV reduction in the superior temporal gyrus (STG) and inferior parietal lobule (Cui et al., 2011).

A meta-analysis found GM loss in the bilateral insula and dorsal ACC across SZ, BD, depression, addiction, anxiety, and obsessive-compulsive disorder (Goodkind et al., 2015). Chang et al. (2018) reported that the SZ, MDD, and BD shared reduced GMV in 87.9% of the whole brain regional volume. In addition, previous studies found functional abnormalities of the insula in MDD (Wang et al., 2018; Wang J. et al., 2020; Wang L. et al., 2020).

However, the common and specific GMV studies of SZ, MDD, and BD are scarce and inconsistent. Therefore, in the present study, we hypothesize that SZ, MDD, and BD may have common specific characteristics that can be explored by brain structure imaging. Further, this study may provide objective image markers for the diagnosis and differential diagnosis of these three psychiatric disorders. Thus, we used VBM analysis to explore possible common and specific changes in neuroimaging features in patients with SZ, MDD, and BD.

MATERIALS AND METHODS

Participants

The participants included four groups of subjects: SZ ($n = 70$), MDD ($n = 85$), BD ($n = 42$), and healthy controls (HCs, $n = 95$). The study was conducted between March 2013 and October 2017 at the Second Affiliated Hospital of Xinxiang Medical University, China. The study was approved by the Ethics Committee of the Second Affiliated Hospital of Xinxiang Medical University. All participants provided written informed consent. All participants were between 18 and 55 years old, Han Chinese in origin, and right-handed. Patients with SZ, MDD, and BD were independently diagnosed by two experienced psychiatrists using the Structured Clinical Interview for Diagnostic and Statistical Manual of Mental Disorders (DSM)-IV Axis I Disorders. Exclusion criteria were the following: heart, kidney, or liver disease; other mental disorders; and the presence of implanted metal frames or electronic devices preventing Magnetic Resonance Imaging (MRI) scanning. Symptoms were measured using the Beck Anxiety Inventory (BAI) (Beck et al., 1988) and Beck Depression Inventory (BDI) (Beck et al., 1961) for patients with MDD, the BDI, BAI, and Young Mania Rating Scale (YMRS) (Young et al., 1978) for patients with BD, and the Positive and Negative Syndrome Scale (PANSS) (Kay et al., 1987) for patients with SZ. Patients with BD were further diagnosed with depression ($n = 15$), mania ($n = 25$), and stable mood ($n = 2$). Cognitive function tests were carried out using the digit symbol substitution test (DSST), forward-digital span (DS), backward-DS, and semantic fluency. None of the HCs had a personal history of psychotic illness or a family history of psychosis in their first-, second-, or third-degree relatives. HCs were excluded if one of the following were present: (1) history of head injury, (2) the presence of a major and unstable physical illness, (3) heart, kidney, or liver disease, (4) pregnant or breast-feeding women, or planning pregnancy, and (5) the presence of implanted metal frames or electronic devices preventing MRI scanning.

Data Acquisition and Pre-processing

All participants underwent T1-weighted imaging using a 3.0 Tesla Siemens Scanner (Siemens, Verio, Germany). Acquisition parameters for T1-weighted scans were as follows: repetition time = 2,530 ms, echo time = 2.43 ms, inversion time = 1,100 ms, flip angle = 7°, matrix size = 256 × 256 × 192, and voxel size = 1 × 1 × 1 mm. Foam pads and earplugs were used to reduce head motion and scanner noise.

All T1-weighted images were processed using Statistical Parametric Mapping (SPM12, Wellcome Department of Imaging Neuroscience, London, United Kingdom)[1] and the Computational Anatomy Toolbox (CAT12). Briefly, the images were bias-corrected and segmented into different tissues, such as GM, white matter, and cerebrospinal fluid images. The tissue images were then spatially normalized and resampled to a resolution of 1.5 × 1.5 × 1.5 mm^3. To preserve regional volumetric information, the images were modulated by the Jacobian determinants of the deformations during the warping. Finally, 6-mm full width at half maximum Gaussian kernel smoothing was performed to generate the voxel-based GMVs for each subject for the subsequent statistical analysis.

Statistical Analysis

The demographic characteristics of the groups were compared using analysis of variance and χ^2-tests. MRI data were analyzed using the CAT12. Group differences in regional GMVs were investigated by comparing the pre-processed GM images from

[1] http://www.fil.ion.ucl.ac.uk/spm/

each pair of groups using a general linear model with age, gender, and total intracranial volume (TIV) as covariates. We performed AlphaSim correction with a threshold of $p < 0.01$ for multiple comparisons. The correction was achieved with a voxelwise threshold of $p < 0.005$ and a minimum cluster extent of 298 voxels. Identification of overlapping regions across mental disorders was performed on the basis of regions showing consistent GM changes after multiple corrections. No statistical method was used to identify overlapping regions. Pearson's correlations were used to assess (i) relationships between GMVs in overlapping regions and digit symbol scores across all groups and (ii) relationships between GMVs and symptom severity as measured by BDI, BAI, and PANSS scales in MDD, BD, and SZ. Partial correlation analysis was performed using age, sex, TIV, and the group as confounding variables.

RESULTS

Sociodemographic and Clinical Characteristics

Sociodemographic and clinical data are presented in **Table 1**. No statistically significant differences in age or sex were noted between each pair of two groups except that patients with SZ were younger than patients with BD (SZ vs. BD, $t = -3.35$, $p = 0.001$) and patients with MDD (SZ vs. MDD, $t = -3.27$, $p = 0.001$). Significant differences were also observed in the duration of illness, age of onset, and medication status across patient groups.

Voxel-Based Morphometry Comparisons

Patients with SZ, MDD, and BD had significantly reduced regional GMVs when compared to HCs. The common GMV was reduced in the orbitofrontal cortex (OFC) region of patients with SZ, MDD, and BD. Specifically, patients with SZ had reduced GM in the frontal lobe, temporal lobe, occipital lobe, thalamus, hippocampus, and cerebellum. For patients with MDD, the differences were most pronounced in the frontal and temporal lobes, insular cortex, and occipital regions. For patients with BD, GM deficits were found in the medial OFC, inferior temporal and fusiform regions, insular cortex, hippocampus, and cerebellum (**Figure 1** and **Supplementary Table 1**). When compared TIV among three patient groups, we found the significant difference between SZ and BD, ($t = -2.184$, $p = 0.029$), BD and DP ($t = 2.009$, $p = 0.047$), and the TIV, there was no significant difference between SZ and DP ($t = 0.143$, $p = 0.886$).

Orbitofrontal cortex GM sizes were correlated with processing speed as assessed with the DSST across four groups and PANSS positive scales only in patients with SZ ($r = 0.17$ and -0.27, both $p < 0.03$; **Figure 1**). In addition, patients with MDD had significantly smaller GM in the superior and middle frontal gyri (SFG/MFG; **Figure 2**). However, GM sizes in SFG/MFG were not significantly correlated with BAI in patients with MDD and BD ($r = -0.10$, $p = 0.360$), or in MDD ($r = 0.11$, $p = 0.301$) or BD ($r = -0.13$, $p = 0.419$) patients only. We also found reduced GMVs in the middle cingulum and middle frontal gyrus in the BD depression subgroup when compared with the BD mania subgroup (**Figure 3**).

Further, we also found common changes in GM size in the insular cortex in MDD and BD, in the frontal lobe, temporal pole, and occipital lobe in MDD and SZ, and in the hippocampus and cerebellum in BD and SZ.

DISCUSSION

In this study, we revealed a transdiagnostic feature of GMV decrease in the OFC across SZ, MDD, and BD. Meanwhile, the specific GMV was decreased in the frontal and temporal lobes, insular cortex, and occipital regions in MDD, in the medial OFC, inferior temporal and fusiform regions, insular cortex, hippocampus, and cerebellum in BD, and in the frontal lobe, temporal pole, occipital lobe, thalamus, hippocampus, and cerebellum in SZ. The present study further provides evidence for the common and specific GMV loss in SZ, MDD, and BD.

The present study is a part of the systematic exploration of the common and specific MRI features of SZ, MDD, and BD in the Chinese population. Our published studies revealed a decreased functional connectivity in the insula (Yang et al., 2019) and reduced white matter integrity in the body and genu of the corpus callosum and corona radiata across these three psychiatric disorders (Cui et al., 2020). The corpus callosum and corona radiata are related to the prefrontal cortex (PFC) and ACC (Goodkind et al., 2015; Dong et al., 2017), and the corona radiata is also related to the pathway of the anterior insula (Nomi et al., 2018). The previous meta-analysis reported common GM loss in the dorsal ACC, right insula, and left insula across six psychiatric disorders that include SZ, MDD, and BD (Goodkind et al., 2015). Meanwhile, a study in the Chinese population found that common GM was decreased in the OFC, dorsolateral PFC, angular gyri, cingulate gyri, parahippocampal gyri, and temporal pole (Chang et al., 2018). Recent meta-analysis found that the decreased GM in the right cerebellum might be a common brain structural abnormality across SZ, BD, and MDD, and the regional GM abnormalities in thalamus, neocortex, and striatum appear to be disorder-specific (Zhang et al., 2020). Interestingly, our finding suggested that the GMV decreased in the OFC, which is part of the PFC, is a common feature of the three psychiatric disorders. Therefore, our finding is consistent with a previous study (Chang et al., 2018) and further supported by the loss of GMV in psychiatric disorders (Goodkind et al., 2015; Chang et al., 2018). Therefore, our findings indicated that OFC impairment may be correlated with brain function in MDD, SZ, and BD. Previous functional connectivity studies have reported that the default mode network (DMN) plays an important role in psychiatric disorders (Meda et al., 2014; Cheng et al., 2022; Pang et al., 2022). Since the OFC is located in the DMN, further research needs to explore the functional abnormalities of the OFC in these three psychiatric disorders.

Orbitofrontal cortex, one of the three main regions of the PFC, plays a role in affective and cognitive processes, such as the integration of multiple sensory information (Forbes and Grafman, 2010). The OFC has been implicated in MDD (Bremner et al., 2002), BD (Konarski et al., 2008), and SZ (Haijma et al., 2013) in previous studies. A previous study found decreased

TABLE 1 | Demographic characteristics of the participants.

	MDD (n = 85)	BD (n = 42)	SZ (n = 70)	HC (n = 95)	F/χ^2-values	P-values
Male (%)	40.0	54.8	44.3	49.5	1.09	0.350
Age (years)	32.44 (8.79)	32.88 (8.79)	28.40 (4.92)[a]	30.21 (6.85)	5.15	0.002*
Education (years)	11.5 (3.60)(n = 84)	10.5 (3.83)(n = 40)	11.48 (2.76)(n = 64)	13.80 (2.88)(n = 94)	13.89	<0.001
Age of onset (years)	29.18 (9.32)(n = 84)	26.25 (8.88)(n = 40)	24.54 (4.86)(n = 64)	N/A	6.61	0.002
Medication (Yes/No)	66/19	37/5	44/26	N/A	9.55	0.008
Antipsychotics (Yes)	5	24	44	N/A	62.66	<0.001
Antidepressants (Yes)	64	15	0	N/A	91.03	<0.001
Mood stabilizer	1	24	0	N/A	95.25	<0.001
Duration of illness (months)	40.81 (55.87)(n = 84)	77.10 (77.16)(n = 40)	43.26 (43.28)(n = 64)	N/A	5.89	0.003
Digit symbol	48.56 (13.40)(n = 81)	47.53 (15.25)(n = 40)	38.18 (10.47)(n = 57)	62.31 (11.92)(n = 94)	11.6	<0.001
BDI	18.60 (7.66)(n = 68)	9.95 (11.71)(n = 40)	N/A	N/A	21.55	<0.001
BAI	42.83 (11.41)(n = 48)	31.85 (13.75)(n = 39)	N/A	N/A	16.59	<0.001
PANSS total	N/A	N/A	78.5 (18.15)	N/A	N/A	N/A
PANSS positive	N/A	N/A	22.74 (3.75)	N/A	N/A	N/A
PANSS negative	N/A	N/A	19.86 (5.29)	N/A	N/A	N/A

Values are mean (SD) unless otherwise indicated.
BAI, Beck Anxiety Inventory; BD, bipolar disorder; BDI, Beck Depression Inventory; HC, healthy control; MDD, major depressive disorder; N/A, not applicable; PANSS, Positive and Negative Syndrome Scale; SZ, schizophrenia.
**SZ had significantly younger age in years than BD and MDD. No significant differences were found in age or gender between three mental disorders (MDD, BD, and SZ) and HC.*

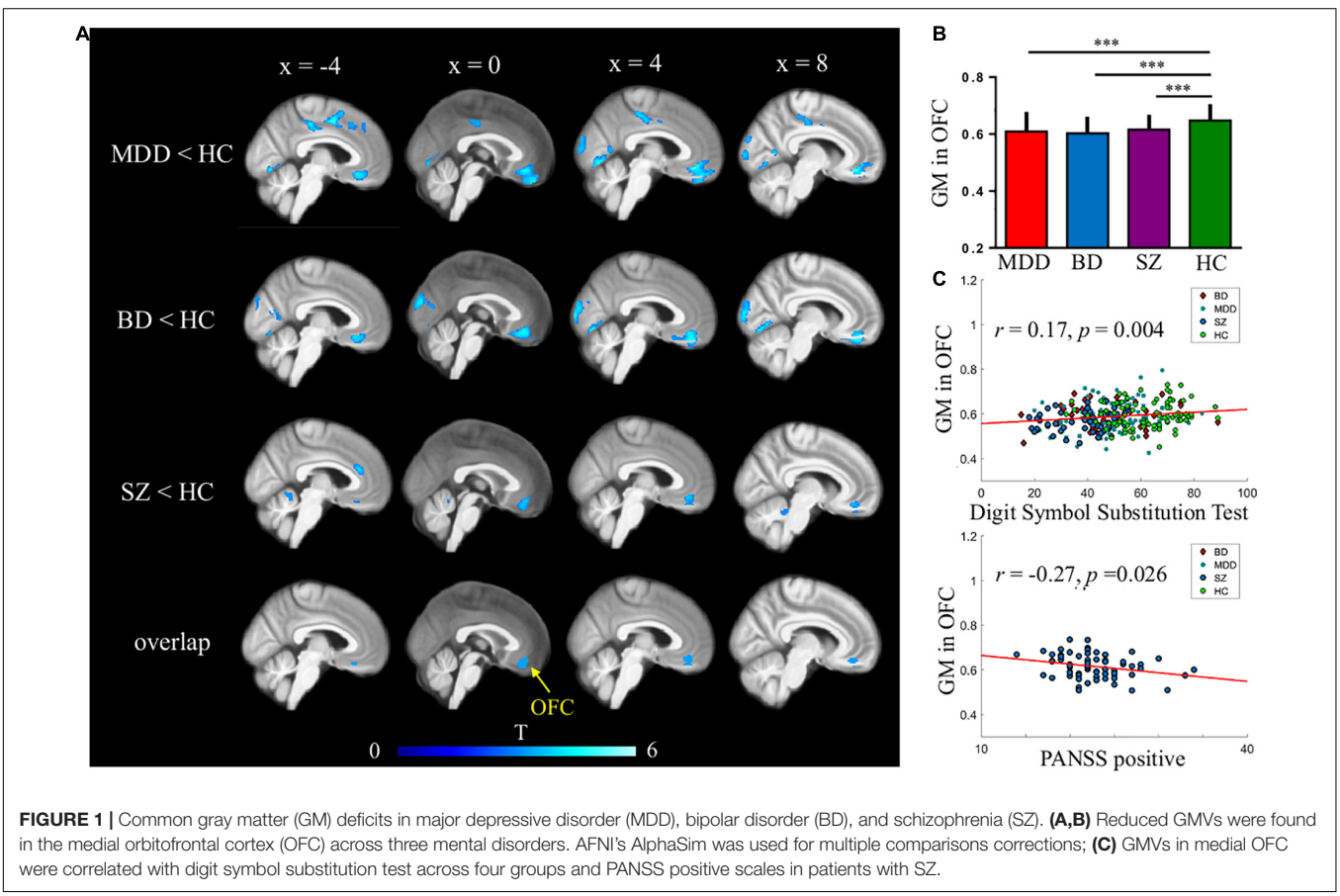

FIGURE 1 | Common gray matter (GM) deficits in major depressive disorder (MDD), bipolar disorder (BD), and schizophrenia (SZ). **(A,B)** Reduced GMVs were found in the medial orbitofrontal cortex (OFC) across three mental disorders. AFNI's AlphaSim was used for multiple comparisons corrections; **(C)** GMVs in medial OFC were correlated with digit symbol substitution test across four groups and PANSS positive scales in patients with SZ.

GMVs in the OFC, dorsolateral PFC, insula, temporal pole, cingulate gyri, parahippocampal gyri, and angular gyri across SZ, MDD, and BD (Chang et al., 2018). The present study is consistent with this study, as we found a decreased GMV of the OFC in these three psychiatric disorders. In the present study, 65.9% of all patients had a recurrent episode and had a long illness

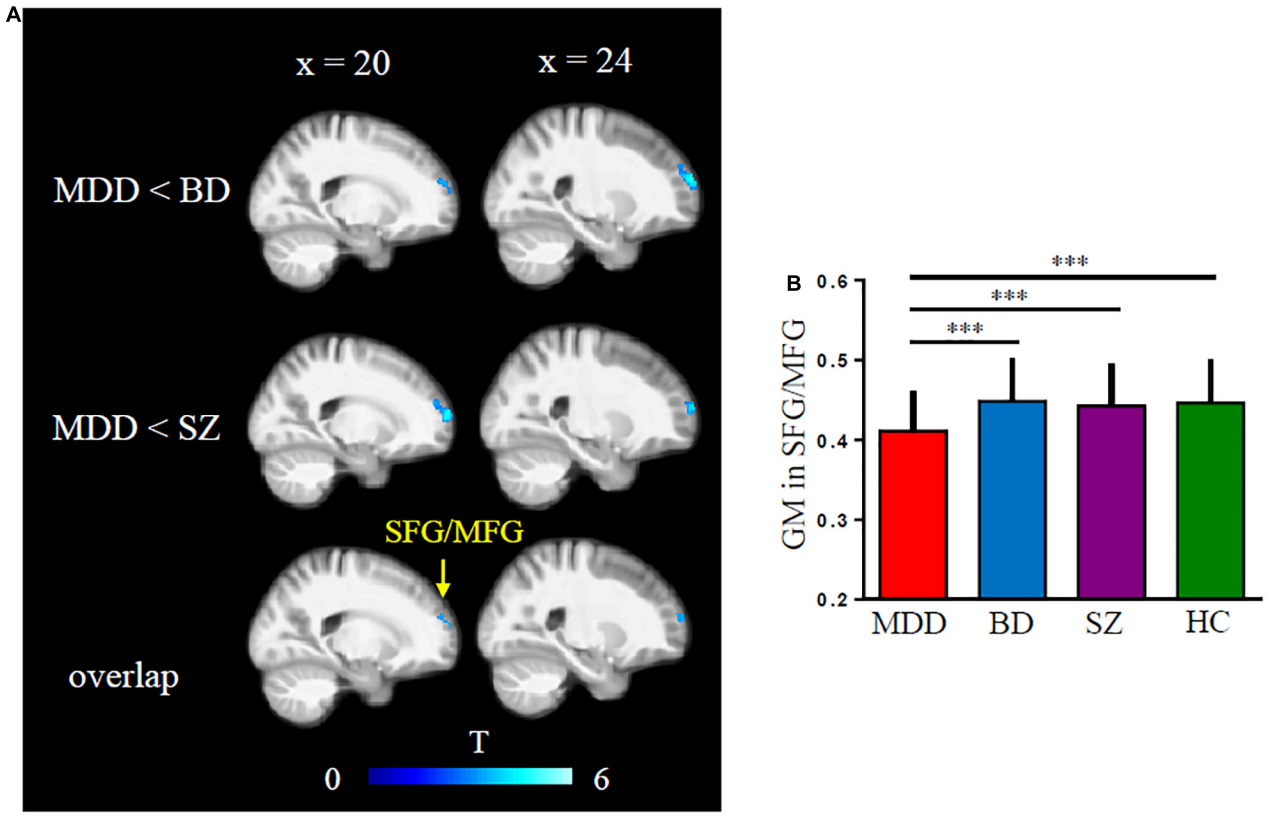

FIGURE 2 | Major depressive disorder (MDD) showed reduced gray matter (GM) volumes in superior and middle frontal gyri (SFG/MFG) compared with bipolar disorder (BD) and schizophrenia (SZ) patients **(A,B)**.

duration, whereas, in previous studies, 72.9% (Chang et al., 2018) and 67.8% (Xia et al., 2018) of all patients had the first episode and short illness duration. Meanwhile, the common genetic variations are 15% for SZ and BD, 10% for MDD and BD, and 9% for MDD and SZ (Lee et al., 2013). This may explain why our findings with respect to morphology in these three psychiatric disorders were different from those of a previous study on six psychiatric disorders (Goodkind et al., 2015).

Previous studies have confirmed that the insula plays an important role in patients with depression or BD, both from structural (Wise et al., 2016) and functional imaging (Wang et al., 2019), and may be a potential biomarker. In the present study, we found a common decrease in GMV in the insular in MDD and BD. This was in line with previous studies (Bora et al., 2012; Wise et al., 2016). Further, common decreases in GMV between SZ and BD were observed in the hippocampus and cerebellum, which is inconsistent with the common decreased GMV in the STG and inferior parietal lobule (Cui et al., 2011). Meanwhile, our study provided further evidence that the GMV was decreased in the frontal lobe, temporal pole, and occipital lobe in MDD and SZ.

Specifically, we revealed GM deficits in the frontal and temporal lobes, insular cortex, and occipital regions in MDD. These results are partly supported by a previous study, which reported that the GMV was reduced in the lateral temporal and occipital cortices in MDD (Frodl et al., 2008). One study also found that GM decreases in the right precentral gyrus in BD (Chang et al., 2018). Further, our study is in line with the founding of GM deficits in the bilateral insular cortex in BD (Wise et al., 2016). Meanwhile, specific GM deficits in the temporal pole (Colibazzi et al., 2017), thalamus (Anticevic et al., 2015; Zhang et al., 2020), PFC, and hippocampus (Ganzola et al., 2014) in SZ were also in consistence with our findings. Therefore, those specific reduced GMV brain regions may provide objective biological markers for image diagnosis and discriminate SZ, MDD, and BD.

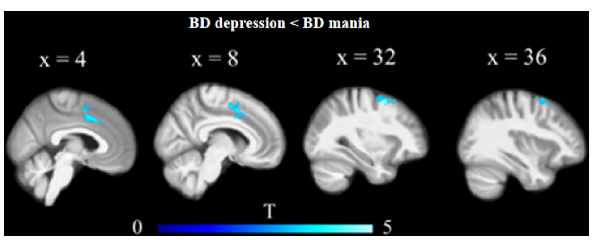

FIGURE 3 | Reduced GM volumes in the middle cingulum and middle frontal gyrus in the BD depression subgroup when compared with the BD mania subgroup.

A recent study found the associations between psychopathological syndromes and regional GMV across affective and psychotic disorders. Especially found positive formal thought disorder was correlated with the GMV of bilateral OFC (Stein et al., 2021). There was also a follow-up study in SZ that showed the important role of OFC in SZ. They found that greater pre-treatment OFC GMV was associated with greater post-treatment improvement in positive symptoms, particularly in hallucinations and persecutory beliefs (Premkumar et al., 2015). Therefore, our result was obtained at baseline MRI and also supports that the decreased GMV of OFC was correlated with positive symptoms in SZ. Executive function is related to the fronto-cingulo-parietal network (van Amelsvoort and Hernaus, 2016) and includes basic cognitive processes, such as attentional control, working memory, cognitive inhibition, and flexibility. It is impaired in multiple disorders, such as MDD, BD, and SZ (Hosenbocus and Chahal, 2012; Etkin et al., 2013). The OFC is related to the visual cortex, and decreased GM of the visual cortex is significantly associated with poor executive function (Goodkind et al., 2015). In the present study, we found that the OFC was correlated with processing speed as assessed with the DSST. Meanwhile, processing speed is considered as a part of cognitive processes. Therefore, our study suggested that OFC impairment may be related to executive function deficits.

Our study had some limitations. Firstly, compared with a previous study (Chang et al., 2018), the sample size of our BD patient group was relatively small. Future studies of the Chinese population will need to include multi-site samples to enlarge the sample sizes. Secondly, factors, such as duration of illness and age of onset, are difficult to control and match between the three groups. Previous research (Chang et al., 2018) was also difficult to achieve such an ideal state and reported that there had significant differences in duration (months), and the first episode (years) among SZ, MDD, and BD. Finally, most patients in the present study were treated with medication. Of 197 patients, 147 (74.6%) used at least one type of medication, such as antipsychotics, antidepressants, and mood stabilizers. The effects of the medication may have influenced the results. However, a recent study reported no significant difference in SZ, MDD, and BD between patients with and without medication (Chang et al., 2018). Moreover, data on medication-free patients are not easily available. Future studies will be needed to analyze the effects of medication.

CONCLUSION

In conclusion, our findings of common OFC alterations in SZ, MDD, and BD provided evidence that this region dysregulation may play a critical role in the pathophysiology of these three psychiatric disorders. In addition, our findings indicated that based on reduced GMV in specific regions, we were able to discriminate MDD from SZ and BD, SZ from MDD and BD, or BD from MDD and SZ. Future studies will need to make a verification for these findings and evaluate the common and specific connection features at the brain network level and in different ethnic groups.

DATA AVAILABILITY STATEMENT

The datasets presented in this article are not readily available because the datasets generated and/or analyzed during the current study are not publicly available due to privacy. Requests to access the datasets should be directed to corresponding authors.

ETHICS STATEMENT

The studies involving human participants were reviewed and approved by the Ethics Committee of the Second Affiliated Hospital of Xinxiang Medical University. The patients/participants provided their written informed consent to participate in this study. Written informed consent was obtained from the individual(s) for the publication of any potentially identifiable images or data included in this article.

AUTHOR CONTRIBUTIONS

LL and JS designed the study protocol. YY, YL, and YZ conducted sample selection and data management. YY, WL, KL, and YC managed the literature searches and analysis. YY, YC, LZ, and XL wrote the first draft of the manuscript. All authors contributed to and have approved the final manuscript.

FUNDING

This work was supported in part by the National Natural Science Foundation of China (81971252 to LL and U1904130 and 82171498 to WL), Science and Technology Research Project of Henan Province (212102310589 to YY), Open Program of Henan Key Laboratory of Biological Psychiatry (ZDSYS2018002 to YC and ZDSYS2019002 to YY), Medical Science and Technology Research Project of Henan Province (LHGJ20200528 to LZ), Postgraduate Education Reform and Quality Improvement Project of Henan Province (YJS2021JD12), and College Students' Innovative Entrepreneurial Training Plan Program (S202010472033).

ACKNOWLEDGMENTS

We thank the patient, their families, and the healthy volunteers for their participation and the physicians who collect the MRI and clinical data in the Second Affiliated Hospital of Xinxiang Medical University. We thank the International Science Editing (http://www.internationalscienceediting.com) for editing our manuscript.

SUPPLEMENTARY MATERIAL

The Supplementary Material for this article can be found online at: https://www.frontiersin.org/articles/10.3389/fnins.2022.919272/full#supplementary-material

REFERENCES

Anticevic, A., Haut, K., Murray, J. D., Repovs, G., Yang, G. J., Diehl, C., et al. (2015). Association of thalamic dysconnectivity and conversion to psychosis in youth and young adults at elevated clinical risk. *JAMA Psychiatry* 72, 882–891. doi: 10.1001/jamapsychiatry.2015.0566

Beck, A. T., Epstein, N., Brown, G., and Steer, R. A. (1988). An inventory for measuring clinical anxiety: psychometric properties. *J. Consult. Clin. Psychol.* 56, 893–897.

Beck, A. T., Ward, C. H., Mendelson, M., Mock, J., and Erbaugh, J. (1961). An inventory for measuring depression. *Arch. Gen. Psychiatry* 4, 561–571.

Bora, E., Fornito, A., Yucel, M., and Pantelis, C. (2012). The effects of gender on grey matter abnormalities in major psychoses: a comparative voxelwise meta-analysis of schizophrenia and bipolar disorder. *Psychol. Med.* 42, 295–307. doi: 10.1017/S0033291711001450

Bremner, J. D., Vythilingam, M., Vermetten, E., Nazeer, A., Adil, J., Khan, S., et al. (2002). Reduced volume of orbitofrontal cortex in major depression. *Biol. Psychiatry* 51, 273–279. doi: 10.1016/s0006-3223(01)01336-1

Cai, Y., Liu, J., Zhang, L., Liao, M., Zhang, Y., Wang, L., et al. (2015). Grey matter volume abnormalities in patients with bipolar I depressive disorder and unipolar depressive disorder: a voxel-based morphometry study. *Neurosci. Bull.* 31, 4–12. doi: 10.1007/s12264-014-1485-5

Chang, M., Womer, F. Y., Edmiston, E. K., Bai, C., Zhou, Q., Jiang, X., et al. (2018). Neurobiological commonalities and distinctionsamong three major psychiatric diagnostic categories: a structural MRI study. *Schizophr. Bull.* 44, 65–74. doi: 10.1093/schbul/sbx028

Chen, L., Wang, Y., Niu, C., Zhong, S., Hu, H., Chen, P., et al. (2018). Common and distinct abnormal frontal-limbic system structural and functional patterns in patients with major depression and bipolar disorder. *Neuroimage Clin.* 20, 42–50. doi: 10.1016/j.nicl.2018.07.002

Cheng, B., Wang, X., Roberts, N., Zhou, Y., Wang, S., Deng, P., et al. (2022). Abnormal dynamics of resting-state functional activity and couplings in postpartum depression with and without anxiety. *Cereb. Cortex* 1–12. doi: 10.1093/cercor/bhac038

Colibazzi, T., Yang, Z., Horga, G., Chao-Gan, Y., Corcoran, C. M., Klahr, K., et al. (2017). Aberrant temporal connectivity in persons at clinical high risk for psychosis. *Biol. Psychiatry Cogn. Neurosci. Neuroimaging* 2, 696–705. doi: 10.1016/j.bpsc.2016.12.008

Cross-Disorder Group of the Psychiatric Genomics Consortium (2019). Genomic relationships, novel loci, and pleiotropic mechanisms across eight psychiatric disorders. *Cell* 179, 1469–1482.e1411. doi: 10.1016/j.cell.2019.11.020

Cui, L., Li, M., Deng, W., Guo, W., Ma, X., Huang, C., et al. (2011). Overlapping clusters of gray matter deficits in paranoid schizophrenia and psychotic bipolar mania with family history. *Neurosci. Lett.* 489, 94–98. doi: 10.1016/j.neulet.2010.11.073

Cui, Y., Dong, J., Yang, Y., Yu, H., Li, W., Liu, Y., et al. (2020). White matter microstructural differences across major depressive disorder, bipolar disorder and schizophrenia: a tract-based spatial statistics study. *J. Affect. Disord.* 260, 281–286. doi: 10.1016/j.jad.2019.09.029

Dong, D., Wang, Y., Chang, X., Jiang, Y., Klugah-Brown, B., Luo, C., et al. (2017). Shared abnormality of white matter integrity in schizophrenia and bipolar disorder: a comparative voxel-based meta-analysis. *Schizophr. Res.* 185, 41–50. doi: 10.1016/j.schres.2017.01.005

Etkin, A., Gyurak, A., and O'Hara, R. (2013). A neurobiological approach to the cognitive deficits of psychiatric disorders. *Dialogues Clin. Neurosci.* 15, 419–429. doi: 10.31887/DCNS.2013.15.4/aetkin

Forbes, C. E., and Grafman, J. (2010). The role of the human prefrontal cortex in social cognition and moral judgment. *Annu. Rev. Neurosci.* 33, 299–324. doi: 10.1146/annurev-neuro-060909-153230

Frodl, T., Jager, M., Smajstrlova, I., Born, C., Bottlender, R., Palladino, T., et al. (2008). Effect of hippocampal and amygdala volumes on clinical outcomes in major depression: a 3-year prospective magnetic resonance imaging study. *J. Psychiatry Neurosci.* 33, 423–430.

Ganzola, R., Maziade, M., and Duchesne, S. (2014). Hippocampus and amygdala volumes in children and young adults at high-risk of schizophrenia: research synthesis. *Schizophr. Res.* 156, 76–86. doi: 10.1016/j.schres.2014.03.030

Goodkind, M., Eickhoff, S. B., Oathes, D. J., Jiang, Y., Chang, A., Jones-Hagata, L. B., et al. (2015). Identification of a common neurobiological substrate for mental illness. *JAMA Psychiatry* 72, 305–315. doi: 10.1001/jamapsychiatry.2014.2206

Haijma, S. V., Van Haren, N., Cahn, W., Koolschijn, P. C., Hulshoff Pol, H. E., and Kahn, R. S. (2013). Brain volumes in schizophrenia: a meta-analysis in over 18 000 subjects. *Schizophr. Bull.* 39, 1129–1138. doi: 10.1093/schbul/sbs118

Hosenbocus, S., and Chahal, R. (2012). A review of executive function deficits and pharmacological management in children and adolescents. *J. Can. Acad. Child. Adolesc. Psychiatry* 21, 223–229.

Kay, S. R., Fiszbein, A., and Opler, L. A. (1987). The positive and negative syndrome scale (PANSS) for schizophrenia. *Schizophr. Bull.* 13, 261–276. doi: 10.1093/schbul/13.2.261

Knochel, C., Stablein, M., Prvulovic, D., Ghinea, D., Wenzler, S., Pantel, J., et al. (2016). Shared and distinct gray matter abnormalities in schizophrenia, schizophrenia relatives and bipolar disorder in association with cognitive impairment. *Schizophr. Res.* 171, 140–148. doi: 10.1016/j.schres.2016.01.035

Konarski, J. Z., McIntyre, R. S., Kennedy, S. H., Rafi-Tari, S., Soczynska, J. K., and Ketter, T. A. (2008). Volumetric neuroimaging investigations in mood disorders: bipolar disorder versus major depressive disorder. *Bipolar. Disord.* 10, 1–37. doi: 10.1111/j.1399-5618.2008.00435.x

Lee, S. H., Ripke, S., Neale, B. M., Faraone, S. V., Purcell, S. M., Perlis, R. H., et al. (2013). Genetic relationship between five psychiatric disorders estimated from genome-wide SNPs. *Nat. Genet.* 45, 984–994. doi: 10.1038/ng.2711

Meda, S. A., Ruano, G., Windemuth, A., O'Neil, K., Berwise, C., Dunn, S. M., et al. (2014). Multivariate analysis reveals genetic associations of the resting default mode network in psychotic bipolar disorder and schizophrenia. *Proc. Natl. Acad. Sci. U. S. A.* 111, E2066–E2075. doi: 10.1073/pnas.1313093111

Nenadic, I., Maitra, R., Langbein, K., Dietzek, M., Lorenz, C., Smesny, S., et al. (2015). Brain structure in schizophrenia vs. psychotic bipolar I disorder: a VBM study. *Schizophr. Res.* 165, 212–219. doi: 10.1016/j.schres.2015.04.007

Niida, A., Niida, R., Matsuda, H., Motomura, M., and Uechi, A. (2014). Analysis of the presence or absence of atrophy of the subgenual and subcallosal cingulate cortices using voxel-based morphometry on MRI is useful to select prescriptions for patients with depressive symptoms. *Int. J. Gen. Med.* 7, 513–524. doi: 10.2147/IJGM.S72736

Niida, R., Yamagata, B., Matsuda, H., Niida, A., Uechi, A., Kito, S., et al. (2019). Regional brain volume reductions in major depressive disorder and bipolar disorder: an analysis by voxel-based morphometry. *Int. J. Geriatr. Psychiatry* 34, 186–192. doi: 10.1002/gps.5009

Nomi, J. S., Schettini, E., Broce, I., Dick, A. S., and Uddin, L. Q. (2018). Structural connections of functionally defined human insular subdivisions. *Cereb. Cortex* 28, 3445–3456. doi: 10.1093/cercor/bhx211

Pang, Y., Wei, Q., Zhao, S., Li, N., Li, Z., Lu, F., et al. (2022). Enhanced default mode network functional connectivity links with electroconvulsive therapy response in major depressive disorder. *J. Affect. Disord.* 306, 47–54. doi: 10.1016/j.jad.2022.03.035

Premkumar, P., Fannon, D., Sapara, A., Peters, E. R., Anilkumar, A. P., Simmons, A., et al. (2015). Orbitofrontal cortex, emotional decision-making and response to cognitive behavioural therapy for psychosis. *Psychiatry Res.* 231, 298–307. doi: 10.1016/j.pscychresns.2015.01.013

Stein, F., Meller, T., Brosch, K., Schmitt, S., Ringwald, K., Pfarr, J. K., et al. (2021). Psychopathological syndromes across affective and psychotic disorders correlate with gray matter volumes. *Schizophr. Bull.* 47, 1740–1750. doi: 10.1093/schbul/sbab037

van Amelsvoort, T., and Hernaus, D. (2016). Effect of pharmacological interventions on the fronto-cingulo-parietal cognitive control network in psychiatric disorders: a transdiagnostic systematic review of fMRI studies. *Front. Psychiatry* 7:82. doi: 10.3389/fpsyt.2016.00082

Wang, C., Wu, H., Chen, F., Xu, J., Li, H., Li, H., et al. (2018). Disrupted functional connectivity patterns of the insula subregions in drug-free major depressive disorder. *J. Affect. Disord.* 234, 297–304. doi: 10.1016/j.jad.2017.12.033

Wang, J., Ji, Y., Li, X., He, Z., Wei, Q., Bai, T., et al. (2020). Improved and residual functional abnormalities in major depressive disorder after electroconvulsive therapy. *Prog. Neuropsychopharmacol. Biol. Psychiatry* 100:109888. doi: 10.1016/j.pnpbp.2020.109888

Wang, L., Wei, Q., Wang, C., Xu, J., Wang, K., Tian, Y., et al. (2020). Altered functional connectivity patterns of insular subregions in major depressive disorder after electroconvulsive therapy. *Brain Imaging Behav.* 14, 753–761. doi: 10.1007/s11682-018-0013-z

Wang, L., Wei, Q., Wang, C., Xu, J., Wang, K., Tian, Y., et al. (2019). Altered functional connectivity patterns of insular subregions in major depressive disorder after electroconvulsive therapy. *Brain Imaging Behav.* 14, 753–761. doi: 10.1007/s11682-018-0013-z

Wang, T., Zhang, X., Li, A., Zhu, M., Liu, S., Qin, W., et al. (2017). Polygenic risk for five psychiatric disorders and cross-disorder and disorder-specific neural connectivity in two independent populations. *Neuroimage Clin.* 14, 441–449. doi: 10.1016/j.nicl.2017.02.011

Watson, D. R., Anderson, J. M., Bai, F., Barrett, S. L., McGinnity, T. M., Mulholland, C. C., et al. (2012). A voxel based morphometry study investigating brain structural changes in first episode psychosis. *Behav. Brain Res.* 227, 91–99. doi: 10.1016/j.bbr.2011.10.034

Wise, T., Radua, J., Via, E., Cardoner, N., Abe, O., Adams, T. M., et al. (2016). Common and distinct patterns of grey-matter volume alteration in major depression and bipolar disorder: evidence from voxel-based meta-analysis. *Mol. Psychiatry* 22, 1455–1463. doi: 10.1038/mp.2016.72

Xia, M., Womer, F. Y., Chang, M., Zhu, Y., Zhou, Q., Edmiston, E. K., et al. (2018). Shared and distinct functional architectures of brain networks across psychiatric disorders. *Schizophr. Bull.* 45, 450–463. doi: 10.1093/schbul/sby046

Yang, Y., Liu, S., Jiang, X., Yu, H., Ding, S., Lu, Y., et al. (2019). Common and specific functional activity features in schizophrenia, major depressive disorder, and bipolar disorder. *Front. Psychiatry* 10:52. doi: 10.3389/fpsyt.2019.00052

Young, R. C., Biggs, J. T., Ziegler, V. E., and Meyer, D. A. (1978). A rating scale for mania: reliability, validity and sensitivity. *Br. J. Psychiatry* 133, 429–435. doi: 10.1192/bjp.133.5.429

Yuksel, C., McCarthy, J., Shinn, A., Pfaff, D. L., Baker, J. T., Heckers, S., et al. (2012). Gray matter volume in schizophrenia and bipolar disorder with psychotic features. *Schizophr. Res.* 138, 177–182. doi: 10.1016/j.schres.2012.03.003

Zhang, W., Sweeney, J. A., Yao, L., Li, S., Zeng, J., Xu, M., et al. (2020). Brain structural correlates of familial risk for mental illness: a meta-analysis of voxel-based morphometry studies in relatives of patients with psychotic or mood disorders. *Neuropsychopharmacology* 45, 1369–1379. doi: 10.1038/s41386-020-0687-y

Conflict of Interest: The authors declare that the research was conducted in the absence of any commercial or financial relationships that could be construed as a potential conflict of interest.

Publisher's Note: All claims expressed in this article are solely those of the authors and do not necessarily represent those of their affiliated organizations, or those of the publisher, the editors and the reviewers. Any product that may be evaluated in this article, or claim that may be made by its manufacturer, is not guaranteed or endorsed by the publisher.

frontiers | Frontiers in Neuroscience

ORIGINAL RESEARCH
published: 20 June 2022
doi: 10.3389/fnins.2022.879703

Exploring Brain Structural and Functional Biomarkers in Schizophrenia *via* Brain-Network-Constrained Multi-View SCCA

Peilun Song[1], *Yaping Wang*[1]*, *Xiuxia Yuan*[2,3], *Shuying Wang*[2,3] *and Xueqin Song*[2,3]*

[1] School of Information Engineering, Zhengzhou University, Zhengzhou, China, [2] Department of Psychiatry, The First Affiliated Hospital of Zhengzhou University, Zhengzhou, China, [3] Biological Psychiatry International Joint Laboratory of Henan/Zhengzhou University, Zhengzhou, China

OPEN ACCESS

Edited by:
Zhifen Liu,
First Hospital of Shanxi Medical University, China

Reviewed by:
Huiling Wang,
Renmin Hospital of Wuhan University, China
Ling Qin Wei,
Third Affiliated Hospital of Sun Yat-sen University, China

***Correspondence:**
Yaping Wang
ieypwang@zzu.edu.cn
Xueqin Song
fccsongxq@zzu.edu.cn

Specialty section:
This article was submitted to Brain Imaging Methods, a section of the journal Frontiers in Neuroscience

Received: 20 February 2022
Accepted: 04 April 2022
Published: 20 June 2022

Citation:
Song P, Wang Y, Yuan X, Wang S and Song X (2022) Exploring Brain Structural and Functional Biomarkers in Schizophrenia via Brain-Network-Constrained Multi-View SCCA. Front. Neurosci. 16:879703. doi: 10.3389/fnins.2022.879703

Recent studies have proved that dynamic regional measures extracted from the resting-state functional magnetic resonance imaging, such as the dynamic fractional amplitude of low-frequency fluctuation (d-fALFF), could provide a great insight into brain dynamic characteristics of the schizophrenia. However, the unimodal feature is limited for delineating the complex patterns of brain deficits. Thus, functional and structural imaging data are usually analyzed together for uncovering the neural mechanism of schizophrenia. Investigation of neural function-structure coupling enables to find the potential biomarkers and further helps to understand the biological basis of schizophrenia. Here, a brain-network-constrained multi-view sparse canonical correlation analysis (BN-MSCCA) was proposed to explore the intrinsic associations between brain structure and dynamic brain function. Specifically, the d-fALFF was first acquired based on the sliding window method, whereas the gray matter map was computed based on voxel-based morphometry analysis. Then, the region-of-interest (ROI)-based features were extracted and further selected by performing the multi-view sparse canonical correlation analysis jointly with the diagnosis information. Moreover, the brain-network-based structural constraint was introduced to prompt the detected biomarkers more interpretable. The experiments were conducted on 191 patients with schizophrenia and 191 matched healthy controls. Results showed that the BN-MSCCA could identify the critical ROIs with more sparse canonical weight patterns, which are corresponding to the specific brain networks. These are biologically meaningful findings and could be treated as the potential biomarkers. The proposed method also obtained a higher canonical correlation coefficient for the testing data, which is more consistent with the results on training data, demonstrating its promising capability for the association identification. To demonstrate the effectiveness of the potential clinical applications, the detected biomarkers were further analyzed on a schizophrenia-control classification task and a correlation analysis task. The experimental results showed that our method had a superior performance with a 5–8% increment in accuracy and 6–10% improvement in

area under the curve. Furthermore, two of the top-ranked biomarkers were significantly negatively correlated with the positive symptom score of Positive and Negative Syndrome Scale (PANSS). Overall, the proposed method could find the association between brain structure and dynamic brain function, and also help to identify the biological meaningful biomarkers of schizophrenia. The findings enable our further understanding of this disease.

Keywords: multimodal brain image analysis, brain network constraint, sparse canonical correlation analysis, schizophrenia, biomarker

INTRODUCTION

Schizophrenia (SCZ) is a severe psychiatric disorder, which is characterized by cognitive dysfunction, delusions, hallucinations, and personality disturbance (Ventura et al., 2009). It has affected about 1% of the population throughout the world, and has potentially become a lifetime burden for the patients and their families (McGrath et al., 2008). Finding objective biomarkers for the accurate diagnosis and effective intervention in the early stage of SCZ is of great importance for the neuroscience and medical science. However, it is still challenging to identify the accurate biomarkers of SCZ as the pathological mechanism of this disease is unclear yet (Insel, 2010). In the recent decades, the advancements in magnetic resonance imaging (MRI) techniques have provided an alternative opportunity to search for SCZ-related biomarkers. Using the non-invasive MRI, such as functional MRI (fMRI), structural MRI (sMRI), and diffusion tensor imaging (DTI), the brain functional and structural abnormalities can be detected, facilitating the understanding about the pathophysiology of SCZ (Ding et al., 2019; Steardo et al., 2020,Sagarwala and Nasrallah, 2021).

A lot of literatures proved that fMRI has played an important role in the analysis of SCZ (Wang et al., 2018; Steardo et al., 2020). Based on the resting-state fMRI (rs-fMRI), the static functional measures are commonly extracted to find the abnormal patterns in brain, and then, the disease-related biomarkers are identified for further analysis. Currently, beyond the traditional static analysis of functional brain activity, the temporal dynamic features of brain have attracted more and more attention, which can depict the temporal alteration of brain function (Filippi et al., 2019). Dynamic regional measurements at resting-state were widely investigated on brain disorders, demonstrating their sensitive detection capability for the abnormal characteristics of brain (Tang et al., 2018). Dynamic fractional amplitude of low-frequency fluctuation (d-fALFF) is one of the popularly used dynamic regional measurements in SCZ research, which can reflect the temporal variability of the amplitude of intrinsic neural activity (Yan et al., 2017; Zhang et al., 2019). However, as a complex brain disorder, such single-modality data cannot adequately depict the defective pattern caused by SCZ. Recently, an increasing number of evidences have shown that the combination of multimodal imaging data might provide distinct and complementary information, contributing to the comprehensive investigation of SCZ (Zhuang et al., 2019; Lei et al., 2020a). Among these multimodal studies, the fMRI and sMRI were most commonly combined, following with a machine learning method, to conduct the subsequent analysis such as the classification of healthy controls (HCs) and SCZ (Cao et al., 2020). Even though the improved performances were obtained based on these multimodal methods, the inter-modality relationships were inevitably overlooked in most of these studies, which are also important for the multimodal analysis.

In the neuroscience field, researchers have been aware of the importance of exploring the inter-modality associations (Du et al., 2020). Various types of correlation analysis method have been proposed to identify the relationship between different modalities (Shen and Thompson, 2020). Within them, the sparse canonical correlation analysis (SCCA) is one of the most popular methods (Witten et al., 2009). The SCCA could identify multivariate associations between two sets of variables, while it is an unsupervised approach, indicating that it cannot utilize the diagnosis information to guide the exploration of disease-related associations. So, it is limited to find the disease-related and biologically interpretable biomarkers. To overcome this shortcoming, the multi-view SCCA (e.g., three-view SCCA) was adopted by including the diagnosis information as the third type of data, with the aim of simultaneously maximizing the pairwise correlations among diagnosis information and other two sets of variables. By introducing the diagnosis information, the disease-related biomarkers could be detected based on this kind of methods (Hao et al., 2017; Won et al., 2020). However, from the point of view of biologically meaningful interpretation, it still remains a challenge to obtain biologically interpretable findings for the current multi-view SCCA method. To incorporate the biologically meaningful structure knowledge, simplify the model complexity, and reduce the risk of overfitting, different regularization methods were used in the SCCA, such as lasso penalty (Witten et al., 2009), graph-constrained elastic net (Kim et al., 2021), group lasso regularization (Du et al., 2014), and so on. Recent studies have tried to associate the detected brain regions with a certain brain network, and found network-level aberrant alterations in SCZ (Li et al., 2019; Supekar et al., 2019). Based on the observations above, it is hypothesized that this brain-network-based structural information might be helpful for the exploration of SCZ-related biomarkers. To our best knowledge, this kind of structure information has not been utilized in SCCA yet. Thus, a novel multi-view SCCA method, which could simultaneously utilize the brain-network-based structural information and the diagnosis information to help to explore the disease-related biomarkers, is needed for

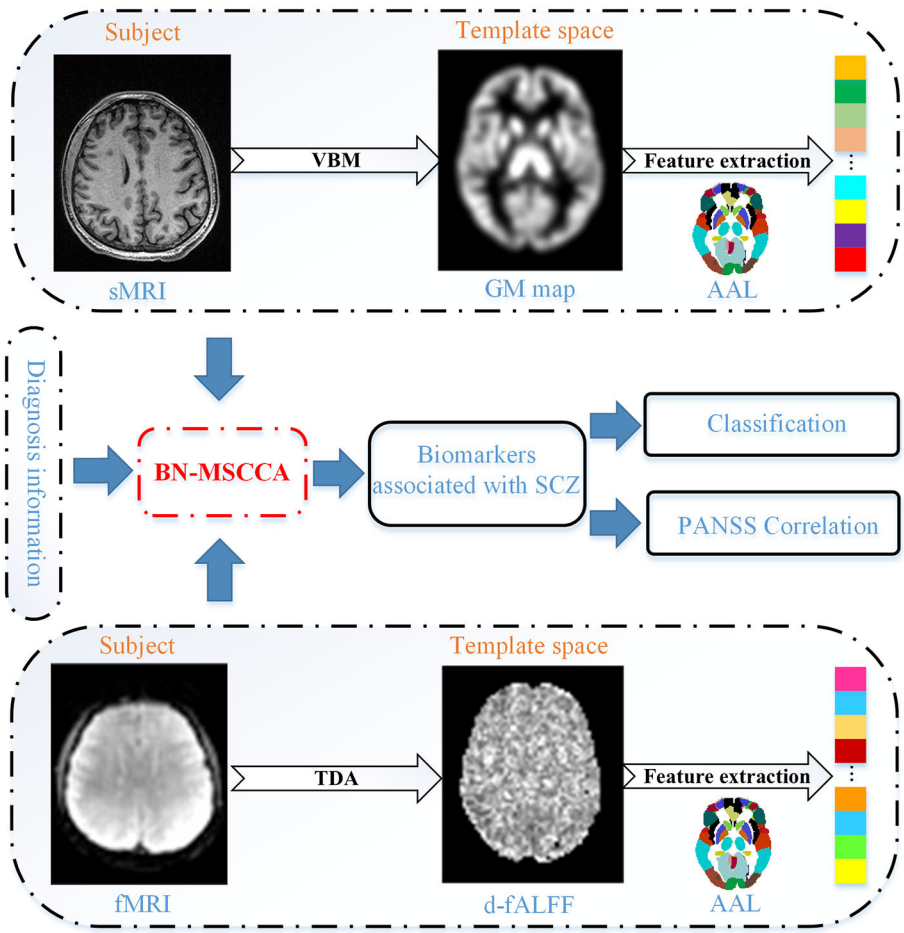

FIGURE 1 | The flowchart of our proposed method.

better identifying disease-related multivariate associations and producing biologically meaningful findings.

In this study, we proposed a novel brain-network-constrained multi-view SCCA (BN-MSCCA) to explore the complex relationships between brain structure and dynamic brain function, and subsequently identify the SCZ-related biomarkers. The temporal dynamic analysis (TDA) was first performed to compute the dynamic brain functional measurement (e.g., d-fALFF) using the sliding window method. Then, voxel-based morphometry (VBM) analysis was performed to obtain the gray matter (GM) map. After that, the region of interest (ROI)-based features were further extracted from these two measurements. Finally, the three-view canonical correlation analysis jointly with the diagnosis information was performed. Moreover, the brain-network-based structural constraint was introduced into the model to prompt the detected biomarkers more interpretable. Using 191 SCZ and 191 HC data, BN-MSCCA obtained more sparse canonical weight patterns and higher canonical correlation coefficients (CCCs). The subsequent classification and PANSS correlation experiments also proved the capability of detected biomarkers for depicting the abnormalities of SCZ.

The rest of this article is organized as follows. Section Materials and Methods describes the materials used in this study and the proposed BN-MSCCA method following with its optimization algorithm. The specific experimental settings and the results are introduced in Section Experiments and Results. In Section Discussion, a comprehensive discussion about the results is presented. Section Conclusion concludes this article.

MATERIALS AND METHODS

The proposed method comprised of four main steps, such as (1) data preprocessing and feature extraction, (2) identifying associations using the proposed BN-MSCCA method, (3) detecting SCZ-related biomarkers, and (4) subsequent analysis based on the detected biomarkers. **Figure 1** presents the overall flowchart of the proposed BN-MSCCA method. In this section, we mainly introduce the data preprocessing,

TABLE 1 | Participant demographics.

Characteristic	SCZ ($N = 191$)	HC ($N = 191$)	p-value*
Age (mean ± sd, year)	23.16 ± 8.45	23.28 ± 4.69	0.863
Gender (M/F)	91/100	89/102	0.838

*t-test is used for comparison of age, and χ^2 test is used for gender comparison.

feature extraction, the proposed BN-MSCCA method, and its optimization algorithm.

Data Preprocessing and Feature Extraction

Data Acquisition

The dataset used in this study was collected at the First Affiliated Hospital of Zhengzhou University, Zhengzhou, China. For the patients with SCZ, the psychiatric diagnoses were based on the USA manual of the Diagnostic and Statistical Manual of Mental Disorders IV (DSM-IV) (Guze, 1995). The exclusion criteria included the presence of traumatic brain injury, severe endocrine diseases, anemia, hematological diseases or other mental diseases, a history of excessive drinking or abuse of psychotropic substances, or the incompletion of MRI examination. Finally, 191 patients with SCZ were enrolled in this work, in which 108 patients have the complete PANSS score.

A total of 191 healthy subjects with matched age and gender were recruited as the HC group. The subjects were able to complete the MR scanning and had no history of organic brain disease or other chronic diseases and mental disorders, nor a family history of psychosis. The demographic information of the studied subjects is summarized in **Table 1**. The study procedures have passed the approval of the ethics committee of the First Affiliated Hospital of Zhengzhou University. All the participants and their legal guardian have consented and signed the informed consent.

The T1-weighted MRI and rs-fMRI were acquired on a GE Discovery 750 3T MRI scanner with an 8-channel head coil. The T1 images were acquired with repetition time (TR) = 8.2 ms, echo time (TE) = 3.2 ms, field of view (FOV) = 256 mm × 256 mm, slice number = 188, slice thickness = 1 mm, flip angle = 12°, and 256 × 256 matrix. The rs-fMRIs were collected using the echo planar imaging sequence (EPI) with TR = 2,000 ms, TE = 30 ms, FOV = 220 mm × 220 mm, slice number = 32, slice thickness = 4 mm, inter-slice gap = 0.5 mm, flip angle = 90°, and 64 × 64 matrix, and the scanning time for each subject is about 6 min (resulting in 188 volumes). During the scanning, the participants were required to think about nothing in particular and keep their head still and eyes closed at the same time.

Data Pre-processing

CAT12 (http://www.neuro.uni-jena.de/cat), an extension toolkit of SPM12, provides a platform for both surface-based morphometry and VBM analysis. Using the T1-weighted MRI data, we followed the standard pipeline of the CAT12 to conduct the VBM analysis. The main steps included the correction of bias-field inhomogeneities, segmentation of brain tissues (gray matter, white matter and cerebrospinal fluid), spatial normalization into the Montreal Neurological Institute (MNI) space, resampling to 1.5 mm × 1.5 mm × 1.5 mm, and non-linear modulation. Finally, the obtained GM maps were smoothed using an 8 mm full width at half maximum (FWHM) Gaussian kernel.

The rs-fMRI data were preprocessed using the DPABI (http://www.rfmri.org/dpabi) software. The processing steps are as follows. First, the initial 10 volumes were removed, followed by the slice-timing correction. Then, the time series of each subject were realigned by a linear transformation. After the realignment, the mean functional image was co-registered to the corresponding T1 image, which had been segmented into gray matter, white matter, and cerebrospinal fluid using a unified segment method (http://www.fil.ion.ucl.ac.uk/spm). Finally, the functional images were resampled to 3 mm × 3 mm × 3 mm and then normalized into the MNI space using the DARTEL (Ashburner, 2007). To alleviate the influence of noise, the images were smoothed by a 4-mm FWHM Gaussian kernel and band-pass filtered within 0.01–0.1 HZ. The nuisance regression was used to regress out the irrelevant variable interferences, including the Friston-24 parameters, white matter signal, cerebrospinal fluid signal, and global signal.

Feature Extraction

Based on the GM images, the ROI-based features were extracted for the subsequent analysis. First, the normalized and modulated GM maps were resampled to 3 mm × 3 mm × 3 mm using the trilinear method. Then, the whole GM map was divided into 116 ROIs according to the AAL atlas. Finally, we averaged the values within each ROI to obtain the ROI-based measurements.

As for the rs-fMRI, we computed the d-fALFF through the TDA module in DPABI. First, we divided all BOLD time series of the whole brain into multiple overlapping windows. In this study, we empirically set the width of each sliding window as 60 s and the interval between time windows as 10 s. Second, the fALFF was calculated based on the time series in a specific time window. The time series was converted to the frequency domain using the fast Fourier transform, and the square root of power spectrum was computed. Then, the sum of amplitude in 0.01–0.1 HZ was divided by the entire frequency range to obtain the fALFF map. Subsequently, the mean and standard deviation of each voxel in the fALFF maps of all sliding windows were computed. Finally, we obtained the coefficient of variation (CV) of these fALFF maps, which was usually regarded as d-fALFF and it was acquired by dividing the standard deviation by the mean in details. The raw d-fALFF of each voxel was further divided by the mean value of the whole brain to reduce the global effects of variability across the subjects (Wang et al., 2020). Similar to T1 image, the d-fALFF of each ROI was also obtained based on the AAL template. To remove the possible effects of age and gender, we pre-adjusted all these imaging features using the regression.

Methods

In this article, we define a matrix using the uppercase letter and a vector using the lowercase letter. Specifically, let $X \in \mathbb{R}^{n\times p}$ and $Y \in \mathbb{R}^{n\times q}$ represent the data matrices, where X corresponds to the d-fALFF-based features with n samples and p variables, and

Y corresponds to the GM volume-based features with n samples and q variables.

SCCA

For identifying the complex multivariate associations, SCCA was proposed with the aim to find the linear transformation of X and Y and obtain the maximal correlation between these two transformed variables. Meanwhile, the penalty terms were introduced to make the variables more sparse and avoid the overfitting (Witten et al., 2009). The SCCA could be formulated as follows.

$$\max_{u,v} u^T X^T Y v \tag{1}$$

$$s.t.\ u^T X^T X u \leq 1,\ \ v^T Y^T Y v \leq 1,\ \ \|u\|_1 \leq a_1,\ \ \|v\|_1 \leq a_2$$

where u and v are the canonical weights for the corresponding data modalities (X and Y), showing the contribution of each feature in this canonical correlation. In this model, the $u^T X^T X u \leq 1$ and $v^T Y^T Y v \leq 1$ are used to describe the covariance structure of the data. The $\|u\|_1 \leq a_1$ and $\|v\|_1 \leq a_2$ are constraints for controlling the sparsity and selecting the most relevant features from the d-fALFF-based and GM volume-based features, respectively. However, the SCCA can only capture associations between two distinct types of data, which cannot meet the demand for identifying multi-view associations among more than two different types of modalities. On the other hand, the SCCA is an unsupervised method indicating that it cannot make full use of the diagnosis information.

Multi-View SCCA

Recently, to uncover the complex associations among multiple types of data, a variant of SCCA, called multi-view SCCA (MSCCA), was proposed to include more than two types of data (Witten and Tibshirani, 2009; Hao et al., 2017). Using the MSCCA, some studies were performed to investigate relationships among three modalities (Du et al., 2021). The MSCCA could be formulated as follows:

$$\max_{u,v,w} u^T X^T Y v + v^T Y^T Z w + w^T Z^T X u \tag{2}$$

$$s.t.\ u^T X^T X u \leq 1,\ \ v^T Y^T Y v \leq 1,\ w^T Z^T Z w \leq 1,$$
$$\|u\|_1 \leq a_1,\ \ \|v\|_1 \leq a_2, \|w\|_1 \leq a_3$$

Note that $Z \in \mathbb{R}^{n \times r}$ is the third type of data, where r is its feature dimension and w is the canonical weight of Z. As a special case of MSCCA, the task-oriented MSCCA was used to incorporate the supervision information as the third type of data, which is from the target task (Hao et al., 2017; Won et al., 2020). According to these studies, the MSCCA has demonstrated its promising capacity for uncovering the disease-related biomarkers. However, the data structure information was overlooked in these methods as the L1-norm penalty can only enforce the individual sparsity without considering the internal structure of the data.

BN-MSCCA

In this work, we focused on association identification among the GM volume-based and d-fALFF-based features. The diagnosis information was also introduced into the model, so that we can find the brain functional and structural biomarkers that are relevant to the disease. Considering the brain structure information as prior information, we further embedded the brain-network-based structural constraint of both imaging features into the MSCCA model, which is formulated as Equation (3). We call it the BN-MSCCA.

$$\max_{u,v,w} u^T X^T Y v + v^T Y^T Z w + w^T Z^T X u \tag{3}$$

$$s.t.\ u^T X^T X u \leq 1,\ v^T Y^T Y v \leq 1, w^T Z^T Z w \leq 1,$$
$$\|u\|_1 + \|u\|_{bn} \leq a_1,\ \|v\|_1 + \|v\|_{bn} \leq a_2,$$
$$\|w\|_1 \leq a_3$$

Here $\|u\|_{bn}$ and $\|v\|_{bn}$ are the brain-network-based structural penalties, introducing the brain-network-based prior information. Their definitions were given in Equations (4) and (5), respectively.

$$\|u\|_{bn} = \sum_{k=1}^{K} \sqrt{\sum_{j \in k} u_j^2} = \sum_{k=1}^{K} \left\| U^k \right\|_2 \tag{4}$$

$$\|v\|_{bn} = \sum_{k=1}^{K} \sqrt{\sum_{j \in k} v_j^2} = \sum_{k=1}^{K} \left\| V^k \right\|_2 \tag{5}$$

Specifically, the ROI-based GM volume and d-fALFF features were extracted based on the same AAL template (116 ROIs). We manually grouped these 116 regions into $K = 15$ brain networks (including both left and right hemispheres) according to a previous study (Han et al., 2019). In our work, the cerebellum was divided into two networks (each in one hemisphere), and the whole vermis was treated as a single brain network. Thus, the objective function for BN-MSCCA was rewritten as follows.

$$\begin{aligned} \min_{u,v,w} & -u^T X^T Y v - v^T Y^T Z w - w^T Z^T X u + \frac{1}{2} \|Xu\|_2^2 \\ & + \frac{1}{2} \|Yv\|_2^2 + \frac{1}{2} \|Zw\|_2^2 + \lambda_1 \alpha \|u\|_{bn} + \lambda_1 (1-\alpha) \|u\|_1 \\ & + \lambda_2 \beta \|v\|_{bn} + \lambda_2 (1-\beta) \|v\|_1 + \lambda_3 \|w\|_1 \end{aligned} \tag{6}$$

In this function, λ_1, λ_2, λ_3, α, and β are the non-negative tuning parameters. λ_1, λ_2, and λ_3 are used to balance between the penalty and the loss function, whereas α and β are used to balance the brain-network-based and individual ROI-based feature selections for the functional and structural modalities respectively.

Algorithm 1 | BN-MSCCA.

Require:
d-fALFF-based features $X = [x_1, \ldots, x_n]^T \in \mathbb{R}^{n \times p}$,
GM volume-based features $Y = [y_1, \ldots, y_n]^T \in \mathbb{R}^{n \times q}$, $p = q = 116$ in our study,
diagnosis information $Z = [z_1, \ldots, z_n]^T \in \mathbb{R}^{n \times r}, r = 1$
Ensure: canonical weights u, v, w
Initialization: $u \in \mathbb{R}^{p \times 1}$, $v \in \mathbb{R}^{q \times 1}$, $w \in \mathbb{R}^{r \times 1}$
While not converged **do**
  Calculate the diagonal matrix $\overline{D}_1$ and D_1;
  Update $u = \left(X^T X + \lambda_1 \alpha \overline{D}_1 + \lambda_1 (1-\alpha) D_1\right)^{-1} X^T (Yv + Zw)$;
  Scale u so that $\|Xu\|_2^2 = 1$;
  Calculate the diagonal matrix $\overline{D}_2$ and D_2;
  Update $v = \left(Y^T Y + \lambda_2 \beta \overline{D}_2 + \lambda_2 (1-\beta) D_2\right)^{-1} Y^T (Xu + Zw)$;
  Scale v so that $\|Yv\|_2^2 = 1$;
  Calculate the diagonal matrix D_3;
  Update $w = \left(Z^T Z + \lambda_3 D_3\right)^{-1} Z^T (Xu + Yv)$;
  Scale w so that $\|Zw\|_2^2 = 1$;
End while

Optimization Algorithm

In this study, we used the alternative iteration algorithm to optimize the BN-MSCCA. To minimize the equation, we take the derivate of the objective function with respect to u, v, and w separately and make them approach zero. Then, we arrive at

$$u = \left(X^T X + \lambda_1 \alpha \overline{D}_1 + \lambda_1 (1-\alpha) D_1\right)^{-1} X^T (Yv + Zw) \quad (7)$$

D_1 is a diagonal matrix with the j-th diagonal entry being $\frac{1}{|u_j|}$. $\overline{D}_1$ is a block diagonal matrix of the k-th diagonal block as $\frac{1}{2\|U^k\|_2}$. Using the same procedure, we can obtain the solution of v and w:

$$v = \left(Y^T Y + \lambda_2 \beta \overline{D}_2 + \lambda_2 (1-\beta) D_2\right)^{-1} Y^T (Xu + Zw) \quad (8)$$

$$w = \left(Z^T Z + \lambda_3 D_3\right)^{-1} Z^T (Xu + Yv) \quad (9)$$

During each iterative procedure, we first fix v and w to solve u, then fix u and w to solve v, and finally fix u and v to solve w. The process stops until meeting the stopping criterion. **Algorithm 1** shows the pseudocode of the BN-MSCCA algorithm.

EXPERIMENTS AND RESULTS

Experimental Setup

To evaluate the effectiveness of the proposed BN-MSCCA, we chose three closely related methods as the benchmarks. They are SCCA (Witten et al., 2009), MSCCA (Hao et al., 2017), and SCCAR (Du et al., 2019). These three methods could find the associations between GM volume-based and d-fALFF-based features. However, the SCCA ignores the diagnosis information. SCCAR combines the linear regression with SCCA to guide the correlation analysis using the diagnosis information, and the discriminative biomarkers could be detected. Both MSCCA and BN-MSCCA extend the SCCA into three-view condition, so that it could introduce the diagnosis information into model for guiding the association identification; meanwhile, BN-MSCCA further incorporated the brain-network-based structure information as prior.

There are five parameters λ_1, λ_2, λ_3, α, and β in the proposed BN-MSCCA method. The α and β were fixed as 0.5 to balance the brain-network-based and individual ROI-based feature selections for the functional and structural modalities respectively. Such settings simplified the parameter tuning procedure and reduced the time consumption without affecting the performance significantly. The optimal values of λ_1, λ_2, and λ_3 were found by the grid searching strategy during a nested 5-fold cross-validation. For MSCCA and BN-MSCCA, we tuned λ_1, λ_2, and λ_3 in the range of [0.01, 0.1, 1, 10, 100]. As for SCCA and SCCAR, due to the limitation of sparse parameter values by applying the soft-thresholding function (Parkhomenko et al., 2009), we tuned the parameters in the range of [0.01: 0.05: 0.5], according to the strategy in the study of Du et al. (2019). For these four methods, the corresponding optimal parameters were determined by minimizing the differences between training and validating canonical correlation coefficients (CCCs). For each comparison method, the overall procedure was repeated for five times to ensure the robustness of results; meanwhile, the time consumption was acceptable. In addition, the data partition and termination condition were same for all comparison methods. The experiments of all comparison methods were executed on the same software platform.

Multivariate Association Identification

In the field of medical image analysis, the detected imaging biomarkers are of great importance. In this work, we compared the amplitude of the canonical weight, which indicated the importance of the biomarkers. After the cross-validation, the canonical weights were averaged for each ROI. The heatmaps of canonical weights U of d-fALFF and V of GM volume for different methods are shown in **Figures 2**, **3**, respectively. In these figures, each row stands for the canonical weights for one method, in which the deeper color indicates the features corresponding to the canonical weights more important. From **Figures 2**, **3**, it can be seen that the SCCA and SCCAR methods identified too many signals, which may misguide the subsequent investigation. MSCCA and our proposed method detected more sparse canonical weight patterns than SCCA and SCCAR methods. Moreover, our method obtained more interesting canonical weight patterns compared with the MSCCA. As shown in **Figure 2**, the largest weight consistently located in left putamen for the MSCCA and BN-MSCCA methods. What is more, the d-fALFF in left hippocampus is also detected by our proposed BN-MSCCA method. Both of them belong to the subcortical network in left hemisphere. As for the canonical weight V in **Figure 3**, the greatest signal in right pallidum is found by the MSCCA and BN-MSCCA methods. Besides this, the right middle cingulate and right hippocampus are also identified by our proposed method. These three ROIs are within the right subcortical

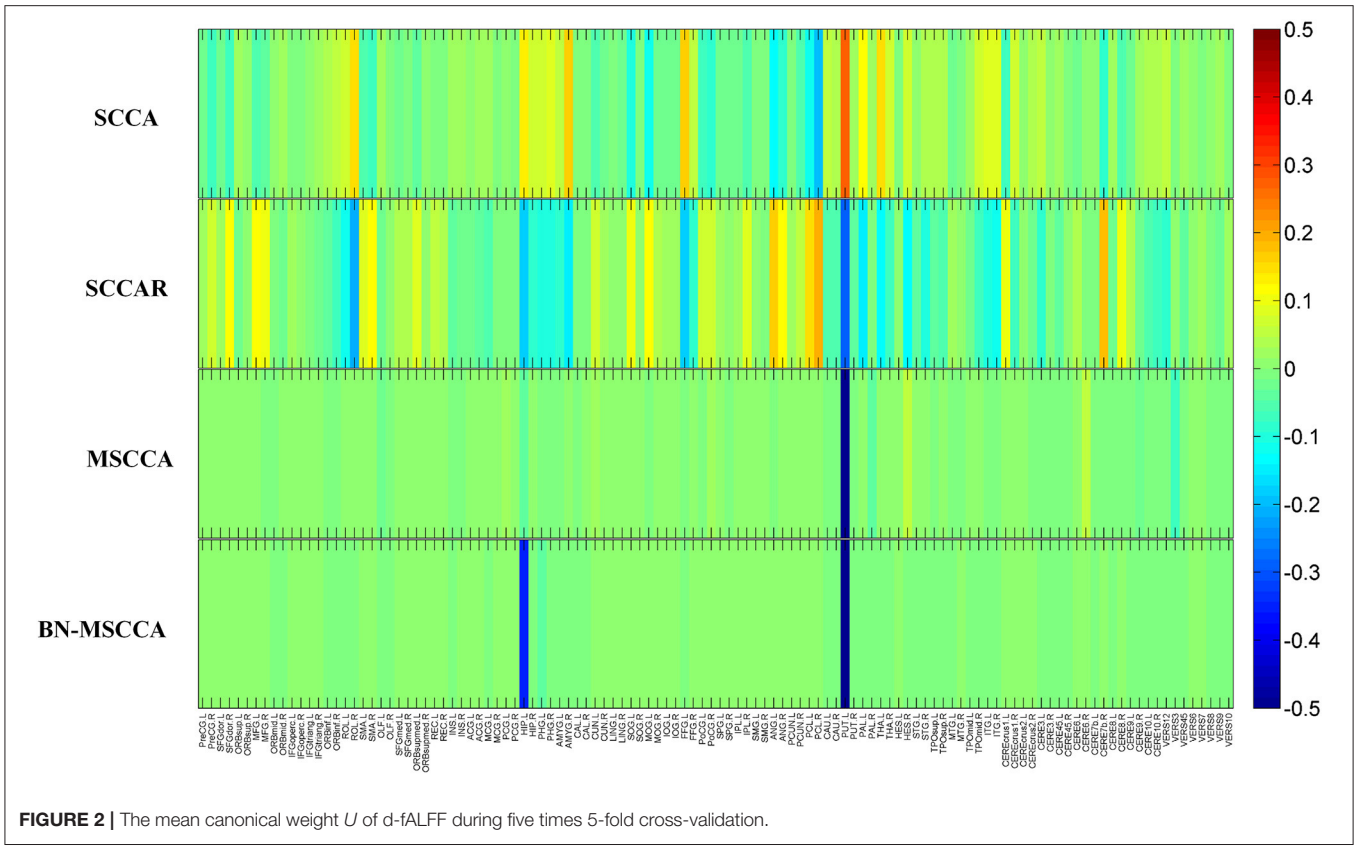

FIGURE 2 | The mean canonical weight *U* of d-fALFF during five times 5-fold cross-validation.

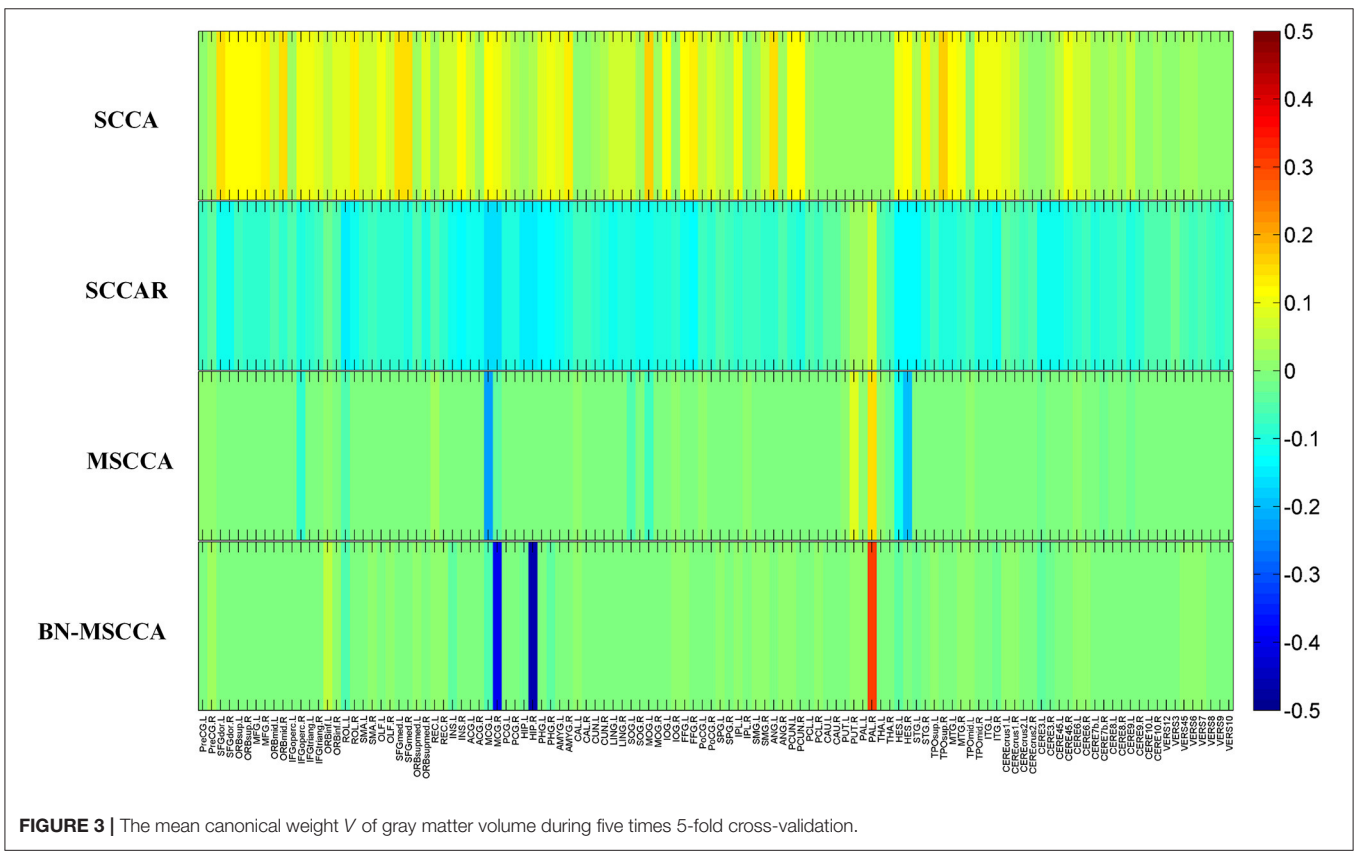

FIGURE 3 | The mean canonical weight *V* of gray matter volume during five times 5-fold cross-validation.

TABLE 2 | Comparison of CCCs on different methods (mean ± standard deviation).

Method	CCC (training)	CCC (testing)
SCCA	0.25 ± 0.02	0.09 ± 0.06
SCCAR	0.26 ± 0.03	0.08 ± 0.06
MSCCA	0.22 ± 0.08	0.11 ± 0.07
BN-MSCCA	0.16 ± 0.03	0.14 ± 0.08

network. These results demonstrated that the proposed BN-MSCCA is very promising in finding the biologically meaningful imaging biomarkers by introducing the brain-network-based structural information.

We also compared BN-MSCCA with other methods in terms of CCCs between d-fALFF-based and GM volume-based features. For each method, the CCCs across the cross-validation were averaged for the training and testing data respectively, and their corresponding mean and standard deviation were calculated. From **Table 2**, we can see that our method achieved the best CCC result in the testing data, which is also more consistent with the CCC result in the training data. This indicates that our method may have better generalization performance compared with the other competing methods.

Classification Setting and Results

To investigate the effectiveness of the identified biomarkers for assisting the diagnosis of SCZ, we performed the classification task based on different feature selection methods. In this study, we compared our BN-MSCCA method with five competing methods, including the method with the original features (without feature selection), the method with two-sample *t*-test feature selection, SCCA, SCCAR, and MSCCA. The details of these methods are summarized as follows.

Original features: In this method, the GM volume-based and d-fALFF-based features were directly concatenated as a feature vector to fit the classifier. Two-sample *t*-test feature selection: Similar to the method with original features, we first obtained the feature vector for each subject. Then, two-sample *t*-test was used to find the most discriminative features. A threshold of *p*-value was set for feature selection. The selected features were used for further model training and testing. The optimal threshold for selecting the features was determined from a set of 10 predefined *p*-values of [0.01–0.1] with the step of 0.01. SCCA: In this method, the GM volume-based and d-fALFF-based features were analyzed using SCCA. According to the absolute value of canonical weights, the top ten features were selected in each imaging modality for the classification. SCCAR: Similarly, the GM volume-based and d-fALFF-based features were analyzed using SCCAR. According to the absolute value of canonical weights, the top ten features were selected for the classification. MSCCA: The GM volume-based and d-fALFF-based features were selected using MSCCA method. Different with SCCA, the diagnosis information was treated as the third type of data to guide the feature selection. We used the features with top ten absolute value of canonical weights in each imaging modality for the classification. BN-MSCCA: The GM volume-based and d-fALFF-based features were selected using BN-MSCCA, with the guidance of diagnosis information for feature selection. And the features corresponding to the top ten absolute value of canonical weights were used to conduct the classifier.

In our study, all the methods used the linear kernel-based support vector machine (SVM) with the same default setting to perform the classification. The 10-fold cross-validation was repeated ten times to ensure the robustness of the model. Finally, the classification performance was evaluated by computing metrics such as the accuracy (ACC), specificity (SPE), sensitivity (SEN), and area under the curve (AUC). As shown in **Table 3**, we can see that the two-sample *t*-test based method, SCCAR, MSCCA, and BN-MSCCA outperform the method with original features. However, the classification performance of SCCAR and MSCCA methods are slightly worse than that of two-sample *t*-test based method, as the latter one is directly designed for finding the discriminative features between two classes. Apparently, our BN-MSCCA method achieves the best performance, and also has the increments of 5.33%, 5.01%, 5.63%, and 6.77% on ACC, SEN, SPE, and AUC respectively, compared with the two-sample *t*-test based method. Overall, we can conclude from these results that the GM volume-based and d-fALFF-based features are effective for the classification of SCZ. After using the feature selection, the performance could be improved. In addition, our proposed BN-MSCCA particularly takes both the diagnosis information and the brain-network-based structural information into consideration, achieving the best classification performance.

Correlation With PANSS Score

The correlation analysis between the detected biomarkers and the PANSS score has been regarded as a proof for the effectiveness of the feature selection in this SCZ research. We used the adjusted features to conduct the correlation with the PANSS scores based on 108 patients with SCZ, whose PANSS scores were available and complete for this analysis. **Figure 4** shows that significant correlations exist between the PANSS scores and two of the detected biomarkers respectively. It is obvious that the d-fALFF of left cerebellum shows a significant negative correlation with the positive symptom score of PANSS ($R = -0.2$, $p = 0.035$). Additionally, the gray matter volume of left heschl is negatively correlated with positive symptom score of PANSS at a significant level ($R = -0.21$, $p = 0.026$).

DISCUSSION

In this section, we summarized the main idea and contributions of this study and further discussed the top 10 identified brain regions of d-fALFF and gray matter volume respectively, following with the investigation about their pairwise correlations. Then, both the classification with the identified biomarkers and the correlation between PANSS score and the detected

TABLE 3 | Comparison of classification performance on different feature selection methods (mean ± standard deviation).

Method	ACC (%)	SEN (%)	SPE (%)	AUC (%)
Original features	62.98 ± 7.96	63.28 ± 12.04	62.62 ± 10.80	67.90 ± 8.30
Two-sample *t*-test	65.17 ± 7.24	64.72 ± 10.70	65.63 ± 10.34	69.77 ± 7.36
SCCA	62.04 ± 8.02	62.39 ± 11.30	61.73 ± 12.13	66.20 ± 8.27
SCCAR	64.92 ± 7.33	63.89 ± 11.05	65.95 ± 9.69	68.63 ± 8.03
MSCCA	64.47 ± 7.42	64.32 ± 11.82	64.57 ± 10.69	70.54 ± 8.20
BN-MSCCA	**70.50 ± 7.43**	**69.73 ± 10.31**	**71.26 ± 10.76**	**76.54 ± 7.46**

Bold values indicate the best results.

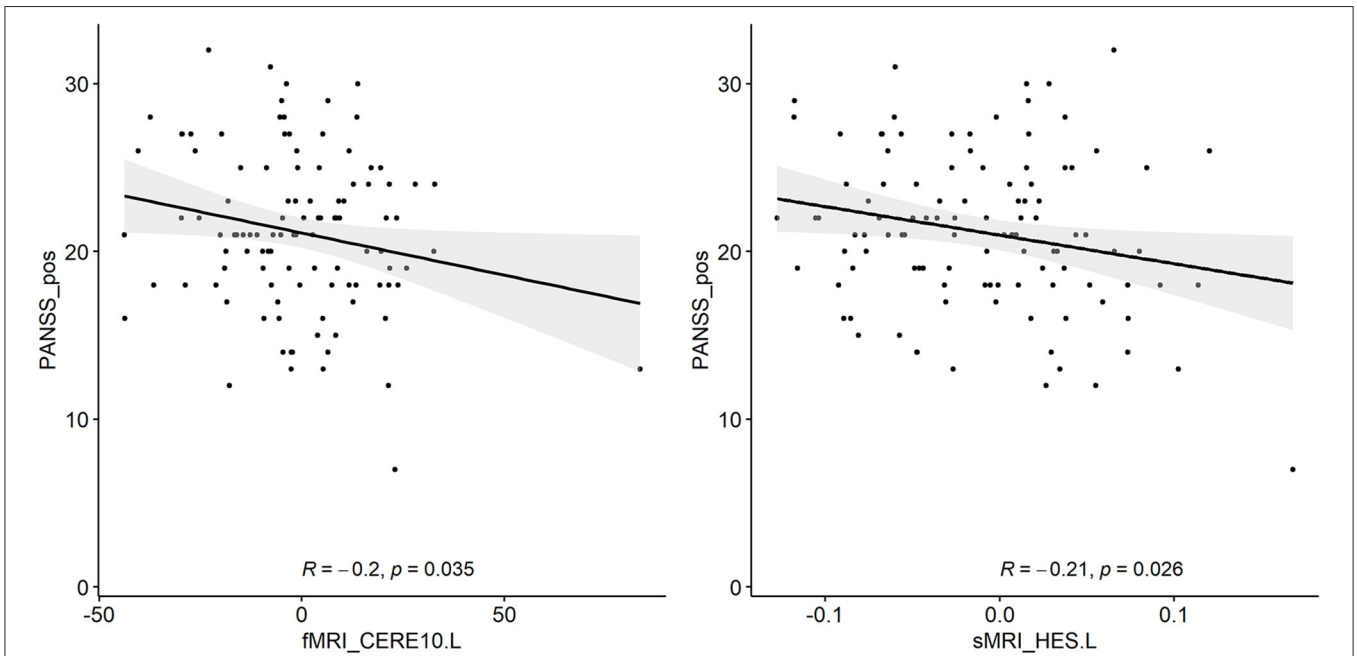

FIGURE 4 | Two detected biomarkers (adjusted values) which have significant correlations with the positive symptom score of PANSS.

TABLE 4 | Top 10 ROIs of d-fALFF identified by our method.

ROI	Related brain network	Weight
PUT.L	SN.L	0.72464
HIP.L	SN.L	0.354
PHG.L	SN.L	0.04529
CEREcrus1.L	CN.L	0.014084
PAL.L	SN.L	0.012935
CERE10.L	CN.L	0.012429
CERE3.L	CN.L	0.0094317
VERS12	VN	0.0060698
ORBinf.L	ATN.L	0.0053477
OLF.L	SN.L	0.0050575

R, right; L, left; PUT, putamen; HIP, hippocampus; PHG, parahippocampal gyrus; CEREcrus, cerebellum_crus; PAL, pallidum; CERE10, cerebellum_10; CERE3, cerebellum_3; VERS12, vermis_1_2; ORBinf, inferior orbitofrontal cortex; OLF, olfactory; SN, subcortical network; CN, cerebellum network; VN, vermis network; ATN, attention network.

biomarkers are analyzed. Finally, the limitations of our method and the potential future study directions are presented.

Main Idea and Contributions

In this study, a brain-network-constrained multi-view SCCA was proposed. It has been demonstrated that the proposed method has significantly improved performance for the identification of brain structural and functional biomarkers, compared with the other competing methods. The main idea and key contributions of this study are summarized as follows: (1) a novel model was proposed to jointly analyze the d-fALFF, gray matter volume, and diagnosis information for the identification of SCZ-related biomarkers; (2) the brain-network-based structural constraint was introduced into the model, so that the detected biomarkers were interpretable; (3) the experiments were performed on 191 patients with SCZ and 191 matched healthy controls, and the proposed method achieved superior performance for the biomarker detection, compared with the other methods; (4) the

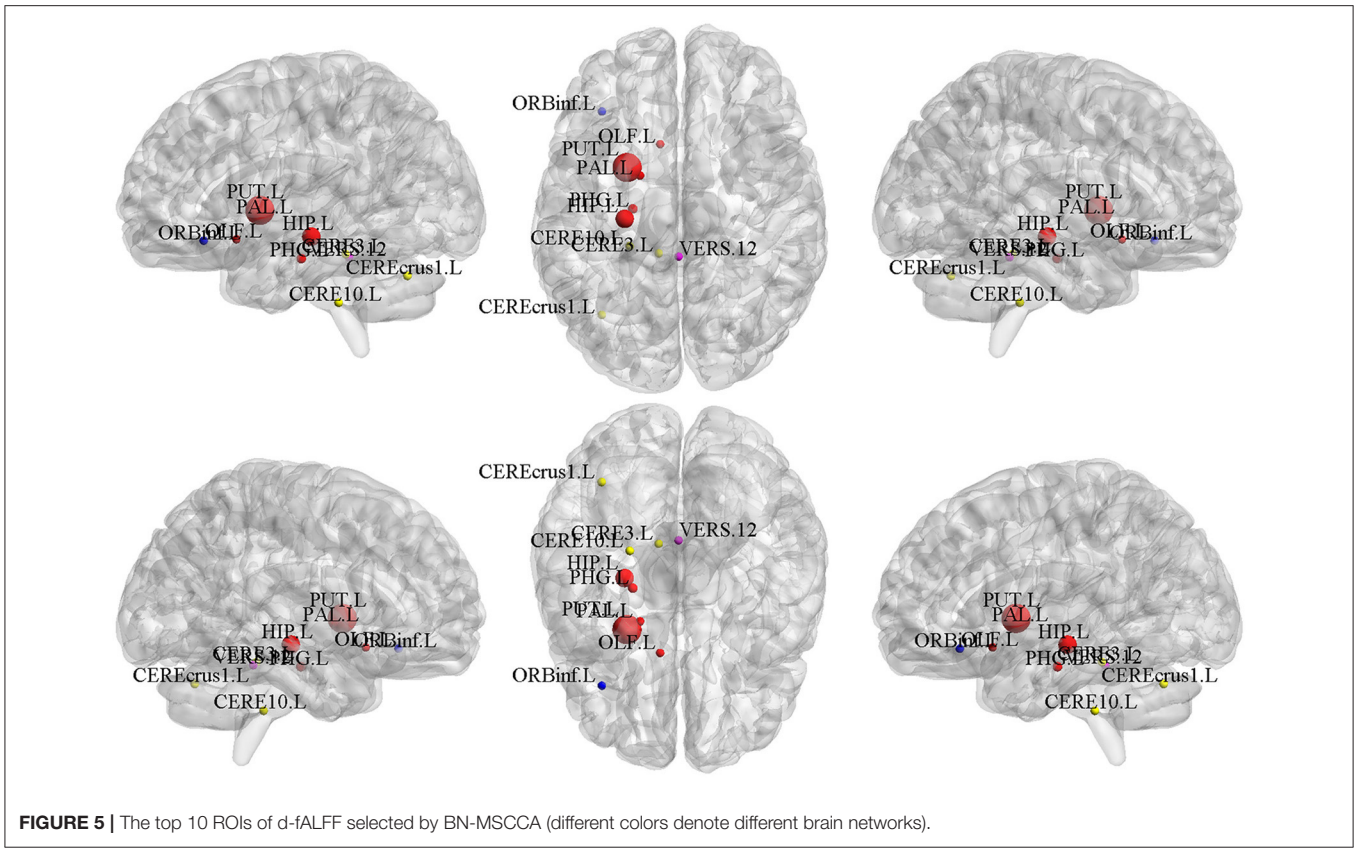

FIGURE 5 | The top 10 ROIs of d-fALFF selected by BN-MSCCA (different colors denote different brain networks).

effectiveness of detected biomarkers was further verified on two subsequent analysis tasks, including the SCZ-HC classification and the PANSS correlation analysis. The results proved the potential usage of these biomarkers for the clinical applications. Overall, the proposed method would be a powerful alternative method for multimodal analysis. In addition, the findings in this study could be supplementaries and verifications to the exploration of biomarkers for SCZ.

Top-10 Selected Brain Regions of d-FALFF

We calculated the mean values of the canonical weights across the five times 5-fold cross-validation to select the top brain regions of d-fALFF. The top ten ROIs are shown in **Table 4**. We also visualized these top-10 selected regions in **Figure 5**. According to **Table 4** and **Figure 5**, we observed that multiple detected regions belong to a certain brain network. For example, five detected regions are within the left subcortical network, including the putamen, hippocampus, parahippocampal, pallidum, and olfactory gyrus in left hemisphere. Previous studies about SCZ have demonstrated the increased functional connectivities between certain subcortical regions and cortical ROIs, showing the important role of the subcortical network in SCZ (Zhang et al., 2012). And the cerebellum might be another key brain region involved in the cognitive function. A study has suggested the functional abnormalities of the cerebellum in a cerebellar-subcortical-cortical loop in the brains of SCZ patients, and it may be the underlying mechanism of SCZ (Zhuo et al., 2018). A total of three ROIs which located in left cerebellum were found in our study, which might be support for this previous finding. The above findings have verified the effectiveness of BN-MSCCA for identifying the interpretable biomarkers of SCZ. With the help of the L1-norm, the proposed method also detected some individual-level SCZ-related ROIs, such

TABLE 5 | Top 10 ROIs of gray matter volume identified by our method.

ROI	Related brain network	Weight
HIP.R	SN.R	0.46577
MCG.R	SN.R	0.39399
PAL.R	SN.R	0.30736
ROL.L	AUN.L	0.060209
MCG.L	SN.L	0.052595
ORBinf.L	ATN.L	0.047987
CERE3.L	CN.L	0.045651
INS.L	AUN.L	0.038043
PHG.R	SN.R	0.035748
HES.L	AUN.L	0.032479

R, right; L, left; HIP, hippocampus; MCG, middle cingulate gyrus; PAL, pallidum; ROL, rolandic operculum; ORBinf, inferior orbitofrontal cortex; CERE3, cerebellum_3; INS, insular; PHG, parahippocampal gyrus; HES, heschl; SN, subcortical network; AUN, auditory network; ATN, attention network; CN, cerebellum network.

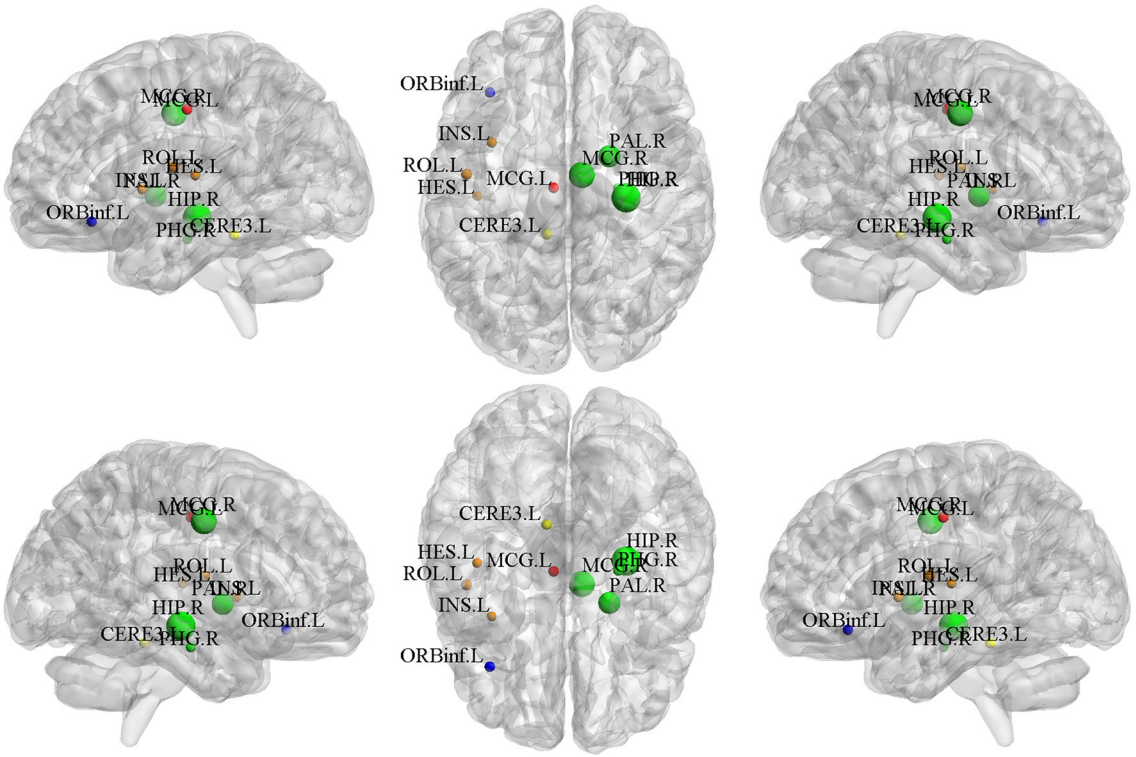

FIGURE 6 | The top 10 ROIs of gray matter volume selected by BN-MSCCA (different colors denote different brain networks).

as vermis and the left inferior frontal gyrus, which is also consistent with the findings in the previous studies (Jeong et al., 2009,Collin, 2011).

Top-10 Selected Brain Regions of Gray Matter Volume

The top-10 selected brain regions of gray matter volume based on their respective average canonical weights are shown in **Table 5**. Accordingly, four ROIs in right subcortical network and three ROIs in left auditory network are detected as the most important biomarkers, proving the effectiveness of introducing the brain-network-based structural constraint. The left middle cingulate gyrus, left inferior frontal gyrus, and left cerebellum were also detected in the GM volume-based features, which is prompted by the L1-norm. **Figure 6** shows the visualization of these top 10 selected regions. As can be seen in **Table 5** and **Figure 6**, we obtained consistent results with the previous studies about these most important ROIs for SCZ (Witthaus et al., 2009; Kubera et al., 2014; Krause and Pogarell, 2017; He et al., 2019).

Refined Correlation Analysis

After identifying SCZ-related biomarkers for each single modality, we further conducted a refined correlation analysis between d-fALFF-based and GM volume-based biomarkers to explain their relationships. We here present the pairwise correlation results between top 10 ROIs of d-fALFF and top 10 ROIs of gray matter volume. **Figure 7** shows the heatmap of this correlation analysis of each pair, where circles labeled with "*" indicate that the correlations between the d-fALFF and gray matter volume of their corresponding regions are significant ($p < 0.05$). As shown in **Figure 7**, when looking horizontally, the d-fALFF of left putamen is significantly correlated with most (seven out of ten) of the GM volume-based biomarkers. The d-fALFF in left hippocampus is positively correlated with three brain regions of gray matter volume (left rolandic operculum, right parahippocampal, and left heschl gyrus) at significant level. When looking vertically, six regions of gray matter volume (bilateral middle cingulate, right pallidum, left rolandic operculum, right parahippocampal, and left heschl gyrus) are significantly correlated with at least two regions of d-fALFF. These pairwise correlation results show that our proposed method could identify the brain regions where the brain function and structure are significantly associated with each other, and these significant correlations might reflect the abnormal brain regions of SCZ.

SCZ-HC Classification and PANSS Correlation

By now, we have selected the SCZ-related ROIs of d-fALFF and gray matter volume respectively based on our method. To investigate the effectiveness of their potential clinical applications, we performed two subsequent analyses, including the SCZ-HC classification and the correlation with PANSS score. According to the classification results, these two types of features

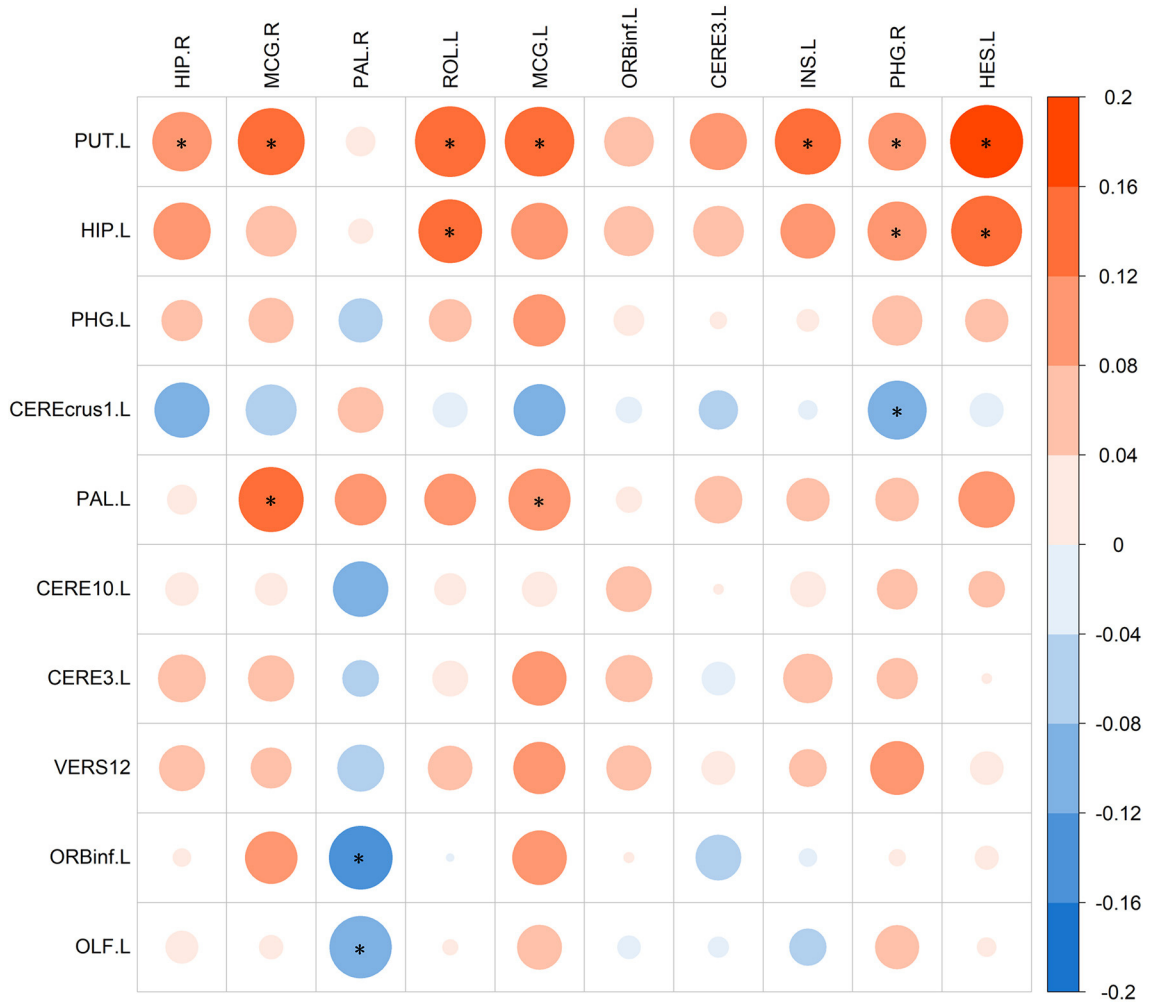

FIGURE 7 | The pairwise correlations between top 10 ROIs of d-fALFF (column) and top 10 ROIs of gray matter volume (row). Here * denotes $p < 0.05$.

could classify the SCZ from the HC with a reasonable accuracy. By performing the feature selection, we also found that the most discriminative features were retained and the redundant features were discarded, which helped achieve significant improvements in the classification performance. Multiple studies have proved SCZ is a disorder with brain network abnormalities (Rubinov and Bullmore, 2013; Li et al., 2019). The detection of such brain network abnormalities could help capture the different patterns between SCZ and HC. Thus, various studies performed the SCZ-HC classification using the brain network-based measurements, which depicted the abnormal alterations of brain functional or structural network (Han et al., 2019; Lei et al., 2020b). Our method can take both the diagnosis information and the brain-network-based prior information into consideration for the selection of the most discriminative features. The biomarkers detected by the proposed method have strong discriminative power, and the classification performance outperforms all comparison methods.

We also conducted the PANSS correlation analysis based on the detected biomarkers. Two significant negative correlations were found in our study, which included the correlation between the d-fALFF of cerebellum and the positive symptom score of PANSS, and the correlation between the gray matter volume of left heschl and the positive symptom score of PANSS. Interestingly, previous studies have proved the same negative correlation trend between the positive symptom score of PANSS score and these two brain regions in SCZ (Narayanaswamy et al., 2015; Du et al., 2017), demonstrating the reasonability of our findings. Here only two detected biomarkers showed significant correlation with the positive symptom score of PANSS. The potential reason may be that the diagnosis information was used as the target to guide the canonical correlation in this study, which might lead to the detected biomarkers not specific to the PANSS score.

Limitations and Future Directions

Based on the above experimental results and discussion, we could conclude that our proposed BN-MSCCA has a great capability for the biomarker identification. However, there are also some

limitations in this study. First, only two imaging modalities were included in this work. In fact, SCZ is a complex and multi-factor induced disease. The other types of data, such as gene and gut microbiome, were also investigated for SCZ (Guan et al., 2021; Li et al., 2021). These different modalities could provide useful and complementary information, which would be considered in our future work. Second, due to the proposed method is based on the MSCCA, it requires that the identified d-fALFF-based biomarkers should be correlated with GM volume-based biomarkers and diagnosis information simultaneously. Thus the modality-specific correlation and its corresponding biomarkers would be overlooked, which might be also valuable for the understanding of the disease. Third, recent studies have proved that SCZ is a heterogeneous disease comprising various symptoms, which could be divided into multiple subtypes (Chand et al., 2020). However, only two diagnostic classes were considered in this work, ignoring the different patterns of abnormalities among different subtypes of patients. Our future direction includes exploring the biomarkers which are oriented to a specific subtype of SCZ, aiming for the accurate diagnosis and treatment of this disease. Fourth, we only used a specific AAL atlas, which may limit the capability of biomarker detection. Future studies should also consider other widely used atlases for feature extraction, such as Power 264 atlas (Power et al., 2011), exploring the influences of different atlases on BN-MSCCA.

CONCLUSION

In this study, we developed a brain-network-constrained multi-view SCCA method namely BN-MSCCA, which could uncover the brain structural and functional associations and identify the potential biomarkers for SCZ. The proposed BN-MSCCA could leverage the inter-modality associations to better find the disease-related multimodal neuroimaging biomarkers, which is achieved by performing the multi-view sparse canonical correlation analysis among brain structural features, functional features, and diagnosis information simultaneously. Moreover, the identified biomarkers were encouraged to locate in multiple predefined brain networks. Thus more biologically interpretable results could be achieved, which was guaranteed by incorporating the brain-network-based structural constraint.

The proposed method was validated on a SCZ dataset, with the aim of mining the relationship between d-fALFF-based features and GM volume-based features and further finding the SCZ-related biomarkers. Compared with the SCCA, SCCAR, and MSCCA method, the BN-MSCCA could not only identify more sparse and meaningful canonical weight patterns, but also obtain the larger testing CCC. Furthermore, the detected biomarkers were evaluated by the subsequent classification and correlation analysis tasks for validating the effectiveness of their clinical applications. Experimental results showed that our method could identify more discriminative biomarkers, achieving the superior classification performance to other competing strategies for feature selection. Moreover, the significant negative correlations were found between the positive symptom score of PANSS and two of the identified biomarkers respectively, demonstrating the promising application of these biomarkers in discovering the severity of SCZ symptoms.

DATA AVAILABILITY STATEMENT

The original contributions presented in the study are included in the article/supplementary material, further inquiries can be directed to the corresponding author/s.

ETHICS STATEMENT

The studies involving human participants were reviewed and approved by the Human Ethics Committee of the First Affiliated Hospital of Zhengzhou University, China (Approval No. 2016-LW-17). Written informed consent to participate in this study was provided by the participants' legal guardian/next of kin. Written informed consent was obtained from the individual(s), and minor(s)' legal guardian/next of kin, for the publication of any potentially identifiable images or data included in this article.

AUTHOR CONTRIBUTIONS

PS and YW designed the study and revised the manuscript. YW provided guidance and suggestions for the study. PS performed experiments and drafted the manuscript. XS, XY, and SW collected the imaging and clinical data, and provided these data along with the description of the data. All authors read and approved the submitted manuscript.

FUNDING

This study was supported by the National Natural Science Foundation of China (U1504606, U21A20367, and 81971253), China Postdoctoral Science Foundation (2016T90679 and 2015M582201), Key Research Projects of Henan Higher Education Institutions (20A510009), Science and Technology Development Plan of Henan Province (172102310270), and Zhong Yuan Technological Innovation leading Talents (204200510019).

REFERENCES

Ashburner, J. (2007). A fast diffeomorphic image registration algorithm. *Neuroimage* 38, 95–113. doi: 10.1016/j.neuroimage.2007.07.007

Cao, B., Cho, R. Y., Chen, D., Xiu, M., Wang, L., Soares, J. C., et al. (2020). Treatment response prediction and individualized identification of first-episode drug-naïve schizophrenia using brain functional connectivity. *Mol. Psychiatry* 25, 906–913. doi: 10.1038/s41380-018-0106-5

Chand, G. B., Dwyer, D. B., Erus, G., Sotiras, A., Varol, E., Srinivasan, D., et al. (2020). Two distinct neuroanatomical subtypes of schizophrenia revealed using machine learning. *Brain* 143, 1027–1038. doi: 10.1093/brain/awaa025

Collin, G. (2011). Impaired cerebellar functional connectivity in schizophrenia patients and their healthy siblings. *Front. Psychiatry* 2, 73. doi: 10.3389/fpsyt.2011.00073

Ding, Y., Ou, Y., Pan, P., Shan, X., Chen, J., Liu, F., et al. (2019). Brain structural abnormalities as potential markers for detecting

individuals with ultra-high risk for psychosis: a systematic review and meta-analysis. *Schizophr. Res.* 209, 22–31. doi: 10.1016/j.schres.2019.05.015

Du, L., Liu, K., Yao, X., Risacher, S. L., Guo, L., Saykin, A. J., et al. (2019). "Diagnosis status guided brain imaging genetics via integrated regression and sparse canonical correlation analysis," in *2019 IEEE 16th International Symposium on Biomedical Imaging (ISBI 2019)* (Venice: IEEE), 356–359. doi: 10.1109/ISBI.2019.8759489

Du, L., Yan, J., Kim, S., Risacher, S. L., Huang, H., Inlow, M., et al. (2014). "A Novel Structure-Aware Sparse Learning Algorithm for Brain Imaging Genetics," in *Medical Image Computing and Computer-Assisted Intervention – MICCAI 2014 Lecture Notes in Computer Science*, eds P. Golland, N. Hata, C. Barillot, J. Hornegger, and R. Howe (Cham: Springer International Publishing), 329–336. doi: 10.1007/978-3-319-10443-0_42

Du, L., Zhang, J., Liu, F., Wang, H., Guo, L., Han, J., et al. (2021). Identifying associations among genomic, proteomic and imaging biomarkers via adaptive sparse multi-view canonical correlation analysis. *Med. Image Anal.* 70, 102003. doi: 10.1016/j.media.2021.102003

Du, L., Zhang, J., Liu, F., Zhang, M., Wang, H., Guo, L., et al. (2020). "Mining high-order multimodal brain image associations via sparse tensor canonical correlation analysis," in *2020 IEEE International Conference on Bioinformatics and Biomedicine (BIBM)* (Seoul: IEEE), 570–575. doi: 10.1109/BIBM49941.2020.9313503

Du, Y., Pearlson, G. D., Lin, D., Sui, J., Chen, J., Salman, M., et al. (2017). Identifying dynamic functional connectivity biomarkers using GIG-ICA: application to schizophrenia, schizoaffective disorder, and psychotic bipolar disorder. *Hum. Brain Mapp.* 38, 2683–2708. doi: 10.1002/hbm.23553

Filippi, M., Spinelli, E. G., Cividini, C., and Agosta, F. (2019). Resting state dynamic functional connectivity in neurodegenerative conditions: a review of magnetic resonance imaging findings. *Front. Neurosci.* 13, 657. doi: 10.3389/fnins.2019.00657

Guan, F., Ni, T., Zhu, W., Williams, L. K., Cui, L.-B., Li, M., et al. (2021). Integrative omics of schizophrenia: from genetic determinants to clinical classification and risk prediction. *Mol. Psychiatry*. doi: 10.1038/s41380-021-01201-2

Guze, S. B. (1995). Diagnostic and statistical manual of mental disorders, 4th ed. (DSM-IV). *AJP* 152, 1228–1228. doi: 10.1176/ajp.152.8.1228

Han, S., Wang, Y., Liao, W., Duan, X., Guo, J., Yu, Y., et al. (2019). The distinguishing intrinsic brain circuitry in treatment-naïve first-episode schizophrenia: ensemble learning classification. *Neurocomputing* 365, 44–53. doi: 10.1016/j.neucom.2019.07.061

Hao, X., Li, C., Du, L., Yao, X., Yan, J., Risacher, S. L., et al. (2017). Mining outcome-relevant brain imaging genetic associations via three-way sparse canonical correlation analysis in Alzheimer's disease. *Sci. Rep.* 7, 44272. doi: 10.1038/srep44272

He, H., Luo, C., Luo, Y., Duan, M., Yi, Q., Biswal, B. B., et al. (2019). Reduction in gray matter of cerebellum in schizophrenia and its influence on static and dynamic connectivity. *Hum. Brain Mapp.* 40, 517–528. doi: 10.1002/hbm.24391

Insel, T. R. (2010). Rethinking schizophrenia. *Nature* 468, 187–193. doi: 10.1038/nature09552

Jeong, B., Wible, C. G., Hashimoto, R.-I., and Kubicki, M. (2009). Functional and anatomical connectivity abnormalities in left inferior frontal gyrus in schizophrenia. *Hum. Brain Mapp.* 30, 4138–4151. doi: 10.1002/hbm.20835

Kim, M., Min, E. J., Liu, K., Yan, J., Saykin, A. J., Moore, J. H., et al. (2021). Multi-task learning based structured sparse canonical correlation analysis for brain imaging genetics. *Med. Image Anal.* 102297. doi: 10.1016/j.media.2021.102297

Krause, D., and Pogarell, O. (2017). Shrinking brain and schizophrenia: a review of AQQ19current studies on the effect of antipsychotic medication on gray matter volume. *Psych. Mental Disord.* 1, 6.

Kubera, K. M., Sambataro, F., Vasic, N., Wolf, N. D., Frasch, K., Hirjak, D., et al. (2014). Source-based morphometry of gray matter volume in patients with schizophrenia who have persistent auditory verbal hallucinations. *Progr. Neuro Psychopharmacol. Biol. Psychiatry* 50, 102–109. doi: 10.1016/j.pnpbp.2013.11.015

Lei, D., Pinaya, W. H. L., van Amelsvoort, T., Marcelis, M., Donohoe, G., Mothersill, D. O., et al. (2020b). Detecting schizophrenia at the level of the individual: relative diagnostic value of whole-brain images, connectome-wide functional connectivity and graph-based metrics. *Psychol. Med.* 50, 1852–1861. doi: 10.1017/S0033291719001934

Lei, D., Pinaya, W. H. L., Young, J., Amelsvoort, T., Marcelis, M., Donohoe, G., et al. (2020a). Integrating machining learning and multimodal neuroimaging to detect schizophrenia at the level of the individual. *Hum Brain Mapp* 41, 1119–1135. doi: 10.1002/hbm.24863

Li, S., Hu, N., Zhang, W., Tao, B., Dai, J., Gong, Y., et al. (2019). Dysconnectivity of multiple brain networks in schizophrenia: a meta-analysis of resting-state functional connectivity. *Front. Psychiatry* 10, 482. doi: 10.3389/fpsyt.2019.00482

Li, S., Song, J., Ke, P., Kong, L., Lei, B., Zhou, J., et al. (2021). The gut microbiome is associated with brain structure and function in schizophrenia. *Sci. Rep.* 11, 9743. doi: 10.1038/s41598-021-89166-8

McGrath, J., Saha, S., Chant, D., and Welham, J. (2008). Schizophrenia: a concise overview of incidence, prevalence, and mortality. *Epidemiol. Rev.* 30, 67–76. doi: 10.1093/epirev/mxn001

Narayanaswamy, J. C., Kalmady, S. V., Venkatasubramanian, G., and Gangadhar, B. N. (2015). Clinical correlates of superior temporal gyrus volume abnormalities in antipsychotic-naïve schizophrenia. *JNP* 27, e128–e133. doi: 10.1176/appi.neuropsych.14030049

Parkhomenko, E., Tritchler, D., and Beyene, J. (2009). Sparse canonical correlation analysis with application to genomic data integration. *Stat. Appl. Genet. Mol. Biol.* 8, 1–34. doi: 10.2202/1544-6115.1406

Power, J. D., Cohen, A. L., Nelson, S. M., Wig, G. S., Barnes, K. A., Church, J. A., et al. (2011). Functional network organization of the human brain. *Neuron* 72, 665–678. doi: 10.1016/j.neuron.2011.09.006

Rubinov, M., and Bullmore, E. (2013). Schizophrenia and abnormal brain network hubs. *Clin. Res.* 15, 11. doi: 10.31887/DCNS.2013.15.3/mrubinov

Sagarwala, R., and Nasrallah, H. A. (2021). The effect of antipsychotic medications on white matter integrity in first-episode drug-naïve patients with psychosis: a review of DTI studies. *Asian J. Psychiatr.* 61, 102688. doi: 10.1016/j.ajp.2021.102688

Shen, L., and Thompson, P. M. (2020). Brain imaging genomics: integrated analysis and machine learning. *Proc. IEEE* 108, 125–162. doi: 10.1109/JPROC.2019.2947272

Steardo, L., Carbone, E. A., de Filippis, R., Pisanu, C., Segura-Garcia, C., Squassina, A., et al. (2020). Application of support vector machine on fMRI data as biomarkers in schizophrenia diagnosis: a systematic review. *Front. Psychiatry* 11, 588. doi: 10.3389/fpsyt.2020.00588

Supekar, K., Cai, W., Krishnadas, R., Palaniyappan, L., and Menon, V. (2019). Dysregulated brain dynamics in a triple-network saliency model of schizophrenia and its relation to psychosis. *Biol. Psychiatry* 85, 60–69. doi: 10.1016/j.biopsych.2018.07.020

Tang, C., Wei, Y., Zhao, J., and Nie, J. (2018). "The dynamic measurements of regional brain activity for resting-state fMRI: d-ALFF, d-fALFF and d-ReHo," in *Medical Image Computing and Computer Assisted Intervention – MICCAI 2018 Lecture Notes in Computer Science*, eds A. F. Frangi, J. A. Schnabel, C. Davatzikos, C. Alberola-López, and G. Fichtinger (Cham: Springer International Publishing), 190–197. doi: 10.1007/978-3-030-00931-1_22

Ventura, J., Hellemann, G. S., Thames, A. D., Koellner, V., and Nuechterlein, K. H. (2009). Symptoms as mediators of the relationship between neurocognition and functional outcome in schizophrenia: a meta-analysis. *Schizophr. Res.* 113, 189–199. doi: 10.1016/j.schres.2009.03.035

Wang, S., Zhang, Y., Lv, L., Wu, R., Fan, X., Zhao, J., et al. (2018). Abnormal regional homogeneity as a potential imaging biomarker for adolescent-onset schizophrenia: a resting-state fMRI study and support vector machine analysis. *Schizophr. Res.* 192, 179–184. doi: 10.1016/j.schres.2017.05.038

Wang, Y., Sun, K., Liu, Z., Chen, G., Jia, Y., Zhong, S., et al. (2020). Classification of unmedicated bipolar disorder using whole-brain functional activity and connectivity: a radiomics analysis. *Cerebral Cortex* 30, 1117–1128. doi: 10.1093/cercor/bhz152

Witten, D. M., Tibshirani, R., and Hastie, T. (2009). A penalized matrix decomposition, with applications to sparse principal components and canonical correlation analysis. *Biostatistics* 10, 515–534. doi: 10.1093/biostatistics/kxp008

Witten, D. M., and Tibshirani, R. J. (2009). Extensions of sparse canonical correlation analysis with applications to genomic data. *Stat. Appl. Genet. Mol. Biol.* 8, 1–27. doi: 10.2202/1544-6115.1470

Witthaus, H., Kaufmann, C., Bohner, G., Özgürdal, S., and Gudlowski, Y., Gallinat, J., et al. (2009). Gray matter abnormalities in subjects at ultra-high risk for schizophrenia and first-episode schizophrenic patients compared to healthy controls. *Psychiatry Res. Neuroimaging* 173, 163–169. doi: 10.1016/j.pscychresns.2008.08.002

Won, J. H., Kim, M., Youn, J., and Park, H. (2020). Prediction of age at onset in Parkinson's disease using objective specific neuroimaging genetics based on a sparse canonical correlation analysis. *Sci. Rep.* 10, 11662. doi: 10.1038/s41598-020-68301-x

Yan, C.-G., Yang, Z., Colcombe, S. J., Zuo, X.-N., and Milham, M. P. (2017). Concordance among indices of intrinsic brain function: insights from inter-individual variation and temporal dynamics. *Science Bulletin* 62, 1572–1584. doi: 10.1016/j.scib.2017.09.015

Zhang, D., Guo, L., Hu, X., Li, K., Zhao, Q., and Liu, T. (2012). Increased cortico-subcortical functional connectivity in schizophrenia. *Brain Imaging Behav.* 6, 27–35. doi: 10.1007/s11682-011-9138-z

Zhang, Y., Guo, G., and Tian, Y. (2019). Increased temporal dynamics of intrinsic brain activity in sensory and perceptual network of schizophrenia. *Front. Psychiatry* 10, 484. doi: 10.3389/fpsyt.2019.00484

Zhuang, H., Liu, R., Wu, C., Meng, Z., Wang, D., Liu, D., et al. (2019). Multimodal classification of drug-naïve first-episode schizophrenia combining anatomical, diffusion and resting state functional resonance imaging. *Neurosci. Lett.* 705, 87–93. doi: 10.1016/j.neulet.2019.04.039

Zhuo, C., Wang, C., Wang, L., Guo, X., Xu, Q., Liu, Y., et al. (2018). Altered resting-state functional connectivity of the cerebellum in schizophrenia. *Brain Imaging Behav.* 12, 383–389. doi: 10.1007/s11682-017-9704-0

Conflict of Interest: The authors declare that the research was conducted in the absence of any commercial or financial relationships that could be construed as a potential conflict of interest.

frontiers | Frontiers in Neuroscience

ORIGINAL RESEARCH
published: 19 July 2022
doi: 10.3389/fnins.2022.937145

Aberrant Dynamic Functional Connectivity of Posterior Cingulate Cortex Subregions in Major Depressive Disorder With Suicidal Ideation

Weicheng Li[1,2,3], Chengyu Wang[1,3], Xiaofeng Lan[1,3], Ling Fu[1,2,3], Fan Zhang[1,2,3], Yanxiang Ye[1,3], Haiyan Liu[1,3], Kai Wu[1,3,4], Guohui Lao[1,3], Jun Chen[5], Guixiang Li[6], Yanling Zhou[1,3] and Yuping Ning[1,2,3]**

[1] The Affiliated Brain Hospital of Guangzhou Medical University, Guangzhou, China, [2] The First School of Clinical Medicine, Southern Medical University, Guangzhou, China, [3] Guangdong Engineering Technology Research Center for Translational Medicine of Mental Disorders, Guangzhou, China, [4] School of Biomedical Sciences and Engineering, South China University of Technology, Guangzhou, China, [5] Guangdong Institute of Medical Instruments, Guangzhou, China, [6] Institute of Biological and Medical Engineering, Guangdong Academy of Sciences, Guangzhou, China

OPEN ACCESS

Edited by:
Zaixu Cui,
Chinese Institute for Brain Research (CIBR), China

Reviewed by:
Xia Liang,
Harbin Institute of Technology, China
Shaoling Peng,
Beijing Normal University, China

***Correspondence:**
Yanling Zhou
zhouylivy@aliyun.com
Yuping Ning
ningjeny@126.com

Specialty section:
This article was submitted to Brain Imaging Methods, a section of the journal Frontiers in Neuroscience

Received: 05 May 2022
Accepted: 17 June 2022
Published: 19 July 2022

Citation:
Li W, Wang C, Lan X, Fu L, Zhang F, Ye Y, Liu H, Wu K, Lao G, Chen J, Li G, Zhou Y and Ning Y (2022) Aberrant Dynamic Functional Connectivity of Posterior Cingulate Cortex Subregions in Major Depressive Disorder With Suicidal Ideation. Front. Neurosci. 16:937145. doi: 10.3389/fnins.2022.937145

Accumulating evidence indicates the presence of structural and functional abnormalities of the posterior cingulate cortex (PCC) in patients with major depressive disorder (MDD) with suicidal ideation (SI). Nevertheless, the subregional-level dynamic functional connectivity (dFC) of the PCC has not been investigated in MDD with SI. We therefore sought to investigate the presence of aberrant dFC variability in PCC subregions in MDD patients with SI. We analyzed resting-state functional magnetic resonance imaging (fMRI) data from 31 unmedicated MDD patients with SI (SI group), 56 unmedicated MDD patients without SI (NSI group), and 48 matched healthy control (HC) subjects. The sliding-window method was applied to characterize the whole-brain dFC of each PCC subregion [the ventral PCC (vPCC) and dorsal PCC (dPCC)]. In addition, we evaluated associations between clinical variables and the aberrant dFC variability of those brain regions showing significant between-group differences. Compared with HCS, the SI and the NSI groups exhibited higher dFC variability between the left dPCC and left fusiform gyrus and between the right vPCC and left inferior frontal gyrus (IFG). The SI group showed higher dFC variability between the left vPCC and left IFG than the NSI group. Furthermore, the dFC variability between the left vPCC and left IFG was positively correlated with Scale for Suicidal Ideation (SSI) score in patients with MDD (i.e., the SI and NSI groups). Our results indicate that aberrant dFC variability between the vPCC and IFG might provide a neural-network explanation for SI and may provide a potential target for future therapeutic interventions in MDD patients with SI.

Keywords: major depressive disorder, posterior cingulate cortex, magnetic resonance imaging, suicidal ideation, dynamic functional connectivity (dFC)

INTRODUCTION

Suicide presents a heavy burden on public health, resulting in nearly one million deaths each year worldwide (Turecki and Brent, 2016). Important contributors to suicide include familial, social, cultural, genetic vulnerability, psychological, and psychiatric factors (Turecki and Brent, 2016). It is reported that up to 80% of people who die by suicide have mental disorders (Ilgen et al., 2010) and more than half of suicide attempters suffered from depression at the time of the attempt (Chahine et al., 2020). Suicidal ideation (SI), described as the consideration or plan to commit suicide (Klonsky and May, 2014), is a significant risk factor for suicide among patients with major depressive disorder (MDD) (Klonsky et al., 2016). Therefore, efforts to achieve a better comprehension of the neurobiological mechanisms underlying SI in patients with MDD are crucial to make progress in the treatment and prevention of suicide.

The posterior cingulate cortex (PCC), which forms a key part of the default mode network (Buckner et al., 2008), demonstrates different brain activity and increased functional connectivity during the resting state than during cognitive tasks (Greicius et al., 2003; Pfefferbaum et al., 2011). The PCC forms a key hub for self-referential processing (Johnson et al., 2009), cognitive control (Vanyukov et al., 2015), and emotion processing and underlies multidomain cognitive functions by linking to distal cortical areas, such as the prefrontal cortex (Leech et al., 2011). In the last decade, much neuroimaging literature has reported structural and functional changes in the PCC of MDD patients with SI (Schmaal et al., 2020). A structural study found increased PCC volume in MDD patients with SI when compared with MDD patients with suicide attempts (SAs) (Hong et al., 2021). Functional magnetic resonance imaging (fMRI) has been widely used to investigate aberrant brain activity in the PCC in MDD patients with SI, and brain dysfunction has been related to cognitive control (Minzenberg et al., 2015) and self-referential (Quevedo et al., 2016) observations in these patients. For instance, Marchand et al. (2013) reported aberrant functional connectivity between the PCC and dorsolateral prefrontal cortex and inferior frontal gyrus (IFG) during motor control tasks in MDD patients with SI. Additionally, this aberrant functional connectivity was positively correlated with SI intensity (Marchand et al., 2013). Analogous to this, decreased resting-state functional connectivity between the PCC and habenula has also been detected in MDD patients with SI (Ambrosi et al., 2019).

The abovementioned studies were conducted from the viewpoint that the PCC is a single homogeneous structure; however, accumulating evidence indicates that the PCC is not homogeneous, either structurally or functionally (Leech et al., 2011). On the basis of the cytoarchitectonic characteristics of the PCC, Fan et al. (2016) recommended that the PCC should be divided into two major subregions, the ventral PCC (vPCC) and dorsal PCC (dPCC) nuclei. The dPCC is reported to play an important role in the orientation of the self and body in visual space (Vogt et al., 2006), whereas the vPCC is at an intermediate stage of information processing between visual recognition and emotion-related substrate and plays a key role in self-reflective function (Johnson et al., 2002; Uddin et al., 2005). PCC subregion-based network abnormalities or volume differences have been reported in schizophrenia (Ebisch et al., 2018), epilepsies (Parvizi et al., 2021), autism spectrum disorders (Lau et al., 2019), obsessive-compulsive disorder (Matsumoto et al., 2010), Alzheimer's disease (Xu et al., 2009), and chronic pain (Yoshino et al., 2018). Nevertheless, PCC dysfunction at the subregional level has been little studied in MDD patients with SI. Therefore, we still know little about whether PCC subregion-based dysfunction is disrupted in MDD patients with SI.

Using the approach of static functional connectivity, aberrant brain activity in PCC subregions was reported in MDD patients with SI (Chase et al., 2021, 2017). Of note, resting-state functional connectivity has traditionally relied on static analytic approaches that assume stable patterns of connectivity across the entire resting scan period. However, human brain connectivity shows time-varying profiles across periods of unconstrained rest (Allen et al., 2014; Zalesky et al., 2014). Analysis of the variability of functional connectivity (dFC) may therefore enable a more sophisticated demonstration of the spontaneous fluctuating nature of neural signals (Vidaurre et al., 2021) and their association with cognition and behavioral performance (Kucyi et al., 2017). Thus, investigation from the perspective of temporal dynamics is needed to explore aberrant dFC in MDD patients with SI. Recently, dFC is increasingly being suggested as a prognostic indicator of disease (Preti et al., 2017; Lurie et al., 2020), such as Parkinson's disease (Kim J. et al., 2017), Huntington's disease (Espinoza et al., 2019), and depression (Liao et al., 2018). Moreover, a prior study reported that patients with depression with SI revealed increased dynamic connectomics relative to patients with depression without SI and healthy controls (HCs) (Liao et al., 2018). Thus, a better understanding of dFC variability may offer nuanced insights into brain activity in MDD patients with SI, further improving our understanding of the psychopathological mechanisms underlying MDD with SI. Up to now, no study has investigated dFC variability differences in PCC subregions in MDD patients with SI.

In the current study, we analyzed resting-state fMRI data from 31 unmedicated MDD patients with SI, 56 unmedicated MDD patients without SI, and 48 matched healthy subjects. The sliding-window method was applied to characterize the whole-brain dFC of each PCC subregion. We generated the following hypotheses: (i) relative to HCs and MDD patients without SI, MDD patients with SI would exhibit anomalous dFC patterns in PCC subregions; and (ii) the aberrant dFC variability would show associations with clinical variables. With these hypotheses, we sought to identify aberrant dFC variability in PCC subregions in MDD patients with SI. In addition, we evaluated correlations between clinical variables and the aberrant dFC variability of brain regions showing significant between-group differences.

MATERIALS AND METHODS

Participants

In total, 89 unmedicated patients with MDD between the ages of 18 and 65 years were drawn from the Molecular Biomarkers of Antidepressant Response study (clinical trial number: ChiCTR1800017626) cohort, the data of which were

published in our previous study (Lan et al., 2021). For all patients, the entrance criteria were (i) meeting the criteria for MDD according to the Diagnostic and Statistical Manual of Mental Disorders, 5th edition; (ii) available imaging data and data on symptoms; (iii) a score $\geq$ 17 on the 17-item Hamilton Depression Rating Scale (HAMD-17) (Helmreich et al., 2012); and (iv) medication-free for at least 4 weeks before inclusion in the trial.

The exclusion criteria included a history of other major psychiatric disorders meeting the criteria of axis I of the Diagnostic and Statistical Manual of Mental Disorders, 5th edition, current serious and unstable somatic disease or a history of neurologic or other chronic medical conditions, a history of substance abuse or dependence, breast-feeding, and pregnancy. Recruitment was carried out at the Affiliated Brain Hospital of Guangzhou Medical University, Guangzhou, China. Ethics approval was obtained from the ethics committees of the Affiliated Brain Hospital of Guangzhou Medical University. In addition, healthy volunteers (n = 48) recruited from the local community served as HCs. Informed consent was signed by all participants before participating in this study.

Assessment of Suicidal Ideation and Depression

The severity of depressive symptoms was assessed using the 17-item HAMD. All raters were masters- or doctoral-level psychiatrists who had undergone training on performing the HAMD-17 before the study to maintain inter-rater reliability, and they all showed an intra-class correlation coefficient > 0.9. The Scale for Suicidal Ideation (SSI) was used to assess the presence and intensity of SI according to 19 items (Beck et al., 1979). Each item has three alternative statements graded from 0 to 2, with the total score ranging from 0 to 38 points, with higher scores indicating greater SI. In this study, the patients with MDD were classified into an SI group (SSI > 3) and a no SI (NSI) group (SSI $\leq$ 3). This threshold has been described as a clinically significant cutoff for SI in previous studies (Holi et al., 2005; Ballard et al., 2015; Grunebaum et al., 2018).

Magnetic Resonance Imaging Data Acquisition

Participants underwent resting-state fMRI on a 3T Philips Achieva MRI Scanner (Philips, Netherlands). Whole-brain fMRI was acquired using a gradient-echo echo planar imaging sequence with the following parameters: repetition time (TR) = 2,000 ms, echo time = 30 ms, flip angle = 90°, slice thickness = 4 mm, number of slices = 33, and field of view = 220 mm × 220 mm. A total of 240 functional volumes were acquired in 8 min. During the MRI scans, all participants were instructed to keep their eyes closed but stay awake.

Resting-State Functional Magnetic Resonance Imaging Preprocessing

Functional image preprocessing was performed using the Data Processing Assistant for Resting-State fMRI (DPARSF[1]) implemented in MATLAB (version R2013b). For each participant, the first 10 functional volumes were removed to ensure signal stabilization, then the remaining 230 volumes were corrected for timing differences between slices. The motion-corrected functional images were conducted using a six motion parameter (rigid body). Notably, the mean framewise displacement (FD) based on the Jenkinson model (FD-Jenkinson) was computed by averaging the FD from every time point for each participant (Jenkinson et al., 2002). Participants with more than 3 mm of head movement or 3° of rotation were excluded. The images were then spatially normalized to the standard Montreal Neurological Institute echo planar imaging template and resampled to 3 mm × 3 mm × 3 mm. After spatial normalization, the images were smoothed using a 4-mm full-width at half-maximum Gaussian kernel. Subsequently, we treated the six parameters from the rigid-body translation, the white matter signal, and the CSF signal as nuisance covariates to be regressed out. Finally, the images were filtered with a temporal band-pass filter of 0.01–0.08 Hz.

Dynamic Functional Connectivity Analysis

Bilateral dPCC and bilateral vPCC regions of interest (ROIs) were derived from the Brainnetome Atlas ([2]**Figure 1**). dFC analysis was conducted using a sliding-window approach in the DPABI software[3]. The sliding-window method was performed to explore time-varying changes in functional connectivity during resting-state fMRI scans. The resting-state blood oxygenation level-dependent (BOLD) time series was segmented into 50 TR windows with a size of 100 s. A sliding window with a step size of 1 TR was applied, resulting in 181 consecutive windows across the entire scan. We chose a window length of 50 TR (100 s) with a step size of 1 TR (2 s) because it has been shown to be able to maintain a balance between capturing rapidly shifting dynamic relationships and obtaining steady correlations (Leonardi and Van De Ville, 2015; Shunkai et al., 2021). For each window, correlation z maps were calculated between the truncated time course of the ROI and all other voxels using Fisher's z—transformed Pearson correlation coefficient, resulting in 181 sliding-window correlation z maps across the entire scan for each participant. Consequently, the dFC was estimated by calculating the standard deviation (SD) of the z maps across the 181 windows, and z-standardization was then applied to the dFC maps. Finally, all dFC maps were spatially smoothed using a Gaussian kernel of 4 mm × 4 mm × 4 mm full-width at half maximum. To further validate the reliability of the results, we also analyzed other window sizes of 30 and 70 TR (Liao et al., 2014).

Statistical Analyses

Demographic and clinical data were tested for normality using the Shapiro–Wilk or Kolmogorov–Smirnov normality test. If demographic and clinical data passed the normality test, a Student's t-test or one-way ANOVA was used, whereas a Mann–Whitney test was performed if data were not normally

[1]http://rfmri.org/DPARSF

[2]http://www.brainnetome.org/

[3]http://rfmri.org/dpabi

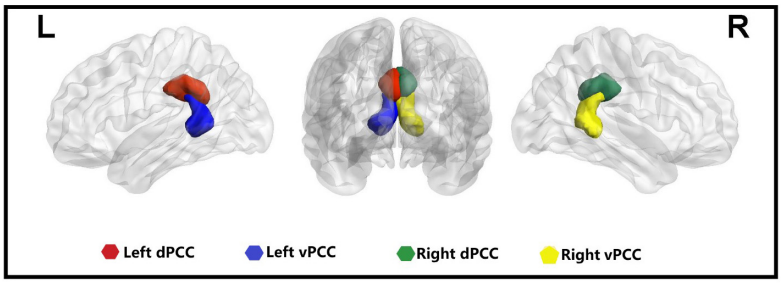

FIGURE 1 | Four seeds of the posterior cingulate cortex in the bilateral hemisphere. L, left; R, right; dPCC, dorsal posterior cingulate cortex; vPCC, ventral posterior cingulate cortex.

distributed. Chi-square tests or Fisher exact tests were used for categorical variables. Statistical calculations were carried out using Statistical Package for the Social Sciences 24.0 (SPSS Inc., NY, United States).

To identify the within-group dFC patterns of each PCC subregion, one-sample *t*-tests were conducted in the SI, NSI, and HC groups ($p < 0.05$, uncorrected). For each PCC subregion, analysis of covariance (ANCOVA) was used to test for between−group differences in dFC maps within the union mask of one-sample *t*-tests of the SI, NSI, and HC groups. Age, gender, and mean FD were treated as covariates. All statistical maps were corrected for multiple comparisons using Gaussian random field (GRF) correction (cluster significance $p < 0.05/4 = 0.0125$, voxel significance $p < 0.005$) performed using DPABI software. The mean *z*-scores of brain regions showing significant differences among the three groups were extracted for further *post hoc* analyses ($p < 0.05$, Bonferroni correction test). Finally, correlations between clinical variables (SSI scores and HAMD without suicide) and the aberrant dFC variability measurements were performed in the patients with MDD using Spearman correlation ($p < 0.05$, Bonferroni-corrected test).

RESULTS

Demographic and Clinical Characteristics

There were no significant differences in gender, mean FD, and age between the SI, NSI, and HC groups (all $p > 0.05$). In addition, no significant differences were found in education, duration of illness, and age of onset between the SI and NSI groups (all $p > 0.05$). However, we found significant differences in the scores of HAMD-17, HAMD-17 without suicide, and SSI between the SI and NSI groups (all $p < 0.05$). The detailed demographic and clinical features of the participants are presented in **Table 1**.

Dynamic Functional Connectivity Variability in the Posterior Cingulate Cortex Subregions

The dFC variability of each PCC subregion, as derived from the one-sample *t*-tests, is shown separately for the three groups in **Figure 2** ($p < 0.05$, uncorrected). Significant differences in dFC variability between the three groups were observed between the left dPCC and left fusiform gyrus, left vPCC and left IFG, and right vPCC and left IFG (**Table 2** and **Figure 3A**; GRF corrected, cluster significance $p < 0.0125$, voxel significance $p < 0.005$). However, no significant differences were found in the whole-brain dFC variability of the right dPCC between the three groups. The results of the *post hoc* analysis on the brain regions showing significant differences are shown in **Figure 3B** ($p < 0.05$, Bonferroni-corrected test). Compared with the HCs, the SI and NSI groups showed higher dFC variability between the left dPCC and left fusiform gyrus and between the right vPCC and left IFG. The SI group exhibited higher dFC variability between the left vPCC and left IFG than the NSI group.

Correlation Analyses

The dFC variability between the left vPCC and left IFG was positively correlated with the SSI scores of all patients with MDD (i.e., the SI group and NSI group combined; $r = 0.254$, Bonferroni-corrected $p = 0.048$; **Figure 4**). However, no correlation was observed between dFC and SSI scores within the SI group ($r = 0.102$, $p = 0.572$) or within the NSI group ($r = 0.020$, $p = 0.886$). There were no significant correlations between HAMD without suicide scores and dFC variability between the left vPCC and left IFG in patients with MDD. Furthermore, no significant correlations were found between other significantly different dFC variability subregions and the scores of SSI and HAMD without suicide in patients with MDD.

Validation Analysis

The results of the 30-TR sliding-window length analysis validated the main results (50 TRs; see **Supplementary Figure 1** and **Supplementary Table 1**). However, no significant differences were observed with the 70-TR sliding-window length.

DISCUSSION

To our knowledge, this study is the first to report aberrant dFC variability of PCC subregions in MDD patients with SI. Aberrant dFC variability between the left vPCC and left IFG was observed in MDD patients with SI in comparison with those with

TABLE 1 | Demographic and clinical features of subjects.

Variables	SI	NSI	HCs	*T*/*Z*/*F*/χ^2	*P*-value
Numbers of subjects	33	56	48		–
Gender (male/female)	10/23	27/29	23/25	3.216	0.200[a]
Age (years)	24.52 ± 5.82	26.04 ± 5.13	27.54 ± 5.95	2.900	0.059[b]
Education (years)	13.09 ± 2.98	13.14 ± 3.00	NA	−0.079	0.937[c]
Duration of illness (month)	30.17 ± 24.06	23.26 ± 21.89	NA	1.618	0.106[d]
Age of onset	22.03 ± 6.26	24.21 ± 5.09	NA	−1.793	0.076[c]
HAMD-17	26.21 ± 5.32	22.21 ± 4.23	NA	3.685	0.001[c]**
HAMD-17 without suicide	23.61 ± 5.37	21.23 ± 4.21	NA	2.177	0.034[c]*
SSI	15.88 ± 5.69	0.95 ± 1.05	NA	7.971	<0.001[d]***
Mean framewise displacement	0.05 ± 0.02	0.05 ± 0.02	0.06 ± 0.02	0.419	0.658[b]

SI, major depressive patients with suicidal ideation; NSI, major depressive patients without suicidal ideation; HCs, healthy controls; HAMD-17, the 17-item Hamilton Depression Rating Scale; SSI, scale for suicide ideation.
[a]*Chi-square test.*
[b]*One-way ANOVA.*
[c]*Two-sample t-test.*
[d]*Mann–Whitney U test.*
**p < 0.05, **p < 0.01, ***p < 0.001.*

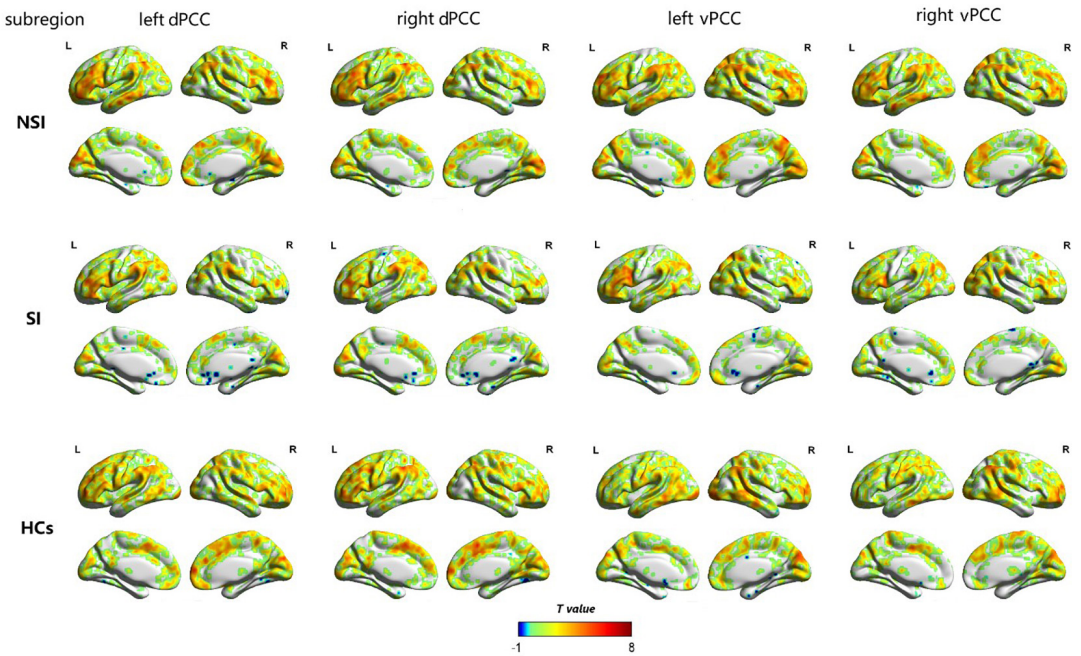

FIGURE 2 | The dFC variability patterns of the bilateral dorsal posterior cingulate cortex (dPCC) and the bilateral ventral posterior cingulate cortex (vPCC) within NSI, SI and HCs groups ($p < 0.05$, uncorrected). The color bar represents a dynamic functional connection. dFC, dynamic functional connectivity; dPCC, dorsal posterior cingulate cortex; vPCC, ventral posterior cingulate cortex; SI, major depressive patients with suicidal ideation; NSI, major depressive patients without suicidal ideation; HCs, healthy controls.

MDD patients without SI, while dFC variability abnormalities between the left dPCC and left fusiform gyrus, right vPCC, and left IFG were detected in MDD patients with SI relative to HCs. Furthermore, we confirmed the relationship between dFC abnormalities of the vPCC subregion and SI severity in patients with MDD. Overall, our findings reveal alterations in dFC variability between brain regions and demonstrate that SI is linked to aberrant dFC variability in patients with MDD. Our data advance the understanding of the potential neurobiological mechanisms of MDD with SI and point to options for clinical diagnostic biomarkers in the future.

Aberrant Dynamic Functional Connectivity Variability in dPCC

The PCC has previously been subdivided into dorsal and ventral regions on the basis of post-mortem cytology measurements (Vogt et al., 2006). Each of the PCC subregions has distinct

TABLE 2 | The areas of significantly different dFC among the SI, NSI, and HCs group (voxel $p < 0.005$, cluster $p < 0.0125$, GRF corrected).

Subregion	Significant regions	MNI coordinates			Voxel size (mm^3)	*F*-value
		X	*Y*	*Z*		
Left dPCC	Left Fusiform	−27	−57	−12	486	15.345
Left vPCC	Left inferior frontal gyrus	−45	9	24	513	11.637
Right vPCC	Left inferior frontal gyrus	−42	9	21	459	11.122

SI, major depressive patients with suicidal ideation; NSI, major depressive patients without suicidal ideation; HCs, healthy controls; dPCC, dorsal posterior cingulate cortex; vPCC, ventral posterior cingulate cortex.

cytoarchitecture, patterns of structural connectivity, and resting-state functional connectivity (Vogt and Laureys, 2005; Margulies et al., 2009). It was suggested that the dPCC plays an important role in visual space and executive control of behavior (Vogt et al., 2006). In the current study, relative to HCs, both MDD patients with and without SI showed higher dFC variability between the left dPCC and left fusiform gyrus. However, no significant difference was observed between MDD patients with SI and MDD patients without SI. Our findings reflect the pathological effect of MDD on altered dFC patterns. The dPCC and fusiform gyrus are consistently reported to be involved in many aspects of cognition, such as word recognition, processing of color information (Weiner and Grill-Spector, 2010), and attentional focus (Leech and Sharp, 2014). Since these brain regions play a major role in cognition, the disrupted dFC variability between the left dPCC and left fusiform gyrus might contribute to negative self-perceptions and confer negative emotions (Schniering and Rapee, 2004) in depressed individuals. Our results highlight the idea that the dFC of key brain regions (such as the dPCC and left fusiform gyrus) in patients with MDD might show abnormalities and thus constitute a neurophysiological basis for the decreased ability to react flexibly to external or internal cognitive demands (Hamilton et al., 2011; Hutchison et al., 2013). Scholars have consistently proposed an analogous viewpoint. For example, Luo et al. (2021) detected decreased temporal variability of the dynamic index of bilateral PCC in patients with MDD in comparison with HCs, while other recent studies have reported dynamic alterations in brain activity in the fusiform gyrus in patients with MDD (Hou et al., 2018; Xue et al., 2020; Zhang et al., 2021). Therefore, it is plausible to consider that the observed anomalous dFC between the dPCC and fusiform gyrus is a neurobiological feature of patients with MDD. In conclusion, our findings could further enhance our understanding of how dFC properties support normal brain functions in patients with MDD.

Aberrant Dynamic Functional Connectivity Variability in vPCC

In the current study, when compared with HCs, MDD patients with SI showed higher dFC variability between the left dPCC and the left IFG and between the right vPCC and left IFG. Moreover, relative to MDD patients without SI, MDD patients with SI showed higher dFC between the left vPCC and left IFG. Our data suggest that disrupted dFC between the vPCC and IFG may provide clues to the representation of neurocognition in MDD patients with SI. The vPCC is at an intermediate stage of information processing between visual recognition and emotion-related substrate (Johnson et al., 2002; Uddin et al., 2005). Interestingly, deficits in interference processing and learning/memory constitute an enduring defect in information processing in MDD patients with SI (Keilp et al., 2014). A previous study indicated that MDD patients with suicidal thoughts and behaviors showed structural and functional abnormalities in the PCC (Dombrovski et al., 2013; Peng et al., 2014).

Our findings could also be interpreted from a broader perspective. It is well known that the vPCC plays a key role in the default mode network (responsible for the processing of rumination) (Leech et al., 2011), while the IFG is the center hub of the frontoparietal network (responsible for handling behavioral inhibition) (Corbetta and Shulman, 2002). Thus, aberrant dFC between the vPCC and IFG in MDD patients with SI could constitute a high-risk circumstance in which the SI is converted to lethal action *via* impaired top-down behavior inhibition and impulsive decision-making (Schmaal et al., 2020). Hence, we conclude that the observed abnormal dFC variability in the MDD patients reveals impaired connectivity between the default mode network and frontoparietal network, which might relate to the potential neurobiological mechanisms of SI. In line with our findings, experimental evidence demonstrates altered dFC between the default mode network and frontoparietal network in patients with MDD (Demirtas et al., 2016; Yao et al., 2019). Furthermore, Liao et al. (2018) quantified dynamic connectomic variability using topological properties in patients with MDD with SI and found that the topological properties of dynamic connectomics could not only distinguish MDD patients with and without SI but could also predict the degree of SI. Congruent with previous findings, we suggest that the aberrant dFC might be regarded as a neurobiological feature for use in predictive and diagnostic models in patients with MDD with SI.

Correlations Between Aberrant Dynamic Functional Connectivity Variability and Clinical Variables

We confirmed an association between dFC variability in the left vPCC subregion and SI severity in patients with MDD. However, we observed no correlation between dFC variability in the left vPCC subregion and the scores of HAMD without suicide in the patients with MDD. With regard to our finding that dFC variability is associated with SI severity but not with MDD severity (measured by the HAMD score without the SI part), we speculate that this may reflect the substantial impact

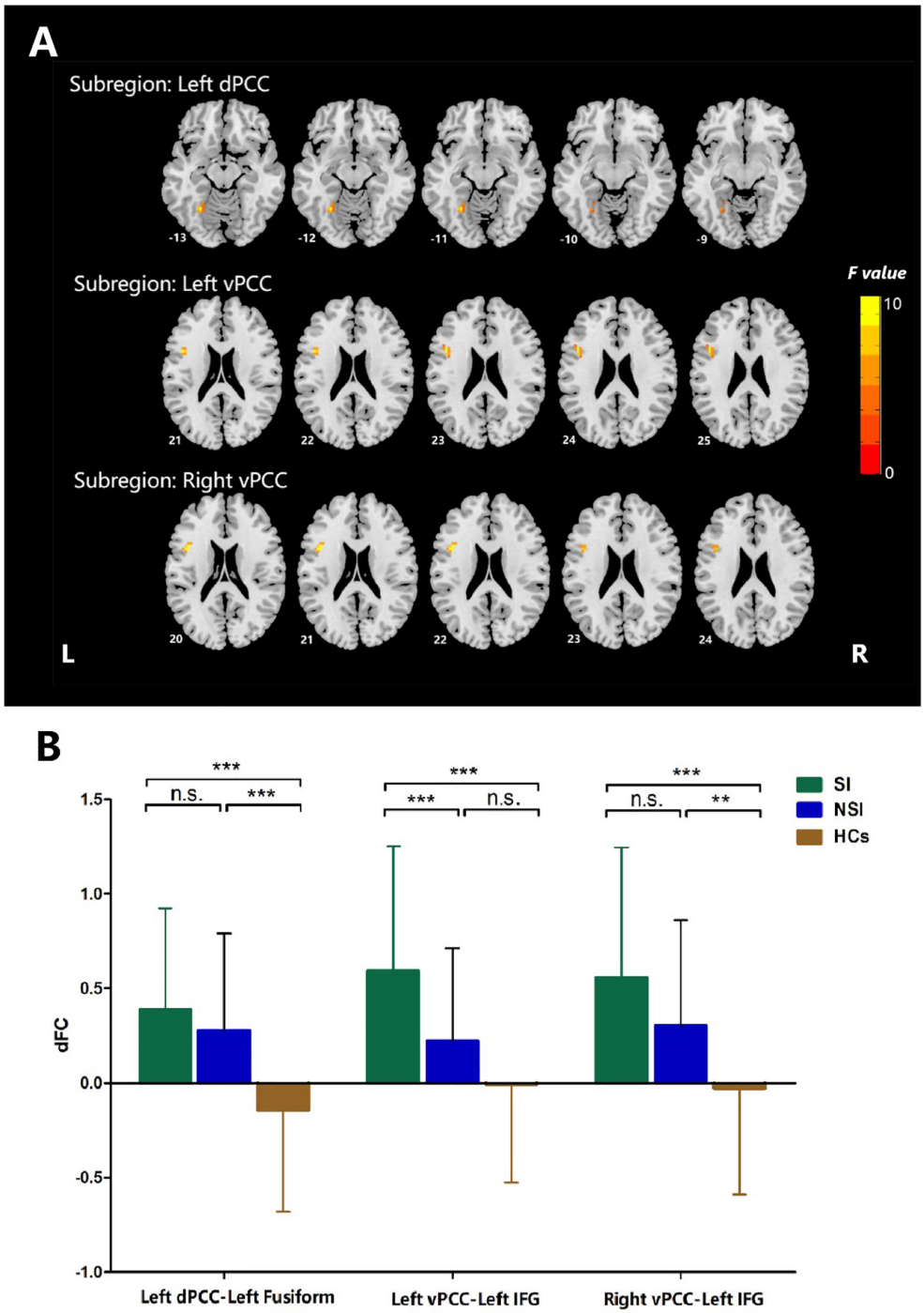

FIGURE 3 | ANCOVA analyses of dFC values among three groups when taking the subregion of posterior cingulate cortex as a seed. **(A)** Brain regions with significant differences among three groups, voxel $p < 0.005$, cluster $p < 0.0125$, GRF corrected. **(B)** *Post hoc* analyses of dFC values among three groups. Bonferroni corrected. dFC, dynamic functional connectivity; vPCC, ventral posterior cingulate cortex; dPCC, dorsal posterior cingulate cortex; IFG, inferior frontal gyrus; SI, major depressive patients with suicidal ideation; NSI, major depressive patients without suicidal ideation; HCs, heathy controls. n.s., not significant. $^{**}p < 0.01$, $^{***}p < 0.001$.

of SI on brain dysfunction, rather than the pathological effects of the disease. Our findings support the idea that SI severity is related to anomalous dFC variability in patients with MDD. Schmaal et al. (2020) reviewed neuroimaging investigations across different mental illnesses for brain function, structural, and molecular alterations showing associations with suicidal thoughts

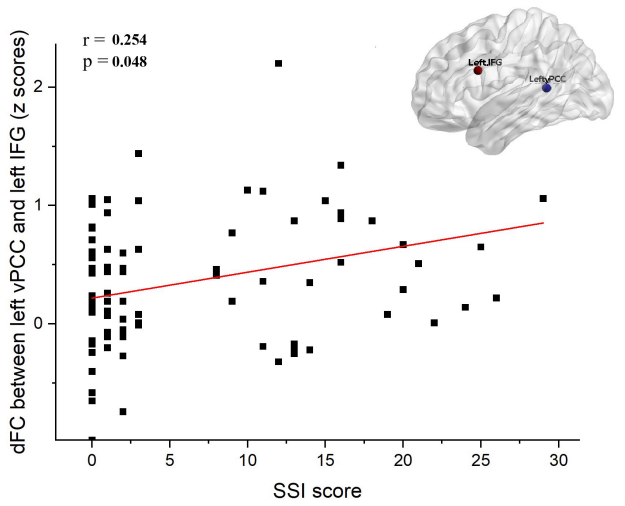

FIGURE 4 | Correlation analysis between dFC and SSI score in depressed subjects (i.e., SI group and NSI group). The dFC between the between left vPCC and left IFG was positively associated with SSI score (r = 0.254, Bonferroni-corrected p = 0.048). SI, major depressive patients with suicidal ideation; NSI, major depressive patients without suicidal ideation; dFC, dynamic functional connectivity; vPCC, ventral posterior cingulate cortex; IFG, inferior frontal gyrus; SSI, scale for suicide ideation.

and behaviors. They found that brain dysfunctions particularly converged in brain areas processing visual recognition and emotion regulation, such as the vPCC. Analogously, Auerbach et al. (2021) reported that altered vPCC volume was associated with SI and non-suicidal self-injury. Overall, we expect that the anomalous dFC variability in the left vPCC subregion underlies an emotional imbalance in individuals with SI. Collectively, the anomalous dFC variability in the left vPCC subregion may reflect SI severity, rather than illness *per se*.

There are several limitations to the current study. First, our study is a cross-sectional analysis, which restricts causal interpretations and longitudinal tracking of SI. Second, we compared the dFC variability differences between HCs and MDD patients with or without SI but did not include MDD patients with SA, who frequently show PCC dysfunction. A previous study reported that young depressed patients with SA exhibited lower PCC gray matter volume relative to HCs (Peng et al., 2014). In addition, decreased activity was found in the PCC during cognitive control in patients with mood disorders with SA (Minzenberg et al., 2015), and patients with MDD with SA exhibited an increased PCC response relative to HCs during the viewing of knives (Kim Y. J. et al., 2017). Furthermore, MDD patients with SA exhibited increased functional connectivity between the dPCC and left IFG when compared with MDD patients but without SA (Kim Y. J. et al., 2017). Thus, it would be meaningful to conduct a direct comparison of the dFC of PCC subregions between patients with SI and those with SA. Third, we acknowledge that our findings must be interpreted with caution because of the relatively small sample size. Finally, because of limitations resulting from the small sample size, we could not confirm the relationship between the dFC of the left vPCC subregion and SI severity in MDD patients with and without SI. The robustness of the left vPCC-left IFG contribution to SI needs further validation. Future studies with greater sample sizes that include longitudinal designs and across different mental illnesses are needed to corroborate our findings.

CONCLUSION

Using dFC variability analyses of PCC subregions, we found that MDD patients with SI showed higher dFC between the left PCC and left IFG than those with MDD without SI. Moreover, the dFC variability positively correlated with SSI scores within all patients with MDD. The observed dFC abnormalities between vPCC and IFG might provide a neural-network explanation for SI and may provide new clues on the potential neurophysiological mechanisms of MDD with SI.

DATA AVAILABILITY STATEMENT

The original contributions presented in this study are included in the article/**Supplementary Material**, further inquiries can be directed to the corresponding authors.

ETHICS STATEMENT

The studies involving human participants were reviewed and approved by the Ethics Committees of Affiliated Brain Hospital of Guangzhou Medical University. The patients/participants provided their written informed consent to participate in this study.

AUTHOR CONTRIBUTIONS

WL: investigation, formal analysis, writing – original draft, and visualization. CW and XL: validation, methodology, and investigation. FZ, LF, YY, and HL: investigation. KW, GHL, JC, and GXL: conceptualization. YZ: validation, project administration, methodology, and investigation. YN: conceptualization, supervision, and writing – review and editing. All authors contributed to the article and approved the submitted version.

FUNDING

This work was supported by the National Natural Science Foundation of China (Grant Number: 81801343), the Guangdong Basic and Applied Basic Research Foundation (Grant Number: 2019A151501136), Science and Technology Plan Project of Guangdong Province (Grant Number: 2019B030316001), Guangdong Medical Science and Technology Research project (Grant Number: B2020178), Guangdong Basic and Applied Basic Research Foundation Outstanding Youth Project (Grant Number: 2021B1515020064), Science

and Technology Plan Project of Guangzhou (Grant Number: 202102020557), and Guangzhou municipal key discipline in medicine (2017–2019). The funding source had no role in the study design, analysis, or interpretation of data or in the preparation of the report or decision to publish.

SUPPLEMENTARY MATERIAL

The Supplementary Material for this article can be found online at: https://www.frontiersin.org/articles/10.3389/fnins.2022.937145/full#supplementary-material

REFERENCES

Allen, E. A., Damaraju, E., Plis, S. M., Erhardt, E. B., Eichele, T., and Calhoun, V. D. (2014). Tracking whole-brain connectivity dynamics in the resting state. *Cereb. Cortex* 24, 663–676. doi: 10.1093/cercor/bhs352

Ambrosi, E., Arciniegas, D. B., Curtis, K. N., Patriquin, M. A., Spalletta, G., Sani, G., et al. (2019). Resting-State functional connectivity of the habenula in mood disorder patients with and without Suicide-Related behaviors. *J. Neuropsychiatr. Clin. Neurosci.* 31, 49–56. doi: 10.1176/appi.neuropsych.17120351

Auerbach, R. P., Pagliaccio, D., Allison, G. O., Alqueza, K. L., and Alonso, M. F. (2021). Neural correlates associated with suicide and nonsuicidal self-injury in youth. *Biol. Psychiatr.* 89, 119–133. doi: 10.1016/j.biopsych.2020.06.002

Ballard, E. D., Luckenbaugh, D. A., Richards, E. M., Walls, T. L., Brutsché, N. E., Ameli, R., et al. (2015). Assessing measures of suicidal ideation in clinical trials with a rapid-acting antidepressant. *J. Psychiatr. Res.* 68, 68–73. doi: 10.1016/j.jpsychires.2015.06.003

Beck, A. T., Kovacs, M., and Weissman, A. (1979). Assessment of suicidal intention: the Scale for Suicide Ideation. *J. Consult. Clin. Psychol.* 47, 343–352. doi: 10.1037//0022-006x.47.2.343

Buckner, R. L., Andrews-Hanna, J. R., and Schacter, D. L. (2008). The brain's default network: anatomy, function, and relevance to disease. *Ann. N. Y. Acad. Sci.* 1124, 1–38. doi: 10.1196/annals.1440.011

Chahine, M., Salameh, P., Haddad, C., Sacre, H., Soufia, M., Akel, M., et al. (2020). Suicidal ideation among Lebanese adolescents: scale validation, prevalence and correlates. *BMC Psychiatr.* 20:304. doi: 10.1186/s12888-020-02726-6

Chase, H. W., Auerbach, R. P., Brent, D. A., Posner, J., Weissman, M. M., and Talati, A. (2021). Dissociating default mode network resting state markers of suicide from familial risk factors for depression. *Neuropsychopharmacology* 46, 1830–1838. doi: 10.1038/s41386-021-01022-5

Chase, H. W., Segreti, A. M., Keller, T. A., Cherkassky, V. L., Just, M. A., Pan, L. A., et al. (2017). Alterations of functional connectivity and intrinsic activity within the cingulate cortex of suicidal ideators. *J. Affect. Disord.* 212, 78–85. doi: 10.1016/j.jad.2017.01.013

Corbetta, M., and Shulman, G. L. (2002). Control of goal-directed and stimulus-driven attention in the brain. *Nat. Rev. Neurosci.* 3, 201–215. doi: 10.1038/nrn755

Demirtas, M., Tornador, C., Falcon, C., Lopez-Sola, M., Hernandez-Ribas, R., Pujol, J., et al. (2016). Dynamic functional connectivity reveals altered variability in functional connectivity among patients with major depressive disorder. *Hum. Brain Mapp.* 37, 2918–2930. doi: 10.1002/hbm.23215

Dombrovski, A. Y., Szanto, K., Clark, L., Reynolds, C. F., and Siegle, G. J. (2013). Reward signals, attempted suicide, and impulsivity in late-life depression. *JAMA Psychiat.* 70:1. doi: 10.1001/jamapsychiatry.2013.75

Ebisch, S., Gallese, V., Salone, A., Martinotti, G., di Iorio, G., Mantini, D., et al. (2018). Disrupted relationship between "resting state" connectivity and task-evoked activity during social perception in schizophrenia. *Schizophr. Res.* 193, 370–376. doi: 10.1016/j.schres.2017.07.020

Espinoza, F. A., Liu, J., Ciarochi, J., Turner, J. A., Vergara, V. M., Caprihan, A., et al. (2019). Dynamic functional network connectivity in Huntington's disease and its associations with motor and cognitive measures. *Hum. Brain Mapp.* 40, 1955–1968. doi: 10.1002/hbm.24504

Fan, L., Li, H., Zhuo, J., Zhang, Y., Wang, J., Chen, L., et al. (2016). The human brainnetome atlas: a new brain atlas based on connectional architecture. *Cereb. Cortex* 26, 3508–3526. doi: 10.1093/cercor/bhw157

Greicius, M. D., Krasnow, B., Reiss, A. L., and Menon, V. (2003). Functional connectivity in the resting brain: a network analysis of the default mode hypothesis. *Proc. Natl. Acad. Sci. U.S.A.* 100, 253–258. doi: 10.1073/pnas.0135058100

Grunebaum, M. F., Galfalvy, H. C., Choo, T. H., Keilp, J. G., Moitra, V. K., Parris, M. S., et al. (2018). Ketamine for rapid reduction of suicidal thoughts in major depression: a Midazolam-Controlled randomized clinical trial. *Am. J. Psychiatr.* 175, 327–335. doi: 10.1176/appi.ajp.2017.17060647

Hamilton, J. P., Chen, G., Thomason, M. E., Schwartz, M. E., and Gotlib, I. H. (2011). Investigating neural primacy in Major Depressive Disorder: multivariate Granger causality analysis of resting-state fMRI time-series data. *Mol. Psychiatr.* 16, 763–772. doi: 10.1038/mp.2010.46

Helmreich, I., Wagner, S., Mergl, R., Allgaier, A. K., Hautzinger, M., Henkel, V., et al. (2012). Sensitivity to changes during antidepressant treatment: a comparison of unidimensional subscales of the Inventory of Depressive Symptomatology (IDS-C) and the Hamilton Depression Rating Scale (HAMD) in patients with mild major, minor or subsyndromal depression. *Eur. Arch. Psychiatry Clin. Neurosci.* 262, 291–304. doi: 10.1007/s00406-011-0263-x

Holi, M. M., Pelkonen, M., Karlsson, L., Kiviruusu, O., Ruuttu, T., Heilä, H., et al. (2005). Psychometric properties and clinical utility of the Scale for Suicidal Ideation (SSI) in adolescents. *BMC Psychiatr.* 5:8. doi: 10.1186/1471-244X-5-8

Hong, S., Liu, Y. S., Cao, B., Cao, J., Ai, M., Chen, J., et al. (2021). Identification of suicidality in adolescent major depressive disorder patients using sMRI: a machine learning approach. *J. Affect. Disord.* 280(Pt), 72–76. doi: 10.1016/j.jad.2020.10.077

Hou, Z., Kong, Y., He, X., Yin, Y., Zhang, Y., and Yuan, Y. (2018). Increased temporal variability of striatum region facilitating the early antidepressant response in patients with major depressive disorder. *Prog. Neuropsychopharmacol. Biol. Psychiatr.* 85, 39–45. doi: 10.1016/j.pnpbp.2018.03.026

Hutchison, R. M., Womelsdorf, T., Allen, E. A., Bandettini, P. A., Calhoun, V. D., Corbetta, M., et al. (2013). Dynamic functional connectivity: promise, issues, and interpretations. *Neuroimage* 80, 360–378. doi: 10.1016/j.neuroimage.2013.05.079

Ilgen, M. A., Bohnert, A. S., Ignacio, R. V., McCarthy, J. F., Valenstein, M. M., Kim, H. M., et al. (2010). Psychiatric diagnoses and risk of suicide in veterans. *Arch. Gen. Psychiatr.* 67, 1152–1158. doi: 10.1001/archgenpsychiatry.2010.129

Jenkinson, M., Bannister, P., Brady, M., and Smith, S. (2002). Improved optimization for the robust and accurate linear registration and motion correction of brain images. *Neuroimage* 17, 825–841. doi: 10.1016/s1053-8119(02)91132-8

Johnson, M. K., Nolen-Hoeksema, S., Mitchell, K. J., and Levin, Y. (2009). Medial cortex activity, self-reflection and depression. *Soc. Cogn. Affect. Neurosci.* 4, 313–327. doi: 10.1093/scan/nsp022

Johnson, S. C., Baxter, L. C., Wilder, L. S., Pipe, J. G., Heiserman, J. E., and Prigatano, G. P. (2002). Neural correlates of self-reflection. *Brain* 125(Pt 8), 1808–1814. doi: 10.1093/brain/awf181

Keilp, J. G., Beers, S. R., Burke, A. K., Melhem, N. M., Oquendo, M. A., Brent, D. A., et al. (2014). Neuropsychological deficits in past suicide attempters with varying levels of depression severity. *Psychol. Med.* 44, 2965–2974. doi: 10.1017/S0033291714000786

Kim, J., Criaud, M., Cho, S. S., Diez-Cirarda, M., Mihaescu, A., Coakeley, S., et al. (2017). Abnormal intrinsic brain functional network dynamics in Parkinson's disease. *Brain* 140, 2955–2967. doi: 10.1093/brain/awx233

Kim, Y. J., Park, H. J., Jahng, G. H., Lee, S. M., Kang, W. S., Kim, S. K., et al. (2017). A pilot study of differential brain activation to suicidal means and DNA methylation of CACNA1C gene in suicidal attempt patients. *Psychiatr. Res.* 255, 42–48. doi: 10.1016/j.psychres.2017.03.058

Klonsky, E. D., and May, A. M. (2014). Differentiating suicide attempters from suicide ideators: a critical frontier for suicidology research. [Introductory Journal Article]. *Suicide Life Threat Behav.* 44, 1–5. doi: 10.1111/sltb.12068

Klonsky, E. D., May, A. M., and Saffer, B. Y. (2016). Suicide, suicide attempts, and suicidal ideation. *Annu. Rev. Clin. Psychol.* 12, 307–330. doi: 10.1146/annurev-clinpsy-021815-093204

Kucyi, A., Hove, M. J., Esterman, M., Hutchison, R. M., and Valera, E. M. (2017). Dynamic brain network correlates of spontaneous fluctuations in attention. *Cereb. Cortex* 27, 1831–1840. doi: 10.1093/cercor/bhw029

Lan, X., Zhou, Y., Wu, F., Wu, K., Zhan, Y., Wang, C., et al. (2021). The relationship between plasma cytokine levels and antidepressant response in patients with first-episode major depressive disorder. *J. Affect. Disord.* 287, 327–333. doi: 10.1016/j.jad.2021.03.036

Lau, W., Leung, M. K., and Lau, B. (2019). Resting-state abnormalities in Autism Spectrum Disorders: a meta-analysis. *Sci. Rep.* 9:3892. doi: 10.1038/s41598-019-40427-7

Leech, R., Kamourieh, S., Beckmann, C. F., and Sharp, D. J. (2011). Fractionating the default mode network: distinct contributions of the ventral and dorsal posterior cingulate cortex to cognitive control. *J. Neurosci.* 31, 3217–3224. doi: 10.1523/JNEUROSCI.5626-10.2011

Leech, R., and Sharp, D. J. (2014). The role of the posterior cingulate cortex in cognition and disease. *Brain* 137(Pt 1), 12–32. doi: 10.1093/brain/awt162

Leonardi, N., and Van De Ville, D. (2015). On spurious and real fluctuations of dynamic functional connectivity during rest. *Neuroimage* 104, 430–436. doi: 10.1016/j.neuroimage.2014.09.007

Liao, W., Li, J., Duan, X., Cui, Q., Chen, H., and Chen, H. (2018). Static and dynamic connectomics differentiate between depressed patients with and without suicidal ideation. *Hum. Brain Mapp.* 39, 4105–4118. doi: 10.1002/hbm.24235

Liao, W., Wu, G. R., Xu, Q., Ji, G. J., Zhang, Z., Zang, Y. F., et al. (2014). DynamicBC: a MATLAB toolbox for dynamic brain connectome analysis. *Brain Connect.* 4, 780–790. doi: 10.1089/brain.2014.0253

Luo, Z., Chen, G., Jia, Y., Zhong, S., Gong, J., Chen, F., et al. (2021). Shared and specific dynamics of brain segregation and integration in bipolar disorder and major depressive disorder: a resting-state functional magnetic resonance imaging study. *J. Affect. Disord.* 280, 279–286. doi: 10.1016/j.jad.2020.11.012

Lurie, D. J., Kessler, D., Bassett, D. S., Betzel, R. F., Breakspear, M., Kheilholz, S., et al. (2020). Questions and controversies in the study of time-varying functional connectivity in resting fMRI. *Netw. Neurosci.* 4, 30–69. doi: 10.1162/netn_a_00116

Marchand, W. R., Lee, J. N., Johnson, S., Gale, P., and Thatcher, J. (2013). Differences in functional connectivity in major depression versus bipolar II depression. *J. Affect. Disord.* 150, 527–532. doi: 10.1016/j.jad.2013.01.028

Margulies, D. S., Vincent, J. L., Kelly, C., Lohmann, G., Uddin, L. Q., Biswal, B. B., et al. (2009). Precuneus shares intrinsic functional architecture in humans and monkeys. *Proc .Natl. Acad. Sci. U.S.A.* 106, 20069–20074. doi: 10.1073/pnas.0905314106

Matsumoto, R., Ito, H., Takahashi, H., Ando, T., Fujimura, Y., Nakayama, K., et al. (2010). Reduced gray matter volume of dorsal cingulate cortex in patients with obsessive-compulsive disorder: a voxel-based morphometric study. *Psychiatr. Clin. Neurosci.* 64, 541–547. doi: 10.1111/j.1440-1819.2010.02125.x

Minzenberg, M. J., Lesh, T. A., Niendam, T. A., Yoon, J. H., Cheng, Y., Rhoades, R. N., et al. (2015). Control-related frontal-striatal function is associated with past suicidal ideation and behavior in patients with recent-onset psychotic major mood disorders. *J. Affect. Disord.* 188, 202–209. doi: 10.1016/j.jad.2015.08.049

Parvizi, J., Braga, R. M., Kucyi, A., Veit, M. J., Pinheiro-Chagas, P., Perry, C., et al. (2021). Altered sense of self during seizures in the posteromedial cortex. *Proc. Natl. Acad. Sci. U S A* 118:e2100522118. doi: 10.1073/pnas.2100522118

Peng, H., Wu, K., Li, J., Qi, H., Guo, S., Chi, M., et al. (2014). Increased suicide attempts in young depressed patients with abnormal temporal-parietal-limbic gray matter volume. *J. Affect. Disord.* 165, 69–73. doi: 10.1016/j.jad.2014.04.046

Pfefferbaum, A., Chanraud, S., Pitel, A. L., Muller-Oehring, E., Shankaranarayanan, A., Alsop, D. C., et al. (2011). Cerebral blood flow in posterior cortical nodes of the default mode network decreases with task engagement but remains higher than in most brain regions. *Cereb. Cortex* 21, 233–244. doi: 10.1093/cercor/bhq090

Preti, M. G., Bolton, T. A., and Van De Ville, D. (2017). The dynamic functional connectome: state-of-the-art and perspectives. *Neuroimage* 160, 41–54. doi: 10.1016/j.neuroimage.2016.12.061

Quevedo, K., Ng, R., Scott, H., Martin, J., Smyda, G., Keener, M., et al. (2016). The neurobiology of self-face recognition in depressed adolescents with low or high suicidality. *J. Abnorm. Psychol.* 125, 1185–1200. doi: 10.1037/abn0000200

Schmaal, L., van Harmelen, A., Chatzi, V., Lippard, E. T. C., Toenders, Y. J., Averill, L. A., et al. (2020). Imaging suicidal thoughts and behaviors: a comprehensive review of 2 decades of neuroimaging studies. *Mol. Psychiatr.* 25, 408–427. doi: 10.1038/s41380-019-0587-x

Schniering, C. A., and Rapee, R. M. (2004). The relationship between automatic thoughts and negative emotions in children and adolescents: a test of the cognitive content-specificity hypothesis. *J. Abnorm. Psychol.* 113, 464–470. doi: 10.1037/0021-843X.113.3.464

Shunkai, L., Su, T., Zhong, S., Chen, G., Zhang, Y., Zhao, H., et al. (2021). Abnormal dynamic functional connectivity of hippocampal subregions associated with working memory impairment in melancholic depression. *Psychol. Med.* 1–13. [Epub ahead of print]. doi: 10.1017/S0033291721004906

Turecki, G., and Brent, D. A. (2016). Suicide and suicidal behaviour. *Lancet.* 387, 1227–1239. doi: 10.1016/S0140-6736(15)00234-2

Uddin, L. Q., Kaplan, J. T., Molnar-Szakacs, I., Zaidel, E., and Iacoboni, M. (2005). Self-face recognition activates a frontoparietal "mirror" network in the right hemisphere: an event-related fMRI study. *Neuroimage.*25, 926–935. doi: 10.1016/j.neuroimage.2004.12.018

Vanyukov, P. M., Szanto, K., Siegle, G. J., Hallquist, M. N., Reynolds, C. R., Aizenstein, H. J., et al. (2015). Impulsive traits and unplanned suicide attempts predict exaggerated prefrontal response to angry faces in the elderly. *Am. J. Geriatr. Psychiatr.* 23, 829–839. doi: 10.1016/j.jagp.2014.10.004

Vidaurre, D., Llera, A., Smith, S. M., and Woolrich, M. W. (2021). Behavioural relevance of spontaneous, transient brain network interactions in fMRI. *Neuroimage* 229:117713. doi: 10.1016/j.neuroimage.2020.117713

Vogt, B. A., and Laureys, S. (2005). Posterior cingulate, precuneal and retrosplenial cortices: cytology and components of the neural network correlates of consciousness. *Prog. Brain Res.* 150, 205–217. doi: 10.1016/S0079-6123(05)50015-3

Vogt, B. A., Vogt, L., and Laureys, S. (2006). Cytology and functionally correlated circuits of human posterior cingulate areas. *Neuroimage* 29, 452–466. doi: 10.1016/j.neuroimage.2005.07.048

Weiner, K. S., and Grill-Spector, K. (2010). Sparsely-distributed organization of face and limb activations in human ventral temporal cortex. *Neuroimage* 52, 1559–1573. doi: 10.1016/j.neuroimage.2010.04.262

Xu, G., McLaren, D. G., Ries, M. L., Fitzgerald, M. E., Bendlin, B. B., Rowley, H. A., et al. (2009). The influence of parental history of Alzheimer's disease and apolipoprotein E epsilon4 on the BOLD signal during recognition memory. *Brain* 132(Pt 2), 383–391. doi: 10.1093/brain/awn254

Xue, K., Liang, S., Yang, B., Zhu, D., Xie, Y., Qin, W., et al. (2020). Local dynamic spontaneous brain activity changes in first-episode, treatment-naive patients with major depressive disorder and their associated gene expression profiles. *Psychol. Med.* 1–10. [Epub ahead of print]. doi: 10.1017/S0033291720003876

Yao, Z., Shi, J., Zhang, Z., Zheng, W., Hu, T., Li, Y., et al. (2019). Altered dynamic functional connectivity in weakly-connected state in major depressive disorder. *Clin. Neurophysiol.* 130, 2096–2104. doi: 10.1016/j.clinph.2019.08.009

Yoshino, A., Okamoto, Y., Okada, G., Takamura, M., Ichikawa, N., Shibasaki, C., et al. (2018). Changes in resting-state brain networks after cognitive-behavioral therapy for chronic pain. *Psychol. Med.* 48, 1148–1156. doi: 10.1017/S0033291717002598

Zalesky, A., Fornito, A., Cocchi, L., Gollo, L. L., and Breakspear, M. (2014). Time-resolved resting-state brain networks. *Proc. Natl. Acad. Sci. U.S.A.* 111, 10341–10346. doi: 10.1073/pnas.1400181111

Zhang, L., Zhang, R., Han, S., Womer, F. Y., Wei, Y., Duan, J., et al. (2021). Three major psychiatric disorders share specific dynamic alterations of intrinsic brain activity. *Schizophr. Res.* 243, 322–329. doi: 10.1016/j.schres.2021.06.014

Conflict of Interest: The authors declare that the research was conducted in the absence of any commercial or financial relationships that could be construed as a potential conflict of interest.

Publisher's Note: All claims expressed in this article are solely those of the authors and do not necessarily represent those of their affiliated organizations, or those of the publisher, the editors and the reviewers. Any product that may be evaluated in this article, or claim that may be made by its manufacturer, is not guaranteed or endorsed by the publisher.

frontiers | Frontiers in Neuroscience

TYPE Original Research
PUBLISHED 25 July 2022
DOI 10.3389/fnins.2022.921547

OPEN ACCESS

EDITED BY
Yuqi Cheng,
The First Affiliated Hospital of Kunming Medical University, China

REVIEWED BY
Ning Sun,
First Hospital of Shanxi Medical University, China
Ling Qin Wei,
Third Affiliated Hospital of Sun Yat-sen University, China

*CORRESPONDENCE
Xijia Xu
xuxijia@c-nbh.com

SPECIALTY SECTION
This article was submitted to Brain Imaging Methods, a section of the journal Frontiers in Neuroscience

RECEIVED 16 April 2022
ACCEPTED 06 July 2022
PUBLISHED 25 July 2022

CITATION
Kong M, Chen T, Gao S, Ni S, Ming Y, Chai X, Ling C and Xu X (2022) Abnormal network homogeneity of default-mode network and its relationships with clinical symptoms in antipsychotic-naïve first-diagnosis schizophrenia.
Front. Neurosci. 16:921547.
doi: 10.3389/fnins.2022.921547

Abnormal network homogeneity of default-mode network and its relationships with clinical symptoms in antipsychotic-naïve first-diagnosis schizophrenia

Mingjun Kong[1], Tian Chen[1], Shuzhan Gao[1], Sulin Ni[1], Yidan Ming[1], Xintong Chai[1], Chenxi Ling[1] and Xijia Xu[1,2]*

[1]Department of Psychiatry, the Affiliated Brain Hospital of Nanjing Medical University, Nanjing Brain Hospital, Nanjing, China, [2]Department of Psychiatry, Nanjing Brain Hospital, Medical School, Nanjing University, Nanjing, China

Schizophrenia is a severe mental disorder affecting around 0.5–1% of the global population. A few studies have shown the functional disconnection in the default-mode network (DMN) of schizophrenia patients. However, the findings remain discrepant. In the current study, we compared the intrinsic network organization of DMN of 57 first-diagnosis drug-naïve schizophrenia patients with 50 healthy controls (HCs) using a homogeneity network (NH) and explored the relationships of DMN with clinical characteristics of schizophrenia patients. Receiver operating characteristic (ROC) curves analysis and support vector machine (SVM) analysis were applied to calculate the accuracy of distinguishing schizophrenia patients from HCs. Our results showed that the NH values of patients were significantly higher in the left superior medial frontal gyrus (SMFG) and right cerebellum Crus I/Crus II and significantly lower in the right inferior temporal gyrus (ITG) and bilateral posterior cingulate cortex (PCC) compared to those of HCs. Additionally, negative correlations were shown between aberrant NH values in the right cerebellum Crus I/Crus II and general psychopathology scores, between NH values in the left SMFG and negative symptom scores, and between the NH values in the right ITG and speed of processing. Also, patients' age and the NH values in the right cerebellum Crus I/Crus II and the right ITG were the predictors of performance in the social cognition test. ROC curves analysis and SVM analysis showed that a combination of NH values in the left SMFG, right ITG, and right cerebellum Crus I/Crus II could distinguish schizophrenia patients from HCs with high accuracy. The results emphasized the vital role of DMN in the neuropathological mechanisms underlying schizophrenia.

KEYWORDS

schizophrenia, cognitive dysfunction, default-mode network, resting-state functional magnetic resonance imaging, network homogeneity

Introduction

Schizophrenia is a chronic psychiatric syndrome impacting around 0.5–1% of the world's population (Smigielski et al., 2020), and disturbances in sensory perception, emotion processing, thought, and social function as well as cognitive deficits, are hallmarks of schizophrenia (Jauhar et al., 2022). With complex heterogeneity in clinical manifestations and the low cure and high recurrence rates, considerable medical resources are devoted to the treatment and rehabilitation of schizophrenia patients, causing an increased economic burden on society and patients' families. Therefore, it is important to further elucidate the potential pathological mechanisms of this disorder to develop effective therapeutic interventions.

Implicated by the disconnection hypothesis, one of the main pathological characteristics of schizophrenia is the disruption of neural synchronization and information integration. Evidence shows that network disruptions might be a biomarker of schizophrenia (van den Heuvel and Fornito, 2014). Among the empirically studied resting-state networks of schizophrenia, it is noteworthy that a set of functionally connected brain regions, comprising the medial prefrontal cortex (MPFC), bilateral posterior cingulate cortex/precuneus (PCC/PCu), lateral posterior cortices, the cerebellum Crus I and Crus II, and parts of the parietal and temporal lobe cortex and the hippocampus, of the default-mode network (DMN), play a key role in the development of schizophrenia (Guo et al., 2014a,c). Several regions of DMN are active at rest and inhibited when the brain is working (Raichle et al., 2001). Previous studies demonstrated that hyperactivity within the DMN played a role in cognitive dysfunction and psychotic symptoms of patients with schizophrenia (Buckner et al., 2008) and that the changes in the DMN were associated with diagnosis (de Filippis et al., 2019) and treatment response of antipsychotic drugs (Mehta et al., 2021; Yang et al., 2021). Healthy individuals at high risk of schizophrenia also showed abnormal levels of functional connectivity (FC) within this network (Shim et al., 2010; Dodell-Feder et al., 2014; Anteraper et al., 2020), which highlighted the importance of the DMN as a potential biomarker of the development of schizophrenia and implied that genetic factors may play a role in the pathogenesis of diseases by interacting with the strength of FC in this network.

Although neuroimaging studies have shown dysfunctions in the network of schizophrenia, the findings are inconsistent. The FC of some regions of the DMN decreased (Camchong et al., 2011) and increased in some other regions (Jamea et al., 2021). Moreover, the relationships between specific regions of the DMN and clinical symptoms also are different (Camchong et al., 2011; Jamea et al., 2021; Roig-Herrero et al., 2022). The heterogeneity of the results may be related to the heterogeneity of factors such as patient characteristics and analytical methods, including those used to analyze the DMN and assess clinical symptoms. Previous studies have widely used the seed-based region of interest (ROI) and independent component analysis (ICA) methodologies to analyze the DMN. While the ROI analysis may be biased to the selection of the predetermined seeds, ICA may fail to identify a direct relationship between extracted components and the previously defined hypothesis. Here, network homogeneity (NH), a voxel-wise measure, provides an unbiased survey of a particular network and identifies abnormal brain regions in network coherence (Uddin et al., 2008). This approach is extensively used to explore the significance of networks in the pathogenesis of psychoses (Guo et al., 2014b; Wei et al., 2016; Zhang et al., 2020), and the findings proved that NH has great potential to explore the pathological mechanisms underlying diseases, including schizophrenia.

In the current study, the FC analysis of the DMN was performed using the NH method in first-diagnosis, drug-naïve schizophrenia patients. We hypothesized that altered NH values within the DMN would be identified in patients in contrast to healthy subjects. Multiple stepwise regression analysis was performed to identify how distinctly altered NH values in these brain regions correlated to cognition dimensions and clinical symptoms differently, to provide a reference for developing better therapeutic interventions targeting specific brain regions to alleviate symptom severity of schizophrenia patients. Additionally, we applied the receiver operating characteristic (ROC) curves analysis and a machine learning approach [support vector machine (SVM)] to identify the brain regions that will help differentiate patients from the healthy subjects.

Materials and methods

Subjects

A total of 57 subjects with schizophrenia treated at the Affiliated Brain Hospital of Nanjing Medical University were recruited between April 2018 and December 2019. The inclusion criteria were as follows: (1) patients who were clinically diagnosed with schizophrenia by two chief psychiatrists based on the diagnostic criteria of schizophrenia of the International Classification of Diseases, 10th Revision; (2) first-diagnosis antipsychotic drug-naïve patients; (3) patients who were 16–60 years old, Han nationals, and right-handed; (4) who had a Wechsler intelligence score $\geq$ 70; and (5) a Positive and Negative Syndrome Scale (PANSS) (Kay et al., 1987) total scores $\geq$ 60. The exclusion criteria were as follows: (1) patients who had other mental disorders or any severe physical diseases or substance abuse ever; (2) severe organic brain disease or brain trauma; (3) contraindications or non-cooperation during magnetic resonance imaging (MRI).

Age- and sex-matched healthy controls (HCs) were recruited via an advertisement during the same period. The inclusion criteria were as follows: (1) no history of

psychotic symptoms assessed using the MINI-International Neuropsychiatric Interview; (2) no familial history of psychiatric illness in two lines and three generations. The exclusion criteria were similar to that of the patient group.

The psychopathology and cognitive performance were measured using the PANSS for patients and MATRICS Consensus Cognitive Battery (Nuechterlein et al., 2008) for all participants. All participants signed written informed consent. The current study was approved by the local Medical Ethics Committee of the Affiliated Brain Hospital of Nanjing Medical University (2017-KY017).

Magnetic resonance imaging acquisition

Images were obtained using a 3T Siemens MRI scanner. Participants were informed to close their eyes, stay awake, and remain motionless. The MRI scanning parameters were as follows: slice thickness = 4 mm; repetition time = 2,000 ms; field of view = 220 × 220 mm; gap = 0.6 mm; flip angle = 90°; matrix size = 64 × 64; time point = 240; echo time = 30 ms; and layers = 33.

Data preprocessing

Data Processing Assistant for Resting-State Functional MRI (DPARSF) in MATLAB (Mathworks) was applied to preprocess the MRI data. If the maximal translation of the participants was over 3 mm and maximal rotation was over 3° in x, y, or z axes after slice timing and head motion correction, the images were excluded. Next, the motion-corrected functional volumes were spatially normalized to the Montreal Neurological Institute (MNI) space and resampled to 3 mm × 3 mm × 3 mm. After normalization, the transformed images were temporally bandpass filtered (0.01–0.08 Hz) and were linearly detrended. Several spurious covariates, including the signal from the 24 head motion parameters acquired by rigid body correction, ventricular seed-based ROI, and the white matter-centered brain region, were removed. The global signal was preserved for further analyses (Hahamy et al., 2014).

Default-mode network identification

The group ICA, in the GIFT toolbox[1], was performed for all subjects (Liu C. H. et al., 2012; Guo et al., 2013). The three main steps followed in the analysis were as follows: (1) reduction of data; (2) the minimum description length criterion was set to 20 to estimate separation of independent components; (3) back reconstruction. Finally, the generated DMN mask was applied in the following NH analyses (Raichle, 2015). More details are provided in the **Supplementary Methods** [Default-Mode Network (DMN) identification].

Network homogeneity analysis

We carried out NH analysis using MATLAB software (Mathworks). For a given voxel with others in a particular whole-brain network, the time series similarity is defined as homogeneity, and the NH value of a voxel is its mean correlation coefficient. The average correlation coefficients were transformed in z-values using Fisher r-to-z transformation (Buckner et al., 2009) to generate the NH maps after being smoothened using a Gaussian kernel of 8-mm full-width at half-maximum for further analyses. Age, sex, and education were regarded as confounders. The two-sample t-test via voxel-wise cross-subject statistics was applied to calculate the differences in NH in the DMN between patients and HCs. A corrected p-value < 0.05 indicated significance for multiple comparisons using the Gaussian Random Field approach (voxel significance, $p < 0.001$; cluster significance, $p < 0.05$).

Statistical analyses

For the demographic and clinical data, the continuous variables were compared using a two-sample independent t-test between patients and HCs. A Chi-square test was employed to identify gender differences. Significance was indicated by a two-tailed p-value < 0.05.

Region of interest were brain regions with aberrant NH values. Mean NH values in these ROIs were calculated for stepwise multiple regression analysis between the NH values in abnormal brain regions and the PANSS scores as well as the cognitive dimension scores, with the aberrant NH values in the DMN regions, age, education, and illness duration as independent variables, and the scores of the subdimensions of PANSS as well as all subsets of cognitive performance as dependent variables in the patient group. The statistical analyses were performed using the Statistical Package for Social Science version 25.0 (SPSS 25.0).

Classification analysis using receiver operating characteristic and support vector machine

Receiver operating characteristic analyses were conducted using SPSS 25.0. The values of Sensitivity + Specificity − 1 were defined as the Youden index to identify the cut-off points.

1 http://mialab.mrn.org/software/

TABLE 1 Characteristics of the subjects.

	Patients (n = 57)	HCs (n = 50)	t/x^2	P
Age (years)	31.63 ± 11.43	28.38 ± 6.87	1.81	0.074[b]
Education (years)	12.86 ± 3.42	15.64 ± 2.26	− 5.02	0.000[b]
Gender (male/female)	20/37	23/27	1.32	0.251[a]
Speed of processing	34.70 ± 12.12	44.28 ± 9.10	− 4.57	0.000[b]
Attention/Vigilance	38.19 ± 13.61	45.56 ± 9.69	− 3.25	0.002[b]
Verbal Learning	37.67 ± 13.66	44.52 ± 7.51	− 3.27	0.002[b]
Visual Learning	42.05 ± 11.61	47.16 ± 9.50	− 2.50	0.014[b]
Reasoning and Problem Solving	38.84 ± 10.78	45.44 ± 9.91	− 3.28	0.001[b]
Working Memory	32.51 ± 12.32	34.28 ± 11.22	− 0.77	0.441[b]
Social Cognition	33.14 ± 8.15	35.32 ± 6.49	− 1.52	0.132[b]
Overall Composite	28.47 ± 13.45	37.60 ± 9.19	− 4.14	0.000[b]
Duration (years)	2.41 ± 2.70			
PANSS				
Positive symptoms	26.39 ± 4.85			
Negative symptoms	20.68 ± 6.89			
General psychopathology	44.79 ± 7.41			
Total	91.84 ± 14.16			

HCs, healthy controls; PANSS, Positive and Negative Syndrome Scale.
[a]The p-value was obtained by x^2 test.
[b]The p-value was gained by two-sample independent t-tests.

Patients could be correctly distinguished from the HCs with optimal sensitivity and specificity using the cut-off points.

To further improve the accuracy of classification, we employed SVM, a method of supervised learning, to test the feasibility and effectiveness of abnormal NH values in the brain regions to differentiate patients from HCs using the LIBSVM software package[2]. The LIBSVM software used the leave-one-out method. The grid search method was applied to search the optimal parameters of the classification model with aberrant NH values in the DMN regions to discriminating patients from HCs. More details are provided in the **Supplementary Methods** [Classification analysis using support vector machine (SVM)].

Results

Demographic distribution and clinical information of subjects

There was no difference between the patients with schizophrenia and HCs in age (t-test, t = 1.808, df = 105, p = 0.074) and gender distribution (Chi-square test, $\chi 2$ = 1.320, df = 1, p = 0.251). However, the years of education of HCs were higher than those of patients (t-test, t = –5.018, df = 105, p = 0.000).

No difference was found in social cognition as well as working memory between patients with schizophrenia and HCs. However, other parameters of cognitive performance were poor in patients with schizophrenia compared to HCs (**Table 1**).

Default-mode network mask

The DMN mask was identified with a template mask using the group ICA method for all participants. The DMN consisted of the ventral anterior cingulate cortex (ACC), bilateral MPFC, PCC/PCu, lateral temporal cortex, cerebellum Crus I/Crus II, and lateral, medial, and inferior parietal lobes (**Figure 1**). The obtained DMN mask was used for NH analyses.

Differences in network homogeneity between patients with schizophrenia and healthy controls

As shown in **Figure 2** and **Table 2**, significant differences in NH values on the DMN mask were identified using the voxel-wise cross-subject comparisons. Compared to HCs, schizophrenia patients showed higher NH values in the left superior medial frontal gyrus (SMFG) and right cerebellum Crus I/Crus II and lower NH values in the right inferior temporal gyrus (ITG) and bilateral PCC.

Correlations between clinical characteristics and network homogeneity values in the brain regions in patients

We calculated the average NH values in the left SMFG, right cerebellum Crus I/Crus II, bilateral PCC, and right ITG. As shown in **Figure 3** and **Table 3**, significant negative correlations were observed between aberrant NH values in the right cerebellum Crus I/Crus II and general psychopathology scores (standardized β coefficients = –0.316, p = 0017), between NH values in the left SMFG and negative symptom scores (standardized β coefficients = –0.284, p = 0.032), and between NH values in the right ITG and speed of processing (standardized β coefficients = –0.270, p = 0.042). Moreover, the patients' age and the NH values in the right cerebellum Crus I/Crus II and the right ITG were the predictors of performance in social cognition test (standardized β coefficients = 0.368, p = 0.002; standardized β coefficients = –0.319, p = 0.008; standardized β coefficients = –0.286, p = 0.017, respectively). Additionally, age explained 12.3% of the variance in attention/vigilance (standardized β coefficients = 0.373,

2 http://www.csie.ntu.edu.tw/~cjlin/libsvm/

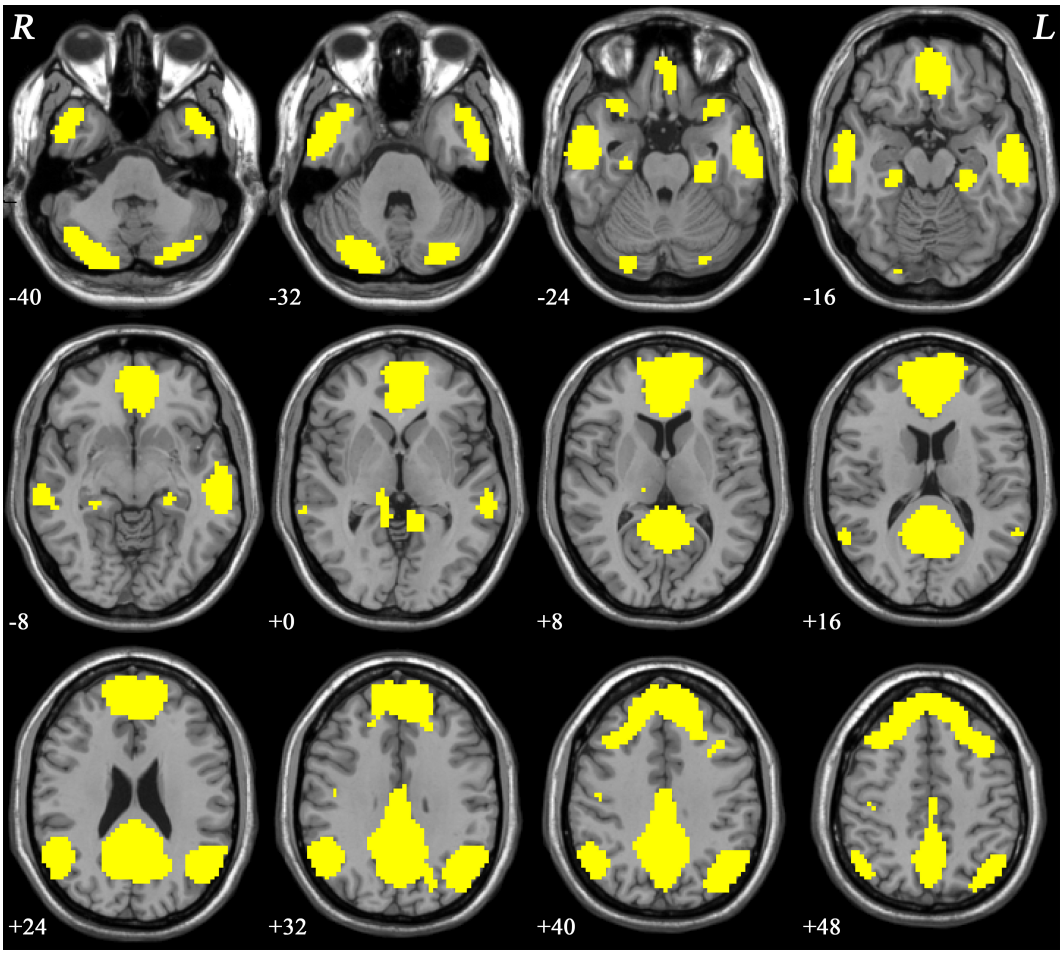

FIGURE 1
The DMN mask was determined using ICA. R and L denote the right and left sides, respectively; DMN, default-mode network; ICA, independent component analysis.

$p = 0.004$), and education accounted for 10.4% of the variance in reasoning and problem solving (standardized β coefficients = –0.346, $p = 0.008$).

Classification results to differentiate patients from healthy controls

As shown in Table 4 and Figure 4, the brain areas with abnormal NH values could distinguish patients from HCs with a relatively high degree of accuracy using ROC analysis. Our results indicated that the NH values in bilateral PCC with an accuracy of 72.30%, a sensitivity of 66.70%, and a specificity of 74.00% discriminated schizophrenia patients from healthy subjects. Moreover, the optimal accuracy, specificity, and sensitivity of the NH values in the left SMFG were 70.70, 50.00, and 86.00%, respectively and those in the right ITG were 73.80, 76.00, and 59.60%, respectively. The right cerebellum Crus I/Crus II NH values showed an accuracy of 71.20%, a specificity of 80.00%, and a sensitivity of 56.10% in differentiating schizophrenia patients from healthy individuals.

The SVM results demonstrated that the NH values in the combined brain regions of the right cerebellum Crus I/Crus II, right ITG, and left SMFG showed an optimal accuracy of 84.11% to distinguish patients from HCs (Table 5 and Figure 5).

Discussion

Our present study demonstrated that the patients with schizophrenia exhibited increased NH values in the left SMFG and right cerebellum Crus I/Crus II, and reduced NH values in the bilateral PCC and right ITG compared to HCs. Moreover, for patients with schizophrenia, we observed negative correlations between the NH values in the left SMFG and negative symptom scores, between the NH values in the right cerebellum Crus

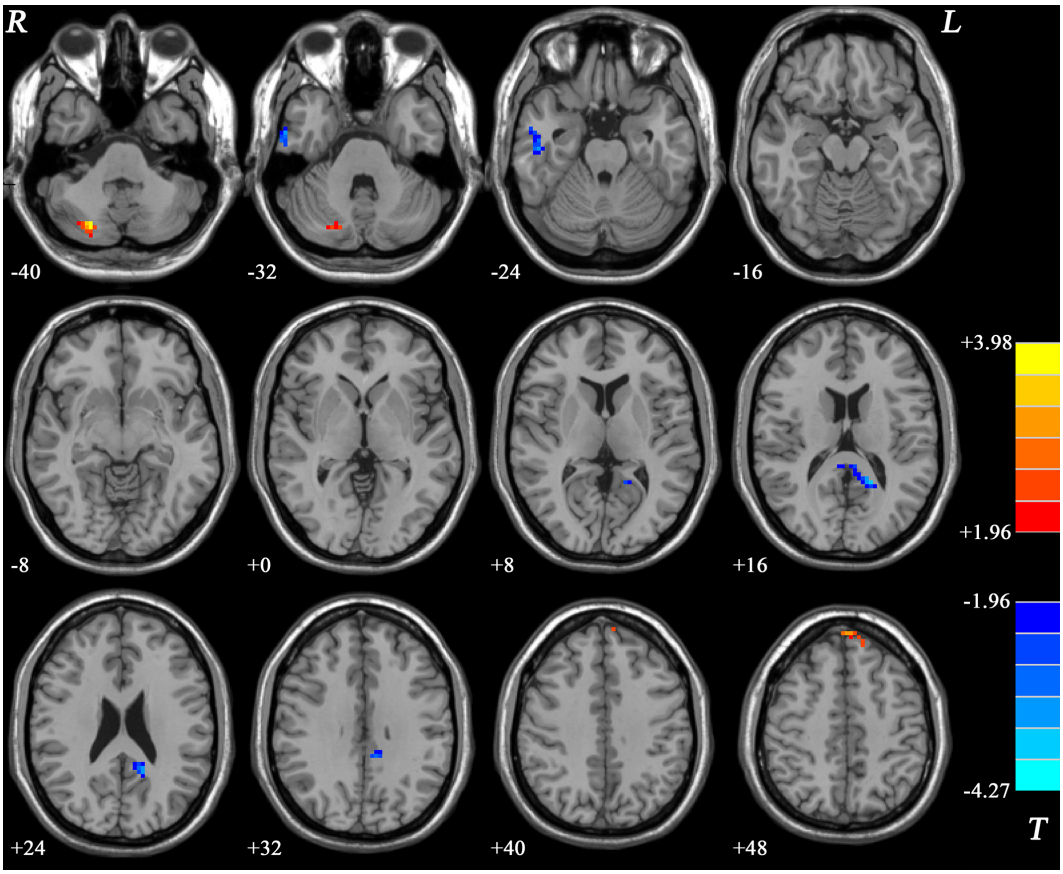

FIGURE 2
Differences in the NH values in the brain regions between patients and HCs. The color of the bars denotes the *t*-values (two-sample *t*-tests). Blue and red represent lower and higher NH, respectively. R and L denote the right and left sides, respectively; HCs, healthy controls; NH, network homogeneity.

I/Crus II and general psychopathology scores, and between the right ITG and the speed of processing scores. Age, NH values in the right cerebellum Crus I/Crus II and the right ITG significantly contributed to the social cognition performance in schizophrenia patients. In conclusion, the correlations between the NH values in these regions and the symptom/cognition dimensions implied that the poor-level coordination in the DMN may be responsible for deficits in cognitive performance and symptoms to some extent.

As a core node of DMN, the MPFC abnormalities have been considered an intrinsic feature of schizophrenia and found to be related to severe psychiatric symptoms like deficits in cognition, especially the execution control function (Li et al., 2019). Our study showed increased NH values in the left SMFG. Zhang et al. (2020) also found increased NH values in the left MPFC, which may help distinguish schizophrenic patients from HCs. In contrast to our results, previous studies also found reduced NH values in left MPFC in the DMN (Guo et al., 2014c) or no difference in NH values in MPFC at baseline in patients with schizophrenia compared to HCs, but after 6 months of treatment with Olanzapine, NH in the left superior MPFC increased in the patient group (Guo et al., 2017). The difference in results may be associated with the heterogeneity of patients with schizophrenia, such as age and sex, illness duration, clinical characteristics, and so on. Moreover, our study showed a negative correlation between the NH values in the left SMFG and the scores of negative

TABLE 2 Differences in DMN NH values between groups.

Cluster location	Peak (MNI)			Number of voxels	*T* value
	x	*y*	*z*		
Left SMFG	−3	54	45	30	3.5043
Right Cerebellum Crus I and II	24	−75	−39	45	3.9834
Bilateral PCC	−18	−51	15	90	−3.6884
Right ITG	51	−18	−27	63	−3.7776

SMFG, superior medial frontal gyrus; PCC, posterior cingulate cortex; ITG, inferior temporal gyrus; MNI, Montreal Neurological Institute; NH, network homogeneity; DMN, default-mode network.

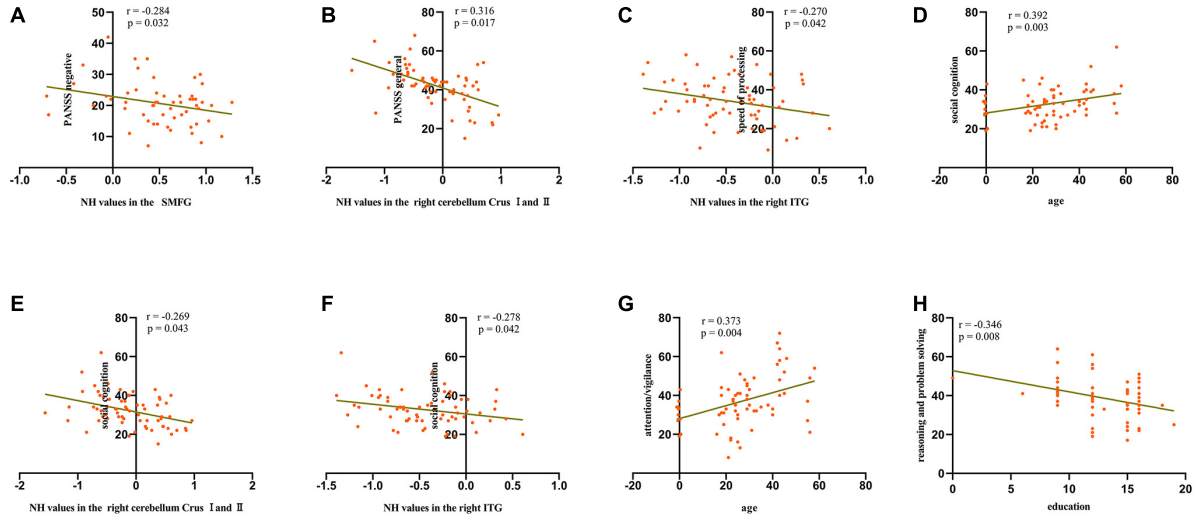

FIGURE 3

Scatterplots of significant associations between NH values in the SMFG and negative symptom scores **(A)**, NH values in the right cerebellum Crus I/Crus II and general psychopathology scores **(B)**, NH values in the right ITG and speed of processing scores **(C)**, age and social cognition scores **(D)**, NH values in the right cerebellum Crus I/Crus II and social cognition scores **(E)**, NH values in the right ITG and social cognition scores **(F)**, age and attention/vigilance scores **(G)**, and education and reasoning and problem-solving scores **(H)** in the patient group. SMFG, superior medial frontal gyrus; ITG, inferior temporal gyrus; PANSS, Positive and Negative Syndrome Scale; NH, network homogeneity.

TABLE 3 Multiple stepwise regression analysis between the abnormal NH values in the brain regions and PANSS dimensions and cognitive tests.

Dependent variable					**Predictive variables**		
	Adj R^2	***B***	***F***	***P***	**Variable**	**Standardized β**	***P***
PANSS							
Negative symptoms	0.081	22.89	4.83	0.032	Left SMFG	− 0.284	0.032
General psychopathology	0.083	43.76	6.10	0.017	Right Cerebellum Crus I and II	− 0.316	0.017
Speed of processing	0.056	31.07	4.33	0.042	Right ITG	− 0.270	0.042
Attention/Vigilance	0.123	24.15	8.89	0.004	Age	0.373	0.004
Reasoning and Problem Solving	0.104	52.87	7.48	0.008	Education	− 0.346	0.008
Social Cognition	0.270	21.11	7.92	0.000	Age	0.368	0.002
					Right Cerebellum Crus I and II	− 0.319	0.008
					Right ITG	− 0.286	0.017

SMFG, superior medial frontal gyrus; ITG, inferior temporal gyrus; PANSS, Positive and Negative Syndrome Scale; NH, network homogeneity.

symptoms. Also, longitudinal brain analysis to elucidate the effects of drug treatment showed that antipsychotic drugs can regulate the functional and connectional integrity of this region to improve the severity of psychotic symptoms, and the levels of FC of the bilateral superior MPFC at baseline could predict the effectiveness of treatments (Guo et al., 2017; Shan et al., 2020). Studies using magnetic resonance spectroscopy further showed that the improvement in symptoms was accompanied by changes in the levels of γ-aminobutyric acid neurotransmitters in the MPFC brain region after antipsychotic drug treatment (Li et al., 2022), further verifying that functional disconnection in MPFC within the whole DMN was involved in the manifestation of clinical symptoms. Taken together, further therapeutic measures targeting the specific brain region containing MPFC are important to improve psychotic symptoms of schizophrenia.

Consistent with the previous reports (Lee et al., 2016), our findings showed a negative correlation between the abnormal neural activity of ITG and neurocognitive performance, especially in speed of processing and social cognition. Using the NH method, previous studies showed no difference between patients with schizophrenia and HCs in the right ITG (Guo et al., 2014c, 2017; Shan et al., 2020; Zhang et al., 2020); however, we found that the NH values in right ITG reduced in the patients. The difference in results may be associated with the heterogeneity of patients with

TABLE 4 ROC analyses for differentiating the schizophrenia patients from the HCs.

Brain regions	Area under the curve	Cut-off point	Sensitivity	Specificity
Right cerebellum Crus I and II	0.712	0.5852	56.10%	80.00%
Bilateral PCC	0.723	0.5622	66.70%	74.00%
Left SMFG	0.707	0.4571	86.00%	50.00%
Right ITG	0.738	0.5678	59.60%	76.00%

SMFG, superior medial frontal gyrus; ITG, inferior temporal gyrus; PCC, posterior cingulate cortex; HCs, healthy controls; ROC, receiver operating characteristic.

schizophrenia. Nevertheless, research comprising functional or structural MRI using different analyses, such as global-brain FC (Zhao et al., 2022), the dynamic amplitude of low-frequency fluctuation (Wang et al., 2021), full- and short-range strength of FC (Miao et al., 2020), and Trace (Lee et al., 2016), have observed aberrant ITG in patients with schizophrenia, which is associated with psychotic (Lee et al., 2016) and cognitive symptoms (Lee et al., 2016) and might predict the response to an antipsychotic drug after 8 weeks (Zhu et al., 2018). Previous studies also showed that both patients with schizophrenia and their unaffected siblings shared similar alterations in the ITG (Liu H. et al., 2012; Zhu et al., 2018), and the neural activity of ITG was regulated by regulating by the Disrupted-in-Schizophrenia-1 gene (Gou et al., 2018), suggesting that the ITG might be a potential biomarker of endophenotype for schizophrenia. Zhu et al. (2020) stated that the right ITG might show unique abnormalities in patients with schizophrenia compared with those with bipolar disorder and attention-deficit/hyperactivity disorder. Moreover, Miao et al. (2020) showed that the functional impairment in this region might be an ongoing pathological process in schizophrenia patients, and it is barely affected by antipsychotic drugs. Above all, to a certain extent, our results provided diverse findings regarding ITG and novel insights into exploring symptomatic and cognitive-related mechanisms in patients with schizophrenia.

In addition to being engaged in motor control and coordination, the cerebellum also plays an important role in emotion and cognitive processing (Stoodley et al., 2012; Sokolov et al., 2017). In line with the results in our study, higher NH values in the right cerebellum Crus I (Guo et al., 2014c) and right cerebellum Crus II (Shan et al., 2020) have been reported in schizophrenia patients. Further, our results of stepwise regression analysis showed that abnormal NH values in both these brain regions were associated with general psychopathology and social cognition. Kuhn et al. (2012) showed that gray matter volume of left cerebellum Crus I/Crus II was related to thought disorder and Trail-making test B. The reduction in general psychopathology was associated with the gray matter volume in the cerebellum (Crus

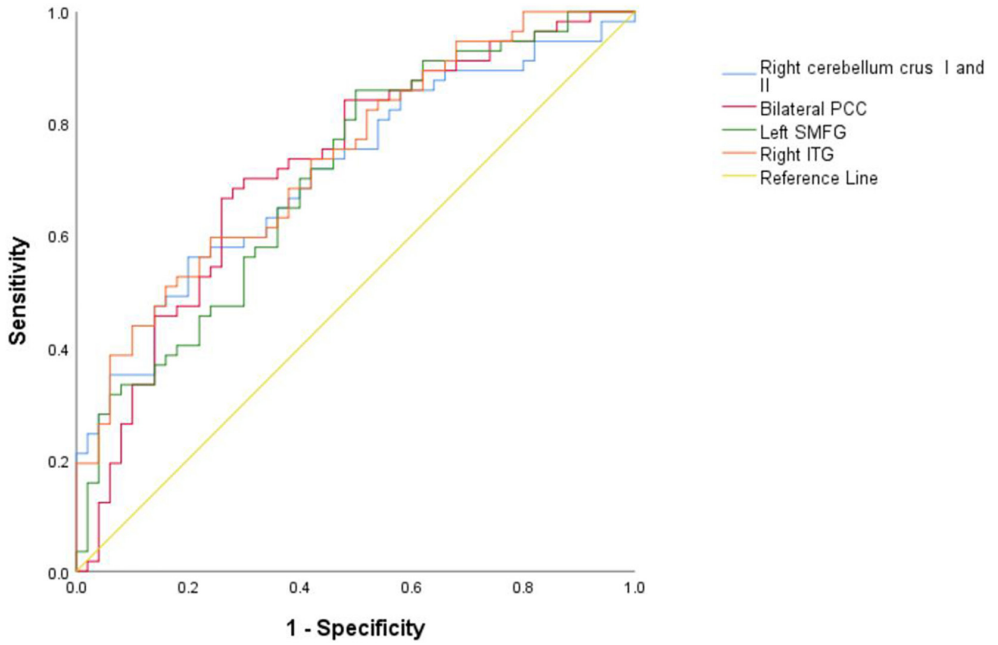

FIGURE 4
Results of the ROC analyses used to differentiate between patients and HCs using the NH values in the different brain regions. NH, network homogeneity; HCs, healthy controls; PCC, posterior cingulate cortex; SMFG, superior medial frontal gyrus; ITG, inferior temporal gyrus; ROC, receiver operating characteristic.

TABLE 5 The results of SVM to classify patients from HCs.

Feature	Accuracy (%)	Feature	Accuracy (%)
1	65.42	123	79.44
2	69.16	124	74.77
3	65.42	134	84.11
4	64.49	234	76.64
12	72.90	1234	74.77
13	72.90		
14	70.09		
23	74.77		
24	73.83		
34	77.57		

1, 2, 3, 4 represent right cerebellum Crus I and II, bilateral posterior cingulate cortex, left superior medial frontal gyrus, right inferior temporal gyrus, respectively.
SVM, support vector machine.

I) (Premkumar et al., 2009), further supporting our results that cerebellum Crus I/Crus II might participate in the pathological mechanism of schizophrenia. The differences among studies might be associated with the heterogeneity of patients and the analysis methods. Laidi et al. (2019) demonstrated that patients with schizophrenia showed a decrease in the cerebellum (Crus II), whereas there was no corresponding alternation in patients with bipolar disorder, indicating that the abnormalities in cerebellum Crus I and/or Crus II might be specific to schizophrenia. According to these reports and our results of SVM, combined with SMFG, right ITG, and right cerebellum Crus I/Crus II might help distinguish between patients with schizophrenia and HCs.

Posterior cingulate cortex, as one of the important nodes of the DMN and limbic system, was associated with cognition, psychotic symptoms, and micro-RNA 137 (Zhang et al., 2018), which might participate in the pathological mechanism of schizophrenia (Leech and Sharp, 2014). Our results showed lower NH values in PCC, which is consistent with previous studies (Shan et al., 2020; Zhang et al., 2020) but in contrast to the study by Guo et al. (2014c). The difference might be related to the heterogeneity of patients with schizophrenia. Several reports showed abnormalities in PCC using different analysis methods in patients with schizophrenia, including aberrant DMN connectivity strength (Hilland et al., 2022), increased global-brain functional connectivity (Ding et al., 2019), and so on. Despite the differences in results, both the studies support that the PCC is involved in the pathological mechanism of schizophrenia. Moreover, PCC is rich in *N*-methyl-D-aspartate (NMDA) receptors (Ma and Leung, 2018), whereas phencyclidine (PCP), an NMDA receptor antagonist, is regarded as a pharmacological model of schizophrenia. He et al. (2006) showed that quetiapine might ameliorate the apoptosis in PCC induced by PCP, implicating that PCC may be a potential target for antipsychotic drugs, such as quetiapine.

Limitations

Several limitations must be taken into account for this study. Firstly, owing to the small sample size, the results herein, cannot be extrapolated to the general population. Secondly, the DMN mask extracted from all the participants using

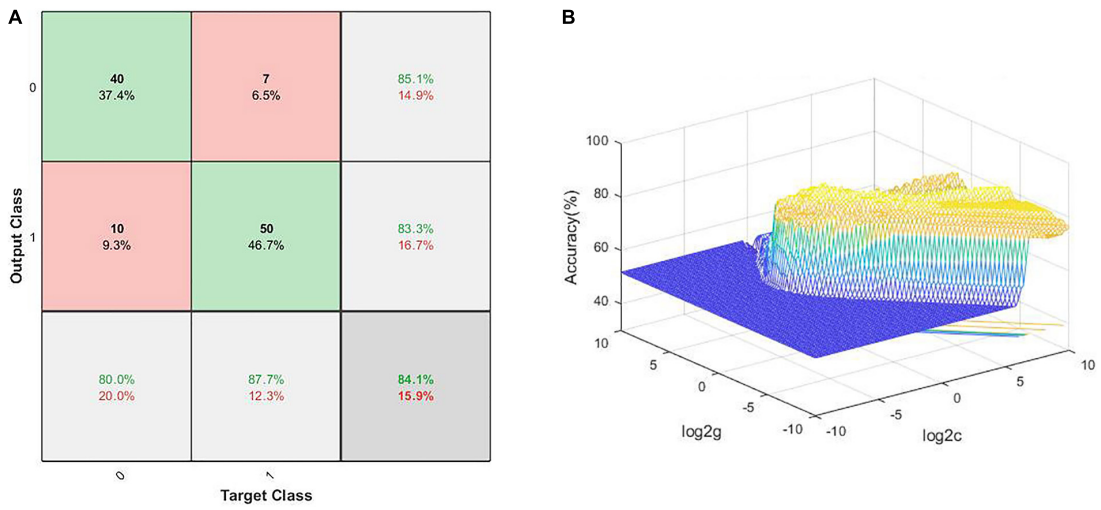

FIGURE 5
Visualization of classification using SVM analysis with the NH values in the combined brain regions, comprising the left SMFG, right cerebellum Crus I/Crus II, and right ITG; **(A)** confusion matrix; **(B)** SVM parameter results of 3D view. Target Class and Output Class represent actual and predicted results of classification, respectively; SMFG, superior medial frontal gyrus; ITG, inferior temporal gyrus; NH, network homogeneity; SVM, support vector machine.

ICA may have affected the analyses (Uddin et al., 2008). Thirdly, we may have neglected the pathophysiology in the other brain regions or networks by focusing on the connective dysfunction of the DMN. Finally, the years of education of schizophrenia patients were different from those of HCs, which may have an effect on the cognitive performance, especially reasoning and problem solving, in schizophrenia patients. The age of patients also affected the clinical characteristics in the patient group although there were no differences in age between patients and HCs. Future studies should consider these confounding effects.

Conclusion

Despite its limitations, our study revealed significantly aberrant intrinsic network organization of the DMN in schizophrenia and demonstrated that the combination of NH values in the SMFG, right ITG, and right cerebellum Crus I/Crus II might help distinguish between patients with schizophrenia and HCs and can be regarded as an underlying biomarker.

Data availability statement

The original contributions presented in this study are included in the article/**Supplementary Material**, further inquiries can be directed to the corresponding author.

Ethics statement

The studies involving human participants were reviewed and approved by Medical Ethics Committee of The Affiliated Nanjing Brain Hospital, Nanjing Medical University (2017-KY017). Written informed consent to participate in this study was provided by the participants or their legal guardian/next of kin. Written informed consent was obtained from the individual(s), and minor(s)' legal guardian/next of kin, for the publication of any potentially identifiable images or data included in this article.

Author contributions

MK wrote the first draft of this manuscript. XX designed the research. SG, TC, MK, YM, SN, XC, and CL collected the clinical and imaging data. XX, MK, and TC analyzed the data. All the authors reviewed and approved the final version of the manuscript.

Funding

This study was supported by the National Natural Science Foundation of China (Grant/Award Numbers: 82172061 and 81771444), the 16th Batch of Six Talent Peak Projects in Jiangsu (Grant/Award Number WSN-166), and the Key Research and Development Plan in Jiangsu (Social Development, Grant/Award Number BE2019707).

Acknowledgments

We thank the subjects who participated in the study and Chaoyong Xiao, Jun Hu, Lanlan Yao, Zonghong Li, and Chenlin Li (Department of Radiology, The Affiliated Nanjing Brain Hospital, Nanjing Medical University, Nanjing, China) for contributing to the imaging data acquisition.

Conflict of interest

The authors declare that the research was conducted in the absence of any commercial or financial relationships that could be construed as a potential conflict of interest.

Publisher's note

Supplementary material

The Supplementary Material for this article can be found online at: https://www.frontiersin.org/articles/10.3389/fnins.2022.921547/full#supplementary-material

References

Anteraper, S. A., Collin, G., Guell, X., Scheinert, T., Molokotos, E., Henriksen, M. T., et al. (2020). Altered resting-state functional connectivity in young children at familial high risk for psychotic illness: a preliminary study. *Schizophr. Res.* 216, 496–503. doi: 10.1016/j.schres.2019.09.006

Buckner, R. L., Andrews-Hanna, J. R., and Schacter, D. L. (2008). The brain's default network: anatomy, function, and relevance to disease. *Ann. N. Y. Acad. Sci.* 1124, 1–38. doi: 10.1196/annals.1440.011

Buckner, R. L., Sepulcre, J., Talukdar, T., Krienen, F. M., Liu, H., Hedden, T., et al. (2009). Cortical hubs revealed by intrinsic functional connectivity: mapping, assessment of stability, and relation to Alzheimer's disease. *J. Neurosci.* 29, 1860–1873. doi: 10.1523/JNEUROSCI.5062-08.2009

Camchong, J., MacDonald, A. W. III, Bell, C., Mueller, B. A., and Lim, K. O. (2011). Altered functional and anatomical connectivity in schizophrenia. *Schizophr. Bull.* 37, 640–650. doi: 10.1093/schbul/sbp 131

de Filippis, R., Carbone, E. A., Gaetano, R., Bruni, A., Pugliese, V., Segura-Garcia, C., et al. (2019). Machine learning techniques in a structural and functional MRI diagnostic approach in schizophrenia: a systematic review. *Neuropsychiatr. Dis. Treat.* 15, 1605–1627. doi: 10.2147/NDT.S202418

Ding, Y., Ou, Y., Su, Q., Pan, P., Shan, X., Chen, J., et al. (2019). Enhanced Global-Brain Functional Connectivity in the Left Superior Frontal Gyrus as a Possible Endophenotype for Schizophrenia. *Front. Neurosci.* 13:145. doi: 10.3389/fnins.2019.00145

Dodell-Feder, D., Delisi, L. E., and Hooker, C. I. (2014). The relationship between default mode network connectivity and social functioning in individuals at familial high-risk for schizophrenia. *Schizophr. Res.* 156, 87–95. doi: 10.1016/j.schres.2014.03.031

Gou, N., Liu, Z., Palaniyappan, L., Li, M., Pan, Y., Chen, X., et al. (2018). Effects of DISC1 Polymorphisms on Resting-State Spontaneous Neuronal Activity in the Early-Stage of Schizophrenia. *Front. Psychiatry* 9:137. doi: 10.3389/fpsyt.2018.00137

Guo, W., Liu, F., Chen, J., Wu, R., Li, L., Zhang, Z., et al. (2017). Olanzapine modulates the default-mode network homogeneity in recurrent drug-free schizophrenia at rest. *Aust. N. Z. J. Psychiatry* 51, 1000–1009. doi: 10.1177/0004867417714952

Guo, W., Liu, F., Yao, D., Jiang, J., Su, Q., Zhang, Z., et al. (2014a). Decreased default-mode network homogeneity in unaffected siblings of schizophrenia patients at rest. *Psychiatry Res.* 224, 218–224. doi: 10.1016/j.pscychresns.2014.08.014

Guo, W., Yao, D., Jiang, J., Su, Q., Zhang, Z., Zhang, J., et al. (2014c). Abnormal default-mode network homogeneity in first-episode, drug-naive schizophrenia at rest. *Prog. Neuropsychopharmacol. Biol. Psychiatry* 49, 16–20. doi: 10.1016/j.pnpbp.2013.10.021

Guo, W., Liu, F., Zhang, J., Zhang, Z., Yu, L., Liu, J., et al. (2014b). Abnormal default-mode network homogeneity in first-episode, drug-naive major depressive disorder. *PLoS One* 9:e91102. doi: 10.1371/journal.pone.0091102

Guo, W., Liu, F., Zhang, J., Zhang, Z., Yu, L., Liu, J., et al. (2013). Dissociation of regional activity in the default mode network in first-episode, drug-naive major depressive disorder at rest. *J. Affect. Disord.* 151, 1097–1101. doi: 10.1016/j.jad.2013.09.003

Hahamy, A., Calhoun, V., Pearlson, G., Harel, M., Stern, N., Attar, F., et al. (2014). Save the global: global signal connectivity as a tool for studying clinical populations with functional magnetic resonance imaging. *Brain Connect.* 4, 395–403. doi: 10.1089/brain.2014.0244

He, J., Xu, H., Yang, Y., Rajakumar, D., Li, X., and Li, X. M. (2006). The effects of chronic administration of quetiapine on the phencyclidine-induced reference memory impairment and decrease of Bcl-XL/Bax ratio in the posterior cingulate cortex in rats. *Behav. Brain Res.* 168, 236–242. doi: 10.1016/j.bbr.2005.11.014

Hilland, E., Johannessen, C., Jonassen, R., Alnaes, D., Jorgensen, K. N., Barth, C., et al. (2022). Aberrant default mode connectivity in adolescents with early-onset psychosis: a resting state fMRI study. *Neuroimage Clin.* 33:102881. doi: 10.1016/j.nicl.2021.102881

Jamea, A. A., Alblowi, M., Alghamdi, J., Alosaimi, F. D., Albadr, F., Abualait, T., et al. (2021). Altered default mode network activity and cortical thickness as vulnerability indicators for SCZ: a preliminary resting state MRI study. *Eur. Rev. Med. Pharmacol. Sci.* 25, 669–677. doi: 10.26355/eurrev_202101_24628

Jauhar, S., Johnstone, M., and McKenna, P. J. (2022). Schizophrenia. *Lancet* 399, 473–486. doi: 10.1016/s0140-6736(21)01730-x

Kay, S. R., Fiszbein, A., and Opler, L. A. (1987). The positive and negative syndrome scale (PANSS) for schizophrenia. *Schizophr. Bull.* 13, 261–276. doi: 10.1093/schbul/13.2.261

Kuhn, S., Romanowski, A., Schubert, F., and Gallinat, J. (2012). Reduction of cerebellar grey matter in Crus I and II in schizophrenia. *Brain Struct. Funct.* 217, 523–529. doi: 10.1007/s00429-011-0365-2

Laidi, C., Hajek, T., Spaniel, F., Kolenic, M., d'Albis, M. A., Sarrazin, S., et al. (2019). Cerebellar parcellation in schizophrenia and bipolar disorder. *Acta Psychiatr. Scand.* 140, 468–476. doi: 10.1111/acps.13087

Lee, J. S., Kim, C. Y., Joo, Y. H., Newell, D., Bouix, S., Shenton, M. E., et al. (2016). Increased diffusivity in gray matter in recent onset schizophrenia is associated with clinical symptoms and social cognition. *Schizophr. Res.* 176, 144–150. doi: 10.1016/j.schres.2016.08.011

Leech, R., and Sharp, D. J. (2014). The role of the posterior cingulate cortex in cognition and disease. *Brain* 137, 12–32. doi: 10.1093/brain/awt162

Li, M., Li, X., Das, T. K., Deng, W., Li, Y., Zhao, L., et al. (2019). Prognostic Utility of Multivariate Morphometry in Schizophrenia. *Front. Psychiatry* 10:245. doi: 10.3389/fpsyt.2019.00245

Li, W., Xu, J., Xiang, Q., Zhuo, K., Zhang, Y., Liu, D., et al. (2022). Neurometabolic and functional changes of default-mode network relate to clinical recovery in first-episode psychosis patients: a longitudinal (1)H-MRS and fMRI study. *Neuroimage Clin.* 34:102970. doi: 10.1016/j.nicl.2022.102970

Liu, C. H., Ma, X., Li, F., Wang, Y. J., Tie, C. L., Li, S. F., et al. (2012). Regional homogeneity within the default mode network in bipolar depression: a resting-state functional magnetic resonance imaging study. *PLoS One* 7:e48181. doi: 10.1371/journal.pone.0048181

Liu, H., Kaneko, Y., Ouyang, X., Li, L., Hao, Y., Chen, E. Y., et al. (2012). Schizophrenic patients and their unaffected siblings share increased resting-state connectivity in the task-negative network but not its anticorrelated task-positive network. *Schizophr. Bull.* 38, 285–294. doi: 10.1093/schbul/sbq074

Ma, J., and Leung, L. S. (2018). Involvement of posterior cingulate cortex in ketamine-induced psychosis relevant behaviors in rats. *Behav. Brain Res.* 338, 17–27. doi: 10.1016/j.bbr.2017.09.051

Mehta, U. M., Ibrahim, F. A., Sharma, M. S., Venkatasubramanian, G., Thirthalli, J., Bharath, R. D., et al. (2021). Resting-state functional connectivity predictors of treatment response in schizophrenia - A systematic review and meta-analysis. *Schizophr. Res.* 237, 153–165. doi: 10.1016/j.schres.2021.09.004

Miao, Q., Pu, C., Wang, Z., Yan, C. G., Shi, C., Cao, Q., et al. (2020). Influence of More Than 5 Years of Continuous Exposure to Antipsychotics on Cerebral Functional Connectivity of Chronic Schizophrenia. *Can. J. Psychiatry* 65, 463–472. doi: 10.1177/0706743720904815

Nuechterlein, K. H., Green, M. F., Kern, R. S., Baade, L. E., Barch, D. M., Cohen, J. D., et al. (2008). The MATRICS Consensus Cognitive Battery, part 1: test selection, reliability, and validity. *Am. J. Psychiatry* 165, 203–213. doi: 10.1176/appi.ajp.2007.07010042

Premkumar, P., Fannon, D., Kuipers, E., Peters, E. R., Anilkumar, A. P., Simmons, A., et al. (2009). Structural magnetic resonance imaging predictors of responsiveness to cognitive behaviour therapy in psychosis. *Schizophr. Res.* 115, 146–155. doi: 10.1016/j.schres.2009.08.007

Raichle, M. E. (2015). The brain's default mode network. *Annu. Rev. Neurosci.* 38, 433–447. doi: 10.1146/annurev-neuro-071013-014030

Raichle, M. E., MacLeod, A. M., Snyder, A. Z., Powers, W. J., Gusnard, D. A., and Shulman, G. L. (2001). A default mode of brain function. *Proc. Natl. Acad. Sci. U.S.A.* 98, 676–682. doi: 10.1073/pnas.98.2.676

Roig-Herrero, A., Planchuelo-Gomez, A., Hernandez-Garcia, M., de Luis-Garcia, R., Fernandez-Linsenbarth, I., Beno-Ruiz-de-la-Sierra, R. M., et al. (2022). Default mode network components and its relationship with anomalous self-experiences in schizophrenia: a rs-fMRI exploratory study. *Psychiatry Res. Neuroimaging* 324:111495. doi: 10.1016/j.pscychresns.2022.111495

Shan, X., Liao, R., Ou, Y., Ding, Y., Liu, F., Chen, J., et al. (2020). Metacognitive Training Modulates Default-Mode Network Homogeneity During 8-Week Olanzapine Treatment in Patients With Schizophrenia. *Front. Psychiatry* 11:234. doi: 10.3389/fpsyt.2020.00234

Shim, G., Oh, J. S., Jung, W. H., Jang, J. H., Choi, C. H., Kim, E., et al. (2010). Altered resting-state connectivity in subjects at ultra-high risk for psychosis: an fMRI study. *Behav. Brain Funct.* 6:58. doi: 10.1186/1744-9081-6-58

Smigielski, L., Jagannath, V., Rossler, W., Walitza, S., and Grunblatt, E. (2020). Epigenetic mechanisms in schizophrenia and other psychotic disorders: a systematic review of empirical human findings. *Mol. Psychiatry* 25, 1718–1748. doi: 10.1038/s41380-019-0601-3

Sokolov, A. A., Miall, R. C., and Ivry, R. B. (2017). The cerebellum: adaptive prediction for movement and cognition. *Trends Cogn. Sci.* 21, 313–332. doi: 10.1016/j.tics.2017.02.005

Stoodley, C. J., Valera, E. M., and Schmahmann, J. D. (2012). Functional topography of the cerebellum for motor and cognitive tasks: an fMRI study. *Neuroimage* 59, 1560–1570. doi: 10.1016/j.neuroimage.2011.08.065

Uddin, L. Q., Kelly, A. M., Biswal, B. B., Margulies, D. S., Shehzad, Z., Shaw, D., et al. (2008). Network homogeneity reveals decreased integrity of default-mode network in ADHD. *J. Neurosci. Methods* 169, 249–254. doi: 10.1016/j.jneumeth.2007.11.031

van den Heuvel, M. P., and Fornito, A. (2014). Brain networks in schizophrenia. *Neuropsychol. Rev.* 24, 32–48. doi: 10.1007/s11065-014-9248-7

Wang, Y., Jiang, Y., Liu, D., Zhang, J., Yao, D., Luo, C., et al. (2021). Atypical Antipsychotics Mediate Dynamics of Intrinsic Brain Activity in Early-Stage Schizophrenia? A Preliminary Study. *Psychiatry Investig.* 18, 1205–1212. doi: 10.30773/pi.2020.0418

Wei, S., Su, Q., Jiang, M., Liu, F., Yao, D., Dai, Y., et al. (2016). Abnormal default-mode network homogeneity and its correlations with personality in drug-naive somatization disorder at rest. *J. Affect. Disord.* 193, 81–88. doi: 10.1016/j.jad.2015.12.052

Yang, C., Tang, J., Liu, N., Yao, L., Xu, M., Sun, H., et al. (2021). The effects of antipsychotic treatment on the brain of patients with first-episode schizophrenia: a selective review of longitudinal MRI Studies. *Front. Psychiatry* 12:593703. doi: 10.3389/fpsyt.2021.593703

Zhang, S., Yang, G., Ou, Y., Guo, W., Peng, Y., Hao, K., et al. (2020). Abnormal default-mode network homogeneity and its correlations with neurocognitive deficits in drug-naive first-episode adolescent-onset schizophrenia. *Schizophr. Res.* 215, 140–147. doi: 10.1016/j.schres.2019.10.056

Zhang, Z., Yan, T., Wang, Y., Zhang, Q., Zhao, W., Chen, X., et al. (2018). Polymorphism in schizophrenia risk gene MIR137 is associated with the posterior cingulate Cortex's activation and functional and structural connectivity in healthy controls. *Neuroimage Clin.* 19, 160–166. doi: 10.1016/j.nicl.2018.03.039

Zhao, J., Zhang, Y., Liu, F., Chen, J., Zhao, J., and Guo, W. (2022). Abnormal global-brain functional connectivity and its relationship with cognitive deficits in drug-naive first-episode adolescent-onset schizophrenia. *Brain Imaging Behav.* 16, 1303–1313. doi: 10.1007/s11682-021-00597-3

Zhu, F., Liu, F., Guo, W., Chen, J., Su, Q., Zhang, Z., et al. (2018). Disrupted asymmetry of inter- and intra-hemispheric functional connectivity in patients with drug-naive, first-episode schizophrenia and their unaffected siblings. *EBioMedicine* 36, 429–435. doi: 10.1016/j.ebiom.2018.09.012

Zhu, J., Zhang, S., Cai, H., Wang, C., and Yu, Y. (2020). Common and distinct functional stability abnormalities across three major psychiatric disorders. *Neuroimage Clin.* 27:102352. doi: 10.1016/j.nicl.2020.102352

frontiers | Frontiers in Neuroscience

TYPE Original Research
PUBLISHED 09 August 2022
DOI 10.3389/fnins.2022.930997

OPEN ACCESS

EDITED BY
Zaixu Cui,
Chinese Institute for Brain Research, Beijing (CIBR), China

REVIEWED BY
Xinyu Liang,
Fudan University, China
Suyu Zhong,
Beijing University of Posts and Telecommunications (BUPT), China

*CORRESPONDENCE
Hongjun Peng
pengdoctor2@163.com
Huawang Wu
Huawangwu@126.com

†These authors have contributed equally to this work

SPECIALTY SECTION
This article was submitted to Brain Imaging Methods, a section of the journal Frontiers in Neuroscience

RECEIVED 28 April 2022
ACCEPTED 11 July 2022
PUBLISHED 09 August 2022

CITATION
Chen J, Luo Q, Li Y, Wu Z, Lin X, Yao J, Yu H, Nie H, Du Y, Peng H and Wu H (2022) Intrinsic brain abnormalities in female major depressive disorder patients with childhood trauma: A resting-state functional magnetic resonance imaging study. *Front. Neurosci.* 16:930997. doi: 10.3389/fnins.2022.930997

Intrinsic brain abnormalities in female major depressive disorder patients with childhood trauma: A resting-state functional magnetic resonance imaging study

Juran Chen[1†], Qianyi Luo[1†], Yuhong Li[1], Zhiyao Wu[1], Xinyi Lin[1], Jiazheng Yao[1], Huiwen Yu[1], Huiqin Nie[1], Yingying Du[1], Hongjun Peng[1*] and Huawang Wu[2*]

[1]Department of Clinical Psychology, The Affiliated Brain Hospital of Guangzhou Medical University, Guangzhou, China, [2]Department of Radiology, The Affiliated Brain Hospital of Guangzhou Medical University, Guangzhou, China

Objective: Childhood trauma is a strong predictor of major depressive disorder (MDD). Women are more likely to develop MDD than men. However, the neural basis of female MDD patients with childhood trauma remains unclear. We aimed to identify the specific brain regions that are associated with female MDD patients with childhood trauma.

Methods: We recruited 16 female MDD patients with childhood trauma, 16 female MDD patients without childhood trauma, and 20 age- and education level-matched healthy controls. All participants underwent resting-state functional magnetic resonance imaging (MRI). Regional brain activity was evaluated as the amplitude of low-frequency fluctuation (ALFF). Furthermore, functional connectivity (FC) analyses were performed on areas with altered ALFF to explore alterations in FC patterns.

Results: There was increased ALFF in the left middle frontal gyrus (MFG) and the right postcentral gyrus (PoCG) in MDD with childhood trauma compared with MDD without childhood trauma. The areas with significant ALFF discrepancies were selected as seeds for the FC analyses. There was increased FC between the left MFG and the bilateral putamen gyrus. Moreover, ALFF values were correlated with childhood trauma severity.

Conclusion: Our findings revealed abnormal intrinsic brain activity and FC patterns in female MDD patients with childhood trauma, which provides new possibilities for exploring the pathophysiology of this disorder in women.

KEYWORDS

childhood trauma, amplitude of low-frequency fluctuation, functional connectivity, middle frontal gyrus, postcentral gyrus, putamen

Introduction

Major depressive disorder (MDD) is a serious mental disorder that affects mood, interest, and cognitive function (Otte et al., 2016). It has enduring impacts throughout life (Kessler et al., 2007) and heavy economic and social burdens (Murray et al., 2012; Ferrari et al., 2013). Women are approximately twice as likely to experience MDD as men (Seedat et al., 2009). Thus, being a woman is a risk factor for developing MDD (Otte et al., 2016). Researchers have speculated that the sex differences in MDD development might relate to variations in susceptibility (both physical and psychological) as well as environmental factors that work at both the micro and macro levels (Kuehner, 2017). However, the neural mechanisms underlying female MDD patients remain unclear.

Childhood trauma is a common psychological stressor and includes experiences of abuse and neglect (Bernstein et al., 2003). Multiple studies have reported that childhood trauma can predict psychiatric disorders such as bipolar disorder, anxiety, substance use disorder, post-traumatic stress disorder, and MDD (Baldwin et al., 2019; Hailes et al., 2019; McKay et al., 2021). There are sex differences in childhood trauma. Compared with men, the impact of childhood trauma is even more profound in women. Women also have more complex patterns of childhood trauma (Haahr-Pedersen et al., 2020), and the female sex also plays a synergistic role with childhood trauma in certain mental disorders (e.g., anxiety and depressive episodes) (Whitaker et al., 2021). Previous studies of childhood trauma have focused on neuroendocrinology (Silva et al., 2021; Tan et al., 2021), neuroinflammation (Andersen, 2022), and neuroimaging (Tozzi et al., 2020; Ma et al., 2021) to analyze the intrinsic biological mechanisms of MDD. However, trauma-related brain dysfunction is not fully understood. In particular, brain neuroimaging studies of women with childhood trauma experience remain severely lacking. It is, therefore, important to investigate the pathophysiology and etiology of MDD in women who have experienced childhood trauma.

A growing body of evidence indicates that the amplitude of the low-frequency fluctuation (ALFF) method can be used to capture local brain activity and identify various physiological conditions in the brain (Yang et al., 2007; Yan et al., 2009). Previous studies have detected ALFF alterations in MDD with childhood trauma, including in the left insula, right dorsal anterior cingulate cortex, bilateral amygdala, and left orbital/cerebellum (Du et al., 2016; Wu et al., 2020). Moreover, functional connectivity (FC) methods have been developed to measure both the temporal correlations (Du et al., 2016; Wu et al., 2020) and the coordination of brain activity (Biswal et al., 1995; Noble et al., 2019) among multiple brain regions. Yu et al. (2019) reported that childhood trauma across different dimensions of symptoms is associated with abnormal network architecture in patients with MDD. A combination of ALFF and FC has been recommended to investigate abnormal intrinsic brain function in patients with MDD (Hu et al., 2019; Ebneabbasi et al., 2021; Yan et al., 2022). However, ALFF and FC alterations in female MDD patients with childhood trauma have not yet been investigated. To address this gap, we used ALFF and FC methods to explore brain function and FC patterns in female MDD patients with childhood trauma. The aim of this study was to provide new insights into the underlying neurobiological mechanisms of the disease.

Materials and methods

Participants

Individual mentalization in early adulthood is not yet fully matured, and individuals in early adulthood are more vulnerable to childhood traumatic experiences (Sonu et al., 2019; Hamlat et al., 2021). Interestingly, the scholar found that early adulthood is the peak period of MDD onset (Kessler et al., 2007). However, mental illness in early adulthood did not raise major attention and age has not been well controlled in previous studies. Thus, we only included female participants in early adulthood (18–35) in this research.

A total of 52 early adulthood women were recruited. The diagnosis of MDD was made by professional psychiatrists referring to the Diagnostic and Statistical Manual of Mental Disorders–Fourth Edition (DSM-V) criteria. The 17-item Hamilton Depression Scale (HAMD) (Zimmerman et al., 2013) was used to measure depression severity. The Childhood Trauma Questionnaire (CTQ) was employed to evaluate the negative impact of childhood trauma. The CTQ can be divided into 5 subscales, including emotional abuse (EA), emotional neglect (EN), sexual abuse (SA), physical abuse (PA), and physical neglect (PN). The cutoff points for the CTQ subscale are as follows: (i) EA $\geq$ 13, (ii) EN $\geq$ 15, (iii) SA $\geq$ 8, (iv) PA $\geq$ 10, and (v) PN $\geq$ 10 (Xie et al., 2018; Georgieva et al., 2021). Childhood trauma history was considered to exist in participants scoring over the subscale threshold (moderate–severe). The HAMD and CTQ were only used for the assessment of patients with MDD.

According to the above criterion, participants were divided into MDD with the childhood trauma group (n = 16), MDD without the childhood trauma group (n = 16), and the healthy control group (n = 20). Subjects with MDD were recruited from the outpatient clinics of the Affiliated Brain Hospital of Guangzhou Medical University. We recruited healthy participants from the local community with matching age and education levels. In this study, the exclusion criteria are as follows: (i) any other physical and mental illness except for MDD; (ii) history of seizures, head trauma, or unconsciousness; (iii) received electroconvulsive therapy

TABLE 1 Characteristics of MDD with childhood trauma, MDD without childhood trauma, and HC groups.

Characteristics	MDD with childhood trauma (n = 16)	MDD without childhood trauma (n = 15)	HC (n = 20)	F/T	P-value
Age, years	24.93 ± 3.73	24.26 ± 3.17	23.40 ± 3.16	0.94	0.39[a]
Education, years	13.93 ± 3.76	14.66 ± 2.76	14.35 ± 1.81	0.26	0.77[a]
HAMD	30.00 ± 6.39	30.20 ± 4.97	–	0.64	0.92[b]
CTQ score					
Emotional abuse	11.37 ± 4.67	6.73 ± 1.79	–	3.60	<0.01[b]
Physical abuse	7.00 ± 2.87	6.13 ± 1.55	–	1.03	0.31[b]
Sexual abuse	7.56 ± 4.17	5.26 ± 0.59	–	2.10	0.04[b]
Emotional neglect	18.37 ± 3.11	8.00 ± 2.10	–	10.78	<0.01[b]
Physical neglect	11.31 ± 3.07	5.86 ± 0.91	–	6.59	<0.01[b]
Total	55.62 ± 11.15	32.00 ± 4.32	–	7.67	<0.01[b]

CTQ, Childhood Trauma Questionnaire; HAMD, Hamilton Depression Rating Scale; plus-minus values are means ± S.D.
[a] *The P-values were obtained by one-way analysis of variance test.*
[b] *The P-values were obtained by two sample-test.*

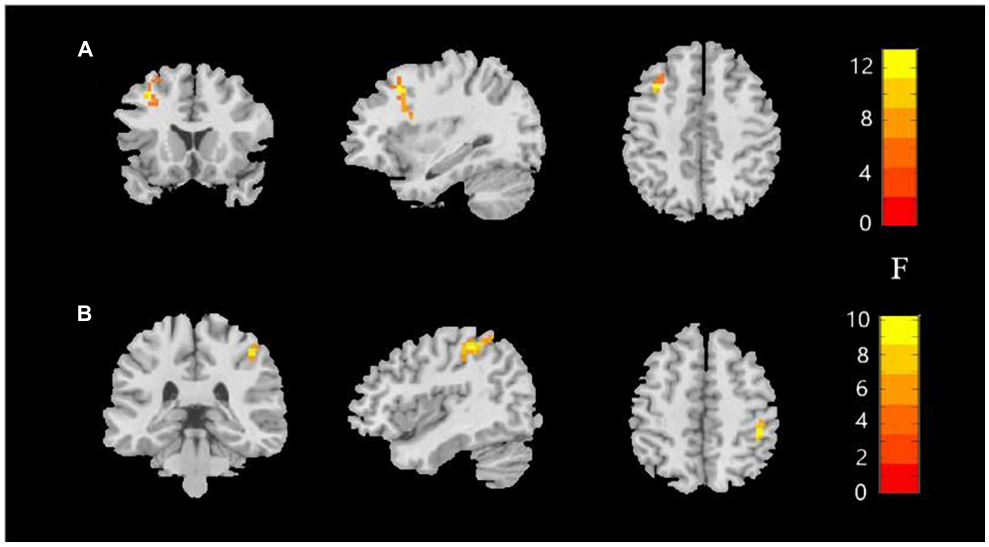

FIGURE 1
Amplitude of low-frequency fluctuations (ALFF) value among the MDD with childhood trauma, MDD without childhood trauma, and HC groups. One-way ANCOVA with age and education as covariates was performed to compare ALFF maps in the experimental groups. Left middle frontal gyrus **(A)** and right postcentral gyrus **(B)** showed the most significant differences according to ALFF analysis (AlphaSim-corrected $p < 0.05$).

TABLE 2 Group differences in amplitude of low-frequency fluctuations in MDD with childhood trauma, MDD without childhood trauma and HC.

Brain regions	Hemisphere	Peak MNI			Cluster size	F
		X	Y	Z		
Middle frontal gyrus	Left	−33	18	45	57	30.40
Postcentral gyrus	Right	42	−33	51	63	16.35

MNI, Montreal Neurological Institute; x, y, z, coordinates of primary peak locations in the MNI space.

within the past 6 months, recently taken contraceptives, and taken psychiatric drugs before; (iv) substance dependence; (v) pregnant, lactating, or menstruating women; and (vi) any contraindications to magnetic resonance imaging (MRI). All participants were fully informed and written informed consent was obtained before enrollment. This study was approved by the Ethics Committee of the Affiliated Brain Hospital of Guangzhou Medical University.

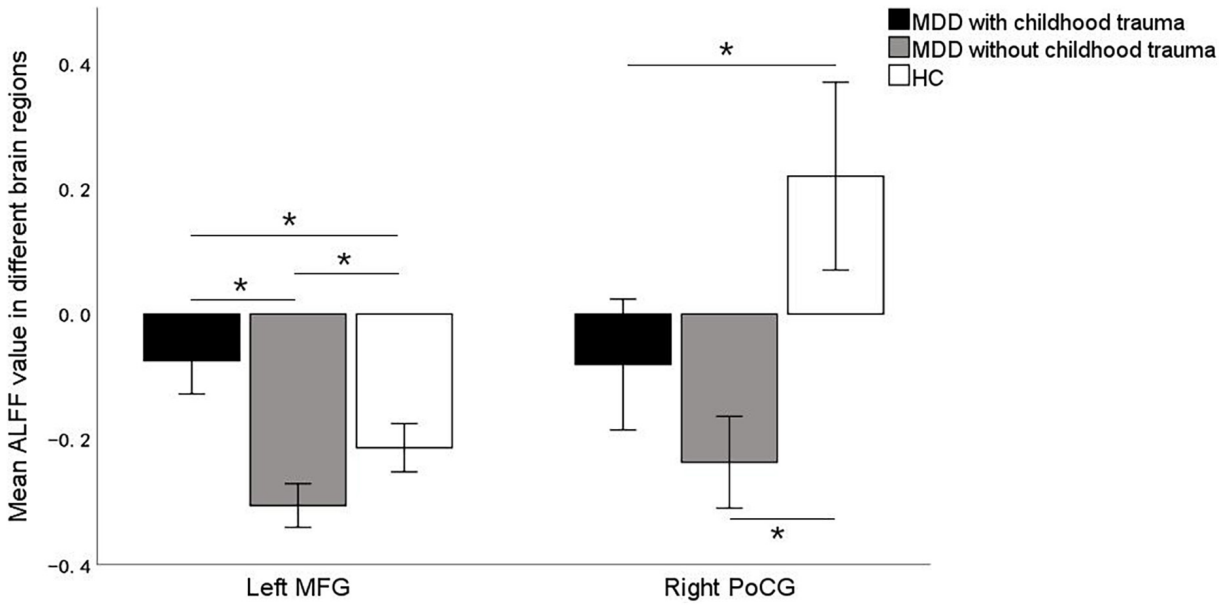

FIGURE 2
Post hoc two samplet—tests were used to determine the between groups differences in ALFF value in left middle frontal gyrus and right postcentral gyrus showing significant differences in ALFF maps in the previous ANOVA. *Bonferroni correction with $P < 0.025$ was set for significance. MFG, middle frontal gyrus; PoCG, postcentral gyrus.

TABLE 3 Multiple comparisons of ALFF in left middle frontal gyrus and right postcentral gyrus.

Brain regions	Pair group (I VS. J)	Mean difference (I–J)	*P*	95%CI	
Left middle frontal gyrus	G1 VS. G2	0.2311	<0.001	0.1567	0.3054
	G1 VS. G3	0.1389	<0.001	0.0695	0.2082
	G2 VS. G3	−0.092	<0.001	−0.1628	−0.0215
Right postcentral gyrus	G1 VS. G2	0.1544	0.242	−0.0603	0.3692
	G1 VS. G3	−0.3008	0.002	−0.5013	−0.1003
	G2 VS. G3	−0.4552	<0.001	−0.6594	−0.2511

G1, MDD with childhood trauma; G2, MDD without childhood trauma; G3, HC.

Magnetic resonance imaging data acquisition

The MRI data were obtained on a 3.0T MRI system (Philips, Best, The Netherlands) in the Affiliated Brain Hospital of Guangzhou Medical University. Tampons were used to reduce noise, while foam pads were used to restrain head movement. During the scan, subjects were asked to remain still and close their eyes, but not fall asleep and think. The parameters of the echo plane imaging (EPI) sequence were as follows: repetition time (TR) = 2,000 ms, echo time (ET) = 30 ms, flip angle = 90°, field of view (FOV) = 220 × 220 mm^2, slices = 33, thickness = 4 mm, inter-slice gap = 0.6 mm, and matrix = 64 × 64. Meanwhile, the parameters of the T1-weighted sagittal images were as follows: TR = 8.2 ms, ET = 3.7 ms, flip angle = 7°, thickness = 1 mm, and matrix = 256 × 256. To strictly control the effect of head movement, we excluded one subject whose head translation was greater than 1.5 mm.

Magnetic resonance imaging data preprocessing

The fMRI data were conducted by a Data Processing Assistant for Resting-State fMRI Advanced Edition V4.5 (DPARSFA)[1] (Yan et al., 2016). In addition to the first 10 volumes being removed, all the images were corrected for temporal differences and head motion. We excluded the participants whose image translation movement was more than 1.5 mm or rotational movement was more than 1.5°. The T1-weighted image was co-registered with the average

1 www.restfmri.net/forum/DPARSF

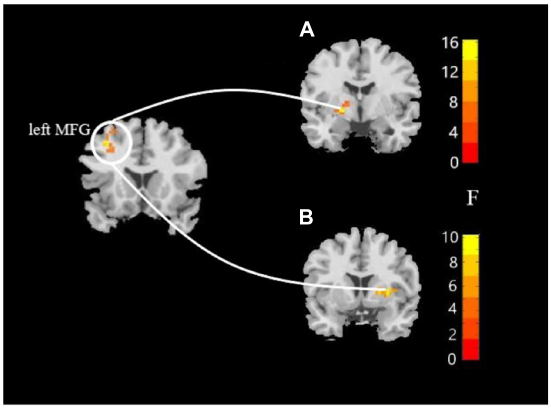

FIGURE 3
Resting-state functional connectivity analyses among MDD with childhood trauma, MDD without childhood trauma, and HC groups. One-way ANCOVA with age and as covariates was performed to compare functional connectivity maps in all the three groups and identified significant differences between left middle frontal gyrus and bilateral putamen (**A**, left putamen gyrus; **B**, right putamen gyrus) (AlphaSim-corrected $p < 0.05$).

functional image after motion correction. Then, the images were normalized to the Montreal Neurological Institute template and resampled to a spatial resolution of $3 \times 3 \times 3$ mm^3. Subsequently, the functional images were smoothed with a Gaussian kernel (full-width half-maximum = 4 mm). In addition, in order to remove the effects of nuisance covariates, we regressed headmotor parameters, white matter signals, and CSF signals. Finally, the time series for each voxel was subjected to linear trend reduction and temporal filtering (0.01–0.08 Hz) to reduce low-frequency drift and high-frequency noise (Biswal et al., 1995; Lowe et al., 1998).

Analysis of amplitude of low-frequency fluctuation

We applied DPASF4.5 to compute ALFF and FC. Briefly, we converted the frequency domain power spectrum of the whole-brain signal with the fast Fourier transform. In addition, based on the power spectrum between 0.01 and 0.08 Hz, we calculated the ALFF. Finally, to minimize variability in general whole-brain ALFF levels between participants, the ALFF value was standardized to the *Z*-value (zALFF).

Analysis of functional connectivity

Subsequently, a seed-based interregional FC analysis was conducted. Seeds were chosen from brain regions correlated with childhood trauma in between-group ALFF discrepancy. FC analysis was calculated after a time series of the seed area average was extracted. The seed area and the rest of the brain were then correlated voxel-by-voxel. Finally, in order to enhance the normality of the correlation coefficient, we performed a Fisher's r to z transformation.

Statistical analysis

Statistical analyses were calculated using Statistical Package for the Social Sciences, version 19.0 (SPSS, Inc., Chicago, United States). Group differences in demographic and clinical data were assessed by one-way analysis of covariance (ANCOVA) or two sample *t*-tests. In this study, significant differences were defined as $p < 0.05$.

To identify the significance of the brain district that had altered ALFF and FC values, a voxel-based ANCOVA was conducted using education and age as covariates. The significance was set with a cluster-level corrected threshold of $p < 0.05$ (cluster-forming threshold at voxel level $p < 0.001$ using the AlphaSim method) (Forman et al., 1995; Poline et al., 1997). Then, to examine group differences in mean ALFF and FC values, two sample *t*-tests were conducted on three groups identified after ANCOVA. Multiple comparison correction was employed with the Bonferroni method, and the significance level was determined at $p < 0.05/2 = 0.025$ (voxel-wise concordance analysis resulting in two significant clusters). In addition, partial correlation analyses were performed to discover the contact of voxel-wise concordance with CTO score in all subjects with MDD [$p < 0.05/12 = 0.0041$ with Bonferroni correction of 12 being due to two clusters and 6 scales (i.e., CTO scale and its 5 subscales)]. Finally, we further explored the association of brain dysfunction with childhood trauma in female patients

TABLE 4 FC differences between left middle frontal gyrus seed and left putamen gyrus and right putamen gyrus in MDD with childhood trauma, MDD without childhood trauma, and HC.

Seed	Brain regions	Peak MNI			Cluster size	*F*
		X	Y	Z		
Left middle frontal gyrus	Left putamen gyrus	−21	−3	−3	74	12.41
	Right putamen gyrus	30	6	3	81	8.57

MNI, Montreal Neurological Institute; x, y, z, coordinates of primary peak locations in the MNI space.

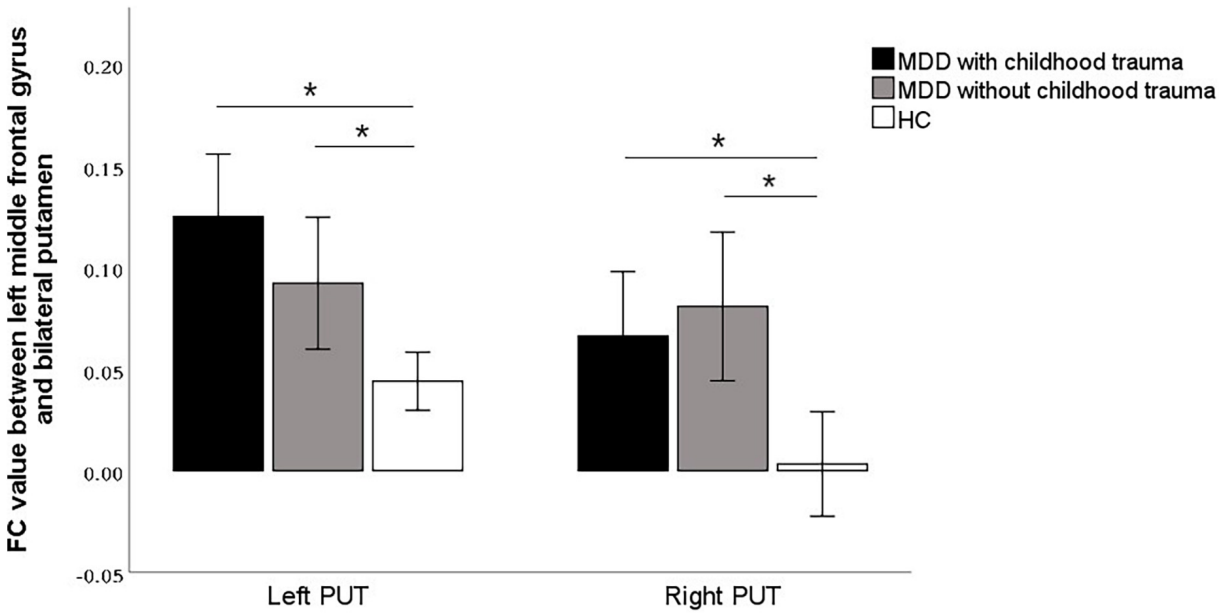

FIGURE 4
Post hoc analyses revealed significant increased functional connectivity of left PUT to left middle frontal gyrus in MDD with childhood trauma compared to both MDD without childhood trauma and HC group. The functional connectivity of right PUT to left middle frontal gyrus in the MMD patient groups were significantly higher than that in the HC group, but there was no significant difference between those with and without childhood trauma. *Bonferroni correction with $P < 0.025$ was set for significance.

TABLE 5 Multiple comparisons of functional connectivity between left middle frontal gyrus seed and left putamen gyrus and right putamen gyrus.

Seed	Brain regions	Pair group (I VS. J)	Mean difference (I–J)	*P*	95%CI	
Left middle frontal gyrus	Left putamen gyrus	G1 VS. G2	0.0328	0.207	−0.0109	0.0766
		G1 VS. G3	0.0810	<0.001	0.0401	0.1219
		G2 VS. G3	0.0482	0.018	0.0065	0.0898
	Right putamen gyrus	G1 VS. G2	−0.0145	1.000	−0.0677	0.0387
		G1 VS. G3	0.0629	0.009	0.0132	0.1126
		G2 VS. G3	0.0774	0.001	0.0268	0.1281

G1, MDD with childhood trauma; G2, MDD without childhood trauma; G3, HC.

with MDD by multiple linear regression with CTQ total scores and the characteristic values of brain region (ALFF and FC). Age and education were considered control variables in partial correlation and multiple linear regression.

Results

Demographic and clinical measures

As shown in Table 1, no significant difference was found in age and education level among the three groups (all $p < 0.05$). Significant differences were detected in CTQ total score and its subscale scores (e.g., EA, EN, SA, and PN) between MDD with the childhood trauma group and MDD without the childhood trauma group.

Assessed by one-way analysis of covariance plus *post hoc* comparisons of amplitude of low-frequency fluctuation

Significant ALFF alterations were found in the left middle frontal gyrus (MFG) (57 voxels) and the right postcentral gyrus (PoCG) (63 voxels) between the three groups (Figure 1 and Table 2). MDD with the childhood trauma group revealed increased ALFF values in the left MFG compared to MDD without the childhood trauma group and the HC group (Figure 2 and Table 3). Moreover, decreased ALFF was detected in the right PoCG in MMD patient groups relative to the HC group. Nonetheless, no significant ALFF difference was discovered among MDD with and without childhood trauma groups (Figure 2 and Table 3).

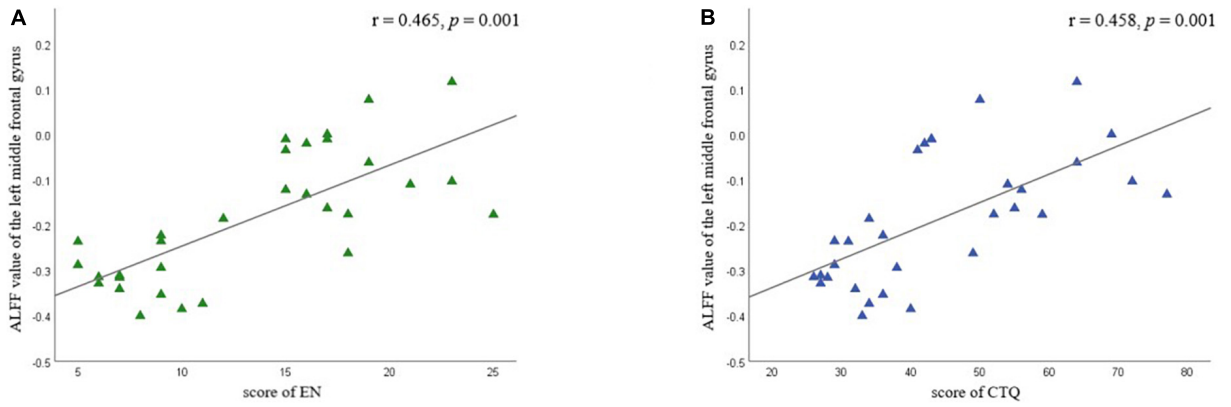

FIGURE 5
Partial correlation analyses between amplitude of low-frequency fluctuation value (ALFF) in left middle frontal gyrus and childhood trauma scores in different subscale were performed by combining all of MDD participants as a whole. Age and education were considered as control variables. **(A)** Shows the correlation between EN scores and ALFF value of the left middle frontal gyrus; **(B)** shows the correlation between CTQ total scores and ALFF value of the left middle frontal gyrus. EA, emotional neglect.

TABLE 6 Partial correlation between CTQ scores and ALFF.

Brain regions	Emotional abuse		Physical abuse		Sexual abuse		Emotional neglect		Physical neglect		Total score of CTQ	
	r	*P*	*r*	*P*	*r*	*P*	*r*	*P*	*r*	*P*	*r*	*P*
Left middle frontal gyrus	0.262	0.068	0.091	0.533	0.352	0.013	0.465*	0.001	0.331	0.020	0.458*	0.001
Right postcentral gyrus	−0.009	0.949	−0.018	0.903	0.025	0.865	0.142	0.329	0.236	0.102	0.116	0.426

ALFF, amplitude of low-frequency fluctuations; CTQ, Childhood Trauma Questionnaire.
Age and education were considered as control variables.
*$p_{adj} < 0.004$, corrected for multiple comparisons.

Functional connectivity analyses

In this study, the brain areas that showed group differences in the ALFF analysis were selected as seed (i.e., left MFG) in the FC analysis. Significant FC difference in the left MFG–bilateral putamen was observed between groups (**Figure 3** and **Table 4**). Compared to the HC group, MDD groups showed increased FC between left MFG and bilateral putamen (**Figure 4** and **Table 5**). However, no observable discrepancy was found between MDD with and without childhood trauma (**Figure 4** and **Table 5**).

Partial correlation analyses and multiple linear regressions analyses

Partial correlation analysis confirmed the positive correlation between ALFF in the left MFG and EN scores ($r = 0.465$ $p = 0.001$) and CTQ total score ($r = 0.458$, $p = 0.001$), respectively (**Figure 5** and **Table 6**). We did not find a significant correlation between FC and CTQ total scores or its subscale scores. Regression analyses further showed the correlation of ALFF value in the left MFG on childhood trauma ($F = 2.476$, $p < 0.05$) (**Table 7**).

Discussion

In this study, we focused on ALFF and FC alterations in female MDD patients with childhood trauma. There was increased ALFF in the left MFG and right PoCG in MDD with childhood trauma compared with MDD without childhood trauma. The brain regions with significant ALFF discrepancies were selected as seeds for the FC analyses. There was increased FC in the left MFG and bilateral putamen gyrus. Moreover, we confirmed an association between altered ALFF and childhood trauma history. Together, our findings indicate the presence of abnormal intrinsic brain activity and FC patterns in female MDD patients with childhood trauma. The results of our research also offer important insights into the neurobiological mechanisms of MDD and childhood trauma.

An interesting finding in this study was that, in the left MFG, ALFF was higher in the MDD group with childhood trauma than in the group without childhood trauma. In addition, ALFF was positively correlated with CTQ scores and EN. Previous studies have reported that left MFG activation is associated with working memory (Zhang et al., 2003), the processing of social information and social perception (Vollm et al., 2006), memory retrieval (Tulving et al., 1994), and emotion

regulation (Ochsner and Gross, 2005; Bermpohl et al., 2006). This area is also associated with rumination (Wang et al., 2018), which in turn increases an individual's risk of MDD (Abela and Hankin, 2011). For example, Shors et al. (2017) reported that interventions targeting rumination generally reduce MDD incidence in women. Furthermore, O'Mahen et al. (2015) revealed that EN and abuse in childhood are associated with depression, with rumination partially mediating this effect. To some extent, our findings support this conjecture. Local brain activity may be affected by previous childhood trauma, especially EN, which in turn affects cognitive processing patterns such as rumination. Notably, Tulving et al. (1994) reported that the left MFG is related to memory retrieval. Thus, abnormal left MFG activation in individuals with childhood trauma may repeatedly trigger traumatic memories and exacerbate rumination. This may be the underlying cause of heightened depressive symptoms in MDD patients with childhood trauma. Overall, our results suggest that abnormal left MFG function might indicate the impact of childhood trauma in young adult women with MDD.

We also revealed that patients with MDD were at a higher risk for dysfunction in the right PoCG; however, there were no significant differences between patients with and without childhood trauma. Numerous studies have noted that the PoCG is mainly involved in the processing of some sensory information (Phillips et al., 2003), cognitive activities (Wager and Smith, 2003), and emotional processing (Luo et al., 2022). Tadayonnejad et al. (2015) reported that regional properties of neural activity in the PoCG are associated with depression severity. Moreover, neuroimaging studies have demonstrated structural and functional changes in the precentral and postcentral gyri of patients with MDD (Guo et al., 2011; Wang et al., 2012). Abnormal brain function in the PoCG may thus be a unique neurobiological feature of MDD; our results support this idea. Together, these findings provide theoretical support for further research into the relationship between the PoCG and MDD.

In this study, we investigated FC patterns in female MDD patients with childhood trauma. We measured the FC of each cluster vs. the rest of the brain using altered ALFF clusters with clinical correlations as the ROIs. The FC between the left MFG and bilateral putamen was observably increased in the MDD group compared with the HC group. The putamen is associated with motor control and learning (Luo et al., 2020), is one of the core regions for emotion production and processing (Wager et al., 2003), and plays an important role in cognitive and executive functions (Peters et al., 2016). Su et al. (2018) reported that a decrease in glucose metabolism in the putamen of patients with MDD impaired FC to key centers, such as the inferior and middle frontal gyri. Although the results of our study differed from those of predecessors, the discrepancies may be caused by differences in sample size, research subjects, or other reasons. Abnormal connectivity between the MFG and the putamen appears to be an important characteristic of MDD. However, our study revealed that the FC between the left MFG and bilateral putamen had no observable discrepancy in the MDD with the childhood trauma group compared with the MDD without the childhood trauma group. Jeong et al. (2021) found that trauma exposure may be related to structural alterations in the MFG and putamen. Thus, trauma exposure may also be an important factor underlying structural abnormalities of the MFG and putamen, but we need further research to find out if there are also functional abnormalities in this brain region. Furthermore, both trauma exposure and MDD appear to be associated with these two cognitively related regions. Thus, perhaps the main crux of depression with childhood trauma is changing in cognition; this may have a certain guiding significance for the clinical treatment of MDD and will be a major direction of our future research. Collectively, our findings provide an important base for investigating the neuropathological mechanisms of MDD as well as those of childhood trauma.

Our study has certain limitations. First, it remains unclear whether self-reported trauma history reflects authentic experiences during childhood and early adolescence. To minimize information bias, we, therefore, conducted in-depth interviews to confirm adverse childhood experiences. In addition, the study age was set at early adulthood (18–35 years of age) to minimize any differences in the duration of childhood trauma. However, this study did not further subdivide the types of childhood trauma. This is also the direction of future research to further analyze the effects of childhood trauma on the brain in terms of different dimensions, intensities, and durations, for example. Second, this study used a cross-sectional approach with small sample size and lacked any comparisons with the male population. The current results should, therefore, be interpreted with caution. Future studies will expand the sample size to further validate the results and add a male control group to investigate whether the identified brain regions are unique to women.

TABLE 7 Multiple linear regressions analyses between childhood trauma and brain dysfunction.

	R^2	F	B	T
Step1				
Age	0.048	1.22	0.136	0.885
Education			−0.236	−1.534
Step2				
Age	0.204*	2.476*	−0.009	−0.055
Education			−0.142	−0.98
ALFF of left MFG			0.452	3.115*
ALFF of right PoCG			0.026	0.176
FC of right PUT			−0.084	−0.433
FC of left PUT			0.049	0.253

*$p < 0.05$.

Conclusion

Overall, after controlling age-related confounding factors as much as possible, our study found that left MFG abnormality and left MFG–putamen dysfunction may be unique neural mechanisms in female MDD patients with childhood trauma. Our findings provide a basis for future research into the relationship between childhood trauma and MDD.

Data availability statement

The raw data supporting the conclusions of this article will be made available by the authors, without undue reservation.

Ethics statement

The studies involving human participants were reviewed and approved by The Affiliated Brain Hospital of Guangzhou Medical University. The patients/participants provided their written informed consent to participate in this study.

Author contributions

HP, HW, and JC designed the experiments. YL, ZW, XL, JY, HY, HN, and YD performed the clinical data collection and assessment. JC and QL performed the neuroimaging data analysis and wrote the draft. All authors discussed the results and reviewed the manuscript.

Funding

The Guangdong Natural Science Foundation, China (2015A030313800 to HP), supported the design of the study. The Guangzhou Municipal Key Discipline in Medicine for Guangzhou Brain Hospital (GBH2014-ZD04 to HP) supported the data collection for the study.

Conflict of interest

The authors declare that the research was conducted in the absence of any commercial or financial relationships that could be construed as a potential conflict of interest.

Publisher's note

References

Abela, J. R., and Hankin, B. L. (2011). Rumination as a vulnerability factor to depression during the transition from early to middle adolescence: A multiwave longitudinal study. *J. Abnorm. Psychol.* 120, 259–271. doi: 10.1037/a0022796

Andersen, S. L. (2022). Neuroinflammation, Early-Life Adversity, and Brain Development. *Harv. Rev. Psychiatry* 30, 24–39. doi: 10.1097/HRP.0000000000000325

Baldwin, J. R., Reuben, A., Newbury, J. B., and Danese, A. (2019). Agreement Between Prospective and Retrospective Measures of Childhood Maltreatment: A Systematic Review and Meta-analysis. *JAMA Psychiatry* 76, 584–593. doi: 10.1001/jamapsychiatry.2019.0097

Bermpohl, F., Pascual-Leone, A., Amedi, A., Merabet, L. B., Fregni, F., Gaab, N., et al. (2006). Attentional modulation of emotional stimulus processing: An fMRI study using emotional expectancy. *Hum. Brain Mapp.* 27, 662–677. doi: 10.1002/hbm.20209

Bernstein, D. P., Stein, J. A., Newcomb, M. D., Walker, E., Pogge, D., Ahluvalia, T., et al. (2003). Development and validation of a brief screening version of the Childhood Trauma Questionnaire. *Child Abuse Negl.* 27, 169–190. doi: 10.1016/s0145-2134(02)00541-0

Biswal, B., Yetkin, F. Z., Haughton, V. M., and Hyde, J. S. (1995). Functional connectivity in the motor cortex of resting human brain using echo-planar MRI. *Magn. Reson. Med.* 34, 537–541. doi: 10.1002/mrm.1910340409

Du, L., Wang, J., Meng, B., Yong, N., Yang, X., Huang, Q., et al. (2016). Early life stress affects limited regional brain activity in depression. *Sci. Rep.* 6:25338. doi: 10.1038/srep25338

Ebneabbasi, A., Mahdipour, M., Nejati, V., Li, M., Liebe, T., Colic, L., et al. (2021). Emotion processing and regulation in major depressive disorder: A 7T resting-state fMRI study. *Hum. Brain Mapp.* 42, 797–810. doi: 10.1002/hbm.25263

Ferrari, A. J., Charlson, F. J., Norman, R. E., Patten, S. B., Freedman, G., Murray, C. J., et al. (2013). Burden of depressive disorders by country, sex, age, and year: Findings from the global burden of disease study 2010. *PLoS Med.* 10:e1001547. doi: 10.1371/journal.pmed.1001547

Forman, S. D., Cohen, J. D., Fitzgerald, M., Eddy, W. F., Mintun, M. A., and Noll, D. C. (1995). Improved assessment of significant activation in functional magnetic resonance imaging (fMRI): Use of a cluster-size threshold. *Magn. Reson. Med.* 33, 636–647. doi: 10.1002/mrm.1910330508

Georgieva, S., Tomas, J. M., and Navarro-Perez, J. J. (2021). Systematic review and critical appraisal of Childhood Trauma Questionnaire - Short Form (CTQ-SF). *Child Abuse Negl.* 120:105223. doi: 10.1016/j.chiabu.2021.105223

Guo, W. B., Liu, F., Xue, Z. M., Yu, Y., Ma, C. Q., Tan, C. L., et al. (2011). Abnormal neural activities in first-episode, treatment-naive, short-illness-duration, and treatment-response patients with major depressive disorder: A resting-state fMRI study. *J. Affect. Disord.* 135, 326–331. doi: 10.1016/j.jad.2011.06.048

Haahr-Pedersen, I., Perera, C., Hyland, P., Vallieres, F., Murphy, D., Hansen, M., et al. (2020). Females have more complex patterns of childhood adversity: Implications for mental, social, and emotional outcomes in adulthood. *Eur. J. Psychotraumatol.* 11:1708618. doi: 10.1080/20008198.2019.1708618

Hailes, H. P., Yu, R., Danese, A., and Fazel, S. (2019). Long-term outcomes of childhood sexual abuse: An umbrella review. *Lancet Psychiatry* 6, 830–839. doi: 10.1016/S2215-0366(19)30286-X

Hamlat, E. J., Prather, A. A., Horvath, S., Belsky, J., and Epel, E. S. (2021). Early life adversity, pubertal timing, and epigenetic age acceleration in adulthood. *Dev. Psychobiol.* 63, 890–902. doi: 10.1002/dev.22085

Hu, L., Xiao, M., Ai, M., Wang, W., Chen, J., Tan, Z., et al. (2019). Disruption of resting-state functional connectivity of right posterior insula in adolescents and young adults with major depressive disorder. *J. Affect. Disord.* 257, 23–30. doi: 10.1016/j.jad.2019.06.057

Jeong, H. J., Durham, E. L., Moore, T. M., Dupont, R. M., McDowell, M., Cardenas-Iniguez, C., et al. (2021). The association between latent trauma and brain structure in children. *Transl. Psychiatry* 11:240. doi: 10.1038/s41398-021-01357-z

Kessler, R. C., Angermeyer, M., Anthony, J. C., De Graaf, R., Demyttenaere, K., Gasquet, I., et al. (2007). Lifetime prevalence and age-of-onset distributions of mental disorders in the World Health Organization's World Mental Health Survey Initiative. *World Psychiatry* 6, 168–176.

Kuehner, C. (2017). Why is depression more common among women than among men? *Lancet Psychiatry* 4, 146–158. doi: 10.1016/S2215-0366(16)30263-2

Lowe, M. J., Mock, B. J., and Sorenson, J. A. (1998). Functional connectivity in single and multislice echoplanar imaging using resting-state fluctuations. *Neuroimage* 7, 119–132. doi: 10.1006/nimg.1997.0315

Luo, Q., Chen, J., Li, Y., Wu, Z., Lin, X., Yao, J., et al. (2022). Altered regional brain activity and functional connectivity patterns in major depressive disorder: A function of childhood trauma or diagnosis? *J. Psychiatry Res.* 147, 237–247. doi: 10.1016/j.jpsychires.2022.01.038

Luo, X., Guo, X., Tan, Y., Zhang, Y., Garcia-Milian, R., Wang, Z., et al. (2020). KTN1 variants and risk for attention deficit hyperactivity disorder. *Am. J. Med. Genet. B Neuropsychiatr. Genet.* 183, 234–244. doi: 10.1002/ajmg.b.32782

Ma, M., Zhang, X., Zhang, Y., Su, Y., Yan, H., Tan, H., et al. (2021). Childhood Maltreatment Was Correlated With the Decreased Cortical Function in Depressed Patients Under Social Stress in a Working Memory Task: A Pilot Study. *Front. Psychiatry* 12:671574. doi: 10.3389/fpsyt.2021.671574

McKay, M. T., Cannon, M., Chambers, D., Conroy, R. M., Coughlan, H., Dodd, P., et al. (2021). Childhood trauma and adult mental disorder: A systematic review and meta-analysis of longitudinal cohort studies. *Acta Psychiatr. Scand.* 143, 189–205. doi: 10.1111/acps.13268

Murray, C. J., Vos, T., Lozano, R., Naghavi, M., Flaxman, A. D., Michaud, C., et al. (2012). Disability-adjusted life years (DALYs) for 291 diseases and injuries in 21 regions, 1990-2010: A systematic analysis for the Global Burden of Disease Study 2010. *Lancet* 380, 2197–2223. doi: 10.1016/S0140-6736(12)61689-4

Noble, S., Scheinost, D., and Constable, R. T. (2019). A decade of test-retest reliability of functional connectivity: A systematic review and meta-analysis. *Neuroimage* 203:116157. doi: 10.1016/j.neuroimage.2019.116157

Ochsner, K. N., and Gross, J. J. (2005). The cognitive control of emotion. *Trends Cogn. Sci.* 9, 242–249. doi: 10.1016/j.tics.2005.03.010

O'Mahen, H. A., Karl, A., Moberly, N., and Fedock, G. (2015). The association between childhood maltreatment and emotion regulation: Two different mechanisms contributing to depression? *J. Affect. Disord.* 174, 287–295. doi: 10.1016/j.jad.2014.11.028

Otte, C., Gold, S. M., Penninx, B. W., Pariante, C. M., Etkin, A., Fava, M., et al. (2016). Major depressive disorder. *Nat. Rev. Dis. Primers* 2:16065. doi: 10.1038/nrdp.2016.65

Peters, S. K., Dunlop, K., and Downar, J. (2016). Cortico-Striatal-Thalamic Loop Circuits of the Salience Network: A Central Pathway in Psychiatric Disease and Treatment. *Front. Syst. Neurosci.* 10:104. doi: 10.3389/fnsys.2016.00104

Phillips, M. L., Drevets, W. C., Rauch, S. L., and Lane, R. (2003). Neurobiology of emotion perception II: Implications for major psychiatric disorders. *Biol. Psychiatry* 54, 515–528. doi: 10.1016/s0006-3223(03)00171-9

Poline, J. B., Worsley, K. J., Evans, A. C., and Friston, K. J. (1997). Combining spatial extent and peak intensity to test for activations in functional imaging. *Neuroimage* 5, 83–96. doi: 10.1006/nimg.1996.0248

Seedat, S., Scott, K. M., Angermeyer, M. C., Berglund, P., Bromet, E. J., Brugha, T. S., et al. (2009). Cross-national associations between gender and mental disorders in the World Health Organization World Mental Health Surveys. *Arch Gen. Psychiatry* 66, 785–795. doi: 10.1001/archgenpsychiatry.2009.36

Shors, T. J., Millon, E. M., Chang, H. Y., Olson, R. L., and Alderman, B. L. (2017). Do sex differences in rumination explain sex differences in depression? *J. Neurosci. Res.* 95, 711–718. doi: 10.1002/jnr.23976

Silva, R. C., Maffioletti, E., Gennarelli, M., Baune, B. T., and Minelli, A. (2021). Biological correlates of early life stressful events in major depressive disorder. *Psychoneuroendocrinology* 125:105103. doi: 10.1016/j.psyneuen.2020.105103

Sonu, S., Post, S., and Feinglass, J. (2019). Adverse childhood experiences and the onset of chronic disease in young adulthood. *Prev. Med.* 123, 163–170. doi: 10.1016/j.ypmed.2019.03.032

Su, H., Zuo, C., Zhang, H., Jiao, F., Zhang, B., Tang, W., et al. (2018). Regional cerebral metabolism alterations affect resting-state functional connectivity in major depressive disorder. *Quant. Imaging Med. Surg.* 8, 910–924. doi: 10.21037/qims.2018.10.05

Tadayonnejad, R., Yang, S., Kumar, A., and Ajilore, O. (2015). Clinical, cognitive, and functional connectivity correlations of resting-state intrinsic brain activity alterations in unmedicated depression. *J. Affect. Disord.* 172, 241–250. doi: 10.1016/j.jad.2014.10.017

Tan, X., Zhang, L., Wang, D., Guan, S., Lu, P., Xu, X., et al. (2021). Influence of early life stress on depression: From the perspective of neuroendocrine to the participation of gut microbiota. *Aging* 13, 25588–25601. doi: 10.18632/aging.203746

Tozzi, L., Garczarek, L., Janowitz, D., Stein, D. J., Wittfeld, K., Dobrowolny, H., et al. (2020). Interactive impact of childhood maltreatment, depression, and age on cortical brain structure: Mega-analytic findings from a large multi-site cohort. *Psychol. Med.* 50, 1020–1031. doi: 10.1017/S003329171900093X

Tulving, E., Kapur, S., Markowitsch, H. J., Craik, F. I., Habib, R., and Houle, S. (1994). Neuroanatomical correlates of retrieval in episodic memory: Auditory sentence recognition. *Proc. Natl. Acad. Sci. U.S.A.* 91, 2012–2015. doi: 10.1073/pnas.91.6.2012

Vollm, B. A., Taylor, A. N., Richardson, P., Corcoran, R., Stirling, J., McKie, S., et al. (2006). Neuronal correlates of theory of mind and empathy: A functional magnetic resonance imaging study in a nonverbal task. *Neuroimage* 29, 90–98. doi: 10.1016/j.neuroimage.2005.07.022

Wager, T. D., and Smith, E. E. (2003). Neuroimaging studies of working memory: A meta-analysis. *Cogn. Affect. Behav. Neurosci.* 3, 255–274. doi: 10.3758/cabn.3.4.255

Wager, T. D., Phan, K. L., Liberzon, I., and Taylor, S. F. (2003). Valence, gender, and lateralization of functional brain anatomy in emotion: A meta-analysis of findings from neuroimaging. *Neuroimage* 19, 513–531. doi: 10.1016/s1053-8119(03)00078-8

Wang, L., Dai, W., Su, Y., Wang, G., Tan, Y., Jin, Z., et al. (2012). Amplitude of low-frequency oscillations in first-episode, treatment-naive patients with major depressive disorder: A resting-state functional MRI study. *PLoS One* 7:e48658. doi: 10.1371/journal.pone.0048658

Wang, Y., Zhu, W., Xiao, M., Zhang, Q., Zhao, Y., Zhang, H., et al. (2018). Hostile Attribution Bias Mediates the Relationship Between Structural Variations in the Left Middle Frontal Gyrus and Trait Angry Rumination. *Front. Psychol.* 9:526. doi: 10.3389/fpsyg.2018.00526

Whitaker, R. C., Dearth-Wesley, T., Herman, A. N., Block, A. E., Holderness, M. H., Waring, N. A., et al. (2021). The interaction of adverse childhood experiences and gender as risk factors for depression and anxiety disorders in US adults: A cross-sectional study. *BMC Public Health* 21:2078. doi: 10.1186/s12889-021-12058-z

Wu, Z., Luo, Q., Wu, H., Wu, Z., Zheng, Y., Yang, Y., et al. (2020). Amplitude of Low-Frequency Oscillations in Major Depressive Disorder With Childhood Trauma. *Front. Psychiatry* 11:596337. doi: 10.3389/fpsyt.2020.596337

Xie, P., Wu, K., Zheng, Y., Guo, Y., Yang, Y., He, J., et al. (2018). Prevalence of childhood trauma and correlations between childhood trauma, suicidal ideation, and social support in patients with depression, bipolar disorder, and schizophrenia in southern China. *J. Affect. Disord.* 228, 41–48. doi: 10.1016/j.jad.2017.11.011

Yan, C. G., Wang, X. D., Zuo, X. N., and Zang, Y. F. (2016). DPABI: Data Processing & Analysis for (Resting-State) Brain Imaging. *Neuroinformatics* 14, 339–351. doi: 10.1007/s12021-016-9299-4

Yan, C., Liu, D., He, Y., Zou, Q., Zhu, C., Zuo, X., et al. (2009). Spontaneous brain activity in the default mode network is sensitive to different resting-state conditions with limited cognitive load. *PLoS One* 4:e5743. doi: 10.1371/journal.pone.0005743

Yan, R., Huang, Y., Shi, J., Zou, H., Wang, X., Xia, Y., et al. (2022). Alterations of regional spontaneous neuronal activity and corresponding brain circuits related to non-suicidal self-injury in young adults with major depressive disorder. *J. Affect. Disord.* 305, 8–18. doi: 10.1016/j.jad.2022.02.040

Yang, H., Long, X. Y., Yang, Y., Yan, H., Zhu, C. Z., Zhou, X. P., et al. (2007). Amplitude of low frequency fluctuation within visual areas revealed by resting-state functional MRI. *Neuroimage* 36, 144–152.

Yu, M., Linn, K. A., Shinohara, R. T., Oathes, D. J., Cook, P. A., Duprat, R., et al. (2019). Childhood trauma history is linked to abnormal brain connectivity in major depression. *Proc. Natl. Acad. Sci. U.S.A.* 116, 8582–8590. doi: 10.1073/pnas.1900801116

Zhang, J. X., Leung, H. C., and Johnson, M. K. (2003). Frontal activations associated with accessing and evaluating information in working memory: An fMRI study. *Neuroimage* 20, 1531–1539. doi: 10.1016/j.neuroimage.2003.07.016

Zimmerman, M., Martinez, J. H., Young, D., Chelminski, I., and Dalrymple, K. (2013). Severity classification on the Hamilton Depression Rating Scale. *J. Affect. Disord.* 150, 384–388. doi: 10.1016/j.jad.2013.04.028

frontiers | Frontiers in Neuroscience

TYPE Original Research
PUBLISHED 23 August 2022
DOI 10.3389/fnins.2022.929383

OPEN ACCESS

EDITED BY
Zhifen Liu,
First Hospital of Shanxi Medical University, China

REVIEWED BY
Yi Zhao,
Sichuan University, China
Zhenbiao Wu,
The Fourth Military Medical University, China
Jiuliang Zhao,
Peking Union Medical College Hospital (CAMS), China
Afis Ajala,
GE Global Research, United States

*CORRESPONDENCE
Jian Xu
jianxu777@126.com

†These authors have contributed equally to this work

SPECIALTY SECTION
This article was submitted to Brain Imaging Methods, a section of the journal Frontiers in Neuroscience

RECEIVED 26 April 2022
ACCEPTED 01 August 2022
PUBLISHED 23 August 2022

CITATION
Yang Y, Zhao R, Zhang F, Bai R, Li S, Cui R, Liu S and Xu J (2022) Dynamic changes of amplitude of low-frequency in systemic lupus erythematosus patients with cognitive impairment.
Front. Neurosci. 16:929383.
doi: 10.3389/fnins.2022.929383

Dynamic changes of amplitude of low-frequency in systemic lupus erythematosus patients with cognitive impairment

Yifan Yang[1†], Ruotong Zhao[1†], Fengrui Zhang[2†], Ru Bai[1], Shu Li[1], Ruomei Cui[1], Shuang Liu[1] and Jian Xu[1*]

[1]Department of Rheumatology and Immunology, First Affiliated Hospital of Kunming Medical University, Kunming, China, [2]Department of Magnetic Resonance Imaging, First Affiliated Hospital of Kunming Medical University, Kunming, China

Background: Cognitive dysfunction (CI) is frequently reported in patients with systemic lupus erythematosus (SLE), but the identification and assessment of SLE-related CI remain challenging. Previous studies have focused on changes in static brain activity, and no studies have investigated the characteristics of dynamic brain activity in SLE patients with CI.

Objects: We calculated the dynamic amplitude of low-frequency fluctuation (dALFF) by combining the ALFF with a sliding window method to assess the temporal variability of brain functional activity in SLE patients with and without CI.

Methods: Thirty-eight SLE with CI, thirty-eight SLE without CI, and thirty-eight healthy controls (HCs) were recruited. By comparing static ALFF (sALFF) and dALFF among the three groups, changes in brain activity intensity and its temporal variability were assessed in patients with SLE with or without CI. Spearman correlation coefficients were calculated between the brain function indicator and Mini-mental State Examination (MMSE) scores of SLE with CI.

Results: Subjects among the three groups exhibited significant sALFF differences in the right parahippocampal gyrus, left caudate nucleus, right putamen, and left cuneus. Compared to the SLE without CI, the right parahippocampal gyrus exhibited higher sALFF in the SLE with CI group. Compared to the HCs, the left caudate nucleus exhibited increased sALFF in the SLE with CI group. Participants in the three groups exhibited significant dALFF variability in the right parahippocampal gyrus, right lingual gyrus, and bilateral inferior occipital gyrus. Compared to the HCs, the right lingual gyrus exhibited reduced dALFF in the SLE without CI group. Compared to the HCs, the right parahippocampal gyrus exhibited increased dALFF, left calcarine fissure, and the surrounding cortex exhibited reduced dALFF in the SLE with CI group. There was no significant correlation between the MMSE score, sALFF, and dALFF in the SLE with CI group.

Conclusion: SLE patients with CI have abnormal brain activity intensity and stability. By analyzing the dynamics of intrinsic brain activity, it provides a new idea for evaluating SLE-related CI. However, more research and validation with multiple metrics are needed to determine the link between the severity of cognitive impairment (CI) and brain activity in patients with SLE.

KEYWORDS

systemic lupus erythematosus, cognitive impairment, resting-state fMRI, dynamic amplitude of low-frequency fluctuation, static amplitude of low-frequency fluctuation

Introduction

Systemic lupus erythematosus (SLE) is a typical autoimmune disease with a global prevalence rate of 0–241/100,000 (Rees et al., 2017). When SLE involves the central and/or peripheral nervous system, it is called neuropsychiatric systemic lupus erythematosus (NPSLE). The clinical manifestations of NPSLE are complex, ranging from mild headache, cognitive impairment (CI), mood disturbance, a series of neurological symptoms, and mental disorders ranging from subtle abnormalities, such as neuritis, to severe manifestations such as epilepsy, cerebrovascular accident, and myelopathy are considered to be the most serious complications and poor prognostic factors of SLE. NPSLE is the second leading cause of death after lupus nephritis in patients with SLE (Schwartz et al., 2019), and the mortality rate is 10 times higher than that of the general population (Zirkzee et al., 2014), and it severely damaged the patients' quality of life (Ogunsanya et al., 2018). The prevalence of CI in patients with SLE reported in previous studies was highly heterogeneous, ranging from 6.6 to 80.0% (Schwartz et al., 2019), significantly higher than in healthy individuals (Kozora et al., 1996; Al-Homood et al., 2017; Zhang et al., 2017; Shaban and Leira, 2019; Kim et al., 2021). Identifying and assessing SLE-related CI remains challenging at present due to the lack of sensitive and standardized neuropsychiatric tests and diagnostic biomarkers (Seet et al., 2021).

Functional magnetic resonance (fMRI) is divided into resting-state fMRI (rs-fMRI) and task-state fMRI. The most commonly used method is blood oxygenation level-dependent (BOLD) imaging. When the brain neurons are excited, their oxygen consumption increases and the local blood flow in the brain area increases. This process will lead to changes in the ratio of local oxyhemoglobin and deoxyhemoglobin. Oxyhemoglobin is diamagnetic, while deoxyhemoglobin is paramagnetic. BOLD-fMRI uses hemoglobin as an endogenous contrast agent to measure the BOLD signal generated by the difference in the magnetization vector between the two hemoglobins to observe the activity of the brain indirectly, non-invasively, and non-radioactively (Fox and Raichle, 2007; Liu et al., 2018). The commonly used indicators of fMRI include regional homogeneity (ReHo), low-frequency amplitude (amplitude of low-frequency fluctuation, ALFF), fractional low-frequency amplitude (fractional amplitude of low-frequency fluctuation, fALFF), degree centrality (degree centrality, DC), etc. Local brain activity reflects the intrinsic properties of brain tissue activity and is related to psychological and cognitive processes (Britz et al., 2011; Hutchison and Morton, 2016). ReHo is the similarity of the time series of a given voxel to the time series of its nearest neighbors, i.e., the consistency of the functional activity between the local voxel and the adjacent voxels (Zang et al., 2004); ALFF is an indicator that can reflect the characteristics of spontaneous activity of local neurons in the resting state by calculating the power spectrum of low-frequency fluctuation signals with a frequency of 0.08–0.10 Hz (Zang et al., 2007), and fALFF is the ratio of ALFF to the root mean square of full-spectrum power, which can reduce the sensitivity of ALFF to physiological noise (Zou et al., 2008). fMRI has been used to study brain function in diseases including SLE. For example, a systematic review of fMRI studies in patients with SLE found that 72.7% of the literature reported increased brain activity in SLE, including pediatric patients without neuropsychiatric symptoms and patients with disease duration of less than 2 years (Mikdashi, 2016). A resting-state fMRI study of non-NPSLE patients found that ReHo values in the fusiform gyrus and thalamus were decreased, and ReHo values in the parahippocampal gyrus and uncinate gyrus were increased in patients with SLE. The ReHo value of the cerebellum was positively correlated with disease activity and the ReHo value of the frontal gyrus was negatively correlated with disease activity, and some brain regions showed correlation with depression and anxiety states (Liu et al., 2018). Another similar study also found that non-NPSLE patients had abnormal increases or decreases in ALFF, fALFF, and ReHo in multiple brain regions compared with healthy controls (HCs), and these abnormalities were correlated with self-rating anxiety scales (Piao et al., 2021). A task-state fMRI study of non-NPSLE patients found abnormally reduced activation of the limbic system but higher activation of memory, emotion, and behavioral systems in patients with SLE, suggesting that these patients with SLE have

subclinical cognitive dysfunction and decision-making deficits (Wu et al., 2018).

Previously, common resting-state fMRI studies defaulted to a constant intensity of brain activity throughout the MRI scan, but more and more studies have shown that even during MRI scans, changes in brain activity over time are dynamic. Brain dynamics-based studies can deepen connections to human brain mechanisms and disease-induced brain damage (Allen et al., 1991; Leonardi et al., 2013; Li et al., 2019). Therefore, some studies have proposed using ALFF combined with dynamic ALFF (dALFF) analysis to study the dynamic changes of local brain activity in the human brain, that is, to study the temporal variation of local brain activity amplitude between voxels by calculating the ALFF changes over time, which helps to improve the reliability of research results (Tagliazucchi et al., 2014; Fu et al., 2018; Han et al., 2019; Cui et al., 2020). The study by Cui et al. (2020) found that generalized patients with anxiety disorder have increased dALFF in a wide range of brain regions, such as bilateral dorsomedial prefrontal cortex and hippocampus, which is positively related to the severity of symptoms. Another study found that compared to HCs, dALFF was significantly increased in brain regions such as the bilateral thalamus, the bilateral cerebellum posterior lobe, and the vermis in patients with major depressive disorder, and the dALFF value of some brain regions with abnormal dALFF is positively correlated with the severity of major depressive disorder symptoms (Zheng et al., 2021). However, whether there is abnormal dynamic local brain activity in patients with SLE has not been reported.

In the present study, we used ALFF combined with a sliding window approach to calculate dALFF for assessing the temporal variability of intrinsic brain activity in SLE patients with or without CI. We will preprocess fMRI data to calculate sALFF map and dALFF map of each subject and further verify whether the above two indicators are different in SLE patients with or without CI and HCs to explore potential imaging indicators that can be used to identify and evaluate SLE-related CI and provide a new perspective for a more complete understanding of the underlying neuropathological mechanisms of NPSLE. We expected an altered dALFF pattern in patients with SLE compared with HCs. Furthermore, dALFF can detect a subset of potentially abnormal brain activity that is not available with sALFF, which could deepen our understanding of the pathological mechanisms of NPSLE. We also hypothesized that dALFF might be associated with cognitive function.

Materials and methods

Participants

A total of seventy-six patients with SLE (thirty-eight with and without CI, respectively) were recruited from the outpatient and inpatient departments of the Rheumatology and Immunology Department of the First Affiliated Hospital of Kunming Medical University.

The inclusion criteria for the case group were: (1) patients diagnosed as SLE according to the 1997 revised American college of rheumatology (ACR) SLE classification criteria; (2) age range from 18 to 50 years; (3) CI was confirmed after Mini-mental State Examination (MMSE) scale assessment (A MMSE score $\leq$ 26 was identified as CI); (4) right-handedness.

The exclusion criteria for the case group were: (1) patients with connective tissue disorders such as rheumatoid arthritis, systemic sclerosis, primary or secondary Sjögren's syndrome who meet the ACR classification criteria; (2) patients with epilepsy, severe active mental illness, stroke, traumatic brain injury, history of intracranial surgery, etc. that may interfere with brain structure or functional imaging; (3) patients with a history of drug abuse and alcoholism; (4) women during pregnancy or lactation; (5) patients who have contraindications to MRI (e.g., claustrophobia, metal implants); (6) patients with structural brain abnormalities on conventional T1- or T2-weighted MRI scan.

Thirty-eight gender and age-matched HCs were recruited for this study.

This study has been approved by the Ethics Committee of the First Affiliated Hospital of Kunming Medical University. Before the start of the trial, the subjects and their legal guardians were informed of the trial procedures in detail and they signed the informed consent.

Psychological assessment and disease activity index scale

On the day of the MRI examination, a psychiatrist and a rheumatologist, respectively assessed the cognitive function and SLE disease activity index of each SLE patient using the MMSE scale and SLE disease activity index 2,000 (SLEDAI-2k).

Magnetic resonance imaging data acquisition

An experienced neuroradiologist acquired MRI images of all subjects using a 1.5T MRI scanner with head coils. First, conventional T1WI and T2WI scans were performed to exclude subjects with obvious brain structural abnormalities. No subjects were excluded due to structural brain abnormalities; 3D-MRI uses a 3D-T1-weighted fast phase perturbation gradient echo (3D-T1-fspgr) sequence with the following parameters: repetition time (TR) = 10.5 ms, echo time (TE) = 2.0 ms, inversion time = 350 ms, slice thickness = 1.8 mm and no layer interval, flip angle (FA) = 15°, spatial resolution = 0.94 mm × 0.94 mm × 0.9 mm, scanning matrix = 256 × 256, FOV = 24 cm × 18 cm, layer number = 172, scans cover the entire brain. The resting-state fMRI uses the

TABLE 1 Results of demographic and clinical data of SLE patients with cognitive impairment group, SLE patients without cognitive impairment, and healthy controls.

	SLE with cognitive impairment (n = 38)	SLE without cognitive impairment (n = 38)	HCs (n = 38)	Statistical	P-value
Gender (female/male)	4/34	4/34	4/34	$\chi^2 = 0$	1.000
Age (year)	30.50 ± 6.45	29.55 ± 6.03	31.89 ± 7.53	$F = 1.18$	0.31
Duration of disease (month)	12.00 (3.00, 24.00)	12.50 (1.66, 32.75)	NA	$U = 707.50$	0.88
SLEDAI-2k	10.42 ± 5.07	9.58 ± 6.26	NA	$t = 0.65$	0.52
MMSE scores	24.00 (21.00, 25.00)	29.50 (29.00, 30.00)	NA	U <0.01	<0.01
Antibody, n (%)					
Anti-Sm antibody	20 (52.63)	21 (55.26)	NA	$\chi^2 = 0.05$	0.82
Anti-dsDNA antibody	28 (73.68)	19 (50.00)	NA	$\chi^2 = 4.52$	0.03
Anti-U1RNP antibody	12 (31.58)	14 (36.84)	NA	$\chi^2 = 0.23$	0.63
Anti-P0 antibody	23 (60.53)	16 (42.11)	NA	$\chi^2 = 2.58$	0.11
GC accumulation (g)	2.55 (0, 10.61)	1.64 (0.26, 12.09)	NA	$U = 657.50$	0.50
HCQ accumulation (g)	0 (0, 3.30)	0.35 (0, 11.70)	NA	$U = 604.00$	0.18
CTX accumulation (g)	0 (0, 1.00)	0 (0, 0.25)	NA	$U = 628.50$	0.25

SLEDAI-2k, Systemic Lupus Erythematosus disease activity index 2000; MMSE, Mini-mental State Examination; NA, not applicable; GC, glucocorticoid; HCQ, hydroxychloroquine; CTX, cyclophosphamide.

gradient echo (GRE) sequence of EPI technology, and the specific parameters are as follows: TR = 2,000 ms, TE = 40 ms, NEX = 2.0, imaging matrix = 64 × 64, FOV = 24 cm × 24 cm, FA = 90°, slice thickness = 5 mm, slice interval = 1 mm, slice number = 24, time points = 160, a total of 320 s, and the scanning range covers the whole brain.

The subjects are required to stay awake, rest, lie flat on the examination bed, breathe calmly, fix their head, and minimize the movement of their head and other parts. At the same time, they are required to rest with their eyes closed and try not to do any thinking activities.

Data preprocessing

BOLD-fMRI data were preprocessed using the DPARSF (Data Processing Assistant for Resting-State fMRI) v4.4 software in the DPABI v6.1 (a toolbox for Data Processing and Analysis for Brain Imaging)[1] (Yan et al., 2016) software package in the Windows operating system. The specific data preprocessing includes the following: (1) data organization, where the original fMRI data in the format and structure required by DPABI is organized so that the software can automatically recognize and read the fMRI data; (2) input parameters such as time point (160) and TR (2 s); (3) format conversion, where Dicom files are converted to NIfTI files; (4) the first 10 time points are removed. At several time points at the beginning of the scan, due to factors such as unstable gradient magnetic field and patient incompatibility, the image noise is large. To reduce its influence on the overall image, the data of the first 10 time points were removed; (5) slice timing: to correct the errors caused by different acquisition times between each layer; (6) head movement correction: to calculate, the subject's head movement are reported and corrected. To reduce the impact of head movement on data quality and statistical results, those with translation > 2.0 mm and rotation > 2.0° in the head movement parameters are excluded. (7) The physiological and head movement effects were reduced by removing covariates and linear drift, including white matter and cerebrospinal fluid signal and 24 Friston movement parameters; (8) Register T1 structural image to fMRI: the high resolution of T1 structural image to improve the accuracy of subsequent fMRI data analysis is used; (9) segmentation: the image is segmented into gray matter, white matter, and cerebrospinal fluid; (10) regression of irrelevant covariates and de-linear drift: the influence of machine noise and head movement in the whole brain signal is removed; (11) Filtering: the filtering range of 0.01–0.1 Hz is selected to eliminate the influence of noise other than the BOLD signal frequency; (12) Spatial normalization and resampling: The fMRI images of each subject were registered to the same template for subsequent comparisons. This study used the MNI space-based EPI template and resampled the voxels to 3 × 3 × 3 mm^3; (13) Smoothing: to improve the signal-to-noise ratio, the FWHM selected in this study is "4 4 4."

Static and dynamic amplitude of low-frequency fluctuation computation

The ALFF reflects the low-frequency oscillation strength of spontaneous brain activity (Zang et al., 2007). The calculation of

1 http://rfmri.org/dpabi

TABLE 2 Regions changes in sALFF in SLE with CI group compared with the SLE without CI and HCs groups.

Brain regions	Cluster size (voxels)	xyz-peak (MNI)	*F*/*t*-value
ANCOVA			
Right parahippocampal gyrus	207	−18/−3/−21	12.65
Left caudate nucleus	135	−12/12/6	11.78
Right putamen	59	27/12/-6	7.85
Left cuneus	71	0/-75/18	8.10
HCs vs. SLE with CI			
Left caudate nucleus	169	−12/12/6	−4.151
SLE with CI vs. SLE without CI			
Right parahippocampal gyrus	137	15/6-24	3.80

Statistical significance was set at voxel P < 0.01, cluster P < 0.05, controlling for age, gender and head motion, GRF corrected.
ALFF, amplitudes of low-frequency fluctuation; SLE with CI, Systemic lupus erythematosus patients with cognitive impairment; SLE without CI, Systemic lupus erythematosus patients without cognitive impairment; HCs, Healthy controls; MNI, Montreal Neurological Institute.

sALFF is to Fourier transform the time series eigenvalues of a certain voxel to frequency space to obtain the average amplitude value in a specific frequency range. The frequency range in this study is 0.01–0.10 Hz. A sliding-window method (Leonardi and Van De Ville, 2015) was used to calculate the dALFF maps by the Dynamic and Stability Analyses module in DPABI v6.1 (Yan et al., 2016) software. Existing research believes that the choice of window length will affect the results of sliding window-related research (Shakil et al., 2016), and window sizes in the range of 40–100 s can capture the dynamic changes of the brain well (Zalesky and Breakspear, 2015). The $f$min is interpreted as the minimum frequency of the time series. To minimize spurious fluctuations, the minimum window length should be higher than 1/$f$min (Li et al., 2018). Thus, we select the optimal window width of 50 TRs (100 s) and a window with a step size of 1 TR (2 s) to dynamically intercept the fMRI time signal and finally apply the variance to quantify the difference between the average ALFF values to obtain the mean dALFF value. The standard deviation (SD) of the measured values in all time windows was calculated by using the mean value of dALFF to quantitatively analyze and compare the time dynamic characteristics of dALFF. Finally, a z-transformation was conducted on the individual sALFF maps and dALFF maps to generate normally distributed zsALFF and zdALFF maps.

Statistical analysis

All demographics and clinical characteristics data were analyzed by SPSS 23.0 software package. Non-parametric K-S test was used to test the normality of the data, and the data distributed normally were expressed as mean ± standard deviation ($\bar{x} \pm s$), while the data with skewed distribution were expressed as median (p25%, p75%). One-way analysis of variance (ANCOVA) was used to compare the age differences among the three groups. Chi-square test (χ^2) was used to compare the gender composition ratio among the three groups. Duration of the disease, MMSE score, and drug accumulation were compared between the SLE with CI and SLE without CI groups by Mann–Whitney U-test. Independent-sample t-test was used to compare SLEDAI-2K scores in SLE with and without CI groups. For each test statistic, a two-tailed probability value of < 0.05 was considered as significant. To further investigate differences in changes in dALFF temporal variability, data statistics module in DPABI software was used to conduct a voxel-based ANCOVA to compare the difference of dALFF value across the three groups with age, gender, and head motion (mean framewise displacement, FD) as covariate, multiple comparisons were performed using the LSD method. To reduce the family-wise error rate (FWER), we adopted a conservative approach with Gaussian random field (GRF) theory (voxel level $P < 0.01$, cluster level $P < 0.01$). *Post-hoc* pairwise comparisons were performed by a two-sample t-test if ANCOVA yielded significant results and a GRF correction was used at the cluster threshold of $P < 0.01$ and a voxel-wise threshold of $P < 0.01$. The sALFF of the three groups were compared using the same method. Each brain region was found to be significant different in dALFF and sALFF between SLE with CI group and SLE without CI group or HCs group was identified as the region of interest (ROI). We used DPABI software (Yan et al., 2016) to extract the mean value of dALFF and sALFF of each ROI, respectively. Spearman correlation analysis was applied between dALFF and sALFF for each ROI and MMSE scores in the SLE with CI group by using GraphPad 8.0.2 software.[2] The threshold for significance was set at $P < 0.05$.

Results

Demographics and clinical characteristics

The demographics and clinical characteristics of the three groups are summarized in **Table 1**. No significant differences were detected among SLE patients with CI, SLE patients without CI, and HCs in age and gender. SLE patients with CI and SLE patients without CI groups showed no significant difference in duration of disease, SLEDAI-2k scores, anti-Sm antibody, anti-U1RNP antibody, drug accumulation of glucocorticoids, hydroxychloroquine, and cyclophosphamide, but significant difference in anti-dsDNA antibody and MMSE scores. For SLE patients with CI, the MMSE scores ranged from 17 to 26.

2 https://www.graphpad.com/

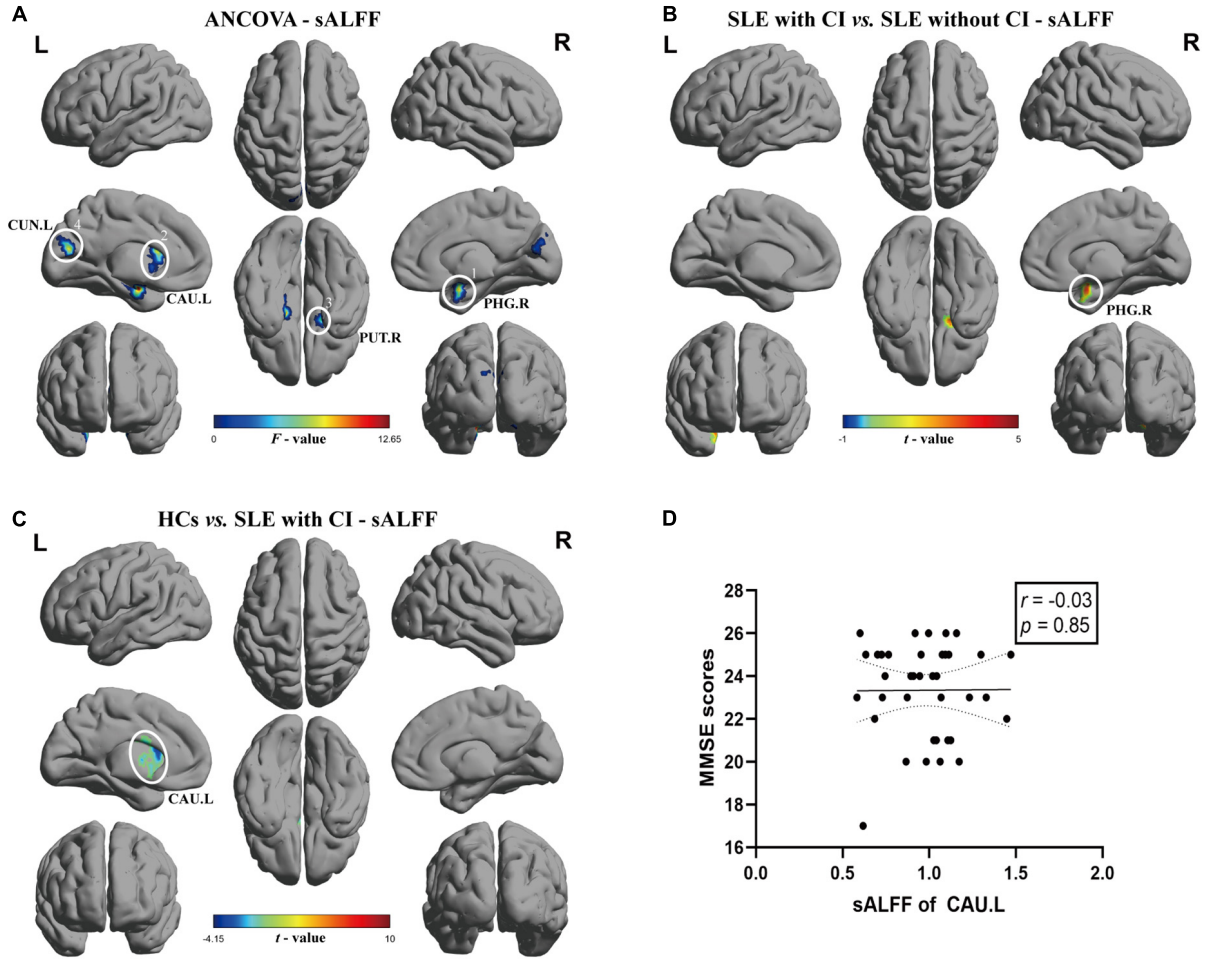

FIGURE 1
Brain regions with significant differences of sALFF among SLE with CI, SLE without CI and HCs. Specifically, **(A)** ANCOVA results of sALFF among three groups (voxel $P < 0.01$, cluster $P < 0.05$, controlling for age, gender and head motion, GRF corrected), **(B,C)** Differences between the groups were calculated using *post-hoc* analysis based on a two-sample *t*-test (voxel $P < 0.01$, cluster $P < 0.05$, controlling for age, gender, and head motion, GRF corrected). **(D)** Correlation analysis showed no significant correlation was found between sALFF and MMSE scores in SLE with CI groups. Color bars represent statistical value; the solid lines and dashed lines represented the linear regression fitted line and 95% confidence interval of the Spearman correlation analysis, respectively, SLE with CI, systemic lupus erythematosus patients with cognitive impairment; SLE without CI, systemic lupus erythematosus patients without cognitive impairment; HCs, healthy controls; sALFF, static amplitudes of low-frequency fluctuation; MMSE, Mini-mental State Examination; L, left hemisphere; R, right hemisphere; PHG, parahippocampal gurys; CAU, caudate nucleus; PUT, lenticular nucleus, putamen; CUN, Cuneus.

Static amplitude of low-frequency fluctuation result

The results of ANCOVA revealed that subjects in the SLE with CI, SLE without CI, and HC groups exhibited significant sALFF variability in the right parahippocampal gyrus, left caudate nucleus, right putamen and left cuneus (voxel $P < 0.01$, cluster $P < 0.05$, controlling for age, gender and head motion, GRF corrected) (Table 2 and Figure 1A). Compared to the SLE without CI, the right parahippocampal gyrus exhibited higher sALFF in the SLE with CI group (Figure 1B). Compared to the HC, the left caudate nucleus exhibited increased sALFF in the SLE with CI group (Figure 1C). There was no significant difference in the sALFF between the HC group and the SLE without CI group.

Dynamic amplitude of low-frequency fluctuation variance result

The results of ANCOVA revealed that participants in the SLE with CI, SLE without CI, and HCs groups exhibited significant dALFF variability in the right parahippocampal gyrus, right lingual gyrus, and bilateral inferior occipital gyrus (voxel $P < 0.01$, cluster $P < 0.05$, controlling for age, gender, and head motion, GRF corrected) (Table 3 and Figure 2A).

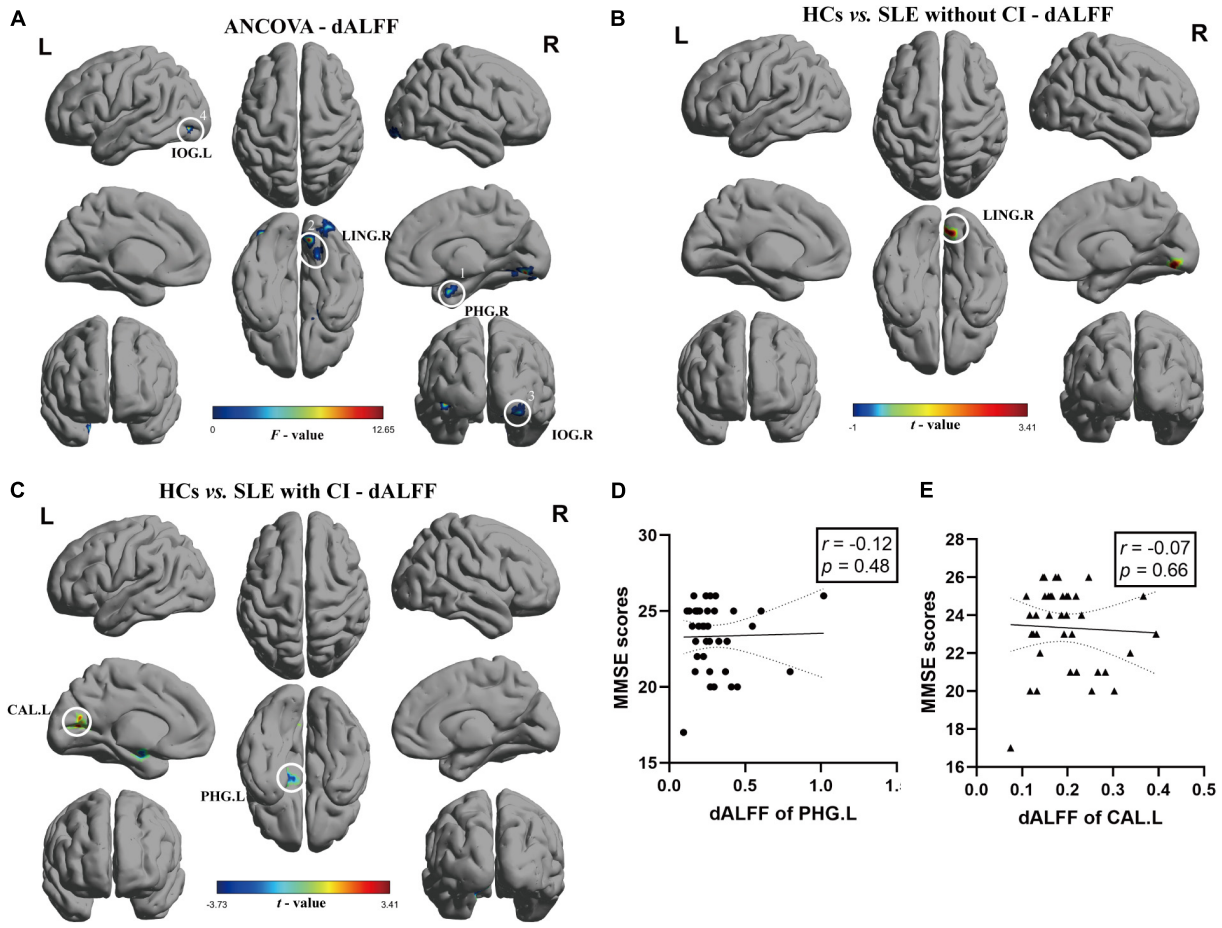

FIGURE 2
Brain regions with significant differences of dALFF among SLE with CI, SLE without CI, and HCs. Specifically, **(A)** ANCOVA results of dALFF among three groups (voxel $P < 0.01$, cluster $P < 0.05$, controlling for age, gender, and head motion, GRF corrected). **(B,C)** Differences between the groups were calculated using *post-hoc* analysis based on a two-sample *t*-test (voxel $P < 0.01$, cluster $P < 0.05$, controlling for age, gender, and head motion, GRF corrected). **(D,E)** Correlation analysis showed no significant correlation was found between dALFF and MMSE scores in SLE with CI groups. Color bars represent statistical value; the solid lines and dashed lines represented the linear regression fitted line and 95% confidence interval of the Spearman correlation analysis, respectively, SLE with CI, systemic lupus erythematosus patients with cognitive impairment; SLE without CI, systemic lupus erythematosus patients without cognitive impairment; HCs, healthy controls; dALFF, dynamic amplitudes of low-frequency fluctuation; MMSE, Mini-mental State Examination; L, left hemisphere; R, right hemisphere; PHG, para hippocampal gurys; LING, lingual gyrus; IOG, inferior occipital, putamen; CAL, calcarine fissure and surrounding cortex.

Compared to the HCs, the right lingual gyrus exhibited reduced dALFF in the SLE without CI group (Figure 2B). Compared to the HC, the right parahippocampal gyrus exhibited increased dALFF and left calcarine fissure, and the surrounding cortex exhibited reduced dALFF in the SLE with CI group (Figure 2C). No significant differences were found in the dALFF between the SLE with CI group and the SLE without CI group.

Correlation analysis results

There was no significant correlation between sALFF, dALFF values and MMSE scores for each ROI in the SLE with CI group (Figures 1D, 2D,E).

Discussion

So far, this is the first fMRI study in patients with SLE that uses both the sALFF and dALFF analysis. We also performed correlation analyses on the sALFF and dALFF abnormalities and MMSE scores. Our study found that compared with HCs and SLE patients without CI, SLE patients with CI showed different characteristics of brain intrinsic functional connectivity strength and stability, among which, the sALFF of SLE with CI was increased in the right parahippocampal gyrus compared with SLE patients without CI, and increased in the left caudate nucleus compared with HCs. In terms of temporal variability in the amplitude of local brain activity, the dALFF of SLE with CI was increased in the right parahippocampal gyrus, but

TABLE 3 Regions changes in dALFF in SLE with CI group compared with the SLE without CI and HCs groups.

Brain regions	Cluster size (voxels)	xyz-peak (MNI)	*F*/*t*-value
ANCOVA			
Right parahippocampal gyrus	29	18/3/−30	10.87
Right lingual gyrus	60	12/-72/-12	13.60
Right inferior occipital gyrus	37	33/−90/−15	7.44
Left inferior occipital gyrus	34	−36/−78/−6	13.67
HCs vs. SLE with CI			
Right parahippocampal gyrus	59	−9/−6/−18	−3.73
Left calcarine fissure and surrounding cortex	48	−15/−69/6	3.41
HCs vs. SLE without CI			
Right lingual gyrus	56	12/−72/−12	4.12

Statistical significance was set at voxel $P < 0.01$, cluster $P < 0.05$, controlling for age, gender, and head motion, GRF corrected.
ALFF, amplitudes of low-frequency fluctuation; SLE with CI, Systemic lupus erythematosus patients with cognitive impairment; SLE without CI, Systemic lupus erythematosus patients without cognitive impairment; HCs, Healthy controls; MNI, Montreal Neurological Institute.

reduced in the left calcarine fissure and surrounding cortex compared with HCs. Compared to the HCs, the right lingual gyrus exhibited reduced dALFF in the SLE without CI group. We did not find a correlation between abnormal sALFF and dALFF in SLE patients with CI and their cognitive performance.

Several previous studies have investigated the intensity of intrinsic brain activity in patients with SLE within the scope of sALFF. These studies found that non-NPSLE patients showed a decrease of sALFF in the bilateral precuneus and an increase in the right cuneus and the right calcarine fissure surrounding cortex, respectively (Yu H. et al., 2019). Another study found increased standardized ALFF in the left inferior temporal gyrus and left putamen in non-NPSLE patients compared with HCs (Yu Y. et al., 2019). A previous study by our research group found that, compared with HCs group, the ALFF values of the bilateral postcentral gyrus in the non-NPSLE group were lower than those in the HCs group, while the ALFF values in the bilateral inferior temporal gyrus, left putamen, and bilateral precuneus were higher than those in the HCs group (Piao et al., 2021). Our study included SLE patients with CI and found that these patients had two brain regions with different sALFF values than HCs and SLE patients without CI. The caudate nucleus participates in cognitive processes by stimulating the correct movement patterns and selecting appropriate secondary targets based on the assessment of the action outcome (Grahn et al., 2008). The parahippocampal gyrus is located in the medial under the occipital and temporal lobes, is the main cortical input to the hippocampus, is considered to play an important role in high cognitive functions including memory coding retrieval and visuospatial processing, and is an important center for memory processing (Lin et al., 2021). This study found that the sALFF in the above two brain regions of SLE patients with CI was higher than that of HCs and SLE patients without CI, respectively, suggesting that the local brain activity intensity of these two brain regions increased, which may be related to the compensation of cognitive dysfunction. Similar results have also been reported in studies of major depressive disorder (Liu et al., 2014), and amnestic CI (Zhang et al., 2021) and its specific mechanism still needs further research.

Previous studies assumed that ALFF was static throughout the rs-fMRI scan, but recent studies confirmed that ALFF is time-varying (Fu et al., 2018). To better understand the mechanism of cognitive dysfunction in patients with SLE, we used a sliding window approach for the first time on the basis of sALFF to study the brain dynamics describing temporal changes in energy expenditure (temporal variability of dALFF). We found that SLE patients with CI did indeed have temporal ALFF alterations. Specifically, compared with HCs, the SLE patient group with CI had a brain region that showed increased (right parahippocampal gyrus) and decreased (left calcarine fissure and surrounding cortex) dALFF, respectively. Brain dynamics reflect functional capabilities of the nervous system (Kucyi et al., 2017), and may more sensitively reflect disruption of cognitive function in multiple diseases (Cui et al., 2020; Lu et al., 2020; Zheng et al., 2021). The results obtained by this innovative dALFF method have led us to realize that in addition to the abnormal local activity intensity of the brain, there are also changes in the stability of local activity dynamics in patients with SLE. As mentioned above, the right parahippocampal gyrus is involved in memory and other cognitive functions (Lin et al., 2021), and the abnormal enhancement of the intensity variability of brain functional activity in this brain region may be one of the mechanisms of CI in patients with SLE. Similar results have been reported in chronic obstructive pulmonary disease patients with semantic-memory impairments. Calcarine fissure and the surrounding cortex is responsible for receiving and transmitting visual signals (Huang et al., 2020), changes in the stability of functional activity in this brain region have been reported in studies on non-NPSLE (Chen et al., 2021), but its exact effect on CI needs more studies to clarify. Notably, the brain regions with abnormal sALFF and dALFF values did not overlap, which may reflect that the intensity and stability of brain activity affect cognitive function in patients with SLE through different neuropathological pathways, suggesting that the assessment of dALFF can complement the results of traditional sALFF and promote our understanding of the pathological mechanism. Future studies can explore the possibility of dALFF as a new biomarker for SLE patients with CI by imaging machine learning or receiver operator characteristic (ROC) curve analysis.

Unfortunately, we did not find a correlation between abnormal sALFF values, dALFF values, and cognitive function scores in the SLE patient group with CI, other than possibly

due to our relatively small sample size and the use of only one scale to assess cognitive function in patients with SLE, it may also be related to the properties of fMRI and the pathogenesis of SLE-related CI. Researchers have tried to use neuroimaging, immunology (Varley et al., 2020), bioinformatics (Geng et al., 2020), and other methods to study NPSLE. Considering the diversity of its clinical manifestations, the pathogenesis of NPSLE is generally considered to be the result of the interaction of multiple pathological processes. Some studies have found that certain autoantibodies and cytokines may lead to cerebrovascular lesions and/or interfere with neuronal connections by mediating immune responses (Bertsias and Boumpas, 2010; Borowoy et al., 2012; Schwartz et al., 2019), and genetic factors and disruption of the blood–brain barrier may also be involved in the pathogenesis of NPSLE (Schwartz et al., 2019). The confounding caused by this heterogeneity in etiology may cause differences in the performance of individual brain functions, and ultimately the sALFF and dALFF values of the regions with the most obvious differences between groups are not significantly related to individual cognitive function. On the other hand, the changes of sALFF and dALFF may be more sensitive than MMSE in distinguishing SLE from CI, that is, the changes of these two indicators can help to identify subclinical CI patients in SLE earlier. In the future, we also need to group the etiology as much as possible through the detection of autoantibodies (such as antiphospholipid antibodies, etc.) and cerebrospinal fluid and obtain more representative subgroups to study the correlation between CI and brain function in a more targeted manner. Future research can perform other scales that reflect neuronal function such as Montreal Cognitive Assessment (MoCA), mini-Cog, etc. and analyze the correlation with sALFF and dALFF values, which may reveal more about the relationship between cognitive function and its fMRI indicators in patients with SLE. In addition to ALFF, fALFF, ReHo, and other fMRI indicators can also complement ALFF to help us understand NPSLE more comprehensively.

This study also has some limitations. First of all, the field strength of the magnetic resonance scanner used in this study (1.5T) is lower than that currently mainstream in brain imaging research (3.0T), so our results may be biased due to the smaller signal-to-noise ratio. We actually started this research 10 years ago and continued the same 1.5T MRI scanner and scanning parameters to build the database. In this study, we conducted strict quality control, including manual visual inspection and software quality control. We also hope to use new magnetic resonance scanners in the future to obtain more accurate results. Secondly, we only used a window length and step size recommended by previous studies and did not use other methods to validate the main results. Finally, this study only applied dALFF to examine the temporal dynamics of local brain activity. However, future work can also explore the changes in fMRI indicators such as dfALFF and dReHo in patients with SLE.

Conclusion

In conclusion, SLE patients with CI not only have abnormal brain activity intensity but also have changes in brain activity stability. By describing the dynamic changes in the intrinsic brain activity, it provides a new idea for elucidating the pathophysiological mechanism of cognitive dysfunction in SLE. However, more research and validation with multimodal data are needed to determine the link between the severity of CI and brain activity in patients with SLE.

Data availability statement

The raw data supporting the conclusions of this article will be made available by the authors, without undue reservation.

Ethics statement

The studies involving human participants were reviewed and approved by the Institutional Review Board of Kunming Medical University. The patients/participants provided their written informed consent to participate in this study. Written informed consent was obtained from the individual(s) for the publication of any potentially identifiable images or data included in this article.

Author contributions

YY, RZ, and FZ were responsible for the management of the research and writing the article. RB and SLi were responsible for recruiting and following up with the patients. RC and SLu were responsible for the consultation of the research. JX was responsible for the whole research and article. All authors contributed to the article and approved the submitted version.

Funding

This work was supported by the National Natural Science Foundation of China (81760296 and 81460256), the Yunnan Province High-level Health Technical Talents (leading talents) (L-2019004), the Yunnan Province Special Project for Famous Medical Talents of the "Ten Thousand Talents Program" (YNWRMY-2018-040), the Funding of Yunnan Provincial Health Science and Technology Plan (2017NS051 and

2018NS0133), the Funding of Ministry of Science and Technology of Yunnan Province (2018ZF016), the Yunnan Province Clinical Research Center for Skin Immune Diseases (2019ZF012), the Yunnan Province Clinical Center for Skin Immune Diseases (ZX2019-03-02), and the Graduate Innovation Fund of Kunming Medical University (2021D08).

Conflict of interest

The authors declare that the research was conducted in the absence of any commercial or financial relationships that could be construed as a potential conflict of interest.

The reviewers JZ and ZW declared a past co-authorship with the author, JX to the handling editor.

Publisher's note

References

Al-Homood, I. A., Omran, N. E., Alwahibi, A. S., Aldosoghy, M., Alharthy, A., and Aljohani, G. S. (2017). Depression in patients with systemic lupus erythematosus: a multicenter study. *Saudi J. Med. Med. Sci.* 5, 248–253. doi: 10.4103/sjmms.sjmms_79_16

Allen, E. A., Damaraju, E., Plis, S. M., Erhardt, E. B., Eichele, T., and Calhoun, V. D. (1991). Tracking whole-brain connectivity dynamics in the resting state. *Cereb. Cortex* 24, 663–676. doi: 10.1093/cercor/bhs352

Bertsias, G. K., and Boumpas, D. T. (2010). Pathogenesis, diagnosis and management of neuropsychiatric SLE manifestations. *Nat. Rev. Rheumatol.* 6, 358–367. doi: 10.1038/nrrheum.2010.62

Borowoy, A. M., Pope, J. E., Silverman, E., Fortin, P. R., Pineau, C., Smith, C. D., et al. (2012). Neuropsychiatric lupus: the prevalence and autoantibody associations depend on the definition: results from the 1000 faces of lupus cohort. *Semin. Arthritis Rheum.* 42, 179–185. doi: 10.1016/j.semarthrit.2012.03.011

Britz, J., Pitts, M. A., and Michel, C. M. (2011). Right parietal brain activity precedes perceptual alternation during binocular rivalry. *Hum. Brain Mapp.* 32, 1432–1442. doi: 10.1002/hbm.21117

Chen, L., Sun, J., Wang, Q., Hu, L., Zhang, Y., Ma, H., et al. (2021). Altered temporal dynamics of brain activity in multiple-frequency bands in non-neuropsychiatric systemic lupus erythematosus patients with inactive disease. *Neuropsychiatr. Dis. Treat.* 17, 1385–1395. doi: 10.2147/NDT.S292302

Cui, Q., Sheng, W., Chen, Y., Pang, Y., Lu, F., Tang, Q., et al. (2020). Dynamic changes of amplitude of low-frequency fluctuations in patients with generalized anxiety disorder. *Hum. Brain Mapp.* 41, 1667–1676. doi: 10.1002/hbm.24902

Fox, M. D., and Raichle, M. E. (2007). Spontaneous fluctuations in brain activity observed with functional magnetic resonance imaging. *Nat. Rev. Neurosci.* 8, 700–711. doi: 10.1038/nrn2201

Fu, Z., Tu, Y., Di, X., Du, Y., Pearlson, G. D., Turner, J. A., et al. (2018). Characterizing dynamic amplitude of low-frequency fluctuation and its relationship with dynamic functional connectivity: an application to schizophrenia. *Neuroimage* 180, 619–631. doi: 10.1016/j.neuroimage.2017.09.035

Geng, L., Xu, X., Zhang, H., Chen, C., Hou, Y., Yao, G., et al. (2020). Comprehensive expression profile of long non-coding RNAs in Peripheral blood mononuclear cells from patients with neuropsychiatric systemic lupus erythematosus. *Ann. Transl. Med.* 8:349. doi: 10.21037/atm.2020.03.25

Grahn, J. A., Parkinson, J. A., and Owen, A. M. (2008). The cognitive functions of the caudate nucleus. *Prog. Neurobiol.* 86, 141–155. doi: 10.1016/j.pneurobio.2008.09.004

Han, S., Wang, X., He, Z., Sheng, W., Zou, Q., Li, L., et al. (2019). Decreased static and increased dynamic global signal topography in major depressive disorder. *Prog. Neuro Psychopharmacol. Biol. Psychiatry* 94:109665. doi: 10.1016/j.pnpbp.2019.109665

Huang, X., Wen, Z., Qi, C. X., Tong, Y., Dan, H. D., Xie, B. J., et al. (2020). Altered temporal dynamic intrinsic brain activity in late blindness. *BioMed Res. Int.* 2020:1913805. doi: 10.1155/2020/1913805

Hutchison, R. M., and Morton, J. B. (2016). It's a matter of time: reframing the development of cognitive control as a modification of the brain's temporal dynamics. *Dev. Cogn. Neurosci.* 18, 70–77. doi: 10.1016/j.dcn.2015.08.006

Kim, M. Y., Sen, D., Drummond, R. R., Brandenburg, M. C., Biesanz, K. L., Kim, A. H., et al. (2021). Cognitive dysfunction among people with systemic lupus erythematosus is associated with reduced participation in daily life. *Lupus* 30, 1100–1107. doi: 10.1177/09612033211006187

Kozora, E., Thompson, L. L., West, S. G., and Kotzin, B. L. (1996). Analysis of cognitive and psychological deficits in systemic lupus erythematosus patients without overt central nervous system disease. *Arthritis Rheum.* 39, 2035–2045. doi: 10.1002/art.1780391213

Kucyi, A., Hove, M. J., Esterman, M., Hutchison, R. M., and Valera, E. M. (2017). Dynamic brain network correlates of spontaneous fluctuations in attention. *Cereb. Cortex* 27, 1831–1840. doi: 10.1093/cercor/bhw029

Leonardi, N., and Van De Ville, D. (2015). On spurious and real fluctuations of dynamic functional connectivity during rest. *Neuroimage* 104, 430–436. doi: 10.1016/j.neuroimage.2014.09.007

Leonardi, N., Richiardi, J., Gschwind, M., Simioni, S., Annoni, J. M., Schluep, M., et al. (2013). Principal components of functional connectivity: a new approach to study dynamic brain connectivity during rest. *Neuroimage* 83, 937–950. doi: 10.1016/j.neuroimage.2013.07.019

Li, J., Duan, X., Cui, Q., Chen, H., and Liao, W. (2019). More than just statics: temporal dynamics of intrinsic brain activity predicts the suicidal ideation in depressed patients. *Psychol. Med.* 49, 852–860. doi: 10.1017/S0033291718001502

Li, R., Liao, W., Yu, Y., Chen, H., Guo, X., Tang, Y. L., et al. (2018). Differential patterns of dynamic functional connectivity variability of striato-cortical circuitry in children with benign epilepsy with centrotemporal spikes. *Hum. Brain Mapp.* 39, 1207–1217. doi: 10.1002/hbm.23910

Lin, Y. H., Dhanaraj, V., Mackenzie, A. E., Young, I. M., Tanglay, O., Briggs, R. G., et al. (2021). Anatomy and white matter connections of the parahippocampal gyrus. *World Neurosurg.* 148, e218–e226. doi: 10.1016/j.wneu.2020.12.136

Liu, J., Ren, L., Womer, F. Y., Wang, J., Fan, G., Jiang, W., et al. (2014). Alterations in amplitude of low frequency fluctuation in treatment-naïve major depressive disorder measured with resting-state fMRI. *Hum. Brain Mapp.* 35, 4979–4988. doi: 10.1002/hbm.22526

Liu, S., Cheng, Y., Xie, Z., Lai, A., Lv, Z., Zhao, Y., et al. (2018). A conscious resting state fMRI study in SLE patients without major neuropsychiatric manifestations. *Front. Psychiatry* 9:677. doi: 10.3389/fpsyt.2018.00677

Lu, F., Liu, P., Chen, H., Wang, M., Xu, S., Yuan, Z., et al. (2020). More than just statics: abnormal dynamic amplitude of low-frequency fluctuation in adolescent patients with pure conduct disorder. *J. Psychiatr. Res.* 131, 60–68. doi: 10.1016/j.jpsychires.2020.08.027

Mikdashi, J. A. (2016). Altered functional neuronal activity in neuropsychiatric lupus: a systematic review of the fMRI investigations. *Semin. Arthritis Rheum.* 45, 455–462. doi: 10.1016/j.semarthrit.2015.08.002

Ogunsanya, M. E., Brown, C. M., Lin, D., Imarhia, F., Maxey, C., and Chong, B. F. (2018). Understanding the disease burden and unmet needs among patients with cutaneous lupus erythematosus: a qualitative study. *Int. J. Womens Dermatol.* 4, 152–158. doi: 10.1016/j.ijwd.2018.01.002

Piao, S., Wang, R., Qin, H., Hu, B., Du, J., Wu, H., et al. (2021). Alterations of spontaneous brain activity in systematic lupus erythematosus patients without neuropsychiatric symptoms: a resting-functional MRI study. *Lupus* 30, 1781–1789. doi: 10.1177/09612033211033984

Rees, F., Doherty, M., Grainge, M. J., Lanyon, P., and Zhang, W. (2017). The worldwide incidence and prevalence of systemic lupus erythematosus: a systematic review of epidemiological studies. *Rheumatology* 56, 1945–1961. doi: 10.1093/rheumatology/kex260

Schwartz, N., Stock, A. D., and Putterman, C. (2019). Neuropsychiatric lupus: new mechanistic insights and future treatment directions. *Nat. Rev. Rheumatol.* 15, 137–152. doi: 10.1038/s41584-018-0156-8

Seet, D., Allameen, N. A., Tay, S. H., Cho, J., and Mak, A. (2021). Cognitive dysfunction in systemic lupus erythematosus: immunopathology, clinical manifestations, neuroimaging and management. *Rheumatol. Ther.* 8, 651–679. doi: 10.1007/s40744-021-00312-0

Shaban, A., and Leira, E. C. (2019). Neurological complications in patients with systemic lupus erythematosus. *Curr. Neurol. Neurosci. Rep.* 19:97. doi: 10.1007/s11910-019-1012-1

Shakil, S., Lee, C. H., and Keilholz, S. D. (2016). Evaluation of sliding window correlation performance for characterizing dynamic functional connectivity and brain states. *Neuroimage* 133, 111–128. doi: 10.1016/j.neuroimage.2016.02.074

Tagliazucchi, E., Carhart-Harris, R., Leech, R., Nutt, D., and Chialvo, D. R. (2014). Enhanced repertoire of brain dynamical states during the psychedelic experience. *Hum. Brain Mapp.* 35, 5442–5456. doi: 10.1002/hbm.22562

Varley, J. A., Andersson, M., Grant, E., Berretta, A., Zandi, M. S., Bondet, V., et al. (2020). Absence of neuronal autoantibodies in neuropsychiatric systemic lupus erythematosus. *Ann. Neurol.* 88, 1244–1250. doi: 10.1002/ana.25908

Wu, B. B., Ma, Y., Xie, L., Huang, J. Z., Sun, Z. B., Hou, Z. D., et al. (2018). Impaired decision-making and functional neuronal network activity in systemic lupus erythematosus. *J. Magn. Reson. imaging* 48, 1508–1517. doi: 10.1002/jmri.26006

Yan, C. G., Wang, X. D., Zuo, X. N., and Zang, Y. F. (2016). DPABI: data processing & analysis for (resting-state) brain imaging. *Neuroinformatics* 14, 339–351. doi: 10.1007/s12021-016-9299-4

Yu, H., Qiu, X., Zhang, Y. Q., Deng, Y., He, M. Y., Zhao, Y. T., et al. (2019). Abnormal amplitude of low frequency fluctuation and functional connectivity in non-neuropsychiatric systemic lupus erythematosus: a resting-state fMRI study. *Neuroradiology* 61, 331–340. doi: 10.1007/s00234-018-2138-6

Yu, Y., Chen, L., Wang, Q., Hu, L., Ding, Q., Jia, X., et al. (2019). Altered amplitude of low-frequency fluctuations in inactive patients with nonneuropsychiatric systemic lupus erythematosus. *Neural Plast.* 2019:9408612. doi: 10.1155/2019/9408612

Zalesky, A., and Breakspear, M. (2015). Towards a statistical test for functional connectivity dynamics. *Neuroimage* 114, 466–470. doi: 10.1016/j.neuroimage.2015.03.047

Zang, Y. F., He, Y., Zhu, C. Z., Cao, Q. J., Sui, M. Q., Liang, M., et al. (2007). Altered baseline brain activity in children with ADHD revealed by resting-state functional MRI. *Brain Dev.* 29, 83–91. doi: 10.1016/j.braindev.2006.07.002

Zang, Y., Jiang, T., Lu, Y., He, Y., and Tian, L. (2004). Regional homogeneity approach to fMRI data analysis. *Neuroimage* 22, 394–400. doi: 10.1016/j.neuroimage.2003.12.030

Zhang, L., Fu, T., Yin, R., Zhang, Q., and Shen, B. (2017). Prevalence of depression and anxiety in systemic lupus erythematosus: a systematic review and meta-analysis. *BMC Psychiatry* 17:70. doi: 10.1186/s12888-017-1234-1

Zhang, X., Xue, C., Cao, X., Yuan, Q., Qi, W., Xu, W., et al. (2021). Altered patterns of amplitude of low-frequency fluctuations and fractional amplitude of low-frequency fluctuations between amnestic and vascular mild cognitive impairment: an ALE-Based comparative meta-analysis. *Front. Aging Neurosci.* 13:711023. doi: 10.3389/fnagi.2021.711023

Zheng, R., Chen, Y., Jiang, Y., Wen, M., Zhou, B., Li, S., et al. (2021). Dynamic altered amplitude of low-frequency fluctuations in patients with major depressive disorder. *Front. Psychiatry* 12:683610. doi: 10.3389/fpsyt.2021.683610

Zirkzee, E. J., Huizinga, T. W., Bollen, E. L., van Buchem, M. A., Middelkoop, H. A., van der Wee, N. J., et al. (2014). Mortality in neuropsychiatric systemic lupus erythematosus (NPSLE). *Lupus* 23, 31–38. doi: 10.1177/0961203313511254

Zou, Q. H., Zhu, C. Z., Yang, Y., Zuo, X. N., Long, X. Y., Cao, Q. J., et al. (2008). An improved approach to detection of amplitude of low-frequency fluctuation (ALFF) for resting-state fMRI: fractional ALFF. *J. Neurosci. Methods* 172, 137–141. doi: 10.1016/j.jneumeth.2008.04.012

frontiers | Frontiers in Neuroscience

TYPE Original Research
PUBLISHED 15 September 2022
DOI 10.3389/fnins.2022.956056

OPEN ACCESS

EDITED BY
Zaixu Cui,
Chinese Institute for Brain Research, Beijing (CIBR), China

REVIEWED BY
Jiaojian Wang,
Kunming University of Science and Technology, China
Zhiqiang Sha,
Max Planck Institute for Psycholinguistics, Netherlands

*CORRESPONDENCE
Yuping Ning
ningjeny@126.com

SPECIALTY SECTION
This article was submitted to Brain Imaging Methods, a section of the journal Frontiers in Neuroscience

RECEIVED 29 May 2022
ACCEPTED 15 August 2022
PUBLISHED 15 September 2022

CITATION
Zhang F, Wang C, Lan X, Li W, Fu L, Ye Y, Liu H, Wu K, Zhou Y and Ning Y (2022) The functional connectivity of the middle frontal cortex predicts ketamine's outcome in major depressive disorder.
Front. Neurosci. 16:956056.
doi: 10.3389/fnins.2022.956056

The functional connectivity of the middle frontal cortex predicts ketamine's outcome in major depressive disorder

Fan Zhang[1,2,3], Chengyu Wang[2,3], Xiaofeng Lan[2,3], Weicheng Li[1,2,3], Ling Fu[1,2,3], Yanxiang Ye[2,3], Haiyan Liu[2,3], Kai Wu[4], Yanling Zhou[2,3] and Yuping Ning[1,2,3]*

[1]The First School of Clinical Medicine, Southern Medical University, Guangzhou, China, [2]The Affiliated Brain Hospital of Guangzhou Medical University, Guangzhou, China, [3]Guangdong Engineering Technology Research Center for Translational Medicine of Mental Disorders, Guangzhou, China, [4]School of Biomedical Sciences and Engineering, South China University of Technology, Guangzho, China

Background: Ketamine, a robust antidepressant, has promising potential in the treatment of major depressive disorder (MDD). However, it does not work for all MDD patients, and the mechanism underlying its anti-depressive effects is unclear. Researchers have explored the mechanisms of ketamine action in MDD patients through MRI, a technique that measures brain activity intuitively. Notably, many MRI results were inconsistent because they selected different brain regions as seeds, particularly with respect to functional connectivity (FC) analysis. To eliminate the influence of prior seeds as much as possible, we used the significantly different results in degree centrality (DC) analysis as seeds to explore the FC changes in MDD patients to identify an imaging biomarker of ketamine's effect.

Methods: Forty-four MDD patients and 45 healthy controls (HCs) were included in the study. Patients, aged 18–65, received six intravenous ketamine injections over 12 days. Depressive symptoms were estimated and MRI scans were performed at baseline and the day after the sixth infusion. We estimated FC differences between responders, non-responders and HCs using the region that showed significant differences between responders and non-responders in DC analysis as the seed. The correlation between the MADRS changes and zFC values was performed, and the potential of zFC values to be a neuroimaging biomarker was explored using the receiver operating characteristic curve.

Result: Compared with non-responders, responders had significantly decreased DC values in the right middle frontal gyrus (MFG). In the analysis of FC using the region that showed significant differences in DC as a seed, there was a significant difference in the region of the right supplementary motor area (SMA) among responders, non-responders, and HCs. This region also overlapped with the bilateral median cingulate gyrus. In *post hoc*

analysis, responders had higher FC than non-responders and HCs, and non-responders had lower FC than HCs. Importantly, the FC between the MFG and SMA (overlapping bilateral median cingulate gyrus) was correlated with the improvement of symptoms, which was estimated by the Mongomery-Asberg Depression Scale (MADRS). FC has the potential to be an imaging biomarker that can predict the ketamine effect in MDD patients according to the receiver operating characteristic curve analysis.

Conclusion: Our results revealed that FC between the SMG and SMA and mACC was highly correlated with depressive symptoms and has the potential to be a neuroimaging biomarker to predict the effect of ketamine in MDD.

KEYWORDS

ketamine, major depressive disorder, degree centrality (DC), functional connectivity, default mode network, biomarker

Introduction

Ketamine, an N-methyl-D-aspartate receptor (NMDAR) antagonist, provides hope for patients with major depressive disorder (MDD) due to its quick and potent antidepressant effects (Serafini et al., 2014). Studies demonstrated that a single intravenous infusion of ketamine (0.5 mg/kg) had an antidepressant effect 40 min post-infusion, and the crest value occurred 1 day after infusion (Berman et al., 2000; Zarate et al., 2006; Murrough et al., 2013a). Previous studies have shown that MDD patients had a prolonged response after receiving a total of 6 ketamine injections (Murrough et al., 2013b; Zheng et al., 2018). Nevertheless, the mechanism of the antidepressant effect of ketamine is not known.

Recently, an increasing number of researchers have used neuroimaging to explore the mechanism of ketamine action in MDD through functional connectivity (FC), a neuroimaging analysis using blood oxygenation level-dependent (BOLD) signals obtained from the *in vivo* brain (Scheidegger et al., 2016; Kraguljac et al., 2017; Teng et al., 2018; Chen et al., 2019; Mkrtchian et al., 2021; Rivas-Grajales et al., 2021). Mkrtchian et al. (2021) revealed that FC between the ventral striatum-left dorsolateral prefrontal cortex, dorsal caudate-right ventrolateral prefrontal cortex, dorsal caudal putamen-pregenual anterior cingulate cortex, and ventral rostral putamen-orbitofrontal cortex increased in treat-resistant depressive participants after ketamine treatment. However, Kraguljac et al. (2017) found that there were no areas that showed increased hippocampus connectivity during a ketamine challenge. Thus, these results are often inconsistent.

These heterogeneous results are due to the different "seeds" in FC analysis, *a priori* brain regions selected based on information obtained from task activation studies, functional neuroanatomy, or even structural deficits (Craddock et al., 2009; Zhang et al., 2016). To avoid this influence, we used the degree centrality (DC) to select the seed (Zuo et al., 2012), which is a kind of network analysis that estimates each node's correlation with the others to measure the importance of each node (Wang et al., 2011; Yang et al., 2014). This is a measure of the importance of each voxel from a whole-brain network perspective, and getting seeds from it can partly reduce the influence (Cheng et al., 2022). Increased DC values in a brain region mean this region plays a key role in brain activity.

In the present study, we obtained seed from DC analysis to reduce bias based on previous brain regions. Then we estimated the different FC among responders, non-responders, and HCs at baseline. The relationship between Mongomery-Asberg Depression Scale (MADRS) score changes and FC values was investigated. In addition, the receiver operating characteristic curve analysis was used to explore the potential of the zFC values as a neuroimaging biomarker of ketamine's antidepressant effect in MDD patients. We wish we could find a reliable neuroimaging biomarker to predict the effect of ketamine in MDD patients.

Patients and method

Study participants

Participants were recruited from a clinical trial (ChiCTR-OOC-17012239) in the Affiliated Brain Hospital of Guangzhou Medical University. Two experienced psychiatrists used the Diagnostic and Statistical Manual of Mental Disorders-5 (DSM-5, SCID) to screen patients. Our study was approved by the Clinical Research Ethics Committee of the Affiliated Brain Hospital of Guangzhou Medical University.

The inclusion criteria for the MDD group were as follows: (a) aged 18–65, (b) 17-item Hamilton Depression Rating Scale (HAMD-17) score $\geq$ 17 at baseline, (c) failure of two adequate antidepressant treatments or Beck Scale for Suicide Ideation-Part I score $\geq$ 2 at baseline.

Healthy controls (HCs) and their family members must have had no DSM-5 diagnosis.

The exclusion criteria for both MDD patients and HCs were as follows: (a) psychotic symptoms; (b) alcohol or substance abuse, (c) any serious or unstable medical conditions at present, or (d) MRI contraindications.

Patients with psychiatric medication treatment, were required to maintain a stable dosage over 4 weeks before ketamine infusion and take stable medications throughout the infusion period.

Forty-four patients were recruited and all signed the consent form. Excluding four patients with maximum head motion parameters over 2 mm or 2°, finally, 40 patients were included in the analysis. Forty-five MRI scans from HCs were also included in the analysis.

Study design

Forty-four MDD patients received six ketamine infusions in 12 days, they were on days 1, 3, 5, 8, 10, and 12, respectively. After an overnight fast, ketamine (0.5 mg/kg) was diluted in saline and injected intravenously through a pump over 40 min. Depressive symptoms and MRI scans were collected at baseline (1 day before the first infusion), and post-treatment (1 day after the sixth infusion). The detailed study design has been described in our previous studies (Zheng et al., 2018; Zhou et al., 2018a,b).

Rating scales

Depressive symptoms were estimated using the Montgomery-Asberg Scale (MADRS) and the responders were defined as having an improvement in MADRS scores (ΔMADRS%) $\geq$ 50%. This was calculated as follows: baseline MADRS score minus posttreatment MADRS score, then divided by the baseline MADRS, and finally multiplied by 100%.

Acquisition of MRI data

Participants completed fMRI scans at baseline and posttreatment. Participants were required to close their eyes but stay awake during the scans. BOLD signals were collected using a 3.0-T Philips Achieva MRI scanner (Philips, the Netherlands). An eight-channel SENSE head coil was used to record fast field echo (FFE) echo-planar images (EPI), the parameters were as follows: repetition time = 2,000 ms; echo time = 30 ms; flip angle = 90°; 33 slices; matrix = 64 × 64; field-of-view = 220 × 220 × 150 mm^3; voxel size = 3.44 × 3.44 × 4 mm^3; gap = 0.6 mm; and the number of signal averages (NSA) = 1. The resting fMRI scan (8 min, 43 s) comprised 240 contiguous volumes.

Preprocessing of MRI data

The MRI data were preprocessed using the toolbox of data processing and analysis for (resting-state) Brain Imaging (DPABI version 6.0),[1] running in MATLAB R2019b (The Mathworks, Natick, MA, USA).

We converted the data from the digital imaging and communications in medicine (DICOM) to a standard format (Neuroimaging Informatics Technology Initiative). The first 10 time points were removed to keep the signal stable. The remaining images were corrected using slice timing and realignment to reduce the interval scanning time difference and head motion. Four images were excluded for their maximum head motion parameter of over 2 mm or 2°. The remaining images were normalized to the Montreal Neurological Institute (MNI) using EPI templates. Nuisance signals from 24-parameter head motion profiles, white matter signals, cerebrospinal fluid signals, and global signals were removed using linear regression. Detrending was performed to remove the linear drift. To decrease physiological noise, images were filtered at 0.01–0.08 Hz.

Degree centrality

After preprocessing, the DC value was calculated using DPABI software. The BOLD signal of each voxel was extracted and collected with every other voxel. The number of correlations, which was over 0.25 ($r > 0.25$), was the DC value (Buckner et al., 2009; Wang et al., 2021). Then the DC values were z-transformed to acquire the Z score DC value images. Finally, these images were smoothed using a 6 mm × 6 mm × 6 mm full width at half the maximum Gaussian kernel.

Functional connectivity

The significantly different clusters in the DC map were used as seeds. The average time series of these regions were separately correlated with the remaining voxels to calculate the FC values and then z-transformed to obtain zFC maps of all MDD patients and HCs.

1 http://rfmri.org/DPARSF

Statistical analysis

Demographic characteristics, including educational level, duration of illness, baseline MADRS score, posttreatment MADRS score, and the dose of antidepressant (converted to standard fluoxetine equivalents) were compared between responders and non-responders using the Kruskal–Wallis H test. Body mass index (BMI) between responders and non-responders was analyzed using two-sample *t*-tests, and the gender was compared using the chi-square test. The age data and head motion were analyzed among responders, non-responders and HCs using analysis of variance (ANOVA). All of the above were run on SPSS 25.0 software, and the significance threshold was $p < 0.05$.

DC values were compared between responders and non-responders using a two-sample *t*-test analysis with age, BMI, and head motion as covariates in SPM12. AAL 90 was used as a mask in the analysis.

A one-way ANOVA with age, gender, and head motion as covariates was used in SPM12 to explore zFC differences among responders, non-responders, and HCs. The mean zFC values in the different clusters were extracted to conduct a *post hoc* analysis.

Moreover, we explored the relationship between the mean zFC values of MDD patients and ΔMADRS% using Spearman's correlation analysis. The mean zFC values of responders and non-responders were extracted separately and assessed the diagnostic efficiency using the receiver operating characteristic curve analysis in GraphPad Prism 5 (GraphPad Software Inc., USA).

Results

Demographic characteristics and clinical symptoms

The demographic and clinical results are shown in Table 1. There was no significant difference in gender, educational level, duration of illness, head motion, dose of antidepressant, or baseline MADRS score. However, responders were older and had a higher BMI than non-responders ($p < 0.05$). As expected, the responder group showed a higher posttreatment MADRS score than the non-responder group ($p < 0.05$).

Degree centrality analysis

Compared with responders, non-responders had higher values in the DC map (voxel-level $p < 0.001$; peak-level $p < 0.05$ corrected by FDR). It is a cluster located in the right middle frontal gyrus (MFG; $x = 36$, $y = 15$, $z = 45$, $k = 32$), shown in Figure 1.

Functional connectivity analysis

Among the 3 groups, MFG-related zFC maps were different in a region centered in the right supplementary motor area (SMA) ($x = 6$, $y = 3$, $z = 45$, $k = 90$; voxel-level $P < 0.001$, cluster-level $P < 0.05$ corrected by FDR). This region also contained parts of the bilateral median cingulate gyrus (SMA and mACC), as shown in Figure 2. The *post hoc* analysis revealed that responders had higher zFC values than non-responders and HCs, and non-responders had lower zFC values than HCs (Figure 3).

Relationship between the zFC value and ΔMADRS%

As Figure 4 shows, Spearman's correlation analysis revealed that the zFC values between MFG and SMA and mACC were positively correlated with ΔMADRS% in MDD patients ($r = 0.495$, $P < 0.05$). Importantly, the zFC value has the potential to be a predictor of the effect of ketamine (AUC = 0.872, $P < 0.001$).

TABLE 1 Demographics and clinical characteristics of the MDD and HCs at baseline.

	Responders	Non-responders	HCs	*P*
Subjects	24	16	45	–
Gender (female/male)	15/9	9/7	27/18	0.925
Age (Year, mean ± *SD*)	39.79 ± 11.58	30.69 ± 11.09	31.44 ± 7.98	0.002
Education (year)	12 (9, 15)	13.5 (9, 15)	–	0.594
Duration (month)	60 (24, 153)	42 (8.25, 105)	–	0.345
BMI (mean ± *SD*)	24.23 ± 2.70	21.36 ± 3.24	–	0.004
Baseline MADRS	31.5 (26, 34.75)	33 (23.5, 39.25)	–	0.503
Post-treatment MADRS	8 (4.25, 11)	27 (20, 31.5)	–	0.000
Head motion (FD)	0.048 (0.039, 0.063)	0.044 (0.035, 0.055)	0.052 (0.047, 0.066)	0.05
The dose of antidepressant (convert to standard fluoxetine equivalents)	51 (20, 60)	35 (20, 63.75)	–	0.733

HCs, healthy control.

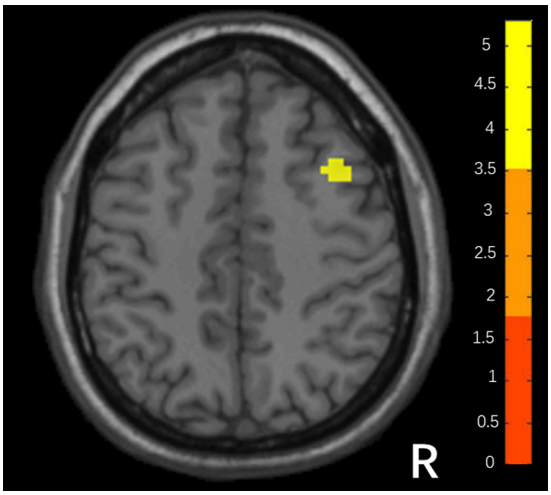

FIGURE 1
Differences in DC between responders and non-responders. (Two sample *t*-test, voxel- level $p < 0.001$, peak $p < 0.05$ corrected by FDR).

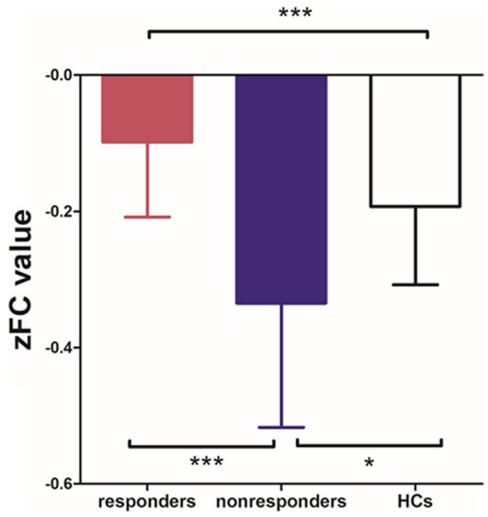

FIGURE 3
Differences in zFC values among responders, non-responders and HCs. (one-way ANOVA, Bonferroni's Multiple Comparison Test. *$p < 0.05$, ***$p < 0.0001$).

Discussion

In this study, we used the seed obtained from the DC map to explore the FC alterations in patients with MDD. The results revealed that the non-responder group had increased DC compared with the responder group in the region of the right MFG, a part of the DMN. The seed-based FC analysis showed a significant difference in the SMA and mACC among responders, non-responders, and HCs. The zFC in this region had a highly sensitive response to ketamine in MDD after six infusions. It can be used as a neuroimaging biomarker.

The MFG was a major part of the default mode network (DMN). The DMN is a key network in MDD and plays the role of cognitive control and integrating information (Yeshurun et al., 2021; Liu et al., 2022; Pang et al., 2022b). According to the prevalent triple network model, the symptoms of depression can be explained by dysfunction between the DMN, salience network, and central executive network, especially the increased FC in the DMN (Hamilton et al., 2015; Kaiser et al., 2015; Li et al., 2022). Using graph theory-based methods in the data of 821 MDD and 765 HCs, Yang et al. (2021) revealed that patients with MDD were characterized by decreased nodal efficiency in the DMN. Another study compared 848 MDD patients with 794 HCs and also found decreased FC in the DMN (Yan et al., 2019). Our results went one step further and revealed a difference within the MDD group. Liang et al. found two MDD subgroups with differing FC profiles of the DMN from 690 MDD patients; one group exhibited increases in connectivity, and the other subgroup showed decreases in connectivity (Liang et al., 2020). Price et al. (2017) also revealed two subgroups in MDD patients by assessing the difference in connectivity patterns across DMN

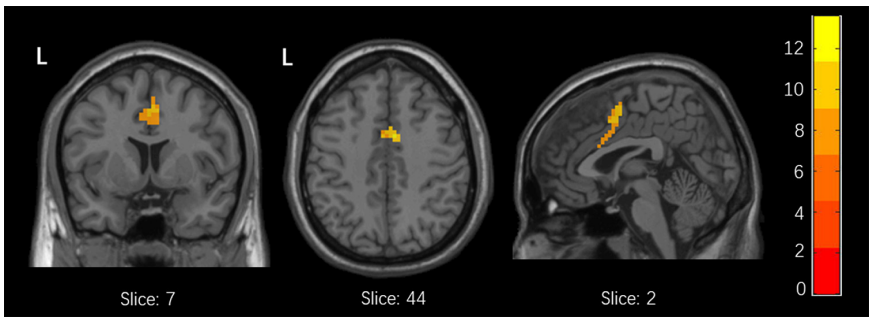

FIGURE 2
Differences in xFC among responders, non-responders and HCs. (one- Way ANOVA, voxel-level $p < 0.001$, cluster-level $p < 0.05$ corrected by FDR).

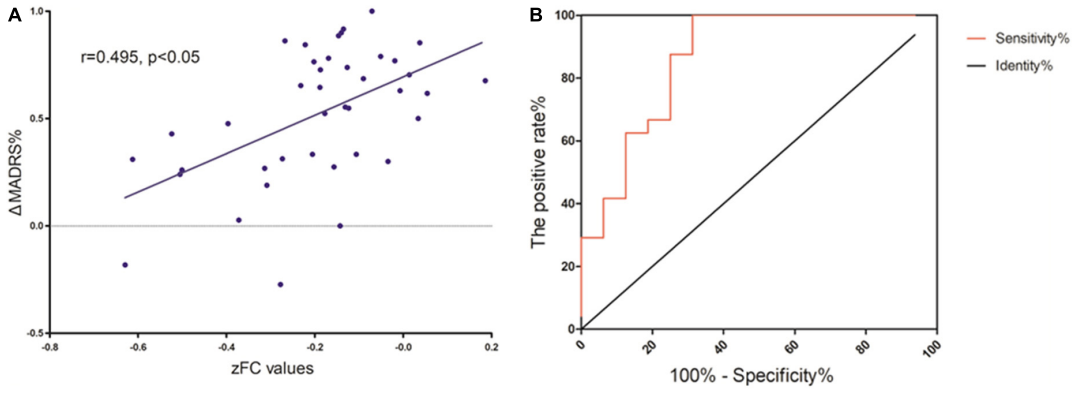

FIGURE 4
(A) Correlation between zFC values and L'lMADRS% in MOD patients. **(B)** ROC curve showing an area under the curve (AUC) of 0.8672 ($p < 0.001$) for the zFC values, with a sensitivity of 100%, and specificity of 68.75%.

nodes. A prior study found that ketamine can reduce FC (Price et al., 2017). Moreover, research has found that changes in FC at baseline could predict the effect of ECT (Pang et al., 2022a). In our results, the FC of responders will be toward HCs while non-responders will be far away from HCs if the FC has been reduced. It seems that the two groups qualitatively had different FC in the DMN, although the FC was negative in both groups. This finding supports the theory mentioned above: there were two subgroups in MDD, one of which is sensitive to ketamine while the other is not.

An increasing number of studies have partly revealed the function of the SMA. Gabbay et al. (2013) revealed that anhedonia scores were positively correlated with the intrinsic FC strength of the SMA; Westlund Schreiner et al. (2017) revealed a hyperconnectivity between the amygdala in self-injured adolescents without suicidal, which may show that negative effects have an important link with habitual behaviors; while other researchers showed that the FC value of the right SMA was negatively correlated with depressive symptoms in depressed patients with irritable bowel syndrome (Li et al., 2021). There were also some results regarding the cortical thickness in the SMA. Some studies have shown depressed patients had significantly smaller volumes of the right pre-SMA than control subjects (Exner et al., 2009; Cheng et al., 2010; Gabbay et al., 2013; Westlund Schreiner et al., 2017). Salomons et al. (2012) revealed fractional anisotropy of connected white matter tracts along the corticospinal tract were associated with helplessness and mediated the relationship between the SMA cortical thickness and helplessness. Besteher et al. (2017) revealed that somatization symptoms showed a negative correlation with the gray matter volume of the right SMA. Moreover, Li et al. (2015) found that regional cerebral glucose metabolism (rCMglu) in the bilateral SMA was decreased in the medication-resistant depression (MRD) group than in the non-MRD group, the MRD group patients also had decreased rCMglu in the SMA than the control group, while Chen et al. (2018) revealed that TRD patients who received the 0.5 mg/kg ketamine infusion had significantly higher glucose metabolism in the SMA than those who received the 0.2 mg/kg ketamine infusion, these authors suggest that the persistent antidepressant effect of a 0.5 mg/kg ketamine infusion may be mediated by increased activation in the SMA. These results indicate that the SMA has a tighter connection with MDD and plays an important role in habitual behaviors, depressive symptoms, and helpless feelings.

It's worth noting that the significant cluster located in the right SMA also overlapped with the bilateral median cingulate gyrus. The cingulate participates in the control of cognition and emotion, and executive attention (Botvinick et al., 2004; Etkin et al., 2006). Recently, an increasing number of studies have shown that the cingulate plays a key role in MDD and bipolar disorder (BP). A large meta-analysis, including 148 MDD patients and 7,957 HCs, indicated that patients with MDD had a thinner cortical anterior cingulate cortex and posterior cingulate cortex (Schmaal et al., 2017). Several studies indicated that the volume of the anterior cingulate cortex was associated with BP, the volume of the anterior midcingulate cortex at baseline was associated with greater symptom improvement after follow-up and patients who remitted had less volume decline than non-remitted patients in the left anterior cingulate cortex during a 3-year follow-up period (Lochhead et al., 2004; McDonald et al., 2004; Frodl et al., 2008; Phillips et al., 2015). Regarding FC, Greicius et al. (2007) found that the FC of the subgenual anterior cingulate cortex was correlated with the depressive episode length. A study using rTMS to treat treatment-resistant depression used sgACC-DLPFC and rACC-IPL connectivity as features, and found responder-non-responder classification accuracies of 84 and 76% (end-of-treatment), 88 and 81% (3-month follow-up)

(Ge et al., 2020). Enhanced FC between the right middle cingulum and right medial prefrontal cortex was positively correlated with the duration of depression since onset (Marazzi et al., 2021). This region is a key node in MDD that we cannot ignore.

Our findings should be considered with some limitations. First, patients took antidepressants and received ketamine injections at the same time. Although there was no difference in the dose, it may have affected the FC in the whole brain, thereby, impacting our final result. However, in the present study, it was closer to a real situation in patients' daily lives. Second, we only explored the FC values in the cerebrum (using the mask of AAL90), excluding the cerebellum. This may cause us to ignore the role of the cerebellum in brain activity. Third, we did not include the baseline MADRS score as a covariate because we did not collect it from HCs. It may improve results in our future studies. Finally, the MDD patients in our study include treatment-resistant depressive patients and patients with suicidal ideation. This could have biased our results.

Our results partially support the DMN's key role of the DMN in MDD and MDD patients could be identified as two subgroups by FC in the DMN. We also revealed that FC between the DMN and SMA and mACC was more highly correlated with depressive symptoms. In addition, FC has the potential to be a neuroimaging biomarker to predict the ketamine effect.

Data availability statement

The raw data supporting the conclusions of this article will be made available by the authors, without undue reservation.

Ethics statement

This study was approved and reviewed by the Clinical Research Ethics Committee of the Affiliated Brain Hospital of Guangzhou Medical University. Written informed consent was obtained from the individual(s) for the publication of any potentially identifiable images or data included in this article.

Author contributions

FZ: investigation, formal analysis, writing—original drafting, and visualization. YZ: validation, project administration, methodology, and investigation. CW and XL: validation, methodology, and investigation. WL, LF, YY, and HL: investigation. KW: conceptualization. YN: conceptualization, supervision, writing—review and editing. All authors contributed to the article and approved the submitted version.

Funding

This work was supported by the National Natural Science Foundation of China (grant no. 81801343), the Guangdong Basic and Applied Basic Research Foundation (grant no. 2019A1515011366), the National Key Research and Development Program of China (grant no. 2016YFC0906300), and Science and Technology Plan Project of Guangdong Province (grant no. 2019B030316001), Science and Technology Plan Project of Guangzhou (grant no. 202102020557).

Conflict of interest

The authors declare that the research was conducted in the absence of any commercial or financial relationships that could be construed as a potential conflict of interest.

The reviewer JW declared a past co-authorship with one of the authors YN to the handling editor.

Publisher's note

All claims expressed in this article are solely those of the authors and do not necessarily represent those of their affiliated organizations, or those of the publisher, the editors and the reviewers. Any product that may be evaluated in this article, or claim that may be made by its manufacturer, is not guaranteed or endorsed by the publisher.

Author disclaimer

The views expressed in this article are those of the authors and do not necessarily reflect the position or policy of the funders.

References

Berman, R. M., Cappiello, A., Anand, A., Oren, D. A., Heninger, G. R., Charney, D. S., et al. (2000). Antidepressant effects of ketamine in depressed patients. *Biol. Psychiatry* 47, 351–354. doi: 10.1016/S0006-3223(99)00230-9

Besteher, B., Gaser, C., Langbein, K., Dietzek, M., Sauer, H., and Nenadić, I. (2017). Effects of subclinical depression, anxiety and somatization on brain structure in healthy subjects. *J. Affect. Disord.* 215, 111–117. doi: 10.1016/j.jad.2017.03.039

Botvinick, M. M., Cohen, J. D., and Carter, C. S. (2004). Conflict monitoring and anterior cingulate cortex: An update. *Trends Cogn. Sci.* 8, 539–546. doi: 10.1016/j.tics.2004.10.003

Buckner, R. L., Sepulcre, J., Talukdar, T., Krienen, F. M., Liu, H., Hedden, T., et al. (2009). Cortical hubs revealed by intrinsic functional connectivity: Mapping, assessment of stability, and relation to Alzheimer's disease. *J. Neurosci.* 29, 1860–1873. doi: 10.1523/JNEUROSCI.5062-08.2009

Chen, M., Li, C., Lin, W., Hong, C., Tu, P., Bai, Y., et al. (2018). Persistent antidepressant effect of low-dose ketamine and activation in the supplementary motor area and anterior cingulate cortex in treatment-resistant depression: A randomized control study. *J. Affect. Disord.* 225, 709–714. doi: 10.1016/j.jad.2017.09.008

Chen, M. H., Lin, W. C., Tu, P. C., Li, C. T., Bai, Y. M., Tsai, S. J., et al. (2019). Antidepressant and antisuicidal effects of ketamine on the functional connectivity of prefrontal cortex-related circuits in treatment-resistant depression: A double-blind, placebo-controlled, randomized, longitudinal resting fMRI study. *J. Affect. Disord.* 259, 15–20. doi: 10.1016/j.jad.2019.08.022

Cheng, B., Roberts, N., Zhou, Y., Wang, X., Li, Y., Chen, Y., et al. (2022). Social support mediates the influence of cerebellum functional connectivity strength on postpartum depression and postpartum depression with anxiety. *Transl. Psychiatry* 12:54. doi: 10.1038/s41398-022-01781-9

Cheng, Y., Xu, J., Chai, P., Li, H., Luo, C., Yang, T., et al. (2010). Brain volume alteration and the correlations with the clinical characteristics in drug-naïve first-episode MDD patients: A voxel-based morphometry study. *Neurosci. Lett.* 480, 30–34. doi: 10.1016/j.neulet.2010.05.075

Craddock, R. C., Holtzheimer, P. R., Hu, X. P., and Mayberg, H. S. (2009). Disease state prediction from resting state functional connectivity. *Magn. Reson. Med.* 62, 1619–1628. doi: 10.1002/mrm.22159

Etkin, A., Egner, T., Peraza, D. M., Kandel, E. R., and Hirsch, J. (2006). Resolving Emotional Conflict: A Role for the Rostral Anterior Cingulate Cortex in Modulating Activity in the Amygdala. *Neuron* 51, 871–882. doi: 10.1016/j.neuron.2006.07.029

Exner, C., Lange, C., and Irle, E. (2009). Impaired implicit learning and reduced pre-supplementary motor cortex size in early-onset major depression with melancholic features. *J. Affect. Disord.* 119, 156–162. doi: 10.1016/j.jad.2009.03.015

Frodl, T. S., Koutsouleris, N., Bottlender, R., Born, C., Jäger, M., Scupin, I., et al. (2008). Depression-related variation in brain morphology over 3 years: Effects of stress? *Arch. Gen. Psychiatry* 65, 1156–1165. doi: 10.1001/archpsyc.65.10.1156

Gabbay, V., Ely, B. A., Li, Q., Bangaru, S. D., Panzer, A. M., Alonso, C. M., et al. (2013). Striatum-Based Circuitry of Adolescent Depression and Anhedonia. *J. Am. Acad. Child Adolesc. Psychiatr.* 52, 628–641. doi: 10.1016/j.jaac.2013.04.003

Ge, R., Downar, J., Blumberger, D. M., Daskalakis, Z. J., and Vila-Rodriguez, F. (2020). Functional connectivity of the anterior cingulate cortex predicts treatment outcome for rTMS in treatment-resistant depression at 3-month follow-up. *Brain Stimul.* 13, 206–214. doi: 10.1016/j.brs.2019.10.012

Greicius, M. D., Flores, B. H., Menon, V., Glover, G. H., Solvason, H. B., Kenna, H., et al. (2007). Resting-state functional connectivity in major depression: Abnormally increased contributions from subgenual cingulate cortex and thalamus. *Biol. Psychiatr.* 62, 429–437. doi: 10.1016/j.biopsych.2006.09.020

Hamilton, J. P., Farmer, M., Fogelman, P., and Gotlib, I. H. (2015). Depressive Rumination, the Default-Mode Network, and the Dark Matter of Clinical Neuroscience. *Biol. Psychiatry* 78, 224–230. doi: 10.1016/j.biopsych.2015.02.020

Kaiser, R. H., Andrews-Hanna, J. R., Wager, T. D., and Pizzagalli, D. A. (2015). Large-Scale Network Dysfunction in Major Depressive Disorder: A Meta-analysis of Resting-State Functional Connectivity. *JAMA Psychiat.* 72, 603–611. doi: 10.1001/jamapsychiatry.2015.0071

Kraguljac, N. V., Frolich, M. A., Tran, S., White, D. M., Nichols, N., Barton-McArdle, A., et al. (2017). Ketamine modulates hippocampal neurochemistry and functional connectivity: A combined magnetic resonance spectroscopy and resting-state fMRI study in healthy volunteers. *Mol. Psychiatry* 22, 562–569. doi: 10.1038/mp.2016.122

Li, C., Su, T., Wang, S., Tu, P., and Hsieh, J. (2015). Prefrontal glucose metabolism in medication-resistant major depression. *Brit. J. Psychiat.* 206, 316–323. doi: 10.1192/bjp.bp.113.140434

Li, J., He, P., Lu, X., Guo, Y., Liu, M., Li, G., et al. (2021). A Resting-state Functional Magnetic Resonance Imaging Study of Whole-brain Functional Connectivity of Voxel Levels in Patients With Irritable Bowel Syndrome With Depressive Symptoms. *J. Neurogastroenterol.* 27, 248–256. doi: 10.5056/jnm20209

Li, Y., Li, Y., Wei, Q., Bai, T., Wang, K., Wang, J., et al. (2022). Mapping intrinsic functional network topological architecture in major depression disorder after electroconvulsive therapy. *J. Affect. Disord.* 311, 103–109. doi: 10.1016/j.jad.2022.05.067

Liang, S., Deng, W., Li, X., Greenshaw, A. J., Wang, Q., Li, M., et al. (2020). Biotypes of major depressive disorder: Neuroimaging evidence from resting-state default mode network patterns. *Neuroimage Clin.* 28:102514. doi: 10.1016/j.nicl.2020.102514

Liu, C., Han, T., Xu, Z., Liu, J., Zhang, M., Du, J., et al. (2022). Modulating Gamma Oscillations Promotes Brain Connectivity to Improve Cognitive Impairment. *Cereb. Cortex* 32, 2644–2656. doi: 10.1093/cercor/bhab371

Lochhead, R. A., Parsey, R. V., Oquendo, M. A., and Mann, J. J. (2004). Regional brain gray matter volume differences in patients with bipolar disorder as assessed by optimized voxel-based morphometry. *Biol. Psychiat.* 55, 1154–1162. doi: 10.1016/j.biopsych.2004.02.026

Marazzi, S., Kiper, P., Palmer, K., Agostini, M., and Turolla, A. (2021). Effects of vibratory stimulation on balance and gait in Parkinson's disease: A systematic review and meta-analysis. *Eur. J. Phys. Rehab. Med.* 57, 254–264. doi: 10.23736/S1973-9087.20.06099-2

McDonald, C., Bullmore, E. T., Sham, P. C., Chitnis, X., Wickham, H., Bramon, E., et al. (2004). Association of genetic risks for schizophrenia and bipolar disorder with specific and generic brain structural endophenotypes. *Arch. Gen. Psychiatr.* 61, 974–984. doi: 10.1001/archpsyc.61.10.974

Mkrtchian, A., Evans, J. W., Kraus, C., Yuan, P., Kadriu, B., Nugent, A. C., et al. (2021). Ketamine modulates fronto-striatal circuitry in depressed and healthy individuals. *Mol. Psychiatr.*26, 3292–3301. doi: 10.1038/s41380-020-00878-1

Murrough, J. W., Iosifescu, D. V., Chang, L. C., Al, J. R., Green, C. E., Perez, A. M., et al. (2013a). Antidepressant efficacy of ketamine in treatment-resistant major depression: A two-site randomized controlled trial. *Am. J. Psychiatr.* 170, 1134–1142. doi: 10.1176/appi.ajp.2013.13030392

Murrough, J. W., Perez, A. M., Pillemer, S., Stern, J., Parides, M. K., Aan, H. R. M., et al. (2013b). Rapid and longer-term antidepressant effects of repeated ketamine infusions in treatment-resistant major depression. *Biol. Psychiatr.*74, 250–256. doi: 10.1016/j.biopsych.2012.06.022

Pang, Y., Wei, Q., Zhao, S., Li, N., Li, Z., Lu, F., et al. (2022a). Enhanced default mode network functional connectivity links with electroconvulsive therapy response in major depressive disorder. *J. Affect. Disord.* 306, 47–54. doi: 10.1016/j.jad.2022.03.035

Pang, Y., Zhao, S., Li, Z., Li, N., Yu, J., Zhang, R., et al. (2022b). Enduring effect of abuse: Childhood maltreatment links to altered theory of mind network among adults. *Hum. Brain Mapp.* 43, 2276–2288. doi: 10.1002/hbm.25787

Phillips, J. L., Batten, L. A., Tremblay, P., Aldosary, F., and Blier, P. (2015). A Prospective, Longitudinal Study of the Effect of Remission on Cortical Thickness and Hippocampal Volume in Patients with Treatment-Resistant Depression. *Int. J. Neuropsychoph.* 18:v37. doi: 10.1093/ijnp/pyv037

Price, R. B., Gates, K., Kraynak, T. E., Thase, M. E., and Siegle, G. J. (2017). Data-Driven Subgroups in Depression Derived from Directed Functional Connectivity Paths at Rest. *Neuropsychopharmacology* 42, 2623–2632. doi: 10.1038/npp.2017.97

Rivas-Grajales, A. M., Salas, R., Robinson, M. E., Qi, K., Murrough, J. W., and Mathew, S. J. (2021). Habenula Connectivity and Intravenous Ketamine in Treatment-Resistant Depression. *Int. J. Neuropsychopharmacol.* 24, 383–391. doi: 10.1093/ijnp/pyaa089

Salomons, T. V., Moayedi, M., Weissman-Fogel, I., Goldberg, M. B., Freeman, B. V., Tenenbaum, H. C., et al. (2012). Perceived helplessness is associated with individual differences in the central motor output system. *Eur. J. Neurosci.* 35, 1481–1487. doi: 10.1111/j.1460-9568.2012.08048.x

Scheidegger, M., Henning, A., Walter, M., Lehmann, M., Kraehenmann, R., Boeker, H., et al. (2016). Ketamine administration reduces amygdalo-hippocampal reactivity to emotional stimulation. *Hum. Brain Mapp.* 37, 1941–1952. doi: 10.1002/hbm.23148

Schmaal, L., Hibar, D. P., Samann, P. G., Hall, G. B., Baune, B. T., Jahanshad, N., et al. (2017). Cortical abnormalities in adults and adolescents with major depression based on brain scans from 20 cohorts worldwide in the ENIGMA Major Depressive Disorder Working Group. *Mol. Psychiatry* 22, 900–909. doi: 10.1038/mp.2016.60

Serafini, G., Howland, R. H., Rovedi, F., Girardi, P., and Amore, M. (2014). The role of ketamine in treatment-resistant depression: A systematic review. *Curr. Neuropharmacol.* 12, 444–461. doi: 10.2174/1570159X12666140619204251

Teng, C., Zhou, J., Ma, H., Tan, Y., Wu, X., Guan, C., et al. (2018). Abnormal resting state activity of left middle occipital gyrus and its functional connectivity in female patients with major depressive disorder. *BMC Psychiatry* 18:370. doi: 10.1186/s12888-018-1955-9

Wang, J. H., Zuo, X. N., Gohel, S., Milham, M. P., Biswal, B. B., and He, Y. (2011). Graph theoretical analysis of functional brain networks: Test-retest

evaluation on short- and long-term resting-state functional MRI data. *PLoS One* 6:e21976. doi: 10.1371/journal.pone.0021976

Wang, L., Hu, F., Wang, W., Li, Q., Li, Y., Zhu, J., et al. (2021). Altered brain intrinsic functional hubs and connectivity associated with relapse risk in heroin dependents undergoing methadone maintenance treatment: A resting-state fMRI study. *Drug Alcohol Depend.* 219:108503. doi: 10.1016/j.drugalcdep.2020.108503

Westlund Schreiner, M., Klimes-Dougan, B., Mueller, B. A., Eberly, L. E., Reigstad, K. M., Carstedt, P. A., et al. (2017). Multi-modal neuroimaging of adolescents with non-suicidal self-injury: Amygdala functional connectivity. *J. Affect. Disord.* 221, 47–55. doi: 10.1016/j.jad.2017.06.004

Yan, C. G., Chen, X., Li, L., Castellanos, F. X., Bai, T. J., Bo, Q. J., et al. (2019). Reduced default mode network functional connectivity in patients with recurrent major depressive disorder. *Proc. Natl. Acad. Sci. U.S.A.* 116, 9078–9083.

Yang, H., Chen, X., Chen, Z. B., Li, L., Li, X. Y., Castellanos, F. X., et al. (2021). Disrupted intrinsic functional brain topology in patients with major depressive disorder. *Mol. Psychiatry* 26, 7363–7371. doi: 10.1038/s41380-021-01247-2

Yang, Y., Dong, Y., and Chawla, N. V. (2014). Predicting node degree centrality with the node prominence profile. *Sci. Rep.* 4:7236. doi: 10.1038/srep07236

Yeshurun, Y., Nguyen, M., and Hasson, U. (2021). The default mode network: Where the idiosyncratic self meets the shared social world. *Nat. Rev. Neurosci.* 22, 181–192. doi: 10.1038/s41583-020-00420-w

Zarate, C. J., Singh, J. B., Carlson, P. J., Brutsche, N. E., Ameli, R., Luckenbaugh, D. A., et al. (2006). A randomized trial of an N-methyl-D-aspartate antagonist in treatment-resistant major depression. *Arch. Gen. Psychiatry* 63, 856–864. doi: 10.1001/archpsyc.63.8.856

Zhang, B., Li, M., Qin, W., Demenescu, L. R., Metzger, C. D., Bogerts, B., et al. (2016). Altered functional connectivity density in major depressive disorder at rest. *Eur. Arch. Psychiatry Clin. Neurosci.* 266, 239–248. doi: 10.1007/s00406-015-0614-0

Zheng, W., Zhou, Y., Liu, W., Wang, C., Zhan, Y., Li, H., et al. (2018). Rapid and longer-term antidepressant effects of repeated-dose intravenous ketamine for patients with unipolar and bipolar depression. *J. Psychiatr. Res.* 106, 61–68. doi: 10.1016/j.jpsychires.2018.09.013

Zhou, Y., Zheng, W., Liu, W., Wang, C., Zhan, Y., Li, H., et al. (2018a). Antidepressant effect of repeated ketamine administration on kynurenine pathway metabolites in patients with unipolar and bipolar depression. *Brain Behav. Immun.* 74, 205–212. doi: 10.1016/j.bbi.2018.09.007

Zhou, Y., Zheng, W., Liu, W., Wang, C., Zhan, Y., Li, H., et al. (2018b). Neurocognitive effects of six ketamine infusions and the association with antidepressant response in patients with unipolar and bipolar depression. *J. Psychopharmacol.* 32, 1118–1126. doi: 10.1177/0269881118798614

Zuo, X. N., Ehmke, R., Mennes, M., Imperati, D., Castellanos, F. X., Sporns, O., et al. (2012). Network centrality in the human functional connectome. *Cereb. Cortex* 22, 1862–1875. doi: 10.1093/cercor/bhr269

frontiers | Frontiers in Neuroscience

TYPE Original Research
PUBLISHED 21 October 2022
DOI 10.3389/fnins.2022.1010488

OPEN ACCESS

EDITED BY
Yuqi Cheng,
First Affiliated Hospital of Kunming Medical University, China

REVIEWED BY
Xu Han,
Shanghai Jiao Tong University, China
Zhifen Liu,
First Hospital of Shanxi Medical University, China

*CORRESPONDENCE
Shixiong Tang
Tangsx1990@csu.edu.cn

†These authors have contributed equally to this work

SPECIALTY SECTION
This article was submitted to Brain Imaging Methods, a section of the journal Frontiers in Neuroscience

RECEIVED 03 August 2022
ACCEPTED 07 October 2022
PUBLISHED 21 October 2022

CITATION
Liu D, Liu X, Long Y, Xiang Z, Wu Z, Liu Z, Bian D and Tang S (2022) Problematic smartphone use is associated with differences in static and dynamic brain functional connectivity in young adults. *Front. Neurosci.* 16:1010488. doi: 10.3389/fnins.2022.1010488

Problematic smartphone use is associated with differences in static and dynamic brain functional connectivity in young adults

Dayi Liu[1†], Xiaoxuan Liu[2†], Yicheng Long[1], Zhibiao Xiang[1], Zhipeng Wu[1], Zhening Liu[1], Dujun Bian[3] and Shixiong Tang[3*]

[1]Department of Psychiatry, National Clinical Research Center for Mental Disorders, The Second Xiangya Hospital, Central South University, Changsha, Hunan, China, [2]Department of Neurology, The Second Xiangya Hospital, Central South University, Changsha, China, [3]Department of Radiology, Clinical Research Center for Medical Imaging in Hunan Province, The Second Xiangya Hospital, Central South University, Changsha, Hunan, China

Introduction: This study aimed to investigate the possible associations between problematic smartphone use and brain functions in terms of both static and dynamic functional connectivity patterns.

Materials and methods: Resting-state functional magnetic resonance imaging data were scanned from 53 young healthy adults, all of whom completed the Short Version of the Smartphone Addiction Scale (SAS-SV) to assess their problematic smartphone use severity. Both static and dynamic functional brain network measures were evaluated for each participant. The brain network measures were correlated the SAS-SV scores, and compared between participants with and without a problematic smartphone use after adjusting for sex, age, education, and head motion.

Results: Two participants were excluded because of excessive head motion, and 56.9% (29/51) of the final analyzed participants were found to have a problematic smartphone use (SAS-SV scores $\geq$ 31 for males and $\geq$ 33 for females, as proposed in prior research). At the global network level, the SAS-SV score was found to be significantly positively correlated with the global efficiency and local efficiency of static brain networks, and negatively correlated with the temporal variability using the dynamic brain network model. Large-scale subnetwork analyses indicated that a higher SAS-SV score was significantly associated with higher strengths of static functional connectivity within the frontoparietal and cinguloopercular subnetworks, as well as a lower temporal variability of dynamic functional connectivity patterns within the attention subnetwork. However, no significant differences were found when directly comparing between the groups of participants with and without a problematic smartphone use.

Conclusion: Our results suggested that problematic smartphone use is associated with differences in both the static and dynamic brain network

organizations in young adults. These findings may help to identify at-risk population for smartphone addiction and guide targeted interventions for further research. Nevertheless, it might be necessary to confirm our findings in a larger sample, and to investigate if a more applicable SAS-SV cutoff point is required for defining problematic smartphone use in young Chinese adults nowadays.

KEYWORDS

addiction, problematic smartphone use, mobile phone use, fMRI, dynamic functional connectivity

Introduction

In the past years, the popularity and availability of smartphones have been increasing worldwide, and such a trend is accompanied by increased concerns regarding the potential overuse of smartphones (Horvath et al., 2020; Ratan et al., 2021). Recently, the term "problematic smartphone use" (or also called "problematic mobile phone use" by some researchers) has been introduced, which is defined as excessive use of smartphones with features of craving, dependence, loss of control, and potentially related physical and mental health problems (Long et al., 2016; Harris et al., 2020; Zou et al., 2021). These problems include, for instance, bodily pain (Ng et al., 2020), poor sleep quality (Huang et al., 2020), reduced physical fitness (Wacks and Weinstein, 2021), as well as mental problems such as depressive symptoms (Elhai et al., 2017; Yang X. et al., 2021) and even major depressive disorder (Alageel et al., 2021).

Identifying factors associated with problematic smartphone use can help identify at-risk population and guide targeted interventions for further research (Luk et al., 2018; Roh et al., 2018). Resting-state functional magnetic resonance imaging (rs-fMRI) offers a promising approach for characterizing the intrinsic brain functional organizations (Canario et al., 2021; Lin et al., 2021). Using rs-fMRI, a growing body of neuroimaging studies has suggested that problematic smartphone use is associated with brain dysfunction even in non-clinical samples with no diagnosis of psychiatric disorders (Chun et al., 2018; Paik et al., 2019; Horvath et al., 2020; Ahn et al., 2021; Pyeon et al., 2021; Zou et al., 2022). For example, the severity of problematic smartphone use has been reported to be positively associated with functional connectivity between the parahippocampal gyrus and middle temporal gyrus (Zou et al., 2022), and negatively associated with the fronto-limbic functional connectivity (Pyeon et al., 2021) in general populations. In another study, problematic smartphone use was suggested to be related to enhanced functional connectivity within the salience network, as well as between the salience and default-mode networks (Ahn et al., 2021). Importantly, some of these alterations (e.g., parahippocampal gyrus-middle temporal gyrus functional connectivity) have been found to moderate the relationship between problematic smartphone use and depressive symptoms in adolescents (Zou et al., 2022). Appreciably, these findings have advanced our understanding of the potential neurobiological factors associated with problematic smartphone use, which may guide further research on interventions for this problem.

The currently published rs-fMRI studies on problematic smartphone use, however, are limited in several ways. Firstly, most of these studies were focused on connectivity patterns within predefined regions of interest (ROIs). Although there have been some attempts (Ahn et al., 2021), investigations on how problematic smartphone use would affect the large-scale configurations of brain networks are relatively limited. Especially, it has been suggested that graph-theoretical-based features of the whole-brain network (e.g., global and local efficiency) can provide a powerful and reliable framework for understanding the alterations in brain function (Achard and Bullmore, 2007; Cao et al., 2014; Yang H. et al., 2021), but their possible relationships with problematic smartphone use were seldom reported. Secondly and importantly, while conventional rs-fMRI studies were generally performed under the assumption that connectivity patterns between brain areas are static, recent studies have proved that the brain connectivity patterns are actually dynamically changed over time (Hutchison et al., 2013a,b). The "dynamic functional connectivity (dFC)" was suggested to reflect important information ignored by conventional "static functional connectivity (sFC)" (Park et al., 2018; Zhang W. et al., 2018), and has been widely used in recent rs-fMRI studies in both psychiatric (Sheng et al., 2021; Chen et al., 2022) and non-clinical (Long et al., 2019; Huang D. et al., 2021) populations. Nonetheless, whether problematic smartphone use would affect the brain dFC patterns have been barely investigated to our knowledge, and needs further investigation.

To overcome the above limitations, this study aimed to investigate the possible associations between problematic smartphone use and differences in large-scale brain network organizations by combining both sFC and dFC analyzing

methods. We anticipate that the results would provide meaningful information to previous studies focusing on only specific ROIs and/or on only brain sFC patterns, and further improve our understanding of the possible biological factors associated with problematic smartphone use.

Materials and methods

Participants and measures

Fifty-three young healthy adults were recruited from the Changsha city area, Hunan Province, China based on the following inclusion criteria: (1) 18∼25 years of age; (2) native Chinese speakers; (3) right-handed; (4) were never diagnosed with any psychiatric diseases; and (5) had no contraindications to rs-fMRI scanning. All participants had signed informed consent, and the study was proved by the Ethics Committee of Second Xiangya Hospital, Changsha, China.

The participants were asked to complete the Short Version of the Smartphone Addiction Scale (SAS-SV) (Kwon et al., 2013) to assess the problematic smartphone use severity. The SAS-SV was a self-reported scale that contains 10 items, each rated from 1 ("strongly disagree") to 6 ("strongly agree"). Thus, the total score of SAS-SV ranges from 10 to 60, and a higher score indicates a higher level of current problematic smartphone use (Kwon et al., 2013; Luk et al., 2018). The Chinese version of SAS-SV has been proved to be valid (Luk et al., 2018) and was widely applied in Chinese adults (Chen et al., 2017; Guo et al., 2020, 2021; Zhang et al., 2022).

All participants also completed the following scales to estimate their current mental health situations during the past two weeks: (1) the 9-item Patient Health Questionnaire (PHQ-9), a screening instrument for depressive symptoms (Kroenke et al., 2001; Wu et al., 2022); and (2) the seven-item Generalized Anxiety Disorder Scale (GAD-7), a questionnaire to assess anxiety levels (Spitzer et al., 2006; Wu et al., 2022). The Cronbach's α coefficients of the SAS-SV, PHQ-9, and GAD-7 in this study were 0.869, 0.831, and 0.867 respectively, which suggests a good internal consistency (Cronbach's α coefficient > 0.7) (Wu et al., 2022).

Imaging data acquisition and preprocessing

The rs-fMRI data were acquired from each participant using a 3.0 T Siemens scanner with the following key parameters: matrix = 64 × 64, slices = 32, repetition time (TR) = 2,000 ms, echo time (TE) = 30 ms, slice thickness = 5 mm, gap = 0 mm, flip angle = 90°, field of view (FOV) = 240 × 240 mm^2, and total volumes = 216. T1-weighted images were also acquired for registration with the following key parameters: matrix = 256 × 256, slices = 176, TR = 1,900 ms, TE = 2 ms, slice thickness = 1 mm, gap = 0 mm, and FOV = 256 × 256 mm^2. After data acquisition, the images of all participants were preprocessed using the DPARSF software[1] (Chao-Gan and Yu-Feng, 2010; Yan et al., 2016) with the standard pipeline. Briefly, the pipeline includes removing the first 10 time points, slice timing, motion realignment, spatial normalization, temporal filtering (0.01–0.10 Hz), and nuisance regression (including the white matter and cerebrospinal fluid signals) (Yan et al., 2019; Long et al., 2020a). The following procedures were performed to ensure data quality: (1) all preprocessed images were manually checked by trained researchers to rule out overt artifacts or poor registration; (2) data were excluded from the analyses when excessive head motion occurred during scanning, as defined by mean framewise-displacement (FD) > 0.2 mm (Huang X. et al., 2021); (3) the mean FD values were further used as a controlling variable in all the following analyses. More details about the data acquisition parameters and preprocessing steps can be found in a previously published work (Huang D. et al., 2021).

Static and dynamic brain network constructions

The Power functional atlas (Power et al., 2011), which includes a total of 264 ROIs distributed across the brain (see **Figure 1A**), was used to define the nodes in brain networks for each participant. We chose the Power atlas here since it was widely used and validated in both sFC and dFC studies (Cao et al., 2014; Tan et al., 2020; Long et al., 2021). The mean time series were firstly extracted from each of the 264 nodes (ROIs) by averaging rs-fMRI signals within each node. The sFC strength for any pair of two nodes was computed as the Fisher's r-to-z transformed Pearson's correlation coefficients of the extracted time series, yielding a 264*264 sFC matrix which represents the static brain network organization (**Figure 1B**).

To construct dynamic brain networks, the extracted time series were further segmented into a number of continuous time windows using a common sliding-window approach (Long et al., 2020a; Zhao et al., 2021). A window width of 50 TRs (100 s) and a step length of 3 TRs (6 s) were used based on previous recommendations (Sun et al., 2019; Long et al., 2020a; Tang et al., 2022), resulting in a total of 53 time windows. Similar to the sFC matrixes, a 264*264 dFC matrix was then generated for each time window based on the Fisher's r-to-z transformed connection strengths between nodes. These dFC matrices are time-ordered, and thus formed a dynamic brain network $G = (G_t)_{t=1, 2, 3, \ldots, 53}$, in which the tth matrix (G_t) represents the "snapshot" of brain dFC patterns within the tth time window (Sun et al., 2019; Huang D. et al., 2021; **Figure 1B**).

1 http://rfmri.org/DPARSF

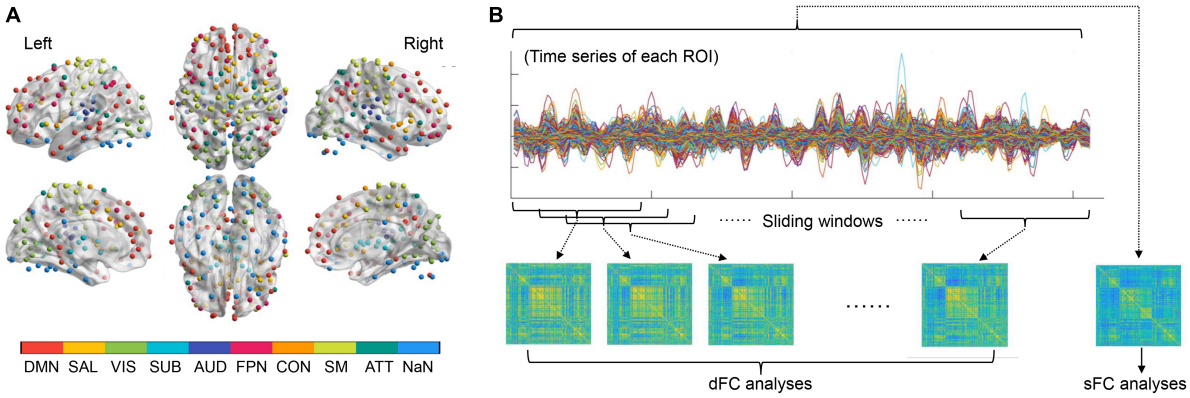

FIGURE 1
(A) The regions of interests (ROIs) used to define the brain nodes and their subnetwork assignments. **(B)** A summary of procedures for static functional connectivity (sFC) and dynamic functional connectivity (dFC) analyses (see details in the Methods section). ATT, attention subnetwork; AUD, auditory subnetwork; CON, cinguloopercular subnetwork; DMN, default-mode subnetwork; FPN, frontoparietal subnetwork; NaN, unassigned; SAL, salience subnetwork; SM, sensorimotor subnetwork; SUB, subcortical subnetwork; VIS, visual subnetwork.

Global and nodal brain network metrics

Several common global and nodal network metrics were calculated for both the static and dynamic (weighted, undirected) brain networks for each participant. Static network metrics included the global efficiency (E_{glob}) and local efficiency (E_{loc}) at the global level, as well as the nodal degree of each node. The E_{glob} and E_{loc} are two of the most intuitive and widely-used metrics to measure the information transfer efficiency of a static brain network (Tan et al., 2020; Yang H. et al., 2021; Liu D. et al., 2022). The nodal degree is a basic measure of the overall connectivity of a node to the rest of the brain (Li T. et al., 2021; Yang H. et al., 2021). The E_{glob} and E_{loc} were calculated in a range of density levels from 0.10 to 0.34 with an interval of 0.01, to avoid possible bias caused by a single density level (Achard and Bullmore, 2007; Lv et al., 2021; Yang H. et al., 2021). This range was chosen because it guaranteed that the network metrics were estimable and there were not too many spurious edges (Achard and Bullmore, 2007; Zhang et al., 2011). For each metric, the area under the curve (AUC) across such a density range (0.10–0.34) was calculated and fed into statistical analyses (Zhang et al., 2011; Yang H. et al., 2021). Referring to the previous work, the characteristic path length (L_p) and clustering coefficient (C_p) were also calculated for the latter validation analyses (Yang H. et al., 2021). The above static brain network metrics were calculated using the Brain Connectivity Toolbox (Rubinov and Sporns, 2010).

The examined dynamic network metrics included the *temporal variability* for the entire brain network and *nodal temporal variability* of each node (Zhang et al., 2016; Dong et al., 2019; Long et al., 2020b; Sun et al., 2022). These two metrics quantify the temporal stability of brain dFC patterns at the global and nodal levels, respectively; higher values of temporal variability indicate more fluctuations of the dFC patterns (less stable dFCs) over time. More details about the calculations of these two metrics can be found in previous publications (Zhang et al., 2016; Dong et al., 2019; Long et al., 2020b; Sun et al., 2022).

Large-scale subnetwork analyses

Besides the global and nodal network metrics, large-scale subnetwork analyses were also performed on both the sFC and dFC architectures strictly following the procedures in previous publications (Dong et al., 2019; Long et al., 2020b; Li L. et al., 2021; Sun et al., 2022). According to prior work (Cole et al., 2013; Mohr et al., 2016; Long et al., 2019, 2021), all ROIs in the Power atlas were firstly assigned into nine large-scale subnetworks including the default-mode, salience, visual, subcortical, auditory, frontoparietal, cinguloopercular, sensorimotor and attention subnetworks (**Figure 1A**). The strengths of within-and between-subnetwork sFC were calculated by averaging the z-transformed sFC values across all involved connections within a specific subnetwork, or between a specific pair of subnetworks (Li L. et al., 2021). Similarly, the temporal variabilities of within- and between-subnetwork dFC were also obtained by calculating the average variabilities of dFC across all involved connections (Dong et al., 2019; Long et al., 2020b; Sun et al., 2022). This resulted in nine within-subnetwork sFC/dFC measures and 36 between-subnetwork sFC/dFC measures.

Statistics

The possible associations between problematic smartphone use and all the sFC/dFC measures were investigated from two

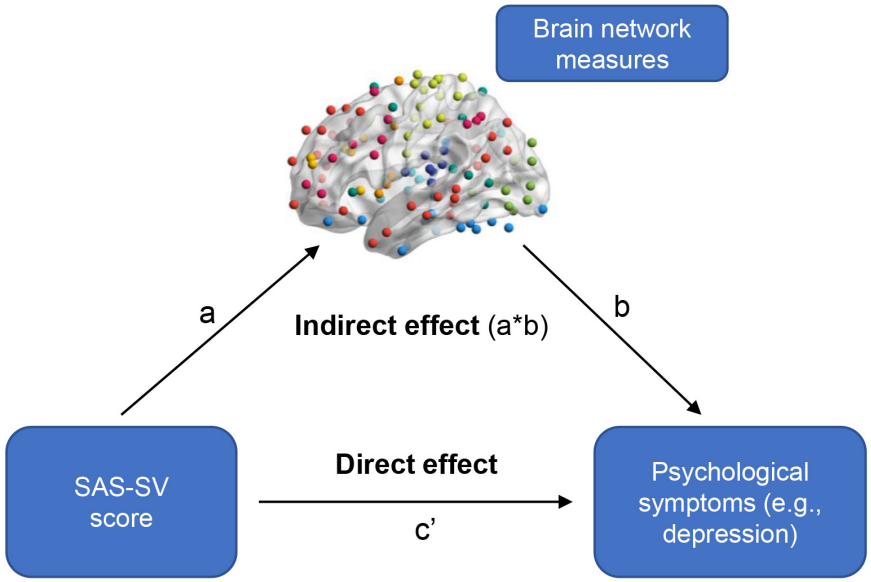

FIGURE 2
A summary of how to test the mediation effects of brain network measures in the relationship between problematic smartphone use severity and psychological symptoms. A significant mediation occurred when the 95% confidence interval for the indirect effect did not include zero.

perspectives. Firstly, relationships between all brain network measures and the SAS-SV score were assessed using the partial Pearson correlations adjusted for age, sex, years of education, and head motion (mean FD value). False discovery rate (FDR) corrections were applied to correct for multiple correlation tests (e.g., across the three global metrics, the 264 nodes, the nine within-subnetwork and 36 between-subnetwork measures). Significance was set at FDR-corrected $p < 0.05$. The results were visualized partly using the BrainNet Viewer (Xia et al., 2013).

Secondly, all brain network measures were compared between the groups of participants with and without a problematic smartphone use, as defined by the commonly-used SAS-SV cutoff points proposed in prior research (SAS-SV scores $\geq$ 31 for males and $\geq$ 33 for females) (Kwon et al., 2013; Luk et al., 2018; Saadeh et al., 2021; Liu H. et al., 2022). All brain network measures were compared between the two groups using the analysis of covariance (ANCOVA) covarying for age, sex, years of education, and head motion. Similarly, FDR corrections were applied to correct for multiple comparisons, and significance was set at FDR-corrected $p < 0.05$.

Validation analyses

Several follow-up analyses were performed to validate the results. Firstly, the associations between the SAS-SV score and L_p/C_p, which have equivalent meanings to the E_{glob} and E_{loc} (Yang H. et al., 2021), were estimated using the same methods. Secondly, since the optimal window width and step length for the sliding-windows method are still being debated (Leonardi and Van De Ville, 2015; Zhang C. et al., 2018), the analyses on all dFC measures were repeatedly with a set of different window and step lengths for the sliding windows [window/step = (80, 100, 120)/(4, 6, 8) s] to see if the results were affected by such analyzing strategies.

Exploratory analyses

In the present study, we performed two-step exploratory analyses to see if those problematic smartphone use-related differences in sFC/dFC would have mediation effects in the relationship between problematic smartphone use and psychological symptoms. Firstly, the linear regression analyses (controlling for age, sex, and education) were used to determine whether an association existed between the SAS-SV score and the GAD-7/PHQ-9 score. Secondly, when significant associations existed ($p < 0.05$), the analyses of mediation effects were further conducted using the PROCESS software (Hayes, 2012) on the sFC/dFC measures. Model 4 in the PROCESS software was used with 5,000 bootstrapping resamples; a significant mediation occurred when the 95% confidence interval (CI) for the indirect effect did not include zero (**Figure 2**; Rhudy et al., 2020; Li J. et al., 2021; Wu et al., 2021).

Additionally, since no significant results were found in group comparisons between the participants with and without a problematic smartphone use (see later in Section "Group comparisons") based on the SAS-SV cutoff points proposed in prior research ($\geq$ 31 for males and $\geq$ 33 for females), we explored whether the results would change when using

TABLE 1 Characteristics of the final analyzed sample (n = 51).

	Mean ± Standard deviation
Age	21.51 ± 1.55
Sex (males/females)	16/35
Year of education	15.65 ± 1.93
SAS-SV score	32.78 ± 9.21
SAS-SV score (in males)	34.69 ± 7.87
SAS-SV score (in females)	31.91 ± 9.74
GAD-7 score	3.12 ± 3.20
PHQ-9 score	4.18 ± 3.66

a different cutoff. Here, referring to some published studies (Mullins et al., 2007; Asarnow et al., 2019; Quintero Garzón et al., 2021), we used a cutoff score estimated based on one standard deviation above the mean of SAS-SV score in the surveyed sample; this resulted a new cutoff score of ≥ 43 for males and ≥ 42 for females. Group comparisons were repeated based on such new cutoff.

Results

Sample characteristics

During data preprocessing, two participants were excluded because of excessive head motion. Thus, the final analyzed sample consisted of 51 subjects and their demographic and clinical characteristics are presented in Table 1.

Correlation analyses

At the global level, significant correlations were found between the SAS-SV score and the E_{glob} of static brain networks (r = 0.288, corrected p = 0.049), as well as between the SAS-SV score and the E_{loc} of static brain networks (r = 0.335, corrected p = 0.032) (Figure 3A). Furthermore, a significant negative correlation was found between the SAS-SV score and the temporal variability of dynamic brain networks (r = −0.354, corrected p = 0.032) (Figure 3B). At the nodal level, however, no significant correlations were found for any metric (all corrected $p > 0.05$).

As shown in the Figure 4, significant positive correlations were found between the SAS-SC score and sFC strength within the frontoparietal subnetwork (r = 0.458, corrected p = 0.011), as well as between the SAS-SC score and sFC strength within the cinguloopercular subnetwork (r = 0.424, corrected p = 0.013); moreover, a significant negative correlation was found between the SAS-SC score and dFC temporal variability within the attention subnetwork (r = −0.409, corrected p = 0.038). No significant results were found on the between-subnetwork sFC/dFC measures (all corrected-$p > 0.05$).

Group comparisons

Based on the cutoff of a SAS-SV score ≥ 31 for males and ≥ 33 for females, 56.9% (29/51) of the participants were found to have a problematic smartphone use. However, no significant group differences were found on any brain network measure between the participants with and without a problematic smartphone use (all corrected $p > 0.05$), even for those measures showing significant correlations with the SAS-SV score (Figure 5A).

Validation analyses

Significant correlations were found between the SAS-SV score and L_p (r = 0.363, corrected p = 0.023), as well as between the SAS-SV score and C_p (r = −0.332, corrected p = 0.023) (Figure 3C), which thus partly validate the findings on E_{glob} and E_{loc}.

The relationships between the SAS-SV score and dFC measures remained significant when repeating the analyses with a set of different window and step lengths (see Supplementary Tables 1, 2). Therefore, the results were unlikely to be largely affected by the analyzing parameters.

Exploratory analyses

The linear regression analyses revealed a significant positive relationship between the SAS-SV score and the PHQ-9 score (β = 0.154, t = 2.787, p = 0.008), suggesting that problematic smartphone use is associated with a higher level of depressive symptoms. However, no significant mediation effects were observed for any sFC/dFC measure in the relationship between problematic smartphone use and depressive symptoms (no significant indirect effects were observed, as shown in Table 2).

When defining problematic smartphone use with a new cutoff (SAS-SV score ≥ 43 for males and ≥ 42 for females), 17.6% (9/51) of the participants were considered to have a problematic smartphone use. When using such new cutoff points, significant group differences were found between the participants with and without a problematic smartphone use on most brain network measures which showed significant correlations with the SAS-SV score (corrected $p < 0.05$, Figure 5B).

Discussion

In this study, we investigated the possible associations between problematic smartphone use and brain functions in young healthy adults combining both the sFC and dFC analyzing methods. Overall, our results suggested

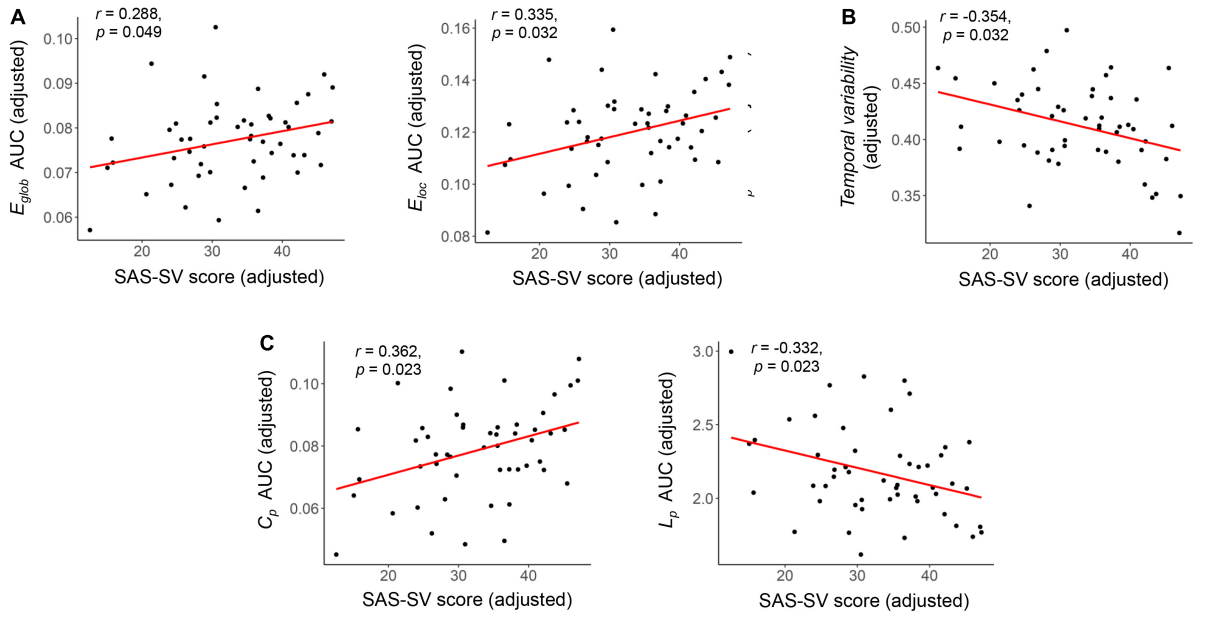

FIGURE 3
Results of the partial correlations between the short version of the smartphone addiction scale (SAS-SC) score and each global brain network metric. **(A)** Results on the E_{glob} and E_{loc} of static brain networks. **(B)** Results on the temporal variability of dynamic brain networks. **(C)** Results on the C_p and L_p of static brain networks (as validation analyses). The partial Pearson correlation coefficients **(*r*)** and corrected *p* values are presented.

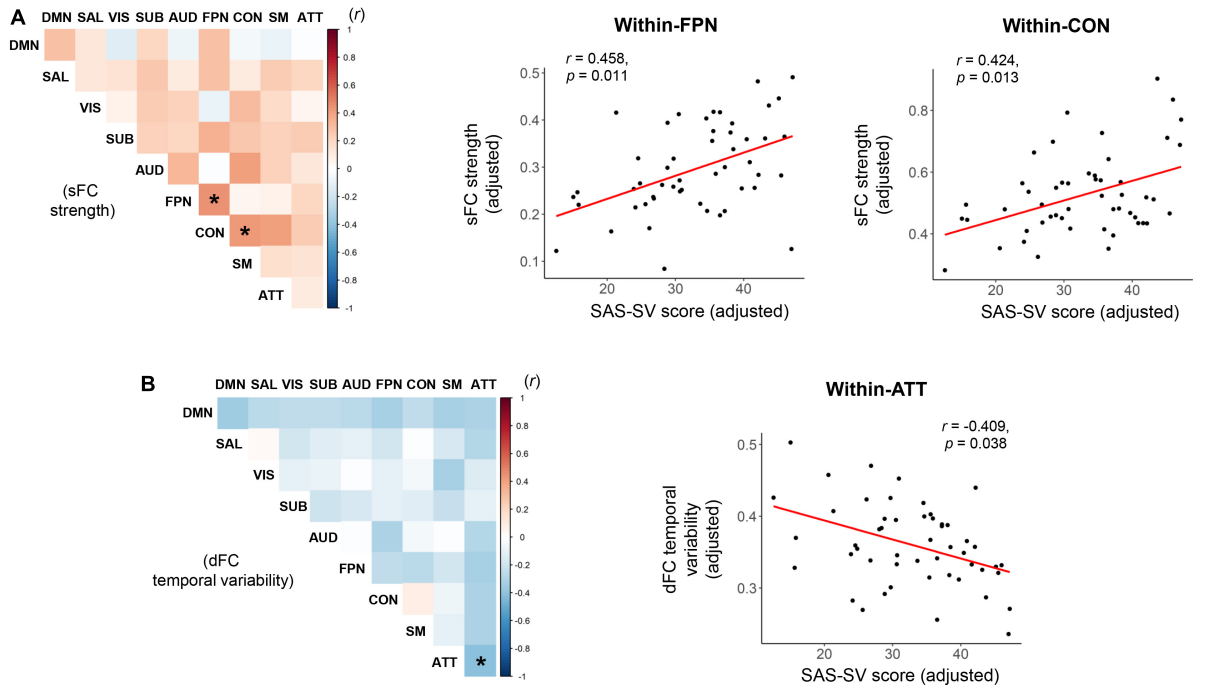

FIGURE 4
Results of partial correlations between the short version of the smartphone addiction scale (SAS-SC) score and the within-or between-subnetwork static functional connectivity (sFC) strength **(A)** and dynamic functional connectivity (dFC) temporal variability **(B)**. The scatter plots for the significant correlations were also presented on the right side. ATT, attention subnetwork; AUD, auditory subnetwork; CON, cinguloopercular subnetwork; DMN, default-mode subnetwork; FPN, frontoparietal subnetwork; SAL, salience subnetwork; SM, sensorimotor subnetwork; SUB, subcortical subnetwork; VIS, visual subnetwork. *Indicates a significant correlation with corrected $p < 0.05$.

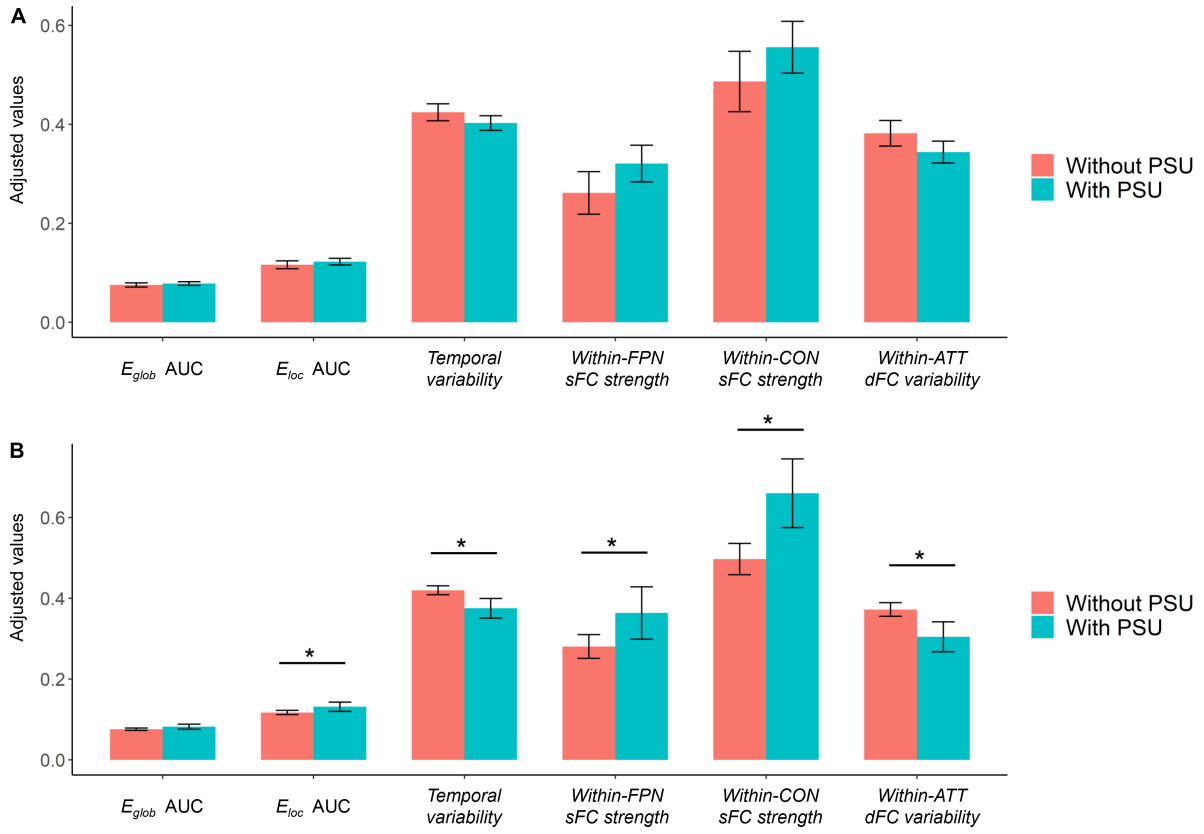

FIGURE 5
(A) Results of group comparisons when defining problematic smartphone use with the cutoff proposed in prior research [short version of the smartphone addiction scale (SAS-SV) score ≥ 31 for males and ≥ 33 for females]. **(B)** Results of exploratory group comparisons when defining problematic smartphone use with a new cutoff (SAS-SV score ≥ 43 for males and ≥ 42 for females, as estimated by one standard deviation above the mean scores). The error bars represent the 95% confidence intervals, and the "*" indicates a significant difference with corrected $p < 0.05$. ATT, attention subnetwork; CON, cinguloopercular subnetwork; PSU, problematic smartphone use.

that the severity of smartphone use is associated with significant differences in both the static and dynamic brain network organizations.

For static brain network properties, our results suggested that higher smartphone use severity is significantly associated with a higher E_{glob} as well as a higher E_{loc} at the global level (**Figure 3A**). Such results were further validated by significant results on the C_p and L_p, which were known to have equivalent meanings to the E_{glob} and E_{loc} (Yang H. et al., 2021; **Figure 3C**). While the neuroimaging studies on problematic smartphone use are growing (Ahn et al., 2021; Pyeon et al., 2021; Zou et al., 2022), the possible effects of problematic smartphone use on these graph-theoretical-based brain network features are still seldom reported. Nevertheless, similar alterations in the brain networks (increased E_{glob} and/or E_{loc}) have been associated with some common psychiatric diseases such as posttraumatic stress disorder (Lei et al., 2015), as well as multiple substance/non-substance addictions such as the nicotine dependence (Lin et al., 2015) and Internet gaming addiction (Park et al., 2017). Our results may thus provide preliminary evidence that higher smartphone use severity could be related to changing trends in topological functional brain organizations, which is similar to changes in patients with these disorders. These findings may help to identify at-risk population for smartphone addiction, and guide targeted interventions for further research.

Using the dynamic network model, our results suggested that problematic smartphone use is associated with a lower temporal variability (**Figure 3B**), which indicates a decreased dynamism of brain networks (Long et al., 2020b). Previous studies have proved that there are unignorable dynamic fluctuations in the human brain's functional organizations (Hutchison et al., 2013a,b), which is closely related to the cognitive (Patil et al., 2021) and emotional (Tobia et al., 2017) processes. Meanwhile, both excessively increased (Long et al., 2020b; Sun et al., 2022) and decreased (Jin et al., 2017; Luo L. et al., 2021; Luo Z. et al., 2021) dynamisms were thought to be reflective of abnormal brain functions. Specially, a decreased dynamism may indicate a disturbance in the information processing across brain regions (Luo Z. et al., 2021). Here, our results therefore provide one of the first

TABLE 2 Results of the mediation effect analyses on each brain network measures in the relationship between the short version of the smartphone addiction scale (SAS-SV) score and patient health questionnaire (PHQ-9) score.

Brain network measures	Direct effects (with 95% confidence intervals)	Indirect effects (with 95% confidence intervals)
Global network metrics		
Global efficiency	0.140 (0.022, 0.259)*	0.015 (−0.013, 0.065)
Local efficiency	0.141 (0.020, 0.261)*	0.015 (−0.021, 0.068)
Temporal variability	0.152 (0.030, 0.275)*	0.003 (−0.040, 0.059)
Characteristic path length	0.142 (0.022, 0.263)*	0.013 (−0.021, 0.066)
Clustering coefficient	0.141 (0.019, 0.263)*	0.014 (−0.025, 0.065)
Subnetwork-level measures		
Within-FPN sFC strength	0.138 (0.010, 0.267)*	0.017 (−0.045, 0.087)
Within-CON sFC strength	0.155 (0.029, 0.282)*	0.000 (−0.060, 0.058)
Within-ATT dFC temporal variability	0.150 (0.025, 0.275)*	0.006 (−0.043, 0.054)

The "*" indicates a significant direct or indirect effect (with a 95% confidence interval not including zero). ATT, attention subnetwork; CON, cinguloopercular subnetwork; FPN, frontoparietal subnetwork.

evidence that problematic smartphone use may decrease the functional brain network dynamism.

At the subnetwork level, it was found that a higher smartphone use severity is associated with increased sFC strengths within the frontoparietal and cinguloopercular subnetworks (**Figure 4A**), as well as decreased dFC temporal variability within the attention subnetwork (**Figure 4B**). The frontoparietal and cinguloopercular subnetworks are known to be implicated in higher-level cognitive functions (Wallis et al., 2015; Schmidt et al., 2016). The attention subnetwork is thought to be responsible for the top-down attentional process, whose abnormality is associated with attention deficits (Vossel et al., 2014; Baldassarre et al., 2016). Therefore, it may be hypothesized that these brain subsystems are prominently disrupted by problematic smartphone use, which may be partially related to the smartphone use-caused cognitive impairments (Wacks and Weinstein, 2021) and attention deficits (Choi et al., 2021). However, this assumption remains speculative and needs to be tested in further studies, since no cognitive or attentional tests were performed in this study. Additionally, it is noteworthy that in the current study, the sFC and dFC analyses suggested significant smartphone use-associated effects in difference brain subnetworks, indicating that they may reflect different aspects of brain function. This may partly support the opinion that dFC can capture important information ignored by conventional static methodology (Hutchison et al., 2013a), and further highlight the value of integrating the sFC and dFC analyses in research on problematic smartphone use.

While significant correlations were found between the brain network metrics and SAS-SV score, no significant differences were obtained when directly comparing between the groups of participants with and without a problematic smartphone use (**Figure 5A**). One possible reason is that our sample size is relatively small, which may limit the statistical power of this research; a larger sample might be needed to detect the between-group differences. We also note that based on the commonly-used SAS-SV cutoff points ($\geq$ 31 for males and $\geq$ 33 for females), a considerable proportion (56.9%) of participants were found to have a problematic smartphone use. However, such a proportion is much higher than most previous research [e.g., 29.8% in Mainland China (Chen et al., 2017), 24.8% in South Korea (Kwon et al., 2013), and 38.5% in Hong Kong populations (Luk et al., 2018)]. Here, we thus propose that such a cutoff may be not optimal for the current sample of young Chinese adults. The previous SAS-SV threshold points proposed by the scale developers (Kwon et al., 2013) may lead to an over-estimated prevalence of problematic smartphone use nowadays, considering that the use of smartphone has been largely increased in recent years and is being frequently engaged with everyday life and work. In fact, such an opinion has also been expressed by other researchers (Saadeh et al., 2021), and may be partly supported by the results of our exploratory analyses using more strict cutoff points (**Figure 5B**). Therefore, further studies may be warranted to investigate if a more applicable SAS-SV cutoff point is required for defining problematic smartphone use in young Chinese nowadays.

Previous studies have reported that alterations in brain structures may act as a moderator of the relationship between problematic smartphone use and depressive symptoms in young adults (Zou et al., 2021). In the current study, on the contrary, no similar mediation effects were found on any sFC/dFC measure (**Table 2**). Nonetheless, it is noteworthy that the sample size is relatively low; moreover, only healthy participants were included whose depressive levels were relatively low. Further studies may be warranted to detect possible mediation effects in a larger sample and in clinical populations.

Some other limitations of this study should be noted. First, because of the nature of cross-sectional research, we are unable to determine the causality relationship between problematic smartphone use and brain dysfunctions. Second, as the SAS-SV is a self-reported scale, the results could be biased by

potential over-or under-reports. Third, while only the sFC/dFC patterns during rest were analyzed, further studies conducted under specific tasks (Choi et al., 2021) may further improve our knowledge. Fourth, in this study, we chose the sliding-window approach to analyze dFC rather than other approaches such as the temporal independent component analysis (tICA), considering that the tICA requires a large number of scanning time points (Li et al., 2020) and the sliding-window approach might be more suitable for the current dataset. Nevertheless, other approaches such as the tICA may provide further important information and can be investigated in the future studies.

In conclusion, this study showed that problematic smartphone use is associated with differences in brain functions in young healthy adults, as characterized by differences in both static and dynamic brain network organizations. These findings may help to improve our understanding of the biological associates of problematic smartphone use. However, further studies may be warranted to confirm our findings in a larger sample, and to investigate if a more applicable SAS-SV cutoff point is required for defining problematic smartphone use in young Chinese nowadays.

Data availability statement

The raw data supporting the conclusions of this article will be made available by the authors, without undue reservation.

Ethics statement

The studies involving human participants were reviewed and approved by The Ethics Committee of Second Xiangya Hospital. The patients/participants provided their written informed consent to participate in this study.

Author contributions

DL, YL, and ST designed the study and carried out the analysis. DL, YL, DB, and ST contributed to the data collection. DL, XL, and YL wrote the first draft of manuscript. ZX, ZW, ZL, and ST contributed to the final manuscript. All authors have read and agreed to the published version of the manuscript.

Funding

This work was supported by the Natural Science Foundation of Hunan Province, China (2021JJ40851 to YL) and the National Natural Science Foundation of China (82071506 to ZL and 82201692 to YL).

Acknowledgments

We would like to thank all subjects who served as research participants.

Conflict of interest

The authors declare that the research was conducted in the absence of any commercial or financial relationships that could be construed as a potential conflict of interest.

Publisher's note

Supplementary material

The Supplementary Material for this article can be found online at: https://www.frontiersin.org/articles/10.3389/fnins.2022.1010488/full#supplementary-material

References

Achard, S., and Bullmore, E. (2007). Efficiency and cost of economical brain functional networks. *PLoS Comput. Biol.* 3:0174–0183. doi: 10.1371/journal.pcbi.0030017

Ahn, J., Lee, D., Namkoong, K., and Jung, Y. C. (2021). Altered functional connectivity of the salience network in problematic smartphone users. *Front. Psychiatry* 12:636730. doi: 10.3389/fpsyt.2021.636730

Alageel, A. A., Alyahya, R. A., Bahatheq, Y. A., Alzunaydi, N. A., Alghamdi, R. A., Alrahili, N. M., et al. (2021). Smartphone addiction and associated factors among postgraduate students in an Arabic sample: A cross-sectional study. *BMC Psychiatry* 21:302. doi: 10.1186/s12888-021-03285-0

Asarnow, L. D., Bei, B., Krystal, A., Buysse, D. J., Thase, M. E., Edinger, J. D., et al. (2019). Circadian preference as a moderator of depression outcome following cognitive behavioral therapy for insomnia plus antidepressant medications: A report from the TRIAD study. *J. Clin. Sleep Med.* 15, 573–580.

Baldassarre, A., Ramsey, L., Rengachary, J., Zinn, K., Siegel, J. S., Metcalf, N. V., et al. (2016). Dissociated functional connectivity profiles for motor and attention deficits in acute right-hemisphere stroke. *Brain* 139, 2024–2038.

Canario, E., Chen, D., and Biswal, B. (2021). A review of resting-state fMRI and its use to examine psychiatric disorders. *Psychoradiology* 1, 42–53. doi: 10.1093/psyrad/kkab003

Cao, H., Plichta, M. M., Schäfer, A., Haddad, L., Grimm, O., Schneider, M., et al. (2014). Test-retest reliability of fMRI-based graph theoretical properties during working memory, emotion processing, and resting state. *Neuroimage* 84, 888–900. doi: 10.1016/j.neuroimage.2013.09.013

Chao-Gan, Y., and Yu-Feng, Z. (2010). DPARSF: A MATLAB toolbox for "pipeline" data analysis of resting-state fMRI. *Front. Syst. Neurosci.* 4:13. doi: 10.3389/fnsys.2010.00013

Chen, B., Liu, F., Ding, S., Ying, X., Wang, L., and Wen, Y. (2017). Gender differences in factors associated with smartphone addiction: A cross-sectional study among medical college students. *BMC Psychiatry* 17:341. doi: 10.1186/s12888-017-1503-z

Chen, G., Chen, P., Gong, J. Y., Jia, Y., Zhong, S., Chen, F., et al. (2022). Shared and specific patterns of dynamic functional connectivity variability of striato-cortical circuitry in unmedicated bipolar and major depressive disorders. *Psychol. Med.* 52, 747–756. doi: 10.1017/S0033291720002378

Choi, J., Cho, H., Choi, J. S., Choi, I. Y., Chun, J. W., and Kim, D. J. (2021). The neural basis underlying impaired attentional control in problematic smartphone users. *Transl. Psychiatry* 11:129. doi: 10.1038/s41398-021-01246-5

Chun, J. W., Choi, J., Cho, H., Choi, M. R., Ahn, K. J., Choi, J. S., et al. (2018). Role of frontostriatal connectivity in adolescents with excessive smartphone use. *Front. Psychiatry* 9:437. doi: 10.3389/fpsyt.2018.00437

Cole, M. W., Reynolds, J. R., Power, J. D., Repovs, G., Anticevic, A., and Braver, T. S. (2013). Multi-task connectivity reveals flexible hubs for adaptive task control. *Nat. Neurosci.* 16, 1348–1355. doi: 10.1038/nn.3470

Dong, D., Duan, M., Wang, Y., Zhang, X., Jia, X., Li, Y., et al. (2019). Reconfiguration of dynamic functional connectivity in sensory and perceptual system in schizophrenia. *Cereb. Cortex* 29, 3577–3589. doi: 10.1093/cercor/bhy232

Elhai, J. D., Dvorak, R. D., Levine, J. C., and Hall, B. J. (2017). Problematic smartphone use: A conceptual overview and systematic review of relations with anxiety and depression psychopathology. *J. Affect. Disord.* 207, 251–259. doi: 10.1016/j.jad.2016.08.030

Guo, N., Luk, T. T., Ho, S. Y., Lee, J. J., Shen, C., Oliffe, J., et al. (2020). Problematic smartphone use and mental health in chinese adults: A population-based study. *Int. J. Environ. Res. Public Health* 17:844. doi: 10.3390/ijerph17030844

Guo, N., Luk, T. T., Wang, M. P., Ho, S. Y., Fong, D. Y. T., Wan, A., et al. (2021). Self-reported screen time on social networking sites associated with problematic smartphone use in Chinese adults: A population-based study. *Front. Psychiatry* 11:614061. doi: 10.3389/fpsyt.2020.614061

Harris, B., Regan, T., Schueler, J., and Fields, S. A. (2020). Problematic mobile phone and smartphone use scales: A systematic review. *Front. Psychol.* 11:672. doi: 10.3389/fpsyg.2020.00672

Hayes, A. F. (2012). *PROCESS: A versatile computational tool for observed variable mediation, moderation, and conditional process modeling*. Available online at: http://www.afhayes.com

Horvath, J., Mundinger, C., Schmitgen, M. M., Wolf, N. D., Sambataro, F., Hirjak, D., et al. (2020). Structural and functional correlates of smartphone addiction. *Addict. Behav.* 105:106334. doi: 10.1016/j.addbeh.2020.106334

Huang, D., Liu, Z., Cao, H., Yang, J., Wu, Z., and Long, Y. (2021). Childhood trauma is linked to decreased temporal stability of functional brain networks in young adults. *J. Affect. Disord.* 290, 23–30. doi: 10.1016/j.jad.2021.04.061

Huang, Q., Li, Y., Huang, S., Qi, J., Shao, T., Chen, X., et al. (2020). Smartphone use and sleep quality in chinese college students: A preliminary study. *Front. Psychiatry* 11:352. doi: 10.3389/fpsyt.2020.00352

Huang, X., Wu, Z., Liu, Z., Liu, D., Huang, D., and Long, Y. (2021). Acute effect of betel quid chewing on brain network dynamics: A resting-state functional magnetic resonance imaging study. *Front. Psychiatry* 12:701420. doi: 10.3389/fpsyt.2021.701420

Hutchison, R. M., Womelsdorf, T., Allen, E. A., Bandettini, P. A., Calhoun, V. D., Corbetta, M., et al. (2013a). Dynamic functional connectivity: Promise, issues, and interpretations. *Neuroimage* 80, 360–378. doi: 10.1016/j.neuroimage.2013.05.079

Hutchison, R. M., Womelsdorf, T., Gati, J. S., Everling, S., and Menon, R. S. (2013b). Resting-state networks show dynamic functional connectivity in awake humans and anesthetized macaques. *Hum. Brain Mapp.* 34, 2154–2177. doi: 10.1002/hbm.22058

Jin, C., Jia, H., Lanka, P., Rangaprakash, D., Li, L., Liu, T., et al. (2017). Dynamic brain connectivity is a better predictor of PTSD than static connectivity. *Hum. Brain Mapp.* 38, 4479–4496. doi: 10.1002/hbm.23676

Kroenke, K., Spitzer, R. L., and Williams, J. B. W. (2001). The PHQ-9: Validity of a brief depression severity measure. *J. Gen. Intern. Med.* 16, 606–613. doi: 10.1046/j.1525-1497.2001.016009606.x

Kwon, M., Kim, D. J., Cho, H., and Yang, S. (2013). The smartphone addiction scale: Development and validation of a short version for adolescents. *PLoS One* 8:e83558. doi: 10.1371/journal.pone.0083558

Lei, D., Li, K., Li, L., Chen, F., Huang, X., Lui, S., et al. (2015). Disrupted functional brain connectome in patients with posttraumatic stress disorder. *Radiology* 276, 818–827. doi: 10.1148/radiol.15141700

Leonardi, N., and Van De Ville, D. (2015). On spurious and real fluctuations of dynamic functional connectivity during rest. *Neuroimage* 104, 430–436. doi: 10.1016/j.neuroimage.2014.09.007

Li, J., Yao, G., Liu, S., Li, X., Zhao, W., Du, X., et al. (2021). Mechanisms of the effects of parental emotional warmth on extraversion in children and adolescents. *Neuroscience* 467, 134–141. doi: 10.1016/j.neuroscience.2021.05.021

Li, L., Lu, B., and Yan, C. G. (2020). Stability of dynamic functional architecture differs between brain networks and states. *Neuroimage* 216:116230. doi: 10.1016/j.neuroimage.2019.116230

Li, L., Su, Y. A., Wu, Y. K., Castellanos, F. X., Li, K., Li, J. T., et al. (2021). Eight-week antidepressant treatment reduces functional connectivity in first-episode drug-naïve patients with major depressive disorder. *Hum. Brain Mapp.* 42, 2593–2605. doi: 10.1002/hbm.25391

Li, T., Yang, Y., Krueger, F., Feng, C., and Wang, J. (2021). Static and dynamic topological organizations of the costly punishment network predict individual differences in punishment propensity. *Cereb. Cortex* 32, 4012–4024. doi: 10.1093/cercor/bhab462

Lin, F., Wu, G., Zhu, L., and Lei, H. (2015). Altered brain functional networks in heavy smokers. *Addict. Biol.* 20, 809–819. doi: 10.1111/adb.12155

Lin, Z., Long, Y., Wu, Z., Xiang, Z., Ju, Y., and Liu, Z. (2021). Associations between brain abnormalities and common genetic variants for schizophrenia: A narrative review of structural and functional neuroimaging findings. *Ann. Palliat. Med.* 10, 10031–10052. doi: 10.21037/apm-21-1210

Liu, D., Tang, S., Wu, Z., Yang, J., Liu, Z., Wu, G., et al. (2022). Changes in brain network properties in major depressive disorder following electroconvulsive therapy: A combined static and dynamic functional magnetic resonance imaging study. *Ann. Palliat. Med.* 11, 1969–1980. doi: 10.21037/apm-21-2723

Liu, H., Zhou, Z., Zhu, E., Huang, L., and Zhang, M. (2022). Smartphone addiction and its associated factors among freshmen medical students in China: A cross-sectional study. *BMC Psychiatry* 22, 1–8. doi: 10.1186/s12888-022-03957-5

Long, J., Liu, T. Q., Liao, Y. H., Qi, C., He, H. Y., Chen, S. B., et al. (2016). Prevalence and correlates of problematic smartphone use in a large random sample of Chinese undergraduates. *BMC Psychiatry* 16:408. doi: 10.1186/s12888-016-1083-3

Long, Y., Cao, H., Yan, C., Chen, X., Li, L., Castellanos, F. X., et al. (2020a). Altered resting-state dynamic functional brain networks in major depressive disorder: Findings from the REST-meta-MDD consortium. *Neuroimage Clin.* 26:102163. doi: 10.1016/j.nicl.2020.102163

Long, Y., Chen, C., Deng, M., Huang, X., Tan, W., Zhang, L., et al. (2019). Psychological resilience negatively correlates with resting-state brain network flexibility in young healthy adults: A dynamic functional magnetic resonance imaging study. *Ann. Transl. Med.* 7, 809–809. doi: 10.21037/atm.2019.12.45

Long, Y., Liu, Z., Chan, C. K. Y., Wu, G., Xue, Z., Pan, Y., et al. (2020b). Altered temporal variability of local and large-scale resting-state brain functional connectivity patterns in schizophrenia and bipolar disorder. *Front. Psychiatry* 11:422. doi: 10.3389/fpsyt.2020.00422

Long, Y., Yan, C., Wu, Z., Huang, X., and Cao, H. (2021). Evaluating test-retest reliability and sex/age-related effects on temporal clustering coefficient of dynamic functional brain networks. *bioRxiv*[Preprint] doi: 10.1101/2021.10.21.465376

Luk, T. T., Wang, M. P., Shen, C., Wan, A., Chau, P. H., Oliffe, J., et al. (2018). Short version of the smartphone addiction scale in Chinese adults: Psychometric properties, sociodemographic, and health behavioral correlates. *J. Behav. Addict.* 7, 1157–1165. doi: 10.1556/2006.7.2018.105

Luo, L., Li, Q., You, W., Wang, Y., Tang, W., Li, B., et al. (2021). Altered brain functional network dynamics in obsessive–compulsive disorder. *Hum. Brain Mapp.* 42, 2061–2076. doi: 10.1002/hbm.25345

Luo, Z., Chen, G., Jia, Y., Zhong, S., Gong, J., Chen, F., et al. (2021). Shared and specific dynamics of brain segregation and integration in bipolar disorder and major depressive disorder: A resting-state functional magnetic resonance imaging study. *J. Affect. Disord.* 280, 279–286. doi: 10.1016/j.jad.2020.11.012

Lv, X., Lu, F., Zhang, J., Chen, H., Zhang, L., Wang, X., et al. (2021). Effects of TIP treatment on brain network topology of frontolimbic circuit in first-episode, treatment-naïve major depressive disorder. *J. Affect. Disord.* 279, 122–130. doi: 10.1016/j.jad.2020.09.127

Mohr, H., Wolfensteller, U., Betzel, R. F., Mišiæ, B., Sporns, O., Richiardi, J., et al. (2016). Integration and segregation of large-scale brain networks during short-term task automatization. *Nat. Commun.* 7:13217. doi: 10.1038/ncomms13217

Mullins, L. L., Wolfe-Christensen, C., Hoff Pai, A. L., Carpentier, M. Y., Gillaspy, S., Cheek, J., et al. (2007). The relationship of parental overprotection, perceived child vulnerability, and parenting stress to uncertainty in youth with chronic illness. *J. Pediatr. Psychol.* 32, 973–982. doi: 10.1093/jpepsy/jsm044

Ng, K. C., Wu, L. H., Lam, H. Y., Lam, L. K., Nip, P. Y., Ng, C. M., et al. (2020). The relationships between mobile phone use and depressive symptoms, bodily pain, and daytime sleepiness in Hong Kong secondary school students. *Addict. Behav.* 101:105975. doi: 10.1016/j.addbeh.2019.04.033

Paik, S.-H., Park, C., Kim, J.-Y., Chun, J.-W., Choi, J.-S., and Kim, D.-J. (2019). Prolonged bedtime smartphone use is associated with altered resting-state functional connectivity of the insula in adult smartphone users. *Front. Psychiatry* 10:516. doi: 10.3389/fpsyt.2019.00516

Park, B. Y., Moon, T., and Park, H. (2018). Dynamic functional connectivity analysis reveals improved association between brain networks and eating behaviors compared to static analysis. *Behav. Brain Res.* 337, 114–121. doi: 10.1016/j.bbr.2017.10.001

Park, C. H., Chun, J. W., Cho, H., Jung, Y. C., Choi, J., and Kim, D. J. (2017). Is the internet gaming-addicted brain close to be in a pathological state? *Addict. Biol.* 22, 196–205. doi: 10.1111/adb.12282

Patil, A. U., Ghate, S., Madathil, D., Tzeng, O. J. L., Huang, H. W., and Huang, C. M. (2021). Static and dynamic functional connectivity supports the configuration of brain networks associated with creative cognition. *Sci. Rep.* 11:165. doi: 10.1038/s41598-020-80293-2

Power, J. D., Cohen, A. L., Nelson, S. M., Wig, G. S., Barnes, K. A., Church, J. A., et al. (2011). Functional network organization of the human brain. *Neuron* 72, 665–678. doi: 10.1016/j.neuron.2011.09.006

Pyeon, A., Choi, J., Cho, H., Kim, J.-Y., Choi, I. Y., Ahn, K.-J., et al. (2021). Altered connectivity in the right inferior frontal gyrus associated with self-control in adolescents exhibiting problematic smartphone use: A fMRI study. *J. Behav. Addict.* 10, 1048–1060. doi: 10.1556/2006.2021.00085

Quintero Garzón, L., Hinz, A., Koranyi, S., and Mehnert-Theuerkauf, A. (2021). Norm values and psychometric properties of the 24-item demoralization scale (DS-I) in a representative sample of the german general population. *Front. Psychol.* 12:681977. doi: 10.3389/fpsyg.2021.681977

Ratan, Z. A., Parrish, A. M., Zaman, S., Bin, Alotaibi, M. S., and Hosseinzadeh, H. (2021). Smartphone addiction and associated health outcomes in adult populations: A systematic review. *Int. J. Environ. Res. Public Health* 18:12257. doi: 10.3390/ijerph182212257

Rhudy, J. L., Huber, F., Kuhn, B. L., Lannon, E. W., Palit, S., Payne, M. F., et al. (2020). Pain-related anxiety promotes pronociceptive processes in native Americans: Bootstrapped mediation analyses from the Oklahoma study of native American pain risk. *Pain Rep.* 5:E808. doi: 10.1097/PR9.0000000000000808

Roh, D., Bhang, S. Y., Choi, J. S., Kweon, Y. S., Lee, S. K., and Potenza, M. N. (2018). The validation of implicit association test measures for smartphone and Internet addiction in at-risk children and adolescents. *J. Behav. Addict.* 7, 79–87. doi: 10.1556/2006.7.2018.02

Rubinov, M., and Sporns, O. (2010). Complex network measures of brain connectivity: Uses and interpretations. *Neuroimage* 52, 1059–1069. doi: 10.1016/j.neuroimage.2009.10.003

Saadeh, H., Fayez, R. Q., Refaei, A., Shewaikani, N., Khawaldah, H., Abu-Shanab, S., et al. (2021). Smartphone use among university students during COVID-19 quarantine: An ethical trigger. *Front. Public Health* 9:600134. doi: 10.3389/fpubh.2021.600134

Schmidt, E. L., Burge, W., Visscher, K. M., and Ross, L. A. (2016). Cortical thickness in frontoparietal and cingulo-opercular networks predicts executive function performance in older adults. *Neuropsychology* 30, 322–331.

Sheng, D., Pu, W., Linli, Z., Tian, G. L., Guo, S., and Fei, Y. (2021). Aberrant global and local dynamic properties in schizophrenia with instantaneous phase method based on Hilbert transform. *Psychol. Med.* 1–11. doi: 10.1017/S0033291721003895 [Epub ahead of print].

Spitzer, R. L., Kroenke, K., Williams, J. B. W., and Löwe, B. (2006). A brief measure for assessing generalized anxiety disorder: The GAD-7. *Arch. Intern. Med.* 166, 1092–1097. doi: 10.1001/archinte.166.10.1092

Sun, J., Zhao, R., He, Z., Chang, M., Wang, F., Wei, W., et al. (2022). Abnormal dynamic functional connectivity after sleep deprivation from temporal variability perspective. *Hum. Brain Mapp.* 43, 3824–3839. doi: 10.1002/hbm.25886

Sun, Y., Collinson, S. L., Suckling, J., and Sim, K. (2019). Dynamic reorganization of functional connectivity reveals abnormal temporal efficiency in schizophrenia. *Schizophr. Bull.* 45, 659–669. doi: 10.1093/schbul/sby077

Tan, W., Liu, Z., Xi, C., Deng, M., Long, Y., Palaniyappan, L., et al. (2020). Decreased integration of the frontoparietal network during a working memory task in major depressive disorder. *Aust. N. Z. J. Psychiatry* 55, 577–587. doi: 10.1177/0004867420978284

Tang, S., Wu, Z., Cao, H., Chen, X., Wu, G., Tan, W., et al. (2022). Age-Related decrease in default-mode network functional connectivity is accelerated in patients with major depressive disorder. *Front. Aging Neurosci.* 13:809853. doi: 10.3389/fnagi.2021.809853

Tobia, M. J., Hayashi, K., Ballard, G., Gotlib, I. H., and Waugh, C. E. (2017). Dynamic functional connectivity and individual differences in emotions during social stress. *Hum. Brain Mapp.* 38, 6185–6205. doi: 10.1002/hbm.23821

Vossel, S., Geng, J. J., and Fink, G. R. (2014). Dorsal and ventral attention systems: Distinct neural circuits but collaborative roles. *Neuroscientist* 20, 150–159. doi: 10.1177/1073858413494269

Wacks, Y., and Weinstein, A. M. (2021). Excessive smartphone use is associated with health problems in adolescents and young adults. *Front. Psychiatry* 12:669042. doi: 10.3389/fpsyt.2021.669042

Wallis, G., Stokes, M., Cousijn, H., Woolrich, M., and Nobre, A. C. (2015). Frontoparietal and cingulo-opercular networks play dissociable roles in control of working memory. *J. Cogn. Neurosci.* 27, 2019–2034. doi: 10.1162/jocn_a_00838

Wu, Z., Liu, Z., Jiang, Z., Fu, X., Deng, Q., Palaniyappan, L., et al. (2022). Overprotection and overcontrol in childhood: An evaluation on reliability and validity of 33-item expanded childhood trauma questionnaire (CTQ-33), Chinese version. *Asian J. Psychiatr.* 68:102962. doi: 10.1016/j.ajp.2021.102962

Wu, Z., Zou, Z., Wang, F., Xiang, Z., Zhu, M., Long, Y., et al. (2021). Family functioning as a moderator in the relation between perceived stress and psychotic-like experiences among adolescents during COVID-19. *Compr. Psychiatry* 111:152274. doi: 10.1016/j.comppsych.2021.152274

Xia, M., Wang, J., and He, Y. (2013). BrainNET viewer: A network visualization tool for human brain connectomics. *PLoS One* 8:e68910. doi: 10.1371/journal.pone.0068910

Yan, C. G., Chen, X., Li, L., Castellanos, F. X., Bai, T. J., Bo, Q. J., et al. (2019). Reduced default mode network functional connectivity in patients with recurrent major depressive disorder. *Proc. Natl. Acad. Sci. U.S.A.* 116, 9078–9083. doi: 10.1073/pnas.1900390116

Yan, C. G., Wang, X., di, Zuo, X. N., and Zang, Y. F. (2016). DPABI: Data processing & analysis for (resting-state) brain imaging. *Neuroinformatics* 14, 339–351. doi: 10.1007/s12021-016-9299-4

Yang, H., Chen, X., Chen, Z. B., Li, L., Li, X. Y., Castellanos, F. X., et al. (2021). Disrupted intrinsic functional brain topology in patients with major depressive disorder. *Mol. Psychiatry* 26, 7363–7371. doi: 10.1038/s41380-021-01247-2

Yang, X., Hu, H., Zhao, C., Xu, H., Tu, X., and Zhang, G. (2021). A longitudinal study of changes in smart phone addiction and depressive symptoms and potential risk factors among Chinese college students. *BMC Psychiatry* 21:252. doi: 10.1186/s12888-021-03265-4

Zhang, C., Baum, S. A., Adduru, V. R., Biswal, B. B., and Michael, A. M. (2018). Test-retest reliability of dynamic functional connectivity in resting state fMRI. *Neuroimage* 183, 907–918. doi: 10.1016/j.neuroimage.2018.08.021

Zhang, C., Hao, J., Liu, Y., Cui, J., and Yu, H. (2022). Associations between online learning, smartphone addiction problems, and psychological symptoms in chinese college students after the COVID-19 pandemic. *Front. Public Health* 10:881074. doi: 10.3389/fpubh.2022.881074

Zhang, J., Cheng, W., Liu, Z., Zhang, K., Lei, X., Yao, Y., et al. (2016). Neural, electrophysiological and anatomical basis of brain-network variability and its characteristic changes in mental disorders. *Brain* 139, 2307–2321. doi: 10.1093/brain/aww143

Zhang, J., Wang, J., Wu, Q., Kuang, W., Huang, X., He, Y., et al. (2011). Disrupted brain connectivity networks in drug-naive, first-episode major depressive disorder. *Biol. Psychiatry* 70, 334–342. doi: 10.1016/j.biopsych.2011.05.018

Zhang, W., Li, S., Wang, X., Gong, Y., Yao, L., Xiao, Y., et al. (2018). Abnormal dynamic functional connectivity between speech and auditory areas in schizophrenia patients with auditory hallucinations. *Neuroimage Clin.* 19, 918–924. doi: 10.1016/j.nicl.2018.06.018

Zhao, Z., Zhang, Y., Chen, N., Li, Y., Guo, H., Guo, M., et al. (2021). Altered temporal reachability highlights the role of sensory perception systems in major depressive disorder. *Prog. Neuropsychopharmacol. Biol. Psychiatry* 112:110426. doi: 10.1016/j.pnpbp.2021.110426

Zou, L., Wu, X., Tao, S., Yang, Y., Zhang, Q., Hong, X., et al. (2021). Anterior cingulate gyrus acts as a moderator of the relationship between problematic mobile phone use and depressive symptoms in college students. *Soc. Cogn. Affect. Neurosci.* 16, 484–491. doi: 10.1093/scan/nsab016

Zou, L., Wu, X., Tao, S., Yang, Y., Zhang, Q., Hong, X., et al. (2022). Functional connectivity between the parahippocampal gyrus and the middle temporal gyrus moderates the relationship between problematic mobile phone use and depressive symptoms: Evidence from a longitudinal study. *J. Behav. Addict.* 11, 40–48. doi: 10.1556/2006.2021.00090

frontiers | Frontiers in Neuroscience

TYPE Original Research
PUBLISHED 03 November 2022
DOI 10.3389/fnins.2022.972870

OPEN ACCESS

EDITED BY
Bradley G. Goodyear,
University of Calgary, Canada

REVIEWED BY
Nabi Zorlu,
İzmir Kâtip Çelebi University, Turkey
Zhiqiang Sha,
Max Planck Institute
for Psycholinguistics, Netherlands

*CORRESPONDENCE
Gaizhi Li
13190608531@163.com
Zhifen Liu
zhifenliu@sxmu.edu.cn

†These authors have contributed equally to this work

SPECIALTY SECTION
This article was submitted to Brain Imaging Methods, a section of the journal Frontiers in Neuroscience

RECEIVED 19 June 2022
ACCEPTED 15 September 2022
PUBLISHED 03 November 2022

CITATION
Liu H, Wen Y, Liang X, Xu Y, Qiao D, Yang C, Han M, Li H, Ren T, Zhang X, Li G and Liu Z (2022) Prefrontal cortex neural activity predicts reduction of non-suicidal self-injury in adolescents with major depressive disorder: An event related potential study.
Front. Neurosci. 16:972870.
doi: 10.3389/fnins.2022.972870

Prefrontal cortex neural activity predicts reduction of non-suicidal self-injury in adolescents with major depressive disorder: An event related potential study

Huishan Liu†, Yujiao Wen†, Xiumei Liang, Yifan Xu, Dan Qiao, Chunxia Yang, Min Han, Hong Li, Tian Ren, Xuemin Zhang, Gaizhi Li* and Zhifen Liu*

Department of Psychiatry, The First Hospital of Shanxi Medical University, Taiyuan, China

Background: Non-suicidal self-injury (NSSI) is common in adolescent MDD, which is also a risk factor for suicide. However, there is few research on biomarkers and predictors about treatment response of NSSI. The purpose of this study was to find the difference of P300 between adolescent MDD with NSSI and healthy controls, and to explore whether the baseline electrophysiological level can predict the change of NSSI after treatment.

Methods: We collected 62 first-episode drug-naïve MDD adolescents with NSSI (MDD with NSSI group) and 44 healthy controls (HC group). The demographic data, HAMD score, self-injury frequency and electrophysiological level of NSSI group and HC group were collected. The HAMD score, frequency of NSSI in was also collected after 8 weeks of antidepressant treatment.

Results: Compared to HC, the latency of the N2, P3a, and P3b components were significantly prolonged, whereas the amplitude of P3a and P3b were decreased in the MDD with NSSI group ($P < 0.001$). The frequency of self-injury decreased significantly after treatment ($P < 0.001$). Regression analysis showed that the amplitudes of P3b had a significant positive predictive effect on the rate of change of NSSI frequency after 8 weeks.

Conclusion: P3b at baseline can be used as potential predictor for the reduction of NSSI in adolescent MDD.

KEYWORDS

non-suicidal self-injury behavior, adolescent, major depressive disorder, ERP, P300

Introduction

Non-suicidal self-injury (NSSI) behavior refers to those behaviors that directly and intentionally damage one's body without the purpose of suicide, and is socially and culturally unacceptable (Ross and Heath, 2002). Common forms of NSSI include pulling hair, scalding, cutting skin, scratching, hitting oneself, preventing wounds from healing, biting, pricking needles, and swallowing dangerous substances, et al. (Saraff and Pepper, 2014). NSSI behavior is listed as an independent clinical disorder in the Diagnostic and Statistical Manual of Mental Disorders, 5th Edition (DSM-5) (Andover, 2014; Zetterqvist, 2015).

Adolescent with NSSI behavior is common in the world, and its incidence is increasing year by year. About 14–15% of global adolescents have experienced NSSI behavior at least once (Liu et al., 2018). According to the results of a survey, 13.5% of girls and 4.3% of boys aged 14–17 said they had experienced NSSI at least once in their lifetime. The incidence of NSSI behaviors varies in different countries. The incidence of NSSI behaviors is 13.8% in Scotland, 15.3% in the United States and 24% in New Zealand, and only 3.1% in Germany. Adolescent in different regions of China have different degrees of NSSI behaviors, and the incidence is gradually increasing (Whitlock et al., 2011; Fleming et al., 2014; Rasmussen and Hawton, 2014; Cimen et al., 2017; Zhang et al., 2018).

Investigations have found that adolescent with major depressive disorder (MDD) are prone to risk behaviors such as self-injury and suicide (Jacobson and Gould, 2007), NSSI may be a unique and important risk factor for suicide (Klonsky et al., 2013). Suicide is the third major cause of death among adolescents (Centers for Disease Control and Prevention [CDC], 2009). The detection rate of suicidal ideation among adolescents is 10.72–12.1%, and that there are suicide attempts and plans for adolescents is 8.1% (Laye-Gindhu and Schonert-Reichl, 2005). In addition, NSSI is also common among adolescents with MDD, but little attention had been paid to it in clinical studies. NSSI will have a great impact on adolescents and seriously harm their physical and mental health.

Treatment for adolescents MDD with NSSI behavior include drug therapy, psychotherapy, physical therapy, combined therapy, etc. A non-RCT study found that ziprasidone was effective in reducing the incidence of NSSI behavior in adolescents compared with risperidone, olanzapine, and promethazine (Libal et al., 2005). A systematic review indicated the effectiveness of dialectical behavioral therapy, cognitive behavioral therapy, and psychosocial basic therapy in the treatment of adolescent NSSI (Ougrin et al., 2014). Sertraline is one of the first selective serotonin reuptake inhibitors (SSRIs) approved for the treatment of childhood and adolescent depression, and it is also the most widely used drug (Gómez-Lumbreras et al., 2021). It can effectively relieve the depressive symptoms in a short time, improve the cognitive function of the patients, and improve the quality of life of the patients (Kaštelan et al., 2019). Currently, there are a variety of treatment methods for adolescent with MDD with NSSI behavior, however, the treatment response varies, so it is critical to find an effective predictor of treatment response.

Previous studies on NSSI behavior mostly focused on emotion regulation, ignoring the role of cognition. On the basis of summarizing four emotion regulation models, Hasking et al. (2017) combined cognitive model and emotion model to construct a new cognitive emotion model related to NSSI, which reflects the important role of cognition. At present, the research on cognitive factors of self-injury behavior mostly adopts neuropsychological test or scale, and research on objective predictors are still lacking. Event related potential (ERP) is a suitable choice due to its high time resolution, simplicity, convenience and cheapness. One component related to cognitive function is P300, which is considered to reflect cognitive processes, including attention distribution, executive function and memory (Polich, 2012). The cerebral cortex of suicidal depressed patients showed a decrease in serotonin-activated neurological function and a significant increase in the amplitude of prefrontal P300, so P300 can be regarded as a reference index to predict the risk of suicide in suicidal depressed patients (Chen et al., 2005). The previous research group found that, compared with the HC group, the adolescent with MDD with NSSI behavior significantly prolonged the incubation period on P300, significantly reduced the amplitude, and had significant cognitive dysfunction, such as executive dysfunction and memory impairment (Wen et al., 2021). Based on this, sertraline was selected as the treatment drug in this study. The incubation period and amplitude of P300 at baseline were used as predictors, and the scores of Hamilton Depression Scale (HAMD) and NSSI Diary Card at baseline and 8 weeks were used as indicators. To observe whether the changes of ERP can predict the clinical efficacy of sertraline in the treatment of adolescent with MDD with NSSI behavior.

The purposes of this study are: firstly, to explore the difference between NSSI group and HC group by the related indicators of ERP, HAMD scores and the NSSI frequency; secondly to examine whether the changes of ERP can predict the clinical efficacy of sertraline in the treatment of adolescent MDD with NSSI.

Materials and methods

Participants

The study included 106 subjects aged 10–23 years: 62 unmedicated patients with first-episode adolescent MDD with

NSSI and 44 healthy control (HC) subjects. All NSSI group patients were from the Department of psychiatry and mental health, the First Hospital of Shanxi Medical University. All HC group subjects were recruited from Taiyuan City, Shanxi Province, China, using community advertisements. All subjects were independently evaluated by two trained psychiatrists using structured clinical interviews for DSM-5, Research Version (SCID-5-RV). The Research Ethics Committee of the First Hospital of Shanxi Medical University approved this study.

Inclusion and exclusion criteria for patients with MDD

The inclusion criteria for MDD patients were as follows: (1) age between 10 and 23 years with no restrictions on gender; (2) DSM-5 diagnostic criteria for MDD; (3) right handed; (4) first-episode MDD with no previous use of antidepressant or other psychotropic medications; and (5) volunteered to participate in the study and signed the informed consent form. The exclusion criteria were as follows: (1) patients with severe or unstable heart, liver, kidney, endocrine, blood and other internal diseases and nervous system diseases; (2) any cooccurring mental disorder; (3) alcohol dependence or abuse; (4) previous history of nervous system disease or brain injury; (5) personal or family history of epileptic seizures; (6) other situations that are not suitable to participate in this study.

Inclusion and exclusion criteria for HCs

Inclusion criteria for HCs were as follows: (1) age 10–23 years; (2) no mental disorder found in the initial screening; (3) matched to the MDD patients in terms of sex and education level; and (4) participated voluntarily and signed the informed consent form. The exclusion criteria were as follows: (1) organic disease; (2) alcohol abuse within 30 days or alcohol or drug dependence within 6 months prior to the screening; (3) participation in other clinical trials in the previous 3 months; and (4) other conditions that disqualified the subject from the study, as determined by the investigators.

Measures

Eligible participants were asked to provide sociodemographic information including name, gender, age. For clinically related variables measures, we used the Hamilton depression scale-24 (HAMD-24) to assess the severity of depressive symptom. NSSI Diary Card was used to record the frequency of NSSI. Most items in HAMD-24 adopt a 5-level scoring method of 0–4 points. The criteria at all levels are: 0-none, 1-mild, 2-moderate, 3-severe, 4-extremely severe. A few items adopt a three-level scoring method of 0–2 points, and the grading standards are: 0-none, 1-mild-moderate, and 2-severe. If the total score exceeds 35, it may be severe depression; More than 20 points may be mild or moderate depression; If less than 8 points, there is no depressive disorder. NSSI diary card was used to record the number of self-injuries in the past month and 1 week.

For eligible adolescents with MDD, sertraline was used for treatment, with a daily dose of 50–200 mg and an initial dose of 25–50 mg.

Event related potential parameters

Event related potential data were collected using the 128-electrode NEMUS 2 system (Brain products GmbH, Germany). Recording electrodes were placed at the Fz, Cz, and Pz positions; the electrode at the Cz position was the standard and those at the Fz and Pz positions were references for waveform identification. Reference electrodes are TP9 and TP10, and the ground electrode (GND) are placed in the middle of the parietal lobe.

P300 detection

The task employed the classic Oddball experimental paradigm. The stimulus sequence was composed of a target stimulus (T) and non-target stimulus (NT) at a probability ratio of 0.2/0.8; T was randomly interspersed among NT, and the task consisted of 60 T and 240 NT. Subjects were required to press a key as soon as T appeared. The stimulus frequency was 0.5–1 time/s; stimulus interval was 1–3 s; and total task duration was 14 min. Electrode resistance was <5 kΩ; the time window for data segmentation was -200 to 1500 ms.

Statistical analysis

Data were analyzed using SPSS 22.0 (SPSS Inc., Chicago, IL, USA). The threshold of statistical significance was set as $\alpha = 0.05$ for all the analyses. For the demographic data, categorical variables were compared with the χ^2 test and continuous variables were compared using the two independent sample t test, which was used for HAMD-24, NSSI diary card scores. Mann-Whitney U test was also used to analyze ERP indicators, the major components of ERPs were identified and their index values determined according to the internationally recognized maximum waveforms of the time analysis window. Linear regression analysis was used to predict the improvement of depression and NSSI frequency in the NSSI group. The results were

considered significant if $P < 0.05$, corrected by false discovery rate (FDR).

Results

Demographics and clinical characteristics of all participants

There were no significant differences between the two groups in terms of age, gender, and education years ($P > 0.05$). The NSSI and HC groups showed significant differences in HAMD-24 and NSSI frequency (both 1 mouth and 1 week) ($P < 0.001$) (Table 1).

Event related potential results analysis between the two groups

Compared with HC subjects, the latency of N2, P3a, and P3b in NSSI group were significantly prolonged; the amplitude of P3a and P3b decreased ($P < 0.001$). In other ERP components, there was no significant difference between the two groups (Table 2 and Figures 1, 2).

Changes of clinical symptoms after treatment

The results of paired sample *t*-test showed that HAMD-24 total score and the frequency of NSSI decreased significantly after 8 weeks of treatment (Table 3).

TABLE 1 Demographic and clinical of all participants.

Variable	MDD with NSSI ($n = 62$)	HC ($n = 44$)	$\chi^2/F/t$	*P*
Gender				
Male	16	11	0.009	0.925
Female	46	33		
Age, years	16.74 ± 2.72	17.34 ± 2.85	−1.093	0.277
Education, years	9.66 ± 2.61	10.34 ± 2.92	−1.254	0.213
HAMD-24	25.74 ± 6.35	2.00 ± 2.83	23.18	<0.001***
NSSI diary card (1 mouth)	2.44 ± 1.78	0.00 ± 0.000	9.96	<0.001***
NSSI diary card (1 week)	1.52 ± 1.91	0.00 ± 0.000	5.803	<0.001***

***Indicates $p < 0.001$.
All subjects were students of Han ethnicity, not married, with no religious affiliation.
Data represent number, mean ± standard deviation.
HAMD, Hamilton Depression Scale; HC, healthy control; NSSI, non-suicidal self-injury.
The frequency of NSSI in the NSSI group in the past 1 month was assessed at baseline (0 week) using NSSI diary card.
The frequency of NSSI in the NSSI group in the past 1 week was assessed at baseline (0 week) using NSSI diary card.

Regression analysis of event related potential index and clinical symptom improvement

Taking the latency and amplitude of N1, P2, N2, P3a, and P3b and total score of HAMD-24 after 8 weeks as independent variables and the rate of change of NSSI frequency between 8 weeks and baseline as dependent variables, the linear regression results show that:

In the assessment of NSSI frequency, the amplitude of P3b ($t = 5.242$, $P < 0.001$) has significant positive prediction effect on the change of NSSI frequency. Other indexes in the independent variable have no significant difference in the prediction effect on the dependent variable (Table 4).

Discussion

In this study, 62 first-episode adolescent MDD with NSSI behavior and 44 healthy controls were included. The oddball task was used to observe the difference of electrophysiological level between the two groups. Regression analysis was used to explore whether baseline P300 can be used as a neural marker to predict the clinical efficacy of sertraline tablets in the treatment of adolescent MDD with NSSI behavior.

TABLE 2 P300 value between the NSSI and HC groups.

P300		NSSI	HC	*Z*	*P*
		Md (P25, P75)	Md (P25, P75)		
Latency, ms	N1	105.5 (99.25, 119)	109 (102.75, 118)	−0.712	0.476
	P2	206.5 (200, 220.75)	202 (195.75, 208.75)	−1.745	0.135
	N2	243.5 (231.25, 258.75)	232 (218, 252.25)	−2.318	0.04*
	P3a	343 (332, 356)	316 (306.75, 332.25)	−5.668	<0.001***
	P3b	370.5 (363.25, 386)	331 (323, 345)	−7.638	<0.001***
Amplitude, μV	N1	−2.81 (−6.12, 0.52)	−3.425 (−5.795, −1.44)	−0.933	0.39
	P2	2.195 (0.15, 4.42)	3.18 (0.325, 5.86)	−1.064	0.36
	N2	−0.3 (−3.385, 3.38)	−0.91 (−4.22, 0.81)	−1.363	0.25
	P3a	7.47 (3.725, 11.58)	11.76 (9.58, 14.25)	−4.29	<0.001***
	P3b	8.315 (3.45, 11.26)	12.76 (9.36, 14.73)	−4.796	<0.001***

*Indicates $p < 0.05$; ***indicates $p < 0.001$.
Data represent Median (quartile, third quartile).
ERP, event-related potential; HC, healthy control; NSSI, non-suicidal self-injury.

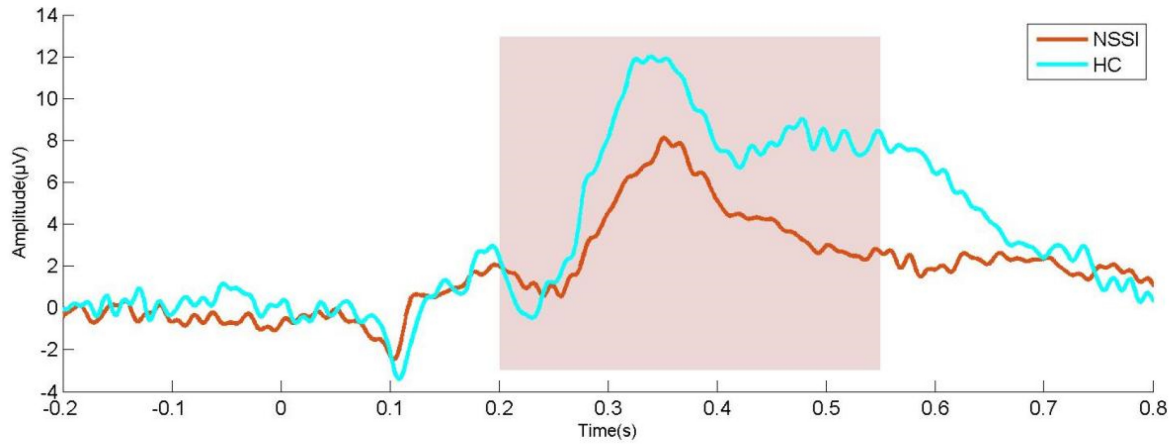

FIGURE 1
Waveform diagram of P300 in CZ channel; NSSI, non-suicidal self-injury (n = 62); HC, healthy control (n = 44).

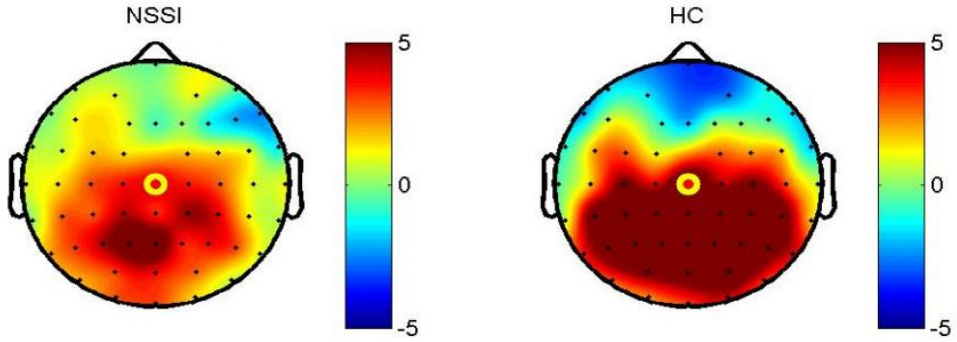

FIGURE 2
Topographic map of P300 in CZ channel 200–500 ms; NSSI, non-suicidal self-injury (n = 62); HC, healthy control (n = 44).

In this study, the MDD adolescents with self-injury behavior is mainly in the middle school stage, which is basically consistent with previous research results (Swannell et al., 2014; Gao et al., 2021; Jiang et al., 2021).

P300 incubation period is an electrophysiological index reflecting the speed of mental activities, and its amplitude can reflect the utilization of effective resources by the brain in information processing, which mainly depends on the sensitivity of the patient to stimulation (Duncan et al., 2005). This study found that compared with HC group, NSSI group had significantly longer N2, P3a, and P3b latency and significantly lower P3a and P3b amplitude, indicating that patients with depression had lower brain nerve excitability and cognitive speed, suggesting that NSSI group may have cognitive impairment. This is consistent with previous study, as Zhou et al. (2022) used oddball paradigm to compare the differences of P3b components among NSSI + MDD, MDD and HC groups. Leone et al. (2021) used laser evoked potential as an index to study the suicide risk of NSSI adolescents suggest that the amplitude of N2 component in NSSI patients is reduced, which is different from our study, may be due to different experimental paradigms. In this study, no significant difference was found in the latency of N1 between the two groups, which was different from Wen's study (Wen et al., 2021). Which may be related to the age of healthy subjects. Some studies suggest that N2 represents reaction inhibition and conflict monitoring, P3a is related to automatic attention capture, and P3b is related to stimulus classification and processing, working memory, reaction inhibition and executive function

TABLE 3 NSSI frequency and HAMD-24 score before and after treatment.

	Baseline	8 week	t	P
HAMD-24	25.74 ± 6.35	12.11 ± 6.75	12.012	<0.001***
NSSI diary card (1 mouth)	2.44 ± 1.78	0.08 ± 0.33	9.962	<0.001***
NSSI diary card (1 week)	1.52 ± 1.91	0.08 ± 0.33	5.619	<0.001***

***Indicates $p < 0.001$.

TABLE 4 Regression analysis of the reduction rate of NSSI after 8 weeks of treatment.

Variable		B	B 95% CI		Beta	*t*	*P*
Latency, ms	N1	−0.001	−0.014	0.012	−0.025	−0.191	0.849
	P2	0.001	−0.01	0.019	0.230	1.917	0.063
	N2	0.000	−0.08	0.007	−0.006	−0.061	0.952
	P3a	0.002	−0.014	0.018	0.045	0.275	0.785
	P3b	0.002	−0.012	0.017	0.055	0.328	0.745
Amplitude, μV	N1	−0.029	0.073	0.014	−0.164	−1.372	0.178
	P2	−0.043	−0.09	0.04	−0.195	−1.852	0.072
	N2	0.02	−0.014	0.18	0.109	0.957	0.785
	P3a	−0.011	−0.046	0.024	−0.077	−0.62	0.539
	P3b	0.112	0.069	0.155	0.672	5.242	<0.001***
HAMD-24 (8 week)		−0.015	−0.039	0.010	−0.126	−1.234	0.225

$R^2 = 0.666$, $F = 6.693$, $df = 11$, $P < 0.001$.

***Indicates $p < 0.001$.

R^2, coefficient of determination; F, statistics in F, Fisher–Snedecor test; df, degrees of freedom; P, probability in the test; B, unstandardized parameter; CI, confidence interval; Beta standardized parameter (size of effect); t, statistics in *t* test.

NSSI, non-suicidal self-injury.

(Bareš et al., 2007; Albert et al., 2010; Sanger and Dorjee, 2015; Deiber et al., 2021; Penengo et al., 2022), which seems to explain the results of this study. One study found that the main effect of N2 component was significant under whether self-injury cues were present, and N2 represented conflict detection and monitoring, which may indicate that greater conflicts were generally detected during exposure to self-injury cues (Zhou et al., 2022). Under the self-injury cue, the P3 amplitude of NSSI group was larger than that of HC group, and the P3 amplitude with the self-injury cue was significantly larger than that with the neutral cue, indicating that the neural response of NSSI adolescents changed during exposure to the self-injury cue (Zhou et al., 2022). Allen found difficulty in response inhibition in the group of eating disorders with NSSI (Allen et al., 2020), Nilsson also found that compared with healthy people (Nilsson et al., 2021), patients with intentional self-mutilation had defects in cognitive flexibility and response inhibition, and Zhang also found executive dysfunction in the group of MDD adolescents with NSSI (Zhang et al., 2022). Our study find neuroelectrophysiological evidence in the adolescent MDD with NSSI compared with HC.

At present, there is no effective drug treatment option for adolescent NSSI. According to the treatment guidelines for adolescent MDD (Cheung et al., 2018; American Psychological Association [APA], 2019) and the treatment guidelines for adolescent NSSI (National Institute for Health and Care Excellence [NICE], 2011; Plener et al., 2016), SSRI seems to be the preferred treatment for adolescent MDD with NSSI behavior, because they are beneficial to alleviate depressive symptoms and do not seem to increase the rate of NSSI (Cheung et al., 2018; American Psychological Association [APA], 2019). Based on this, sertraline was selected as drug treatment in this study. The results showed that the frequency of self-injury behavior decreased significantly after the sertraline treatment. Previous studies have different evidence. The results of a study in the group of adolescent refractory depression show that the subjects who choose SSRI for intervention have the lowest incidence of self-injury behavior (Brent et al., 2009). Glenn found that among adolescents with anxiety disorder, the frequency of self-injury in the intervention group combined with fluoxetine decreased significantly compared with adolescents who only used cognitive behavioral therapy (Melvin et al., 2019). However, a recent meta-analysis of psychotropic drugs for the treatment of NSSI in children and adolescents showed that there was no statistically significant difference in the occurrence of NSSI in adolescents between SSRI and the control group (drug or placebo) (Eggart et al., 2022). Whether there is a recommended drug choice for NSSI behavior of adolescents needs to be carried out in a larger randomized controlled study in the future.

The results of regression analysis showed that baseline P3b amplitudes had a significant positive predictive effect on the 8 week NSSI frequency, which indicated that the higher the baseline amplitude, the higher the reduction rate of 8 week NSSI behavior frequency. Many studies suggest that P3 components are related to response inhibition and executive function (Zhang et al., 2021; Egbert et al., 2022; Reed et al., 2022), which indicates that subjects with higher response inhibition and executive function at baseline, the NSSI behavior are more likely to reduce significantly after treatment. The results of a systematic review of neuroimaging of NSSI behavior showed that the activation of brain areas related to executive function decreased in NSSI samples (Brañas et al., 2021). The results of a near infrared spectroscopy study suggest that NSSI patients show the deactivation of the dorsolateral prefrontal cortex (DLPFC), which plays a key role in the executive regulation of cognitive

and behavioral responses to the environment (Zahid et al., 2020). The results of a cross-sectional resting state fMRI study in MDD samples of adolescents with NSSI behavior also provide supporting evidence (Huang et al., 2021). In the past, most studies on self-injury behavior focused on the use of scale evaluation to find mediators or regulatory variables, and most studies on neuroimaging were cross-sectional studies. To our knowledge, this study found neurophysiological markers that can predict the reduction of self-injury behavior in adolescent MDD with NSSI for the first time.

This study has some limitations. firstly, the sample size is relative small. Although we found that the baseline P300 index can predict the reduction of adolescent MDD patients self-injury frequency, this needs to be verified in a larger cohort; adolescent MDD group without NSSI behavior was not included in this study, which is also a limitation; 8 weeks follow-up is relatively short, we will continue to follow up.

Conclusion

Compared with HC subjects, the cognitive impairment of adolescent MDD with NSSI patients was mainly manifested in response inhibition, decreased executive function and poor anti-interference ability. Baseline P300 can be used as a potential predictor of the improvement of 8 week NSSI frequency in MDD adolescents with NSSI behavior.

Data availability statement

The datasets presented in this article are not readily available because they contain sensitive patient information. The data supporting the conclusions of this article will be made available upon reasonable request by any qualified researcher. Requests to access the datasets should be directed to the corresponding author.

Ethics statement

The studies involving human participants were reviewed and approved by Ethics Committee of the First Hospital of Shanxi Medical University. Written informed consent to participate in this study was provided by the participants' legal guardian/next of kin.

Author contributions

HSL and YW designed the study and involved in data acquisition, analysis, and interpretation. XL and TR contributed to the data acquisition. GL, YX, DQ, and CY contributed to the study design and data interpretation. XZ involved in clinical assessment of participants and involved in patient follow up. ZL served as advisors and were responsible for overall oversight of the study. All authors participated in the drafting or critical review of the article, gave final approval of the version to be published, and agreed to be accountable for all aspects of the work.

Funding

This work was supported by the National Natural Science Foundation of China (Grant nos. 82171534 and 81601193), the Key Research and Development Project (International Cooperation) of Shanxi Province (Grant no. 201903D421059), the Shanxi Province Science Foundation for Youths (Grant no. 2015021204), the Research Project Supported by Shanxi Scholarship Council of China (Grant no. 2015-100), and the First Hospital of Shanxi Medical University Foundation for Youths Innovation (Grant no. YC1409).

Conflict of interest

The authors declare that the research was conducted in the absence of any commercial or financial relationships that could be construed as a potential conflict of interest.

Publisher's note

References

Albert, J., López-Martín, S., and Carretié, L. (2010). Emotional context modulates response inhibition: Neural and behavioral data. *Neuroimage* 49, 914–921. doi: 10.1016/j.neuroimage.2009.08.045

Allen, K. J., Sammon, M. M., Fox, K. R., and Stewart, J. G. (2020). Emotional response inhibition: A shared neurocognitive deficit in eating disorder symptoms and nonsuicidal self-injury. *Brain Sci.* 10:104. doi: 10.3390/brainsci10020104

American Psychological Association [APA] (2019). *Clinical practice guideline for the treatment of depression across three age cohorts*. Washington, DC: Author.

Andover, M. S. (2014). Non-suicidal self-injury disorder in a community sample of adults. *Psychiatry Res.* 219, 305–310. doi: 10.1016/j.psychres.2014.06.001

Bareš, M., Nestrašil, I., and Rektor, I. (2007). The effect of response type (motor output versus mental counting) on the intracerebral distribution of the slow cortical potentials in an externally cued (CNV) paradigm. *Brain Res. Bull.* 71, 428–435. doi: 10.1016/j.brainresbull.2006.10.012

Brañas, M. J., Croci, M. S., Ravagnani Salto, A. B., Doretto, V. F., Martinho, E., Macedo, M., et al. (2021). Neuroimaging studies of nonsuicidal self-injury in youth: A systematic review. *Life* 11:729. doi: 10.3390/life11080729

Brent, D. A., Emslie, G. J., Clarke, G. N., Asarnow, J., Spirito, A., Ritz, L., et al. (2009). Predictors of spontaneous and systematically assessed suicidal adverse events in the treatment of SSRI-resistant depression in adolescents (TORDIA) study. *Am. J. Psychiatry* 166, 418–426. doi: 10.1176/appi.ajp.2008.08070976

Centers for Disease Control and Prevention [CDC] (2009). *Web-based injury statistics query and reporting system (WISQARS)*. Atlanta, GA: Centers for Disease Control and Prevention.

Chen, T.-J., Yu, Y. W.-Y., Chen, M.-C., Wang, S.-Y., Tsai, S.-J., and Lee, T.-W. (2005). Serotonin dysfunction and suicide attempts in major depressives: An auditory event-related potential study. *Neuropsychobiology* 52, 28–36. doi: 10.1159/000086175

Cheung, A. H., Zuckerbrot, R. A., Jensen, P. S., Laraque, D., Stein, R. E., Levitt, A., et al. (2018). Guidelines for adolescent depression in primary care (GLAD-PC): Part II. Treatment and ongoing management. *Pediatrics* 141:e20174082.

Cimen, I., Coşkun, A., and Etiler, N. (2017). Non-suicidal self-injury behaviors' features and relationship with adolescents' daily life activities and mental status. *Turk. J. Pediatr.* 59, 113–121 doi: 10.24953/turkjped.2017.02.002

Deiber, M.-P., Ammann, C., Hasler, R., Colin, J., Perroud, N., and Ros, T. (2021). Electrophysiological correlates of improved executive function following EEG neurofeedback in adult attention deficit hyperactivity disorder. *Clin. Neurophysiol.* 132, 1937–1946. doi: 10.1016/j.clinph.2021.05.017

Duncan, C. C., Kosmidis, M. H., and Mirsky, A. F. (2005). Closed head injury-related information processing deficits: An event-related potential analysis. *Int. J. Psychophysiol.* 58, 133–157. doi: 10.1016/j.ijpsycho.2005.05.011

Egbert, A. H., Stockdale, L. A., Nicholson, L. M., Sroka, A., Szpak, V., Morrison, R. G., et al. (2022). Delicious and difficult to resist?: Inhibitory control differs in young women after exposure to food and non-food commercials. *Appetite* 173:105993. doi: 10.1016/j.appet.2022.105993

Eggart, V., Cordier, S., Hasan, A., and Wagner, E. (2022). Psychotropic drugs for the treatment of non-suicidal self-injury in children and adolescents: A systematic review and meta-analysis. *Eur. Arch. Psychiatry Clin. Neurosci.* [Epub ahead of print]. doi: 10.1007/s00406-022-01385-w

Fleming, T. M., Clark, T., Denny, S., Bullen, P., Crengle, S., Peiris-John, R., et al. (2014). Stability and change in the mental health of New Zealand secondary school students 2007–2012: Results from the national adolescent health surveys. *Austr. N.Z. J. Psychiatry* 48, 472–480. doi: 10.1177/0004867413514489

Gao, Y., Xiong, Y., Liu, X., and Wang, H. (2021). The effects of childhood maltreatment on non-suicidal self-injury in male adolescents: The moderating roles of the monoamine oxidase a (MAOA) gene and the catechol-o-methyltransferase (comt) gene. *Int. J. Environ. Res. Public health* 18:2598. doi: 10.3390/ijerph18052598

Gómez-Lumbreras, A., Sangenis, A. G., Vallverdú, O., Carbó, A., and Pedrós, R. (2021). Psychotropic use in children and adolescents in Scandinavia and Catalonia: A 10-year Population-Based Study. *Psychopharmacology* 238, 1805–1815. doi: 10.1007/s00213-021-05809-8

Hasking, P., Whitlock, J., Voon, D., and Rose, A. (2017). A cognitive-emotional model of NSSI: Using emotion regulation and cognitive processes to explain why people self-injure. *Cogn. Emot.* 31, 1543–1556. doi: 10.1080/02699931.2016.1241219

Huang, Q., Xiao, M., Ai, M., Chen, J., Wang, W., Hu, L., et al. (2021). Disruption of neural activity and functional connectivity in adolescents with major depressive disorder who engage in non-suicidal self-injury: A resting-state fMRI study. *Front. Psychiatry* 12:571532. doi: 10.3389/fpsyt.2021.571532

Jacobson, C. M., and Gould, M. (2007). The epidemiology and phenomenology of non-suicidal self-injurious behavior among adolescents: A critical review of the literature. *Arch. Suicide Res.* 11, 129–147. doi: 10.1080/13811110701247602

Jiang, Y., Ren, Y., Liu, T., and You, J. (2021). Rejection sensitivity and adolescent non-suicidal self-injury: Mediation through depressive symptoms and moderation by fear of self-compassion. *Psychol. Psychother.* 94, 481–496. doi: 10.1111/papt.12293

Kaštelan, A., Hladnik, A., Petrić, D., Gudelj, L., and Graovac, M. (2019). Prescribing patterns in adolescent psychiatric practice: An important role of antipsychotics. *Psychiatr. Danub.* 31, 153–161.

Klonsky, E. D., May, A. M., and Glenn, C. R. (2013). The relationship between nonsuicidal self-injury and attempted suicide: Converging evidence from four samples. *J. Abnorm. Psychol.* 122:231. doi: 10.1037/a0030278

Laye-Gindhu, A., and Schonert-Reichl, K. A. (2005). Nonsuicidal self-harm among community adolescents: Understanding the "Whats" and "Whys" of self-harm. *J. Youth Adolesc.* 34, 447–457. doi: 10.1007/s10964-005-7262-z

Leone, C., Galosi, S., Mollica, C., Fortunato, M., Possidente, C., Milone, V., et al. (2021). Dissecting pain processing in adolescents with non-suicidal self injury: Could suicide risk lurk among the electrodes? *Eur. J. Pain* 25, 1815–1828. doi: 10.1002/ejp.1793

Libal, G., Plener, P. L., Ludolph, A. G., and Fegert, J. M. (2005). Ziprasidone as a weight-neutral alternative in the treatment of self-injurious behavior in adolescent females. *Child Adolesc. Psychopharmacol. News* 10, 1–6. doi: 10.1521/capn.2005.10.4.1

Liu, Z.-Z., Chen, H., Bo, Q.-G., Chen, R.-H., Li, F.-W., Lv, L., et al. (2018). Psychological and behavioral characteristics of suicide attempts and non-suicidal self-injury in Chinese adolescents. *J. Affect. Disord.* 226, 287–293. doi: 10.1016/j.jad.2017.10.010

Melvin, G. A., Finnin, L., Taffe, J., Dudley, A. L., Klimkeit, E. I., Gordon, M. S., et al. (2019). Adverse events reported by anxious school refusing adolescents receiving cognitive behavioral therapy with and without fluoxetine. *Clin. Child Psychol. Psychiatry* 24, 892–905. doi: 10.1177/1359104518822681

National Institute for Health and Care Excellence [NICE] (2011). *Self-harm in over 8s: long-term management. Clinical guideline CG133*. London: NICE.

Nilsson, M., Lundh, L., Westrin, Å, and Westling, S. (2021). Executive functioning in psychiatric patients with deliberate self-harm, as compared with a psychiatric and a healthy comparison group. *J. Clin. Exp. Neuropsychol.* 43, 225–237. doi: 10.1080/13803395.2021.1894094

Ougrin, D., Tranah, T., Stahl, D., Moran, P., and Asarnow, J. R. (2014). Therapeutic Interventions for Suicide Attempts and Self-Harm in Adolescents: Systematic Review and Meta-Analysis. *J. Am. Acad. Child Adolesc. Psychiatry* 54, 97–107. doi: 10.1016/j.jaac.2014.10.009

Penengo, C., Colli, C., Bonivento, C., Boscutti, A., Balestrieri, M., Delvecchio, G., et al. (2022). Auditory event-related electroencephalographic potentials in borderline personality disorder. *J. Affect. Disord.* 296, 454–464. doi: 10.1016/j.jad.2021.09.096

Plener, P. L., Brunner, R., Fegert, J. M., Groschwitz, R. C., In-Albon, T., Kaess, M., et al. (2016). Treating nonsuicidal self-injury (NSSI) in adolescents: Consensus based German guidelines. *Child Adolesc. Psychiatry Ment. Health* 10:46. doi: 10.1186/s13034-016-0134-3

Polich, J. (2012). "Neuropsychology of P300," in *The Oxford handbook of eventrelated potential components*, eds S. J. Luck and E. S. Kappenman (Oxford: Oxford University Press), 159–188.

Rasmussen, S., and Hawton, K. (2014). Adolescent self-harm: A school-based study in Northern Ireland. *J. Affect. Disord.* 159, 46–52.

Reed, C. L., Siqi-Liu, A., Lydic, K., Lodge, M., Chitre, A., Denaro, C., et al. (2022). Selective contributions of executive function ability to the P3. *Int. J. Psychophysiol.* 176, 54–61. doi: 10.1016/j.ijpsycho.2022.03.004

Ross, S., and Heath, N. (2002). A study of the frequency of self-mutilation in a community sample of adolescents. *J. Youth Adolesc.* 31, 67–77. doi: 10.1023/A:1014089117419

Sanger, K. L., and Dorjee, D. (2015). Mindfulness training for adolescents: A neurodevelopmental perspective on investigating modifications in attention and emotion regulation using event-related brain potentials. *Cogn. Affect. Behav. Neurosci.* 15, 696–711. doi: 10.3758/s13415-015-0354-7

Saraff, P. D., and Pepper, C. M. (2014). Functions, lifetime frequency, and variety of methods of non-suicidal self-injury among college students. *Psychiatry Res.* 219, 298–304. doi: 10.1016/j.psychres.2014.05.044

Swannell, S. V., Martin, G. E., Page, A., Hasking, P., and St John, N. J. (2014). Prevalence of nonsuicidal self-injury in nonclinical samples: Systematic review,

meta-analysis and meta-regression. *Suicide Life Threat. Behav.* 44, 273–303. doi: 10.1111/sltb.12070

Wen, Y., Zhang, X., Xu, Y., Qiao, D., Guo, S., Sun, N., et al. (2021). Cognitive impairment in adolescent major depressive disorder with nonsuicidal self-injury: Evidence based on multi-indicator ERPs. *Front. Hum. Neurosci.* 15:81. doi: 10.3389/fnhum.2021.637407

Whitlock, J., Muehlenkamp, J., Purington, A., Eckenrode, J., Barreira, P., Baral Abrams, G., et al. (2011). Nonsuicidal self-injury in a college population: General trends and sex differences. *J. Am. Coll. Health* 59, 691–698. doi: 10.1080/07448481.2010.529626

Zahid, Z., Mcmahon, L., and Lynch, M. (2020). Neural activity across the dorsolateral prefrontal cortex and risk for suicidal ideation and self-injury. *Archives of Suicide Research* 26, 187–207. doi: 10.1080/13811118.2020.1779154

Zetterqvist, M. (2015). The DSM-5 diagnosis of nonsuicidal self-injury disorder: A review of the empirical literature. *Child Adolesc. Psychiatry Ment. Health* 9:31. doi: 10.1186/s13034-015-0062-7

Zhang, S. S., Zhang, Y., and Fang, J. (2018). Childhood psychological maltreatment,neglect and self-injury behavior of college students: The mediating effect of social support. *Mod. Prev. Med.* 45, 824–827.

Zhang, Y., Lai, S., Wu, W., Wang, Y., Zhu, Y., Chen, G., et al. (2022). Associations between executive function impairment and biochemical abnormalities in depressed adolescents with non-suicidal self-injury. *J. Affect. Disord.* 298, 492–499. doi: 10.1016/j.jad.2021.10.132

Zhang, Y., Ou, H., Yuan, T.-F., and Sun, J. (2021). Electrophysiological indexes for impaired response inhibition and salience attribution in substance (stimulants and depressants) use disorders: A meta-analysis. *Int. J. Psychophysiol.* 170, 133–155. doi: 10.1016/j.ijpsycho.2021.10.008

Zhou, D.-D., Zhao, L., Ma, L.-L., Hu, J.-H., Chen, R., Jiang, Z.-H., et al. (2022). Altered neural reactivity in adolescents with nonsuicidal self-injury during exposure to self-injury related cues: Electrophysiological evidence from a two-choice oddball paradigm. *Front. Psychiatry* 13:649. doi: 10.3389/fpsyt.2022.827480

Frontiers in Neuroscience

Provides a holistic understanding of brain function from genes to behavior

Part of the most cited neuroscience journal series which explores the brain - from the new eras of causation and anatomical neurosciences to neuroeconomics and neuroenergetics.

Discover the latest Research Topics

See more →

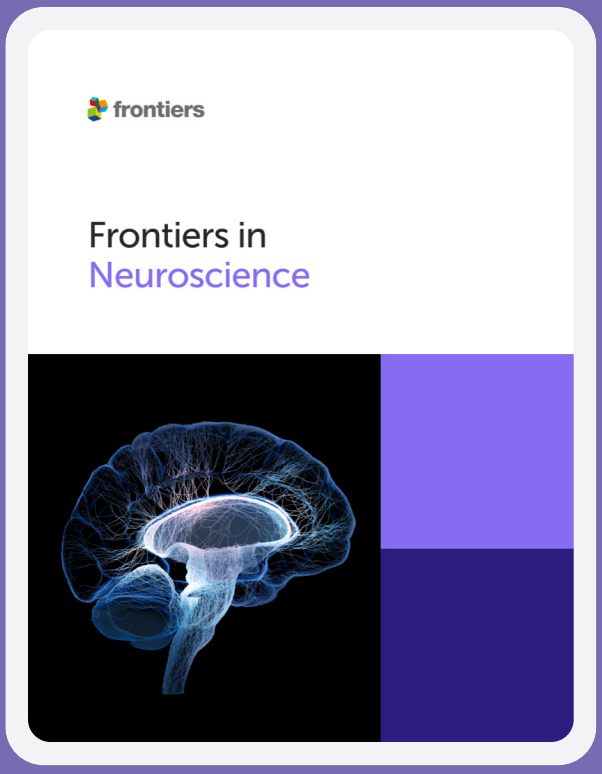

Frontiers

Avenue du Tribunal-Fédéral 34
1005 Lausanne, Switzerland
frontiersin.org

Contact us

+41 (0)21 510 17 00
frontiersin.org/about/contact